TRANSACTIONS
OF THE ASME
Series E

Journal of APPLIED MECHANICS

December 1960

DYNAMICS • VIBRATIONS • ELASTICITY • LUBRICATION AND WEAR
RHEOLOGY • FRACTURES • STRUCTURES • HYDRAULICS • AERODYNAMICS
INTERNAL FLOW • MECHANICAL PROPERTIES OF METALS • THERMODYNAMICS
TURBULENCE • HEAT TRANSFER • COMPUTING DEVICES AND METHODS
BOUNDARY LAYERS • AEROELASTICITY • EXPERIMENTAL STRESS ANALYSIS

Published Quarterly by
THE AMERICAN SOCIETY OF MECHANICAL ENGINEERS

TRANSACTIONS
OF THE ASME
Series E

EDITORIAL DEPARTMENT

Editor, J. J. JAKLITSCH, JR.
Consulting Editor, LEO BLODGETT
Art Editor, HENRY BALFOUR
Production, HILDA E. WILSON

APPLIED MECHANICS DIVISION

Chairman, S. S. RATKOWSKY
Secretary, A. M. WAHL
Technical Editor, D. C. DRUCKER
Technical Editor, J. KESTIN
Honorary Editor, JOHN E. LESSELLS

OFFICERS OF THE ASME

President, W. L. CESLER
Secretary, O. B. SCHIER, II
Treasurer, E. J. KATES
Assistant Treasurer, H. J. BAUER

PUBLICATIONS COMMITTEE

Chairman, R. A. BENOTZKI
HENDLEY N. BLACKMON
R. D. BINDLIN
MARTIN GOLAND
VITO L. SALERNO

Junior Representatives
A. S. GOLDSTEIN
J. W. POLLAMBEE

REGIONAL ADVISORY BOARD

Region I, M. E. REISS, JR.
Region II, GLENN E. FIFLING
Region III, F. J. HENZIE
Region IV, FRANCIS C. SMITH
Region V, H. M. CATHER
Region VI, C. R. EARLE
Region VII, R. E. GIBBENHAUER
Region VIII, CARL J. ECKHARDT

Published quarterly by The American Society of Mechanical Engineers. Publication office at 20th and Northampton Streets, Easton, Pa. The editorial department is located at the headquarters of the Society, 29 West Thirty-Ninth Street, New York 18, N. Y. Cable address, "Dyneer," New York. Price $3.00 a copy, $10.00 annually to members, $3.00 a copy, $8.00 annually. Add 50 cents for postage to all countries outside the United States and Canada. Changes of address must be received at Society headquarters seven weeks before they are to be effective on the mailing list. Please send old as well as new address. . . . By-Laws: The Society shall not be responsible for statements or opinions advanced in papers or . . . printed in its publications (B13, Par. 4). . . . Second-class mail privileges authorized at Easton, Penna. . . . This publication is authorized to be mailed at the special rates of postage prescribed by Section 132.122 . . . © Copyright, 1960, by The American Society of Mechanical Engineers. Reprints from this publication may be made on condition that full credit be given the TRANSACTIONS of the ASME, Series E—Journal of Applied Mechanics, and the author, and that date of publication be stated.

TRANSACTIONS OF THE ASME
is indexed by the Engineering Index, Inc.

Journal of APPLIED MECHANICS

VOLUME 27 • SERIES E • NUMBER 4

December 1960

CONTENTS

TECHNICAL PAPERS

603 **Two-Dimensional Gas Jets** (60—APM-27)
M. J. Cohen

609 **On the Compressibility Effects of the Lubricant for Two-Dimensional Slider Bearings** (60—WA-29)
K. T. Yen

613 **Heat Transfer and Sublimation at a Stagnation Point in Potential Flow** (60—WA-20)
W. W. Short

617 **Transient Heat Conduction in a Rod of Finite Length With Variable Thermal Properties** (60—WA-25)
W. H. Chu and H. N. Abramson

623 **Transient Conduction in Coaxial Cylinders With Relative Motion and Heat Generation** (60—APM-24)
V. S. Arpaci

629 **Thermal Stresses in an Elastic, Work-Hardening Sphere** (60—APMW-8)
Chintsun Hwang

635 **Thermal Stresses Due to Disturbance of Uniform Heat Flow by an Insulated Ovaloid Hole** (60—APMW-6)
A. L. Florence and J. N. Goodier

640 **Sinusoidal Excitation of a System With Bilinear Hysteresis** (60—APM-8)
T. K. Caughey

644 **Forced Oscillations of a Semi-Infinite Rod Exhibiting Weak Bilinear Hysteresis** (60—WA-28)
T. K. Caughey

649 **Random Excitation of a System With Bilinear Hysteresis** (60—WA-27)
T. K. Caughey

653 **Vibrations of Elastic Sandwich Cylindrical Shells** (60—WA-21)
Yi-Yuan Yu

663 **Free, Transverse Vibrations of a Solid Elastic Mass in an Infinitely Long, Rigid, Circular-Cylindrical Tank** (60—APMW-12)
J. H. Baltrukonis

669 **Free Vibration of Continuous Skin-Stringer Panels**
Y. K. Lin

677 **On a Class of Nonlinear Axisymmetric Plate Problems** (60—APMW-7)
F. Essenburg

681 **Flexural Stress Waves in an Infinite Elastic Plate Due to a Suddenly Applied Concentrated Transverse Load** (60—APMW-11)
Julius Miklowitz

690 **Propagation of Axisymmetric Waves in an Unlimited Elastic Shell** (60—WA-22)
A. Kalnins and P. M. Naghdi

696 **Plastic Analysis of Circular Conical Shells** (60—APM-31)
P. G. Hodge, Jr.

701 **The Elastic Half Plane Subjected to Surface Tractions With Random Magnitude or Separation** (60—APMW-10)
A. C. Eringen and J. W. Dunkin

CONTENTS

710 **On the Response of an Elastic Half-Space to a Moving Blast Wave** (60—APMW-9)
J. W. Miles

717 **The Penetration of Hard-Steel Spheres Into Plane Metal Surfaces** (60—WA-15)
Werner Goldsmith and Peter T. Lyman

726 **Stress Distributions Analyzed in Bispherical Co-Ordinates** (60–APMW-4)
T. P. Mitchell and J. A. Weese

DESIGN DATA AND METHODS

733 **Elastic-Plastic Bending of Curved Bars of Constant and Variable Thickness,** *H. D. Conway*

BRIEF NOTES

Graphical Investigation of Geometric Aspects of the Hertz Problem 735 *D. C. Gazis*

Effect of Axial Constraint on Instability of Thin Circular Shells 737 *J. Singer*

Coupled Bending and Torsional Vibrations of Restrained Thin-Walled Beams 739 *Y. K. Lin*

Energy Absorption of Aluminum Tubing 740 *L. D. Mutchler*

743 Vibrations of Thin Paraboloidal Shells of Revolution *Y. K. Lin and F. A. Lee*

744 The Lowest Natural Frequency of Elastic Arcs *E. Volterra and J. D. Morell*

747 An Accurate Expression for Gas-Pressure Drop *R. H. Foz*

749 Flow of Liquid Metal Past a Porous Flat Plate *G. Horvay*

DISCUSSION

751 Discussion of previously published papers by *W. E. Baker; B. Paul; B. Saelman; Akira Atsumi; R. Skalak and M. I. Yarymovych; P. R. Sethna; S. L. Soo and C. L. Tien; B. W. Shaffer and E. E. Ungar; J. Denavit and R. S. Hartenberg; Eugene Sevin*

BOOK REVIEWS

Advances in Applied Mechanics 759
Evaporation and Droplet Growth 759
760 Incompressible Aerodynamics
760 The Theory of Linear Viscoelasticity

TRANSACTIONS OF THE ASME Series B

Journal of
ENGINEERING FOR INDUSTRY

Volume 82 • Series B • Number 4

CONTENTS FOR NOVEMBER, 1960

283 Tensile and Short-Time Creep Properties of N-155 Alloy Sheet, by E. C. Bernett. (59—A-27)

303 A Photoelastic Analysis of Machining Stresses, by E. Usui and H. Takeyama. (59—A-37)

309 Correlation of Bendability of Materials With Their Tensile Properties, by J. Datsko and C. T. Yang. (59—A-110)

315 Comparisons Between the Shearing Properties of Alpha-Brass as Derived From the Cutting Process and From Static and Impact Torsion Tests, by S. S. Chang and W. B. Heginbotham. (59—A-38)

324 The Role of Friction in Metal Cutting, by S. Kobayashi and E. G. Thomsen. (59—A-132)

333 A Critical Comparison of Metal-Cutting Theories With New Experimental Data, by S. Kobayashi, R. P. Herzog, D. M. Eggleston, and E. G. Thomsen. (59—A-131)

348 New Developments in the Theory of the Metal-Cutting Process, Part I, by P. Albrecht. (59—A-243)

359 Structural Weight Approximation for a Bell-Nozzle Divergent Section, by G. D. Brewer and E. Levin. (59—A-69)

363 Optimum Tolerances of Sheet Materials for Flight Vehicles, by G. A. Hoffman. (59—A-70)

369 Mechanical Vibration Filters With Nonlinear Characteristics, by W. J. Worley. (59—A-42)

377 Refinement of Finite Difference Calculations in Kinematic Analysis, by B. W. Shaffer and I. Krause. (59—A-53)

382 The Measurement of Very Low Frictional Torques in Rotating Equipment, by M. Zaid and I. S. Tolins. (59—A-43)

387 Design by Quantitative Factor of Safety, by Hsuan-Loh Su. (59—A-48)

393 Study of Critical Velocity of Stick-Slip Sliding, by B. R. Singh. (59—A-146)

399 Inertial Effects in a Multiple-Ball Transmission, by W. S. Rouverol. (59—A-14)

407 Some Applications of the Cycloid in Machine Design, by E. P. Pollitt. (59—A-134)

415 A Discussion of the Vibration Characteristics of a Simple Mechanical Connection, by Arthur Sorensen, Jr. (59—A-41)

423 Deformation and Moments in Elastically Restrained Circular Plates Under Arbitrary Load or Linear Thermal Gradient, by M. Zaid and M. Farray. (59—A-39)

439 Dimensionless Parameters for Helical Compression Springs, by R. J. Erisman. (59—A-30)

444 Errata on previously published paper by R. C. Brewer.

TRANSACTIONS OF THE ASME Series A

Journal of
ENGINEERING FOR POWER
Volume 82 • Series A • Number 4

CONTENTS FOR OCTOBER, 1960

247 Throat Tap Nozzles Used for Accurate Flow Measurements, by K. C. Cotton and J. C. Westcott. (59—A-174)

264 Water-Treatment, Corrosion, and Internal-Deposit Studies for Eddystone, by R. C. Ulmer, H. A. Grabowski, and R. C. Patterson. (59—A-147)

275 The Selection of Materials and Fabricating Techniques for the Eddystone Boiler and Sulzer Control Valves, by E. C. Chapman and R. E. Lorentz, Jr. (59—A-318)

286 Development Associated With the Superpressure Turbine for Eddystone Station Unit No. 1, by W. E. Trumpler, Jr., A. F. LeBreton, E. A. Fox, and R. B. Williamson. (59—A-288)

293 Material Selection and Fabrication, Main Steam Piping for Eddystone No. 1, 1200-F and 5000-Psi Service, by R. H. Caughey and W. G. Benz, Jr. (59—A-327)

315 Solar Turbo Power Plant Design, by D. B. Mackay and E. L. Leventhal. (59—A-74)

325 Analysis of Solar-Furnace Performance in Mechanical Testing at Extremely High Temperatures, by G. S. Leon and M. E. Shank. (59—A-79)

TRANSACTIONS OF THE ASME Series C

Journal of
HEAT TRANSFER
Vol 82 • Series C • No. 4

CONTENTS FOR NOVEMBER, 1960

265 A Variable Density Single-Fluid Model for Two-Phase Flow With Particular Reference to Steam-Water Flow, by S. G. Bankoff. (59—HT-7)

273 Transient Temperatures and Thermal Stresses in Hollow Cylinders Due to Heat Generation, by John E. Schmidt and George Sonnemann. (59—A-144)

279 Thermal-Contact Resistance in Finned Tubing, by Karl A. Gardner and T. C. Carnavos. (59—A-135)

294 Mass Transfer, Flow, and Heat Transfer About a Rotating Disk, by E. M. Sparrow and J. L. Gregg. (58—A-107)

303 Heat Transfer and Effectiveness for a Turbulent Boundary Layer With Tangential Fluid Injection, by R. A. Seban. (59—A-177)

313 Sublimation Mass Transfer Through Compressible Boundary Layers on a Flat Plate, by T. K. Sherwood and Olev Trass. (59—A-137)

325 Laminar Skin Friction and Heat Transfer on Flat Plates With Wedge-Shaped Grooves in Flow Direction, by T. F. Irvine, Jr., and E. R. G. Eckert. (59—A-143)

333 Heat Transfer to Liquid Metals With Variable Properties, by R. Viskanta and Y. S. Touloukian. (59—A-148)

341 A Summary of Experiments on Turbulent Heat Transfer From a Nonisothermal Flat Plate, by W. C. Reynolds, W. M. Kays, and S. J. Kline. (59—A-157)

349 An Experimental Study of the Effects of Nonuniform Wall Temperature on Heat Transfer in Laminar and Turbulent Axisymmetric Flow Along a Cylinder, by R. Eichhorn, E. R. G. Eckert, and A. D. Anderson. (59—A-151)

360 Geometric Factors for Radiative Heat Transfer Through an Absorbing Medium in Cartesian Coordinates, by A. K. Oppenheim and J. T. Bevans. (59—A-206)

369 Thermal Radiation From a Cylindrical Enclosure With Specified Wall Heat Flux, by C. M. Usiskin and R. Siegel. (59—A-159)

375 Application of Variational Methods to Radiation Heat-Transfer Calculations, by E. M. Sparrow. (59—A-120)

381 Certain Thermodynamic and Transport Properties of the Atmospheres of Venus, Mars, and Jupiter, by W. E. Ibele and T. F. Irvine, Jr. (59—A-102)

M. J. COHEN
Senior Lecturer,
Northampton College
of Advanced Technology,
London, England

Two-Dimensional Gas Jets

A method is described for solving certain problems of subsonic aerodynamic design where flow boundaries in the physical plane are required to have specific dynamic characteristics. The method is tested on two type-problems with known exact solutions: the two-dimensional gas jet and the flow in the neighborhood of stagnation points. It has been found to give the solution with a degree of accuracy acceptable for practical design.

THIS paper illustrates in a particular instance the application of an approximate and simple approach to many problems of subsonic gas dynamics. The particular problem is Chaplygin's classical one on gas jets and has been chosen to check the degree of the approximation involved. The new solution technique, which is generally applicable to such problems of the indirect variety, has been developed elsewhere [1][1] and the solution is given here without elaboration. The immediate practical results appear in the form of contraction ratios for the complete range of nozzle angles and of subcritical exit-pressure conditions. The degree of the approximation is very close as can be gaged from the values given by Chaplygin [2].

An Approximate Solution to Gas-Jet Problem

Fundamentals. The two-dimensional gas jet issuing from a nozzle with an included angle of 2α between its straight walls, Fig. 1, possesses the familiar hodograph representation shown in Fig. 2. The log-modified hodograph plane, $\zeta = \Lambda + i\theta$, (LMH plane) obtained from the true hodograph plane ($q'e^{i\theta}$-plane) by means of the nonconformal transformation

$$\Lambda = \log\left(\frac{1}{\lambda}\right) = -\int \frac{(1 - \mathbf{M}^2)^{1/2}}{q'}\, dq', \qquad \theta = \theta \tag{1}$$

[1] Numbers in brackets designate References at end of paper.

Presented at the Summer Conference of the Applied Mechanics Division, University Park, Pa., June 20–22, 1960, of THE AMERICAN SOCIETY OF MECHANICAL ENGINEERS.

Discussion of this paper should be addressed to the Secretary, ASME, 29 West 39th Street, New York, N. Y., and will be accepted until January 10, 1961 for publication at a later date. Discussion received after the closing date will be returned.

First draft of manuscript received by ASME Applied Mechanics Division, October 17, 1958; final draft received, November 19, 1959. Paper No. 60—APM-27.

will exhibit the flow configuration for the gas jet shown in Fig. 3. In the ζ-plane, the field equations are the canonical forms [3]

$$\frac{\partial \phi}{\partial \Lambda} = T\,\frac{\partial \psi}{\partial \theta}$$
$$\frac{\partial \phi}{\partial \theta} = -T\,\frac{\partial \psi}{\partial \Lambda} \tag{2}$$

which can be written as

$$\frac{\partial^2 W}{\partial \zeta\, \partial \bar{\zeta}} = \tfrac{1}{2}\,\frac{\partial \log T}{\partial \zeta}\,\frac{\partial \bar{W}}{\partial \Lambda} \tag{3}$$

where

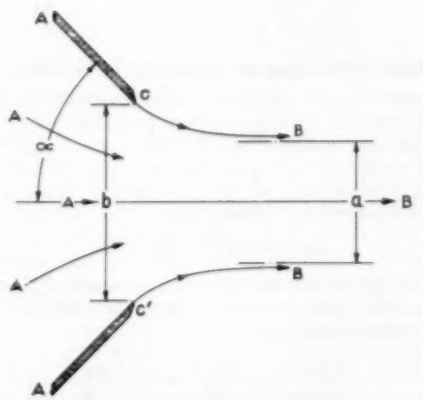

Fig. 1 Two-dimensional gas jet in physical plane; $r = a/b$

Nomenclature

I_r = I-function. $I_r = \oint \log T (d\Lambda)^r$, where $r = 1, 2, 3 \ldots$.
$\mathbf{M}$ = Mach number
q' = velocity in jet relative to sonic throat velocity: $q' = \frac{q}{a^*}$
q_0' = relative velocity at infinity downstream in jet or along free streamline of jet
r = jet-contraction ratio
T = $(1 - \mathbf{M}^2)^{1/2}/\rho'$
W = $\phi + i\psi$
W_0 = $\phi_0 + i\psi_0$, potential function of equivalent incompressible flow
z = complex variable in physical plane, $z = x + iy$
ds = element of streamline in physical plane
α = one half the included angle of a two-dimensional straight-walled nozzle
λ = velocity parameter defined by $d\lambda/\lambda = (1 - \mathbf{M}^2)^{1/2} dq'/q'$
Λ = velocity parameter defined by: $\Lambda = \log(1/\lambda)$
θ = angle of fluid velocity vector with datum
ϕ = velocity potential of flow
ψ = stream function of flow
ϕ_0 = velocity potential of equivalent incompressible flow
ψ_0 = stream function of equivalent incompressible flow
ζ = complex variable in log-modified hodograph plane: $\zeta = \Lambda + i\theta$
ζ_0 = position of sink singularity in the ζ-plane
ζ_1 = plane obtained from the ζ-plane by a conformal transformation
ρ = density in jet
ρ' = density in jet relative to stagnation or reservoir density ρ_s; i.e., $\rho' = \rho/\rho_s$
ρ_0' = relative density at infinity downstream in jet or along free streamline of jet
$d\sigma$ = element of a streamline in ζ-plane

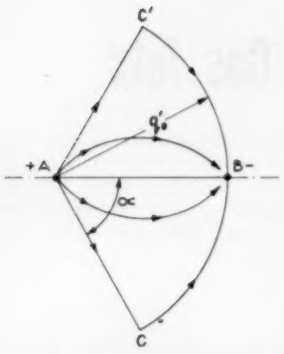

Fig. 2 Hodograph configuration for two-dimensional gas jet

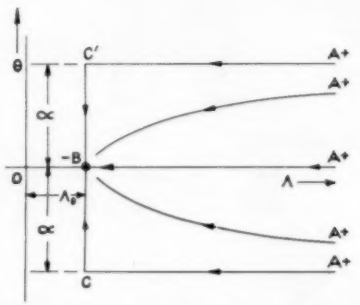

Fig. 3 Log-modified hodograph configuration for two-dimensional gas jet

$$W = \phi + i\psi$$

$$\bar{\zeta} = \Lambda - i\theta$$

and $\log T$ is a function of Λ only; i.e.,

$$\log T = \log T\,\{{}^1/_2(\zeta + \bar{\zeta})\}$$

It can be shown [1] that, if $W = W_0$ is a solution of the Laplace equation, $\partial^2 W/\partial\zeta\partial\bar{\zeta} = 0$, this being considered a first approximation to the solution of (3), since

$$\frac{\partial \log T}{\partial \zeta} = \frac{\partial \log T}{\partial \bar{\zeta}} = {}^1/_2 \frac{\partial \log T}{\partial \Lambda}$$

is small in the lower subsonic region, then

$$W = W_0 + {}^1/_2 \int \log T \frac{\partial \bar{W}_0}{\partial \bar{\zeta}}\, d\zeta \qquad (4)$$

is the solution of

$$\frac{\partial^2 W}{\partial \zeta \partial \bar{\zeta}} = {}^1/_2 \frac{\partial \log T}{\partial \zeta} \frac{\partial \bar{W}_0}{\partial \bar{\zeta}}$$

in closed form and a second and higher approximation to the exact solution of (3). This approach suggests a process of iteration in the derivation of higher and closer approximations, but the result so derived from even one further such step loses more from the increased mathematical complexity than it gains from additional accuracy. Equation (4) has the simplicity of formulation necessary to, and all the accuracy required for, practical application.

The integral in (4) can be integrated by parts in an infinite series which is absolutely convergent everywhere in the ζ-plane except in small regions near the singularities of W_0. Thus

$$W = W_0 - I_1 \frac{d\bar{W}_0}{d\bar{\zeta}} - 2I_2 \frac{d^2\bar{W}_0}{d\bar{\zeta}^2} + 2^2 I_3 \frac{d^3\bar{W}_0}{d\bar{\zeta}^3} + \cdots \qquad (5)$$

where

$$I_r = \int_{-}^{\Lambda} \log T (d\Lambda)^r \qquad (6)$$

The repeated integrations (6) are performed by assuming for $\log T$ the purely empirical representation, $-0.0350\,\{\log(\Lambda - a)\}^3$, which gives a very close approximation to its exact value, i.e.,

$$\log\,[(1 - \mathbf{M}^2)^{1/2}/\rho']$$

in the subsonic region; a is the value of Λ at sonic speed when $\mathbf{M} = 1$ and is numerically equal to 0.2775. These I_r-functions were observed [1] to obey closely the following sequential law throughout the subsonic range:

$$I_r = \frac{(-1)^{r+1}}{r^2\, r!} I_1, \qquad r \geq 1 \qquad (7)$$

and this observation has enabled (5) to be contracted, following a further approximation, to

$$W = W_0 + {}^1/_2 I_1 \left[\frac{d\bar{W}_0}{d\bar{\zeta}} + \bar{W}_0(\bar{\zeta} + 1) - W_0\right] \qquad (8)$$

or,

$$W = W_0 + {}^1/_2 I_1 \left[\frac{\partial}{\partial \Lambda} + e^{\frac{\partial}{\partial \Lambda}} - 1\right] \bar{W}_0$$

using an alternative operator form.

Equation (5) or (8) can be split into real and imaginary parts to give the velocity potential and stream functions, respectively.

Test Example. As an example, consider a type-solution of

$$\frac{\partial^2 W_0}{\partial \zeta \partial \bar{\zeta}} = 0,$$

such as $W_0 = e^{-n\zeta}$. This is of particular interest because it is the element solution in the LMH-plane corresponding to each term of the exact solution of any problem in the hodograph plane when expanded in a series in $e^{-\zeta}$. A better approximation to a solution of (3) would be, using (8) say,

$$W = \{e^{-n\zeta} - {}^1/_2 I_1(\overline{n+1} e^{-n\bar{\zeta}} - e^{-n(\bar{\zeta}+1)})\} \qquad (9)$$

which, split into its real and imaginary parts, yields

$$\phi = \{1 - {}^1/_2 I_1(\overline{n+1} - e^{-n})\}\phi_0,$$

and (10)

$$\psi = \{1 + {}^1/_2 I_1(\overline{n+1} - e^{-n})\}\psi_0$$

where

$$\phi_0 = \lambda^n \cos n\theta = \left(\frac{\lambda}{q'}\right)^n q'^n \cos n\theta,$$

and

$$\psi_0 = \lambda^n \sin n\theta = \left(\frac{\lambda}{q'}\right)^n q'^n \sin n\theta$$

Equations (10) can be rewritten as

$$\phi = Z_n q'^n \cos n\theta$$

$$\psi = Y_n q'^n \sin n\theta \qquad (11)$$

where

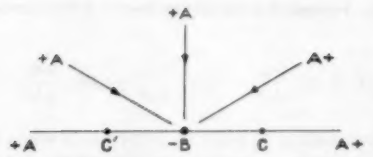

Fig. 4 ζ_1-plane configuration for two-dimensional gas jet

$$Y_n = \left(\frac{\lambda}{q'}\right)^n [1 + {}^1/_2 I_1(\overline{n+1} - e^{-n})] \tag{12}$$

Y_n has been checked for values of n up to $n = 6$ and found to be a very close approximation throughout the subsonic range to the hypergeometric-function equivalent appearing in the exact solution of (3) for this problem, Fig. 5. Equation (9) represents a close solution in the subsonic region to the flow in the neighborhood of a stagnation point at a solid corner which includes an angle of $2\pi/n$.

Two-Dimensional Gas Jet

Classical Solution. The exact solution for the two-dimensional gas jet was given by Chaplygin [2] for the case of the two-dimensional slot in a straight wall, and the solution extended to cover the whole range of jet angles, $0 \leq \alpha \leq 180$ deg, by C. Jacob [5] 32 years later. The problem is now treated by the method outlined in this paper. W_0, in a ζ_1-plane, Fig. 4, obtained from the ζ-plane by means of the conformal transformation

$$\zeta_1 = i \sinh \frac{\pi}{2\alpha}(\zeta - \zeta_0), \tag{13}$$

is

$$W_0 = \frac{m}{\pi} \log \zeta_1 \tag{14}$$

Substituting for ζ_1 from (13) in (14), gives the equivalent incompressible solution of the problem in the ζ-plane

$$W_0 = \frac{m}{\pi} \log \left\{ i \sinh \frac{\pi}{2\alpha}(\zeta - \zeta_0) \right\} \tag{15}$$

i.e.,

$$W_0 = \frac{m}{\pi} \left\{ \frac{\pi}{2\alpha}[(\Lambda - \Lambda_0) + i(\alpha + \theta)] - \sum_1^\infty \frac{e^{-\frac{\pi r}{\alpha}(\zeta - \zeta_0)}}{r} \right\} \tag{16}$$

Each of the terms under the summation sign is of the form $e^{-n\zeta}$ studied as an example earlier, and following the subsequent argument, (16) can be interpreted in terms of the compressible-flow problem using (10) or (11) to give

$$\psi = \frac{m}{\pi} \left\{ \frac{\pi}{2\alpha}(\alpha + \theta) + \sum_1^\infty \frac{1}{r} \frac{Y_{\pi r/\alpha}}{Y_{\pi r/\alpha, 0}} \left(\frac{q'}{q_0'}\right)^{\frac{r\pi}{\alpha}} \sin \frac{\pi r \theta}{\alpha} \right\} \tag{17}$$

This is the general solution by the method presented for the two-dimensional gas jet which, when $\alpha = \pi/2$, corresponds to the problem treated by Chaplygin [2]. $Y_{\pi r/\alpha}$ is given by (12) and corresponds to the exact hypergeometric function of the speed q' in Chaplygin's paper, which it closely approximates. $Y_{\pi r/\alpha, 0}$, which appears in the denominator of each term in the summation, is a constant; i.e., the value of $Y_{\pi r/\alpha}$ when $q' = q_0'$ on the free streamlines of the jet. These have been introduced to satisfy the boundary conditions on the free streamlines. The appearance of these factors leads to the question of boundary-condition satisfaction by the solution (8) proposed.

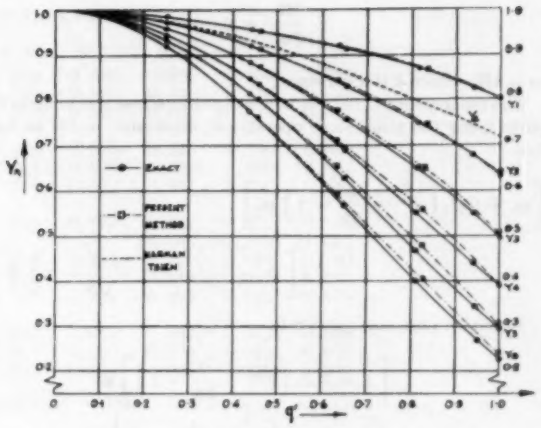

Fig. 5 Y_n-functions

Boundary Conditions. The necessity of satisfying the boundary conditions of the jet in the hodograph plane, i.e.,

$$\begin{aligned} \psi &= 0, \quad \text{when} \quad \theta = -\alpha,\ q' \text{ variable}, \\ &\qquad\qquad q' = q_0',\ \theta \text{ variable}, (<0) \\ \psi &= m, \quad \text{when} \quad \theta = \alpha,\ q' \text{ variable}, \\ &\qquad\qquad q' = q_0',\ \theta \text{ variable}, (>0) \end{aligned} \tag{18}$$

introduces the need for suitably modifying the coefficients of the terms in the summation as was done in (17). This implies that at least whenever one is dealing with problems involving both constant-velocity (free streamline) and constant-inclination boundaries in the hodograph plane the derivation of an approximate solution such as (8) is in itself not enough, since it should be expanded in a power series in $e^{-\zeta}$; that accomplished, its coefficients must then be suitably modified to satisfy the boundary conditions as was done in the case of the jet. The reason for this limitation on (8) is not far to seek. If W_0 is a solution within some boundaries in the equivalent incompressible hodograph field, then W, as given by (8), will be the approximate solution within the *same* boundaries in the compressible hodograph field only if these boundaries are constant-θ lines, as a brief study of (8) will show. If parts of the hodograph boundaries are not constant-θ lines, these parts will be distorted and the solution obtained, equation (8), will hold within, not the original boundaries, but within the boundaries so distorted. In order to overcome this effect and bring within the scope of the method proposed a large range of problems, for example the many problems involving a free-streamline boundary, the following quite formal and practical operational method is suggested; it is applied to the two-dimensional gas-jet problem in the following paragraph.

To investigate conditions near the free-streamline boundary, write instead of (8),

$$W = \frac{W_0 + {}^1/_2 I_1 \left[\frac{d\bar{W}_0}{d\bar{\zeta}} + \bar{W}_0(\bar{\zeta} + 1) - \bar{W}_0\right]}{\left[1 - {}^1/_2 I_1 \left(e^{\frac{\partial}{\partial \Lambda}} + \frac{\partial}{\partial \Lambda} - 1\right)\right]_0} \tag{19}$$

where the denominator is an "operational constant"; the suffix 0 denotes constant free-streamline conditions, and hence does not invalidate the general solution (8) since if W_0 is a solution of

$$\frac{\partial^2 W}{\partial\zeta\partial\bar{\zeta}} = 0,$$

so is kW_0 where k is a constant.

The numerator in (19) can now be split into real and imaginary parts using the alternative operational expression in (8) as follows:

$$\left[\phi_0 + {}^1/_2 I_1\left(e^{\frac{\partial}{\partial\Lambda}} + \frac{\partial}{\partial\Lambda} - 1\right)\phi_0\right] + i\left[\psi_0 - {}^1/_2 I_1\left(e^{\frac{\partial}{\partial\Lambda}} + \frac{\partial}{\partial\Lambda} - 1\right)\psi_0\right]$$

Equation (19) now splits into

$$\phi = \frac{\left[1 + {}^1/_2 I_1\left(e^{\frac{\partial}{\partial\Lambda}} + \frac{\partial}{\partial\Lambda} - 1\right)\right]\phi_0}{\left[1 - {}^1/_2 I_1\left(e^{\frac{\partial}{\partial\Lambda}} + \frac{\partial}{\partial\Lambda} - 1\right)\right]_0} \tag{20}$$

and

$$\psi = \frac{\left[1 - {}^1/_2 I_1\left(e^{\frac{\partial}{\partial\Lambda}} + \frac{\partial}{\partial\Lambda} - 1\right)\right]\psi_0}{\left[1 - {}^1/_2 I_1\left(e^{\frac{\partial}{\partial\Lambda}} + \frac{\partial}{\partial\Lambda} - 1\right)\right]_0}$$

which, on the boundary streamline, reduce to

$$\phi = \left\{\left[1 + I_1\left(e^{\frac{\partial}{\partial\Lambda}} + \frac{\partial}{\partial\Lambda} - 1\right)\right]\phi_0\right\}_0 \tag{21}$$

and

$$\psi = \psi_0$$

since ${}^1/_2 I_1$ is small throughout the subsonic range. The effect of the operator in brackets on ϕ_0 has been assumed to be at most of the order of ϕ_0 itself, except perhaps near the singularities of W_0.

Free-Streamline Boundary in the Physical Plane. Along a streamline the relation between a streamline element ds in the physical plane or z-plane and a streamline element $d\sigma$ in the LMH or ζ-plane is

$$ds = \frac{1}{q'}\frac{d\phi}{d\sigma}\,d\sigma$$

(i) Along $q' = \text{const}$, lines, i.e., free streamlines,

$$ds = \frac{1}{q'}\frac{\partial\phi}{\partial\theta}\,d\theta \tag{22}$$

i.e., from (21)

$$ds = \left\{(1 - I_1)\frac{\partial\phi_0}{\partial\theta} + \frac{\partial\phi_0(\Lambda + 1)}{\partial\theta}\right\}\frac{d\theta}{q'}, \quad \text{since} \quad \frac{\partial^2\phi_0}{\partial\Lambda\partial\theta} = 0 \tag{22a}$$

In the gas-jet case, $\partial\phi_0(\Lambda + 1)/\partial\theta \approx 0$, i.e., the flow at a large distance upstream of the orifice is nearly radial and therefore,

$$ds = (1 - I_1)\frac{d\phi_0}{q'} \tag{22b}$$

(ii) Along $\theta = \text{const}$, lines, i.e., along the straight walls of the jet,

$$ds = \frac{1}{q'}\frac{\partial\phi}{\partial\Lambda}\,d\Lambda \tag{23}$$

Using the expanded form of the first of (21) corresponding to (5), i.e.,

$$\phi = \phi_0 + 2I_1\frac{\partial\phi_0}{\partial\Lambda} - 2^2 I_2\frac{\partial^2\phi_0}{\partial\Lambda^2} + 2^3 I_3\frac{\partial^3\phi_0}{\partial\Lambda^3} - \ldots.$$

before differentiating, to avoid the error which would have arisen from differentiating an approximate equivalent, and reintroducing the approximation after the differentiation, (23) becomes

$$ds = \left\{1 + 2I_0 - I_1\left(\frac{\dfrac{\partial^2\phi_0}{\partial\Lambda^2}}{\dfrac{\partial\phi_0}{\partial\Lambda}} + \frac{\dfrac{\partial\phi_0(\Lambda + 1)}{\partial\Lambda}}{\dfrac{\partial\phi_0}{\partial\Lambda}} - 1\right)\right\}\frac{d\phi_0}{q'} \tag{23a}$$

In the gas-jet case

$$\frac{\partial\phi_0(\Lambda + 1)}{\partial\Lambda} \approx \frac{\rho'_0 q'_0}{\alpha},$$

assuming radial flow at a large distance upstream of the orifice, and therefore,

$$ds = \frac{(1 + 2I_0)d\phi_0}{q'} - I_1\left(\frac{\rho'_0 q'_0}{\alpha} - \frac{\partial\phi_0}{\partial\Lambda} + \frac{\partial^2\phi_0}{\partial\Lambda^2}\right)\frac{d\Lambda}{q'} \tag{23b}$$

or

$$ds \approx \frac{(1 + 2I_0)}{q'}\,d\phi_0, \quad \text{since} \quad I_1 \ll I_0$$

and assuming the terms in the second bracket to be of the same order. The free-streamline boundary is obtained from an integration of (22b), since it is a $q' = \text{const}$ line in the hodograph plane. If q_0' is this free-streamline velocity,

$$s = \frac{(1 - I_{1,0})}{q'_0}\int_0^\alpha\left(\frac{\partial\phi_0}{\partial\theta}\right)_0 e^{i\theta}\,d\theta \tag{24}$$

where again the suffix 0 refers the various quantities to their free-streamline values.

Contraction Ratios of Two-Dimensional Jets. This is defined as

$$\tau = \frac{1}{1 + \int_0^\alpha dy(\theta)} \tag{25}$$

where

$$dy(\theta) = ds\sin\theta$$

i.e.,

$$dy(\theta) = \frac{(1 - I_{1,0})}{q_0'}\left(\frac{\partial\phi_0}{\partial\theta}\right)_0\sin\theta d\theta \tag{26}$$

from equation (22b).

But on this particular streamline,

$$\frac{\partial\phi_0}{i\partial\theta}\,id\theta = \frac{dW_0}{d\zeta}\,d\zeta$$

and, hence, using (15) for the differentiation,

$$\frac{dW_0}{d\zeta}\,d\zeta = \frac{m}{2\alpha}\frac{\cos\dfrac{\pi\theta}{2\alpha}}{\sin\dfrac{\pi\theta}{2\alpha}}\,d\theta \tag{27}$$

Also consistent with (25), $m = 2\rho_0' q_0'$, since the breadth of the

Table 1 Jet contraction ratios, $r(\alpha, M_0) = a/b$

M_0 / α, deg	0	0.3	0.4	0.5	0.6	0.7	0.8	0.9	1.0
180	0.500	0.511	0.519	0.531	0.546	0.564	0.584	0.606	0.630
165	0.510	0.520	0.529	0.541	0.556	0.573	0.593	0.615	0.638
150	0.522	0.530	0.539	0.551	0.566	0.583	0.602	0.624	0.647
135	0.537	0.548	0.557	0.569	0.583	0.600	0.619	0.640	0.663
120	0.556	0.570	0.578	0.590	0.604	0.620	0.639	0.660	0.682
105	0.580	0.594	0.602	0.613	0.627	0.643	0.661	0.682	0.703
90	0.611	0.622	0.630	0.640	0.654	0.670	0.687	0.707	0.728
(90)	...	...	...	...	...	...	(0.688)	(0.713)	(0.74.)
75	0.648	0.660	0.668	0.678	0.691	0.705	0.722	0.740	0.760
60	0.693	0.703	0.710	0.720	0.732	0.745	0.760	0.777	0.793
45	0.748	0.758	0.764	0.772	0.783	0.795	0.808	0.822	0.836
30	0.815	0.823	0.828	0.835	0.843	0.851	0.861	0.872	0.883
15	0.897	0.903	0.905	0.908	0.914	0.920	0.925	0.931	0.938
0	1.000	1.000	1.000	1.000	1.000	1.000	1.000	1.000	1.000

( ), Values obtained by interpolation from Chaplygin's paper [2].

jet at infinity downstream has been taken as two units. Therefore,

$$r(\alpha, q_0') = \frac{1}{1 + \frac{2}{\pi}\rho_0'(1 - I_{1.0})\left\{\int_0^\alpha \cot\frac{\pi\theta}{2\alpha}\sin\theta\, d\left(\frac{\pi\theta}{2\alpha}\right)\right\}}$$

i.e.,

$$r(\alpha, q_0') = \frac{1}{1 + \frac{2}{\pi}\rho_0' K(\alpha)(1 - I_{1.0})} \tag{28}$$

where

$$K(\alpha) = \int_0^\alpha \cot\frac{\pi\theta}{2\alpha}\sin\theta\, d\left(\frac{\pi\theta}{2\alpha}\right)$$

When $\alpha = \pi/2$, $K(\alpha) = 1$ and

$$r\left(\frac{\pi}{2}, q_0'\right) = \frac{1}{1 + \frac{2}{\pi}\rho_0'(1 - I_{1.0})},$$

compared with $1\Big/\left(1 + \frac{2}{\pi}\rho_0'\right)$, which is equivalent to Demtchenko's [4] result. Equation (28) gives values of contraction ratios for the full range of values of α and exit pressure conditions in closed form provided the pressure at exit is subcritical. $K(\alpha)$ is a function of the jet-wall angle α only, whereas $\rho_0'(1 - I_{1.0})$ is a function of exit and reservoir pressure conditions only. Values of r are given in Table 1 for values of $0 < \alpha \leq 180$ deg and free-streamline Mach number $0 < M_0 \leq 1$. These show the closeness of the approximation in the case of the jet issuing from a slot in a plane wall even at the limiting value of $M = 1$. The error is everywhere less than 2 per cent. Demtchenko [4] who tackled the Chaplygin problem using an approximation of the von Karman-Tsien order obtained a result with an error over twice as large as that recorded here. The small error observed is due to (*a*) nonexact satisfaction of the boundary condition, and (*b*) the presence of a flow singularity on the hodograph boundary which makes the use of expansions like (5) and contractions such as (8) unjustified near the singularity, i.e., as one proceeds farther along the free streamline of the jet in the physical plane on its near parallel portion.

Conclusions

As explained at the beginning of the paper the two-dimensional gas-jet problem has been selected as a vehicle for the practical method proposed here for solving two-dimensional subsonic fluid-flow problems of the indirect variety. Problems of the indirect variety are, of course, problems involving the design of aerodynamic objects to perform specified practical functions, and hence, theoretically, the problem is set and solved in the hodograph plane which involves the dynamic parameters of the flow; the resultant physical boundary which will achieve the specific boundary conditions in the hodograph plane is derived by means of the standard transformation linking hodograph and physical planes.

The gas-jet problem and solution representing a classical advance in the field of high subsonic aerodynamics was chosen to ease an apprehension of the present method and also on account of the vast amount of research carried out on that particular topic. The method has also been used by the author for the design of wind-tunnel contractions (noncirculatory flow) and for the design of cascade blading (circulatory flow) but in this latter case not ignoring the hodograph-boundary distortion.

This last problem involves a study of the criterion for profile closure in the physical plane which can easily be achieved from considerations of continuity in that plane. In all the relevant cases the profiles were found to close practically exactly. The wind-tunnel solution was found to involve an over-all error of less than 2 per cent, measured by comparing contraction ratios for given inlet and outlet velocities, with sonic conditions at the throat. Because of the presence of flow singularities on the boundary in the hodograph plane, i.e., a source to represent conditions at infinity upstream in the tunnel and a sink to represent conditions at infinity downstream in the throat of the tunnel, this error was not unexpected and is of the same order as that observed in the case of the two-dimensional jet.

In short, the method is applicable whenever the equivalent incompressible-flow problem of the indirect variety, involving constant-inclination and constant-velocity boundaries in the hodograph plane, is soluble by standard conformal techniques except where there are singularities on the hodograph boundaries; even then the errors involved are of such an order as to be often acceptable for practical purposes.

Acknowledgment

The author wishes to thank Miss E. Dewdney for the speed, efficiency, and patience shown in providing the typescripts, and Mr. J. Hearnden for kindly drawing the figures and graphs illustrating the paper.

References

1 M. J. Cohen, "On the Solution of Compressible Flow Problems by an Analytic Method and by the Electric Network Analogue," Doctor's thesis, University of London, London, England, 1953.

2 A. Chaplygin, "Sur les jets gazeux," *Annales Scientifiques de l'Université de Moscou*, Phys. Maths. Div., vol. 21, 1904, pp. 1–121; also, "Gas Jets," NACA TM 1063, 1944.

3 C. C. Chang, "General Considerations of Problems in Compressible Flow Using the Hodograph Method," NACA TN 2582, January, 1952.

4 B. Demtchenko, "Sur les mouvements lents des fluides compressibles: Quelques problems d'hydrodynamique bi-dimensionelle des fluides compressibles," *Comptes-Rendus Academie des Sciences*, vol. 194, 1932, pp. 1218–1220; also PST Ministère de l'air, No. 144, 1939.

5 Caius Jacob, "Sur un jet gazeux," *Comptes-Rendus Academie des Sciences*, vol. 203, 1936, pp. 423–425.

On the Compressibility Effects of the Lubricant for Two-Dimensional Slider Bearings

K. T. YEN[1]
Professor,
Department of Aeronautical Engineering,
Rensselaer Polytechnic Institute,
Troy, N. Y.

An analytical study of the compressibility effects on the characteristics of two-dimensional slider bearings is made. By the variational method, it is shown that, for a given bearing length, no optimal film shape of the bearing can be found to yield a maximum total load. Analysis of the numerical results carried out for stepped films with a compressible lubricant under isothermal compression or expansion indicates that this anomaly is due to the nonlinear nature of the compressible problem. By considering a modified variational problem, it is further shown that stepped-film bearings with isothermal lubricant still yield the maximum total load for a given mass flow rate passing through the bearings, but the exact shape of the optimal stepped film is found to depend on the value of the maximum pressure.

A STUDY of the compressibility effects of the lubricant for two-dimensional slider bearings is made in this paper. When the lubricant is considered as incompressible, Lord Rayleigh [1][2] has shown that a stepped film yields the maximum total load for a given bearing length. Attempts have been made by Osterle and Saibel [2] to extend Rayleigh's analysis to other cases of interest. It will be shown in this paper, however, that for a "polytropic" compressible lubricant, no optimal shape of the film thickness can be found under the same given conditions as in the incompressible case.

This anomaly is apparently due to the nonlinear character of the compressible problem. For an incompressible lubricant the pressure distribution in the bearing is linear and varies linearly with the bearing length. In addition, when reduced to a nondimensional form, it depends only on the location of the step and the film-thickness ratio. When the flow is compressible, however, the pressure distribution depends not only on the location of the step and the film-thickness ratio, but also on the amount of the minimum film thickness (taken as the reference length) relative to the bearing length. Thus a variational problem for the compressible case formulated in the same manner as that for the incompressible case does not lead to a physically meaningful solution.

The foregoing variational problem can be modified to yield the result that, for a given mass flow rate passing through the bearing, the stepped film still yields the maximum total load. But no single optimal film shape is valid for the entire range of maximum pressure which occurs at the step of the bearing.

[1] Now on leave of absence at Space Sciences Laboratory, General Electric Company.

[2] Numbers in brackets designate References at end of the paper.

Contributed by the Applied Mechanics Division and presented at the Winter Annual Meeting, New York, N. Y., November 27–December 2, 1960, of THE AMERICAN SOCIETY OF MECHANICAL ENGINEERS.

Discussion of this paper should be addressed to the Secretary, ASME, 29 West 39th Street, New York, N. Y., and will be accepted until January 10, 1961, for publication at a later date. Discussion received after the closing date will be returned.

Manuscript received by Applied Mechanics Division, August 28, 1959. Paper No. 60—WA-29.

Some General Relations

The differential equation governing the fluid motion in a slider bearing of length L and with film thickness $h(x)$, Fig. 1, is

$$\rho u = Q, \tag{1}$$

where

$$u = {}^1/_2 Uh + \frac{h^3}{12\mu}\frac{dp}{dx}, \tag{2}$$

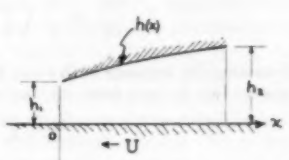

Fig. 1 Two-dimensional slider bearing

Nomenclature

h = film thickness
k = mass flow parameter = $2Q/\rho_0 h_1 U$
L = bearing length
n = exponent in density-pressure relation of lubricant
p = pressure
Q = mass flow rate
r = film-thickness ratio = h_2/h_1
s = step-location ratio = L_2/L_1
t = h/h_1
U = velocity of slider
W = total load of bearing
x = co-ordinate axis
λ = Lagrange multiplier
Λ = $6\mu UL/p_0 h_1^2$
μ = coefficient of viscosity of lubricant
ξ = $6\mu Ux/p_0 h_1^2$
π = p/p_0
ρ = density of lubricant

Subscripts

0 refers to ambient conditions
1 refers to outlet side of bearing
2 refers to inlet side of bearing
i refers to incompressible fluid
m refers to maximum value of pressure

and Q is the mass flow rate passing through the bearing. The direction of positive U is chosen to be along the negative x-axis. The pressure at both the inlet and the outlet of the bearing is equal to p_0, the ambient pressure.

The lubricant is assumed to satisfy the following "polytropic" density-pressure relation

$$\frac{\rho}{\rho_0} = \left(\frac{p}{p_0}\right)^n, \tag{3}$$

where the subscripts 0 refer to the ambient conditions, and the exponent n is a positive quantity. For $n = 0$, the lubricant is incompressible, and for $n = 1$, an isothermal process is assumed. In an actual compressible problem, the value of n is believed to lie between 1 and γ^{-1}, where γ is the ratio of specific heats [3].

For the present study, it is convenient to introduce the following transformations:

$$\pi = \frac{p}{p_0}, \qquad t = \frac{h}{h_1}, \qquad \xi = \frac{6\mu U}{p_0 h_1^2}\, x, \tag{4}$$

where h_1 is the film thickness at $x = 0$. Equation (1) can be written as

$$\pi^n t\left(1 + t^3 \frac{d\pi}{d\xi}\right) = (2Q/\rho_0 h_1 U) = k \tag{5}$$

The boundary conditions are

$$\pi = 1, \qquad \xi = 0, \qquad \text{and} \qquad \xi = \Lambda, \tag{6}$$

where Λ is the value of ξ at $x = L$.

For an incompressible fluid, the differential equation is

$$t\left(1 + t^3 \frac{d\pi_i}{d\xi}\right) = (2Q_i/\rho_0 h_1 U) = k_i, \tag{7}$$

while the boundary conditions are the same as (6). The incompressible problem can be solved easily, but, in general, the solution of the nonlinear differential equation (5) cannot be obtained in closed form. Based on the equations of motion and the boundary conditions, however, some observations on the compressible effects can be made.

Equations (5) and (7) can be written in the following form:

$$\frac{d\pi}{d\xi} = \frac{1}{t^3}\left(\frac{k}{\pi^n t} - 1\right), \tag{8}$$

$$\frac{d\pi_i}{d\xi} = \frac{1}{t^3}\left(\frac{k_i}{t} - 1\right) \tag{9}$$

Let us consider bearings with $\pi_i \geqslant 1$. Then, for a given value of Λ and t, it can be seen from (6), (8), and (9) that

$$k > k_i \tag{10}$$

This is due to the fact that, if $k \leqslant k_i$, the following relation

$$\frac{d\pi}{d\xi} < \frac{d\pi_i}{d\xi} \quad (0 < \xi < \Lambda) \tag{11}$$

would follow from (8) and (9). Under these circumstances, it is not possible for π to reach the value 1 at $\xi = \Lambda$. Hence $k > k_i$, and it follows that $(d\pi/d\xi)$ at $\xi = 0$ for the compressible case must be larger than that for the incompressible case. (This result has been confirmed by numerical calculations carried out for both stepped and linear films.)

The relation (10) shows that for given values of ρ_0, h_1, and U, the compressible-flow theory predicts a higher mass flow rate. In addition, since at the outlet of the bearing, the slope of the pressure curve for the compressible case is larger than that for the incompressible case, the centroid of the pressure curve for the compressible case is closer to the outlet than that for the incompressible case.

For bearings having pressure distribution with continuous slope, the maximum pressure for the compressible case is, from (5),

$$\pi_m{}^n = \frac{k}{t_m} = \frac{2Q}{\rho_0 h_m U}$$

Thus, to obtain higher π_m, it is desirable to have a large mass flow parameter and a small t_m, where t_m is the value of t at $\pi = \pi_m$. For the incompressible case, no analogous relation for π_{im} exists, but from (7), it is seen that

$$k_i = t_m$$

Thus the slope of the pressure curve for the incompressible case at the outlet of the bearing is determined by the value of t at the location of the maximum pressure.

Variational Problems

To find the optimal film shape for the maximum total load, the variational method is used. The problem is to find the film-thickness function t such that the total load of the bearing W, in a nondimensional form,

$$\frac{6\mu U W}{p_0 h_1^2} = \int_0^\Lambda \pi d\xi \tag{12}$$

is a maximum for a given Λ. The function π satisfies the differential equation (5), and the boundary conditions (6).

This variational problem can be solved by introducing a Lagrange multiplier function $\lambda(\xi)$, reference [4]. Thus the problem is to maximize

$$\int_0^\Lambda (\pi + \lambda G) d\xi, \tag{13}$$

where $G = 0$ is the differential equation satisfied by π.

For the incompressible case,

$$G_i \equiv \frac{dt}{d\xi} + 3t^2 \frac{dt}{d\xi}\frac{d\pi_i}{d\xi} + t^3 \frac{d^2\pi_i}{d\xi^2} = 0 \tag{14}$$

Two Euler's equations are obtained:

$$\left(1 + 3t^2 \frac{d\pi_i}{d\xi}\right)\frac{d\lambda}{d\xi} = 0,$$

$$1 - \frac{d}{d\xi}\left(t^3 \frac{d\lambda}{d\xi}\right) = 0$$

From the foregoing two equations and (7), it is found

$$\frac{d^2\pi_i}{d\xi^2} = 0, \tag{15}$$

$$t = {}^3/_2 k_i \tag{16}$$

For a stepped film, with the step at $\xi = \Lambda_1$ and the film-thickness ratio $r = (h_2/h_1)$, the pressure distribution is, from equation (7),

$$\pi_i - 1 = (k_i - 1)\xi, \qquad 0 \leqslant \xi \leqslant \Lambda_1, \tag{17}$$

$$r^2(\pi_i - 1) = \left(1 - \frac{k_i}{r}\right)(\Lambda - \xi), \qquad \Lambda_1 \leqslant \xi \leqslant \Lambda \tag{18}$$

Since the pressure distribution is continuous at $\xi = \Lambda_1$,

$$k_i = r(r^2 + s^3)/(r^3 + s), \tag{19}$$

where $s = \Lambda_2/\Lambda_1 = L_2/L_1$. The maximum pressure π_{im}, which can be expressed in the following form

$$\frac{\pi_{im} - 1}{\Lambda} = \frac{k_i - 1}{1 + s}, \tag{20}$$

is found to have its maximum, $\pi_{im} = 1 + .75\Lambda$, when $r = 1.866$, $s = 2.54$, and $k_i = 1.266$. These numerical values check with Rayleigh's results [1].

For the compressible case

$$G \equiv \pi^n \frac{dt}{d\xi} + t \frac{d\pi^n}{d\xi} + 3t^2 \frac{dt}{d\xi} (\pi^n) \frac{d\pi}{d\xi} + t^3 \frac{d}{d\xi}\left(\pi^n \frac{d\pi}{d\xi}\right) = 0, \tag{21}$$

and the Euler's equations are

$$\pi^n \left(1 + 3t^2 \frac{d\pi}{d\xi}\right) \frac{d\lambda}{d\xi} = 0,$$

$$1 - n\lambda t \left(1 + t^2 \frac{d\pi}{d\xi}\right) \frac{d\pi^{n-1}}{d\xi} - \left(nt\pi^{n-1} - \frac{dt^3}{d\xi} \pi^n\right) \frac{d\lambda}{d\xi} + t^3\pi^n \frac{d^2\lambda}{d\xi^2} = 0$$

However, no solution of optimal film shape for a maximum total load can be obtained from these equations.

In an attempt to clarify the foregoing anomaly, numerical calculations were carried out for bearings with stepped films and isothermal lubricant. The results obtained indicate that this anomaly is due to the nonlinear nature of the compressible problem. These numerical results are presented in the next section of this paper.

The variational problem for the compressible case can be made "determinate," if a subsidiary condition is imposed. A physically meaningful problem may be posed as follows: For a given mass flow parameter k, i.e., for given ρ_0, h_1, U, and Q, what is the film-thickness function t which would yield a maximum total load (for a given Λ)? The answer to this problem can be obtained easily. From (5),

$$\int_0^\Lambda \pi d\xi = k \int_0^\Lambda \frac{\pi^{1-n}}{t} d\xi - \int_0^\Lambda \pi t^2 \frac{d\pi}{d\xi} d\xi \tag{22}$$

Thus the problem is to maximize the right-hand side of equation (22). The Euler's equation is found to be

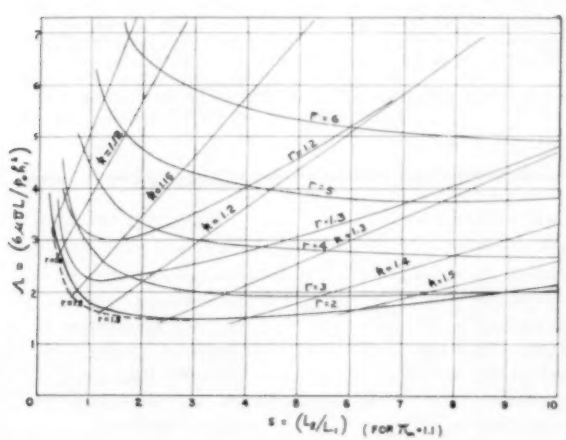

Fig. 2 Maximum pressure chart

$$(1 - n)k + \pi^{1+n} t \frac{dt^2}{d\xi} = 0 \tag{23}$$

For isothermal lubricant, i.e., $n = 1$, the result is $t = \text{const}$. Hence the stepped-film bearings are shown to be the optimal ones to use for this problem. The total load is found to be

$$\frac{6\mu UW}{p_0 h_1^2} = \tfrac{1}{2}(s^2 - 1)(\pi_m^2 - 1) + k\Lambda \frac{r + s}{r(1 + s)}$$

It is easy to see that no single stepped-film shape can be considered as optimal. Instead, the optimal values of r and s will depend on the maximum pressure in addition to k and Λ. This question of optimal film shape will be discussed in more detail later. For $0 < n < 1$, the stepped film is not the optimal shape, but no simple film shape can be obtained.

Numerical Results for Bearings With Stepped Films[3]

Some numerical results carried out for stepped-film bearings with isothermal lubricant are presented here. One reason that bearings of this type are considered in detail is that, for these bearings, closed-form solutions are possible even though transcendental functions are involved.

For the numerical calculations, it is convenient to proceed in the following manner: Let the solutions be written in the following form:

$$1 - \pi + k \ln\left(\frac{k - 1}{k - \pi}\right) = \xi, \qquad 0 \leqslant \xi \leqslant \Lambda_1, \tag{24}$$

$$r(\pi - 1) + k \ln\left(\frac{r\pi - k}{r - k}\right) = \frac{s\Lambda}{r(1 + s)} - \frac{\xi}{r}, \qquad \Lambda_1 \leqslant \xi \leqslant \Lambda \tag{25}$$

The unknown k is determined from the condition that the pressure is continuous at $\xi = \Lambda_1$. Thus

$$1 - \pi_m + k \ln\left(\frac{k - 1}{k - \pi_m}\right) = \frac{\Lambda}{1 + s}, \tag{26}$$

$$r(\pi_m - 1) + k \ln\left(\frac{r\pi_m - k}{r - k}\right) = \frac{s\Lambda}{r(1 + s)} \tag{27}$$

Calculations were carried out by choosing a value for π_m and using equations (26) and (27) to find the values of Λ and s. A typical example is shown in Fig. 2. The co-ordinates used are found to be convenient because, for a fixed π_m, constant k-curves are all straight lines. It may be mentioned that physically meaningful solutions are possible only for $r > k > \pi_m$.

For the incompressible case, as seen from (19), the values of k_i depend only on r and s, but equations (26) and (27) show that in addition to r and s, k now depends also on the maximum pressure π_m, and the parameter Λ. The form of equation (20) makes it possible to maximize the maximum pressure or the total load for the incompressible case. However, for the compressible case, the maximum pressure depends also on the film thickness h_1 relative to the bearing length. When h_1 is decreased, or, in other words, when L is increased, the maximum pressure will increase.

In the incompressible case, the maximum pressure π_{im} varies linearly with Λ, while in the compressible case the dependence of π_m upon Λ is nonlinear (only slightly, however, for small values of $\pi_m - 1$). As Λ increases, the value of π_m tends to drop below the linear law. This implies that the total load will taper off when

[3] After these calculations had been completed, a paper by Kochi [5], with extensive numerical results for the same problem, came to the author's attention. Therefore only typical examples of the numerical results obtained are presented here.

the slider velocity U is gradually increased to large values.

It may be seen from Fig. 2, that, for a given Λ and s, there are two values of r yielding the same π_m. For example, at $\Lambda = 3.2$, and $s = 2.3$, to yield $\pi_m = 1.1$, r may be chosen as either 1.2 or 4. The maximum pressure in the incompressible case is 1.108 when $r = 1.2$, and 1.101 when $r = 4$. It appears, therefore, that the compressibility effects are less noticeable for bearings with large film-thickness ratio ($r > 2$).

Optimal Stepped-Film Shapes for Compressible Isothermal Lubricant

It remains to determine the optimal stepped-film shapes for a compressible isothermal lubricant. The optimal stepped film for the maximum total load has been studied in detail in [5], and will not be discussed here. Instead, the problem of finding the stepped-film shape which would yield a specified value of π_m for the smallest Λ is considered. As can be seen from Fig. 2, for $\pi_m = 1.1$, the values of r and s of this optimal film shape are about 2 and 3, respectively, and the smallest value of Λ is about 1.6. These values of r and s are close to those of the optimal stepped film for the incompressible case (for maximum load).

From equation (26), for $\pi_m - 1 < k - 1$ and $r - k$, it can be easily found by minimizing Λ with respect to r that

$$r \approx \frac{2 + \pi_m}{2\pi_m} k, \tag{28}$$

which is valid for $\pi_m < 2$ (since $r > k$). The similarity between the two equations (16) and (28) is to be noted. From (27), by minimizing Λ with respect to k, it is found

$$2r \approx \frac{k}{(k-1)(k-\pi_m)} \{-(k - \pi_m - 1) + [(k - \pi_m - 1)^2 - 4(k-1)(k-\pi_m)]^{1/2}\} \tag{29}$$

From these two relations, the values of r and k can be found for a given π_m. The values of r and s can then be calculated from (26) and (27). However, (28) tends to underestimate the value of (r/k). For example, for $\pi_m = 1.5$, (28) yields $(r/k) = 1.167$. The exact values are $(r/k) = 1.29$, and $r = 2.04$. In general, the values of r and s are larger than those for the optimal stepped film for the incompressible fluid.

A few remarks on the general compressible problem may be added here. It is of interest to determine the optimal film for the maximum total load when n is not equal to 1. For a given Λ, the differential equations (5) and (23), and the boundary conditions (6) and the condition $t = 1$ at $\xi = 0$ are sufficient to determine the pressure distribution, the film shape, and the mass flow parameter k. The mathematical problem involved appears to be rather complex. It is being planned to use electronic computers for this work.

Acknowledgment

The author wishes to express his gratitude to Prof. E. Saibel, Rensselaer Polytechnic Institute, for his many valuable comments and discussions, and to Mr. K. Toba, Rensselaer Polytechnic Institute, for his help in checking some of the results.

References

1 Lord Rayleigh, "Notes on the Theory of Lubrication," *Philosophical Magazine*, vol. 35, 1918, p. 1.

2 F. Osterle and E. Saibel, "Recent Advances in the Hydrodynamic Theory of Slider-Bearing Lubrication, the Reynolds Equation," ASME Paper No. 54—LUB-15, October, 1954.

3 J. S. Ausman, "The Fluid Dynamic Theory of Gas-Lubricated Bearings," TRANS. ASME, vol. 79, 1957, p. 1218.

4 R. Courant and D. Hilbert, "Methods of Mathematical Physics," vol. 1, Interscience Publishers, New York, N. Y., 1953, p. 221.

5 K. C. Kochi, "Characteristics of a Self-Lubricated Stepped Thrust Pad of Infinite Width With Compressible Lubricant," *Journal of Basic Engineering*—TRANS. ASME, Series D, vol. 81, 1959, p. 135.

Heat Transfer and Sublimation at a Stagnation Point in Potential Flow

W. W. SHORT
Senior Research Engineer,
Convair Division of
General Dynamics Corporation,
San Diego, Calif.

A simple analytical expression is derived which predicts the effect of mass transfer on countercurrent heat transfer to a vaporizing body. In this theory, the fluid stream is assumed to be inviscid and of constant thermal conductivity. The inviscid theory correlates well with heat-transfer data without mass transfer and is believed to predict heat-transfer rates fairly accurately at high mass-transfer rates.

THE EFFECT of mass transfer on the countercurrent heat transfer in vapor-phase boundary layers is discussed. This phenomenon is of current interest as it usually occurs during an ablation process.[1] Analytical solutions of convective heat transfer at a stagnation point without mass transfer have been obtained by Sibulkin [1],[2] Drake [2], Frössling [3], and many others. These solutions compare very well with experimental data. Few theoretical and experimental data concerning simultaneous heat and mass transfer are available, and the agreement between ablation theory and the available experimental data is not good, especially at high mass-transfer rates. Several analytical solutions have been presented [4–8, 16, 17] in the literature. These solutions can only be extrapolated to conditions of high mass-transfer rates. High mass-transfer rates refer to instances where the heat-transfer rate to the body is reduced to less than 20 per cent of the rate in an identical situation without mass transfer.

The heat-transfer solutions in the references cited assume a thin viscous boundary layer at the surface of the body which, in turn, is surrounded by potential flow. These solutions are difficult to obtain; often extensive numerical work is required. Here, the viscous terms are omitted from the flow equations which greatly simplifies the analysis. It is assumed by this omission that the potential flow field applies up to the surface of the body. This assumption is suggested by the fact that the shear forces and boundary-layer thickness are very small at a stagnation point.

[1] Ablation is the process through which hypersonic bodies deteriorate in the atmosphere.

[2] Numbers in brackets designate References at end of paper.

Contributed by the Applied Mechanics Division and presented at the Winter Annual Meeting, New York, N. Y., November 27–December 2, 1960, of THE AMERICAN SOCIETY OF MECHANICAL ENGINEERS.

Discussion of this paper should be addressed to the Secretary, ASME, 29 West 39th Street, New York, N. Y., and will be accepted until January 10, 1961, for publication at a later date. Discussion received after the closing date will be returned.

Manuscript received by ASME Applied Mechanics Division, December 10, 1959. Paper No. 60—WA-20.

Fig. 1 presents a qualitative description of the flow near a three-dimensional stagnation point with mass transfer from the surface where a viscous boundary layer is considered and where the viscous effects are omitted. The inviscid flow field in the vicinity of the stagnation point of a sphere having a uniform blowing velocity normal to the surface will be determined using potential theory. It is assumed that this field is identical to that at the stagnation point on any blunt body of revolution under the same free-stream conditions.

Analysis

This analysis is based on the following assumptions:

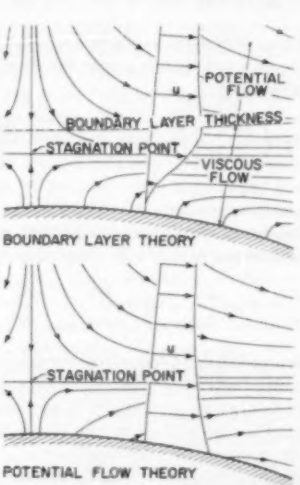

Fig. 1 Streamlines near a three-dimensional stagnation point with a blowing surface

Nomenclature

a = radius of sphere
C_p = specific heat of ablating vapor
g = dimensionless temperature
h = heat-transfer coefficient
H = enthalpy
k = thermal conductivity
K = thermal diffusivity = $k/C_p\rho$
M = dimensionless mass-transfer parameter = $C_p\rho v_0/h^*$
Nu = Nusselt number = ha/k
Pr = Prandtl number = $C_p\mu/k$
r = radial distance
Re = Reynolds number = $aU\rho/\mu$
T = temperature
u = local velocity in x-direction
U = free-stream velocity
v = local velocity in y-direction
x = distance parallel to surface
y = distance normal to surface
θ = heat-transfer ratio h/h^*
ψ = polar angle in spherical co-ordinates
μ = absolute viscosity
ρ = density of ablating vapor
ϕ = potential function
ν = kinematic viscosity

Subscripts

0 = values in vapor phase at surface
* = no mass transfer (nonablating)
∞ = free-stream conditions
i = conditions in interior of body

1 The viscosity of the fluid is negligible (potential flow).
2 The fluid is incompressible.
3 The thermal diffusivities of the fluid and the mass diffusing into the stream are constant and equal.
4 There is no source of energy in the stream.
5 In the stagnation region, $\partial T/\partial x = 0$.

Streeter [9] developed the following potential function, ϕ, in spherical co-ordinates for steady flow of an infinite incompressible fluid around a sphere:

$$\phi = \frac{Ua^3}{2r^2}\cos\psi + Ur\cos\psi \tag{1}$$

The co-ordinates used in this analysis are shown in Fig. 2. The ablation of material from the surface of the sphere can be represented by a source of strength $4\pi a^2 v_0$. The potential function for this source alone is $a^2 v_0/r$. By adding this function to equation (1), the potential function for steady flow of an infinite fluid around an ablating sphere is found to be

$$\phi = \frac{Ua^3}{2r^2}\cos\psi + Ur\cos\psi + \frac{a^2 v_0}{r} \tag{2}$$

Potential functions can be summed because the boundary conditions and Laplace's equation are satisfied by the new equation. The radial component of velocity, v, is obtained by differentiating the potential function in equation (2) as follows:

$$v = -\frac{\partial\phi}{\partial r} = \frac{Ua^3}{r^3}\cos\psi - U\cos\psi + \frac{a^2 v_0}{r^2} \tag{3}$$

The usual linear approximation of the radial velocity represented by equation (3) is assumed to apply near the forward stagnation point of an ablating body:

$$v = v_0 + \left(\frac{\partial v}{\partial r}\right)_{\substack{r=a\\ \psi=0}} y = v_0 - \left(\frac{3U + 2v_0}{a}\right) y, \tag{4}$$

where y is the distance normal to the surface.

In rectilinear co-ordinates the energy equation, neglecting pressure gradients, and variation of K with x and y, is

$$u\frac{\partial T}{\partial x} + v\frac{\partial T}{\partial y} = K\left(\frac{\partial^2 T}{\partial x^2} + \frac{\partial^2 T}{\partial y^2}\right) \tag{5}$$

It is further assumed that $\partial T/\partial x = 0$ in the neighborhood of the stagnation point on a body of revolution. This assumption states that isotherms in this region are parallel to the surface. The isotherms are parallel to the surface at the stagnation point on a symmetrical body, and will be very nearly so over a much larger area if the vaporization temperature of the surface is a weak function of pressure. The temperature can then be expressed in the dimensionless form

$$g(y) = \frac{T - T_0}{T_\infty - T_0} \tag{6}$$

and equation (5) is simplified to

$$v\frac{\partial T}{\partial y} = K\left(\frac{\partial^2 T}{\partial y^2}\right) \tag{7}$$

Substituting equations (4) and (6) into equation (7) gives

$$\left[v_0 - \left(\frac{3U + 2v_0}{a}\right) y\right] g' = Kg'' \tag{8}$$

where the primes denote differentiation with respect to y. The boundary conditions are

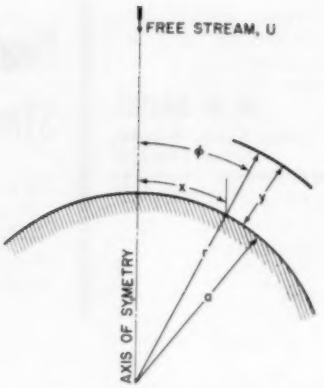

Fig. 2 Co-ordinate system

$$g = 0, \quad g' = g_0' \quad \text{when} \quad y = 0 \tag{9}$$

and

$$g = 1, \quad g' = 0 \quad \text{when} \quad y = \infty \tag{10}$$

Integrating equation (8) and applying boundary condition equation (9) give

$$g' = g_0' e^{\frac{y}{K}\left[v_0 - \left(\frac{3U+2v_0}{2a}\right) y\right]} \tag{11}$$

Integrating a second time and using boundary condition equation (10) give the following normal probability integral

$$\frac{1}{g_0'} = \int_0^\infty e^{\frac{y}{K}\left[v_0 - \left(\frac{3U+2v_0}{2a}\right) y\right]} dy \tag{12}$$

The solution to this equation is

$$g_0' = \left[\frac{2(3U + 2v_0)}{\pi K a}\right]^{1/2} e^{-\frac{av_0^2}{2K(3U+2v_0)}} \tag{13}$$

The heat-transfer coefficient h, as defined by equation (14), is equal to kg_0' when the dimensionless temperature g is substituted in the definition:

$$h = \frac{k\left(\frac{\partial T}{\partial y}\right)_{y=0}}{(T_\infty - T_0)} \tag{14}$$

Under conditions of mass transfer, the heat-transfer coefficient is, therefore,

$$h = k\left[\frac{2(3U + 2v_0)}{\pi k a}\right]^{1/2} e^{-\frac{av_0^2}{2K(3U+2v_0)}} \tag{15}$$

The foregoing equation also predicts heat transfer under conditions of no mass transfer by letting $v_0 = 0$. Combining equation (15) with the definitions of Nusselt, Reynolds, and Prandtl numbers, the heat transfer at the stagnation point of a nonablating body is

$$\mathrm{Nu}_* = 1.38\mathrm{Re}^{1/2}\mathrm{Pr}^{1/2} \tag{16}$$

The asterisk denotes no mass transfer; i.e., $v_0 = 0$. The similar relation developed by Sibulkin [1] for heat transfer at a stagnation point in viscous flow is

$$\mathrm{Nu}_* = 0.93\ \mathrm{Re}^{1/2}\mathrm{Pr}^{0.4} \tag{17}$$

The value of the coefficient in equation (17) is 1.32 in the work of Sibulkin because Re and Nu_* were based on the sphere diameter.

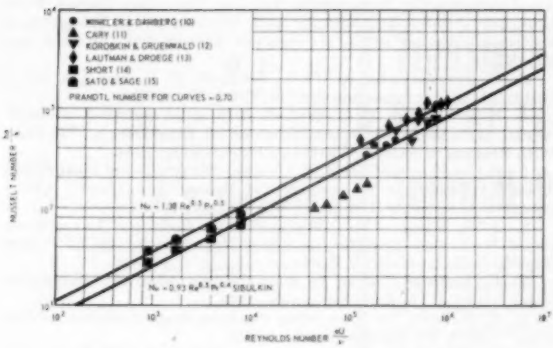

Fig. 3 Heat transfer at stagnation point of a sphere

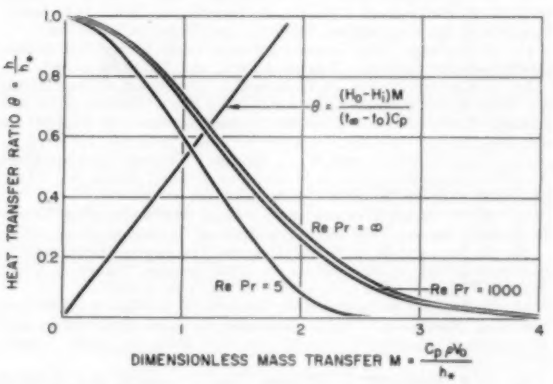

Fig. 4 Effect of mass transfer on heat transfer in potential flow at a stagnation point

Equations (16) and (17) are plotted in Fig. 3 along with experimental data on stagnation heat transfer.

The reduction in heat transfer caused by simultaneous mass transfer can be expressed by the ratio $\theta = h/h_*$

$$\theta = \left(1 + \frac{2v_0}{3U}\right)^{1/2} e^{-\frac{ar_0^2}{2K(3U+2v_0)}} \tag{18}$$

Using the dimensionless mass-transfer parameter, $M = \rho c_p v_0/h_*$, the heat-transfer ratio can be reduced to

$$\theta = \left(1 - {}^2/_3 \frac{M}{\mathrm{Re}^{1/2}\mathrm{Pr}^{1/2}}\right)^{1/2} e^{-\frac{M^2}{2\left(1 - {}^2/_3 \frac{M}{\mathrm{Re}^{1/2}\mathrm{Pr}^{1/2}}\right)}} \tag{19}$$

This relation is plotted in Fig. 4 with Reynolds number times Prandtl number as a parameter. Fig. 4 shows that the heat-transfer reduction is nearly independent of the parameter, Reynolds number times Prandtl number, when its value is greater than 1000. For values of this parameter greater than 1000, which will usually be the case during aerodynamic ablation, the following form of equation (19) for Re Pr = ∞ can be used

$$\theta = e^{-\frac{M^2}{2}} \tag{20}$$

The curves in Fig. 4 provide a simple means of determining the steady-state mass-transfer rate for a particular subliming material. An energy balance at the ablating surface can be written for the case in which all the mass is converted to vapor,

$$h(T_\infty - T_0) = (H_0 - H_i)v_0\rho \tag{21}$$

Here, H_0 and H_i are the enthalpy of the vapor at the interface and at the initial enthalpy of the vaporizing material, respectively. This energy balance assumes that the heat conduction into the solid is constant. Combining this equation with the definitions of θ and M gives

$$\theta = \frac{(H_0 - H_i)}{(T_\infty - T_0)C_p} M \tag{22}$$

Equation (22) is plotted in Fig. 4. The intersection of this straight line with the appropriate theoretical curve determines the heat and mass-transfer rates for the particular material described by equation (22).

Discussion of Theories

The potential-flow theory of sublimation at first glance may appear to be a very rough approximation to the ablation problem; however, this solution has some unique characteristics that make it applicable to situations involving turbulent flow or high blowing rates. Since viscous terms are omitted in determining the flow field, potential flow does not predict a momentum boundary layer; however, this theory does predict a thermal boundary layer similar to that found using viscous boundary-layer theory. At low blowing rates, the thickening of the momentum-transfer boundary layer rather than convection of the subliming material away from the surface reduces the heat transfer toward the surface. Because of the omission of the momentum boundary layer by potential-flow theory, the curves illustrating the reduction in heat transfer in Fig. 4 have zero slope at $M = 0$. The velocity component normal to the surface, v, exerts a strong influence on the energy transfer at the stagnation point as shown by equation (7). At high blowing rates, v is strongly dependent on the blowing rates, v_0, and the external flow, and only weakly dependent upon the viscous forces. The distribution of the velocity component parallel to the surface, u, is almost entirely dependent upon the viscous forces; however, u does not enter the simplified energy equation. The streamlines in potential flow and in viscous flow near a stagnation point with a blowing surface are shown qualitatively in Fig. 1. It will be noted that in the stagnation region the flows are similar. At very high blowing rates $M > 2$, the boundary layer "separates" from the surface and gives rise to pressure gradients normal to the surfaces. This pressure gradient invalidates the usual assumption required to obtain the boundary-layer solutions. Separation, however, does not complicate the potential-flow solution. For this reason, it is believed that the theory presented here describes heat transfer at high blowing rates more accurately than does boundary-layer theory.

The heat-transfer rates without mass transfer predicted by the present potential-flow theory, equation (16), are 48 per cent higher than those of Sibulkin based on a laminar boundary-layer solution, equation (17). Most experimental data lie between these two curves, as turbulence, which is usually present in the experimental air streams employed, produces larger heat-transfer rates than those predicted by equation (17). Experimental data obtained from others [10–15] are also plotted in Fig. 3. Heat-transfer rates measured by Sato and Sage [15] in air streams with 15 per cent turbulence agree well with those of equation (16). This is not surprising as turbulent streams have velocity profiles similar to that of potential flow. It is believed that turbulence will produce this same effect when simultaneous mass transfer is present. If this is the case, equation (19) will best predict the heat-shielding effect and mass-transfer rate during ablation under conditions of turbulent flow.

The potential theory is compared with ablation theories developed by several authors in Fig. 5. It will be noted that boundary-layer theory predicts a greater reduction in heat transfer than does film or potential theories. This reduction partly re-

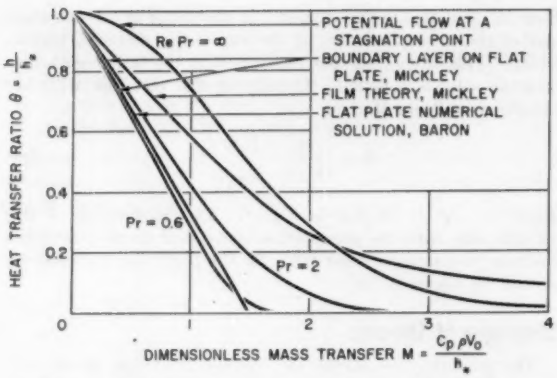

Fig. 5 Theories predicting combined heat and mass transfer

sults from the fact that boundary-layer theory takes into account changes in boundary-layer thickness caused by flow normal to the wall whereas film theory ignores such changes. Film theory assumes a stagnate film of constant thickness adjacent to the surface through which heat and material diffuse. Potential theory does not consider a boundary layer at all; but does consider the change in the external or potential flow caused by the ablating material. Film theory correlates well with experimental data obtained from transpiration cooling in turbulent flow [4] just as potential theory was shown to correlate with turbulent heat-transfer data.

References

1 M. Sibulkin, "Heat Transfer Near the Forward Stagnation Point of a Body of Revolution," *Journal of the Aeronautical Sciences*, vol. 19, 1952, pp. 570–571.

2 Robert M. Drake, "Calculation Method for Three-Dimensional Rotationally Symmetrical Laminar Boundary Layers With Arbitrary Free-Stream Velocity and Arbitrary Wall-Temperature Variation," *Journal of the Aeronautical Sciences*, vol. 20, 1953, pp. 309–316.

3 N. Frössling, Lunds. Univ. Arsskrift, N. F. Ard 2.36, No. 4 (1940); English translation NACA TM 1432, 1953.

4 H. S. Mickley, R. C. Ross, A. L. Squyers, and W. E. Stewart, "Heat, Mass, and Momentum Transfer for Flow Over a Flat Plate With Blowing or Suction," NACA TN 3028, July, 1954.

5 S. Georgiev and M. B. T. George, "Evaluation of Heat Shield Ablation During the Re-entry of the Jupiter Nose Cone," AVCO Research Laboratory, Research Note 81, July, 1958.

6 J. R. Baron, "The Binary-Mixture Boundary Layer Associated With Mass Transfer Cooling at High Speeds," M.I.T. Naval Supersonic Laboratory, T.R. 160.

7 L. Roberts, "Mass Transfer Cooling Near the Stagnation Point," NACA TN 4391, September, 1958.

8 L. Roberts, "A Theoretical Study of Stagnation-Point Ablation," NACA TN 4392, September, 1958.

9 V. L. Streeter, "Fluid Dynamics," McGraw-Hill Book Company, Inc., New York, N. Y., 1948, p. 67.

10 E. M. Winkler and J. E. Danberg, "Heat Transfer Characteristics of Hemisphere Cylinder at Hypersonic Mach Numbers," Institute of the Aeronautical Sciences, Inc., Preprint 622, 1956.

11 J. R. Cary, "The Determination of Local Forced-Convection Coefficients for Spheres," TRANS. ASME, vol. 75, 1953, p. 483.

12 I. Korobkin and K. H. Gruenwald, "Discussion of Local Laminar Heat Transfer Coefficients for Spheres and Cylinders in Incompressible Flow," *Journal of the Aeronautical Sciences*, vol. 24, 1957, p. 3.

13 L. G. Lautman and W. C. Droege, "Thermal Conductances About a Sphere Subjected to Forced Convection," Serial No. AIRL A6118 50-15-3, Air Material Command, 1950.

14 W. W. Short, Thesis, Part II, "Local Convective Heat Transfer From a Sphere," California Institute of Technology, June, 1958.

15 K. Sato and B. H. Sage, "Thermal Transfer in Turbulent Gas Streams—Effect of Turbulence on Macroscopic Transport From Spheres," TRANS. ASME, vol. 80, 1958, pp. 1380–1388.

16 L. Lees, "Convective Heat Transfer With Mass Addition and Chemical Reactions," Paper presented at third Combustion and Propulsion Colloquium, AGARD, NATO, Palermo, Sicily, March 17–21, 1958.

17 J. F. Gross, D. J. Masson, and C. Gazley, Jr., "General Characteristics of Binary Boundary Layers With Application to Sublimation Cooling," RAND Corp. Report, May, 1958, p. 1371.

W. H. CHU
Senior Research Engineer,
Department of Applied Mechanics,
Southwest Research Institute,
San Antonio, Texas

H. N. ABRAMSON
Director,
Department of Applied Mechanics,
Southwest Research Institute,
San Antonio, Texas.
Mem. ASME

Transient Heat Conduction in a Rod of Finite Length With Variable Thermal Properties[1]

This paper presents a theoretical solution for transient heat conduction in a rod of finite length with variable thermal properties. A numerical procedure is developed and the results of one example are presented and compared with the corresponding solution for the case of constant properties. Application to the problem of determination of thermophysical properties is discussed briefly.

Previous methods of determining the temperature-dependent diffusivity of materials [1–4][2] are based almost entirely on analytical solutions for constant thermophysical properties [5, 6], from which relations for the evaluation of thermal diffusivity can be deduced. However, in order to evaluate the thermophysical properties of materials from measurements of idealized one-dimensional transient heat flow (conduction) with large temperature variation, it is more desirable to have available sufficiently accurate solutions based on temperature-dependent thermal properties. Unfortunately, when the thermal properties are considered to be variable, the mathematical analysis leads to a difficult nonlinear integral equation.

For semi-infinite bodies with constant or variable thermal properties, a variety of possible methods of solution have been proposed [7–12]. The heat-balance integral method of Goodman [7, 8], utilizing temperature profiles approximated by polynomials, has been employed to solve integral equations applicable to problems involving a phase change, by reducing the mathematical problem to the solution of an ordinary differential equation which can be solved analytically or numerically. Reynolds and Dolton [9] have presented a more general analysis applicable to a variety of conduction problems, also employing temperature polynomials, but this analysis does not seem adequate for large dependence of thermal properties on temperature. An exact solution for the problem of a stepwise change in surface temperature on a semi-infinite body was given by Yang [10], and later used to evaluate the accuracy of an approximate solution obtained by using a two-parameter representation of the temperature distribution to reduce the mathematical problem to the numerical solution of an ordinary differential equation [11]. A somewhat different approach has been discussed in [12], in which variational methods are applied to problems involving a melting body.

In the case of a rod of finite length with temperature-dependent properties, none of the foregoing methods appears to be adequate. As an approach to this problem, the present paper is concerned with a method based on replacing the one-dimensional heat-conduction equation by a difference equation.[3] The thermophysical properties are then to be determined from numerical solutions of this difference equation by appropriate curve-fitting techniques.

Formulation of Problem

Assuming that the heat flow is one-dimensional, the conduction equation is

[1] This research was supported in part by the U. S. Air Force under Contract No. AF 33(616)-6233, monitored by the Materials Laboratory, Wright Air Development Division, Wright-Patterson Air Force Base, Ohio.

[2] Numbers in brackets designate References at end of paper.

Contributed by the Applied Mechanics Division and presented at the Winter Annual Meeting, New York, N. Y., November 27–December 2, 1960, of The American Society of Mechanical Engineers.

Discussion of this paper should be addressed to the Secretary, ASME, 29 West 39th Street, New York, N. Y., and will be accepted until January 10, 1961, for publication at a later date. Discussion received after the closing date will be returned.

Manuscript received by ASME Applied Mechanics Division, December 14, 1959. Paper No. 60—WA-25.

[3] An extensive review of the literature on linear and quasi-linear heat flow is given in [13].

Nomenclature

c = specific heat at constant pressure
$e_b = K^* - \bar{K}^*$
$E(t)$ = an upper bound of $|e_b|$
$E_1(t)$ = truncation error with exact boundary values
$\bar{E}_1(n) = E_1(n\Delta t)$
$E_2(t)$ = inherited truncation error due to approximate boundary condition
$\bar{E}_2(n) = E_2(n\Delta t)$
$E_R(t)$ = an upper bound of round-off error
$E_R(n) = E_R(n\Delta t)$
$f(n)$ = defined in equation (16a)
$g(n)$ = defined in equation (16b)
H = heat flux
H_0, H_1 = heat input at $x^* = 0, x^* = 1$, respectively
k = thermal conductivity
$k^* = k/k_i$
$K = \int_{T_i}^{T} k dT$
$K^* = K/(k_i T_s)$
L = total length
$m_b(t^*)$ = defined by equation (18), an upper bound of ϵ_b
$M_1(t^*)$ = maximum value or an upper bound of $|\kappa^* R_2 - R_1|$ at t^*
M_2 = maximum value or an upper bound of $|d\kappa^*/dK^*|$ in temperature range covered
$M_3(t^*)$ = an upper bound of either $\frac{\Delta^2 \bar{K}^*}{\Delta x^{*2}}$ or $\frac{\Delta^2 K^*}{\Delta x^{*2}}$ in $\Delta x^* \leqslant x^* \leqslant 1 - \Delta x^*$
$r = \Delta t^*/(\Delta x^*)^2$
n = integer, number of time increment

(*Continued on next page*)

$$\rho c \frac{\partial T}{\partial t} = \frac{\partial}{\partial x}\left(k \frac{\partial T}{\partial x}\right) \tag{1}$$

where $k(\partial T/\partial x)$ is the heat flux in the negative x-direction. The right-hand side of this equation represents the heat flow into a infinitesimal element of volume per unit time and the left-hand side represents the increase of energy inside the element per unit time.

The temperature must satisfy the initial condition

$$T(x, 0) = T_i(x), \quad 0 \leqslant x \leqslant L \tag{2}$$

and one boundary condition at each end of the bar. If the temperature is measured at the end, then

$$T_{end}(t) = T(x_{end}, t) \tag{3a}$$

and if the amount of heat flow in the positive x-direction at the end ($x_{end} = 0$ or L) is known to be H, then

$$-\left[k\left(\frac{\partial T}{\partial x}\right)\right]_{end} = H \tag{3b}$$

Let

$$K = \int_{T_i}^{T} k(T)dT \tag{4}$$

so that equation (1) reduces to the simplified form

$$\frac{\partial K}{\partial t} = \kappa \frac{\partial}{\partial x}\left(\frac{\partial K}{\partial x}\right) \tag{5a}$$

or

$$\frac{\partial K^*}{\partial t^*} = \kappa^* \frac{\partial}{\partial x^*}\left(\frac{\partial K^*}{\partial x^*}\right) = \kappa^* \frac{\partial^2 K^*}{\partial x^{*2}} \tag{5b}$$

where κ^* is an assumed function of K^*.

Numerical Solution

Well-known numerical methods [14] can be applied to the nondimensional equation (5b) to obtain an approximate solution, $\bar{K}^*$. Let $\bar{K}^*$ be governed by the difference equation

$$\bar{K}^*(t^* + \Delta t^*) - \bar{K}^*(x^*, t^*) = [\kappa^*(\bar{K}^*)]\left[\frac{\Delta t^*}{(\Delta x^*)^2}\right][\bar{K}^*(x^* + \Delta x^*, t^*) - 2\bar{K}^*(x^*, t^*) + \bar{K}^*(x^* - \Delta x^*, t^*)] \tag{6}$$

The basic truncation error, $\bar{K}^* - K^*$, due to the approximate equation (6) is given in Appendix 1.

For the first boundary-value problem, prescribed by equation (3a) at both ends ($x^* = 0$, $x^* = 1$), there is no additional truncation error. However, in the second boundary-value problem, there is additional error due to truncation of the first derivative at either end or at both ends. Therefore instead of employing only the first difference for the first derivative, the form which includes also the second difference will be employed. Thus

$$\bar{K}^*(x^*, t^*) = \tfrac{1}{3}\left[4\bar{K}^*(x^* + \Delta x^*, t^*) - \bar{K}^*(x^* + 2\Delta x^*, t^*) - 2(\Delta x^*)\frac{\partial \bar{K}^*(x^*, t^*)}{\partial x^*}\right] \tag{7}$$

where $x^* = 0$ or $x^* = 1$. A more detailed discussion of the reasons for choosing this form is given in Appendix 2.

The heat input at $x^* = 0$ is H_0,

$$-\left[k\left(\frac{\partial T}{\partial x}\right)\right]_{x=0} = H_0 \quad \text{or} \quad \left(\frac{\partial \bar{K}^*}{\partial x^*}\right)_{x^*=0} = -\frac{LH_0}{k_i T_i} \tag{8a}$$

and the heat input in the negative x^*-direction at $x^* = 1$ is H_1 ($= -H_{x^*=1}$),

$$\left[k\left(\frac{\partial T}{\partial x}\right)\right]_{x=L} = H_1 \quad \text{or} \quad \left(\frac{\partial \bar{K}^*}{\partial x^*}\right)_{x^*=1} = \frac{LH_1}{k_i T_i} \tag{8b}$$

Example

A numerical example has been carried out on a medium-sized digital computer (NCR 102A) and is given in detail as follows.

A copper bar is assumed to be 5 cm long, initially at a uniform temperature of 300 deg K, insulated at $x^* = 1$, ($H_1 = 0$), and heated by an input $H_0 = 500$ cal/cm²-sec. The diffusivity and conductivity are assumed to be linear functions of the temperature T, and the value of $\partial\kappa/\partial T$ is assumed to be that given by Butler and Inn [1]. The value of $\partial k/\partial T$ is assumed to be that given by [15]. In nondimensional form, the appropriate quantities are

$$\kappa^* = 1 + a_1^*(\Delta T^*) = 1 - 0.1069(\Delta T^*) \tag{9a}$$

$$\Delta T^* = \frac{1 - (1 + 2a_1^* K^*)^{1/2}}{(-a_1^*)} = \frac{1 - (1 - 0.0798K^*)^{1/2}}{0.03990} \tag{9b}$$

where the constants depend on the initial temperature, since

$$a_1^* = \frac{T_i}{k_i}\frac{dk}{dT},$$

$$\frac{dk}{dT} \cong -1.2195 \times 10^{-4} \text{ cal/deg K-cm-sec} \tag{10a}$$

Nomenclature

$M_4(t^*) = rm_b(t^*)$
R_1 = defined in equation (13a)
R_2 = defined in equation (13b)
t = time
$t^* = \kappa_i t/L^2$
T = temperature
$T^* = T/T_i$
x = distance along bar
$x^* = x/L$
Δt^* = increment of t^*
$\Delta T^* = (T - T_i)/T_i$
Δx^* = spacing along bar
$\Delta^2 K^* = K^*(x^* + \Delta x^*, t) - 2K^*(x, t^*) + K^*(x^* - \Delta x^*, t^*)$
ϵ_b = maximum direct round-off error in absolute value
$\kappa = k/\rho c$ = diffusivity
$\kappa^* = \kappa/\kappa_i$
ρ = density of material

Superscripts

$(\bar{\ })$ = approximation of ( )
$(\ )^*$ = nondimensional quantity of ( )

Subscripts

$(\ )_i$ = initial value of ( ). If the initial temperature is nonuniform, take the value of ( ) corresponding to average initial temperature.
$(\ )_a$ = quantities in analytic solution with assumption of constant properties
$(\ )_c$ = quantities in numerical solution with assumption of constant properties
$(\ )_v$ = quantities in numerical solution with assumed temperature-dependent properties
$(\ )_e$ = exact value of ( )

$$a_2^* = \frac{T_i}{\kappa_i}\frac{d\kappa}{dT}, \quad \frac{d\kappa}{dT} \cong -4.033 \times 10^{-4} \text{ cm}^2/\text{deg K-sec} \quad (10b)$$

Finally, the increments $\Delta t^* = 0.001$, $\Delta x^* = 0.05$ are used so that

$$r = \frac{\Delta t^*}{(\Delta x^*)^2} = 0.4 < 1/2$$

When $k^* \equiv 1$, $\kappa^* \equiv 1$ (constant properties), it is necessary that $r < 1/2$ for convergence of the error [14]. When k^*, κ^* are functions of T^*, $r < 1/2$ is also sufficient for convergence of the error (Appendix 1).

Solutions for both constant properties and temperature-dependent properties have been carried out on the computer, subject to the conditions

$$\left(\frac{\partial K^*}{\partial x^*}\right)_{x^*=0} = -9.09, \quad \left(\frac{\partial K^*}{\partial x^*}\right)_{x^*=1} = 0, \quad K^*(x^*, 0) = 0$$

After a change in co-ordinates, the known analytic solution for the case of constant properties [5] takes the nondimensional form

$$\Delta T^* = T^* - 1 = \frac{H_0 L}{kT_i}\left\{t^* + 1/3 - x^* + 1/2 x^{*2} - \frac{2}{\pi^2}\sum_{n=1}^{\infty}\frac{1}{n^2}\, e^{-n^2\pi^2 t^*}\cos(n\pi x^*)\right\} \quad (11)$$

The numerical results and the analytic results for constant thermal properties are compared in Table 1, for $t^* = 0.100$. The maximum deviation in temperature from the "exact" value (analytic solution) is less than 0.5 per cent.

The numerical results for temperature distribution for both constant and temperature-dependent properties, at $t^* = 0.100$ and $t^* = 0.118$, are compared in Figs. 1(*a*) and 1(*b*), respectively. The absolute and percentage errors for assuming constant properties, at $t^* = 0.001$ and $t^* = 0.118$, are given in Figs. 2(*a*) and 2(*b*).

From graphical interpolation and extrapolation, the time at which the left end ($x^* = 0$) begins to melt are $t^* = 0.1176$ for constant thermal physical properties and $t^* = 0.1185$ for temperature-dependent properties.

A complete solution of one case, on the computer, requires a minimum of 2 hr and an average of 4 hr. The effort required to program the calculation of the bound on the error, equation (17*b*), is quite substantial, and therefore, for present purposes, the amplification factor (Appendix 1) can be utilized, since the solution for temperature-dependent properties, in this example, is quite close to the solution for constant properties. An approximate value for this factor is found in Appendix 3 to be less than 1.5. Therefore,

$$|K_v^* - K_e^*| < 1.57 \times .006, \quad |T_v^* - T_e^*|_{mx} = \left|T_i\left[\frac{(1 + 2a_1^* K_v^*)^{1/2} - (1 + 2a_1^* K_e^*)^{1/2}}{(-a_1^*)}\right]\right| < 1.64 \times 2 \text{ deg C}$$

which occurs at $t^* = 0.118$. The absolute error is therefore quite satisfactory.

Discussion

In the foregoing example, the temperature dependency seems to be rather small, and therefore one might expect that values of the thermal properties determined by one of the previous methods, e.g., [1], would be satisfactory. However, in cases of more rapid

Table 1 Comparison of analytic and numerical results for constant thermal physical properties $t^* = 0.100$

x^*	T_a^*	T_c^*	$\frac{T_c^* - T_a^*}{T_a^*}$	$\frac{K_c^* - K_a^*}{K_a^*}$	$\frac{K_c^* - K_a^*}{T_c^* - T_a^*}$
0	4.243	4.248	0.001	0.002	0.005
0.2	2.745	2.756	0.004	0.002	0.001
0.5	1.539	1.533	0.004	0.007	0.006
0.8	1.131	1.126	0.004	0.03	0.005
1.0	1.072	1.067	0.005	0.07	0.005

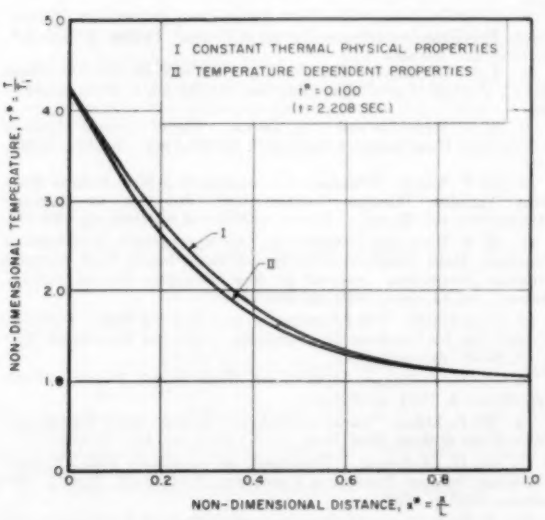

Fig. 1(*a*) Comparison of temperature distribution at $t^* = 0.100$

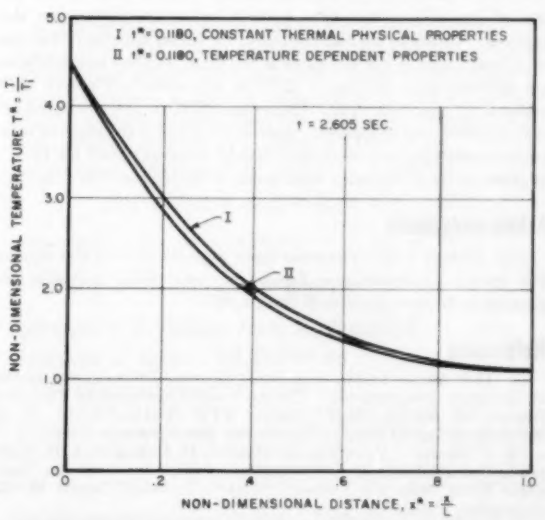

Fig. 1(*b*) Comparison of distribution at $t^* = 0.118$ (left-end temperature near melting point $T^* = 4.52$)

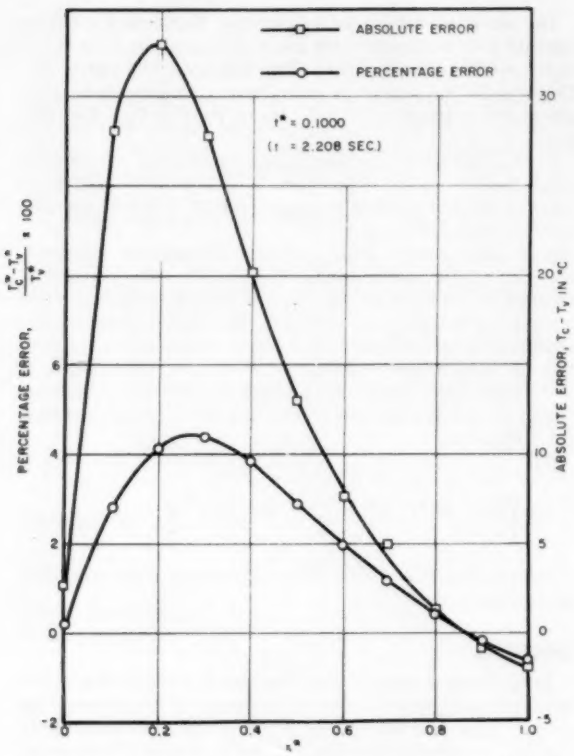

Fig. 2(a) Error owing to assumption of constant thermal-physical properties

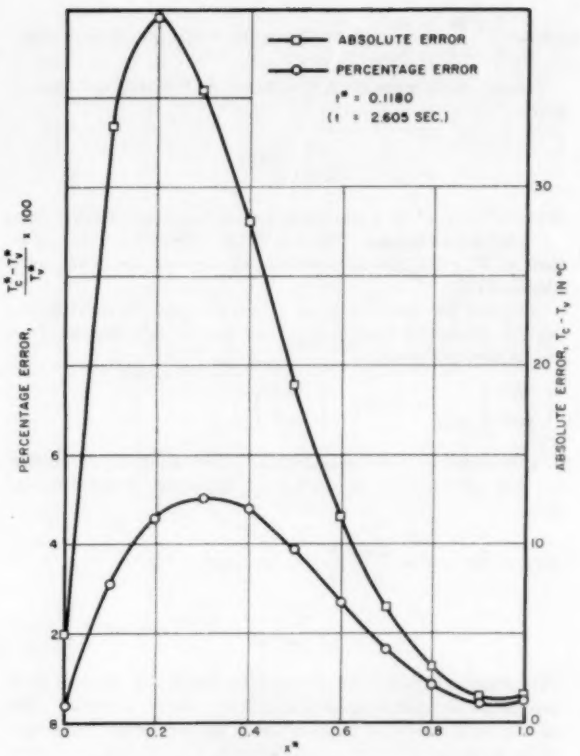

Fig. 2(b) Error owing to assumption of constant thermal-physical properties

or extremely high heat input for this material, or in cases of other materials where the temperature dependence is more pronounced, the present method will be better able to predict the temperature dependence of the thermal properties and can be used to check the accuracy of the results obtained by other methods.

It may be of some interest to point out that, in Figs. 1(*a*) and 1(*b*), the equivalence in nondimensional temperature at the left end of the rod in the two cases is not contradictory to this analysis. It must, on the contrary, be noted carefully that the total heat input in the two cases is the same, but the temperatures are different since in Case I, $\Delta T^* = K^*$, while in Case II, ΔT^* is given by equation (9*b*). The values of K in the two cases are also different. Qualitatively, since $k(T) \leq k(T_i)$ the slope of temperature-distribution curve for Case II is steeper than for Case I in order to have the same heat input, $k(\partial T/\partial x)$ or $(\partial K^*/\partial x^*)$.

Acknowledgments

The authors wish to express their appreciation to the staff of the SwRI Computations Laboratory for their valuable assistance in the preparation of this paper.

References

1 C. P. Butler and E. C. Y. Inn, "Thermal Diffusivity of Metals at Elevated Temperatures," Research and Development Technical Report US NRDL-TR-177, BuAer TFD NRDL-AE4101, U. S. Naval Radiological Defense Laboratory, San Francisco, Calif.

2 C. Sheer, C. D. Fitz, L. H. Mead, J. D. Holmgren, L. D. Rothacker, and D. Allmand, "Investigation of High Intensity Arc Technique From Materials Testing," WADC Technical Report 58-142, November, 1958.

3 S. T. Hsu, "Determination of Thermal Conductivities of Metals by Measuring Transient Temperatures in Semi-Infinite Solids," TRANS. ASME, vol. 79, 1957, pp. 1197–1201.

4 M. A. Kaganov, "The Problem of Utilizing the Method of an 'Instantaneous' Heat Source for Determining the Thermal Characteristics of Heat Insulators," *Soviet Physics, Technical Physics*, 1, 1957, pp. 650–653.

5 H. S. Carslaw and J. C. Jaeger, "Conduction of Heat in Solids," Oxford Press, Oxford, England, 1947, p. 104.

6 A. Sommerfeld, "Partial Differential Equations in Physics," Academic Press, Inc., Publishers, New York, N. Y., chapter 3, 1949.

7 T. R. Goodman, "The Heat-Balance Integral and Its Application to Problems Involving a Change of Phase," TRANS. ASME, vol. 80, 1958, pp. 335–342.

8 T. R. Goodman, "The Heating of Slabs With Arbitrary Heat Input," *Journal of Aero/Space Sciences*, vol. 26, no. 3, 1959, pp. 187–188.

9 W. C. Reynolds and T. A. Dolton, "Use of Integral Methods in Transient Heat-Transfer Analysis," ASME Paper No. 58—A-248, 1958.

10 K. T. Yang, "Transient Conduction in a Semi-Infinite Solid With Variable Thermal Conductivity," JOURNAL OF APPLIED MECHANICS, vol. 25, no. 1, TRANS. ASME, vol. 80, 1958, pp. 146–147.

11 K. T. Yang and A. Szewczyk, "An Approximate Treatment of Unsteady Heat Conduction in Semi-Infinite Solids With Variable Thermal Properties," *Journal of Heat Transfer*—TRANS. ASME, Series C, vol. 81, no. 3, 1959, pp. 251–252.

12 S. J. Citron, "Heat Conduction in a Melting Slab," Technical Report No. 15, Contract Nonr-266(20), Columbia University, New York, N. Y., January, 1959.

13 N. E. Friedman, "Quasilinear Heat Flow," TRANS. ASME, vol. 80, no. 4, 1958, pp. 635–645.

14 W. E. Milne, "Numerical Solution of Differential Equations," John Wiley & Sons, New York, N. Y., 1953, pp. 49, 120–122.

15 C. D. Hodgman, "Handbook of Chemistry and Physics," Chemical Rubber Publishing Company, New York, N. Y., 35th edition, 1952, p. 2086.

16 T. Fort, "Finite Differences and Difference Equations in the Real Domain," Oxford at the Clarendon Press, Oxford, England, 1948, pp. 123, 242–243.

APPENDIX 1

Error Analysis of Numerical Method[4]

The purpose of this analysis is to find an upper bound for the total error, which is simple enough to facilitate computation and yet accurate enough to avoid an unnecessarily refined mesh size.

Truncation Error. The exact solution satisfies the following relation

$$\frac{K(x, t + \Delta t) - K(x, t)}{\Delta t} + R_1 = \kappa[K(x, t)] \left[\frac{K(x + \Delta x, t) - 2K(x, t) + K(x - \Delta x, t)}{(\Delta x)^2} + R_2\right] \quad (12)$$

where the remainders are

$$R_1 = -\frac{1}{2!}(\Delta t)\frac{\partial^2 K(x', t')}{\partial t'^2}, \quad t \leqslant t' \leqslant t + \Delta t \quad (13a)$$

$$R_2 = -\frac{1}{4!}(\Delta x)^2\left[\frac{\partial^4 K(x', t)}{\partial x'^4} + \frac{\partial^4 K(x'', t)}{\partial x''^4}\right], \quad \begin{matrix} x - \Delta x \leqslant x'' \leqslant x \\ x \leqslant x' \leqslant x + \Delta x \end{matrix} \quad (13b)$$

Let the truncation error be $e_a(x, t)$. By subtraction of equations (12) and (6), it is found that

$$e_a(x, t + \Delta t) = e_a(x, t) + r\kappa[\bar{K}(x, t)] [e_a(x + \Delta x, t) - 2e_a(x, t) + e_a(x - \Delta x_1 t)] - \left[e_a(x, t)\frac{d\kappa(K')}{dK'}\right]\left[\frac{\Delta^2 \bar{K}}{\Delta x^2}\right](\Delta t) + (\kappa R_2 - R_1)(\Delta t) \quad (14a)$$

or

$$e_a(x, t + \Delta t) = e_a(x, t) + r\kappa[\bar{K}(x, t)] [e_a(x + \Delta x, t) - 2e_a(x, t) + e_a(x - \Delta x, t)] + \left[e_a(x, t)\frac{d\kappa(K')}{dK'}\right]\left[\frac{\Delta^2 K}{\Delta x^2}\right](\Delta t) + (\kappa R_2 - R_1)(\Delta t) \quad (14b)$$

where K' is some value between $K(x, t)$ and $\bar{K}(x, t)$.

When $\kappa \equiv 1$, it is necessary to have $r < 1/2$ to insure convergence of error [14]. In the present temperature range κ is monotonically decreasing and $\kappa \leqslant 1$. Let $r < 1/2$.

(*a*) If the boundary condition is exact, then $|e_a(x, t)| < E_1(t)$, which satisfies the dominant difference equation. Thus

$$E_1(t + \Delta t) = E_1(t) + M_2 M_3(t)(\Delta t) + M_1(t)\Delta t, \quad \Delta x \leqslant x \leqslant 1 - \Delta x \quad (15a)$$

Let

$$\left.\begin{aligned} t = n\Delta t, \quad E_1(n\Delta t) &= \bar{E}_1(n) \\ \bar{E}_1(n + 1) &= \bar{E}_1(n)f(n) + g(n) \end{aligned}\right\} \quad (15b)$$

where

$$f(n) = M_2 M_3(n\Delta t)(\Delta t) + 1 \geqslant 1 \quad (16a)[5]$$

$$g(n) = M_1(n\Delta t)(\Delta t) \geqslant 0 \quad (16b)$$

At

$$t = 0, \quad E_1(t) = M_2(t) = M_1(t) = 0, \quad \bar{E}_1(n) = 0, \quad f(0) = 1, \quad g(0) = 0$$

Analogous to the technique of variation of parameters [16], the solution of equation (15*b*) is found to be

$$\bar{E}_1(n) = \prod_{m'=0}^{n-1} f(m')\left[\sum_{m=0}^{n-1}\frac{g(m)}{\prod_{l=0}^{m} f(l)}\right] \quad (17a)$$

$$\leqslant \prod_{m'=0}^{n-1} f(m')\left[\sum_{m=0}^{n-1} g(m)\right] \quad (17b)$$

Assume that the effect of temperature-dependent thermal properties is small, so that the quantity

$$\sum_{m=0}^{n-1} g(m)$$

is close to that in the same problem with constant thermal properties. Hence one may define

$$\prod_{m'=0}^{n-1} f(m')$$

as an amplification factor.

(*b*) If the boundary condition is approximate, there is a direct truncation error ϵ_b at the boundary. If equation (3) is applied on the boundary, there is a remainder

$$|\epsilon_b| \leqslant {}^1/_3(\Delta x)^3\left|\frac{\partial^3 K}{\partial \xi^3}\right|_{max} = m_b(t), \quad 0 \leqslant \xi \leqslant 2\Delta x \quad \text{or} \quad 1 - 2\Delta x \leqslant \xi \leqslant 1 \quad (18)$$

Next to the boundary there is an additional error introduced into the difference equation (6), which is $r\kappa\epsilon_b(t)$. At any interior point an upper bound to the additional error, $E_2(t)$ or $\bar{E}_2(n)$ can be calculated from equation (17*a*) in place of $\bar{E}_1(n)$, with M_1 replaced by M_4 in equation (16*b*). On the boundary, the error is less than or equal to

$$E(t) = E_1(t) + E_2(t) + m_b(t)$$

Round-Off Error. It is difficult to find a general solution of the nonlinear difference equation (14*a*). If the absolute value of the direct round-off error of each number is less than or equal to ϵ_R, the upper bound $E_R(t)$ may be sufficient for many applications. $\bar{E}_R(n)$ can be calculated from equation (17*a*) in place of $\bar{E}_1(n)$, but replacing $M_1\Delta t$ by ϵ_R in equation (16*b*).

Total Error. The total error is less than or equal to

$$E(t) = E_1(t) + E_2(t) + m_b(t) + \epsilon_R + E_R(t) \quad (19)$$

where $m_b(t) = 0$ at interior points.

APPENDIX 2

Selection of Difference Form for Boundary Condition of Given First Derivative

Since the basic difference equation is

$$\bar{K}^*(x^*, t^* + \Delta t^*) = \bar{K}^*(x^*, t^*) + \frac{\Delta t^*}{(\Delta x^*)^2}[\bar{K}^*(x^* + \Delta x^*, t^*) - 2\bar{K}^*(x^*, t^*) + \bar{K}^*(x^* - \Delta x^*, t^*)]$$

the error continuously introduced from the boundary should be of the order $(\Delta x^*)^2$, or higher, so that the error will decrease with Δx^*.

---

[4] The superscript * will be omitted for convenience. All of the quantities in this Appendix are nondimensionalized quantities.

[5] A closer estimation can be obtained by substituting

$$M_2(n\Delta t) = \left|\frac{d\kappa[K(x_1 t)]}{dK}\right|_{max\, at\, t}$$

for M_2.

The simplest form satisfying this requirement should include the second differences; namely,

$$\frac{\partial K^*}{\partial x^*} = \frac{K^*(x^* + \Delta x^*, t^*) - K^*(x^*, t^*)}{\Delta x^*} - \frac{\Delta x^*}{2}\left[\frac{K^*(x^* + 2\Delta x^*, t^*) - 2K^*(x^* + \Delta x^*, t^*) + K^*(x^*, t^*)}{(\Delta x^*)^2}\right] \tag{20}$$

instead of the approximation

$$\frac{\partial K^*}{\partial x^*} = \frac{K^*(x^* + \Delta x^*, t^*) - K^*(x^*, t^*)}{\Delta x^*} \tag{21}$$

For t^* small, the solution for a semi-infinite bar with constant thermal properties indicates that there is little advantage in employing an approximation of higher order than equation (20). In order to compare equations (20) and (21), the results of an example, near the initial time, is shown in Table 2. In this example, it is assumed that $T_i = 672°\text{R}$ (373°K), $K^*(x^*, 0) = 0$

$$\left(\frac{\partial K^*}{\partial x^*}\right)_{x^*=0} = -2.6, \quad \left(\frac{\partial K^*}{\partial x^*}\right)_{x^*=1} = 0,$$

$$\Delta t^* = 0.001, \quad \Delta x^* = 0.05$$

Table 2

t^*	I	II	III	IV
0.005	0.26419	0.26312	0.20951	0.2080
0.010	0.35325	0.35188		

I—Numerical, copper: $K^*(0, t^*) = K^*(\Delta x^*, t^*) - \dfrac{\partial K^*(o, t^*)}{\partial x^*}(\Delta x^*)$, $\kappa^* = 1 - 0.1365(\Delta T^*)$, $\Delta T^* = [1 - (1 - 0.10182K^*)^{1/2}]/0.05091$

II—Numerical, constant properties: $K^*(0, t^*) = K^*(\Delta x^*, t^*) - \dfrac{\partial K^*}{\partial x^*}(\Delta x^*)$

III—Numerical constant properties: equation (7)

IV—Analytic, constant properties, exact boundary conditions: equation (11)

APPENDIX 3

Estimation of Amplification Factor

Assume that the effect of the temperature dependency of the thermal properties is small. From the numerical error found of the case in which the thermal properties are treated as constant, an error estimate can be obtained by multiplying that error by the amplification factor,

$$\prod_{m=0}^{n-1} f(m) = e^{\sum_{m=1}^{n-1} \ln f(m)}$$

which can be calculated approximately by integration. For instance, let $n = 119$ be the value corresponding to the "melting time." Thus

$$\sum_{m=0}^{n-1} \ln f(m) \leq \int_0^{n+1=120} \ln f(m)dm - \ln f(n+1)$$

where $f(m)$ is given in equation (16a).

In the first example,

$$M_2 = \left|\frac{dk^*}{dK^*}\right|_{mx} = 0.1447, \quad \text{since} \quad K_{mx}{}^* = 3.273$$

$$f(n) = 1 + M_2\Delta t\left|\frac{\Delta^2 K^*}{\Delta x^{*2}}\right|_{mx \text{ at } t^* \text{ in } \Delta x^* \leq x^* \leq 1} \quad \text{(temperature-dependent properties}$$

$$\cong 1 + M_2\Delta t\left|\frac{\partial^2 T^*}{\partial x^{*2}}\right|_{mx \text{ at } t^* \text{ in } \Delta x^* \leq x^* \leq 1-\Delta x^*} \quad \text{(constant properties)}$$

From the analytic solution,

$$\left|\frac{\partial^2 T^*}{\partial x^{*2}}\right|_{mx} = \left|\frac{\partial^2 T^*}{\partial x^{*2}}\right|_{x^*=\Delta x^*}$$

can be calculated and is

$$M_2 = \left|\frac{\partial^2 T^*}{\partial x^{*2}}\right|_{x^*=\Delta x^*} = 9.09\left\{1 + 2\sum_{n=1}^{\infty} e^{-n^2\pi^2 t^*}\cos(n\pi\Delta x^*)\right\}, \quad t^* \geqslant \nabla_* t$$

$$M_2 = \tilde{M}_2 = 0 \quad \text{when} \quad t^* = 0$$

If the integration is then carried out by Simpson's rule with twelve intervals, the amplification factor is found to be approximately less than 1.50.

Transient Conduction in Coaxial Cylinders With Relative Motion and Heat Generation

V. S. ARPACI[1]

Instructor,
Mechanical Engineering Department,
Istanbul Technical University,
Istanbul, Turkey

Transient temperatures in a coaxially moving tube and a stationary rod resulting from a step change in the rate of energy generation within the rod are obtained. For the small values of time, the use of finite Hankel transforms reduces the problem to the solution of an integrodifferential equation. In the solution of this equation, Laplace transforms have been used considering the convolutive property of the kernel involved. For the large values of time, this method is not convenient, and the asymptotic behavior of the temperature functions is given by means of the classical approach which requires the use of Laplace transforms. For a given time, it is found that the interface temperature gradient is inversely proportional to the axial distance.

THE system under consideration is shown in Fig. 1, and consists of a constant-diameter tube moving coaxially on a stationary rod. The rod is subjected to a transient effect throughout its volume. The temperature field in the tube and rod, and the temperature gradient on the interface, are desired.

The following assumptions are made:

(*a*) The outer surface of the tube is adiabatic.

(*b*) Mechanical friction along the interface is negligible.

(*c*) The clearance between the tube and rod is negligible and does not have any thermal resistance.

(*d*) Axial heat conduction is negligible, both in the tube and rod.

(*e*) Radial heat conduction is infinite in the tube. Therefore the tube temperature is not a function of radial distance.

(*f*) The physical properties ρ', c_p', ρ, c_p, k of the tube and rod are constant.

(*g*) Initially both tube and rod have the same temperature, which may be taken equal to zero.

(*h*) The transient effect is introduced by a sudden and uniform heat generation in the rod.

(*i*) The tube velocity U is taken to be constant.

A system of co-ordinates fixed to the rod is chosen. Then the application of the first law of thermodynamics to a rod element (a closed system) and a tube control volume, Fig. 2, results in the following two partial differential equations:

For the rod

$$\rho c_p \frac{\partial \theta^*}{\partial t} = k\left(\frac{\partial^2 \theta^*}{\partial r^2} + \frac{1}{r}\frac{\partial \theta^*}{\partial r}\right) + q''' \qquad (1)$$

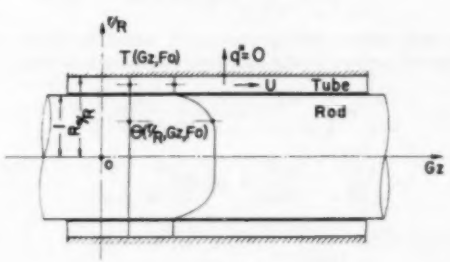

Fig. 1

[1] Currently, Assistant Professor of Mechanical Engineering, University of Michigan, Ann Arbor, Mich.

Presented at the Summer Conference, of the Applied Mechanics Division, University Park, Pa., June 20–22, 1960, of THE AMERICAN SOCIETY OF MECHANICAL ENGINEERS.

Discussion of this paper should be addressed to the Secretary, ASME, 29 West 39th Street, New York, N. Y., and will be accepted until January 10, 1961, for publication at a later date. Discussion received after the closing date will be returned.

Manuscript received by ASME Applied Mechanics Division, August 17, 1959. Paper No. 60—APM-24.

Nomenclature

α = thermal diffusivity of rod
A = cross-sectional area of tube
B = function of axial distance
C = const
c_p = specific heat of rod at constant pressure
c_p' = specific heat of tube at constant pressure
D = const
e = internal energy of rod
e' = internal energy of tube
$\epsilon = \dfrac{PR}{A}\dfrac{(\rho c_p)}{(\rho' c_p')}$, dimensionless number
$\operatorname{erf}(x) = \dfrac{2}{\pi^{1/2}}\displaystyle\int_0^x e^{-\xi^2} d\xi$, error function,
$\operatorname{erfc}(x)$ = $1 - \operatorname{erf}(x)$, complementary error function
$\mathrm{i}^0 \operatorname{erfc}(x)$ = $\operatorname{erfc}(x)$
$\mathrm{i}^m \operatorname{erfc}(x)$ = $\displaystyle\int_x^\infty \mathrm{i}^{m-1} \operatorname{erfc}(\xi) d\xi$
Fo = $\alpha t/R^2$, Fourier number
Fo* = dummy variable
ϕ = temperature function defined in (23)
Gz = $(x/R)/\mathrm{Pe}$, Graetz number
h^0 = stagnation enthalpy of tube
I_0 = modified Bessel function of first kind, of order zero
I_1 = modified Bessel function of first kind, of order first
J_0 = Bessel function of first kind, of order zero
J_1 = Bessel function of first kind, of order first
k = thermal conductivity of rod

(Continued on next page)

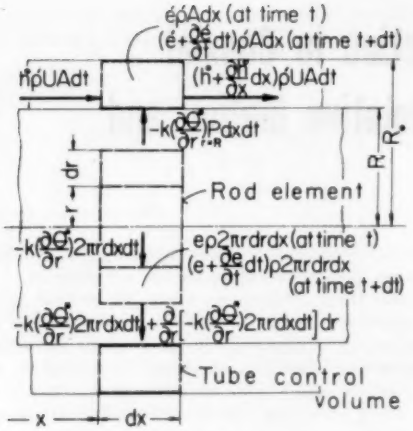

Fig. 2

For the tube

$$(\rho' c_p')A\left(\frac{\partial T^*}{\partial t} + U\frac{\partial T^*}{\partial x}\right) = -Pk\left(\frac{\partial \theta^*}{\partial r}\right)_{r=R} \tag{2}$$

The initial and boundary conditions to be taken according to the outline of this problem are

$$\text{Initial}\begin{cases}\theta^*(r, x, 0) = 0 & (3)\\ T^*(x, 0) = 0 & (4)\end{cases}$$

$$\text{Boundary}\begin{cases}\dfrac{\partial\theta^*(0, x, t)}{\partial r} = 0 & (5)\\ \theta^*(R, x, t) = T^*(x, t) & (6)\\ T^*(0, t) = 0. & (7)\end{cases}$$

The same differential equations and initial boundary conditions can be written in the following dimensionless form:

$$\frac{\partial\theta}{\partial \text{Fo}} = \left[\frac{\partial^2\theta}{\partial(r/R)^2} + \frac{1}{(r/R)}\frac{\partial\theta}{\partial(r/R)}\right] + 1 \tag{8}$$

$$\frac{\partial T}{\partial \text{Fo}} + \frac{\partial T}{\partial \text{Gz}} = -\left[\frac{\partial\theta}{\partial(r/R)}\right]_{r/R=1} \tag{9}$$

$$\text{Initial}\begin{cases}\theta(r/R, \text{Gz}, 0) = 0 & (10)\\ T(\text{Gz}, 0) = 0 & (11)\end{cases}$$

$$\text{Boundary}\begin{cases}\dfrac{\partial\theta(0, \text{Gz}, \text{Fo})}{\partial(r/R)} = 0 & (12)\\ \theta(1, \text{Gz}, \text{Fo}) = T(\text{Gz}, \text{Fo}) & (13)\\ T(0, \text{Fo}) = 0. & (14)\end{cases}$$

The similar problem in the semi-infinite Cartesian co-ordinates was solved previously [1].[2] In the same work the difficulty for finite co-ordinates is also indicated. Here, by the use of another approach which is outlined in the next section, the temperatures for finite circular geometry and for the small values of time are given.

Method of Study

Denoting by $\bar{\vartheta}(\lambda_k, \text{Gz}, \text{Fo})$ the finite Hankel transform of order zero of the dimensionless rod temperature $\theta(r/R, \text{Gz}, \text{Fo})$, then

$$\bar{\vartheta}(\lambda_k, \text{Gz}, \text{Fo}) = \int_0^1 (r/R)\theta(r/R, \text{Gz}, \text{Fo})J_0(\lambda_k r/R)d(r/R). \tag{15}$$

After two integrations by parts this becomes

$$\int_0^1 (r/R)\left[\frac{\partial^2\theta}{\partial(r/R)^2} + \frac{1}{(r/R)}\frac{\partial\theta}{\partial(r/R)}\right]J_0(\lambda_k r/R)d(r/R) = \lambda_k J_1(\lambda_k)T(\text{Gz}, \text{Fo}) - \lambda_k^2\bar{\vartheta}, \tag{16}$$

where λ_k is the kth root of the Bessel function of first kind, of order zero. $T(\text{Gz}, \text{Fo})$ is the dimensionless tube temperature. It may be noted that, for a radially symmetric problem (12) is identically satisfied.

Multiplying (8) and (10) throughout by $(r/R)J_0(\lambda_k r/R)$ and integrating with respect to (r/R) over the range (0, 1) it is found that $\bar{\vartheta}(\lambda_k, \text{Gz}, \text{Fo})$ is determined by the solution of the first-order linear differential equation

$$\frac{\partial\bar{\vartheta}}{\partial \text{Fo}} + \lambda_k^2\bar{\vartheta} = \lambda_k J_1(\lambda_k)T(\text{Gz}, \text{Fo}) + \frac{J_1(\lambda_k)}{\lambda_k} \tag{17}$$

with the initial condition

$$\bar{\vartheta}(\lambda_k, \text{Gz}, 0) = 0. \tag{18}$$

The solution of this differential equation is in the form

$$\bar{\vartheta}(\lambda_k, \text{Gz}, \text{Fo}) = \frac{J_1(\lambda_k)}{\lambda_k}\int_0^{\text{Fo}} e^{-\lambda_k^2(\text{Fo}-\text{Fo}^*)}\,d\text{Fo}^* + \lambda_k J_1(\lambda_k)\int_0^{\text{Fo}} e^{-\lambda_k^2(\text{Fo}-\text{Fo}^*)}T(\text{Gz}, \text{Fo}^*)d\text{Fo}^*. \tag{19}$$

[2] Numbers in brackets designate References at end of paper.

Nomenclature

λ_k = kth term of eigenvalues
Nu = modified Nusselt number
p = Laplace transform variable
P = periphery of rod
Pe = UR/α, Péclèt number
q''' = heat generation per unit volume
r = radial variable
r/R = dimensionless radial variable
R = radius of rod
R_0 = outer radius of tube
ρ = density of rod
ρ' = density of tube
t = time
T^* = temperature of tube
$T = T^*\Big/\left(\dfrac{eq'''R^2}{k}\right)$, dimensionless temperature of tube
$\bar{T}$ = Laplace transform of tube temperature
θ^* = temperature of rod
$\theta = \theta^*\Big/\left(\dfrac{q'''R^2}{k}\right)$, dimensionless temperature of rod
$\bar{\theta}$ = Laplace transform of rod temperature
$\bar{\vartheta}$ = Hankel transform of rod temperature
U = uniform velocity of tube
x = axial distance
x/R = dimensionless axial distance
ξ = dummy variable
z = complex variable

On the other hand, by means of the following theorem [2]:

$$\theta(r/R, \text{Gz}, \text{Fo}) = 2\sum_{k=0}^{\infty} \bar{\vartheta}(\lambda_k, \text{Gz}, \text{Fo}) \frac{J_0(\lambda_k r/R)}{J_1^2(\lambda_k)} \tag{20}$$

equation (9) can be written as follows:

$$\frac{\partial T}{\partial \text{Fo}} + \frac{\partial T}{\partial \text{Gz}} = 2\sum_{k=0}^{\infty} \frac{\lambda_k}{J_1(\lambda_k)} \bar{\vartheta}(\lambda_k, \text{Gz}, \text{Fo}). \tag{21}$$

Now, by using (19) and (21), an integrodifferential equation is obtained in which $T(\text{Gz}, \text{Fo})$ is the only unknown function. This equation is

$$\frac{\partial T}{\partial \text{Fo}} + \frac{\partial T}{\partial \text{Gz}} = 2\int_0^{\text{Fo}} \sum_{k=0}^{\infty} e^{-\lambda_k^2(\text{Fo}-\text{Fo}^*)}\, d\text{Fo}^* + 2\int_0^{\text{Fo}} \sum_{k=0}^{\infty} \lambda_k^2 e^{-\lambda_k^2(\text{Fo}-\text{Fo}^*)}\, T(\text{Gz}, \text{Fo}^*) d\text{Fo}^*. \tag{22}$$

Inspection reveals that for the values of $\text{Fo} \leq 0.04$, the right-hand side of this equation converges very slowly. Therefore an asymptotic solution is needed.

Let an infinite rod be subjected to a step temperature change on its surface. If the initial temperature is assumed to be zero, the well-known solution of this new problem is

$$\phi(r/R, \text{Fo}) = 1 - 2\sum_{k=0}^{\infty} e^{-\lambda_k^2 \text{Fo}} \frac{J_0(\lambda_k r/R)}{\lambda_k J_1(\lambda_k)}, \tag{23}$$

where ϕ is the rod temperature.

It may be shown that for the small values of (Fo) the same solution can be written as [3]

$$\phi(r/R, \text{Fo}) \cong \frac{1}{(r/R)^{1/2}} \operatorname{erfc}\left(\frac{1 - r/R}{2\text{Fo}^{1/2}}\right) + \frac{(1 - r/R)\text{Fo}^{1/2}}{4(r/R)^{3/2}}\, i\operatorname{erfc}\left(\frac{1 - r/R}{2\text{Fo}^{1/2}}\right) + \dots \tag{24}$$

Equating the radial gradients of (23) and (24) at the rod surface,

$$\sum_{k=0}^{\infty} e^{-\lambda_k^2 \text{Fo}} \cong \frac{1}{2\pi^{1/2}\text{Fo}^{1/2}} - \frac{1}{4} \tag{25}$$

is obtained if only the first term of (24) is taken into account. Then differentiating with respect to (Fo) results in

$$\sum_{k=0}^{\infty} \lambda_k^2 e^{-\lambda_k^2 \text{Fo}} \cong \frac{1}{4\pi^{1/2}\text{Fo}^{3/2}} \tag{26}$$

If $\text{Fo} \leq 0.04$, the error of the right-hand side of (25) is at most 1.52 per cent, assuming this latter value when the equality holds. On the other hand, the maximum error in (26) is 1.54 per cent. If the constant term (1/4) in (25) is neglected, the maximum error is increased to 23.4 per cent. However, the assumption of the equal effect of each term on the integrodifferential equation (22) reduces this error to 6 per cent approximately. For the sake of simplicity, this term is omitted in the following study, but it has been included in the Appendix.

Substituting the asymptotic values of (25) and (26) into (22)

$$\frac{\partial T}{\partial \text{Fo}} + \frac{\partial T}{\partial \text{Gz}} = \int_0^{\text{Fo}} \frac{d\text{Fo}^*}{\pi^{1/2}(\text{Fo} - \text{Fo}^*)^{1/2}} + \int_0^{\text{Fo}} \frac{T(\text{Gz}, \text{Fo}^*) d\text{Fo}^*}{2\pi^{1/2}(\text{Fo} - \text{Fo}^*)^{3/2}} \tag{27}$$

is obtained. This equation includes two ordinary convolution integrals on its right-hand side. If use is made of the fact that the Laplace transform of the convolution of two functions is equal to the product of the transforms of these functions, the problem of solving the foregoing equation is reduced to that of determining the solution of an ordinary differential equation and the inverse transformation of this solution.

Multiplying both sides of (27) and (14) by $e^{-p\text{Fo}}$ and integrating with respect to (Fo) from 0 to ∞ gives

$$p\bar{T} + \frac{d\bar{T}}{d\text{Gz}} = \frac{1}{p^{3/2}} - p^{1/2}\bar{T} \tag{28}$$

which can be put into the following form:

$$\frac{d\bar{T}}{d\text{Gz}} + p^{1/2}(1 + p^{1/2})\bar{T} = \frac{1}{p^{3/2}} \tag{29}$$

and

$$\bar{T}(0, p) = 0. \tag{30}$$

The solution of this equation is in the form

$$\bar{T} = \frac{1}{p^2(1 + p^{1/2})} - \frac{e^{-p^{1/2}\text{Gz}}}{p^2(1 + p^{1/2})}\, e^{-p\text{Gz}} \tag{31}$$

The use of transform pair No. 16 in reference [1][3] results in the tube temperature

$$T(\text{Fo}) = 1 - e^{\text{Fo}} \operatorname{erfc}(\text{Fo}^{1/2}) - 2\left(\frac{\text{Fo}}{\pi}\right)^{1/2} + \text{Fo}, \qquad \text{Fo} \leq \text{Gz} \tag{32}$$

$$T(\text{Gz}, \text{Fo}) = T(\text{Fo}) + e^{\text{Fo}} \operatorname{erfc}\left[\frac{\text{Gz}}{2(\text{Fo} - \text{Gz})^{1/2}} + (\text{Fo} - \text{Gz})^{1/2}\right] - \sum_{m=0}^{2} [-2(\text{Fo} - \text{Gz})^{1/2}]^m i^m \operatorname{erfc}\left[\frac{\text{Gz}}{2(\text{Fo} - \text{Gz})^{1/2}}\right], \qquad \text{Fo} \geq \text{Gz} \tag{33}$$

which is valid for $\text{Fo} \leq 0.04$.

Inverting (19) by means of (20) gives

$$\theta(r/R, \text{Gz}, \text{Fo}) = \int_0^{\text{Fo}} 2\sum_{k=0}^{\infty} e^{-\lambda_k^2(\text{Fo}-\text{Fo}^*)} \frac{J_0(\lambda_k r/R)}{\lambda_k J_1(\lambda_k)}\, d\text{Fo}^* + \int_0^{\text{Fo}} 2\sum_{k=0}^{\infty} \lambda_k e^{-\lambda_k^2(\text{Fo}-\text{Fo}^*)} \frac{J_0(\lambda_k r/R)}{J_1(\lambda_k)}\, T(\text{Gz}, \text{Fo}^*) d\text{Fo}^*, \tag{34}$$

which is the rod temperature in terms of the tube temperature. On the other hand, for the small values of time, equality of (23) and (24) results in

$$2\sum_{k=0}^{\infty} e^{-\lambda_k^2 \text{Fo}} \frac{J_0(\lambda_k r/R)}{\lambda_k J_1(\lambda_k)} \cong 1 - \frac{1}{(r/R)^{1/2}} \operatorname{erfc}\left(\frac{1 - r/R}{2\text{Fo}^{1/2}}\right) \tag{35}$$

Then differentiating with respect to (Fo) gives

$$2\sum_{k=0}^{\infty} \lambda_k e^{-\lambda_k^2 \text{Fo}} \frac{J_0(\lambda_k r/R)}{J_1(\lambda_k)} \cong \frac{2}{\pi^{1/2}(r/R)^{1/2}} \frac{(1 - r/R)}{4\text{Fo}^{3/2}}\, e^{-\frac{(1-r/R)^2}{4\text{Fo}}} \tag{36}$$

If the right-hand sides of equations (35) and (36) are substituted into (32),

[3] Reference [1], Appendix 5, p. 495.

$$\theta(r/R, \mathrm{Gz}, \mathrm{Fo}) = \int_0^{\mathrm{Fo}} \left\{1 - \frac{1}{(r/R)^{1/2}} \operatorname{erfc}\left[\frac{1 - r/R}{2(\mathrm{Fo} - \mathrm{Fo}^*)^{1/2}}\right]\right\} d\mathrm{Fo}^* + \frac{1}{(r/R)^{1/2}} \int_0^{\mathrm{Fo}} \frac{(1 - r/R)e^{-\frac{(1-r/R)^2}{4(\mathrm{Fo}-\mathrm{Fo}^*)}}}{2\pi^{1/2}(\mathrm{Fo} - \mathrm{Fo}^*)^{3/2}} T(\mathrm{Gz}, \mathrm{Fo}^*) d\mathrm{Fo}^* \quad (37)$$

is obtained. Multiplying this equation by $e^{-p\mathrm{Fo}}$, integrating with respect to (Fo) from 0 to ∞, and using (30) gives

$$\bar{\theta}(r/R, \mathrm{Gz}, p) = \frac{1}{p^2} - \frac{1}{(r/R)^{1/2}} \frac{e^{-(1-r/R)p^{1/2}}}{p^2} + \frac{1}{(r/R)^{1/2}} \frac{e^{-(1-r/R)p^{1/2}}}{p^2(1 + p^{1/2})} - \frac{1}{(r/R)^{1/2}} \frac{e^{-(1-r/R+\mathrm{Gz})p^{1/2}}}{p^2(1 + p^{1/2})} e^{-p\mathrm{Gz}} \quad (38)$$

Again the use of transform pair No. 16 in reference [1][3] results in the rod temperature

$$\theta(r/R, \mathrm{Fo}) = -e^{(1-r/R+\mathrm{Fo})} \operatorname{erfc}\left(\frac{1 - r/R}{2\mathrm{Fo}^{1/2}} + \mathrm{Fo}^{1/2}\right) + \sum_{m=0}^{2} (-2\mathrm{Fo}^{1/2})^m i^m \operatorname{erfc}\left(\frac{1 - r/R}{2\mathrm{Fo}^{1/2}}\right), \qquad \mathrm{Fo} \leq \mathrm{Gz} \quad (39)$$

$$\theta(r/R, \mathrm{Gz}, \mathrm{Fo}) = \theta(r/R, \mathrm{Fo}) + \frac{1}{(r/R)^{1/2}} \left\{e^{(1-r/R+\mathrm{Fo})} \operatorname{erfc}\left[\frac{1 - r/R + \mathrm{Gz}}{2(\mathrm{Fo} - \mathrm{Gz})^{1/2}} + (\mathrm{Fo} - \mathrm{Gz})^{1/2}\right] - \sum_{m=0}^{2} [-2(\mathrm{Fo} - \mathrm{Gz})^{1/2}]^m i^m \operatorname{erfc}\left[\frac{1 - r/R + \mathrm{Gz}}{2(\mathrm{Fo} - \mathrm{Gz})^{1/2}}\right]\right\}, \qquad \mathrm{Fo} \geq \mathrm{Gz} \quad (40)$$

To calculate the heat flux, the dimensionless temperature gradient along the tube-rod interface can be written as

$$\mathrm{Nu}(\mathrm{Gz}, \mathrm{Fo}) = -\left[\frac{\partial\theta}{\partial(r/R)}\right]_{r/R=1} \quad (41)$$

If this equation is combined with (9),

$$\mathrm{Nu}(\mathrm{Gz}, \mathrm{Fo}) = \frac{\partial T}{\partial \mathrm{Fo}} + \frac{\partial T}{\partial \mathrm{Gz}} \quad (42)$$

is obtained. Taking the Laplace transforms of (40) in the (Fo)-variable, and using (11) gives

$$\overline{\mathrm{Nu}} = p\bar{T} + \frac{d\bar{T}}{d\mathrm{Gz}}. \quad (43)$$

Combining this equation with (28) and (31) results in

$$\overline{\mathrm{Nu}} = \frac{1}{p(1 + p^{1/2})} + \frac{e^{-p^{1/2}\mathrm{Gz}}}{p^{3/2}(1 + p^{1/2})} e^{-p\mathrm{Gz}} \quad (44)$$

Then using the same transform pair,

$$\mathrm{Nu}(\mathrm{Fo}) = 1 - e^{\mathrm{Fo}} \operatorname{erfc}(\mathrm{Fo}^{1/2}), \qquad \mathrm{Fo} \leq \mathrm{Gz} \quad (45)$$

$$\mathrm{Nu}(\mathrm{Gz}, \mathrm{Fo}) = \mathrm{Nu}(\mathrm{Fo}) + \left\{2\left(\frac{\mathrm{Fo} - \mathrm{Gz}}{\pi}\right)^{1/2} e^{-\frac{\mathrm{Gz}^2}{4(\mathrm{Fo}-\mathrm{Gz})}} - (1 + \mathrm{Gz}) \operatorname{erfc}\left[\frac{\mathrm{Gz}}{2(\mathrm{Fo} - \mathrm{Gz})^{1/2}}\right] + e^{\mathrm{Fo}} \operatorname{erfc}\left[\frac{\mathrm{Gz}}{2(\mathrm{Fo} - \mathrm{Gz})^{1/2}} + (\mathrm{Fo} - \mathrm{Gz})^{1/2}\right]\right\}, \qquad \mathrm{Fo} \geq \mathrm{Gz} \quad (46)$$

is obtained for the dimensionless temperature gradient along the tube-rod interface.

The integrodifferential equation (22) has two integrals with zero lower limit, and for the large values of time an integration from (0) to a large (Fo) is necessary. However, the character of the function (23), which is needed for the solution of this integrodifferential equation, is entirely different for the small and large values of time. Therefore the method used in this section is not convenient for the large values of time. For these values of time, the behavior of the tube and rod temperature, and the interface temperature gradient are obtained by the classical method which requires the use of Laplace transforms.

Classical Method

This method is well known and has already been used for a variety of problems. However, to the author's knowledge, for the first time it is applied to the present problem.

Multiplying both sides of equations (8), (9), (12), (13), and (14) by $e^{-p\mathrm{Fo}}$, integrating with respect to (Fo) from 0 to ∞, and using (11) and (12) gives

$$p\bar{\theta} = \frac{\partial^2\bar{\theta}}{\partial(r/R)^2} + \frac{1}{(r/R)} \frac{\partial\bar{\theta}}{\partial(r/R)} + \frac{1}{p} \quad (47)$$

$$p\bar{T} + \frac{d\bar{T}}{d\mathrm{Gz}} = -\left[\frac{\partial\bar{\theta}}{\partial(r/R)}\right]_{r/R=1} \quad (48)$$

$$\frac{\partial\bar{\theta}(0, \mathrm{Gz}, p)}{\partial(r/R)} = 0 \quad (49)$$

$$\bar{\theta}(1, \mathrm{Gz}, p) = \bar{T}(\mathrm{Gz}, p) \quad (50)$$

$$\bar{T}(0, p) = 0. \quad (51)$$

The solution of (47) with (49) may be found as

$$\bar{\theta}(r/R, \mathrm{Gz}, p) = \frac{1}{p^2} + B(\mathrm{Gz}) I_0(p^{1/2} r/R) \quad (52)$$

which is the Laplace transformed (in time) rod temperature. Where B is an integration parameter and depends on (Gz).

By the use of (50)

$$\bar{T}(\mathrm{Gz}, p) = \frac{1}{p^2} + B(\mathrm{Gz}) I_0(p^{1/2}) \quad (53)$$

is obtained for the transformed tube temperature.

Obtaining the values of $(\bar{T})$ and $(d\bar{T}/d\mathrm{Gz})$ from (53), and $[d\bar{\theta}/d(r/R)]_{r/R=1}$ from (52), and substituting into (48) results in

$$\frac{dB(\mathrm{Gz})}{d\mathrm{Gz}} + \left[p + \frac{p^{1/2} I_1(p^{1/2})}{I_0(p^{1/2})}\right] B(\mathrm{Gz}) = -\frac{1}{pI_0(p^{1/2})} \quad (54)$$

The solution of this differential equation is in the form

$$B(\mathrm{Gz}) = -\frac{1}{p^2 I_0(p^{1/2}) + p^{1/2} I_1(p^{1/2})} + Ce^{-\frac{p^{1/2} I_1(p^{1/2})}{I_0(p^{1/2})} \mathrm{Gz}} e^{-p\mathrm{Gz}}, \quad (55)$$

where C is an integration constant.

If the value of $B(\mathrm{Gz})$ is taken from (55) and substituted into (53), and using (51)

$$\bar{T}(\mathrm{Gz}, p) = \left[\frac{1}{p^2} - \frac{I_0(p^{1/2})}{p^2 I_0(p^{1/2}) + p^{1/2} I_1(p^{1/2})}\right] \times \left[1 - e^{-\frac{p^{1/2} I_1(p^{1/2})}{I_0(p^{1/2})} \mathrm{Gz}} e^{-p\mathrm{Gz}}\right] \quad (56)$$

is obtained. Similarly, the use of (50), (51), (52), and (55) results in

$$\bar{\theta}(r/R, \mathrm{Gz}, p) = \left[\frac{1}{p^2} - \frac{I_0(p^{1/2}r/R)}{p^2 I_0(p^{1/2}) + p^{3/2} I_1(p^{1/2})}\right] - \left[\frac{I_0(p^{1/2}r/R)}{p^2 I_0(p^{1/2})} - \frac{I_0(p^{1/2}r/R)}{p^2 I_0(p^{1/2}) + p^{3/2} I_1(p^{1/2})}\right] e^{-\frac{p^{1/2} I_1(p^{1/2})}{I_0(p^{1/2})}\mathrm{Gz}} e^{-p\mathrm{Gz}} \quad (57)$$

So far, there is no difficulty in getting the transformed (in time) temperature functions (56) and (57). However, the inverse transforms of these functions are rather more difficult to obtain. In addition to this difficulty, the solutions would not be suitable for use with small values of time, say, for values less than 0.04. For that reason, in the preceding section, another approach was used for the small values of time. For the large values of time, the asymptotic expansion of the Bessel functions involved in (56) and (57) are considered.

It is a well-known fact that the solution of transient conduction problems in finite regions consists of the summation of an infinite number of exponentials plus a constant, linear, or quadratic term in time, or their combination. The latter results from the residue at the origin and, since for the large values of time the terms involving exponentials are negligible, gives the asymptotic behavior of the temperature function. Having this in mind, in the inversion of

$$\frac{I_0(p^{1/2}r/R)}{p^2 I_0(p^{1/2})} \quad (58)$$

and

$$\frac{I_0(p^{1/2}r/R)}{p^2 I_0(p^{1/2}) + p^{3/2} I_1(p^{1/2})}, \quad (59)$$

only the residues at the origin are considered.

Each of these equations has a double pole at the origin and the corresponding residue can be found by an expansion in terms of $(1/z)$ and taking the coefficient of $(1/z)$. Following the usual procedure

$$\frac{e^{z\mathrm{Fo}} I_0(z^{1/2}r/R)}{z^2 I_0(z^{1/2})} = \frac{1}{z^2} + \left\{\mathrm{Fo} - \frac{1}{4}\left[1 - (r/R)^2\right]\right\}\frac{1}{z} + \ldots \quad (60)$$

and

$$\frac{e^{z\mathrm{Fo}} I_0(z^{1/2}r/R)}{z^2 I_0(z^{1/2}) + z^{3/2} I_1(z^{1/2})} = \frac{2}{3z^2} + 2/3\left\{\mathrm{Fo} - 1/4\left[1 - (r/R)^2\right] + \frac{1}{24}\right\}\frac{1}{z} + \ldots \quad (61)$$

are obtained. Therefore for the large values of time

$$\frac{I_0(p^{1/2}r/R)}{p^2 I_0(p^{1/2})} \subset \mathrm{Fo} - 1/4\left[1 - (r/R)^2\right] \supset \frac{1}{p^2} - \frac{1}{4p}\left[1 - (r/R)^2\right] \quad (62)$$

and

$$\frac{I_0(p^{1/2}r/R)}{p^2 I_0(p^{1/2}) + p^{3/2} I_1(p^{1/2})} \subset 2/3\left\{\mathrm{Fo} - 1/4\left[1 - (r/R)^2\right] + \frac{1}{24}\right\} \supset 2/3\left\{\frac{1}{p^2} - \frac{1}{4p}\left[1 - (r/R)^2\right] + \frac{1}{24p}\right\} \quad (63)$$

Using the foregoing two approximations and the following expansion

$$e^{-\frac{p^{1/2} I_1(p^{1/2})}{I_0(p^{1/2})}\mathrm{Gz}} \cong e^{-\left(\frac{p}{2} - \frac{p^2}{16} + \ldots\right)\mathrm{Gz}} \quad (64)$$

the Laplace transforms of the tube and rod temperatures can be written as

$$\bar{T}(\mathrm{Gz}, p) = 1/3\left(\frac{1}{p^2} - \frac{1}{12p}\right)\left(1 - e^{-\frac{3}{2}\mathrm{Gz}p} e^{\frac{\mathrm{Gz}}{16}p^2}\right) \quad (65)$$

and

$$\bar{\theta}(r/R, \mathrm{Gz}, p) = 1/3\left\{\frac{1}{p^2} + \frac{1}{2p}\left[1 - (r/R)^2\right] - \frac{1}{12p}\right\} - 1/3\left\{\frac{1}{p^2} - \frac{1}{4p}\left[1 - (r/R)^2\right] - \frac{1}{12p}\right\} e^{-\frac{3}{2}p\mathrm{Gz}} e^{\frac{\mathrm{Gz}}{16}p^2} \quad (66)$$

By taking the Laplace transform of (41), and using (66) results in

$$\overline{\mathrm{Nu}}(\mathrm{Gz}, p) = \frac{1}{3p} + \frac{e^{\frac{\mathrm{Gz}}{16}p^2}}{6p} e^{-\frac{3}{2}p\mathrm{Gz}} \quad (67)$$

Then by the use of a transform table [4], for the large values of time, the following temperature functions and the temperature gradient are obtained:

$$T(\mathrm{Gz}, \mathrm{Fo}) = \frac{\mathrm{Gz}}{2} - \frac{1}{12}\left(\frac{\mathrm{Gz}}{\pi}\right)^{1/2} e^{-\frac{4(\mathrm{Fo} - 3/2\,\mathrm{Gz})^2}{\mathrm{Gz}}} + 1/6\left(\mathrm{Fo} - 3/2\,\mathrm{Gz} - \frac{1}{12}\right)\mathrm{erfc}\left[\frac{2(\mathrm{Fo} - 3/2\,\mathrm{Gz})}{\mathrm{Gz}^{1/2}}\right], \quad \mathrm{Fo} \geq 3/2\mathrm{Gz} \quad (68)$$

$$\theta(r/R, \mathrm{Gz}, \mathrm{Fo}) = \frac{\mathrm{Gz}}{2} + 1/4\left[1 - (r/R)^2\right] - \frac{1}{12}\left(\frac{\mathrm{Gz}}{\pi}\right)^{1/2} e^{-\frac{4(\mathrm{Fo} - 3/2\mathrm{Gz})^2}{\mathrm{Gz}}} + 1/6\,(\mathrm{Fo} - 3/2\,\mathrm{Gz} - 1/4[1 - (r/R)^2] - 1/12)\,\mathrm{erfc}\left[\frac{2(\mathrm{Fo} - 3/2\,\mathrm{Gz})}{\mathrm{Gz}^{1/2}}\right], \quad \mathrm{Fo} \geq 3/2\mathrm{Gz} \quad (69)$$

$$\mathrm{Nu}(\mathrm{Gz}, \mathrm{Fo}) = 1/2 - 1/12\,\mathrm{erfc}\left[\frac{2(\mathrm{Fo} - 3/2\,\mathrm{Gz})}{\mathrm{Gz}^{1/2}}\right], \quad \mathrm{Fo} \geq 3/2\mathrm{Gz} \quad (70)$$

Steady Solution

For large values of time, the problem under study approaches a steady-state case which can be expressed by the following differential equations:

$$\frac{1}{(r/R)}\frac{\partial}{\partial(r/R)}\left[(r/R)\frac{\partial\theta}{\partial(r/R)}\right] + 1 = 0 \quad (71)$$

$$\frac{dT}{d\mathrm{Gz}} = -\left[\frac{\partial\theta}{\partial(r/R)}\right]_{r/R=1} \quad (72)$$

and the boundary conditions

$$\frac{\partial\theta(0, \mathrm{Gz})}{\partial(r/R)} = 0 \quad (73)$$

$$\theta(1, \mathrm{Gz}) = T(\mathrm{Gz}) \tag{74}$$

$$T(0) = 0 \tag{75}$$

The solution of the foregoing system can be obtained easily, and the results are

$$T(\mathrm{Gz}) = \frac{\mathrm{Gz}}{2} \tag{76}$$

$$\theta(r/R, \mathrm{Gz}) = \frac{\mathrm{Gz}}{2} + 1/4[1 - (r/R)^2] \tag{77}$$

Then, the use of (41) gives the dimensionless heat flux along the tube-rod interface as

$$\mathrm{Nu}(\mathrm{Gz}) = 1/2 \tag{78}$$

Conclusion

The methods described in the preceding sections have been used to obtain the dimensionless heat flux on the tube-rod interface, and the tube and rod temperatures. In Fig. 3 is shown the interface Nusselt number versus $(\mathrm{Fo}^{1/2})$ for both small and large values of $(\mathrm{Fo}^{1/2})$. It seems important to note that, for a given time, the heat flux is inversely proportional to the axial distance.

Consider a fluid with very low Prandtl number flowing coaxially on a rod. Assume that outer surface of the fluid is insulated. A heat source with constant strength is applied to the rod, and the temperature fields in the fluid and rod and the interface heat flux are required. The present study can be used to investigate this problem which approximates the transient behavior of certain types of nuclear reactors. It is well known that the heat source of a cylindrical fuel element which is proportional to the neutron flux is not uniform [5] within its volume. However, having a linear problem, the other type heat sources can be obtained by simply using the principle of superposition.

APPENDIX

For the small values of Fourier number, the following equality,

$$\sum_{k=0}^{\infty} e^{-\lambda_k^2 \mathrm{Fo}} \cong \frac{1}{2\pi^{1/2}\mathrm{Fo}^{1/2}} - 1/4,$$

previously has been obtained in (25), and to simplify the results the constant term 1/4 was omitted. In this Appendix, the effect of 1/4 to the tube temperature is shown. Taking (25) substituting into (27) results in

$$\frac{\partial T_t}{\partial \mathrm{Fo}} + \frac{\partial T_t}{\partial \mathrm{Gz}} = \int_0^{\mathrm{Fo}} \left[\frac{1}{\pi^{1/2}(\mathrm{Fo} - \mathrm{Fo}^*)^{1/2}} - 1/2\right] d\mathrm{Fo}^* + \int_0^{\mathrm{Fo}} \frac{T_t(\mathrm{Gz}, \mathrm{Fo}^*)d\mathrm{Fo}^*}{2\pi^{1/2}(\mathrm{Fo} - \mathrm{Fo}^*)^{3/2}} \tag{79}$$

where T_t is the tube temperature including the effect of this constant term.

This integrodifferential equation is linear with respect to the first right-hand side term, and can be written as follows:

$$T_t = T + \Delta T, \tag{80}$$

where ΔT shows the effect of 1/4.

Then the integrodifferential equation satisfied by ΔT is found to be

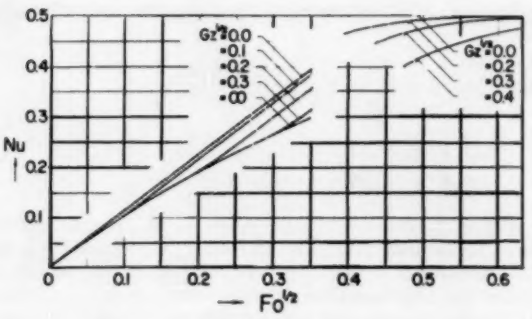

Fig. 3

$$\frac{\partial \Delta T}{\partial \mathrm{Fo}} + \frac{\partial \Delta T}{\partial \mathrm{Gz}} = -1/2\mathrm{Fo} + \int_0^{\mathrm{Fo}} \frac{\Delta T(\mathrm{Gz}, \mathrm{Fo}^*)d\mathrm{Fo}^*}{2\pi^{1/2}(\mathrm{Fo} - \mathrm{Fo}^*)^{3/2}} \tag{81}$$

Following the previous procedure, multiplying each term of (80) and (81) by $e^{-p\mathrm{Fo}}$ and integrating with respect to (Fo) from 0 to ∞, and combining (29) with (80), it is found that $\Delta\bar{T}(\mathrm{Gz}, p)$ is determined by the solution of the following first-order linear differential equation:

$$\frac{d\Delta\bar{T}}{d\mathrm{Gz}} + p^{1/2}(1 + p^{1/2})\Delta\bar{T} = -\frac{1}{2p^2} \tag{82}$$

with the boundary condition

$$\Delta\bar{T}(0, p) = 0 \tag{83}$$

The solution of this equation is in the form

$$\Delta\bar{T} = -1/2\left[\frac{1}{p^{5/2}(1 + p^{1/2})} - \frac{e^{-p^{1/2}\mathrm{Gz}}}{p^{5/2}(1 + p^{1/2})}\, e^{-p\mathrm{Gz}}\right] \tag{84}$$

By the use of the same transform pair No. 16 in reference [1],[3] the following correction term in the tube temperature is obtained

$$\Delta T(\mathrm{Fo}) = -1/2\left[e^{\mathrm{Fo}}\,\mathrm{erfc}\,(\mathrm{Fo}^{1/2}) - 1 + 2\left(\frac{\mathrm{Fo}}{\pi}\right)^{1/2} - \mathrm{Fo} + \frac{4}{3\pi^{1/2}}\mathrm{Fo}^{3/2}\right], \quad \mathrm{Fo} \le \mathrm{Gz} \tag{85}$$

$$\Delta T(\mathrm{Gz}, \mathrm{Fo}) = \Delta T(\mathrm{Fo}) + 1/2\left(e^{\mathrm{Fo}}\,\mathrm{erfc}\left[\frac{\mathrm{Gz}}{2(\mathrm{Fo} - \mathrm{Gz})^{1/2}} + (\mathrm{Fo} - \mathrm{Gz})^{1/2}\right] - \sum_{m=0}^{3}\left[-2(\mathrm{Fo} - \mathrm{Gz})^{1/2}\right]^m i^m\,\mathrm{erfc}\left[\frac{\mathrm{Gz},}{2(\mathrm{Fo} - \mathrm{Gz})^{1/2}}\right]\right), \quad \mathrm{Fo} \ge \mathrm{Gz} \tag{86}$$

References

1 H. S. Carslaw and J. C. Jeager, "Conduction of Heat in Solids," Oxford University Press, Oxford, England, 1959, p. 396.

2 I. N. Sneddon, "Fourier Transforms," McGraw-Hill Book Company, Inc., New York, N. Y., 1952, p. 82.

3 S. Goldstein, "Some Two-Dimensional Diffusion Problems With Circular Symmetry," *Proceedings of the London Mathematical Society*, vol. 34, 1932, p. 51.

4 G. A. Campbell and R. M. Foster, "Fourier Integrals for Practical Applications," D. Van Nostrand Book Company, New York, N. Y., 1954.

5 S. Glasstone and M. C. Edlund, "The Elements of Nuclear Reactor Theory," D. Van Nostrand Book Company, New York, N. Y., 1952, p. 213.

Thermal Stresses in an Elastic, Work-Hardening Sphere

CHINTSUN HWANG[1]

Head, Commercial Systems, The National Cash Register Company, Hawthorne, Calif. Mem. ASME

In this paper, a method is presented for obtaining the transient thermal-stress distribution and the residual stresses in a spherical body where the time-dependent temperature distribution is symmetrical with respect to the center of the sphere. The material is assumed to be elastoplastic, while in the plastic range it work-hardens isotropically. The von Mises yield condition is used. The thermal and mechanical properties of the material are assumed to be temperature independent. The problem is reduced to a single nonlinear differential equation which is solved numerically on the NCR 304 digital computer. Several sets of numerical data representing various degrees of work-hardening in the spherical bodies during a cooling process are presented.

THERMAL-stress problems, which play a significant role in both metal-processing and machine design, have received widespread attention and have been treated at some length by research workers. In most cases, the theoretical treatment on thermal stresses in solids is limited to the elastic or elastic-perfectly plastic cases. For an extensive bibliography on the subject, the reader is referred to [1].[2] Recently, Prager presented a theory of nonisothermal deformation of rigid, work-hardening solids [2]. The constitutive law he proposed contains an unspecified function of temperature, stress, strain, and strain history. The uniqueness of the solution of a typical boundary-value problem is discussed. On the other hand, Weiner and his associates studied the transient and residual stresses in heat-treated plates and cylinders [3–6]. The material assumed in their study is elastic, perfectly plastic. In one case [6], the effect of viscoelasticity is considered.

Lomakin studied the elastic, work-hardening behavior of a sphere in a transient temperature field [7]. In his study the local stresses are assumed to be solely dependent on the local thermal strain. The "secondary strain," which is due to the redistribution of deformations among the spherical elements, is ignored. The resulting stress distribution, though statistically admissible, is therefore arbitrary and may not represent the true stress picture in the sphere. The foregoing statement can be exemplified by the fact that, based on his approach, the residual stresses appear only in the region where the thermal strain has reached a certain value corresponding to the yield condition of the material. No residual stress is encountered in the "elastic" region.

The present paper deals with the transient and residual stresses in a hollow or solid spherical body. The mechanical and thermal properties are assumed to be temperature independent. The temperature distribution, which is symmetrical with respect to the center of the sphere, is determined by the classical solution based on specific boundary conditions [8]. The material of the spherical body is elastic, work-hardening. The von Mises' yield condition is used. In the work-hardening range, the material hardens isotropically. In both the elastic and the work-hardening ranges, appropriate flow rules are used [9], [10]. Based on the equilibrium and compatibility conditions, a nonlinear ordinary differential equation is established which determines the changes in stress deviation in the spherical body as a result of specific temperature changes. The stress distribution, either transient or residual, is then obtained by further integration.

The differential equation is solved by a numerical method through the use of a digital computer. A flow diagram, indicating the computation procedures, is given in the paper. Numerical data are presented which give the thermal stresses in an elastic, work-hardening sphere with uniform initial temperature and cooling in an infinite medium of lower temperature according to Newton's law. Three distinct cases of thermal-stress distribution in the sphere are given, each case representing a different degree of work-hardening in the sphere during the cooling process.

Yield Condition and Stress-Strain Relation

In spherical co-ordinates (r, θ, ϕ), if the stress distribution is symmetrical with respect to the origin, the three principal stresses σ_r, σ_θ, σ_ϕ are functions of the radial position r and time t only. The tangential stresses σ_θ and σ_ϕ are equal.

The von Mises yield condition is represented by

$$(\sigma_1 - \sigma_2)^2 + (\sigma_2 - \sigma_3)^2 + (\sigma_3 - \sigma_1)^2 = 2Y^2 \qquad (1)$$

where σ_1, σ_2, σ_3 are the principal stresses, Y is the yield stress in simple tension. For the special case of symmetrical stress distribution in spherical co-ordinates, we have $(\sigma_1, \sigma_2, \sigma_3) = (\sigma_r, \sigma_\theta, \sigma_\phi)$. Condition (1) is reduced to

$$\sigma_r^2 - 2\sigma_r\sigma_\phi + \sigma_\phi^2 = Y^2 \qquad (2)$$

In Fig. 1 the von Mises yield condition (1) is represented by the cylindrical surface located in the stress space $(\sigma_1, \sigma_2, \sigma_3)$, reference [9]. The axis of the cylindrical surface makes equal angles with the co-ordinate axes, while the radius of the cylindrical surface is equal to $\sqrt{2/3}\,Y$. For an elastic, isotropic-hardening material, yielding is reached when the local stress condition is represented by a point on the cylindrical yield surface of Fig. 1. As the load further increases, the yield surface expands proportionately about its fixed axis AA. The material is in an unloading state when the stress point departs from the yield surface and re-enters the region inscribed by the yield surface. For symmetrical stress distribution in spherical co-ordinates, the foregoing rules apply while the stress point remains on a plane defined by axes AA and σ_r in Fig. 1.

---

[1] Also, Lecturer, University of Southern California.

[2] Numbers in brackets designate References at end of paper.

Presented at the West Coast Conference of the Applied Mechanics Division, Pasadena, Calif., June 27–29, 1960, of THE AMERICAN SOCIETY OF MECHANICAL ENGINEERS.

Discussion of this paper should be addressed to the Secretary, ASME, 29 West 39th Street, New York, N. Y., and will be accepted until January 10, 1961, for publication at a later date. Discussion received after the closing date will be returned.

Manuscript received by ASME Applied Mechanics Division, December 17, 1959. Paper No. 60—APMW-8.

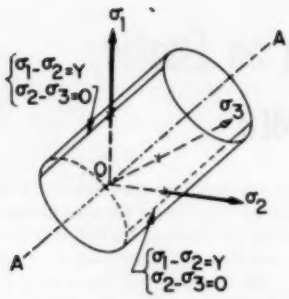

Fig. 1 Von Mises yield surface in a stress space

For the part of the material which has reached the yield condition and is in the work-hardening range, the incremental flow rule gives the plastic strain rates:

$$\dot{e}_i^p = \frac{3\sigma_i'\dot{\bar{\sigma}}}{2H'\bar{\sigma}},$$

where

$$\bar{\sigma} = [3/2 \Sigma (\sigma_i')^2]^{1/2}, \qquad i = 1, 2, 3 \tag{3}$$

In expressions (3), e_i^p are the principal plastic strains, σ_i' are the corresponding components of stress deviation, $\bar{\sigma}$ is called the equivalent stress, H' is the slope of the curve of the equivalent stress versus the equivalent strain. A dot on a variable indicates the time derivative of the variable. For a detailed explanation of the flow rule the reader is referred to [9]. If we apply the foregoing flow rule (3) to a spherical element with symmetrical stress distribution, we obtain the following expressions for the plastic strains of the element:

$$\dot{e}_r^p = \frac{1}{H'}(\dot{\sigma}_r - \dot{\sigma}_\phi)$$

$$\dot{e}_\phi^p = \dot{e}_\theta^p = -\frac{1}{2H'}(\dot{\sigma}_r - \dot{\sigma}_\phi) \tag{4}$$

The foregoing expressions for the plastic strains along the radial and tangential directions apply only when the element is in the loading state of the work-hardening range. Otherwise, the plastic strain rate vanishes. Using expressions (4), and considering the elastic strains and the strain due to thermal expansion, we reach the following expressions for the strain rates in a spherical element:

$$\dot{e}_r = \frac{1}{E}(\dot{\sigma}_r - 2\nu\dot{\sigma}_\phi) + \frac{q}{H'}(\dot{\sigma}_r - \dot{\sigma}_\phi) + \alpha\dot{T}$$

$$\dot{e}_\phi = \dot{e}_\theta = \frac{1}{E}[-\nu\dot{\sigma}_r + (1-\nu)\dot{\sigma}_\phi] - \frac{q}{2H'}(\dot{\sigma}_r - \dot{\sigma}_\phi) + \alpha\dot{T} \tag{5}$$

$q = 1$ if $|\sigma_r - \sigma_\phi| \geqslant Y$, and $(\sigma_r - \sigma_\phi)(\dot{\sigma}_r - \dot{\sigma}_\phi) \geqslant 0$,

$q = 0$ if otherwise

In expressions (5), E is the Young's modulus, ν is Poisson's ratio, α is the coefficient of linear thermal expansion of the material, and $\dot{T} = \dot{T}(r, t)$ is the temperature rate in the spherical element.

Cooling of a Spherical Body

When a spherical body, which has a uniform initial temperature T_1, is immersed in an infinite medium of zero temperature, the temperature of the body decreases with time and eventually reaches the temperature of the surrounding medium. In the cooling process, because of the uneven thermal-strain distribution, stresses are developed in the spherical body. To study the thermal stresses, first we have to find the transient temperature distribution of the body. According to Newton's law of cooling, the equation for the cooling of the spherical body under discussion is

$$\frac{\partial T}{\partial t} = \mathcal{K}\left(\frac{\partial^2 T}{\partial r^2} + \frac{2}{r}\frac{\partial T}{\partial r}\right) \qquad 0 \leqslant r \leqslant R$$

$$\frac{\partial T}{\partial r} + hT = 0 \quad \text{at} \quad r = R \tag{6}$$

$$T = T_1, \text{ when } t = 0$$

where $\mathcal{K} = k/c\rho$, k is the thermal conductivity coefficient of the material, c is the specific heat; ρ is the specific weight; $h = H/k$, H is the surface heat-transfer coefficient; R is the radius of the sphere. The solution [8] of equation (6) is

$$\frac{T}{T_1} = \frac{2\lambda}{r/R}\sum_{n=1}^{\infty}\exp\left(-\frac{\mathcal{K}\gamma_n^2 t}{R^2}\right) \cdot \frac{\gamma_n^2 + (\lambda-1)^2}{\gamma_n^2[\gamma_n^2 + \lambda(\lambda-1)]}\sin\gamma_n \sin\gamma_n\left(\frac{r}{R}\right) \tag{7}$$

where $\lambda = Rh$, and γ_n are the successive positive roots of the equation

$$\gamma\cot\gamma + \lambda - 1 = 0 \tag{8}$$

Formulation of Problem

Based on the temperature distribution $T(r, t)$ as given by expression (7) and the strain rates as given by (5), we are in a position to formulate the problem of the transient and residual stresses in the spherical body during the cooling process. For symmetrical stress distribution, the equilibrium condition of a spherical element yields the following relation:

$$\frac{\partial\dot{\sigma}_r}{\partial r} + \frac{2}{r}(\dot{\sigma}_r - \dot{\sigma}_\phi) = 0 \tag{9}$$

The corresponding strain components in the same element are given by the expressions

$$e_r = \frac{\partial u}{\partial r}$$

$$e_\phi = e_\theta = \frac{u}{r} \tag{10}$$

where $u = u(r, t)$ is the displacement along the radial direction. Elimination of u in expressions (10) yields the compatibility equation in terms of strain rates:

$$\frac{\partial\dot{e}_\phi}{\partial r} = \frac{1}{r}(\dot{e}_r - \dot{e}_\phi) \tag{11}$$

which is true if e_ϕ is small compared with unity. Substituting the expressions (5) in (11) and using the equilibrium equation (9), we reach the following stress equation:

$$\left(\frac{1-\nu}{E} + \frac{q}{2H'}\right)\frac{\partial(\dot{\sigma}_r - \dot{\sigma}_\phi)}{\partial r} + 3\left(\frac{1-\nu}{E} + \frac{q}{2H'}\right)\frac{\dot{\sigma}_r - \dot{\sigma}_\phi}{r} = \frac{\partial(\alpha\dot{T})}{\partial r} \tag{12}$$

which is an equation of the stress deviations of the spherical body due to the temperature changes, as we note that the components of the stress deviation are

$$\sigma_r' = {}^2/_3(\sigma_r - \sigma_\phi)$$
$$\sigma_\phi' = \sigma_\theta' = -{}^1/_3(\sigma_r - \sigma_\phi) \tag{13}$$

In equation (12), the value of q is either 1 or 0 depending on the conditions specified in (5), the value of $\partial(\alpha\hat{T})/\partial r$ as a function of r and t is obtained from equations (7), (8). Furthermore, if we trace the function $(\dot{\sigma}_r - \dot{\sigma}_\phi)$ along the radius at any time t, we note that there should be a jump in the value of $(\dot{\sigma}_r - \dot{\sigma}_\phi)$ when we cross a boundary between the elastic region and the work-hardening region. This jump in the value of $(\dot{\sigma}_r - \dot{\sigma}_\phi)$ is necessary in order to preserve the continuity of the displacement u and the tangential strain e_ϕ in the spherical body. For instance, if we assume $\nu = 1/2$, then based on (5) we have the following expression for $\dot{e}_\phi$:

$$\dot{e}_\phi = -\frac{1}{2E}(\dot{\sigma}_r - \dot{\sigma}_\phi) - \frac{q}{2H'}(\dot{\sigma}_r - \dot{\sigma}_\phi) + \alpha\dot{\hat{T}} \tag{14}$$

The continuity of $\dot{e}_\phi$ is observed if we multiply the value of $(\dot{\sigma}_r - \dot{\sigma}_\phi)$ by a factor $H'/(E + H')$ when a boundary is crossed from the elastic region to the elastic, work-hardening region, and a factor $(E + H')/H'$ is multiplied to $(\dot{\sigma}_r - \dot{\sigma}_\phi)$ when the elastic region is re-entered. In the actual case, the elastic-plastic boundary moves along the r-axis with time unless $(\dot{\sigma}_r - \dot{\sigma}_\phi)$ vanishes at the position where the boundary is located. As a result, the function $(\sigma_r - \sigma_\phi)$, which is the time integral of $(\dot{\sigma}_r - \dot{\sigma}_\phi)$, shows no discontinuities when plotted against the radial axis.

To simplify equation (12), the following nondimensional quantities are introduced:

$$A = \frac{(1-\nu)Y}{E\alpha T_1}$$

$$B = \frac{Y}{2H'\alpha T_1}$$

$$S = (\sigma_r - \sigma_\phi)/Y$$

$$\hat{T} = T/T_1$$

It is also understood that from here on, the symbol r indicates the nondimensional radial position r/R; the symbol t indicates the nondimensional time $\mathcal{K}t/R^2$; a dot on a variable indicates the derivative of the variable with respect to the nondimensional time. Using this nomenclature, equation (12) is reduced to

$$\frac{\partial S}{\partial r} + \frac{3S}{r} = \frac{1}{A + qB}\frac{\partial \hat{T}}{\partial r}$$
$$q = 1 \text{ if } |S| \geq 1 \text{ and } S\dot{S} \geq 0,$$
$$q = 0 \text{ if } |S| < 1 \text{ or } S\dot{S} < 0, \tag{15}$$
$$S = 0, \qquad \dot{S} = 0 \text{ at } r = 0$$

Equation (15) is the basic equation governing the elastoplastic thermal-stress distribution in the spherical body. The equation can be solved by a numerical method if the temperature history of the body is known. After the $\dot{S}$-values are obtained, we can integrate the nondimensional equilibrium equation (16) to find the radial stress in the spherical body:

$$\frac{\partial(\dot{\sigma}_r/Y)}{\partial r} + \frac{2\dot{S}}{r} = 0$$
$$\dot{\sigma}_r/Y = 0 \text{ at } r = 1 \tag{16}$$

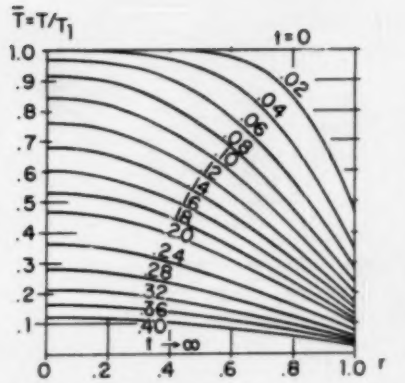

Fig. 2 Transient temperature distribution in a cooling sphere. ($\lambda = HR/k = 5$)

With both S and σ_r/Y available, the tangential stress σ_ϕ/Y is easily computed.

Numerical Data

In a cooling spherical body, we assume $\lambda = HR/k = 5$. Its temperature distribution is computed from equations (7), (8) for various values of r and t. The results are presented in Fig. 2. To obtain $\partial\hat{T}/\partial r$ for a certain time increment, equation (7) is differentiated with respect to r and the derivative is then evaluated at t and $t + \Delta t$. The difference of the two values gives $\partial\hat{T}/\partial r$ for the time increment Δt. A table is prepared which gives the values of $\partial\hat{T}/\partial r$ for various r and t. The table will be used for the solution of equation (15).

We further assume that $T_1 = 250$ F, $\nu = 1/2$, $Y = 36{,}000$ psi, $E = 30 \times 10^6$ psi, $\alpha = 6 \times 10^{-6}$/deg F, and $H'/E = 0.05$. Substituting the assumed values into the nondimensional expressions A, B we obtain:

Case I

$$A = 0.40 \qquad B = 8.0$$

By either increasing the assumed value of T_1, or reducing the assumed Y value, we reach cases where the degree of work-hardening is more severe. In this manner the following sets of conditions are established:

Case II

$$A = 0.25 \qquad B = 5.0$$

Case III

$$A = 0.125 \qquad B = 2.5$$

Based on the assumed values of A, B and the computed values $\partial\hat{T}/\partial r$, equation (15) is integrated in a stepwise manner from the center of the sphere toward its surface starting from $t = 0$ and for a certain time increment Δt. The Runge-Kutta method of integration is used [11]. For each integration step a proper q-value is used according to the values of S, $\dot{S}$ at the starting position of the step. At the end of the integration step a check is made to see if an elastic-plastic boundary has been crossed. If it is found that the elastic-plastic boundary is crossed in the integration step, then the initial value of $\dot{S}$ and the q-value are readjusted and the integration step is repeated. The integration process continues toward the outer surface of the sphere.

After a round of integration is completed for $\dot{S}$ along the radial axis, integration of equation (16) yields the corresponding thermal-stress increments $\dot{\sigma}_r/Y$ and $\dot{\sigma}_\phi/Y$. The $\dot{S}$-values are then added to the corresponding S-values to form the new S. The

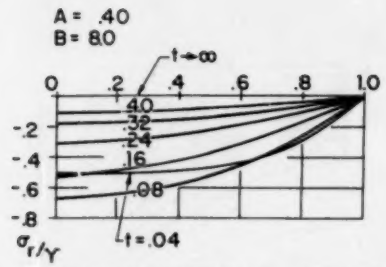

Fig. 3(a) Radial-stress distribution in a cooling sphere

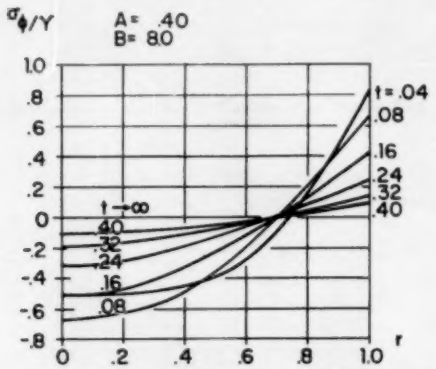

Fig. 3(b) Tangential-stress distribution in a cooling sphere, Case I

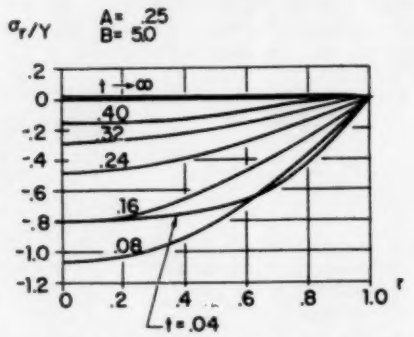

Fig. 4(a) Radial-stress distribution in a cooling sphere

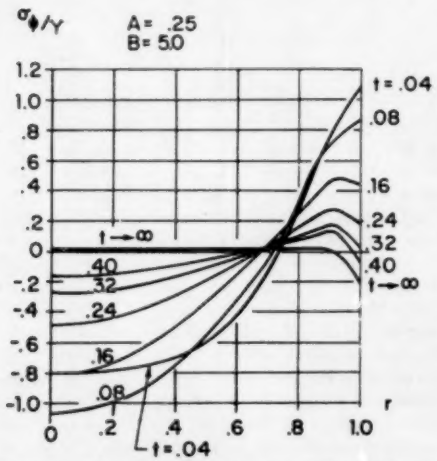

Fig. 4(b) Tangential-stress distribution in a cooling sphere, Case II

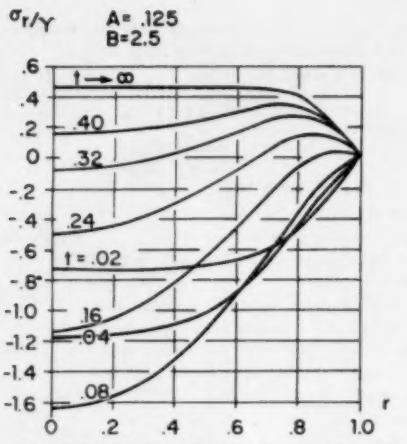

Fig. 5(a) Radial-stress distribution in a cooling sphere

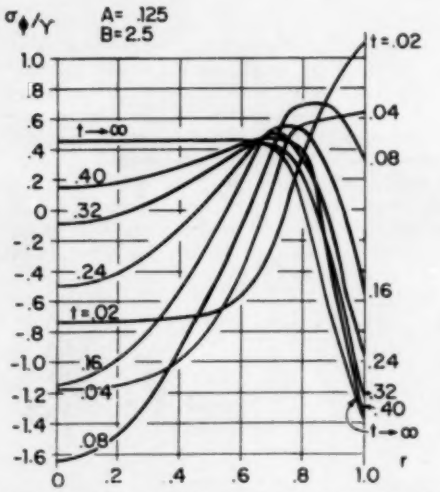

Fig. 5(b) Tangential-stress distribution in a cooling sphere, Case III

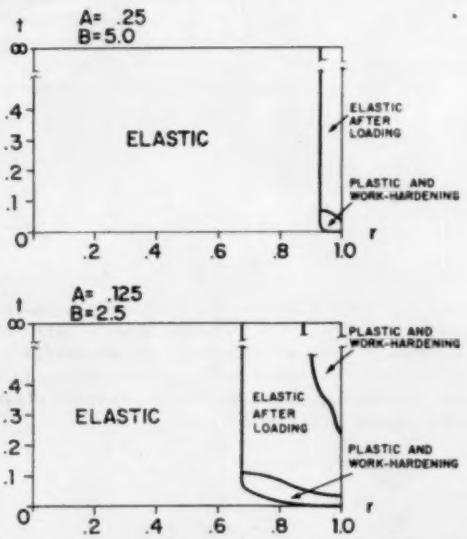

Fig. 6 Elastic-plastic boundaries in a cooling sphere, Cases II, III

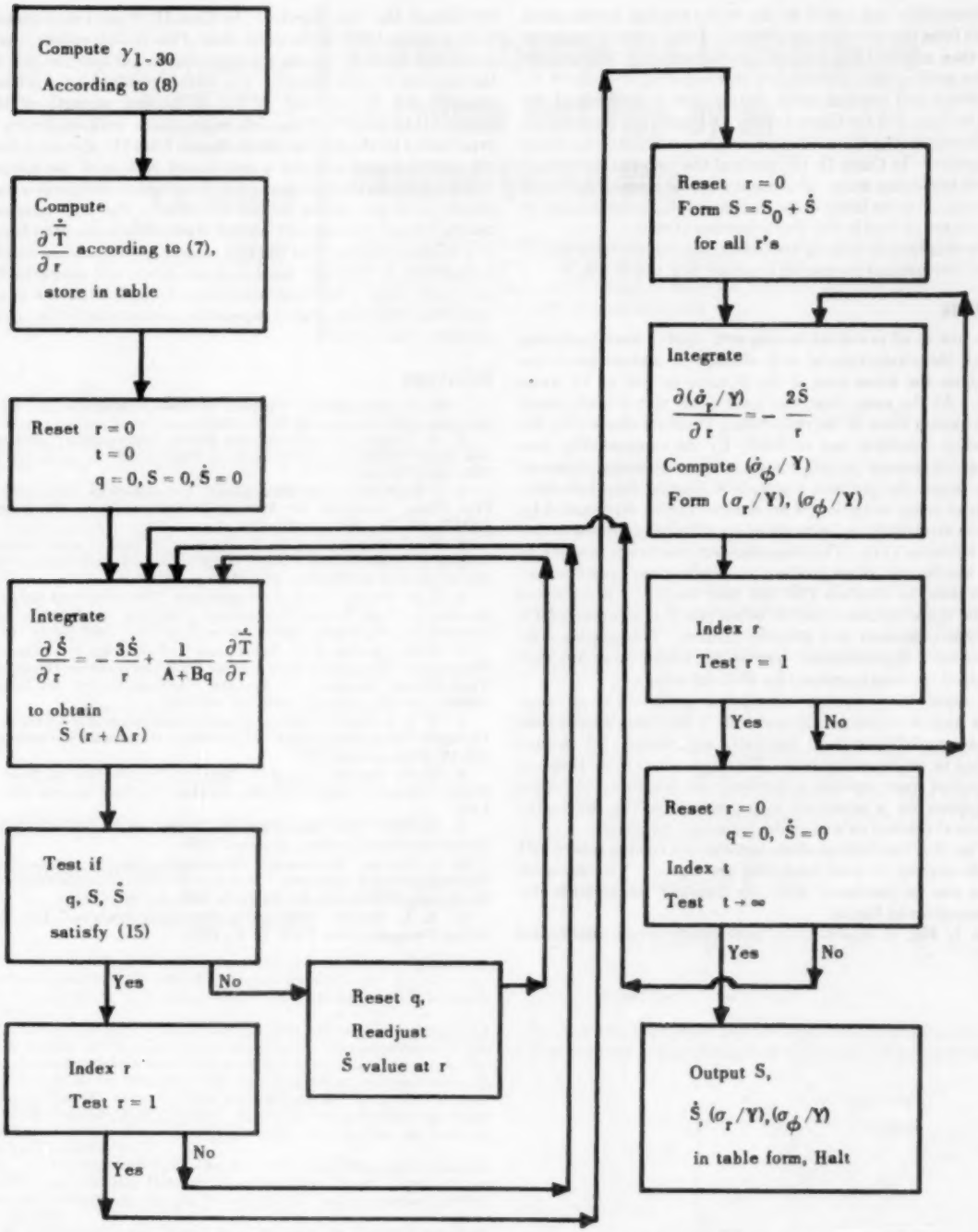
Compute y_{1-30} According to (8)
Compute $\frac{\partial \bar{T}}{\partial r}$ according to (7), store in table
Reset r = 0
t = 0
q = 0, S = 0, $\dot{S}$ = 0
Integrate $\frac{\partial \dot{S}}{\partial r} = -\frac{3\dot{S}}{r} + \frac{1}{A+Bq}\frac{\partial \bar{T}}{\partial r}$ to obtain $\dot{S}(r+\Delta r)$
Test if q, S, $\dot{S}$ satisfy (15)
Yes
No
Reset q, Readjust $\dot{S}$ value at r
Index r
Test r = 1
Yes
No
Reset r = 0
Form $S = S_0 + \dot{S}$ for all r's
Integrate $\frac{\partial(\dot{\sigma}_r/Y)}{\partial r} = -\frac{2\dot{S}}{r}$
Compute $(\dot{\sigma}_\phi/Y)$
Form (σ_r/Y), (σ_ϕ/Y)
Index r
Test r = 1
Yes
No
Reset r = 0
q = 0, $\dot{S}$ = 0
Index t
Test $t \to \infty$
Yes
No
Output S, $\dot{S}$, (σ_r/Y), (σ_ϕ/Y) in table form, Halt

Fig. 7 Flow diagram indicating computation procedures for thermal and residual stresses in a cooling sphere

stress increments are added to the corresponding initial stress values to form the new thermal stresses. Integration of equation (15) is then resumed for another time increment. The process continues until a time increment is reached when $t + \Delta t \rightarrow \infty$. The thermal and residual-stress distribution thus obtained are plotted in Figs. 3–5 for Cases I–III. In Case I the material remains elastic during the cooling process, no residual stress exists in the sphere. In Cases II, III, parts of the material go through the work-hardening state; as a result residual stresses appear in the sphere. For the latter cases the elastic-plastic boundaries in the sphere are plotted in Fig. 6 as a function of time.

A flow diagram, indicating the computation procedures for the thermal and residual stresses in a sphere, is given in Fig. 7.

Conclusion

As is true in all problems dealing with elastic, work-hardening material, the strain rate of each element in a structure is dependent on the stress rate of the element as well as its stress history. At the same time, the local stress rate is interrelated with the stress rates of the neighboring elements directly by the equilibrium condition and indirectly by the compatibility condition which governs the strain rates of the neighboring elements. In this paper, the problem is simplified because the three components of stress deviation of an element can be represented by the same expression, to be modified by different constant multipliers, equation (13). This simplification renders it possible to reduce the thermal-stress problem to a single stress equation (15). Furthermore, in equation (15) the time variable t is separated from the space variable r as the stress rate $\dot{S}$ is computed for a finite time increment in a stepwise fashion. This approach introduces some approximation because the initial value S is used throughout the time increment for the evaluation of q.

In general, the computer technique is applicable to problems dealing with work-hardening materials if the time variable and the space variables can be justifiably separated in the manner described in the foregoing text. For cases where more than one independent space variable is involved, the feasibility of solving the problem by a computer is dependent on the differential equation(s) reached as well as the boundary conditions.

In Figs. 3–5, the thermal-stress histories of a cooling sphere with variable degrees of work-hardening are traced. The stress behaviors can be correlated with the transient temperature distribution given in Fig. 2.

Case I, Fig. 3, represents a pure elastic stress distribution throughout the time interval. In Case II, Figs. 4–6, a plastic state is reached only in the outer shell of the cooling sphere. As a result, the residual stresses exist in a significant amount only in the outer shell of the sphere. The surface residual stress is compressive and is beneficial to the mechanical strength of the sphere. In Case III, Figs. 5-6, more severe work-hardening is experienced by the cooling sphere than in Case II. For some time the plastic region occupies a substantial portion of the sphere. The peak tensile stress is reached at the spherical surface at a time shortly after the cooling process is started. The high transient tensile stress is the cause of surface cracks which are often found in a cooling sphere. The residual stresses, which are essentially compressive in the outer portion of the sphere and tensile in the inner core, form a favorable stress distribution. It is also noted that at one time very high compressive stresses exist in the center portion of the sphere.

References

1 B. E. Gatewood, "Thermal Stresses," McGraw-Hill Book Company, Inc., New York, N. Y., 1957.

2 W. Prager, "Non-Isothermal Plastic Deformation," *Proceedings*, Royal Academy of Sciences of the Netherlands, Series B, vol. 61, 1958, pp. 176–182.

3 J. H. Weiner, "An Elastoplastic Thermal-Stress Analysis of a Free Plate," JOURNAL OF APPLIED MECHANICS, vol. 23, TRANS. ASME, vol. 78, 1956, pp. 395–402.

4 H. G. Landau and J. H. Weiner, "Transient and Residual Stresses in Heat-Treated Plates," JOURNAL OF APPLIED MECHANICS, vol. 25, TRANS. ASME, vol. 80, 1958, pp. 459–465.

5 J. H. Weiner and J. V. Huddleston, "Transient and Residual Stresses in Heat-Treated Cylinders," JOURNAL OF APPLIED MECHANICS, vol. 26, TRANS. ASME, series E, vol. 81, 1959, pp. 31–39.

6 H. G. Landau, J. H. Weiner, and E. E. Zwicky, Jr., "Thermal Stresses in a Viscoelastic-Plastic Plate With Temperature-Dependent Yield Stress," JOURNAL OF APPLIED MECHANICS, vol. 27, TRANS. ASME, vol. 82, Series E, 1960, pp. 297–302.

7 V. A. Lomakin, "Elastic-Plastic Equilibrium of a Sphere in an Unsteady Temperature Field," *Prikladnaya Matematika i Mekhanika*, vol. 19, 1955, pp. 244–248.

8 H. S. Carslaw and J. C. Jaeger, "Conduction of Heat in Solids," Oxford University Press, London, England, second edition, 1959.

9 R. Hill, "The Mathematical Theory of Plasticity," Oxford University Press, London, England, 1950.

10 C. Hwang, "Incremental Stress-Strain Law Applied to Work-Hardening Plastic Materials," JOURNAL OF APPLIED MECHANICS, vol. 26, TRANS. ASME, vol. 81, Series E, 1959, pp. 594–598.

11 K. L. Nielsen, "Methods in Numerical Analysis," The Macmillan Company, New York, N. Y., 1956.

A. L. FLORENCE[2]
Graduate Student and Research Assistant, Stanford University, Stanford, Calif.

J. N. GOODIER
Professor of Engineering Mechanics, Stanford University, Stanford, Calif. Mem. ASME

Thermal Stresses Due to Disturbance of Uniform Heat Flow by an Insulated Ovaloid Hole[1]

The linear thermoelastic problem is solved for a uniform heat flow disturbed by a hole of ovaloid form, which includes the ellipse and circle as special cases. Results for stress and displacement are found in closed form, by reducing the problem to one of boundary loading solvable by a method of Muskhelishvili.

When an infinite plate is under a temperature distribution which is uniform but for the disturbance caused by the presence of an insulated ovaloid hole, thermal stresses are produced.[3] The temperature gradient, τ, considered constant sufficiently far from the hole will be directed at an angle β to the major axis of the ovaloid, Fig. 1.

Here an ovaloid will be defined as the mapping of the unit circle γ in the ζ-plane into the z-plane under the conformal transformation

$$z = \omega(\zeta) = R\left(\zeta + \frac{m}{\zeta} + \frac{n}{\zeta^2}\right) \tag{1}$$

where

$$2Rm = a - b, \qquad 2R(1 + n) = a + b,$$

and

$$\zeta = \rho e^{i\theta} = \xi + i\eta$$

a and b are the major and minor semiaxes of the ovaloid.

Temperature Distribution

In the ζ-plane for heat flow around an insulated circular hole of unit radius, the temperature distribution is

$$T = \tau R\left(\rho + \frac{1}{\rho}\right)\cos(\theta - \beta) \tag{2}$$

the undisturbed flow being at an angle β to the positive ξ-axis.

The complex function W having T as its real part is

$$W = T + iQ = \tau R\left(\zeta e^{-i\beta} + \frac{e^{i\beta}}{\zeta}\right) \tag{3}$$

In the z-plane for steady heat flow past an insulated ovaloid hole the complex temperature function is (3) used in conjunction with the mapping (1). It can be seen that for large $|\zeta|$ and hence large $|z|$ the temperature gradient is ultimately τ directed as shown in Fig. 1.

Thermal Dislocation

If the plate which is in the z-plane is cut along the positive x-axis and allowed to deform freely under the temperature distribution (2) it is in a state of zero stress. Also, the x and y-components of the relative displacements of points 1 $(r, 0)$ and 2 $(r, 2\pi)$, Fig. 1, are given by

$$(u + iv)_2 - (u + iv)_1 = \alpha \int_1^2 W dz$$

$$= \alpha\tau R^2 \oint \left(\zeta e^{-i\beta} + \frac{e^{i\beta}}{\zeta}\right)\left(1 - \frac{m}{\zeta^2} - \frac{3n}{\zeta^4}\right)d\zeta$$

$$= \alpha\tau R^2(e^{i\beta} - me^{-i\beta})2\pi i \tag{4}$$

In (4) u and v are the x and y-components of displacement and will have this meaning throughout the paper. α is the coefficient

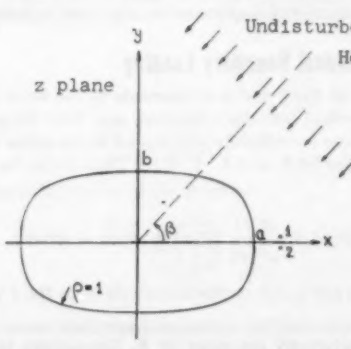

Fig. 1 Heat flow around an insulated ovaloid hole, with uniform temperature gradient at a distance

---

[1] From research sponsored by the Office of Naval Research, through Contract Nonr 225(29) with Stanford University.

[2] Now, Lecturer in Applied Dynamics, University of Edinburgh, Scotland.

[3] Solutions for the corresponding problems of the circular hole and the spherical cavity were given elsewhere.[4] A comprehensive account including solutions not yet published is contained in a report to the Office of Naval Research "Thermal Stress Due to Disturbance of Uniform Heat Flow by Cavities and Inclusions," by A. L. Florence and J. N. Goodier, July 15, 1959. It will be apparent that yet other two-dimensional hole shapes can be dealt with by the methods of Muskhelishvili.[5]

[4] A. L. Florence and J. N. Goodier, "Thermal Stress at Spherical Cavities and Circular Holes in Uniform Heat Flow," JOURNAL OF APPLIED MECHANICS, vol. 26, TRANS. ASME, vol. 81, Series E, 1959, pp. 293–294.

[5] N. I. Muskhelishvili, "Some Basic Problems in the Mathematical Theory of Elasticity" (translated by J. R. M. Radok), Noordhoff, Groningen, Netherlands, 1953.

Presented at the West Coast Conference of the Applied Mechanics Division, Pasadena, Calif., June 27–29, 1960, of THE AMERICAN SOCIETY OF MECHANICAL ENGINEERS.

Discussion of this paper should be addressed to the Secretary, ASME, 29 West 39th Street, New York, N. Y., and will be accepted until January 10, 1961, for publication at a later date. Discussion received after the closing date will be returned.

Manuscript received by ASME Applied Mechanics Division, January 5, 1960. Paper No. 60—APMW-6.

of thermal expansion of the material. The integration is performed along a contour remaining entirely in the material, enclosing the origin of co-ordinates, and taken in a counterclockwise sense.

Continuity of Displacements

To remove the thermal dislocation (4) in the final solution an isothermal state of stress and displacement is sought having an equal and opposite dislocation.

Introducing the complex representation[5] of the elastic state of a body in plane stress, the displacements in particular are expressed by the formula

$$2G(u + iv) = \kappa^* \phi(\zeta) - \frac{\omega(\zeta)}{\overline{\omega'(\zeta)}} \overline{\phi'(\zeta)} - \overline{\psi(\zeta)} \tag{5}$$

For the case of plane stress[6]

$$\kappa^* = \frac{3 - \nu}{1 + \nu} \tag{6}$$

where ν is Poisson's ratio for the material of the plate, G is the shear modulus of the material, and the primes denote differentiation with respect to ζ.

Without regard to the boundary loading, an isothermal state of stress and displacement having a dislocation along the positive x-axis similar to (4) is obtained by choosing

$$\phi(\zeta) = A \log \zeta \tag{7}$$

and

$$\psi(\zeta) = \bar{A} \log \zeta \tag{8}$$

where A is a complex number to be determined.

When the functions (7) and (8) are used in equation (5) the difference between the displacements for points 1 and 2 is found to be

$$(u + iv)_2 - (u + iv)_1 = A \frac{8\pi i}{E} \tag{9}$$

using (6) and the equation $2G(1 + \nu) = E$.

The value of A required to give continuity of displacements is obtained by adding dislocations (4) and (9) and equating their sum to zero.

This gives

$$A = -1/4 E\alpha\tau R^2 (e^{i\beta} - me^{-i\beta}) \tag{10}$$

The state of stress described by the functions (7) and (8) requires loading on the ovaloid boundary. Further functions $\phi(\zeta)$ and $\psi(\zeta)$ which require an equal and opposite loading but which preserve the continuity of displacements must now be determined.

Removal of Residual Boundary Loading

Let X and Y be the x and y-components of the force per unit length on the ovaloid boundary summed, say, from the point $(a, 0)$ to a point whose co-ordinates correspond to the point $(1, \theta)$ in the ζ-plane. Also let $f = i(X + iY)$. Then it can be shown[5] that

$$f = \phi(\sigma) + \frac{\omega(\sigma)}{\overline{\omega'(\sigma)}} \overline{\phi'(\sigma)} + \overline{\psi(\sigma)} + \text{const} \tag{11}$$

where $\sigma = e^{i\theta}$ is any point on the unit circle γ, in the ζ-plane.

[5] The changes required for conversion from plane stress to plane strain in thermoelasticity are given by S. Timoshenko and J. N. Goodier in "Theory of Elasticity," McGraw-Hill Book Company, Inc., New York, N. Y., 1951, p. 408.

The boundary loading required by the state of stress described by the functions (7) and (8) and expressed by means of the function f is found by substituting (7) and (8) in equation (11).

This gives

$$f = \frac{\omega(\sigma)}{\overline{\omega'(\sigma)}} \sigma \bar{A}$$

Further functions $\phi(\zeta)$ and $\psi(\zeta)$ must therefore be found to describe a state of stress which requires a boundary loading given by

$$f = -\frac{\omega(\sigma)}{\overline{\omega'(\sigma)}} \sigma \bar{A}$$

The functions must also preserve the continuity of displacements.

Apart from a constant which has no effect on the stress distribution, the boundary condition to be satisfied by the new functions is

$$\phi(\sigma) + \frac{\omega(\sigma)}{\overline{\omega'(\sigma)}} \overline{\phi'(\sigma)} + \overline{\psi(\sigma)} = -\frac{\omega(\sigma)}{\overline{\omega'(\sigma)}} \sigma \bar{A} \tag{12}$$

The functions $\phi(\zeta)$ and $\psi(\zeta)$ are analytic outside γ and so admit the representations

$$\phi(\zeta) = \frac{a_1}{\zeta} + \frac{a_2}{\zeta^2} + \frac{a_3}{\zeta^3} + \dots \tag{13}$$

and

$$\psi(\zeta) = \frac{b_1}{\zeta} + \frac{b_2}{\zeta^2} + \frac{b_3}{\zeta^3} + \dots \tag{14}$$

The constant terms in the series (13) and (14) have been omitted because they do not affect the stress distribution.

The boundary condition (12) is next multiplied by

$$\left(\frac{1}{2\pi i}\right)\left(\frac{d\sigma}{\sigma - \zeta}\right)$$

where ζ is outside γ, and integrated round γ in an anticlockwise sense. The Cauchy integrals so formed will now be evaluated.[7]

The Cauchy integral formula for external regions is

$$\frac{1}{2\pi i} \int_\gamma \frac{\phi(\sigma) d\sigma}{\sigma - \zeta} = -\phi(\zeta) \tag{15}$$

The function $\overline{\psi(\sigma)}$ is the boundary value on γ of the function

$$\overline{\psi}\left(\frac{1}{\zeta}\right) = \bar{b}_1\zeta + \bar{b}_2\zeta^2 + \bar{b}_3\zeta^3 + \dots$$

which is analytic inside γ. Hence

$$\frac{1}{2\pi i} \int_\gamma \frac{\overline{\psi(\sigma)} d\sigma}{\sigma - \zeta} = 0 \tag{16}$$

On γ, the function $[\omega(\sigma)/\overline{\omega'(\sigma)}]\sigma$ is the boundary value of the function

$$\frac{\omega(\zeta)}{\overline{\omega'}\left(\frac{1}{\zeta}\right)} \zeta$$

which is analytic in γ except at $\zeta = 0$ which is a double pole.

Thus

[7] Footnote 5, chapter 15, section 84.

$$\frac{\bar{A}}{2\pi i}\int_\gamma \frac{\omega(\sigma)\sigma\, d\sigma}{\overline{\omega'(\sigma)}(\sigma-\zeta)} = \frac{\bar{A}}{2\pi i}\int_\gamma \frac{\sigma^4+m\sigma^2+n}{\sigma^2(1-m\sigma^2-3n\sigma^4)}\cdot\frac{d\sigma}{\sigma-\zeta} = -\frac{n\bar{A}}{\zeta^2} \quad (17)$$

On γ,

$$\frac{\omega(\sigma)}{\overline{\omega'(\sigma)}}\,\overline{\phi'(\sigma)}$$

is the boundary value of the function

$$\frac{\omega(\zeta)}{\overline{\omega'}\left(\frac{1}{\zeta}\right)}\,\overline{\phi'}\left(\frac{1}{\zeta}\right)$$

which is analytic in γ except at $\zeta = 0$, which is a simple pole.

Hence

$$\frac{1}{2\pi i}\int_\gamma \frac{\omega(\sigma)}{\overline{\omega'(\sigma)}}\,\overline{\phi'(\sigma)}\,\frac{d\sigma}{\sigma-\zeta} = \frac{na_1}{\zeta} \quad (18)$$

using the transformation (1) and the series (13).

Substituting the values (15)–(18) into the integral form of the boundary condition (12) yields

$$\phi(\zeta) = \frac{\bar{a}_1 n}{\zeta} - \frac{\bar{A}n}{\zeta^2} \quad (19)$$

To find a_1 in (19) the boundary condition (12) is multiplied by

$$\frac{1}{2\pi i}\frac{\sigma\, d\sigma}{\sigma-\zeta}$$

where ζ is again outside γ, and integrated around γ in an anticlockwise sense.

Using arguments similar to the foregoing, the evaluation of the integrals results in the following:

$$\frac{1}{2\pi i}\int_\gamma \frac{\phi(\sigma)\sigma\, d\sigma}{\sigma-\zeta} = -\zeta\phi(\zeta) + a_1 \quad (20)$$

$$\frac{1}{2\pi i}\int_\gamma \frac{\overline{\psi(\sigma)}\sigma\, d\sigma}{\sigma-\zeta} = 0 \quad (21)$$

$$\frac{\bar{A}}{2\pi i}\int_\gamma \frac{\omega(\sigma)\sigma^2 d\sigma}{\overline{\omega'(\sigma)}(\sigma-\zeta)} = -\frac{\bar{A}n}{\zeta} \quad (22)$$

and

$$\frac{1}{2\pi i}\int_\gamma \frac{\omega(\sigma)\overline{\phi'(\sigma)}\sigma\, d\sigma}{\overline{\omega'(\sigma)}(\sigma-\zeta)} = 0 \quad (23)$$

These values (20)–(23) substituted into the integral form of the boundary condition (12) lead to

$$\phi(\zeta) = \frac{a_1}{\zeta} - \frac{\bar{A}n}{\zeta^2} \quad (24)$$

Comparison of the forms of $\phi(\zeta)$ given by (19) and (24) shows that $a_1 = 0$ and hence

$$\phi(\zeta) = -\frac{\bar{A}n}{\zeta^2} \quad (25)$$

To find $\psi(\zeta)$ the complex conjugate of the boundary condition (12) is considered. This is

$$\overline{\phi(\sigma)} + \frac{\overline{\omega(\sigma)}}{\omega'(\sigma)}\phi'(\sigma) + \psi(\sigma) = -\frac{\overline{\omega(\sigma)}}{\omega'(\sigma)}\frac{A}{\sigma} \quad (26)$$

As in the determination of $\phi(\zeta)$, the procedure is to multiply (26) by

$$\frac{1}{2\pi i}\frac{d\sigma}{\sigma-\zeta}$$

where ζ is outside γ, and integrate around γ in an anticlockwise sense. The resulting integrals are now evaluated. We have,

$$\frac{1}{2\pi i}\int_\gamma \frac{\psi(\sigma)d\sigma}{\sigma-\zeta} = -\psi(\zeta) \quad (27)$$

and

$$\frac{1}{2\pi i}\int_\gamma \frac{\overline{\phi(\sigma)}d\sigma}{\sigma-\zeta} = 0 \quad (28)$$

On γ,

$$\frac{\overline{\omega(\sigma)}}{\omega'(\sigma)}\left(\frac{1}{\sigma}\right)$$

is the boundary value of the function

$$\frac{\bar{\omega}\left(\frac{1}{\zeta}\right)}{\omega'(\zeta)}\left(\frac{1}{\zeta}\right)$$

This is analytic outside γ except at $\zeta = \infty$ which is a double pole.

Hence

$$\frac{A}{2\pi i}\int_\gamma \frac{\overline{\omega(\sigma)}}{\omega'(\sigma)}\cdot\frac{d\sigma}{\sigma(\sigma-\zeta)} = -A\frac{\bar{\omega}\left(\frac{1}{\zeta}\right)}{\omega'(\zeta)}\frac{1}{\zeta} + AG_\infty(\zeta)$$

where $G_\infty(\zeta)$ is the principal part of the pole at infinity.[8]

Now

$$\frac{\bar{\omega}\left(\frac{1}{\zeta}\right)}{\omega'(\zeta)\zeta} = n\zeta^2 + m(1+n) + 0\left(\frac{1}{\zeta^2}\right)$$

Therefore

$$G_\infty(\zeta) = m(1+n) + n\zeta^2$$

After neglecting constants since they do not influence the stress, and using the transformation (1), it follows that

$$\frac{A}{2\pi i}\int_\gamma \frac{\overline{\omega(\sigma)}d\sigma}{\omega'(\sigma)\sigma(\sigma-\zeta)} = -\frac{A\zeta^2(1+m\zeta^2+n\zeta^4)}{\zeta^4-m\zeta^2-3n} + An\zeta^2 \quad (29)$$

On γ

$$\frac{\overline{\omega(\sigma)}}{\omega'(\sigma)}\,\phi'(\sigma)$$

is the boundary value of the function

$$\frac{\bar{\omega}\left(\frac{1}{\zeta}\right)}{\omega'(\zeta)}\cdot\phi'(\zeta)$$

which is analytic outside γ except at $\zeta = \infty$ which is a simple pole.

[8] Footnote 5, chapter 12, section 70.

Hence

$$\frac{1}{2\pi i}\int_\gamma \frac{\overline{\omega(\sigma)}}{\omega'(\sigma)}\frac{\phi'(\sigma)d\sigma}{(\sigma-\zeta)} = -\frac{\bar{\omega}\left(\frac{1}{\zeta}\right)}{\omega'(\zeta)}\phi'(\zeta) + G_\infty(\zeta)$$

where $G_\infty(\zeta)$ is the principal part of the pole at infinity.

In fact

$$G_\infty(\zeta) = -a_1 n\zeta - 2a_2 n$$

and since $a_1 = 0$, $G_\infty(\zeta)$ is a constant which will be neglected.

Using the transformation (1) and the function $\phi(\zeta)$ given by (25) it follows that

$$\frac{1}{2\pi i}\int_\gamma \frac{\overline{\omega(\sigma)}}{\omega'(\sigma)}\frac{\phi'(\sigma)d\sigma}{(\sigma-\zeta)} = 2\bar{A}n\frac{1+m\zeta^2+n\zeta^4}{\zeta^4-m\zeta^2-3n} \quad (30)$$

The results (27)–(30) with the integral form of the boundary condition (26) yield

$$\psi(\zeta) = An\zeta^2 - (A\zeta^2 - 2\bar{A}n)\frac{1+m\zeta^2+n\zeta^4}{\zeta^4-m\zeta^2-3n} \quad (31)$$

The plate is now free of boundary loading and has continuous displacements everywhere. The state of stress and displacement is described by the temperature (2) and the functions

$$\phi(\zeta) = A\log\zeta - \frac{\bar{A}n}{\zeta^2} \quad (32)$$

and

$$\psi(\zeta) = \bar{A}\log\zeta - (A\zeta^2 - 2\bar{A}n)\frac{1+m\zeta^2+n\zeta^4}{\zeta^4-m\zeta^2-3n} + An\zeta^2 \quad (33)$$

Stress Distribution

Let $\widehat{\rho\rho}$ and $\widehat{\theta\theta}$ be stresses acting normal to the curves ρ = const (ovaloids) and θ = const, respectively, in the directions of ρ and θ increasing, and let $\widehat{\rho\theta}$ be the shear stress.

The stress distribution in the plate is given by the formulas[5]

$$\widehat{\rho\rho} + \widehat{\theta\theta} = 2\left[\frac{\phi'(\zeta)}{\omega'(\zeta)} + \overline{\frac{\phi'(\zeta)}{\omega'(\zeta)}}\right] \quad (34)$$

$$\widehat{\theta\theta} - \widehat{\rho\rho} + 2i\widehat{\rho\theta} = \frac{2\zeta^2}{\rho^2\overline{\omega'(\zeta)}}\left[\overline{\omega(\zeta)}\left\{\frac{\phi'(\zeta)}{\omega'(\zeta)}\right\}' + \psi'(\zeta)\right] \quad (35)$$

The functions (32) and (33) with the stress formulas (34) and (35) give the stress distribution. It can be put in the following form:

$$\frac{RH}{2}(-\widehat{\rho\rho} + i\widehat{\rho\theta}) = a_7\zeta^7 + a_5\zeta^5 + a_3\zeta^3 + a_1\zeta + a_{-1}\bar{\zeta} + a_{-3}\bar{\zeta}^3 + a_{-5}\bar{\zeta}^5 \quad (36)$$

$$\frac{RH}{2}(\widehat{\rho\rho} + \widehat{\theta\theta}) = b_7\rho^7\cos 7\theta + b_5\rho^5\cos 5\theta + b_3\rho^3\cos 3\theta + b_1\rho\cos\theta \quad (37)$$

where

$$H = [\rho^8 + \rho^4 m + 9n^2 - 2\rho^2 m(\rho^4 - 3n)\cos 2\theta - 6\rho^4 n\cos 4\theta]^2$$

$$a_7 = 3An^2(\rho^2 - 1)$$

$$a_5 = Amn(\rho^8 - \rho^4 - 6\rho^2 n + 6n)$$

$$a_3 = An[-\rho^{10} + 4\rho^8 - \rho^6(5m^2 + 3m^2n + 9n^2 + 3) + 5\rho^4 m^2 + 3\rho^2 n(m^2 - 6n) + 27n^2] + 6\bar{A}mn^2[-\rho^6(1+n) + \rho^4 + n]$$

$$a_1 = A\rho^2 n[\rho^{10} - \rho^8(1 + m^2 + m^2n - 2n + 3n^2) + \rho^6(m^2 - 2n) + \rho^4 n(m^2 - 24n - 18n^2) + 27\rho^2 n^2 + 18n^3] + 2\bar{A}n[-\rho^{10}m^2(1+n) + \rho^8(m^2 + 6n) - 6\rho^6 n(1 + 3n^2) + \rho^4 m^2 n + 18n^3]$$

$$a_{-1} = A[-\rho^{14} + \rho^{12}(1 + m^2 + m^2n + 3n^2) - \rho^{10}m^2 - \rho^8 n(7m^2 + 6m^2n - 6n) + 6\rho^6 m^2 n + 3\rho^4 n^2(2m^2 - 3 - 9n^2) + 27n^4] + \bar{A}\rho^8 mn[\rho^{10}(1+n) + \rho^8 - 2\rho^6(1 + 3n^2) - 4\rho^4 n + 3\rho^2 n(1 - 3n) + 15n^2]$$

$$a_{-3} = 3Amn[2\rho^8(1+n) - \rho^6 - \rho^4(1 + 2n + 3n^2) + 3n^2] + 2\bar{A}\rho^2 n[-2\rho^8 + 2\rho^6(1 + 3n^2) - \rho^4 m^2 + \rho^2 m^2(1 - 3n) + 3n(m^2 - 2n)]$$

$$a_{-5} = 3An[-\rho^6 + \rho^4(1 + 3n^2) - 3n^2] + 2\bar{A}\rho^2 mn[\rho^4 - \rho^2(1 - 3n) - 3n]$$

$$b_7 = -3An^2(2\rho^2 - 3)$$

$$b_5 = Amn(-2\rho^6 + 6\rho^4 + 12\rho^2 n - 9n) + 3\bar{A}n(-\rho^6 + 6n^2)$$

$$b_3 = A[2\rho^{10}n + \rho^8(m^2 - 6n) + 4\rho^6 m^2 n - 6\rho^4 m^2 n - 6\rho^2 n^2(m^2 - 6n) - 27n^3] + \bar{A}(-\rho^{10} + 6\rho^6 n + 12\rho^4 n^2 - 18n^2)$$

$$b_1 = A\rho^2 m(\rho^2 + 2n)[-2\rho^8 - \rho^4(m^2 - 6n) - 18n^2] + \bar{A}[\rho^{14} + 2\rho^{10}m^2 + 2\rho^8 n(m^2 - 6n) - 3\rho^6 n(m^2 - 6n) - 12\rho^4 m^2 n^2 - 54n^4]$$

The Insulated Elliptic Hole

The stress distribution for the case of the insulated elliptic hole is obtained by setting $n = 0$ in the stress results (36) and (37). The following stresses are obtained:

$$h\widehat{\rho\rho} = {}^1/_4 E\alpha\tau(a+b)[\rho^4 - \rho^2(1+m^2) + m^2][m(\rho^2+1)\cos(\theta+\beta) - (\rho^2+m^2)\cos(\theta-\beta)] \quad (38)$$

$$h\widehat{\theta\theta} = -{}^1/_2 E\alpha\tau(a-b)[m(\rho^2+1)\cos(3\theta+\beta) - (\rho^2+m^2)\cos(3\theta-\beta)] + {}^1/_4 E\alpha\tau(a+b)[m\{\rho^6 + \rho^4(4+m^2) + \rho^2(1+4m^2) + m^2\}\cos(\theta+\beta) + \{\rho^6 + \rho^4(1+4m^2) + \rho^2 m^2(4+m^2) + m^4\}\cos(\theta-\beta)] \quad (39)$$

$$h\widehat{\rho\theta} = {}^1/_4 E\alpha\tau(a+b)[\rho^4 - \rho^2(1+m^2) + m^2][m(\rho^2-1)\sin(\theta+\beta) - (\rho^2-m^2)\sin(\theta-\beta)] \quad (40)$$

where

$$h = [\rho^4 - 2\rho^2 m\cos 2\theta\cos 2\theta + m^2]^2 \quad (41)$$

If the heat flow far from the hole is parallel to the y-axis and directed in a negative sense, the case $\beta = 0$, Fig. 1, the stress formulas (38)–(40) reduce to

$$h\widehat{\rho\rho} = -{}^1/_2 E\alpha\tau a\rho(\rho^2+m)[\rho^4 - \rho^2(1+m^2) + m^2]\sin\theta$$

$$h\widehat{\theta\theta} = -{}^1/_2 E\alpha\tau a\rho(\rho^2+m)[\{\rho^4 + \rho^2(1+m)^2 + m^2\}\sin\theta - 2\rho^2 m\sin 3\theta]$$

$$h\widehat{\rho\theta} = {}^1/_2 E\alpha\tau a\rho(\rho^2-m)[\rho^4 - \rho^2(1+m^2) + m^2]\cos\theta \quad (42)$$

where h is given by (41).

It can be shown that when $m = 0$ these formulas agree with formulas given in a previous paper[4] for the insulated circular hole.

The Slot

The elliptic hole can be made very narrow and of length $2a$ by letting m approach unity. For $\beta = \pi/2$, the case of heat flow perpendicular to the slot, the stress $\widehat{\theta\theta}$ at the surface of the slot behaves as follows:

$$\text{As} \quad m \to 1 \qquad \widehat{\theta\theta} \to -\frac{E\alpha\tau a}{\sin\theta}$$

Singular points occur at the ends of the slot where $\theta = 0$ and $\theta = \pi$.

Another interesting observation is that, along the positive x-axis ($\theta = 0$) for $\rho > 1$, the shear stress $\widehat{\rho\theta}$ behaves in the following way:

$$\text{As} \quad m \to 1 \qquad \widehat{\rho\theta} \to {}^1/_2\, E\alpha\tau a\, \frac{\rho}{\rho^2 - 1}$$

Again, this shows that the stress becomes infinite at the ends of the slot.

Sinusoidal Excitation of a System With Bilinear Hysteresis

T. K. CAUGHEY
Associate Professor of Applied Mechanics, California Institute of Technology, Pasadena, Calif.

Many physical systems exhibit hysteresis which may be adequately described by a bilinear hysteresis model. This paper considers the response of such a system to sinusoidal excitation. It is shown that the system exhibits a soft-type resonance with stable, single-valued response curves. For such a system it is shown that there exists a critical value of the excitation, above which unbounded resonance occurs.

Introduction

MANY physical systems exhibit bilinear hysteresis of the type illustrated in Fig. 1. Such behavior may be caused by the presence of Coulomb friction in the system or may be due to elastoplastic behavior of the material in the system. The analysis of bilinear hysteresis in built-up structures has received considerable attention in recent years [1–4].[1] Vibration isolators using elastically supported Coulomb friction dampers have been studied both analytically and on an analog computer by J. E. Ruzicka [5]. L. S. Jacobsen [6, 7], and R. Tanabashi [8] have both made graphical studies of the transient response of elastoplastic structures to simple pulses and square waves.

This paper analyzes the response of a single-degree-of-freedom oscillator, having bilinear hysteresis, to sinusoidal excitation. The stability of the resulting motion is analyzed in the case of weak damping.

Formulation

Consider the forced vibrations of a mass m mounted on a spring which exhibits bilinear hysteresis of the type shown in Fig. 1. The equation of motion for the system is

$$m\ddot{x} + kF(x, \mu, t) = P \cos \omega t \tag{1}$$

where $F(x, \mu, t)$ is the hysteresis restoring force. $F(x, \mu, t)$ is such that, as $\mu \to 0$, $F(x, \mu, t) \to x$. Let

$$\frac{k}{m} = \omega_0^2$$

$$\tau = \omega_0 t$$

$$\frac{P}{k} = x_s \tag{2}$$

$$\eta = \frac{\omega}{\omega_0}$$

Substituting (2) into (1)

$$\frac{d^2x}{d\tau^2} + F(x, \mu, \tau) = x_s \cos \eta\tau \tag{3}$$

It should be noted that if $\mu = 0$, equation (2) is linear, hence $x(\tau)$ is sinusoidal. If μ is not zero, but is small, the essentially sinusoidal character of the response will be preserved.

Method of Solution

The method of solution is based on the work of Kryloff and Bogoliuboff in [9] and is sometimes called the method of slowly varying parameters.

$$x(\tau) = R \cos (\eta\tau + \phi) \tag{4}$$

where R and ϕ are slowly varying functions of τ.

Let

$$(\eta\tau + \phi) = \theta \tag{5}$$

Differentiating (4) with respect to τ

$$\frac{dx}{d\tau} = x' = -\eta R \sin \theta + R' \cos \theta - R\phi' \sin \theta \tag{6}$$

By analogy with Lagrange's method of variation of a parameter, set

$$R' \cos \theta - R\phi' \sin \theta = 0 \tag{7}$$

$$\therefore \frac{d^2x}{d\tau^2} = -\eta^2 R \cos \theta - \eta R' \sin \theta - \eta R\phi' \cos \theta \tag{8}$$

Substituting into equation (3)

$$-\eta R' \sin \theta - \eta R\phi' \cos \theta - \eta^2 R \cos \theta + F(R \cos \theta, \mu, \tau) = x_s \cos (\theta - \phi) \tag{9}$$

Multiply (7) by $\eta \cos \theta$, (9) by $\sin \theta$ and subtract.

$$\therefore -\eta R' - \eta^2 R \sin \theta \cos \theta + F(R \cos \theta, \mu, \tau) \sin \theta = x_s \cos (\theta - \phi) \sin \theta \tag{10}$$

Since R and ϕ are by supposition slowly varying, average equation (1) over one cycle of θ. Thus

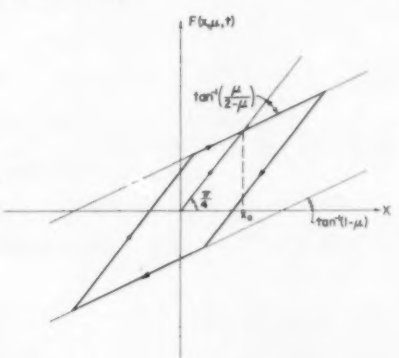

Fig. 1 Bilinear hysteresis

[1] Numbers in brackets designate References at end of paper.

Presented at the Summer Conference of the Applied Mechanics Division, University Park, Pa., June 20–22, 1960, of THE AMERICAN SOCIETY OF MECHANICAL ENGINEERS.

Discussion of this paper should be addressed to the Secretary, ASME, 29 West 39th Street, New York, N. Y., and will be accepted until January 10, 1961, for publication at a later date. Discussion received after the closing date will be returned.

NOTE: Statements and opinions advanced in papers are to be understood as individual expressions of their authors and not those of the Society. Manuscript received by ASME Applied Mechanics Division, August 25, 1959. Paper No. 60—APM-8.

$$-2\eta R' + \frac{1}{\pi}\int_0^{2\pi} F(R\cos\theta, \mu, \tau)\sin\theta d\theta = x_s \sin\phi \quad (11)$$

To simplify notation, no distinction has been made between R and the average value of R over one cycle of θ.

Now, multiply (7) by $\eta \sin\theta$, (9) by $\cos\theta$ and add.

$$\therefore -\eta R\phi' - \eta^2 R\cos^2\theta + F(R\cos\theta, \mu, \tau)\cos\theta = x_s\cos(\theta - \phi)\cos\theta \quad (12)$$

Averaging over one cycle of θ

$$-2\eta R\phi' - \eta^2 R + \frac{1}{\pi}\int_0^{2\pi} F(R\cos\theta, \mu, \tau)\cos\theta d\theta = x_s\cos\phi \quad (13)$$

Let

$$C(R) = \frac{1}{\pi}\int_0^{2\pi} F(R\cos\theta, \mu, \tau)\cos\theta d\theta$$
$$S(R) = \frac{1}{\pi}\int_0^{2\pi} F(R\cos\theta, \mu, \tau)\sin\theta d\theta \quad (14)$$

Hence equations (12) and (13) become

$$-2\eta R' + S(R) = x_s\sin\phi$$
$$-\eta^2 R - 2\eta R\phi' + C(R) = x_s\cos\phi \quad (15)$$

Evaluation of $S(R)$ and $C(R)$

Using Fig. 1, the quantities $C(R)$ and $S(R)$ defined by (14) may be readily evaluated. Let

$$\theta^* = \cos^{-1}\left[1 - \frac{2x_0}{R}\right] \quad (16)$$

$S(R)$

$$S(R) = \frac{2}{\pi}\left[\int_0^{\theta^*}(\mu x_0 - \mu R + R\cos\theta)\sin\theta d\theta + \int_{\theta^*}^{\pi}(-\mu x_0 + R(1-\mu)\cos\theta)\sin\theta d\theta\right] \quad (17)$$

Therefore

$$S(R) = -\frac{\mu R}{\pi}[\sin^2\theta^*] \quad R > x_0$$
$$S(R) = 0 \quad R < x_0 \quad (18)$$

$C(R)$

$$C(R) = \frac{2}{\pi}\left[\int_0^{\theta^*}(\mu x_0 - \mu R + R\cos\theta)\cos\theta d\theta + \int_{\theta^*}^{\pi}(-\mu x_0 + R(1-\mu)\cos\theta)\cos\theta d\theta\right] \quad (19)$$

Therefore

$$C(R) = \frac{R}{\pi}\left[\mu\theta^* + (1-\mu)\pi - \frac{\mu}{2}\sin 2\theta^*\right] \quad R > x_0$$
$$= R \quad R < x_0 \quad (20)$$

Substitution of (18) and (20) into (15) reveals that R and ϕ are indeed slowly varying, if

$$\eta^2 = 0(1)$$
$$\mu < 1$$
$$x_s < x_0 \quad (21)$$

Steady-State Response

The steady-state response is obtained by setting R' and ϕ' equal to zero in (15). Hence equations (15) become

$$S(R_0) = x_s\sin\phi_0$$
$$C(R_0) - \eta^2 R_0 = x_s\cos\phi_0 \quad (22)$$

where the subscript 0 denotes the steady state.

Eliminating ϕ_0 from (22)

$$[C(R_0) - \eta^2 R_0]^2 + [S(R_0)]^2 = [x_s]^2 \quad (23)$$

Eliminating x_s from (22)

$$\tan\phi_0 = \frac{S(R_0)}{C(R_0) - \eta^2 R_0} \quad (24)$$

It is more convenient to specify R_0 in (23) and to solve for η^2; thus

$$\eta^2 = \frac{C(R_0)}{R_0} \pm \left[\left(\frac{x_s}{R_0}\right)^2 - \left(\frac{S(R_0)}{R_0}\right)^2\right]^{1/2} \quad (25)$$

The maximum amplitude will occur at the point where η has a double root, that is at the point where

$$\left(\frac{x_s}{R_0}\right)^2 = \left(\frac{S(R_0)}{R_0}\right)^2 \quad (26)$$

Using (18) and (16)

$$x_s = \frac{4\mu}{\pi}x_0\left(1 - \frac{x_0}{R_0}\right) \quad (27)$$

Hence

$$\frac{R_0}{x_0} = \frac{\frac{4\mu}{\pi}}{\frac{4\mu}{\pi} - \left(\frac{x_s}{x_0}\right)} \quad (28)$$

Since R_0 is by definition positive, bounded response is obtained provided

$$\frac{x_s}{x_0} < \frac{4\mu}{\pi} \quad (29)$$

If $x_s/x_0 > 4\mu/\pi$, the system exhibits an unbounded resonance.

From (25), it will be seen that, at peak response, the frequency is given by

$$\eta^2 = \frac{C(R_0)}{R_0} \quad (30)$$

Hence using (24)

$$\tan\phi_0 = \infty, \phi_0 = \pi/2 \quad (31)$$

Thus for this particular system, phase resonance and amplitude resonance occur at the same frequency. In plotting the responce curves for the system it is convenient to introduce certain dimensionless variables:

Let

$$\frac{x}{\mu x_0} = f$$

$$\frac{\eta^2 - 1}{\mu} = \bar{X} \tag{32}$$

$$A = \frac{R}{x_0}$$

Using the new dimensionless variables, equation (25) may be written in the following way:

$$\bar{X} = -\left\{1 - \frac{\theta^*}{\pi} + \frac{1}{2\pi}\sin 2\theta^* \pm \left[\left(\frac{f}{A}\right)^2 - \left(\frac{\sin^2\theta^*}{\pi}\right)^2\right]^{1/2}\right\}$$

$$A > 1 \tag{33}$$

$$\bar{X} = \pm\frac{f}{A}, \qquad A < 1$$

Fig. 2 shows the steady-state response plotted for several values of the force parameter f. It will be observed that all the curves are single valued, hence jump behavior, characteristic of certain nonlinear systems, is not expected to occur. It will also be observed that if $f < 4/\pi$, the response curves are bounded; however, if $f > 4/\pi$, the system exhibits an unbounded resonance.

Stability of Steady-State Solution

In equations (15), let

$$\begin{aligned} \phi &= \phi_0 + \psi \\ R &= R_0 + \xi \end{aligned} \tag{34}$$

where ψ and ξ are small perturbations on the steady-state values ϕ_0 and R_0. Substituting (34) into equations (15) and making use of the steady-state equations (22),

$$\begin{aligned} -2\eta\xi' + \frac{\partial S}{\partial R}\,\xi &= x_s \cos\phi_0\psi \\ -\eta^3\xi - 2\eta R_0\psi' + \frac{\partial C}{\partial R}\,\xi &= -x_s \sin\phi_0\psi \end{aligned} \tag{35}$$

Using the steady-state equations (22) to replace $x_s \cos\phi_0$ and $x_s \sin\phi_0$, equations (35) become

$$-2\eta\xi' + \frac{\partial S}{\partial R}\,\xi = [-R_0\eta^3 + C(R_0)]\psi \tag{36}$$

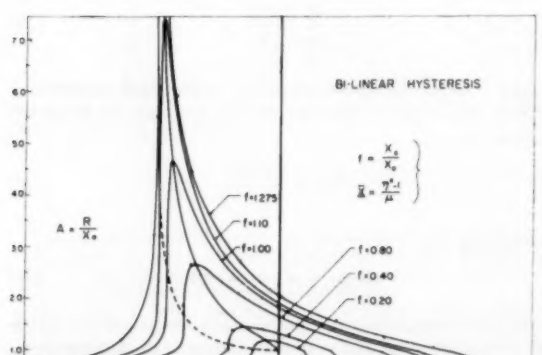

Fig. 2

$$\left(-\eta^2 + \frac{\partial C}{\partial R}\right)\xi = 2\eta R_0\psi' - S(R_0)\psi \tag{36 (cont.)}$$

Let

$$\begin{aligned} \xi &= \xi_0 e^{\lambda t} \\ \psi &= \psi_0 e^{\lambda t} \end{aligned} \tag{37}$$

Substituting (37) in (36), the frequency equation is

$$(2\eta\lambda)^2 - (2\eta\lambda)\left[\frac{S(R_0)}{R_0} + \frac{\partial S}{\partial R}\right] + \frac{S(R_0)}{R_0}\,\frac{\partial S}{\partial R} + \left(\frac{C(R_0)}{R_0} - \eta^2\right)\left(\frac{\partial C}{\partial R} - \eta^2\right) = 0 \tag{38}$$

Now

$$S(R_0) = -\frac{\mu R_0}{\pi}\sin^2\theta^*$$

$$C(R_0) = \frac{R_0}{\pi}\left[\mu\theta^* + (1-\mu)\pi - \frac{\mu}{2}\sin 2\theta^*\right] \tag{39}$$

$$\cos\theta^* = \left(1 - \frac{2x_0}{R_0}\right)$$

$$\therefore \frac{S(R_0)}{R_0} = -\frac{\mu}{\pi}\left[(1 - \cos^2\theta^*)\right] \tag{40}$$

$$S'(R_0) + \frac{S(R_0)}{R_0} = -\frac{2\mu}{\pi}(1 - \cos\theta^*) \tag{41}$$

$$C'(R_0) = \frac{1}{\pi}\left[\mu\theta^* + (1-\mu)\pi + \frac{\mu}{2}\sin 2\theta^* - 2\mu\sin\theta^*\right] \tag{42}$$

$$\therefore \left[\frac{1}{R_0}C(R_0) - \eta^2\right][C'(R_0) - \eta^2] + \frac{1}{R_0}S(R_0)S'(R_0)$$
$$= \eta^4 - \eta^2\left(\frac{2}{\pi}\right)[\mu\theta^* + (1-\mu)\pi - \mu\sin\theta^*]$$
$$+ \frac{1}{\pi^2}\left[\mu\theta^* + (1-\mu)\pi + \frac{\mu}{2}\sin 2\theta^* - 2\mu\sin\theta^*\right]\left[\mu\theta^* + (1-\mu)\pi - \frac{\mu}{2}\sin 2\theta^*\right]$$
$$+ \left(\frac{\mu}{\pi}\right)^2\sin^2\theta^*(1 - \cos\theta^*)^2 \tag{43}$$

$$= \left[\eta^2 - \frac{1}{\pi}(\mu\theta^* + (1-\mu)\pi - \mu\sin\theta^*)\right]^2 \tag{44}$$

Hence

$$(2\eta\lambda)^2 + 2\eta\lambda\left[\frac{2\mu}{\pi}(1 - \cos\theta^*)\right] + \left[\eta^2 - \frac{1}{\pi}(\mu\theta^* + (1-\mu)\pi - \mu\sin\theta^*)\right]^2 = 0 \tag{45}$$

$$\therefore 2\eta\lambda = -\frac{\mu}{\pi}(1 - \cos\theta^*) \pm \left\{\left[\frac{\mu}{\pi}(1 - \cos\theta^*)\right]^2 - \left[\eta^2 - \frac{1}{\pi}(\mu\theta^* + (1-\mu)\pi - \mu\sin\theta^*)\right]^2\right\}^{1/2} \tag{46}$$

Hence

$$R(2\eta\lambda) \leq 0$$

Therefore the system is always stable.

Summary of Results

From the analysis of a single-degree-of-freedom oscillator exhibiting bilinear hysteresis, the following results have been obtained for the case of sinusoidal excitation.

(a) The system exhibits "soft" type resonance; i.e., the resonance peak moves to a lower frequency as the amplitude of the driving force is increased.

(b) The response curves are single valued and stable, and show very steep slopes on the low-frequency side of resonance.

(c) Phase resonance and amplitude resonance occur at the same frequency in this system.

(d) If the driving force exceeds $(4\mu/\pi)kx_0$, the system exhibits undamped resonance.

Computer Studies

Equation (1) was simulated on an electronic differential analyzer (Appendix) and solutions were obtained for various values of f. The results are plotted in Fig. 2 and show good agreement with theory. It was observed that in the frequency range $-1.2 < \bar{X} < 1.2$ the solutions were very close to sinusoidal, thus justifying the assumptions made in [4].

Conclusions

The main findings of the theory were confirmed by the analog studies, which showed that no nonlinear jumps occurred, and that for large enough excitation the system exhibited undamped resonance.

References

1 J. H. Klumpp and B. J. Lazan, "Frictional Damping and Resonant Vibration Characteristics of an Axial Slip Lap Joint," WADC Technical Report No. 54-64, 1954.

2 L. E. Goodman and J. H. Klumpp, "Analysis of Slip Damping With Reference to Turbine-Blade Vibration," JOURNAL OF APPLIED MECHANICS, vol. 23, TRANS. ASME, vol. 78, 1956, pp. 421–429.

3 B. J. Lazan and L. E. Goodman, "Effect of Material and Slip Damping on Resonance Behaviour" from "Shock and Vibration Instrumentation," ASME Publishing Department, New York, N. Y.

4 T. H. Pian and F. C. Hallowell, Jr., "Structural Damping in Simple Built-up Beam," Proceedings of the First U. S. National Congress of Applied Mechanics, 1952, pp. 97–102.

5 J. E. Ruzicka, "Forced Vibrations in Systems with Elastically Supported Dampers," MSc thesis, Massachusetts Institute of Technology, June, 1957.

6 L. S. Jacobsen, "Dynamic Behaviour of Simplified Structures up to the Point of Collapse," *Proceedings*, Symposium Earthquake and Blast Effects on Structures, 1952, pp. 94–113.

7 L. S. Jacobsen and R. S. Ayre, "Engineering Vibrations," McGraw-Hill Book Company, Inc., New York, N. Y., 1958.

8 R. Tanabashi, "Studies on the Non-Linear Vibrations of Structures Subjected to Destructive Earthquakes," World Conference on Earthquake Engineering, 1956.

9 N. Minorski, "Non-Linear Mechanics," J. W. Edwards, Ann Arbor, Mich., 1947.

10 Reference [6], pp. 112 and 113.

11 W. T. Thomson, "Analog Computer for Nonlinear System With Hysteresis," JOURNAL OF APPLIED MECHANICS, vol. 24, TRANS. ASME, vol. 79, 1957, pp. 245–247.

APPENDIX

Analog Simulation of System with Bilinear Hysteresis

The problem of simulating bilinear hysteresis is by no means a simple one. L. S. Jacobsen [10] has made use of mechanical models to simulate elastoplastic behavior in dynamic structures. W. T. Thomson [11] used an electronic differential analyzer in combination with a number of high-speed relays to obtain the positive quadrant of a system with elastoplastic behavior. J. E. Ruzicka [5] used an electronic differential analyzer to simulate a vibration isolator using elastically supported Coulomb friction dampers, thereby accomplishing the same thing as did Jacobsen with his mechanical model.

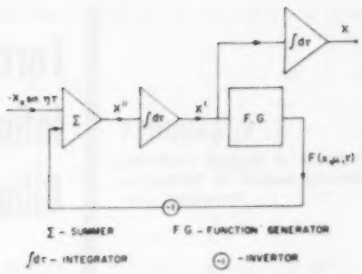

Fig. 3 Schematic computer setup

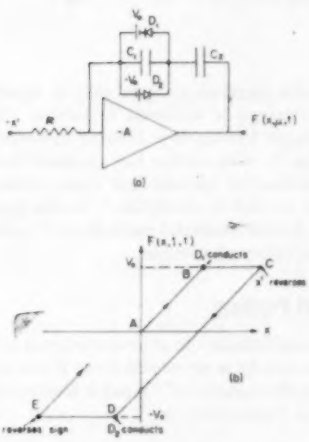

Fig. 4 Hysteresis function generator

The computer setup used by the author is shown schematically in Fig. 3. The component denoted by FG is shown in detail in Fig. 4.

The operation of the bilinear hysteresis component may be explained in the following manner: Consider for simplicity that the capacitor C_2 is shorted out. Suppose that C_1 is discharged initially when $\dot{x}$ is fed into the input. The voltage across C_1 is proportional to the time integral of the input, $\dot{x}$; that is, the voltage across C_1 is proportional to x. For positive $\dot{x}$, x will increase with time until the voltage across C_1 reaches the bias voltage on the diode D_1; further increase of the voltage across C_1 is effectively prevented by conduction of the diode. Hence the output voltage will be held at the level set by the bias voltage V_0. When the velocity $\dot{x}$ reverses direction, current may now flow from the capacitor C_1 and the system will integrate downwards from point C, along a line parallel to A-B, until the voltage on C_1 reaches the negative bias voltage on diode D_2, at which point further decrease in output voltage is prevented by the conduction of the diode. The output voltage will be held at this level until the input reverses sign. The operation of the system is illustrated in Fig. 4(b). The addition of capacitor C_2 allows the slope of the curve B-C to be set arbitrarily.

Forced Oscillations of a Semi-Infinite Rod Exhibiting Weak Bilinear Hysteresis

T. K. CAUGHEY
Associate Professor of Applied Mechanics, California Institute of Technology, Pasadena, Calif.

A first-order nonlinear solution is presented for the problem of forced sinusoidal oscillations of a semi-infinite bar exhibiting weak bilinear hysteresis.

MANY physical systems exhibit hysteresis and frequently the hysteresis is nonlinear in nature. One simple example of nonlinear hysteresis is bilinear hysteresis, which is illustrated in Fig. 1. The author has analyzed the response of a single-degree-of-freedom bilinear hysteresic system to sinusoidal excitation[1] and to random excitation.[2] In this paper an analysis is made of the forced sinusoidal oscillations of a semi-infinite rod exhibiting weak bilinear hysteresis.

Formulation of Problem

Consider a semi-infinite rod of cross-sectional area a, density ρ, excited at one end by a sinusoidal force $P \cos \omega t$. The stress-strain curve for the material of the rod is illustrated in Fig. 1, and is of the bilinear hysteresic type.

Equation of Motion

As in the case of an elastic rod, the equation of motion is given by

$$\rho \frac{\partial^2 u}{\partial t^2} = \frac{\partial \sigma}{\partial x} \tag{1}$$

Let

a = cross-sectional area of bar
ρ = density of bar
σ = stress in bar at distance x from driven end
u = axial displacement of bar at point distance x from driven end
$\epsilon = \partial u/\partial x$ = axial strain
$\sigma = EF(\epsilon, \mu, t)$ (stress-strain law) (2)

where $F(\epsilon, \mu, t)$ is the bilinear hysteresic function shown in Fig. 1.
$F(\epsilon, \mu, t)$ is such that as $\mu \to 0$ $F(\epsilon, \mu, t) \to \epsilon$.
E = Young's modulus for material when $\mu = 0$.
Using (2), equation (1) becomes

$$\rho \frac{\partial^2 u}{\partial t^2} = E \frac{\partial F(\epsilon, \mu, t)}{\partial x} \tag{3}$$

Let

$$E/\rho = v^2 \tag{4}$$

where v = velocity of propagation in bar when $\mu = 0$.

Differentiating (3) with respect to x and using (2), equation (3) becomes

$$\frac{\partial^2 \epsilon}{\partial t^2} = v^2 \frac{\partial^2 F(x, \mu, t)}{\partial x^2} \tag{5}$$

Boundary Conditions

The boundary conditions on equation (5) are:

$$\left.\begin{aligned} &1 \quad \epsilon \text{ bounded.} \\ &2 \quad \sigma|_{x=0} = EF(\epsilon, \mu, t)|_{x=0} = \frac{P}{a} \cos \omega t \end{aligned}\right\} \tag{6}$$

Linear Problem $\mu = 0$

Consider first the linear problem obtained by setting $\mu = 0$ in (5)

$$\frac{\partial^2 \epsilon}{\partial t^2} = v^2 \frac{\partial^2 \epsilon}{\partial x^2} \tag{7}$$

Equation (7) together with the boundary conditions (6) yields the linear solution

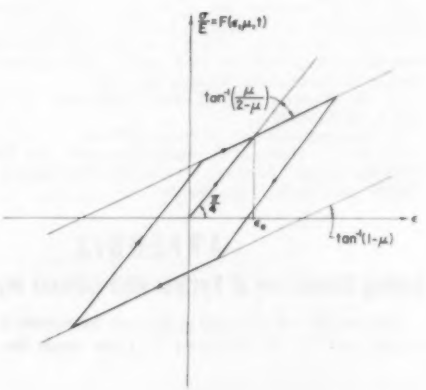

Fig. 1 Bilinear hysteresis

[1] T. K. Caughey, "Sinusoidal Excitation of a System With Bi-Linear Hysteresis," see this issue of the JOURNAL OF APPLIED MECHANICS, pp. 640–643.

[2] T. K. Caughey, "Random Excitation of a System With Bilinear Hysteresis," see this issue of the JOURNAL OF APPLIED MECHANICS, pp. 649–652.

Contributed by the Applied Mechanics Division and presented at the Winter-Annual Meeting, New York, N. Y., November 27–December 2, 1960, of THE AMERICAN SOCIETY OF MECHANICAL ENGINEERS.

Discussion of this paper should be addressed to the Secretary, ASME, 29 West 39th Street, New York, N. Y., and will be accepted until January 10, 1961, for publication at a later date. Discussion received after the closing date will be returned.

Manuscript received by ASME Applied Mechanics Division, February 15, 1960. Paper No. 60—WA-28.

$$\epsilon = \frac{P}{aE} \cos \omega \left(t - \frac{x}{v} \right) \tag{8}$$

Nonlinear Problem $\mu \neq 0$

In the case where $\mu \neq 0$, but is small, it is reasonable to hypothesize a solution of the following type:

$$\epsilon = \epsilon_0 = A(x) \cos \left[\omega \left(t - \frac{x}{v} \right) + \phi(x) \right] \tag{9}$$

where A and ϕ are slowly varying function of x.

Substituting (9) into (5)

$$\frac{\partial^2 \epsilon_0}{\partial t^2} = v^2 \frac{\partial^2}{\partial x^2} [F(\epsilon_0, \mu, t)] \tag{10}$$

Expanding $F(\epsilon_0, \mu, t)$ in a Fourier series in the variable

$$\left[\omega \left(t - \frac{x}{v} \right) + \phi(x) \right]_{x = \text{const}}$$

and retaining only the fundamental terms:

$$F(\epsilon_0, \mu, t) \cong C(A) \cos \psi + S(A) \sin \psi \tag{11}$$

where

$$\psi = \left[\omega \left(t - \frac{x}{v} \right) + \phi(x) \right]$$

$$C(A) = \frac{1}{\pi} \int_0^{2\pi} F(A \cos \psi, \mu, t) \cos \psi d\psi$$

$$S(A) = \frac{1}{\pi} \int_0^{2\pi} F(A \cos \psi, \mu, t) \sin \psi d\psi \tag{12}[3]$$

The functions $C(A)$ and $S(A)$ in (11) are readily evaluated using Fig. 1:

$$\text{Let } \cos \theta^* = \left(1 - \frac{2\epsilon_0}{A} \right) \tag{13}$$

Therefore

$$\left.\begin{aligned} S(A) &= -\frac{\mu A}{\pi} \sin^2 \theta^* \qquad A > \epsilon_0 \\ &= 0 \qquad\qquad\qquad A < \epsilon_0 \end{aligned}\right\} \tag{14}$$

and

$$\left.\begin{aligned} C(A) &= \frac{A}{\pi} \left[\pi + \mu(\theta^* - \pi - \tfrac{1}{2} \sin^2 \theta^*) \right] \qquad A > \epsilon_0 \\ &= A \qquad\qquad\qquad\qquad\qquad\qquad A < \epsilon_0 \end{aligned}\right\} \tag{15}$$

Substituting (11) into (10)

$$\frac{\partial^2}{\partial t^2} [A \cos \psi] = v^2 \frac{\partial^2}{\partial x^2} [C(A) \cos \psi + S(A) \sin \psi] \tag{16}$$

Carrying out the differentiation in (16) and retaining only terms up to first order in μ

$$-\frac{\omega^2}{v^2} A \cos \psi = 2 \frac{\omega}{v} \frac{dC(A)}{dx} \sin \psi - \frac{\omega^2}{v^2} C(A) \cos \psi$$

$$- \frac{\omega^2}{v^2} S(A) \sin \psi + \frac{2\omega}{v} \frac{d\phi}{dx} C(A) \sin \psi + 0(\mu^2) \tag{17}$$

[3] These integrals are evaluated in Reference in footnote 1.

Equating the coefficients of $\cos \psi$ and $\sin \psi$ separately to zero:

$$\frac{\omega^2}{v^2} [C(A) - A] = \frac{2\omega}{v} C(A) \frac{d\phi}{dx} \tag{18}$$

$$\frac{\omega^2}{v^2} S(A) = \frac{2\omega}{v} \frac{dC(A)}{dx} \tag{19}$$

Using (15) and (18)

$$\frac{d\phi}{dx} = \tfrac{1}{2} \frac{\omega}{v} \frac{\frac{\mu A}{\pi} (\theta^* - \pi - \tfrac{1}{2} \sin 2\theta^*)}{A \left[1 + \frac{\mu}{\pi} (\theta^* - \pi - \tfrac{1}{2} \sin 2\theta^*) \right]} \tag{20}$$

Therefore

$$\left.\begin{aligned} \frac{d\phi}{dx} &= \tfrac{1}{2} \frac{\omega}{v} \frac{\mu}{\pi} (\theta^* - \pi - \tfrac{1}{2} \sin 2\theta^*) + 0(\mu^2) \qquad A > x_0 \\ &= 0 \qquad\qquad\qquad\qquad\qquad\qquad\qquad\qquad A < x_0 \end{aligned}\right\} \tag{21}$$

Using (14) and (19)

$$\frac{dA}{dx} \left[1 + \frac{\mu}{\pi} (\theta^* - \pi + \tfrac{1}{2} \sin 2\theta^* - 2 \sin \theta^*) \right] = -\tfrac{1}{2} \frac{\omega}{v} \frac{\mu}{\pi} A \sin^2 \theta^* \tag{22}$$

Therefore

$$\left.\begin{aligned} \frac{dA}{dx} &= -\tfrac{1}{2} \frac{\omega}{v} \frac{\mu}{\pi} A \sin^2 \theta^* + 0(\mu^2) \qquad A > x_0 \\ &= 0 \qquad\qquad\qquad\qquad\qquad\qquad\qquad\qquad A < x_0 \end{aligned}\right\} \tag{23}$$

From (21) and (23) it will be observed that since $0 < \theta^* < \pi$ and $\sin 2\theta^*$ is bounded, both dA/dx and $d\phi/dx$ are of order μ, and since μ is small, it follows that A and ϕ are slowly varying functions of x.

Let

$$X = \mu \frac{4x}{\lambda} \tag{24}$$

where

$$\lambda = \frac{v}{f} \tag{25}$$

λ is the wave length of waves of frequency f traveling with velocity v in the elastic bar obtained by setting $\mu = 0$.

Using (24), equations (21) and (23) become

$$\left.\begin{aligned} \frac{d\phi}{dX} &= \tfrac{1}{4} (\theta^* - \pi - \tfrac{1}{2} \sin 2\theta^*) \qquad A > \epsilon_0 \\ &= 0 \qquad\qquad\qquad\qquad\qquad\qquad A < \epsilon_0 \end{aligned}\right\} \tag{26}$$

$$\left.\begin{aligned} \frac{dA}{dX} &= -\tfrac{1}{4} \sin^2 \theta^* \qquad A > \epsilon_0 \\ &= 0 \qquad\qquad\qquad\qquad\qquad\qquad A < \epsilon_0 \end{aligned}\right\} \tag{27}$$

Consider first equation (27). From equation (13)

$$\sin^2 \theta^* = \frac{4\epsilon_0}{A} \left(1 - \frac{\epsilon_0}{A} \right) \tag{28}$$

Therefore

$$\frac{dA}{dX} = -\frac{\epsilon_0(A - \epsilon_0)}{A} \tag{29}$$

This may be integrated to give (See Appendix 1):

$$X = -\frac{A}{\epsilon_0} - \ln(A - \epsilon_0) + C \tag{30}$$

Now $A = A_0$ at $X = 0$. Therefore

$$X = \frac{A_0 - A}{\epsilon_0} + \ln\left[\frac{A_0 - \epsilon_0}{A - \epsilon_0}\right] \tag{31}$$

Define

$$\eta = \frac{A}{\epsilon_0} \tag{32}$$

Therefore

$$X = (\eta_0 - \eta) + \ln\left(\frac{\eta_0 - 1}{\eta - 1}\right) \tag{33}$$

Hence the distance X from the excited end of the bar to the point having an amplitude ratio η is given parametrically by (33).

It will be observed that as $\eta \to 1$, $X \to \infty$, Fig. 2 shows a plot of η versus X. It will be observed that η falls almost linearly with X until $\eta = 2$, thereafter, η asymptotically approaches unity as X tends to infinity.

Now consider equation (26)

$$\phi = \int {}^1/_4\,(\theta^* - \pi - {}^1/_2 \sin 2\theta^*)dX \tag{34}$$

$$= \int {}^1/_4(\theta^* - \pi - {}^1/_2 \sin 2\theta^*)\,\frac{dA/d\theta^*}{dA/dX}\,d\theta^* \tag{35}$$

but

$$\frac{dA}{dX} = -{}^1/_4\,A \sin^2\theta^* \quad \text{by (27)}$$

and

$$\frac{dA}{d\theta^*} = -\frac{A^2 \sin\theta^*}{2\epsilon_0} \quad \text{from (13)}$$

Hence

$$\phi = \int \frac{[\theta^* - \pi - {}^1/_2 \sin 2\theta^*]}{A \sin^2\theta^*}\,\frac{A^2 \sin\theta^*}{2\epsilon_0}\,d\theta^* \tag{36}$$

Now

$$\frac{2\epsilon_0}{A} = 1 - \cos\theta^* \quad \text{by (13)}$$

Therefore

$$\phi^* = \int \frac{\theta^* - \pi - {}^1/_2 \sin 2\theta^*}{\sin\theta^*(1 - \cos\theta^*)}\,d\theta^* \tag{37}$$

This may be integrated to give (Appendix 2):

$$\phi = \theta^* + \frac{1 + \cos\theta^*}{\sin\theta^*} + \left\{ {}^1/_2\,(\theta^* - \pi)\left[\ln\tan\frac{\theta^*}{2} - \frac{1}{2\sin^2\frac{\theta^*}{2}}\right] - {}^1/_2 \operatorname{cotan}\frac{\theta^*}{2} + \sum_{r=0}^{\infty}\frac{\sin(2r+1)\theta^*}{(2r+1)^2}\right\} + C \tag{38}$$

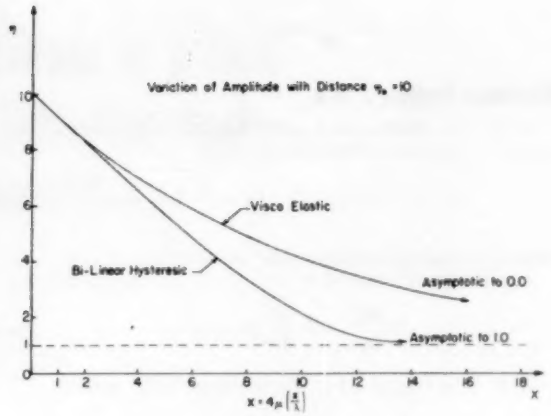

Fig. 2

The constant C may be evaluated by noting that $\phi = \phi_0$ at $X = 0$ and at $\theta^* = \theta_0^*$. The quantities A_0 and ϕ_0 are determined from the conditions at $X = 0$.

Now

$$P \cos\omega t = aEF(\epsilon, \mu, t)\big|_{x=0} \tag{39}$$

Expanding $F(\epsilon, \mu, t)$ in a Fourier series and retaining only the fundamental terms

$$\frac{P}{aE}\cos\omega t = C(A_0)\cos(\omega t + \phi_0) + S(A_0)\sin(\omega t + \phi_0) + 0(\mu^2) \tag{40}$$

Let

$$\psi = \omega t + \phi_0 \tag{41}$$

Then neglecting terms of order μ^2

$$\frac{P}{aE}\cos\phi_0 = C(A_0)$$
$$\frac{P}{aE}\sin\phi_0 = S(A_0) \tag{42}$$

Therefore

$$\{[C(A_0)^2 + S(A_0)]^2\}^{1/2} = \frac{P}{aE} \tag{43}$$

Therefore

$$\tan\phi_0 = \frac{S(A_0)}{C(A_0)} \tag{44}$$

Using (14) and (15)

$$\sqrt{[C(A_0)]^2 + [S(A_0)]^2} = A_0[1 + 0(\mu)] = \frac{P}{aE} \tag{45}$$

Therefore

$$A_0 = \frac{P}{aE} + 0(\mu) \tag{46}$$

Similarly

$$\tan\phi_0 = \frac{S(A_0)}{C(A_0)} = 0(\mu) \tag{47}$$

Therefore

$$\phi_0 = 0(\mu) \tag{48}$$

Thus consistent with the approximations made in the foregoing analysis

$$\phi_0 \simeq 0, \quad A_0 \simeq \frac{P}{aE} \tag{49}$$

Comparison With Viscoelastic Solid

It is interesting to compare the results obtained in the foregoing with those one obtains for a viscoelastic solid. For the viscoelastic solid, replace $F(\epsilon, \mu, t)$ by $[\epsilon + \mu\beta(\partial\epsilon/\partial t)]$. Using the approximate techniques just outlined, it may easily be shown (Appendix 3) that

$$\eta = \eta_0 e^{-\left(\frac{\pi}{4}\omega\beta\right)X} + 0(\mu\omega\beta) \tag{50}$$

$$\phi = C + 0(\mu(\omega\beta)^2 X) \tag{51}$$

Hence the phase shift ϕ is very small except at very large distances from the origin.

Fig. 2 shows a plot of η versus X for the bilinear hysteresic solid and also for the viscoelastic solid. The constant $\omega\beta$ of the viscoelastic solid has been so chosen that the initial slope of both curves is the same. It will be observed that the amplitude decays much faster in the case of the bilinear hysteresic solid; it should of course be noted that the viscoelastic amplitude tends to zero as X tends to infinity.

Fig. 3 shows the variation of ϕ with X for the case of bilinear hysteresis. It will be noted that ϕ is always negative and that it varies almost linearly with X initially, but finally becomes asymptotic to -7.214 as X tends to infinity. It is interesting to note that for the viscoelastic solid ϕ is always positive and varies linearly with X.

APPENDIX 1

Integration of Equation (29)

$$\frac{dA}{dX} = -\epsilon_0 \frac{(A - \epsilon_0)}{A} \tag{52}$$

Hence

$$\frac{A\,dA}{A - \epsilon_0} = -\epsilon_0 dX \tag{53}$$

$$\therefore \quad dA + \frac{\epsilon_0 dA}{A - \epsilon_0} = -\epsilon_0 dX \tag{54}$$

Hence integrating (54)

$$X = -\frac{A}{\epsilon_0} - \ln(A - \epsilon_0) + C \tag{55}$$

where ln is the logarithm to the base e.

APPENDIX 2

Integration of Equation (37)

$$\phi = \int \frac{\theta^* - \pi - \frac{1}{2}\sin 2\theta^*}{\sin\theta^*(1 - \cos\theta^*)}\, d\theta^* \tag{56}$$

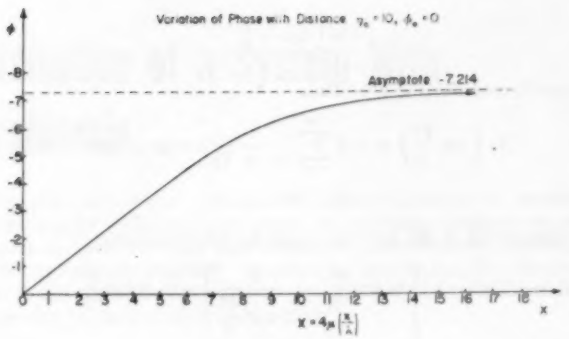

Fig. 3

Expanding the integrand

$$\phi = \int \left\{ \frac{\theta^* - \pi}{\sin\theta^*(1 - \cos\theta^*)} - \frac{\cos\theta^*}{1 - \cos\theta^*} \right\} d\theta^* \tag{57}$$

Let

$$I_1 = \int \frac{\theta^* - \pi}{\sin\theta^*(1 - \cos\theta^*)}\, d\theta^* \tag{58}$$

$$I_2 = -\int \frac{\cos\theta^*}{(1 - \cos\theta^*)}\, d\theta^* \tag{59}$$

Consider I_2 first, using integral 331.17f[4]

$$I_2 = \theta^* + \frac{1 + \cos\theta^*}{\sin\theta^*} + \text{const} \tag{60}$$

Now consider I_1. Let

$$\theta^* = 2x \tag{61}$$

Then I_1 becomes

$$I_1 = \int \frac{2(2x - \pi)dx}{4\sin^2 x \cos x} \tag{62}$$

Integrating by parts using integral 331.15g[4]

$$I_1 = {}^1/_2(2x - \pi)\left[\ln\tan x - \frac{1}{2\sin^2 x}\right] - \int \left[\ln\tan x - \frac{1}{2\sin^2 x}\right] dx \tag{63}$$

Making use of integral 331.6d and (61), equation (63) becomes

$$I_1 = {}^1/_2(\theta^* - \pi)\left[\ln\tan\frac{\theta^*}{2} - \frac{1}{2\sin^2\frac{\theta^*}{2}}\right] - {}^1/_2\cot\frac{\theta^*}{2} - {}^1/_2\int \ln\left(\tan\frac{\theta^*}{2}\right) d\theta^* \tag{64}$$

The integral

$$\int \ln\left(\tan\frac{\theta^*}{2}\right) d\theta^*$$

cannot be evaluated in closed form; to facilitate its evaluation, express

[4] W. Grobner, "Integraltafel, Unbestimmte Integrale," and W. Grabner and N. Hofreiter, "Integrale," Springer-Verlag, Berlin, 1959.

$$\ln\left(\tan\frac{\theta^*}{2}\right)$$

as a Fourier series in θ^*. Thus

$$\ln\left(\tan\frac{\theta^*}{2}\right) = -2\sum_{r=0}^{\infty}\frac{1}{(2r+1)}\cos(2r+1)\theta^* \qquad (65)$$

$$0 < \theta^* < \pi$$

Substitution of (65) into (64) yields the following result:

$$I_1 = {}^1/_2(\theta^* - \pi)\left[\ln\tan\frac{\theta^*}{2} - \frac{1}{2\sin^2\dfrac{\theta^*}{2}}\right] - {}^1/_2\operatorname{cotan}\frac{\theta^*}{2} + \sum_{r=1}^{\infty}\frac{\sin(2r+1)\theta^*}{(2r+1)^2} + \text{const} \qquad (66)$$

$$0 < \theta^* < \pi$$

Hence $\phi = I_1 + I_2$ is given by equation (37).

APPENDIX 3

Solution of Viscoelastic Problem

The viscoelastic problem obtained by replacing $F(\epsilon, \mu, t)$ by $[\epsilon + \mu\beta(\partial\epsilon/\partial t)]$ in equation (5) can be solved exactly, however, if $\mu\omega\beta$ is small, it is somewhat more convenient to solve the problem using the approximate method outlined previously.

Thus equation (5) becomes

$$\frac{\partial^2\epsilon}{\partial t^2} = v^2\left[\frac{\partial^2\epsilon}{\partial x^2} + \mu\beta\frac{\partial^3\epsilon}{\partial x^2\partial t}\right] \qquad (67)$$

Assume a solution of the form

$$\epsilon = A(x)\cos\left[\omega\left(t - \frac{x}{v}\right) + \phi(x)\right] \qquad (68)$$

where A and ϕ are slowly varying functions of x. Substituting (68) into (67) and retaining only first-order terms

$$-\left(\frac{\omega}{v}\right)^2 A\cos\psi = -\left(\frac{\omega}{v}\right)^2 A\cos\psi + 2A'\left(\frac{\omega}{v}\right)\sin\psi + 2A\phi'\left(\frac{\omega}{v}\right)\cos\psi + \mu\omega\beta\left[\left(\frac{\omega}{v}\right)^2 A\sin\psi\right] + 0(\mu^2) \qquad (69)$$

where

$$\psi = \omega\left(t - \frac{x}{v}\right) + \phi \qquad (70)$$

Equating the coefficients of $\sin\psi$ and $\cos\psi$ separately to zero,

$$2A' + \mu\omega\beta\left(\frac{\omega}{v}\right)A = 0 \qquad (71)$$

$$\phi' = 0 \qquad (72)$$

Thus

$$A = A_0 e^{-\frac{\mu}{2}\omega\beta\frac{\omega}{v}x}, \qquad \phi = \text{const} \qquad (73)$$

Let

$$X = 4x/\lambda$$

$$\therefore\ A = A_0 e^{-\frac{\pi}{4}(\omega\beta)X}, \qquad \phi = \text{const} \qquad (74)$$

If second-order terms are retained in (69) it may easily be shown that

$$\phi = C + 0[\mu(\omega\beta)^2 X] \qquad (75)$$

Hence for $\mu(\omega\beta)^2$ small, the phase-correction term will be small except at large distances from the origin.

Random Excitation of a System With Bilinear Hysteresis

T. K. CAUGHEY
Associate Professor of Applied Mechanics, California Institute of Technology, Pasadena, Calif.

An analysis is made of the response of a system with bilinear hysteresis to random excitation. It is shown that for moderately large inputs, the additional damping created by the bilinear hysteresis decreases the mean squared deflection compared with that for a linear system with the same viscous damping. However, for large inputs, the decrease in the stiffness of the system due to the bilinear hysteresis causes the mean squared deflection to increase over that for the equivalent linear system.

MANY physical systems exhibit bilinear hysteresis of the type shown in Fig. 1. Hysteresis may be due to the presence of Coulomb friction in the system, or it may be due to elastoplastic behavior of the material in the system. As an example of hysteresis due to Coulomb friction, consider a steel-framed building with masonry walls. The masonry is held in place primarily by its own weight and the resulting frictional forces developed between the masonry blocks. If the building is caused to vibrate, both the masonry and the structural steel work contribute to the stiffness of the building. For small amplitudes of motion, the shearing forces in the masonry are insufficient to overcome the frictional forces, and the masonry contributes considerable shear rigidity to the building. As the amplitude of the motion is increased a point will be reached at which the shearing forces in the masonry exceed the frictional forces, and relative sliding will then occur. During this portion of the motion the shear rigidity of the building is that of the structural steel work; though the masonry no longer contributes to the rigidity of the structure, the relative sliding of the masonry blocks dissipates energy, thereby providing an additional source of damping. Such a system would exhibit bilinear hysteresis of the type shown in Fig. 1. In the past it has been assumed tacitly that such damping would be beneficial and give an additional factor of safety. As the following analysis will show, hysteresis damping of this type may actually lead to larger displacements than would occur in the linear system.

Formulation of Problem

Consider a dynamic system, the restoring force of which exhibits bilinear hysteresis, subjected to a stationary random Gaussian excitation having a white power spectrum; i.e.,

$$m\ddot{x} + m\beta\dot{x} + kF(x, \mu, t) = N(t) \tag{1}$$

where

$F(x, \mu, t)$ is the hysteresic restoring force of Fig. 1
$F(x, \mu, t)$ is such that as $\mu \to 0$, $F(x, \mu, t) \to x$

Let

$$\begin{aligned} k/m &= \omega_0^2 \\ \omega_0 t &= \tau \\ N(t)/k &= x_s(\tau) \\ \beta/\omega_0 &= \bar{\beta} \end{aligned} \tag{2}$$

Using (2), equation (1) becomes

$$x'' + \bar{\beta}x' + F(x, \mu, \tau) = x_s(\tau) \tag{3}$$

If in (3) $\mu = 0$ and $\bar{\beta}$ is small, the solution may be written

$$x = R(\tau)\cos[\tau + \theta(\tau)] \tag{4}$$

$$x' \doteq -\omega R(\tau)\sin[\tau + \theta(\tau)] \tag{5}$$

where R and θ are slowly varying functions of τ. If in (3) $\mu \neq 0$ but is small, the essentially slowly varying nature of the solution will be preserved.

Method of Solution

The method of solution to be used in this paper is to replace equation (3) by an equivalent linear differential equation, which may then be solved quite readily. Rewrite equation (3) in the following form:

$$x'' + \beta_{eq}x' + \omega_{eq}^2 x + \epsilon(x, x', \tau) = x_s(\tau) \tag{6}$$

where $\epsilon(x, x', \tau)$ is the equation deficiency. If in (6) $\epsilon(x, x', \tau)$ is neglected, the equation is linear and may be solved readily. The smaller $\epsilon(x, x', \tau)$, the smaller the error in neglecting it. Hence the logical choice of the system constants β_{eq} and ω_{eq}^2 are those values which minimize the equation deficiency. For mathemati-

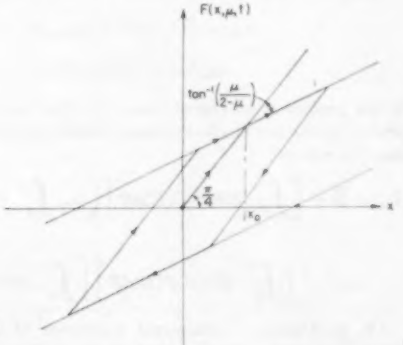

Fig. 1 Bilinear hysteresis

Contributed by the Applied Mechanics Division and presented at the Winter Annual Meeting, New York, N. Y., November 27–December 2, 1960, of THE AMERICAN SOCIETY OF MECHANICAL ENGINEERS.

Discussion of this paper should be addressed to the Secretary, ASME, 29 West 39th Street, New York, N. Y., and will be accepted until January 10, 1961, for publication at a later date. Discussion received after the closing date will be returned.

Manuscript received by ASME Applied Mechanics Division, February 15, 1960. Paper No. 60—WA-27.

cal expediency the minimization of the mean squared error will be used. Thus

$$\overline{\epsilon^2(x, x', \tau)} = \overline{[(\bar{\beta} - \beta_{eq})x' + F(x, \mu, \tau) - \omega_{eq}^2 x]^2} \quad (7)$$

where the bar superscript denotes average with respect to time.

Minimizing (7) with respect to β_{eq} and ω_{eq}^2, gives

$$\beta_{eq} = \overline{[\bar{\beta}(x')^2 + x'F(x, \mu, \tau) - \omega_{eq}^2 xx']}\ \overline{[(x')^2]}^{-1} \quad (8)$$

$$\omega_{eq}^2 = \overline{[(\bar{\beta} - \beta_{eq})x'x + xF(x, \mu, \tau)]}\ \overline{[(x)^2]}^{-1} \quad (9)$$

Now, for a stationary, differentiable random process, the velocity and displacement are uncorrelated at the same time; thus

$$\overline{xx'} = 0 \quad (10)$$

Hence equations (8) and (9) become

$$\beta_{eq} = \bar{\beta} + \overline{[x'F(x, \mu, \tau)]}\ \overline{[(x')^2]}^{-1} \quad (11)$$

$$\omega_{eq}^2 = \overline{[xF(x, \mu, \tau)]}\ \overline{[(x)^2]}^{-1} \quad (12)$$

If in equation (6) $\epsilon(x, x', \tau)$ is neglected, the equation is linear; further, if $\bar{\beta}$ and μ are small, β_{eq} will also be small, hence the solution may be written:

$$\begin{aligned} x &= R(\tau)\cos[\omega_{eq}\tau + \theta(\tau)] \\ x' &= -\omega_{eq}R(\tau)\sin[\omega_{eq}\tau + \theta(\tau)] \end{aligned} \quad (13)$$

where R and θ are slowly varying functions of τ. Since R and θ are slowly varying quantities, the integrands in (11) and (12) may be replaced by their average values over one cycle. Hence

$$\beta_{eq} = \bar{\beta} + \overline{\left[\frac{1}{2\pi}\int_0^{2\pi} -\omega_{eq} R \sin\psi F(R\cos\psi, \mu, \tau)d\psi\right]}\ [{}^1/_2\omega_{eq}^2\overline{R^2}]^{-1} \quad (14)$$

$$\omega_{eq}^2 = \overline{\left[\frac{1}{2\pi}\int_0^{2\pi} R\cos\psi F(R\cos\psi, \mu, \tau)d\psi\right]}\ [{}^1/_2\overline{R^2}]^{-1} \quad (15)$$

where

$$\psi = [\omega_{eq}\tau + \theta] \quad (16)$$

Define

$$C(R) = \frac{1}{\pi}\int_0^{2\pi} \cos\psi\, F(R\cos\psi, \mu, \tau)d\psi \quad (17)$$

$$S(R) = \frac{1}{\pi}\int_0^{2\pi} \sin\psi F(R\cos\psi, \mu, \tau)d\psi \quad (18)$$

These integrals have been evaluated previously by the author[1]

Using (17) and (18) equations (14) and (15) become

$$\beta_{eq} = \bar{\beta} - \overline{[RS(R)]}[\omega_{eq}\overline{R^2}]^{-1} \quad (19)$$

$$\omega_{eq}^2 = \overline{[RC(R)]}[\overline{R^2}]^{-1} \quad (20)$$

If the process is an ergodic one, the time averages may be replaced by the stochastic averages, hence equations (19) and (20) may be written

$$\beta_{eq} = \bar{\beta} - \left[\int_0^\infty RS(R)P(R)dR\right]\left[\omega_{eq}\int_0^\infty R^2P(R)dR\right]^{-1} \quad (21)$$

$$\omega_{eq}^2 = \left[\int_0^\infty RC(R)P(R)dR\right]\left[\int_0^\infty R^2P(R)dR\right]^{-1} \quad (22)$$

[1] T. K. Caughey, "Sinusoidal Excitation of a System With Bilinear Hysteresis," see this issue of the JOURNAL OF APPLIED MECHANICS, pp. 640–643.

where $P(R)dR$ is the probability that R lies in the range R to $R + dR$.

If in equation (6) μ is set equal to zero, the equation is linear, and since $x_s(\tau)$ is Gaussian, $x(\tau)$ and $x'(\tau)$ will also be Gaussian. Further, if the damping is small, such that equations (4) and (5) hold, then the probability density function $(P)R$ will be the Rayleigh distribution. In the nonlinear system the statistics of the solution will not, in general, be Gaussian; however, if the nonlinearity is small the statistics will be approximately Gaussian.

Hence

$$P(R)dR \simeq \frac{R}{\sigma^2}\, e^{-R^2/2\sigma^2}\, dR \quad (23)$$

where

$$\sigma^2 = \overline{x^2} = \langle x^2\rangle_{avg}$$

Equations (21) and (22) now become

$$\beta_{eq} = \bar{\beta} - \left[\int_0^\infty \frac{R^2}{\sigma^2} S(R)e^{-R^2/2\sigma^2}dR\right]\left[\omega_{eq}\int_0^\infty \frac{R^2}{\sigma^2}\, e^{-R^2/2\sigma^2}\, dR\right]^{-1} \quad (24)$$

$$\omega_{eq}^2 = \left[\int_0^\infty \frac{R^2}{\sigma^2}\, C(R)e^{-R^2/2\sigma^2}\, dR\right]\left[\int_0^\infty \frac{R^2}{\sigma^2}\, e^{-R^2/2\sigma^2}\, dR\right]^{-1} \quad (25)$$

Evaluation of $S(R)$ and $C(R)$

Let

$$\cos\theta^* = \left(1 - \frac{x_0}{2R}\right) \quad (26)$$

Using Fig. 1, $S(R)$ and $C(R)$ may be evaluated readily

$$S(R) = \frac{2}{\pi}\left[\int_0^{\theta^*} [\mu x_0 - \mu R + R\cos\psi]\sin\psi d\psi + \int_{\theta^*}^{\pi} [-\mu x_0 + R(1-\mu)\cos\psi]\sin\psi d\psi\right] \quad (27)$$

Therefore

$$\left.\begin{aligned} S(R) &= -\frac{\mu R}{\pi}[\sin^2\theta^*] && R > x_0 \\ &= 0 && R < x_0 \end{aligned}\right\} \quad (28)$$

$$C(R) = \frac{2}{\pi}\left[\int_0^{\theta^*} [\mu x_0 - \mu R + R\cos\psi]\cos\psi d\psi + \int_{\theta^*}^{\pi} [-\mu x_0 + R(1-\mu)\cos\psi]\cos\psi d\psi\right] \quad (29)$$

Therefore

$$\left.\begin{aligned} C(R) &= \frac{R}{\pi}\left[\mu\theta^* + (1-\mu)\pi - \frac{\mu}{2}\sin 2\theta^*\right] && R > x_0 \\ &= R && R < x_0 \end{aligned}\right\} \quad (30)$$

Substituting (28) into (24)

$$\beta_{eq} = \bar{\beta} + \frac{1}{2\sigma^4\omega_{eq}}\int_{x_0}^\infty \frac{\mu R^2}{\pi}\sin^2\theta^* e^{-R^2/2\sigma^2}dR \quad (31)$$

Using (26), (31) may be integrated to give

$$\beta_{eq} = \bar{\beta} + \frac{2}{\sqrt{\pi}} \frac{\mu}{\omega_{eq}} \frac{x_0}{\sqrt{2}\sigma} \operatorname{erfc} \frac{x_0}{\sqrt{2}\sigma} \tag{32}$$

where erfc is the complimentary error function. Let

$$\begin{aligned} n &= \frac{\sqrt{2}\sigma_0}{x_0} \\ y &= \frac{\sigma}{\sigma_0} \\ \lambda &= n^2 y^2 \end{aligned} \tag{33}$$

where $\sigma_0 = \sqrt{\overline{x^2}}$ when $\mu = 0$. Using (33), (32) becomes

$$\beta_{eq} = \bar{\beta} + \frac{2\mu}{\sqrt{\pi}} \frac{1}{\omega_{eq}\lambda^{1/2}} \operatorname{erfc}\left(\frac{1}{\lambda^{1/2}}\right) \tag{34}$$

Equation (34) may be expressed in a more convenient form for plotting as

$$(\beta_{eq} - \bar{\beta})\omega_{eq}/\mu = 2(\pi\lambda)^{-1/2} \operatorname{erfc} (\lambda^{-1/2}) \tag{35}$$

The function defined by equation (35) is shown in Fig. 2. It will be observed that the function is zero when λ is zero, reaches its maximum at about λ equal to 3, then tends asymptotically to zero.

Substituting (30) into equation (25):

$$\omega_{eq}^2 = \frac{1}{2\pi\sigma^4}\left[\int_0^{x_0} R^2\pi e^{-R^2/2\sigma^2}\, dR + \int_{x_0}^{\infty} R^2[\pi - \mu(\pi - \theta^* + {}^1/_2 \sin 2\theta^*)]e^{-R^2/2\sigma^2} dR\right] \tag{36}$$

Let

$$R/x_0 = z \tag{37}$$

Substituting (37) into (36) and integrating the second term by parts, gives

$$\omega_{eq}^2 = 1 - \frac{8\mu}{\pi}\int_1^{\infty} [(z\lambda)^{-1}(z-1)^{1/2} + z^{-3}(z-1)^{1/2}]e^{-z^2/\lambda}\, dz \tag{38}$$

Equation (38) may be written in a more convenient form for plotting as

$$\frac{1 - \omega_{eq}^2}{\mu} = \frac{8}{\pi}\int_1^{\infty} [(z\lambda)^{-1}(z-1)^{1/2} + z^{-3}(z-1)^{1/2}]e^{-z^2/\lambda}\, dz \tag{39}$$

The integral (39) has been evaluated numerically and the results are plotted in Fig. 3. It will be observed that the function starts at zero for λ equal to zero, increases with λ, and tends asymptotically to 1 as λ tends to infinity.

Mean Squared Displacement

If in equation (6), the deficiency term $\epsilon(x, x', \tau)$ is neglected, the equation is linear and may be solved readily.

If $X(\omega)$ is the power spectrum of $x(\tau)$, $X_s(\omega)$ is the power spectrum of $x_s(\tau)$. Then

$$X(\omega) = \frac{X_s(\omega)}{[\omega_{eq}^2 - \omega^2]^2 + [\omega\beta_{eq}]^2} \tag{40}$$

$$\sigma^2 = \overline{x^2} = \int_0^{\infty} X(\omega)d\omega \tag{41}$$

If $x_s(\tau)$ has a white spectrum of density $4D$/cycle, then

$$\sigma^2 = \frac{D}{\omega_{eq}^2\beta_{eq}} \tag{42}$$

Let

$$D/\bar{\beta} = \sigma_0^2 = \overline{x^2}$$

when $\mu = 0$. Hence

$$\frac{\sigma^2}{\sigma_0^2} = y^2 = \frac{\bar{\beta}}{\omega_{eq}^2\beta_{eq}} \tag{43}$$

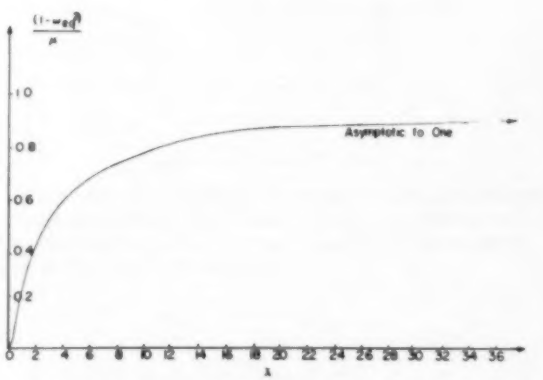

Fig. 3

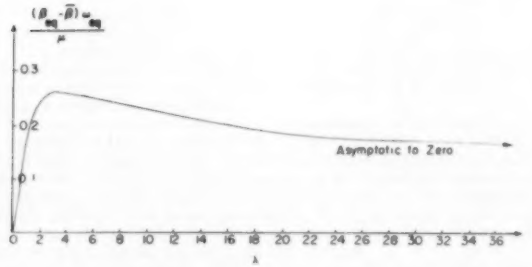

Fig. 2

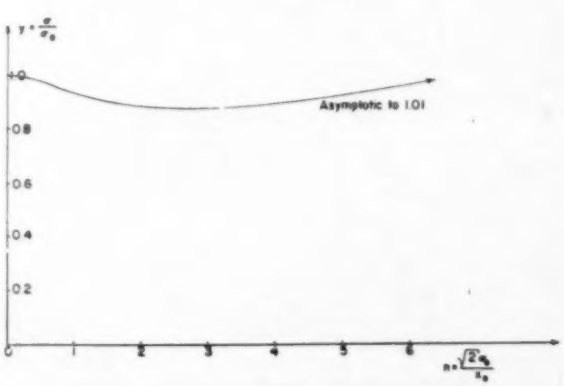

Fig. 4

Method of Solving Equation (43)

In (43), ω_{eq}^2 and β_{eq} are functions of $\lambda = n^2y^2$; therefore, assume a value of λ, obtain ω_{eq}^2 and β_{eq} from Figs. 2 and 3, solve (43) for y^2, then $n^2 = \lambda/y^2$. Repeat for different values of λ, plot y against n.

Results. Fig. 4 shows the results for the case where $\mu = \bar{\beta} = 0.02$. It will be observed that bilinear hysteresis has the following effects:

1 For small values of n, there is no effect.

2 For moderate values of n, there is an appreciable reduction in the rms deflection.

3 For large values of n, y tends asymptotically to $1/(1 - \mu)^{1/2}$.

Conclusions

From the foregoing analysis it will be seen that the effects of bilinear hysteresis are beneficial for small or moderately large random inputs. For large inputs, however, the effect of bilinear hysteresis is to increase root mean square deflection compared with that for the linear system $\mu = 0$. The explanation of this apparent paradox is that for large inputs, the damping tends asymptotically to the linear damping $\bar{\beta}$ while the effective stiffness of the system tends asymptotically to $(1 - \mu)$. The combination of damping $\bar{\beta}$ and stiffness $(1 - \mu)$ results in a mean squared deflection which is $1/(1 - \mu)$ times the mean squared deflection for the linear system ($\mu = 0$). In the case of an elastoplastic structure, $\mu = 1$, the results would be disastrous. It must therefore be concluded that too much reliance should not be placed in the usefulness of bilinear hysteresis as a means of increasing the effective damping in structures subjected to random excitation such as earthquakes.

YI-YUAN YU
Professor,
Department of Mechanical Engineering,
Polytechnic Institute of Brooklyn,
Brooklyn, N. Y.
Mem. ASME

Vibrations of Elastic Sandwich Cylindrical Shells[1]

Previous treatment of vibration of elastic sandwich plates [1–6][2] is extended in this paper to the vibration study of sandwich cylindrical shells. General theory is developed. Simplified equations are applied to the investigation of axially symmetric and torsional vibrations.

In a series of recent papers [1–6] theories of sandwich plates have been developed, and free and forced vibrations of sandwich plates have been investigated. It is the purpose of this paper to extend the treatment to sandwich cylindrical shells. In the following text we develop first a general theory of such shells, which is an extension of the new theory of sandwich plates in references [1] and [6], and from which simplified equations are deduced. On the basis of the latter equations, axially symmetric and torsional vibrations of the infinite sandwich cylindrical shell are investigated, and numerical examples are presented. As in the case of the homogeneous cylindrical shell [7], results for the infinite sandwich shell are also immediately applicable to the simply supported sandwich shell having a finite length.

In presenting the results for the infinite sandwich cylinder we shall concentrate on the frequency rather than the phase velocity, although the latter has been the object of investigation more often chosen by recent authors in discussing the dynamic behavior of the homogeneous cylindrical shell. In the homogeneous case the first three axially symmetric modes for long wave lengths are known to be longitudinal, radial, and thickness shear in nature. When the shell is of sandwich construction of the ordinary type, the cutoff frequency of the radial mode in general becomes higher, and that of the thickness-shear mode becomes lower; it thus becomes possible for the two modes to reverse their relative order near the cutoff. Such interesting features of the frequency spectrum of the sandwich cylindrical shell would not have been revealed, had the phase velocity instead of the frequency been chosen to be the object of our investigation.

Stress Equations of Motion

We consider the sandwich cylindrical shell whose cross-sectional dimensions are shown in Fig. 1. The two face layers have the same thickness and are composed of the same material. As usual, the thickness-radius ratio $2h/a$ is assumed small compared to unity. The displacements in the longitudinal (x), circumferential ($s = a\theta$), and radially outward directions are assumed to be

$$u_i(x, s, z, t) = u_i^{(0)}(x, s, t) + z u_i^{(1)}(x, s, t)$$

$$v_i(x, s, z, t) = v_i^{(0)}(x, s, t) + z v_i^{(1)}(x, s, t) \qquad (i = 1, 2, 3)$$

$$w_i(x, s, z, t) = w_i^{(0)}(x, s, t)$$

or

$$\begin{aligned} u_1 &= u + z\psi_1, & u_2, u_3 &= u \mp h_1(\psi_1 - \psi_2) + z\psi_2 \\ v_1 &= v + z\varphi_1, & v_2, v_3 &= v \mp h_1(\varphi_1 - \varphi_2) + z\varphi_2 \qquad (1) \\ & & w_1 &= w_2 = w_3 = w \end{aligned}$$

which are similar to those assumed for the sandwich plate [6] and in which the subscripts $i = 1, 2, 3$ refer to the core, inner, and outer face layers, respectively. The displacement components are then

$$\begin{aligned} u_1^{(0)} &= u, & u_2^{(0)}, u_3^{(0)} &= u \mp h_1(\psi_1 - \psi_2) \\ u_1^{(1)} &= \psi_1, & u_2^{(1)}, u_3^{(1)} &= \psi_2 \\ v_1^{(0)} &= v, & v_2^{(0)}, v_3^{(0)} &= v \mp h_1(\varphi_1 - \varphi_2) \qquad (2) \\ v_1^{(1)} &= \varphi_1, & v_2^{(1)}, v_3^{(1)} &= \varphi_2 \\ & & w_1^{(0)} &= w_2^{(0)} = w_3^{(0)} = w \end{aligned}$$

By substituting the displacements in the variational equations of motion in cylindrical co-ordinates and carrying out the integration with respect to z, the following equations of motion are obtained for the three individual layers:

$$\frac{\partial \sigma_{xi}^{(0)}}{\partial x} + \frac{\partial \tau_{sxi}^{(0)}}{\partial s} + [\tau_{rxi}]_{a_i}^{b_i} + \frac{1}{a}[z\tau_{rxi}]_{a_i}^{b_i} = \rho_i\left[b_i - a_i - \frac{b_i^2 - a_i^2}{2a}\right]\ddot{u}_i^{(0)} + \rho_i\left[\frac{b_i^2 - a_i^2}{2} + \frac{b_i^3 - a_i^3}{3a}\right]\ddot{u}_i^{(1)}$$

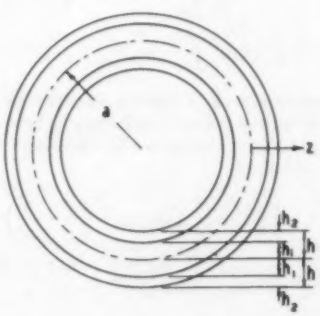

Fig. 1 Cross section of sandwich cylindrical shell. (Scale in thickness direction exaggerated.)

[1] This research, which was carried out when the author was a John Simon Guggenheim Fellow, was supported in part by the United States Air Force under Contract AF49(638)-453 monitored by the Air Force Office of Scientific Research.

[2] Numbers in brackets designate References at end of paper.

Contributed by the Applied Mechanics Division and presented at the Winter Annual Meeting, New York, N. Y., November 27–December 2, 1960, of The American Society of Mechanical Engineers.

Discussion of this paper should be addressed to the Secretary, ASME, 29 West 39th Street, New York, N. Y., and will be accepted until January 10, 1961, for publication at a later date. Discussion received after the closing date will be returned.

Manuscript received by ASME Applied Mechanics Division, February 3, 1960. Paper No. 60—WA-21.

$$\frac{\partial \sigma_{xs}^{(1)}}{\partial x} + \frac{\partial \tau_{zxs}^{(1)}}{\partial s} - \tau_{rzs}^{(0)} + [z\tau_{rxs}]_{a_i}^{b_i} + \frac{1}{a}[z^2\tau_{rzs}]_{a_i}^{b_i} = \rho_i\left[\frac{b_i^2 - a_i^2}{2} + \frac{b_i^3 - a_i^3}{3a}\right]\ddot{u}_i^{(0)} + \rho_i\left[\frac{b_i^3 - a_i^3}{3} + \frac{b_i^4 - a_i^4}{4a}\right]\ddot{u}_i^{(1)}$$

$$\frac{\partial \sigma_{ss}^{(0)}}{\partial s} + \frac{\partial \tau_{xss}^{(0)}}{\partial x} + \frac{\tau_{rss}^{(0)}}{a} + [\tau_{rss}]_{a_i}^{b_i} + \frac{1}{a}[z\tau_{rss}]_{a_i}^{b_i} = \rho_i\left[b_i - a_i + \frac{b_i^2 - a_i^2}{2a}\right]\ddot{v}_i^{(0)} + \rho_i\left[\frac{b_i^2 - a_i^2}{2} + \frac{b_i^3 - a_i^3}{3a}\right]\ddot{v}_i^{(1)} \qquad (i = 1, 2, 3) \quad (3)$$

$$\frac{\partial \sigma_{ss}^{(1)}}{\partial s} + \frac{\partial \tau_{xss}^{(1)}}{\partial x} - \tau_{rss}^{(0)} + [z\tau_{rss}]_{a_i}^{b_i} + \frac{1}{a}[z^2\tau_{rss}]_{a_i}^{b_i} = \rho_i\left[\frac{b_i^2 - a_i^2}{2} + \frac{b_i^3 - a_i^3}{3a}\right]\ddot{v}_i^{(0)} + \rho_i\left[\frac{b_i^3 - a_i^3}{3} + \frac{b_i^4 - a_i^4}{4a}\right]\ddot{v}_i^{(1)}$$

$$\frac{\partial \tau_{xrs}^{(0)}}{\partial x} + \frac{\partial \sigma_{srs}^{(0)}}{\partial s} - \frac{\sigma_{ss}^{(0)}}{a} + [\sigma_{rs}]_{a_i}^{b_i} + \frac{1}{a}[z^2\sigma_{rs}]_{a_i}^{b_i} = \rho_i\left[b_i - a_i + \frac{b_i^2 - a_i^2}{2a}\right]\ddot{w}_i^{(0)}$$

where $z = a_i, b_i$ refer to the inner and outer surfaces of the layer and the shell stresses with reference to the zsz-co-ordinate system are

$$\begin{aligned}
(\sigma_{xs}^{(0)}, \tau_{xzs}^{(0)}, \tau_{xrs}^{(0)}) &= \int_{a_i}^{b_i} (\sigma_{xi}, \tau_{xzi}, \tau_{xri})\left(1 + \frac{z}{a}\right) dz \\
(\sigma_{ss}^{(0)}, \tau_{sxs}^{(0)}, \tau_{srs}^{(0)}) &= \int_{a_i}^{b_i} (\sigma_{xi}, \tau_{xzi}, \tau_{xri}) dz \\
(\sigma_{xs}^{(1)}, \tau_{xzs}^{(1)}) &= \int_{a_i}^{b_i} (\sigma_{xi}, \tau_{xzi})\left(1 + \frac{z}{a}\right) z\, dz \\
(\sigma_{ss}^{(1)}, \tau_{sxs}^{(1)}) &= \int_{a_i}^{b_i} (\sigma_{xi}, \tau_{xzi}) z\, dz
\end{aligned} \qquad (4)$$

For the composite shell, equations (3) may be combined in such a way that the tractions at the interfaces between layers are eliminated. By further making use of equations (2), the following results are obtained:

$$\frac{\partial \sigma_x^{(0)}}{\partial x} + \frac{\partial \tau_{sx}^{(0)}}{\partial s} + \left[\left(1 + \frac{h}{a}\right)(\tau_{rx2})_h - \left(1 - \frac{h}{a}\right)(\tau_{rx2})_{-h}\right] = 2(\rho_1 h_1 + \rho_2 h_2)\ddot{u} + \left[\rho_1\frac{2h_1^3}{3a} + \rho_2\frac{h_1(h^2 - h_1^2)}{a}\right]\ddot{\psi}_1 + \rho_2\left[\frac{2(h^3 - h_1^3)}{3a} - \frac{h_1(h^2 - h_1^2)}{a}\right]\ddot{\psi}_2$$

$$\frac{\partial \sigma_s^{(0)}}{\partial s} + \frac{\partial \tau_{xs}^{(0)}}{\partial x} + \frac{\tau_{rs}^{(0)}}{a} + \left[\left(1 + \frac{h}{a}\right)(\tau_{rs2})_h - \left(1 - \frac{h}{a}\right)(\tau_{rs2})_{-h}\right] = 2(\rho_1 h_1 + \rho_2 h_2)\ddot{v} + \left[\rho_1\frac{2h_1^2}{3a} + \rho_2\frac{h_1(h^2 - h_1^2)}{a}\right]\ddot{\varphi}_1 + \rho_2\left[\frac{2(h^3 - h_1^3)}{3a} - \frac{h_1(h^2 - h_1^2)}{a}\right]\ddot{\varphi}_2$$

$$\frac{\partial \tau_{xr}^{(0)}}{\partial x} + \frac{\partial \sigma_r^{(0)}}{\partial s} - \frac{\sigma_s^{(0)}}{a} + \left[\left(1 + \frac{h}{a}\right)(\sigma_{r2})_h - \left(1 - \frac{h}{a}\right)(\sigma_{r2})_{-h}\right] = 2(\rho_1 h_1 + \rho_2 h_2)\ddot{w} \qquad (5)$$

$$\frac{\partial \sigma_x^{(1)}}{\partial x} + \frac{\partial \tau_{sx}^{(1)}}{\partial s} - \tau_{rx}^{(0)} + h\left[\left(1 + \frac{h}{a}\right)(\tau_{rx2})_h + \left(1 - \frac{h}{a}\right)(\tau_{rx2})_{-h}\right] = \left[\rho_1\frac{2h_1^3}{3a} + \rho_2\frac{2(h^3 - h_1^3)}{3a}\right]\ddot{u} + \left[\rho_1\frac{2h_1^3}{3} + \rho_2 h_1(h^2 - h_1^2)\right]\ddot{\psi}_1 + \rho_2\left[\frac{2(h^3 - h_1^3)}{3} + h_1(h^2 - h_1^2)\right]\ddot{\psi}_2$$

$$\frac{\partial \sigma_s^{(1)}}{\partial s} + \frac{\partial \tau_{xs}^{(1)}}{\partial x} - \tau_{rs}^{(0)} + h\left[\left(1 + \frac{h}{a}\right)(\tau_{rs2})_h + \left(1 - \frac{h}{a}\right)(\tau_{rs2})_{-h}\right] = \left[\rho_1\frac{2h_1^3}{3a} + \rho_2\frac{2(h^3 - h_1^3)}{3a}\right]\ddot{v} + \left[\rho_1\frac{2h_1^3}{3} + \rho_2 h_1(h^2 - h_1^2)\right]\ddot{\varphi}_1 + \rho_2\left[\frac{2(h^3 - h_1^3)}{3} + h_1(h^2 - h_1^2)\right]\ddot{\varphi}_2$$

$$\frac{\partial}{\partial x}[\sigma_{x1}^{(1)} + h_1(\sigma_{x3}^{(0)} - \sigma_{x2}^{(0)})] + \frac{\partial}{\partial s}[\tau_{xz1}^{(1)} + h_1(\tau_{xz3}^{(0)} - \tau_{xz2}^{(0)})] - \tau_{rz1}^{(0)} + h_1\left[\left(1 + \frac{h}{a}\right)(\tau_{rz3})_h + \left(1 - \frac{h}{a}\right)(\tau_{rz2})_{-h}\right] = \left[\rho_1\frac{2h_1^3}{3a} + \rho_2\frac{h_1(h^2 - h_1^2)}{a}\right]\ddot{u} + \left[\rho_1\frac{2h_1^2}{3} + 2\rho_2 h_1^2 h_2\right]\ddot{\psi}_1 + \rho_2[h_1(h^2 - h_1^2) - 2h_1^2 h_2]\ddot{\psi}_2$$

$$\frac{\partial}{\partial s}[\sigma_{z1}^{(1)} + h_1(\sigma_{z3}^{(0)} - \sigma_{z2}^{(0)})] + \frac{\partial}{\partial x}[\tau_{xz1}^{(1)} + h_1(\tau_{xz3}^{(0)} - \tau_{xz2}^{(0)})] - \tau_{rs1}^{(0)} + \frac{h_1}{a}(\tau_{rs3}^{(0)} - \tau_{rs2}^{(0)}) + h_1\left[\left(1 + \frac{h}{a}\right)(\tau_{rs3})_h + \left(1 - \frac{h}{a}\right)(\tau_{rs2})_{-h}\right]$$

$$= \left[\rho_1 \frac{2h_1^3}{3a} + \rho_2 \frac{h_1(h^2 - h_1^2)}{a}\right]\ddot{v} + \left[\rho_1 \frac{2h_1^3}{3} + 2\rho_2 h_1^2 h_2\right]\ddot{\varphi}_1 + \rho_2[h_1(h^2 - h_1^2) - 2h_1^2 h_2]\ddot{\varphi}_2$$

where

$$\sigma_x^{(0)} = \overset{\bullet}{\sigma}_{x1}^{(0)} + \sigma_{x2}^{(0)} + \sigma_{x3}^{(0)}, \quad \sigma_x^{(1)} = \sigma_{x1}^{(1)} + \sigma_{x2}^{(1)} + \sigma_{x3}^{(1)}, \ldots$$

In the axially symmetric case equations (5), with the surface-loading terms disregarded, reduce to

$$\begin{aligned}
\frac{\partial \sigma_x^{(0)}}{\partial x} &= 2(\rho_1 h_1 + \rho_2 h_2)\ddot{u} + \left[\rho_1 \frac{2h_1^3}{3a} + \rho_2 \frac{h_1(h^2 - h_1^2)}{a}\right]\ddot{\psi}_1 + \rho_2\left[\frac{2(h^2 - h_1^2)}{3a} - \frac{h_1(h^2 - h_1^2)}{a}\right]\ddot{\psi}_2 \\
\frac{\partial \tau_{xr}^{(0)}}{\partial x} - \frac{\sigma_s^{(0)}}{a} &= 2(\rho_1 h_1 + \rho_2 h_2)\ddot{w} \\
\frac{\partial \sigma_x^{(1)}}{\partial x} - \tau_{rs}^{(0)} &= \left[\rho_1 \frac{2h_1^3}{3a} + \rho_2 \frac{2(h^3 - h_1^3)}{3a}\right]\ddot{u} + \left[\rho_1 \frac{2h_1^3}{3} + \rho_2 h_1(h^2 - h_1^2)\right]\ddot{\psi}_1 + \rho_2\left[\frac{2(h^3 - h_1^3)}{3} + h_1(h^2 - h_1^2)\right]\ddot{\psi}_2 \\
\frac{\partial}{\partial x}[\sigma_{x1}^{(1)} + h_1(\sigma_{x3}^{(0)} - \sigma_{x2}^{(0)})] &- \tau_{rs1}^{(0)} = \left[\rho_1 \frac{2h_1^3}{3a} + \rho_2 \frac{h_1(h^2 - h_1^2)}{a}\right]\ddot{u} + \left[\rho_1 \frac{2h_1^3}{3} + 2\rho_2 h_1^2 h_2\right]\ddot{\psi}_1 + \rho_2[h_1(h^2 - h_1^2) - 2h_1^2 h_2]\ddot{\psi}_2
\end{aligned} \tag{6}$$

In the torsional case equations (5) yield

$$\begin{aligned}
\frac{\partial \tau_{xs}^{(0)}}{\partial x} + \frac{\tau_{sr}^{(0)}}{a} &= 2(\rho_1 h_1 + \rho_2 h_2)\ddot{v} + \left[\rho_1 \frac{2h_1^3}{3a} + \rho_2 \frac{h_1(h^2 - h_1^2)}{a}\right]\ddot{\varphi}_1 + \rho_2\left[\frac{2(h^2 - h_1^2)}{3a} - \frac{h_1(h^2 - h_1^2)}{a}\right]\ddot{\varphi}_2 \\
\frac{\partial \tau_{xs}^{(1)}}{\partial x} - \tau_{sr}^{(0)} &= \left[\rho_1 \frac{2h_1^3}{3a} + \rho_2 \frac{2(h^3 - h_1^3)}{3a}\right]\ddot{v} + \left[\rho_1 \frac{2h_1^3}{3} + \rho_2 h_1(h^2 - h_1^2)\right]\ddot{\varphi}_1 + \rho_2\left[\frac{2(h^3 - h_1^3)}{3} + h_1(h^2 - h_1^2)\right]\ddot{\varphi}_2 \\
\frac{\partial}{\partial x}[\tau_{xs1}^{(1)} + h_1(\tau_{xs3}^{(0)} - \tau_{xs2}^{(0)})] - \tau_{sr1}^{(0)} &+ \frac{h_1}{a}(\tau_{sr3}^{(0)} - \tau_{sr2}^{(0)}) = \left[\rho_1 \frac{2h_1^3}{3a} + \rho_2 \frac{h_1(h^2 - h_1^2)}{a}\right]\ddot{v} + \left[\rho_1 \frac{2h_1^3}{3} + 2\rho_2 h_1^2 h_2\right]\ddot{\varphi}_1 + \rho_2[h_1(h^2 - h_1^2) - 2h_1^2 h_2]\ddot{\varphi}_2
\end{aligned} \tag{7}$$

Stress-Strain Displacement Relations

To convert the stress equations of motion into displacement equations of motion, the relations between the shell stresses $\sigma_{xi}^{(0)}$, $\sigma_{xi}^{(1)}, \ldots$ and the shell displacements u, ψ_1, $\psi_2, \ldots$ are needed. We shall consider here only the stresses that are present in equations (6) of the symmetric case and (7) of the torsional case. The stresses in the general case may be considered in a similar manner.

First the shell stresses of the xsz-co-ordinate system are related to those of the xsz_i-co-ordinate systems. The latter systems are chosen in a similar manner as the rectangular co-ordinate systems used for sandwich plates [6]; namely, by taking

$$z = z_i + c_i$$

where

$$c_1 = 0, \quad c_2, c_3 = \mp\left(h_1 + \frac{h_2}{2}\right)$$

It may then be shown that the shell stresses in the two systems are related by

$$\begin{aligned}
\sigma_{xi}^{(0)} &= \frac{a_i}{a} N_{xi} \\
\sigma_{si}^{(0)} &= N_{si} \\
\tau_{xri}^{(0)} &= \frac{a_i}{a} Q_{xi} \\
\sigma_{xi}^{(1)} &= \frac{a_i}{a}(M_{xi} + c_i N_{xi})
\end{aligned} \tag{8}$$

where a_i are the radii of the middle surfaces of the individual layers and the shell stresses with reference to xsz_i-co-ordinate systems are defined by

$$\begin{aligned}
N_{xi} &= \int \sigma_{xi}\left(1 + \frac{z_i}{a_i}\right)dz_i \\
N_{si} &= \int \sigma_{si}\,dz_i \\
Q_{xi} &= \int \tau_{xri}\left(1 + \frac{z_i}{a_i}\right)dz_i \\
M_{xi} &= \int \sigma_{xi}\left(1 + \frac{z_i}{a_i}\right)z_i\,dz_i
\end{aligned}$$

the integrals being understood to be evaluated over the thickness of the layer.

Since N_{xi}, N_{si}, Q_{xi}, and M_{xi} refer to the individual layers, the relations for homogeneous cylindrical shells become valid. We may therefore write

$$\begin{aligned}
N_{xi} &= \epsilon_i t_i\left(e_{xi} + \nu_i e_{si} + \frac{t_i^2}{12a_i}k_{xi}\right) \\
N_{si} &= \epsilon_i t_i(e_{si} + \nu_i e_{xi}) \\
Q_{xi} &= \kappa_i \mu_i t_i e_{xri} \\
M_{xi} &= \epsilon_i I_i\left(k_{xi} + \frac{1}{a_i}e_{xi}\right)
\end{aligned} \tag{9}$$

where t_i is the thickness of the layer, I_i the moment of inertia, $\epsilon_i = E_i/(1 - \nu_i^2)$, κ_i the shear coefficient, and the strain components e_{xi}, e_{si}, e_{xri}, and k_{xi} have been introduced in the following manner:

$$\epsilon_{xi} = e_{xi} + z_i k_{xi}$$

$$\epsilon_{xi} = \frac{a_i}{r}\,\epsilon_{x1} \qquad (10)$$

$$\gamma_{xri} = e_{xri}$$

The final step is to relate the strain components to the shell displacements. This is done by making use of the usual strain-displacement relations, without the θ-dependent terms,

$$\epsilon_{xi} = \frac{\partial u_i}{\partial x}, \qquad \epsilon_{\theta i} = \frac{w_i}{r}, \qquad \gamma_{xri} = \frac{\partial u_i}{\partial z_i} + \frac{\partial w_i}{\partial x} \qquad (11)$$

By virtue of equations (10), (11), and (1), there results

$$\begin{aligned}
&e_{x1} = u' && e_{x2},\ e_{x3} = u' \mp (h_1\psi_1' + {}^1/_2 h_2\psi_2') \\
&k_{x1} = \psi_1' && k_{x2} = k_{x3} = \psi_2' \\
&e_{\theta 1} = \frac{w}{a} && e_{\theta 2},\ e_{\theta 3} = \frac{w}{a \mp (h_1 + {}^1/_2 h_2)} \\
&e_{xr1} = \psi_1 + w' && e_{xr2} = e_{xr3} = \psi_2 + w'
\end{aligned} \qquad (12)$$

where primes indicate differentiation with respect to x.

Through substitution of equations (12) in (9) and the result in (8), the stress combinations that are present in equations (6) are found to be

$$\begin{aligned}
\sigma_x^{(0)} &= 2(\epsilon_1 h_1 + \epsilon_3 h_2)u' + 2(\epsilon_1 h_1 \nu_1 + \epsilon_3 h_2 \nu_2)\frac{w}{a} \\
&\quad + \left[\epsilon_1 \frac{2h_1^3}{3} + \epsilon_2 h_1 h_2 (2h_1 + h_2)\right]\frac{1}{a}\,\psi_1' \\
&\quad + \epsilon_3 h_2^2 (h_1 + {}^2/_3 h_2)\,\frac{1}{a}\,\psi_2' \\
\sigma_\theta^{(0)} &= 2(\epsilon_1 h_1 \nu_1 + \epsilon_3 h_2 \nu_2)u' + 2(\epsilon_1 h_1 + \epsilon_3 h_2)\frac{w}{a} \\
\tau_{xr}^{(0)} &= 2\kappa_1 \mu_1 h_1 (\psi_1 + w') + 2\kappa_2 \mu_2 h_2 (\psi_2 + w') \\
\sigma_x^{(1)} &= \left[\epsilon_1 \frac{2h_1^3}{3} + 2\epsilon_3 h_2 \left(h_1 + \frac{h_2}{2}\right)^2\right]\frac{u'}{a} + \left[\epsilon_1 \frac{2h_1^3}{3}\right. \\
&\quad \left. + \epsilon_3 h_1 h_2 (2h_1 + h_2)\right]\psi_1' + \epsilon_3 h_2^2 (h_1 + {}^2/_3 h_2)\psi_2' \\
\sigma_{z1}^{(1)} &= \epsilon_1 \frac{2h_1^3}{3}\left(\frac{u'}{a} + \psi_1'\right) \\
\sigma_{z3}^{(0)} - \sigma_{z2}^{(0)} &= \epsilon_3 h_2 \left[(2h_1 + h_2)\frac{u'}{a} + 2h_1\psi_1' + h_2\psi_2'\right] \\
\tau_{xr1}^{(0)} &= 2\kappa_1 \mu_1 h_1 (\psi_1 + w')
\end{aligned} \qquad (13)$$

In a similar manner the stress combinations that are present in equations (7) are expressible in terms of the shell displacements as follows:

$$\begin{aligned}
\tau_{x\theta}^{(0)} &= 2(\mu_1 h_1 + \mu_2 h_2)v' \\
&\quad + \left[\mu_1 \frac{2h_1^3}{3} + \mu_2 h_1 h_2 (2h_1 + h_2)\right]\frac{\varphi_1'}{a} + \mu_2 h_2^2 (h_1 + {}^2/_3 h_2)\frac{\varphi_2'}{a} \\
\tau_{\theta r}^{(0)} &= 2\kappa_1 \mu_1 h_1 \left(\varphi_1 - \frac{v}{a}\right) \\
&\quad + 2\kappa_2 \mu_2 h_2 \left[\varphi_2 - \frac{v}{a} + \frac{1}{a^2}\left(h_1 + \frac{h_2}{2}\right)(h_1\varphi_1 + {}^1/_2 h_2\varphi_2)\right] \\
\tau_{x\theta}^{(1)} &= \left[\mu_1 \frac{2h_1^3}{3} + \mu_2 \frac{2(h^3 - h_1^3)}{3}\right]\frac{v'}{a} \\
&\quad + \left[\mu_1 \frac{2h_1^3}{3} + \mu_2 h_1 h_2 (2h_1 + h_2)\right]\varphi_1' + \mu_2 h_2^2 \left(h_1 + \frac{2h_2}{3}\right)\varphi_2' \qquad (14) \\
\tau_{x\theta 1}^{(1)} &= \mu_1 \frac{2h_1^3}{3}\left(\varphi_1' + \frac{v'}{a}\right) \\
\tau_{x\theta 3}^{(0)} - \tau_{x\theta 2}^{(0)} &= \mu_2 h_2 \left[(2h_1 + h_2)\frac{v'}{a} + 2h_1\varphi_1' + h_2\varphi_2'\right] \\
\tau_{\theta r 1}^{(0)} &= 2\kappa_1 \mu_1 h_1 \left(\varphi_1 - \frac{v}{a}\right) \\
\tau_{\theta r 3}^{(0)} - \tau_{\theta r 2}^{(0)} &= 2\kappa_2 \mu_2 h_2 \frac{1}{a}\left[\left(h_1 + \frac{h_2}{2}\right)\frac{v}{a}\right. \\
&\quad \left. - (h_1\varphi_1 + {}^1/_2 h_2\varphi_2)\right]
\end{aligned}$$

The reason for adopting the same coefficients κ_1 and κ_2 in the circumferential as in the longitudinal direction will become clear later.

Initial and Boundary Conditions

These conditions may be derived in a similar manner as were those for the sandwich plate [6]. The results for the complete set of equations (5) of the sandwich cylindrical shell are as follows: The initial conditions require the specification of the initial values of u, ψ_1, ψ_2, . . . and $\dot{u}$, $\dot{\psi}_1$, $\dot{\psi}_2$, ... The edge conditions at a circular section (x = const) require the specification of one member of each of the following seven products at each point of the section:

$$\sigma_x^{(0)}u, \qquad \tau_{x\theta}^{(0)}v, \qquad \tau_{xr}^{(0)}w$$

$$[\sigma_{x1}^{(1)} + h_1(\sigma_{x3}^{(0)} - \sigma_{x2}^{(0)})]\psi_1,$$

$$[\sigma_{x2}^{(1)} + \sigma_{x3}^{(1)} - h_1(\sigma_{x3}^{(0)} - \sigma_{x2}^{(0)})]\psi_2$$

$$[\tau_{x\theta 1}^{(1)} + h_1(\tau_{x\theta 3}^{(0)} - \tau_{x\theta 2}^{(0)})]\varphi_1,$$

$$[\tau_{x\theta 2}^{(1)} + \tau_{x\theta 3}^{(1)} - h_1(\tau_{x\theta 3}^{(0)} - \tau_{x\theta 2}^{(0)})]\varphi_2$$

The surface conditions require the specification of one member of each of the following five products at each point of the shell:

$$\left[\left(1 + \frac{h}{a}\right)(\tau_{rx3})_h - \left(1 - \frac{h}{a}\right)(\tau_{rx2})_{-h}\right]u$$

$$\left[\left(1 + \frac{h}{a}\right)(\tau_{rx3})_h + \left(1 - \frac{h}{a}\right)(\tau_{rx2})_{-h}\right](h_1\psi_1 + h_2\psi_2)$$

$$\left[\left(1 + \frac{h}{a}\right)(\tau_{r\theta 3})_h - \left(1 - \frac{h}{a}\right)(\tau_{r\theta 3})_{-h}\right]v$$

$$\left[\left(1 + \frac{h}{a}\right)(\tau_{r\theta 3})_h + \left(1 - \frac{h}{a}\right)(\tau_{r\theta 2})_{-h}\right](h_1\varphi_1 + h_2\varphi_2)$$

$$\left[\left(1 + \frac{h}{a}\right)(\sigma_{r3})_h - \left(1 - \frac{h}{a}\right)(\sigma_{r2})_{-h}\right]w$$

Displacement Equations of Motion

For the axially symmetric case these are obtained by substituting equations (13) in (6); thus,

$$2(\epsilon_1 h_1 + \epsilon_3 h_2)u'' + \left[\epsilon_1 \frac{2h_1^3}{3} + \epsilon_3 h_1 h_2 (2h_1 + h_2)\right]\frac{1}{a}\,\psi_1'' + \epsilon_3 h_2^2 (h_1 + {}^2/_3 h_2)\frac{1}{a}\,\psi_2'' + 2(\epsilon_1 h_1 \nu_1 + \epsilon_3 h_2 \nu_2)\frac{w'}{a}$$

$$= 2(\rho_1 h_1 + \rho_3 h_2)\ddot{u} + \left[\rho_1 \frac{2h_1^3}{3} + \rho_3 h_1 h_2(2h_1 + h_2)\right]\frac{1}{a}\ddot{\psi}_1 + \rho_3 h_2^2(h_1 + {}^1/_3 h_2)\frac{1}{a}\ddot{\psi}_2$$

$$2\kappa_1\mu_1 h_1(\psi_1' + w'') + 2\kappa_3\mu_3 h_2(\psi_2' + w'') - 2(\epsilon_1 h_1\nu_1 + \epsilon_3 h_2\nu_2)\frac{u'}{a} - 2(\epsilon_1 h_1 + \epsilon_3 h_2)\frac{w}{a^2} = 2(\rho_1 h_1 + \rho_1 h_2)\ddot{w}$$

$$\left[\epsilon_1 \frac{2h_1^3}{3} + \epsilon_3 \frac{2(h^3 - h_1^3)}{3}\right]\frac{u''}{a} + \left[\epsilon_1 \frac{2h_1^3}{3} + \epsilon_3 h_1 h_2(2h_1 + h_2)\right]\psi_1'' + \epsilon_3 h_2^2(h_1 + {}^2/_3 h_2)\psi_2'' - 2\kappa_1\mu_1 h_1(\psi_1 + w') - 2\kappa_3\mu_3 h_2(\psi_2 + w') = \left[\rho_1 \frac{2h_1^3}{3} + \rho_2 \frac{2(h^3 - h_1^3)}{3}\right]\frac{\ddot{u}}{a} + \left[\rho_1 \frac{2h_1^3}{3} + \rho_3 h_1 h_2(2h_1 + h_2)\right]\ddot{\psi}_1 + \rho_3 h_2^2(h_1 + {}^2/_3 h_2)\ddot{\psi}_2 \tag{15}$$

$$\left[\epsilon_1 \frac{2h_1^3}{3} + \epsilon_3 h_1 h_2(2h_1 + h_2)\right]\frac{u''}{a} + \left[\epsilon_1 \frac{2h_1^3}{3} + 2\epsilon_3 h_1^2 h_2\right]\psi_1'' + \epsilon_3 h_1 h_2^2\psi_2'' - 2\kappa_1\mu_1 h_1(\psi_1' + w') = \left[\rho_1 \frac{2h_1^3}{3} + \rho_3 h_1 h_2(2h_1 + h_2)\right]\frac{\ddot{u}}{a} + \left[\rho_1 \frac{2h_1^3}{3} + 2\rho_3 h_1^2 h_2\right]\ddot{\psi}_1 + \rho_3 h_1 h_2^2\ddot{\psi}_2$$

Similarly, substitution of equations (14) in (7) results in the following displacement equations of motion for the case of torsion:

$$2(\mu_1 h_1 + \mu_3 h_2)w'' + \left[\mu_1 \frac{2h_1^3}{3} + \mu_3 h_1 h_2(2h_1 + h_2)\right]\frac{1}{r}\varphi_1'' + \mu_3 h_2^2(h_1 + {}^1/_3 h_2)\frac{1}{a}\varphi_2'' + 2\kappa_1\mu_1 h_1\frac{1}{a}\left(\varphi_1 - \frac{v}{a}\right) + 2\kappa_3\mu_3 h_2\frac{1}{a}\left[\varphi_2 - \frac{v}{a} + \frac{1}{a^2}\left(h_1 + \frac{h_2}{2}\right)(h_1\varphi_1 + {}^1/_3 h_2\varphi_2)\right] = 2(\rho_1 h_1 + \rho_3 h_2)\ddot{w} + \left[\rho_1 \frac{2h_1^3}{3} + \rho_3 h_1 h_2(2h_1 + h_2)\right]\frac{1}{a}\ddot{\varphi}_1 + \rho_3 h_2^2(h_1 + {}^2/_3 h_2)\frac{1}{a}\ddot{\varphi}_2$$

$$\left[\mu_1 \frac{2h_1^3}{3} + \mu_3 \frac{2(h^3 - h_1^3)}{3}\right]\frac{v''}{a} + \left[\mu_1 \frac{2h_1^3}{3} + \mu_3 h_1 h_2(2h_1 + h_2)\right]\varphi_1'' + \mu_3 h_2^2\left(h_1 + \frac{2h_2}{3}\right)\varphi_2'' - 2\kappa_1\mu_1 h_1\left(\varphi_1 - \frac{v}{a}\right) - 2\kappa_3\mu_3 h_2\left[\varphi_2 - \frac{v}{a} + \frac{1}{a^2}\left(h_1 + \frac{h_2}{2}\right)(h_1\varphi_1 + {}^1/_3 h_2\varphi_2)\right] = \left[\rho_1 \frac{2h_1^3}{3} + \rho_2 \frac{2(h^3 - h_1^3)}{3}\right]\frac{\ddot{v}}{a} + \left[\rho_1 \frac{2h_1^3}{3} + \rho_3 h_1 h_2(2h_1 + h_2)\right]\ddot{\varphi}_1 + \rho_3 h_2^2\left(h_1 + \frac{2h_2}{3}\right)\ddot{\varphi}_2 \tag{16}$$

$$\left[\mu_1 \frac{2h_1^3}{3} + \mu_3 h_1 h_2(2h_1 + h_2)\right]\frac{v''}{a} + \left[\mu_1 \frac{2h_1^3}{3} + 2\mu_3 h_1^2 h_2\right]\varphi_1'' + \mu_3 h_1 h_2^2\varphi_2'' - 2\kappa_1\mu_1 h_1\left(\varphi_1 - \frac{v}{a}\right) + 2\kappa_3\mu_3 h_2\left[\frac{1}{a^2}h_1\left(h_1 + \frac{h_2}{2}\right)\frac{v}{a} - \frac{h_1}{a^2}(h_1\varphi_1 + {}^1/_3 h_2\varphi_2)\right] = \left[\rho_1 \frac{2h_1^3}{3} + \rho_3 h_1 h_2(2h_1 + h_2)\right]\frac{\ddot{v}}{a} + \left[\rho_1 \frac{2h_1^3}{3} + 2\rho_3 h_1^2 h_2\right]\ddot{\varphi}_1 + \rho_3 h_1 h_2^2\ddot{\varphi}_2$$

When h_1 or $h_2 = 0$, equations (15) and (16) reduce, respectively, to the displacement equations of motion for symmetric and torsional motions of the homogeneous cylindrical shell. On the other hand, as $a \to \infty$, the last three of equations (15) and the last two of (16) become the flexural equations of sandwich plates without the y-dependent terms. The first equations of (15) and (16) reduce to the extensional equations of sandwich plates of the classical type.

Simplified Equations

When the face layers of the sandwich cylindrical shell are very thin, the equations of motion may be simplified in exactly the same manner as were those of the sandwich plate [5, 6]. In such a case the third and fourth of equations (6) or (15) become practically the same, and equations (15) reduce to

$$2(\epsilon_1 h_1 + \epsilon_3 h_2)u'' + \left(\epsilon_1 \frac{2h_1^3}{3} + 2\epsilon_3 h_1^2 h_2\right)\frac{1}{a}\psi_1'' + 2(\epsilon_1 h_1\nu_1 + \epsilon_3 h_2\nu_2)\frac{1}{a}w' = 2(\rho_1 h_1 + \rho_3 h_2)\ddot{u} + \left(\rho_1 \frac{2h_1^3}{3} + 2\rho_3 h_1^2 h_2\right)\frac{1}{a}\ddot{\psi}_1$$

$$2\kappa_1\mu_1 h_1(\psi_1' + w'') - 2(\epsilon_1 h_1\nu_1 + \epsilon_3 h_2\nu_2)\frac{1}{a}u' - 2(\epsilon_1 h_1 + \epsilon_3 h_2)\frac{1}{a^2}w = 2(\rho_1 h_1 + \rho_3 h_2)\ddot{w} \tag{17}$$

$$\left(\epsilon_1 \frac{2h_1^3}{3} + 2\epsilon_3 h_1^2 h_2\right)\left(\frac{u''}{a} + \psi_1''\right) - 2\kappa_1\mu_1 h_1(\psi_1 + w') = \left(\rho_1 \frac{2h_1^3}{3} + 2\rho_3 h_1^2 h_2\right)\left(\frac{\ddot{u}}{a} + \ddot{\psi}_1\right)$$

Comparing with equations (15) we see that ψ_2 has been omitted. Similar to the equations of sandwich plates [5], equations (17) may be modified and improved by further replacing $2h_1^2h_2$ by $2h_2(h_1 + h_2/2)^2$, or, more simply, by $2h_2(h_1^2 + h_1h_2)$ or $2h_1h_2h$; thus,

Equations (17) with $2h_1^2h_2$ replaced by $2h_1h_2h$ (18)

The torsional equations (16) may be simplified in the same manner. Thus we find

$$2(\mu_1 h_1 + \mu_3 h_2)w'' + \left(\mu_1 \frac{2h_1^3}{3} + 2\mu_3 h_1^2 h_2\right)\frac{1}{a}\varphi_1''$$

$$+ 2\kappa_1\mu_1 h_1 \frac{1}{a}\left(\varphi_1 - \frac{v}{a}\right) = 2(\rho_1 h_1 + \rho_2 h_2)\ddot{v} + \left(\rho_1 \frac{2h_1^3}{3} + 2\rho_2 h_1^2 h_2\right)\frac{1}{a}\ddot{\varphi} \quad (19)$$

$$\left(\mu_1 \frac{2h_1^3}{3} + 2\mu_2 h_1^2 h_2\right)\left(\frac{v''}{a} + \varphi''\right) - 2\kappa_1\mu_1 h_1\left(\varphi_1 - \frac{v}{a}\right) = \left(\rho_1 \frac{2h_1^3}{3} + 2\rho_2 h_1^2 h_2\right)\left(\frac{\ddot{v}}{a} + \ddot{\varphi}\right)$$

With $2h_1^2h_2$ in equations (19) replaced by $2h_1h_2h$ we further have the modified and improved version:

Equations (19) with $2h_1^2h_2$ replaced by $2h_1h_2h$ (20)

Equations (17) to (20) are analogous to the corresponding equations of the homogeneous cylindrical shell, just as the simplified sandwich-plate equations are analogous to the homogeneous-plate equations [5, 6]. They are expected to be applicable to frequency ranges somewhat lower than those that can be covered by the more complete equations (15) and (16), also as the simplified sandwich-plate equations [5].

Determination of κ_1 and κ_2

The coefficients κ_1 and κ_2 are determined by matching the simple thickness-shear frequencies calculated from the sandwich-shell theory with those from the exact theory of elasticity. For this purpose solutions are first derived from the latter theory, in the same manner as for the sandwich plate [2]. The frequency equation for the thickness-shear motion in the longitudinal direction is found to be

$$[(r_\rho r_\mu)^{1/2}K_1J_0(\beta_1 r_{12}) - J_1(\beta_1 r_{12})][(r_\rho r_\mu)^{1/2}K_2Y_0(\beta_1 r_{12}) - Y_1(\beta_1 r_{12})] - [(r_\rho r_\mu)^{1/2}K_2J_0(\beta_1 r_{12}) - J_1(\beta_1 r_{12})][(r_\rho r_\mu)^{1/2}K_1Y_0(\beta_1 r_{12}) - Y_1(\beta_1 r_{12})] = 0 \quad (21)$$

where

$$K_1 = \frac{J_1(\beta_2 r_{12})Y_1(\beta_2 r_2) - J_1(\beta_2 r_2)Y_1(\beta_2 r_{12})}{J_0(\beta_2 r_{12})Y_1(\beta_2 r_2) - J_1(\beta_2 r_2)Y_0(\beta_2 r_{12})}$$

$$K_2 = \frac{J_1(\beta_2 r_{12})Y_1(\beta_2 r_h) - J_1(\beta_2 r_h)Y_1(\beta_2 r_{12})}{J_0(\beta_2 r_{12})Y_1(\beta_2 r_h) - J_1(\beta_2 r_h)Y_0(\beta_2 r_{12})}$$

and

$$r_\rho = \rho_2/\rho_1, \quad r_\mu = \mu_2/\mu_1, \quad \beta_1 = \omega(\rho_1/\mu_1)^{1/2}, \quad \beta_2 = \omega(\rho_2/\mu_2)^{1/2}$$

$$r_{12} = a - h_1, \quad r_{12} = a + h_1, \quad r_2 = a - h, \quad r_h = a + h$$

For thin cylindrical shells for which $2h/a \ll 1$, equation (21) is reducible to

$$r_\rho r_\mu \tan^2\left[f\left(\frac{r_\rho r_h^2}{r_\mu}\right)^{1/2}\right]\tan 2f - 2(r_\rho r_\mu)^{1/2}\tan\left[f\left(\frac{r_\rho r_h^2}{r_\mu}\right)^{1/2}\right] - \tan 2f = 0 \quad (22)$$

where

$$r_h = \frac{h_2}{h_1}, \qquad f = \frac{1}{1 + r_h}\left(\frac{\rho_1}{\mu_1}\omega^2 h^2\right)^{1/2}$$

For ordinary sandwiches for which $(r_\rho r_h^2/r_\mu) \ll 1$ so that

$$\tan\left[f\left(\frac{r_\rho r_h^2}{r_\mu}\right)^{1/2}\right]$$

may be replaced by

$$f\left(\frac{r_\rho r_h^2}{r_\mu}\right)^{1/2},$$

equation (22) becomes

$$\tan 2f = \frac{2r_\rho r_h f}{(r_\rho r_h f)^2 - 1} \quad (23)$$

Assume further that $r_\rho r_h$ is large enough so that $(r_\rho r_h f)^2 \gg 1$, and $\tan 2f \approx 2\tan f$, which implies that $\tan^2 f \ll 1$; then the frequency equation takes the final form

$$f\tan f = \frac{1}{r_\rho r_h} \quad (24)$$

which is the same as the result for the sandwich plate [2].

On the basis of the equations of motion (15) of the sandwich cylindrical-shell theory, the frequency equation for the simple thickness-shear mode is found to be

$$\frac{r_\rho r_h^2}{r_\mu}(3r_\rho r_h + 4)f^4 - 12\left[\kappa_1\frac{r_\rho r_h^2}{r_\mu} + \kappa_2(3r_\rho r_h + 1)\right]f^2 + 36\kappa_1\kappa_2 = 0 \quad (25)$$

which is also the same as the corresponding result for the sandwich plate [2, 6]. On the basis of the simplified equations (17) or (18), the frequency equation is again the same as that for the sandwich plate [5].

The situation is now as follows: For thin cylindrical shells of ordinary sandwich construction for which

$$\frac{2h}{a} \ll 1, \qquad \frac{r_\rho r_h^2}{r_\mu} \ll 1$$

κ_1 and κ_2 should be determined in such a way that the two roots of f of equation (25) be made, respectively, the same as the two lowest roots of f of equation (23). If $r_\rho r_h$ is further large enough so that

$$(r_\rho r_h f)^2 \gg 1, \qquad \tan^2 f \ll 1$$

then the situation becomes entirely the same as for the sandwich plate; that is, when equations (15) are employed, roots of f of equation (25) should be matched with the two lowest roots of (24). When equations (17) are employed, κ_1 is given by

$$\kappa_1 = (r_\rho r_h + 1/3)f^2 \quad (26)$$

which may also be adopted for use with equations (15) where κ_2 may be taken equal to κ_1 as was done in reference [2]. Finally, when equations (18) are used, κ_1 is given by

$$\kappa_1 = [(1 + r_h)r_\rho r_h + 1/3]f^2 \quad (27)$$

In both equations (26) and (27) f is the lowest root of equation (24). On the basis of (26) and (27) it may be shown that, when $r_\rho r_h > 2$, we may take $\kappa_1 = 1$ without appreciable error.

The simple thickness-shear mode in the circumferential direction of the cylindrical shell may be investigated similarly. From the exact theory of elasticity the frequency equation may be shown to be reducible to equation (22) for thin shells. From equations (16) of the sandwich-shell theory the frequency equation may be shown to be reducible to equation (25). The results for the circumferential thickness-shear mode of thin sandwich cylindrical shells therefore become entirely the same as those for the longitudinal thickness-shear mode. For this reason, only one set of the coefficients κ_1 and κ_2 has been chosen to be used in the expressions of both Q_{xi} and $Q_{\varphi i}$.

Symmetric Vibration of Infinite Sandwich Cylindrical Shell

For simplicity the investigation will be based upon the simplified equations (18). By the usual procedure the frequency equation is found to be

$$\frac{1}{2\kappa_1\mu_1 h_1}\,4(\rho_1h_1+\rho_2h_2)^2\left(\rho_1\frac{2h_1^3}{3}+2\rho_2h_1h_2h\right)\omega^6$$
$$-\left[\left\{\left(\rho_1\frac{2h_1^3}{3}+2\rho_2h_1h_2h\right)\left(1+\frac{2(\epsilon_1h_1+\epsilon_2h_2)}{2\kappa_1\mu_1h_1}\right)\right.\right.$$
$$+\frac{2(\rho_1h_1+\rho_2h_2)}{2\kappa_1\mu_1h_1}\left(\epsilon_1\frac{2h_1^3}{3}+2\epsilon_2h_1h_2h\right)\Big\}\frac{\lambda^2}{a^2}$$
$$+\left\{2(\rho_1h_1+\rho_2h_2)+\frac{2(\epsilon_1h_1+\epsilon_2h_2)}{2\kappa_1\mu_1h_1}\right.$$
$$\left.\left(\rho_1\frac{2h_1^3}{3}+2\rho_2h_1h_2h\right)\frac{1}{a^2}\right\}\Big]2(\rho_1h_1+\rho_2h_2)\lambda\omega^4$$
$$+\left[\left\{2(\rho_1h_1+\rho_2h_2)\left(\epsilon_1\frac{2h_1^3}{3}+2\epsilon_2h_1h_2h\right)\left(1+\frac{2(\epsilon_1h_1+\epsilon_2h_2)}{2\kappa_1\mu_1h_1}\right)\right.\right.$$
$$+2(\epsilon_1h_1+\epsilon_2h_2)\left(\rho_1\frac{2h_1^3}{3}+2\rho_2h_1h_2h\right)\Big\}\frac{\lambda^4}{a^4}$$
$$+\left\{2(\rho_1h_1+\rho_2h_2)2(\epsilon_1h_1+\epsilon_2h_2)\right.$$
$$+\frac{1}{2\kappa_1\mu_1h_1}2(\rho_1h_1+\rho_2h_2)2(\epsilon_1h_1+\epsilon_2h_2)\left(\epsilon_1\frac{2h_1^3}{3}+2\epsilon_2h_1h_2h\right)\frac{1}{a^2}$$
$$+\frac{1}{2\kappa_1\mu_1h_1}\left(\rho_1\frac{2h_1^3}{3}+2\rho_2h_1h_2h\right)\Big[4(\epsilon_1h_1+\epsilon_2h_2)^2$$
$$\left.-4(\epsilon_1h_1\nu_1+\epsilon_2h_2\nu_2)^2\Big]\frac{1}{a^2}\right\}\frac{\lambda^2}{a^2}$$
$$+2(\rho_1h_1+\rho_2h_2)\cdot2(\epsilon_1h_1+\epsilon_2h_2)\frac{1}{a^2}\Big]\omega^2$$
$$-\left[2(\epsilon_1h_1+\epsilon_2h_2)\left(\epsilon_1\frac{2h_1^3}{3}+2\epsilon_2h_1h_2h\right)\frac{\lambda^6}{a^6}\right.$$
$$+\left(\epsilon_1\frac{2h_1^3}{3}+2\epsilon_2h_1h_2h\right)\left\{\frac{4(\epsilon_1h_1+\epsilon_2h_2)^2-4(\epsilon_1h_1\nu_1+\epsilon_2h_2\nu_2)^2}{2\kappa_1\mu_1h_1}\right.$$
$$\left.\left.-4(\epsilon_1h_1\nu_1+\epsilon_2h_2\nu_2)^2\right\}\frac{1}{a^2}\frac{\lambda^4}{a^4}+\{4(\epsilon_1h_1+\epsilon_2h_2)^2\right.$$
$$\left.-4(\epsilon_1h_1\nu_1+\epsilon_2h_2\nu_2)^2\right\}\frac{1}{a^2}\frac{\lambda^2}{a^2}\Big]=0 \quad (28)$$

or, written in terms of the various ratios which were used before for sandwich plates,

$$\frac{r_1}{\kappa_1}(1+r_\rho r_h)^2[1+3r_\rho r_h(1+r_h)]k\Omega^2$$
$$-\left[\left\{[1+3r_\rho r_h(1+r_h)]\left[1+\frac{r_1+r_2r_h}{\kappa_1}\right]\right.\right.$$
$$+\frac{1+r_\rho r_h}{\kappa_1}[r_1+3r_2r_h(1+r_h)]\Big\}k\lambda^2+\Big\{(1+r_h)^2(1+r_\rho r_h)$$
$$\left.+\frac{r_1+r_2r_h}{\kappa_1}[1+3r_\rho r_h(1+r_h)]k\right\}\Big](1+r_\rho r_h)\Omega^2$$
$$+\left[\left\{(1+r_\rho r_h)\left[1+3\frac{r_2}{r_1}r_h(1+r_h)\right]\left[1+\frac{r_1+r_2r_h}{\kappa_1}\right]\right.\right.$$
$$\left.\left.+\left(1+\frac{r_2r_h}{r_1}\right)[1+3r_\rho r_h(1+r_h)]\right\}k\lambda^4\right.$$
$$+\left\{(1+r_h)^2(1+r_\rho r_h)\left(1+\frac{r_2r_h}{r_1}\right)\right.$$
$$+(1+r_\rho r_h)\frac{r_1+r_2r_h}{\kappa_1}\left[1+3\frac{r_2}{r_1}r_h(1+r_h)\right]k$$
$$+\frac{1}{\kappa_1}[1+3r_\rho r_h(1+r_h)]\{(r_1+r_2r_h)^2$$
$$\left.-(r_1\nu_1+r_2r_h\nu_2)^2]\frac{k}{r_1}\right\}\lambda^2$$
$$+(1+r_h)^2(1+r_\rho r_h)\left(1+\frac{r_2r_h}{r_1}\right)\Big]\Omega$$
$$-\left\{\left(1+\frac{r_2}{r_1}r_h\right)\left[1+3\frac{r_2}{r_1}r_h(1+r_h)\right]k\lambda^6\right.$$
$$+\left[1+3\frac{r_2}{r_1}r_h(1+r_h)\right]$$
$$\left[\frac{(r_1+r_2r_h)^2-(r_1\nu_1+r_2r_h\nu_2)^2}{\kappa_1r_1}-\frac{2(r_1\nu_1+r_2r_h\nu_2)}{r_1}\right]k\lambda^4$$
$$\left.+(1+r_h)^2\left[\left(1+\frac{r_2r_h}{r_1}\right)^2-\left(\nu_1+\frac{r_2}{r_1}r_h\nu_2\right)^2\right]\lambda^2\right\}=0 \quad (29)$$

where

$$r_1=\frac{\epsilon_1}{\mu_1},\qquad r_2=\frac{\epsilon_2}{\mu_1}$$
$$k=\frac{h^2}{3a^2},\qquad \Omega=\frac{\rho_1}{\epsilon_1}a^2\omega^2,\qquad \lambda=\frac{2\pi a}{L}$$

L is the wave length, and $\sqrt{\Omega}$ is proportional to the frequency. Being cubic in Ω, equation (28) or (29) involves three modes. When $r_h=0$, they reduce to the result of the homogeneous cylindrical shell.

A study of the cutoff frequencies presents great interest, since they are the lowest frequencies of the various modes. By putting $\lambda=0$, equation (29) redues to

$$\frac{r_1}{\kappa_1}(1+r_\rho r_h)[1+3r_\rho r_h(1+r_h)]k\Omega^2$$
$$-\left\{(1+r_h)^2(1+r_\rho r_h)+\frac{1}{\kappa_1}(r_1+r_2r_h)[1+3r_\rho r_h(1+r_h)]k\right\}\Omega^2$$
$$+\frac{1}{r_1}(1+r_h)^2(r_1+r_2r_h)\Omega=0 \quad (30)$$

which has the roots

$$\sqrt{\Omega}=0 \qquad \text{(longitudinal)}$$
$$\sqrt{\Omega}=\left(\frac{1}{r_1}\frac{r_1+r_2r_h}{1+r_\rho r_h}\right)^{1/2} \qquad \text{(radial)} \quad (31)$$
$$\sqrt{\Omega}=\left[\frac{\kappa_1}{kr_1}\frac{(1+r_h)^2}{1+3r_\rho r_h(1+r_h)}\right]^{1/2} \qquad \text{(thickness-shear)}$$

When $r_h=0$, these become in order

$$\sqrt{\Omega}=0,\quad 1,\quad \left(\frac{\kappa_1}{kr_1}\right)^{1/2} \quad (32)$$

which are the results for the homogeneous cylindrical shell made of the core material and in which κ_1 now takes the value of $\pi^2/12$. The zero frequency in equations (31) and (32) corresponds to the translation of the cylindrical shell as a whole in the longitudinal direction. The second cutoff frequency in each of these equations corresponds to the purely radial motion of the cylinder vibrating

in the mode of a ring. Since $r_2/r_1 > r_\rho$ for ordinary sandwiches, the second cutoff frequency is higher in the sandwich case than in the homogeneous case. The third cutoff frequencies in equations (31) and (32) are the simple thickness-shear frequencies. In spite of the slight increase in value of κ_1 in the sandwich case, the thickness-shear frequency is much lower than that in the homogeneous case, approximately in the ratio of $1/(1 + 3r_\rho r_h)^{1/2}$.

It is interesting to note the relative magnitudes of the two nonzero cutoff frequencies in equations (31), one of which is independent of the thickness-radius ratio (contained in k) but the other is not. The value of k for the two frequencies to be equal to each other is easily found to be

$$k = \kappa_1 \frac{(1 + r_h)^2}{1 + 3r_\rho r_h(1 + r_h)} \frac{1 + r_\rho r_h}{r_1 + r_2 r_h}$$

For k smaller than this critical value, i.e., thinner shells, the thickness-shear frequency is the highest cutoff frequency. For k greater than this, the shear frequency is only the second highest. The change in order is possible for sandwich cylindrical shells of the ordinary type, which makes it important to include the thickness-shear mode in the sandwich-shell theory. According to equations (32) for homogeneous shells, similar change in order would occur at $k = \kappa_1/r_1 = \pi^2(1 - \nu_1)/24$. Since k is actually much smaller than 1, such change in order will not take place in the case of homogeneous shells.

It is also interesting to examine the effect of curvature, the elimination of which reduces equation (30) to

$$\frac{r_1}{\kappa_1}[1 + 3r_\rho r_h(1 + r_h)]k\Omega^2 - (1 + r_h)^2\Omega^2 = 0$$

This is now for the sandwich plate, and the roots are

$$\sqrt{\Omega} = 0,\ 0,\ \left[\frac{\kappa_1}{kr_1}\frac{(1 + r_h)^2}{1 + 3r_\rho r_h(1 + r_h)}\right]^{1/2}$$

One of the two zero frequencies corresponds to the longitudinal translation of the plate as a whole, as in the case of the shell. The other zero frequency corresponds to the transverse translation of the plate as a whole, which is a degenerate case of the radial motion of the cylindrical shell. The expression of the thickness-shear frequency is the same for sandwich plates as for sandwich cylindrical shells. This frequency is thus independent of the radius a even in the latter case, which is true because of the assumption of a thin shell.

As $\lambda \to \infty$, namely, as the wave length shortens, equation (29) reduces to

$$\begin{aligned}\frac{r_1}{\kappa_1}(1 + r_\rho r_h)^2[1 + 3r_\rho r_h(1 + r_h)]\Omega^2 \\ - \left\{[1 + 3r_\rho r_h(1 + r_h)]\left[1 + \frac{r_1 + r_2 r_h}{\kappa_1}\right]\right. \\ \left. + \frac{1 + r_\rho r_h}{\kappa_1}[r_1 + 3r_2 r_h(1 + r_h)]\right\}(1 + r_\rho r_h)\lambda^2\Omega^2 \\ + \left\{(1 + r_\rho r_h)\left(1 + \frac{r_1 + r_2 r_h}{\kappa_1}\right)\left[1 + 3\frac{r_2}{r_1}r_h(1 + r_h)\right]\right. \\ \left. + \left(1 + \frac{r_2 r_h}{r_1}\right)[1 + 3r_\rho r_h(1 + r_h)]\right\}\lambda^4\Omega \\ - \left(1 + \frac{r_2 r_h}{r_1}\right)\left[1 + 3\frac{r_2}{r_1}r_h(1 + r_h)\right]\lambda^6 = 0\end{aligned}$$

from which

$$\sqrt{\Omega} = \left[\frac{\kappa_1}{r_1(1 + r_\rho r_h)}\right]^{1/2}\lambda$$

$$\sqrt{\Omega} = \left(\frac{1 + \frac{r_2}{r_1}r_h}{1 + r_\rho r_h}\right)^{1/2}\lambda \qquad (33)$$

$$\sqrt{\Omega} = \left[\frac{1 + 3\frac{r_2}{r_1}r_h(1 + r_h)}{1 + 3r_\rho r_h(1 + r_h)}\right]^{1/2}\lambda$$

These are now independent of the thickness-radius ratio, which should be so since they have become also the results for the sandwich plate, which the sandwich shell essentially turns into as the wave length becomes very short. The first and third of equations (33) are associated with flexure and are obtainable from the result in reference [5]. The second of equation (33) is associated with extension and is lower than the third in the case of ordinary sandwiches. For the homogeneous shell, the expressions of the limiting frequencies in (33) become in order

$$\sqrt{\Omega} = \left(\frac{\kappa_1}{r_1}\right)^{1/2}\lambda,\ \lambda,\ \lambda \qquad (34)$$

the second and third of which are now the same. Comparing equations (33) and (34), we see that the first branch is lower in the sandwich case than in the homogeneous case, approximately in the ratio of $1/(1 + r_\rho r_h)^{1/2}$. The second and third branches, on the other hand, are much higher in the sandwich case.

The complete frequency spectrum given by the frequency equation (29) has been calculated for the ratios

$$r_\rho = 34.4,\quad r_\mu = 1683,\quad r_1 = 2.20,\quad r_2 = 4790$$

$$r_h = 1/10 \text{ and } 0$$

$$2h/a = 1/30,\ 1/10, \text{ and } 1/5$$

The value of κ_1 is

$$\kappa_1 = 1.086 \quad \text{for} \quad r_h = 1/10 \text{ (sandwich)}$$

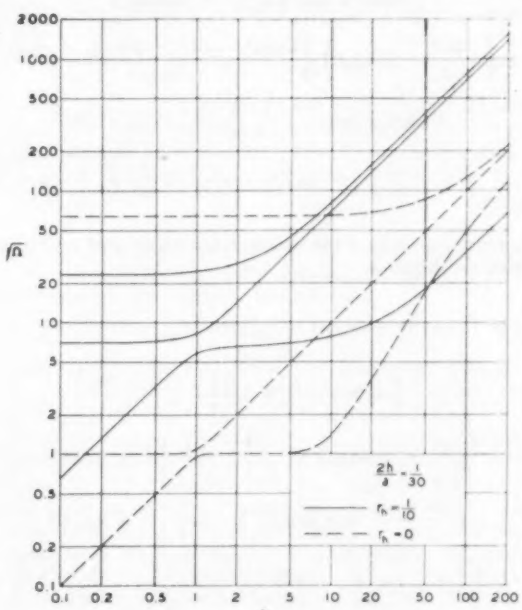

Fig. 2 Axially symmetric vibration of an infinite sandwich cylindrical shell

$$\kappa_1 = \pi^2/12 \quad \text{for} \quad r_h = 0 \text{ (homogeneous)}$$

There are thus six cases, one sandwich case ($r_h = 1/10$) and one homogeneous case ($r_h = 0$) for each of the three values of the thickness-radius ratio $2h/a$. The frequency curves have been plotted in Figs. 2 to 4, in which solid lines represent results of the sandwich cases and dotted lines those of the homogeneous cases. In the cases $2h/a = 1/30$ and $1/10$ in Figs. 2 and 3, the thickness-shear frequency is the highest cutoff frequency for the sandwich shell; in the case $2h/a = 1/5$ in Fig. 4 it is the second highest. As λ becomes large, the results in the three figures approach each other and approach those of the plate. Other features of the spectra are also seen to be in complete agreement with the general discussion just given.

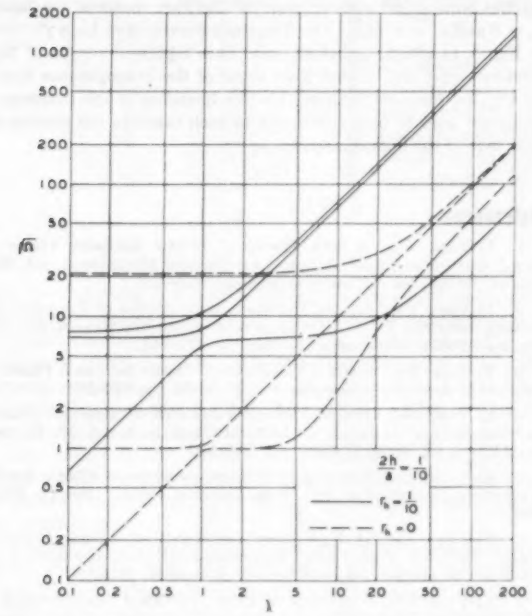

Fig. 3 Axially symmetric vibration of an infinite sandwich cylindrical shell

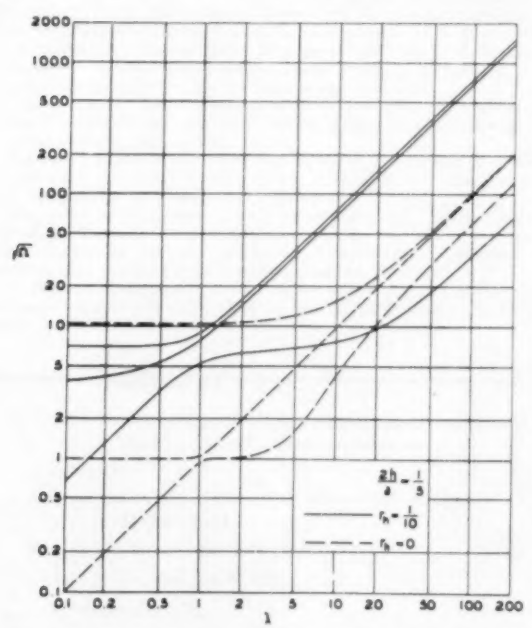

Fig. 4 Axially symmetric vibration of an infinite sandwich cylindrical shell

The accuracy of the results of the simplified equations (18), as well as the accuracy of the other equations for the sandwich cylindrical shell, cannot be ascertained exactly until the corresponding results are also obtained on the basis of the exact theory of elasticity. However, based on the experience obtained from the vibration studies of sandwich plates [5], the accuracy of the results given by equations (18) should be within 10–15 per cent of those given by the exact theory of elasticity as long as the frequency does not exceed the simple thickness-shear frequency. For frequencies lower than one half of the thickness-shear frequency, the accuracy should be within a few per cent. The accuracy for the case $2h/a = 1/5$ is probably lower than for the other cases, since the shell is no longer quite thin; the result is, nevertheless, included to show the reversal in order of the branches near the cutoff.

Torsional Vibration of Infinite Sandwich Cylindrical Shell

This will be analyzed on the basis of the simplified equations (20), from which the frequency equation of the infinite shell is found to be

$$2(\rho_1 h_1 + \rho_2 h_2)\left(\rho_1 \frac{2h_1^3}{3} + 2\rho_2 h_1 h_2 h\right)\omega^4 - \left[\left\{2(\rho_1 h_1 + \rho_2 h_2)\left(\mu_1 \frac{2h_1^3}{3} + 2\mu_2 h_1 h_2 h\right) + 2(\mu_1 h_1 + \mu_2 h_2)\left(\rho_1 \frac{2h_1^3}{3} + 2\rho_2 h_1 h_2 h\right)\right\}\frac{\lambda^2}{a^2} + 2(\rho_1 h_1 + \rho_2 h_2)\cdot 2\kappa_1 \mu_1 h_1\right]\omega^2 + 2(\mu_1 h_1 + \mu_2 h_2)\frac{\lambda^2}{a^2}\left\{\left(\mu_1 \frac{2h_1^3}{3} + 2\mu_2 h_1 h_2 h\right)\frac{\lambda^2}{a^2} + 2\kappa_1 \mu_1 h_1\right\} = 0$$

or

$$[\{1 + 3r_\rho r_h(1 + r_h)\}r_1^2\Omega - \{[1 + 3r_\mu r_h(1 + r_h)]k\lambda^2 + \kappa_1(1 + r_h)^2\}] \times [(1 + r_\rho r_h)r_1\Omega - (1 + r_\mu r_h)\lambda^2] = 0 \quad (35)$$

This reduces to the result of the homogeneous cylindrical shell when $r_h = 0$. The two torsional modes are uncoupled from each other, and their cutoff frequencies are given by

$$\sqrt{\Omega} = 0, \qquad \left[\frac{\kappa_1}{kr_1}\frac{(1 + r_h)^2}{1 + 3r_\rho r_h(1 + r_h)}\right]^{1/2}$$

The first of these corresponds to the rotation of the shell as a whole about its own axis. The second is the circumferential thickness-shear frequency and is the same as the longitudinal thickness-shear frequency in equations (31). As was mentioned before, the thickness-shear frequency is lower in the sandwich case than in the homogeneous case, approximately in the ratio of $1/(1 + 3r_\rho r_h)^{1/2}$.

As $\lambda \to \infty$ for short wave lengths, equation (35) yields

$$\sqrt{\Omega} = \left(\frac{1}{r_1}\frac{1 + r_\mu r_h}{1 + r_\rho r_h}\right)^{1/2}\lambda$$

$$\sqrt{\Omega} = \left[\frac{1}{r_1}\frac{1 + 3r_\mu r_h(1 + r_h)}{1 + 3r_\rho r_h(1 + r_h)}\right]^{1/2}\lambda \quad (36)$$

Since $r_\mu > r_\rho$ for ordinary sandwiches, the first of these is lower than the second. Both are now independent of the thickness-

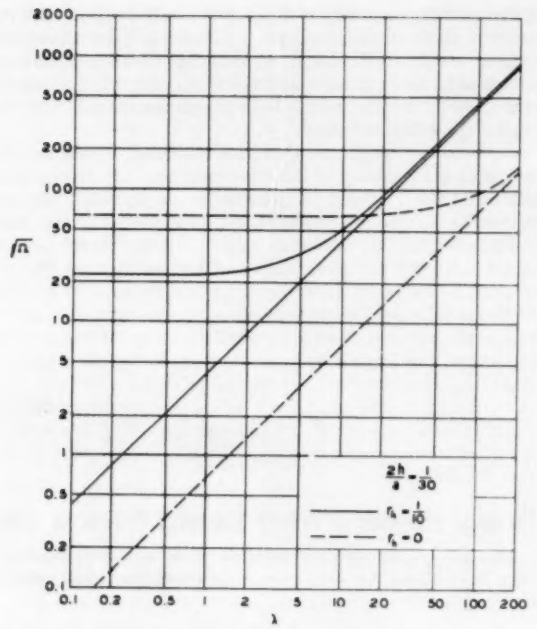

Fig. 5 Torsional vibration of an infinite sandwich cylindrical shell

radius ratio, since, as in the axially symmetric case, they have essentially reduced to the results for the sandwich plate. For the homogeneous shell, equations (36) become

$$\sqrt{\Omega} = \left(\frac{1}{r_1}\right)^{1/2}\lambda, \quad \left(\frac{1}{r_1}\right)^{1/2}\lambda$$

which are equal to each other. At short wave lengths the frequencies are seen to be higher in the sandwich case.

The frequency equation (35) has been computed for two of the previous numerical cases, in which

$$r_\rho = 34.4, \quad r_\mu = 1683, \quad r_1 = 2.20, \quad r_2 = 4790, \quad 2h/a = 1/30$$

For the sandwich shell we have $r_h = 1/10$ and $\kappa_1 = 1.086$, and for the homogeneous shell made of the core material we have $r_h = 0$ and $\kappa_1 = \pi^2/12$. The frequency curves have been plotted in Fig. 5, in which, as before, solid lines represent results of the sandwich case and dotted lines those of the homogeneous case. In the low-frequency range the two branches of the frequency curve are seen to be much closer to each other in the sandwich case than in the homogeneous case.

References

1 Yi-Yuan Yu, "A New Theory of Elastic Sandwich Plates—One-Dimensional Case," JOURNAL OF APPLIED MECHANICS, vol. 26, TRANS. ASME, vol. 81, series E, 1959, pp. 415–421.

2 Yi-Yuan Yu, "Simple Thickness-Shear Modes of Vibration of Infinite Sandwich Plates," JOURNAL OF APPLIED MECHANICS, vol. 26, TRANS. ASME, vol. 81, series E, 1959, pp. 679–681.

3 Yi-Yuan Yu, "Flexural Vibrations of Elastic Sandwich Plates," *Journal of Aero/Space Sciences*, vol. 27, 1960, pp. 272–282.

4 Yi-Yuan Yu, "Forced Flexural Vibrations of Sandwich Plates in Plane Strain," JOURNAL OF APPLIED MECHANICS, vol. 27, TRANS. ASME, vol. 82, Series E, 1960, pp. 535–540.

5 Yi-Yuan Yu, "Simplified Vibration Analysis of Elastic Sandwich Plates," *Journal of Aero/Space Sciences*, vol. 27, 1960, pp. 894–900.

6 Yi-Yuan Yu, "A New Theory of Sandwich Plates—General Case," Technical Note No. 6, Polytechnic Institute of Brooklyn, Department of Mechanical Engineering, November, 1959.

7 Yi-Yuan Yu, "Vibrations of Thin Cylindrical Shells Analyzed by Means of Donnell-Type Equations," *Journal of Aero/Space Sciences*, vol. 25, 1958, pp. 699–715.

Free, Transverse Vibrations of a Solid Elastic Mass in an Infinitely Long, Rigid, Circular-Cylindrical Tank

J. H. BALTRUKONIS
Member of Technical Staff,
Space Technology Laboratories, Inc.,
Los Angeles, Calif.

Making use of the field equations of elasticity, the frequency equation is derived for the free, transverse vibrations of a solid elastic mass contained by an infinitely long, rigid, circular-cylindrical tank. This frequency equation relates the natural circular frequencies and Poisson's ratio. This relationship is plotted revealing a very interesting steplike variation of the natural frequency with Poisson's ratio. Displacement fields are plotted for two natural frequencies in each of the first three modes.

THE present problem was motivated by an interest in the free transverse vibrations of solid-propellant rocket motors consisting of relatively rigid casings with extremely compliant, solid-propellant cores. The problem under consideration should by no means be considered a model of the solid-propellant motor, the present study being only an exploratory consideration. Nonetheless, the results presented herein should shed considerable light on the problem motivating this study.

The history of the problem of the vibrations of elastic, continuous bodies in polar cylindrical co-ordinates has been more than adequately covered by many different authors[1] and need not be repeated here.

Basically, the problem under consideration is essentially that of plane strain vibrations of a solid, elastic cylinder clamped along its cylindrical surface. Solution of the analogous problem for the solid, elastic cylinder with traction-free surface was presented by Gazis.[2] Although, as just mentioned, the present problem is one of plane strain vibrations, in view of its motivation, the author prefers to think of it in the present context.

In the initial section of the paper a short summary is presented, for the sake of completeness and convenience, of the general theory of vibrations of elastic, continuous media in polar, cylindrical co-ordinates. Subsequently, a transcendental frequency equation is derived relating the natural circular frequency coefficients and Poisson's ratio. In the following section this relationship is plotted in the first four modes by means of a plotting method due to Pao and Mindlin.[3] A very interesting steplike variation of the natural frequency with Poisson's ratio is obtained for all branches of this relationship. In the final section of the paper parametric equations defining the displacement fields are derived corresponding to each of the natural frequencies. These displacement fields are plotted for two natural frequencies in each of the first three modes.

[1] For example, see A. E. H. Love, "The Mathematical Theory of Elasticity," Dover Publications, New York, N. Y., fourth edition, 1944, for classical references; and H. N. Abramson, H. J. Plass, and E. A. Ripperger, "Stress Wave Propagation in Rods and Beams," *Advances in Applied Mechanics*, Academic Press, New York, N. Y., vol. 5, 1958, pp. 111–194, for the more recent references.

[2] D. C. Gazis, "Exact Analysis of the Plane-Strain Vibrations of Thick-Walled Hollow Cylinders," *Journal of the Acoustical Society of America*, vol. 30, 1958, p. 786.

Presented at the West Coast Conference of the Applied Mechanics Division, Pasadena, Calif., June 27–29, 1960, of THE AMERICAN SOCIETY OF MECHANICAL ENGINEERS.

Discussion of this paper should be addressed to the Secretary, ASME, 29 West 39th Street, New York, N. Y., and will be accepted until January 10, 1961, for publication at a later date. Discussion received after the closing date will be returned.

First draft of manuscript received by ASME Applied Mechanics Division, January 19, 1959; final draft received, February 26, 1960. Paper No. 60—APMW-12.

Statement and Solution of Problem

It is not difficult to show that the field equations for the vibrations of compressible, elastic continua in polar, cylindrical co-ordinates may be reduced to the following three equations of motion:

$$\nabla^2 u_r - \frac{u_r}{r^2} - \frac{2}{r^2}\frac{\partial u_\theta}{\partial \theta} + \frac{1}{1-2\nu}\frac{\partial \Delta}{\partial r} = \frac{\rho}{G}\frac{\partial^2 u_r}{\partial t^2} \quad (1a)$$

$$\nabla^2 u_\theta - \frac{u_\theta}{r^2} + \frac{2}{r^2}\frac{\partial u_r}{\partial \theta} + \frac{1}{1-2\nu}\frac{1}{r}\frac{\partial \Delta}{\partial \theta} = \frac{\rho}{G}\frac{\partial^2 u_\theta}{\partial t^2} \quad (1b)$$

[3] Y. H. Pao and R. D. Mindlin, "Dispersion of Flexural Waves in an Elastic, Circular Cylinder," JOURNAL OF APPLIED MECHANICS, vol. 27, TRANS. ASME, vol. 82, Series E, 1960, pp. 513–520.

Nomenclature

r, θ, z = radial, circumferential, and axial co-ordinate variables of polar cylindrical co-ordinates

t = time

u_r, u_θ, u_z = radial, circumferential, and axial components of displacement

E, ν = elastic modulus and Poisson's ratio

G = shear modulus $= E/2(1+\nu)$

ρ = mass density

Δ = cubical dilatation $= \dfrac{\partial u_r}{\partial r} + \dfrac{u_r}{r} + \dfrac{1}{r}\dfrac{\partial u_\theta}{\partial \theta} + \dfrac{\partial u_z}{\partial z}$

∇^2 = Laplacian $= \dfrac{\partial^2}{\partial r^2} + \dfrac{1}{r}\dfrac{\partial}{\partial r} + \dfrac{1}{r^2}\dfrac{\partial^2}{\partial \theta^2} + \dfrac{\partial^2}{\partial z^2}$

ω = circular frequency

Ω = circular-frequency coefficient

a = radius of interface between elastic mass and rigid tank

n = order number of vibration mode

m = frequency number within a given mode

J_n = Bessel function of first kind of order n

Primes over a quantity denote the ordinary derivative of the quantity with respect to its argument

$$\nabla^2 u_z + \frac{1}{1-2\nu}\frac{\partial \Delta}{\partial z} = \frac{\rho}{G}\frac{\partial^2 u_z}{\partial t^2} \tag{1c}$$

Solutions of these equations of motion are usually found in terms of three displacement potentials as follows:

$$u_r = \frac{\partial \phi}{\partial r} + \frac{\partial^2 \psi}{\partial r \partial z} + \frac{1}{r}\frac{\partial \chi}{\partial \theta} \tag{2a}$$

$$u_\theta = \frac{1}{r}\frac{\partial \phi}{\partial \theta} + \frac{1}{r}\frac{\partial^2 \psi}{\partial \theta \partial z} - \frac{\partial \chi}{\partial r} \tag{2b}$$

$$u_z = \frac{\partial \phi}{\partial z} - \left(\frac{\partial^2}{\partial r^2} + \frac{1}{r}\frac{\partial}{\partial r} + \frac{1}{r^2}\frac{\partial^2}{\partial \theta^2}\right)\psi \tag{2c}$$

It may be verified by direct substitution that equations (1) are identically satisfied by these displacement components provided we take the displacement potentials as solutions of the following differential equations:

$$\nabla^2 \phi = c_d^{-2}\frac{\partial^2 \phi}{\partial t^2} \tag{3a}$$

$$\nabla^2(\psi, \chi) = c_s^{-2}\frac{\partial^2}{\partial t^2}(\psi, \chi) \tag{3b}$$

wherein c_d and c_s denote the dilatational and shear wave velocities, respectively, and are given by

$$c_d^2 = \frac{1}{k^2}\frac{G}{\rho} \tag{4a}$$

$$c_s^2 = \frac{G}{\rho} \tag{4b}$$

$$k^2 = \frac{1-2\nu}{2(1-\nu)} \tag{4c}$$

We immediately recognize the differential equations given by equations (3) as wave equations, solutions of which are well known.

We now apply this general theory to the problem of the free, lateral vibrations of a solid elastic mass in an infinitely long, rigid, circular-cylindrical tank. We assume that the elastic mass has a perfect bond to the rigid tank and seek solutions in which a generic material point undergoes a steady-state, simple harmonic motion in the $\theta = 0$ direction. We further assume that the tank is at rest so that if the tank is rigid and if there is a perfect bond between the tank and the elastic mass at their interface $r = a$, we must require that the displacements in the elastic mass vanish at $r = a$; i.e.,

$$u_r\Big|_{r=a} = u_\theta\Big|_{r=a} = u_z\Big|_{r=a} = 0 \tag{5}$$

In order to satisfy these boundary conditions we take the displacement potentials in the following form:

$$\phi = C_{n1} J_n\left(k\Omega\frac{r}{a}\right) e^{i\omega t}\cos n\theta \tag{6a}$$

$$\psi = 0 \tag{6b}$$

$$\chi = C_{n2} J_n\left(\Omega\frac{r}{a}\right) e^{i\omega t}\sin n\theta \tag{6c}$$

where C_{n1} and C_{n2} are arbitrary constants and n, in these and all subsequent equations, takes on all positive integer values. It may be verified by direct substitution that these potentials are solutions of equations (3) provided we take

$$\Omega^2 = \frac{\rho\omega^2 a^2}{G} \tag{6d}$$

Because of its relation to the circular frequency ω, Ω will be referred to as the circular frequency coefficient.

Now, substitution from equations (6) into equations (2) results in the following displacement field:

$$u_r = \left[C_{n1}\frac{k\Omega}{a}J_n'\left(k\Omega\frac{r}{a}\right) + C_{n2}\frac{n}{r}J_n\left(\Omega\frac{r}{a}\right)\right]e^{i\omega t}\cos n\theta \tag{7a}$$

$$u_\theta = -\left[C_{n1}\frac{n}{r}J_n\left(k\Omega\frac{r}{a}\right) + C_{n2}\frac{\Omega}{a}J_n'\left(\Omega\frac{r}{a}\right)\right]e^{i\omega t}\sin n\theta \tag{7b}$$

$$u_z = 0 \tag{7c}$$

We make note of the fact that by taking the displacement potentials ϕ and χ independent of z and ψ to vanish, a plane strain displacement field results immediately. Substitution from equations (7) into the boundary conditions given by equations (5) results in the following system of equations:

$$C_{n1}(k\Omega)J_n'(k\Omega) + C_{n2}nJ_n(\Omega) = 0 \tag{8a}$$

$$C_{n1}nJ_n(k\Omega) + C_{n2}\Omega J_n'(\Omega) = 0 \tag{8b}$$

This homogeneous system of linear, algebraic equations in the unknown constants can have a solution only if the determinant of the coefficients of the unknowns vanishes. Thus we obtain the following frequency equation:

$$k\Omega^2 J_n'(\Omega)J_n'(k\Omega) - n^2 J_n(\Omega)J_n(k\Omega) = 0 \tag{9a}$$

which may also be written as follows if we take advantage of the recurrence relations for the Bessel functions:

$$J_{n-1}(\Omega)J_{n+1}(k\Omega) + J_{n+1}(\Omega)J_{n-1}(k\Omega) = 0 \tag{9b}$$

These transcendental frequency equations define a doubly infinite set of natural circular frequency coefficients Ω_{nm} which depend on Poisson's ratio. In the following section we investigate this dependency further.

The Natural Frequencies

In order to investigate the dependency of the natural circular frequencies on Poisson's ratio we have taken advantage of a plotting method due to Pao and Mindlin.[2] The method was originally demonstrated in plotting the branches of a transcendental dispersion equation in a wave-propagation problem, but it is equally applicable to equations (9) and, in fact, it would appear to be applicable and advantageous for most transcendental equations. In this method a system of bounds, barriers, and intersectors of the branches is constructed for the branches of the transcendental equation under consideration. Bounds are defined as a family of curves with the following properties:

(i) Their construction requires less computation than that required for plotting the branches directly.

(ii) Their co-ordinates satisfy the transcendental equation only at certain, readily determined points.

(iii) They pass through a family of solutions at the extreme values of the independent variable.

Curves that satisfy conditions (i) and (ii) but not (iii) are called *barriers*. Curves that intersect the bounds or barriers are called *intersectors*. Branches can cross bounds or barriers only at the points of intersection of the latter with intersectors.

We now apply this method to plotting the variation of the nat-

ural circular frequency coefficients as functions of k, this dependency being defined by equations (9). We begin the process by determining the values of the frequency coefficients at the extreme values of the independent variable, the ratio k. Poisson's ratio is defined in a physical sense only over the range from 0 to 1/2 so that by equation (4c) we see that k is defined physically only over the range from 0 to $1/\sqrt{2}$, $k = 0$ corresponding to $\nu = 1/2$ which defines the incompressible material. However, k can be defined in a mathematical sense over a much larger range and still meaningful solutions of equations (9) will result. It will be convenient to consider k defined over the range $0 - 1$. This will in no manner affect the dependency of Poisson's ratio on k or the dependency of Ω on k.

If we denote the left-hand side of equations (9) with P, we readily obtain the following results at the extremes of k:

$$P \Big|_{k=0} \equiv J_{n+1}(\Omega) = 0 \tag{10a}$$

$$P \Big|_{k=1} \equiv \begin{cases} J_{n+1}(\Omega) = 0 \\ J_{n-1}(\Omega) = 0 \end{cases} \tag{10b}$$

Accordingly, we define the following systems of bounds, barriers, and intersectors:

$$\left.\begin{aligned} B_1 &\equiv J_{n+1}(\Omega) = 0 \\ I_1 &\equiv J_{n+1}(k\Omega) = 0 \end{aligned}\right\} \tag{11a}$$

$$\left.\begin{aligned} B_2 &\equiv J_{n-1}(\Omega) = 0 \\ I_2 &\equiv J_{n-1}(k\Omega) = 0 \end{aligned}\right\} \tag{11b}$$

$$\left.\begin{aligned} C_3 &\equiv J_n(\Omega) = 0 \\ I_3 &\equiv J_n'(k\Omega) = 0 \end{aligned}\right\} \tag{11c}$$

$$\left.\begin{aligned} C_4 &\equiv J_n'(\Omega) = 0 \\ I_4 &\equiv J_n(k\Omega) = 0 \end{aligned}\right\} \tag{11d}$$

In the foregoing the symbols B, C, and I have been used to denote bounds, barriers, and intersectors, respectively. The indices have been appended to associate a bound or a barrier with its intersector. We note that each of the bounds or barriers above is a straight line parallel to the k-axis while each of the intersectors is an hyperbola.

On plotting equations (11) many points of intersection occur, each such point of intersection constituting a point on a branch of equations (9). Thus the various branches are readily plotted. An additional refinement has been added to aid in plotting the branches since the frequency coefficient-k relationship is an unusual one including many very rapid variations. This refinement is to plot the slope of the branch at each point of intersection of the bounds or barriers with their intersectors and at the values of the frequency coefficient for the extreme values of k. By the rule of differentiation of implicit functions we readily obtain the following expression for the slope of a branch at a generic point (Ω, k):

$$\frac{d\Omega}{dk} = -\left(\frac{\partial P}{\partial k}\right) \Big/ \frac{\partial P}{\partial \Omega} \tag{12a}$$

And so it follows from equation (9a) that

$$\frac{d\Omega}{dk} = -\frac{1}{k^2\Omega} \frac{\begin{matrix}(k^2\Omega^2 - n^2)J_n'(\Omega)J_n(k\Omega) \\ + n^2kJ_n(\Omega)J_n'(k\Omega)\end{matrix}}{\begin{matrix}kJ_n'(\Omega)J_n(k\Omega) \\ + J_n(\Omega)J_n'(k\Omega)\end{matrix}} \tag{12b}$$

Now, we readily obtain the following results:

$$\frac{d\Omega}{dk}\Big|_{k=0} = 0 \tag{13a}$$

$$\frac{d\Omega}{dk}\Big|_{k=1} = -\frac{\Omega}{2} \tag{13b}$$

$$\left(\frac{d\Omega}{dk}\right)_1 = \left(\frac{d\Omega}{dk}\right)_2 = -\frac{k\Omega}{1+k^2} \tag{13c}$$

$$\left(\frac{d\Omega}{dk}\right)_3 = -\frac{\Omega}{k}\left[1 - \left(\frac{n}{k\Omega}\right)^2\right] \tag{13d}$$

$$\left(\frac{d\Omega}{dk}\right)_4 = -\frac{n^2}{k\Omega} \tag{13e}$$

Equations (13c)–(13e) give the slopes of the branches of equations (9) at the points of intersection of the bounds or barriers and their intersectors. The subscripts have been appended to associate the slope given with the appropriate system given by equations (11).

By plotting the bounds or barriers and their intersectors to obtain points of intersection and then by plotting the slope of the branch at these intersections, Fig. 1 was obtained. We note a very interesting, pronounced steplike variation of the frequency coefficients with k. Pao and Mindlin[3] also noted a variation of this general nature in their solutions of the dispersion equation for flexural waves in an elastic, circular cylinder with traction-free surfaces. The author also has obtained this type of variation in other problems, some of which were much more complicated than the present problem. It would seem therefore that this type of variation may be typical of problems of this type which are defined by a transcendental equation similar to equations (9). We call attention to the plotted points in Fig. 1 that were calculated directly.

The Displacement Field

To complete the solution of the present problem we must investigate the nature of the displacement field. In order to plot the displacement field corresponding to a given natural frequency, we assume that a generic material point (r, θ) in the undeformed body assumes the new position under the deformation given by (r^*, θ^*) wherein

$$\frac{r^*}{a} = \left[\left(\frac{r}{a} + \frac{u_r}{a}\right)^2 + \left(\frac{u_\theta}{a}\right)^2\right]^{1/2} \tag{14a}$$

$$\theta^* = \theta + \tan^{-1}\left(\frac{u_\theta}{a}\right)\left(\frac{r}{a} + \frac{u_r}{a}\right)^{-1} \tag{14b}$$

From equation (7) we readily obtain the following expressions for the components of displacement:

$$u_r = S\left[\left(k\Omega\frac{r}{a}\right)J_n'\left(k\Omega\frac{r}{a}\right) - \frac{(k\Omega)J_n'(k\Omega)}{J_n(\Omega)}J_n\left(\Omega\frac{r}{a}\right)\right]\frac{a}{r}\cos n\theta \tag{15a}$$

$$u_\theta = -S\left[J_n\left(k\Omega\frac{r}{a}\right) - \frac{J_n(k\Omega)}{\Omega J_n'(\Omega)}\left(\Omega\frac{r}{a}\right)J_n'\left(\Omega\frac{r}{a}\right)\right]\frac{a}{r}\sin n\theta \tag{15b}$$

wherein S is a scale factor depending on time given by

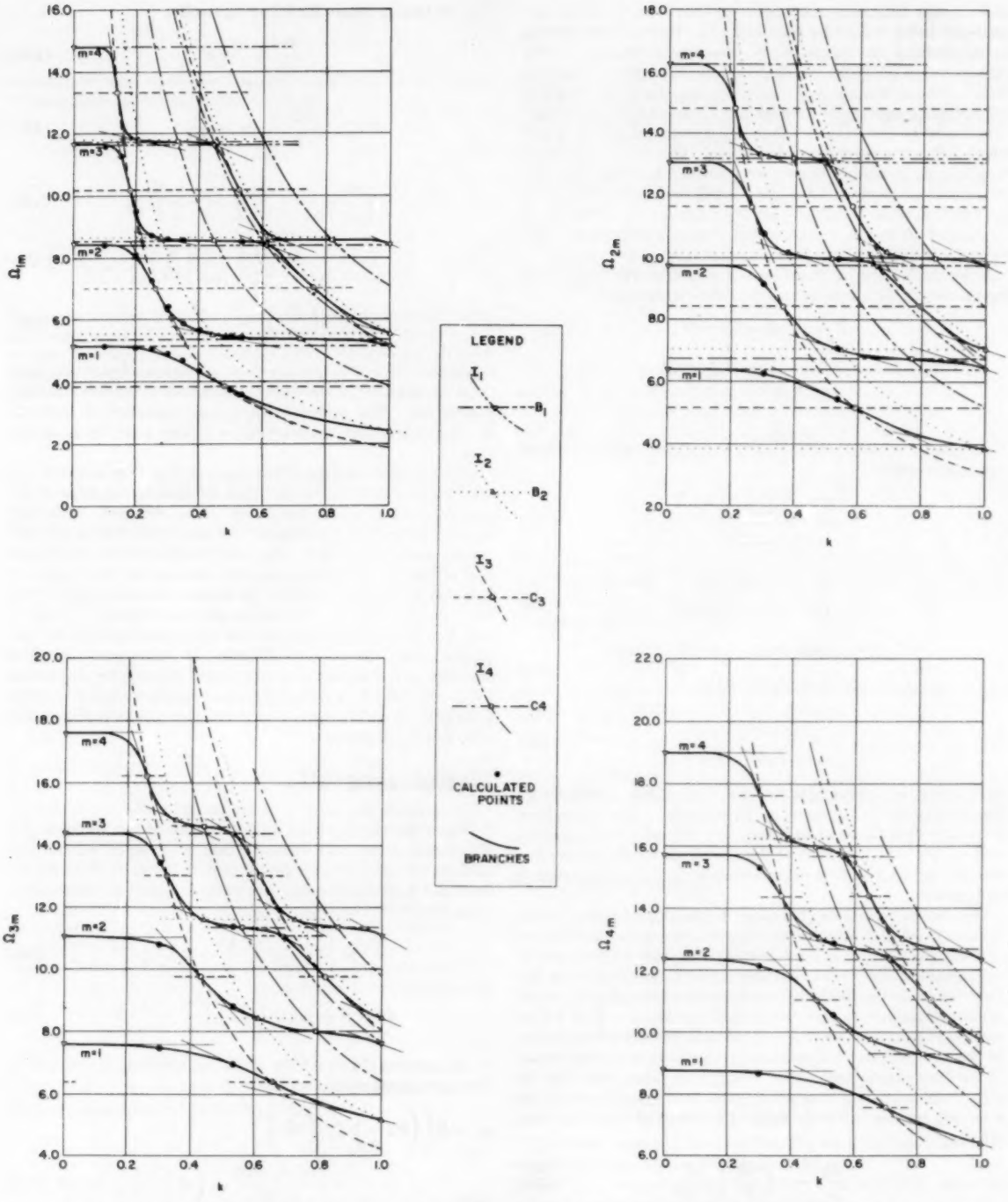

Fig. 1 Variation of the circular frequency coefficients as functions of Poisson's ratio for free, transverse vibrations of a solid elastic core contained by an infinitely long, rigid, circular-cylindrical tank

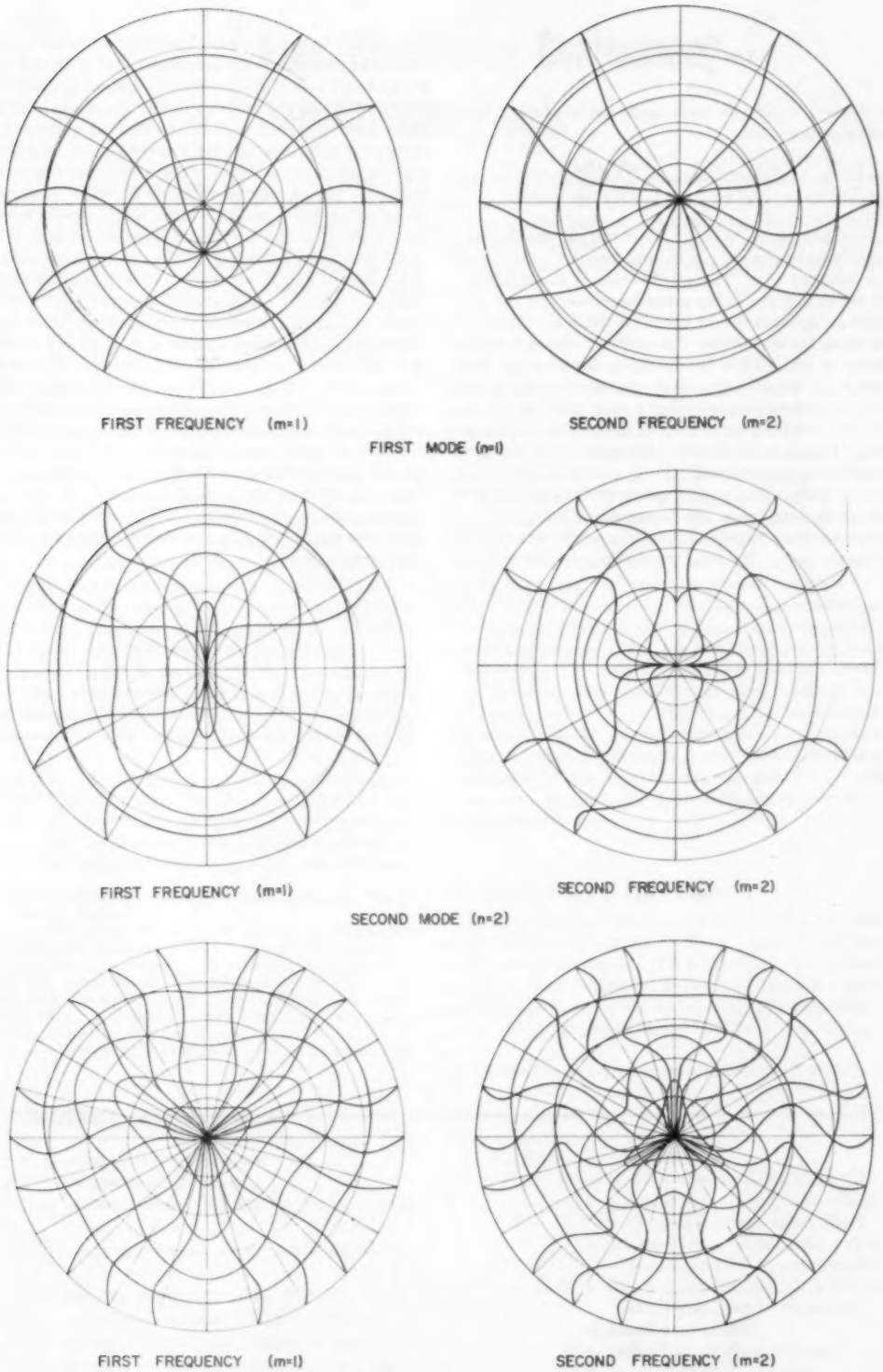

Fig. 2 Displacement fields corresponding to the natural circular frequency ω_{mn} of free vibration in the $\theta = 0$ direction of a solid elastic mass ($\nu = 0.45$) in an infinitely long, rigid, circular-cylindrical tank. (NOTE: Line at bottom should read: Third Mode ($n = 3$).)

$$S = \frac{C_{n1}}{a^2} e^{i\omega t} \tag{15c}$$

In arriving at these results we have made use of the following obtained from equations (8):

$$\frac{C_{n2}}{C_{n1}} = -\frac{(k\Omega)J_n'(k\Omega)}{J_n(\Omega)} = -\frac{n^2 J_n(k\Omega)}{\Omega J_n'(\Omega)} \tag{15d}$$

By making use of equations (14) and (15) we can plot the displacement field corresponding to a given natural frequency apart from the arbitrary constant C_{n1}. The actual value of C_{n1} is indeterminate from the data given in the present problem and can only be determined on specification of initial conditions. Therefore, for arbitrary time, the scale factor S is arbitrary also and we can assign its value at will. Thus the resulting displacement fields will be correct in shape only, since the amplitudes of the displacements are indeterminate. Fig. 2 show plots of the displacement fields corresponding to a few of the natural frequencies as indicated. These plots illustrate the deformed shape of a given network of circles (r = const) and rays (θ = const) imbedded in the undeformed body. These plots are more than sufficient to illustrate the general nature of the displacement fields.

It is rather interesting to note that no true nodal lines occur in the displacement fields. Instead, we obtain two different loci that should be mentioned. The first line is the locus of points that have only radial displacement. For want of a better name we shall call such loci *nodal diameters*, it being clearly understood that they are not nodal lines in the true sense. Similarly, there occur lines that are loci of points that have circumferential displacement only. Such a locus occurs in the displacement field corresponding to ω_{23} between $r/a = 0.4$ and $r/a = 0.6$, Fig. 2. Such loci will be referred to as *nodal circles*, it being clear that along nodal circles only the radial displacement vanishes. It is clear from equations (15) that n is associated with the number of nodal diameters occurring in the displacement field. Thus, as illustrated in Fig. 2, when $n = 1$, there will be only one nodal diameter; when $n = 2$, there will be two; when $n = 3$, there are three; and so on. Further, if we examine Fig. 2 closely we observe that the frequency number m is associated with the number of nodal circles, provided we count the outer boundary as a nodal circle. Thus if $m = 1$, we have only one nodal circle, the outer boundary; but if $m = 2$, we have two nodal circles, the outer boundary plus one other; and so on. As a result, it is clear that the displacement field corresponding to ω_{11} will have one nodal diameter and one nodal circle while the displacement field corresponding to ω_{23} will have three nodal diameters and two nodal circles. It is clear that a plot showing only the nodal circles and the nodal diameters would suffice to demonstrate the general nature of the displacement field.

Free Vibration of Continuous Skin-Stringer Panels

Y. K. LIN[1]
Assistant Professor of Aeronautical Engineering, University of Illinois, Urbana, Ill.

The determination of the natural frequencies and normal modes of vibration for continuous panels, representing more or less typical fuselage skin-panel construction for modern airplanes, is discussed in this paper. The time-dependent boundary conditions at the supporting stringers are considered. A numerical example is presented, and analytical results for a particular structural configuration agree favorably with available experimental measurements.

KNOWLEDGE is often required of the natural frequencies and normal modes of vibration for typical skin-stringer fuselage panels of flight vehicles for studies in sonic fatigue, sound transmission, and panel flutter. It appears that analyses in the literature for panel vibration characteristics are based on oversimplified boundary conditions, corresponding either to knife-edge or clamped types of supports without consideration of the dynamic behavior of the structural members supporting the skin. This assumption is not justifiable at the longitudinal stringers, since they are generally fairly flexible both in bending and in torsion, and absorb a significant amount of energy in the over-all system. On the other hand, the exact nature of the boundary conditions at the circumferential frames are not normally critical in the study of panel vibrations, because the frames are generally spaced farther apart than are the stringers and are much more rigid in radial deformation. By assuming the boundary conditions at the frames as simple supports, only small errors will be introduced.

The objective is to develop a vibration theory for typical airplane skin-stringer panels considering the time-dependent nature of the restraints due to the stringers. The mathematical model of the structure is chosen as a row of panels between two frames. The skin is assumed to be continuous over the intermediate stringers which, in turn, are simply supported on both sides by rigid structure. The ends of the panels are assumed to be simply supported.

The differential equation of motion is solved for individual panels. However, the boundary conditions are so specified that the continuity of the neighboring panels in the row is insured. The vibrations of the skin and stringers are coupled because both the skin and the stringers are integral parts of the structure. The natural frequencies for a row of identical panels will fall in frequency groups, similar to the groups described by Miles [1][2] in his study of the vibration characteristics of continuous beams. The upper and lower limits of each modal frequency group are definite and independent of the number of panels for a given type of construction. Frequency equations and the normal modes for these limits are given herein. An energy method is used to investigate the effect of curvature on the vibration characteristics of a circumferential band of panels around an airplane fuselage. Finally, a numerical example is presented. The limits of modal frequencies for the first two groups and the associated mode shapes are computed, and the results are compared with experimental measurements.

Vibration of a Row of Flat Panels

Consider the free vibration of a row of N flat skin-stringer panels, such as that shown in Fig. 1. Specifically, the pth panel in the row has a constant skin thickness h_p, a constant skin mass density ρ_p, and a constant width b_p. This panel is simply supported at $x = 0$, and $x = l$, and is elastically supported by the pth and $(p + 1)_{th}$ stringers at $y = (b_1/2) + \ldots + b_{p-1}$ and $y =$

[1] Formerly Research Engineer, Boeing Airplane Company, Transport Division, Renton, Wash.

Presented at the West Coast Conference of the Applied Mechanics Division, Stanford, Calif., September 9–11, 1959, of THE AMERICAN SOCIETY OF MECHANICAL ENGINEERS. This paper was not preprinted.

Discussion of this paper should be addressed to the Secretary, ASME, 29 West 39th Street, New York, N. Y., and will be accepted until January 10, 1961, for publication at a later date. Discussion received after the closing date will be returned.

Manuscript received by ASME Applied Mechanics Division, June 11, 1959.

[2] Numbers in brackets designate References at end of paper.

Nomenclature

A = cross-sectional area of stringer
$A_{1p}, A_{2p}, A_{3p}, A_{4p}$ = constants of integration
C = uniform torsion constant of stringer cross section
C_{ss} = warping constant of stringer cross section with respect to S
D = bending stiffness for skin, $Eh^3/12(1 - \nu^2)$
E = modulus of elasticity of skin material
E_b, G_b = moduli of elasticity of stringer material
$I_\eta, I_{\eta\zeta}$ = moment of inertia and product of inertia of stringer cross section, respectively
I_s = polar moment of inertia of stringer cross section about S
K_0, K_1, K_2, K_3 = coefficients
N = number of continuous spans
S = point on skin directly beneath shear center of stringer cross section, Fig. 2
T = kinetic energy (subscripts, s or b, referring to skin or stringer, respectively)
U = strain energy (subscripts, s or b, referring to skin or stringer, respectively)
Y_m = function of y only
a = radius of curvature of panel
b = width of individual panel
h = thickness of skin
l = length of individual panel

(Continued on next page)

$(b_1/2) + \ldots b_p$, respectively. h_p, ρ_p, and b_p may be different for each panel. Also, the supporting stringers may all be different in size and shape, although it is assumed that each is uniform along its span. It is assumed further that the stringers are the commonly used thin-walled members of open cross section.

The equation of motion for any panel in the row is the well-known

$$\nabla^2\nabla^2 w_p = -\frac{h_p\rho_p}{D_p}\ddot{w}_p \tag{1}$$

Introducing a dimensionless local co-ordinate,

$$\bar{y} = \frac{y - \left(\frac{b_1}{2} + b_2 + \ldots + b_{p-1} + \frac{b_p}{2}\right)}{b_p}$$

$$\frac{b_1}{2} + \ldots + b_{p-1} \leq y \leq \frac{b_1}{2} + \ldots + b_p \tag{2}$$

Equation (1) is transformed to

$$\frac{\partial^4 w_p}{\partial x^4} + \frac{2}{b_p^2}\frac{\partial^4 w_p}{\partial x^2\partial\bar{y}^2} + \frac{\partial^4 w_p}{b_p^4\partial\bar{y}^4} = -\frac{h_p\rho_p}{D_p}\ddot{w}_p \tag{3}$$

The general solution of equation (3) may be written in the form according to Levy as the following:

$$w_p = \sum_{m=1}^{\infty} Y_{mp}\sin\frac{m\pi x}{l}\sin\omega_m t \tag{4}$$

where

$$Y_{mp} = A_{1p}\cosh k_{1p}\bar{y} + A_{2p}\sinh k_{1p}\bar{y} + A_{3p}\cos k_{2p}\bar{y} + A_{4p}\sin k_{2p}\bar{y} \tag{5}$$

and

$$k_{1p} = b_p\left[\omega_m\left(\frac{h_p\rho_p}{D_p}\right)^{1/2} + \left(\frac{m\pi}{l}\right)^2\right]^{1/2}$$
$$k_{2p} = b_p\left[\omega_m\left(\frac{h_p\rho_p}{D_p}\right)^{1/2} - \left(\frac{m\pi}{l}\right)^2\right]^{1/2} \tag{6}$$

Boundary Conditions

The determination of natural frequencies and normal modes of vibration for the system requires the number of boundary conditions to be equal to 4 times the number of spans. Each interior support furnishes 4 boundary conditions resulting from compatibility and equilibrium considerations. Compatibility dictates unique deflection and unique slope at any point on an interior stringer; and equilibrium demands that the unbalanced bending moments and shear forces from two neighboring panels

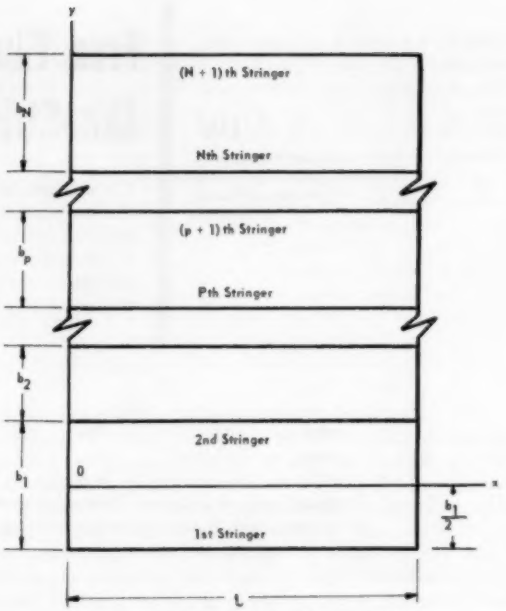

Fig. 1 Continuous skin-stringer panels

act on the stringer as twisting moment and vertical load, respectively. For each exterior stringer, the compatibility criteria do not exist, and only two boundary conditions stemming from equilibrium requirements need be satisfied. In mathematical language, these boundary conditions are written as follows:

$$Y_{m,(p-1)}(1/2) = Y_{m,p}(-1/2), \quad p = 2, 3, \ldots N \tag{7}$$

$$\frac{Y'_{m,(p-1)}(1/2)}{b_{p-1}} = \frac{Y'_{m,p}(-1/2)}{b_p}, \quad p = 2, 3, \ldots N \tag{8}$$

$$\left[\frac{(E_bC_{ws})_p}{b_{p-1}}\cdot\frac{\partial^3 w_{p-1}}{\partial x^4\partial\bar{y}} - \frac{(G_bC)_p}{b_{p-1}}\cdot\frac{\partial^3 w_{p-1}}{\partial x^2\partial\bar{y}} - (E_bI_{\eta\zeta s_s})_p\frac{\partial^4 w_{p-1}}{\partial x^4} + \frac{(\rho_bI_s)_p}{b_{p-1}}\cdot\frac{\partial\ddot{w}_{p-1}}{\partial\bar{y}} - (\rho_bAc_y)_p\ddot{w}_{p-1}\right]_{\bar{y}=1/2}$$
$$= -D_{p-1}\left(\frac{\partial^2 w_{p-1}}{b_{p-1}^2\partial\bar{y}^2} + \nu_{p-1}\frac{\partial^2 w_{p-1}}{\partial x^2}\right)_{\bar{y}=1/2} + D_p\left(\frac{\partial^2 w_p}{b_p^2\partial\bar{y}^2} + \nu_p\frac{\partial^2 w_p}{\partial x^2}\right)_{\bar{y}=-1/2},$$
$$p = 2, 3, \ldots N+1, \text{ and } D_{N+1} = 0 \tag{9}$$

Nomenclature

c_y, s_z = distances as shown in Fig. 2
k_{1p}, k_{2p} = functions of natural frequency ω_m, as defined in equations (6)
m, n = positive integers
p, $(p-1)$, etc. = sequence of spans or stringers (used as subscripts only)
ω_m = natural frequency for flat continuous panels, radians/sec
ω_{mn} = natural frequency for curved continuous panels
q = generalized co-ordinate, function of t
t = time, sec
u, v, w = displacements
x, y, $\bar{y}$ = independent variables or corresponding co-ordinates
β = $h^2/12a^2$
η, ζ = centroidal axes of stringer cross section
ν = Poisson's ratio of skin material
ρ = mass density of skin material
ρ_b = mass density of stringer material
ϕ = independent variable or corresponding co-ordinate
Δ = $\frac{\rho a^2(1-\nu^2)}{E}\omega_{mn}^2$
θ = central angle for curved panel, Fig. 4
Φ = function of ϕ

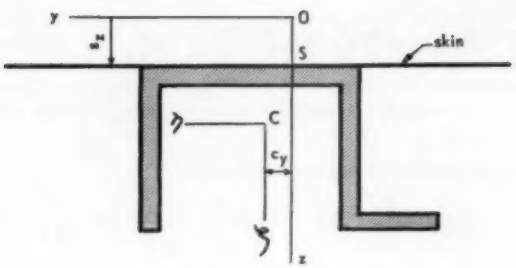

Fig. 2 Stringer cross section

$$\left[(E_bI_\eta)_p \frac{\partial^4 w_{p-1}}{\partial x^4} - \frac{(E_bI_{\eta\zeta}s_s)_p}{b_{p-1}} \cdot \frac{\partial^3 w_{p-1}}{\partial x^4 \partial \bar{y}} + (\rho_b A)_p \ddot{w}_{p-1} - \frac{(\rho_b A c_y)_p}{b_{p-1}} \cdot \frac{\partial \ddot{w}_{p-1}}{\partial \bar{y}}\right]_{\bar{y}=1/2}$$

$$= \frac{D_{p-1}}{b_{p-1}} \left\{\frac{\partial}{\partial \bar{y}}\left[\frac{\partial^2 w_{p-1}}{b_{p-1}^2 \partial \bar{y}^2} + (2 - \nu_{p-1}) \frac{\partial^2 w_{p-1}}{\partial x^2}\right]\right\}_{\bar{y}=1/2} - \frac{D_p}{b_p} \cdot \left\{\frac{\partial}{\partial \bar{y}}\left[\frac{\partial^2 w_p}{b_p^2 \partial \bar{y}^2} + (2 - \nu_p) \frac{\partial^2 w_p}{\partial x^2}\right]\right\}_{\bar{y}=-1/2}$$

$$p = 2, 3, \ldots N + 1; \text{ and } D_{N+1} = 0 \quad (10)$$

$$\left[\frac{(E_bC_{ws})_1}{b_1} \frac{\partial^3 w_1}{\partial x^4 \partial \bar{y}} - \frac{(G_bC)_1}{b_1} \frac{\partial^3 w_1}{\partial x^2 \partial \bar{y}} - (E_bI_{\eta\zeta}s_s)_1 \frac{\partial^4 w_1}{\partial x^4} + \frac{(\rho_bI_s)_1}{b_1} \frac{\partial \ddot{w}_1}{\partial \bar{y}} - (\rho_bAc_y)_1 \ddot{w}\right]_{\bar{y}=-1/2} = D_1 \left(\frac{\partial^2 w_1}{b_1^2 \partial \bar{y}^2} + \nu_1 \frac{\partial^2 w_1}{\partial x^2}\right)_{\bar{y}=-1/2} \quad (11)$$

$$\left[(E_bI_\eta)_1 \frac{\partial^4 w}{\partial x^4} - \frac{(E_bI_{\eta\zeta}s_s)_1}{b_1} \cdot \frac{\partial^3 w_1}{\partial x^4 \partial \bar{y}} + (\rho_bA)_1 \ddot{w}_1 - \frac{(\rho_bAc_y)_1}{b_1} \cdot \frac{\partial \ddot{w}_1}{\partial \bar{y}}\right]_{\bar{y}=-1/2} = -\frac{D_1}{b_1} \left\{\frac{\partial}{\partial \bar{y}}\left[\frac{\partial^2 w_1}{b_1^2 \partial \bar{y}^2} + (2 - \nu_1) \frac{\partial^2 w_1}{\partial x^2}\right]\right\}_{\bar{y}=-1/2} \quad (12)$$

The left-hand sides of equations (9) through (12) are taken from [2],[3] with $\partial w/b\partial\bar{y}$ substituting for the angle of sectional rotation. The sectional properties I_η, I_ζ, $I_{\eta\zeta}$, I_s, and C_{ws} of the stringers are referred to the centroidal axes η, ζ (of the stringer cross section) and the point S on the skin, directly under the shear center of the cross section, as shown in Fig. 2.

Equations (7) through (12) provide for $4N$ independent equations, which, in turn, lead to an eigenvalue equation involving a determinant of the order $4N$. Numerical handling of the resulting determinant is very laborious when N is not a reasonably small number.

It is not necessary, of course, to have any exterior stringers or end panels. The two end panels may actually meet, as those on a typical fuselage section or on a box-type structure. For such cases equations (11) and (12) must be discarded, and the two new boundary conditions are formulated from continuity of deflection and slope resulting from joining the 1st and the Nth panels. These equations would be the same as those given in (7) and (8), except for appropriate subscripts. It is also evident that $D_{N+1} = D_1 \neq 0$, and $b_{N+1} = b_1$ should be used in the application of equations (9) and (10) for $p = N + 1$. The order of the resulting determinant of the eigenvalue equation will remain $4N$.

[3] Difference in the orientation of co-ordinate axes should be noted.

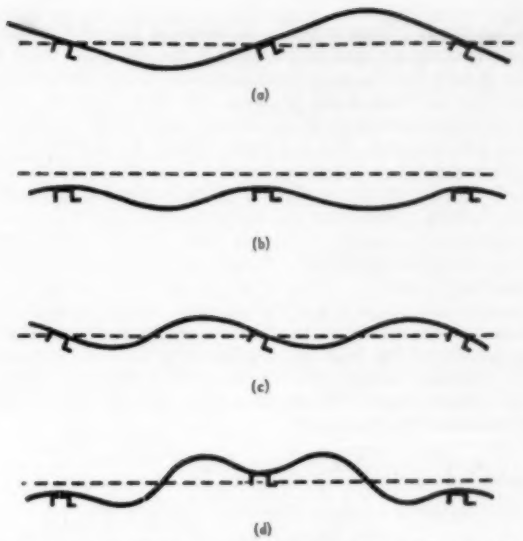

Fig. 3 Normal modes corresponding to limits of first and second frequency bands for continuous identical panels. Dotted lines indicate static equilibrium position.

Identically Constructed Panels and Modal Frequency Groups

For typical modern aircraft body construction, the number of panels on a fuselage section are numerous. It may be impractical to solve a very high order determinant by an iteration process even with high-speed digital computers. However, important information can be obtained by considering a special case, for which each panel is identically constructed in every structural aspect.

Consider a typical aircraft fuselage section made of uniform skin and uniformly spaced identical stringers; and assume, for the present, that the curvature of the panels is negligible so that the equations based on the plate theory given previously are still applicable. It has been shown by Miles [1], for a one-dimensional case of continuous beam arrays supported on rigid knife edges, that the natural frequencies of each array will fall in frequency groups with distinct upper and lower limits for each group. The beam problem treated by Miles may be considered as a special case. The frequency-grouping phenomenon is true for the more general case of continuous panels on flexible supports considered herein. As the number of panels in an array becomes larger, the discrete modal frequencies become more closely spaced until finally the structure exhibits characteristics of "filter bands" to imposed excitations.

Equations for Limiting Frequencies and the Associated Normal Modes

The normal modes associated with the limiting frequencies for the afore-mentioned filter bands are those having identical shapes for all the panels. Sketches of these limiting modes for the first and second frequency bands are shown in Fig. 3. When the alternate panels vibrate out of phase, as illustrated in Figs. 3(*a*) and (*c*), there are only twisting deformations in the supporting stringers. Any bending deformation in the stringers would either disturb the continuity between neighboring panels, or the neighboring panels would vibrate in different shapes. Similarly, when

all the panels vibrate in phase, as shown in Figs. 3(*b*) and (*d*), there are only bending deformations in the stringers. Also, for any of these limiting cases the dynamic and elastic restraints provided by all stringers are identical. We have, therefore, much simpler situations with which to deal when only the limiting cases are examined. For such cases, definition of the behavior of a single panel is sufficient to describe the over-all system, since all the panels vibrate identically, either in phase or alternately out of phase. Advantage also can be taken of the symmetry or antisymmetry of mode shapes with respect to the center of panel span. Only the even-function terms or the odd-function terms in equation (5) need be retained at a time, and the boundary conditions are considered at one stringer only. The frequency equations and normal modes can be obtained by a straightforward application of the boundary conditions for these limiting cases. The frequency equation is as follows for alternate panels vibrating out of phase, wherein the vibration modes are symmetrical about the center of the panel span:

$$\cosh\frac{k_1}{2}\left\{\left[E_bC_{ss}\left(\frac{m\pi}{l}\right)^4+G_bC\left(\frac{m\pi}{l}\right)^2-\rho_bI_s\omega_m^2\right]k_2\sin\frac{k_2}{2}+2\frac{D}{b}k_2^2\cos\frac{k_2}{2}\right\}+\cos\frac{k_2}{2}\left\{\left[E_bC_{ss}\left(\frac{m\pi}{l}\right)^4+G_bC\left(\frac{m\pi}{l}\right)^2-\rho_bI_s\omega_m^2\right]k_1\sinh\frac{k_1}{2}+2\frac{D}{b}k_1^2\cosh\frac{k_1}{2}\right\}=0 \quad (13a)$$

The corresponding normal modes are

$$Y_m=A_1\left[\cosh k_1\bar{y}-\left(\cosh\frac{k_1}{2}\Big/\cos\frac{k_2}{2}\right)\cos k_2\bar{y}\right] \quad (14a)$$

One of these modes is shown in Fig. 3(*a*).

The subscripts p, $(p-1)$, and so on, indicating different panels are no longer needed in equation (13*a*). Omission of these subscripts will be continued for the remainder of the paper, since the following discussion will be limited to the case of identical panels.

When the vibration modes remain symmetrical about the center of span, but all the panels are vibrating in phase, as illustrated in Fig. 3(*b*), the frequency equation is

$$k_1\sinh\frac{k_1}{2}\left\{\left[E_bI_y\left(\frac{m\pi}{l}\right)^4-\rho_bA\omega_m^2\right]\cos\frac{k_2}{2}-2\frac{D}{b^3}k_2^3\sin\frac{k_2}{2}\right\}+k_2\sin\frac{k_2}{2}\left\{\left[E_bI_y\left(\frac{m\pi}{l}\right)^4-\rho_bA\omega_m^2\right]\cosh\frac{k_1}{2}-2\frac{D}{b^3}k_1^3\sinh\frac{k_1}{2}\right\}=0 \quad (13b)$$

and the corresponding normal modes are

$$Y_m=A_1\left[\cosh k_1\bar{y}+\left(k_1\sinh\frac{k_1}{2}\Big/k_2\sin\frac{k_2}{2}\right)\cos k_2\bar{y}\right] \quad (14b)$$

Fig. 3(*c*) gives an example of the antisymmetrical modes about the center of span, with alternating panels vibrating out of phase. The frequency equation corresponding to this mode type is

$$\sinh\frac{k_1}{2}\left\{-\left[E_bC_{ss}\left(\frac{m\pi}{l}\right)^4+G_bC\left(\frac{m\pi}{l}\right)^2-\rho_bI_s\omega_m^2\right]k_2\cos\frac{k_2}{2}+2\frac{D}{b}k_2^3\sin\frac{k_2}{2}\right\}+\sin\frac{k_2}{2}\left\{\left[E_bC_{ss}\left(\frac{m\pi}{l}\right)^4+G_bC\left(\frac{m\pi}{l}\right)^2-\rho_bI_s\omega_m^2\right]k_1\cosh\frac{k_1}{2}+2\frac{D}{b}k_1^3\sinh\frac{k_1}{2}\right\}=0 \quad (13c)$$

and the corresponding normal modes are

$$Y_m=A_2\left[\sinh k_1\bar{y}-\left(\sinh\frac{k_1}{2}\Big/\sin\frac{k_2}{2}\right)\sin k_2\bar{y}\right] \quad (14c)$$

One of the antisymmetrical modes about the center of span with all panels vibrating in phase is shown in Fig. 3(*d*). The corresponding frequency equation for this type of mode is

$$k_1\cosh\frac{k_1}{2}\left\{\left[E_bI_y\left(\frac{m\pi}{l}\right)^4-\rho_bA\omega_m^2\right]\sin\frac{k_2}{2}+2\frac{D}{b^3}k_2^3\cos\frac{k_2}{2}\right\}+k_2\cos\frac{k_2}{2}\left\{-\left[E_bI_y\left(\frac{m\pi}{l}\right)^4-\rho_bA\omega_m^2\right]\sinh\frac{k_1}{2}+2\frac{D}{b^3}k_1^3\cosh\frac{k_1}{2}\right\}=0 \quad (13d)$$

and the corresponding normal modes are

$$Y_m=A_2\left[\sinh k_1\bar{y}-\left(k_1\cosh\frac{k_1}{2}\Big/k_2\cos\frac{k_2}{2}\right)\sin k_2\bar{y}\right] \quad (14d)$$

Since equations (13*a*)–(13*d*) are highly transcendental, they can only be solved by successive iteration. However, the number of iterations can be reduced greatly if the quadrant and approximate position of the angle $k_2/2$ are estimated after the first trial. Normally, equations (13*a*) and (13*c*) will give the lower limits for the frequency groups, and equations (13*b*) and (13*d*) will give the upper limits. The former equations correspond to minimum restraint from the neighboring panels and the latter correspond to maximum restraint. If the stringers were extremely flexible in bending but extremely stiff in torsion, equations (13*a*) and (13*c*) might give the upper limits, and equations (13*b*) and (13*d*) might give the lower limits. However, this situation is most unlikely.

It will be noted that each frequency equation has an infinite number of roots, corresponding to an infinite number of mode shapes in each category. Only the fundamental ones are illustrated in Fig. 3.

Frequency Equation for Curved Panels

Thus far the discussion has been limited to flat panels. However, the theoretical determination of the approximate natural frequencies for curved panels by the energy method is straightforward. The method consists of expressing the strain and

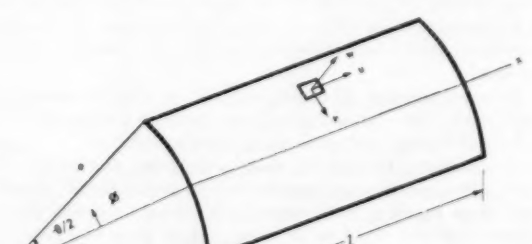

Fig. 4 A single curved panel

kinetic energies for the system in terms of the generalized co-ordinates and the normal functions. The equations of motion are derived by a Lagrangian formulation. Corresponding to the co-ordinate system shown in Fig. 4, the strain and kinetic energies of the vibrating skin are, respectively [3],

$$U_s = \frac{Eh}{2a(1-\nu^2)} \iint \left\{ a^2 \left(\frac{\partial u}{\partial x} \right)^2 + \left(\frac{\partial v}{\partial \phi} + w \right)^2 + 2\nu a \frac{\partial u}{\partial x} \left(\frac{\partial v}{\partial \phi} + w \right) + \frac{1-\nu}{2} \left(\frac{\partial u}{\partial \phi} + a \frac{\partial v}{\partial x} \right)^2 + \beta \left[a^4 \frac{\partial^2 w}{\partial x^2} \left(a \frac{\partial^2 w}{\partial x^2} - 2 \frac{\partial u}{\partial x} \right) + \left(w + \frac{\partial^2 w}{\partial \phi^2} \right)^2 + 2\nu a^2 \frac{\partial^2 w}{\partial x^2} \left(\frac{\partial^2 w}{\partial \phi^2} - \frac{\partial v}{\partial \phi} \right) + \frac{1-\nu}{2} \left(a \frac{\partial^2 w}{\partial x \partial \phi} + \frac{\partial u}{\partial \phi} \right)^2 + {}^1/_2 (1-\nu) a^2 \left(\frac{\partial^2 w}{\partial x \partial \phi} - \frac{\partial v}{\partial x} \right)^2 \right] \right\} d\phi \, dx \quad (15)$$

$$T_s = \frac{\rho h a}{2} \iint \left\{ \dot{u}^2 + \dot{v}^2 + \dot{w}^2 + \beta \left[a \frac{\partial \dot{w}}{\partial x} \left(a \frac{\partial \dot{w}}{\partial x} - 2\dot{u} \right) + \left(\frac{\partial \dot{w}}{\partial \phi} - \dot{v} \right) \left(\frac{\partial \dot{w}}{\partial \phi} - 3\dot{v} \right) \right] \right\} d\phi \, dx \quad (16)$$

If the computations are limited to a determination of the limiting frequencies of the frequency bands, the double integrations indicated in the foregoing need be carried out only over the surface of one single panel.[4]

Expressions for the strain and kinetic energies of each stringer, which is attached to the skin, are the following [2]:

$$U_b = {}^1/_2 \left[E_b C_{w_b} \int_0^l \left(\frac{\partial^2 w}{a \partial x^2 \partial \phi} \right)^2 dx + E_b I_{v_b} \int_0^l \left(\frac{\partial^2 w}{\partial x^2} \right)^2 dx + G_b C \int_0^l \left(\frac{\partial^2 w}{a \partial x \partial \phi} \right)^2 dx - 2E_b I_{v_b^0} \int_0^l \left(\frac{\partial^2 w}{a \partial x^2 \partial \phi} \right) \left(\frac{\partial^2 w}{\partial x^2} \right) dx \right]_{\phi = \frac{\theta}{2}} \quad (17)$$

$$T_b = \frac{\rho_b A}{2} \left[\int_0^l \dot{w}^2 dx - 2c_{v_b} \int_0^l \dot{w} \left(\frac{\partial \dot{w}}{a \partial \phi} \right) dx + \frac{I_v}{A} \int_0^l \left(\frac{\partial \dot{w}}{a \partial \phi} \right)^2 dx \right]_{\phi = \frac{\theta}{2}} \quad (18)$$

It is noted that the angle of rotation of the stringer cross section is represented by $\partial w/a\partial\phi$, according to the co-ordinate system specified in Fig. 4, and that the deflections along the stringer are equal to those of the skin at $\phi = \theta/2$.

The deformations of the panel for a particular mode of vibration are assumed as follows:

$$u = q_u \Phi_u \cos \frac{m\pi x}{l}$$

$$v = q_v \Phi_v \sin \frac{m\pi x}{l} \quad (19)$$

$$w = q_w \Phi_w \sin \frac{m\pi x}{l}$$

[4] The double integrations would be carried out over the entire surface of the system if all the frequencies were desired.

Since the vibrations are predominantly bending, it is reasonable to use the bending-mode shapes obtained for the flat panels as the approximate normal functions in the radial or w-direction for the curved panels. This is accomplished by transforming Y_m for the flat panels to Φ_w by substituting ϕ/θ for ϑ. The continuity of the neighboring panels will be maintained by this simple transformation. The mode shapes for the circumferential and longitudinal vibrations, Φ_v and Φ_u, are approximated by choosing Φ_v to be the same as that of longitudinal vibrations in a bar, and Φ_u to be the same as the transverse vibration in a beam with a large depth-to-span ratio wherein the deformations are mainly attributed to shear. It is interesting to note that this "shear" type of transverse vibration in a beam can be represented by a second-order differential equation and results in mode shapes with maximum slopes at the supports.

When the deformations are symmetrical about the center of span, we may write

$$\Phi_u = \cos \frac{(2n-1)\pi\phi}{\theta}$$

$$\Phi_v = \begin{cases} \sin \dfrac{(2n-1)\pi\phi}{\theta} & \text{Alternating panels vibrating out of phase} \\ \sin \dfrac{2n\pi\phi}{\theta} & \text{All panels vibrating in phase} \end{cases} \quad (20)$$

$$\Phi_w = Y_m \left(\frac{\phi}{\theta} \right) \qquad Y_m \text{ an even function}$$

When the deformations are antisymmetrical about the center of span,

$$\Phi_u = \sin \frac{2n\pi\phi}{\theta}$$

$$\Phi_v = \begin{cases} \cos \dfrac{2n\pi\phi}{\theta} & \text{Alternating panels vibrating out of phase} \\ \cos \dfrac{(2n+1)\pi\phi}{\theta} & \text{All panels vibrating in phase} \end{cases} \quad (21)$$

$$\Phi_w = Y_m \left(\frac{\phi}{\theta} \right) \qquad Y_m \text{ an odd function}$$

The Lagrange equation for a conservative system is

$$\frac{d}{dt} \left[\frac{\partial}{\partial \dot{q}} (T_s + T_b) \right] + \frac{\partial}{\partial q} (U_s + U_b) = 0 \quad (22)$$

It is assumed that the contribution from shear stresses to the deformations in the w-direction are small. This is true if

$$\beta \left(\frac{m\pi a}{l} \right)^2 \ll 1 \quad \text{and} \quad \beta \left(\frac{n\pi}{\theta} \right)^2 \ll 1$$

With the foregoing restrictions, many of the β-terms may be neglected when equations (15) through (21) are substituted into equation (22). Having done this, we obtain

$$\begin{aligned} m_u \ddot{q}_u + C_{1q} q_u + C_{2q} q_v + C_{3q} q_w &= 0 \\ m_v \ddot{q}_v + C_{2q} q_u + C_{4q} q_v + C_{5q} q_w &= 0 \\ m_w \ddot{q}_w + C_{3q} q_u + C_{5q} q_v + C_{6q} q_w &= 0 \end{aligned} \quad (23)$$

where

$$
\left.
\begin{aligned}
m_u &= \frac{\rho a^2(1-\nu^2)}{E}\int \Phi_u^2 d\phi \\
m_v &= \frac{\rho a^2(1-\nu^2)}{E}\int \Phi_v^2 d\phi \\
m_w &= \frac{\rho a^2(1-\nu^2)}{E}\int \Phi_w^2 d\phi \\
&\quad + \frac{\rho_b A a(1-\nu^2)}{Eh}\left[\Phi_w^2 - \frac{2c_y}{a}\Phi_w\Phi_w' \right. \\
&\quad \left. + \frac{I_x}{Aa^2}(\Phi_w')^2\right]_{\phi=\frac{\theta}{2}} \\
C_1 &= \left(\frac{m\pi a}{l}\right)^2\int \Phi_u^2 d\phi + \frac{1-\nu}{2}\int (\Phi_u')^2 d\phi \\
C_2 &= -\left(\frac{m\pi a}{l}\right)\nu\int \Phi_u\Phi_v' d\phi \\
&\quad + \left(\frac{1-\nu}{2}\right)\left(\frac{m\pi a}{l}\right)\int \Phi_u'\Phi_v d\phi \\
C_3 &= -\left(\frac{m\pi a}{l}\right)\nu\int \Phi_u\Phi_w d\phi \\
C_4 &= \int (\Phi_v')^2 d\phi + \left(\frac{1-\nu}{2}\right)\left(\frac{m\pi a}{l}\right)^2\int \Phi_v^2 d\phi \\
C_5 &= \int \Phi_v'\Phi_w d\phi \\
C_6 &= \int \Phi_w^2 d\phi + \beta\left[\left(\frac{m\pi a}{l}\right)^4\int \Phi_w^2 d\phi \right. \\
&\quad + \int (\Phi_w'')^2 d\phi - 2\left(\frac{m\pi a}{l}\right)^2\nu\int \Phi_w\Phi_w'' d\phi \\
&\quad \left. + 2(1-\nu)\left(\frac{m\pi a}{l}\right)^2\int (\Phi_w')^2 d\phi\right] \\
&\quad + \frac{(1-\nu^2)a}{Eh}\left\{E_b I_\eta\left(\frac{m\pi}{l}\right)^4\Phi_w^2 \right. \\
&\quad + \left[\frac{G_b C}{a^2}\left(\frac{m\pi}{l}\right)^2 + \frac{E_b C_{ws}}{a^2}\left(\frac{m\pi}{l}\right)^4\right](\Phi_w')^2 \\
&\quad \left. - \frac{2EI_{\eta\xi}s_z}{a}\left(\frac{m\pi}{l}\right)^4\Phi_w\Phi_w'\right\}_{\phi=\frac{\theta}{2}}
\end{aligned}
\right\} \quad (24)
$$

The integrations in Equation (24) are carried out from $-\theta/2$ to $\theta/2$ when we are concerned only with the limiting frequencies of the frequency bands. For these limiting cases, either Φ_w or Φ_w' vanishes at $\phi = \theta/2$ and the terms involving $\Phi_w \cdot \Phi_w'$, appearing in the expressions for m_w and C_6, are identically zero. However, these terms are purposely retained, as presented, to enable the computation of other intermediate frequencies if so desired. Also, in the general case, the latter portions of the expressions for m_w and C_6, corresponding to stringer inertia and stringer stiffness, would be written for each and every stringer, and the integrations indicated in equations (24) would cover the whole surface domain of the system.

The natural frequencies for continuous curved skin-stringer panels are obtained from the following characteristic equation:

$$
\begin{vmatrix}
(-m_u\omega_{mn}^2 + C_1) & C_2 & C_3 \\
C_2 & (-m_v\omega_{mn}^2 + C_4) & C_5 \\
C_3 & C_5 & (-m_w\omega_{mn}^2 + C_6)
\end{vmatrix} = 0 \quad (25)
$$

Expansion of equation (25) results in a cubic equation for the frequency parameter Δ,

$$K_3\Delta^3 - K_2\Delta^2 + K_1\Delta - K_0 = 0 \quad (26)$$

The solution of this equation gives three positive real roots. The lowest root generally corresponds to the vibration deformations predominantly in the radial, w-direction. This lowest root is normally the only one of practical importance. Usually K_1 and K_0 are much larger than K_3 and K_2; therefore the lowest root for (26) can actually be computed from dividing K_0 by K_1.

The application of equation (25) or (26) is limited to the relatively lower modes, since the contribution of shearing deformations in the radial direction is assumed negligible. The validity of equation (25) or (26) is assured, however, when the quantities $\beta(m\pi a/l)^2$ and $\beta(n\pi/\theta)^2$ are both much smaller than unity.

Correlation of Test Results and Theory

To substantiate the theory, advantage is taken of available stress records (more precisely, the strain records) obtained in engine noise tests on a large jet airplane. These records were the outputs of wire-resistance strain gages which were mounted on the outer-skin surface of the nearly flat side-body panels. They were of 2 sec duration, and were taken when the airplane was on the ground with the engines operating at maximum take-off power without sound suppressors, so that the panels were subjected to maximum noise pressure fluctuations. The strain gages were oriented normal to the stringers, and they were located near the mid-span of the stringers. Frequency analyses were made of the stress records to obtain stress power spectra. Two typical stress power spectra are shown in Fig. 5.

Since the stress measurements were obtained from the side-body panels, which are nearly flat, it is believed that the equations for flat continuous panels are more applicable. Equations (13a) through (13d) were used to compute the limiting frequencies of the theoretical frequency bands, and equations (14a) through (14d) were used to compute the associated mode shapes. The following dimensional and physical constants needed in the calculation were taken from the actual structure:

$$
\begin{aligned}
b &= 8.2 \text{ in.} \\
c_y &= 0 \\
h &= 0.04 \text{ in.} \\
A &= 0.2302 \text{ in.} \\
C_{ws} &= 0.01649 \text{ in.}^6 \\
C &= 2.263\ (10^{-4}) \text{ in.}^4 \\
E = E_b &= 10.5\ (10^6) \text{ psi} \\
I_x &= 0.254 \text{ in.}^4 \\
I_\eta &= 0.122 \text{ in.}^4 \\
I_{\eta\xi} &= 0 \\
\nu &= 0.3 \\
\rho = \rho_b &= \frac{0.101}{386} \text{ lb-sec}^2/\text{in.}^4
\end{aligned}
$$

Table 1 gives the analytical results for the first two frequency bands.

A study of Fig. 5 along with Table 1 reveals that the two major response bands agree closely with the theoretical filter bands, 98.9 to 130.2 cps and 228.9 to 323.0 cps, respectively. It is surprising to find a "dip" near the middle of each response band. However, this effect becomes more obvious with the following explanation.

It is well known that the response of a lightly damped single-degree-of-freedom system is either approximately in phase or approximately out of phase with the excitation, depending upon whether the frequency of excitation is lower or higher than the natural frequency. Using the concept of normal modes, a complicated system, such as that considered in the example, can be treated as a number of single-degree-of-freedom systems superimposed on one another. Consider the forcing frequency being gradually increased to the lower limit of a filter band; all the corresponding modes within that band respond in phase with the excitation. When the forcing frequency is increased beyond the upper limit of the band, all the corresponding modes within that band respond out of phase with the excitation. In terms of the total stress at a certain reference point in the structure, the contributions from these modes are more or less additive for both cases. However, when the frequency of excitation is located within the two limits, contributions from the lower modes tend to cancel the contributions from the higher modes, or vice versa; hence a "dip" in each response band is exhibited in the stress power spectral plots.

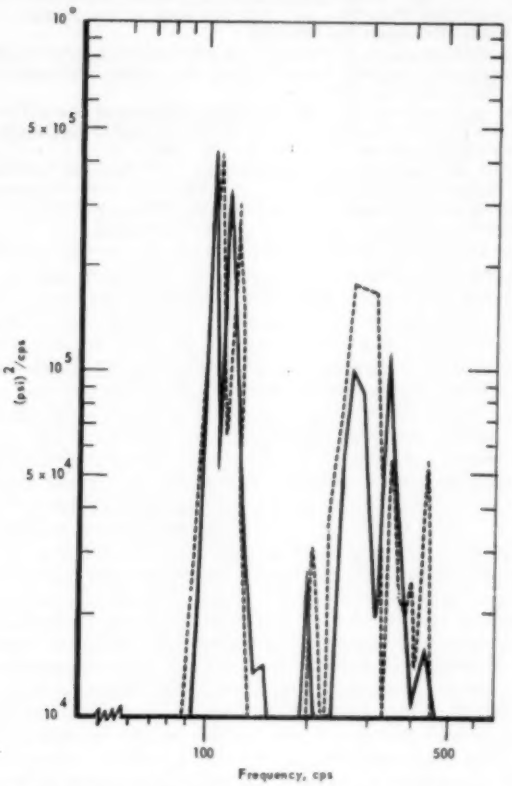

Fig. 5 Typical power spectra of skin stresses near stringer resulting from engine noise excitation

Equation (26) for curved continuous panels was used to investigate the effect of curvature at other locations on the fuselage, where the curvature is not negligible. A typical radius of curvature of 72 in. was assumed, other data being the same as those for flat panels. The results are presented in the column of computed frequency of Table 2. It is interesting to note that a curvature of such magnitude is sufficient to broaden greatly the width of each filter band, and to cause overlapping neighboring bands.

To verify the applicability of the equations for curved panels, shake tests were performed on an assembly of curved skin-stringer panels, consisting of six continuous skin-panel spans. All the dimensional and physical constants of the assembly were identical to those used in the previous calculation. The specimen was excited by an electronic shaker, which was situated either at a mid-span or a quarter-span point depending on whether a symmetrical mode or an antisymmetrical mode was to be excited. The amplitudes of vibration were "sensed" by a special point-sensitive microphone which was connected to a decibel meter and an oscilloscope. The frequency of the shaker was first set near each computed natural frequency and then changed slightly back and forth until resonances were noted on the decibel meter. The resonance frequencies obtained from the tests are given in the last column of Table 2. They compare remarkably well with the analytical results.

Concluding Remarks

The theory presented herein will give a rather accurate description of the vibration characteristics of typical airplane skin-stringer panels. In the example, good agreement was noted be-

Table 1 Limiting frequencies and mode shapes for first two frequency bands, flat continuous panels

Mode type	Motion of neighboring panels	Frequency, cps	Mode shape, Y_1
(*a*) Symmetrical about center of span	Out of phase	98.9	$\cosh(4.345\bar{y}) + 11.38\cos(3.945\bar{y})$
(*b*) Symmetrical about center of span	In phase	130.2	$\cosh(4.934\bar{y}) + 8.386\cos(4.585\bar{y})$
(*c*) Antisymmetrical about center of span	Out of phase	228.9	$\sinh(6.444\bar{y}) - 245.9\sin(6.181\bar{y})$
(*d*) Antisymmetrical about center of span	In phase	323.0	$\sinh(7.615\bar{y}) + 27.31\sin(7.349\bar{y})$

Table 2 Limiting frequencies for first two frequency bands, curved continuous panels

Mode Type	Motion of neighboring panels	Frequency, cps	
		Computed	Observed
(*a*) Symmetrical about center of span	Out of phase	104.5	102
(*b*) Symmetrical about center of span	In phase	414.0	420
(*c*) Antisymmetrical about center of span	Out of phase	232.3	237
(*d*) Antisymmetrical about center of span	In phase	496.6	490

tween the experimental measurements and the computed frequencies for both flat and curved continuous panels.

The present theory should provide adequate information for determining optimum skin gages to withstand a noise environment when used in conjunction with Powell's method [4]. It would also be useful in the study of panel flutter for supersonic-flight vehicles [5].

Acknowledgment

The work reported herein is a part of a continuing research effort to assess the endurance of airplane structure under engine noise excitation. The author is grateful to the Boeing Airplane Company, Transport Division, for permission to present this paper, to Mr. E. L. Webb, Unit Chief of Structural Dynamics, and to Mr. R. B. Skoog, Unit Supervisor in Structural Dynamics for their encouragement in this effort. His most sincere thanks are due to Dr. J. R. Fuller for many valuable discussions and suggestions in the course of this study. The help extended to him from Mr. A. Holden in performing the shake tests is also gratefully acknowledged.

References

1 J. W. Miles, "Vibrations of Beams on Many Supports," *Proceedings, ASCE*, vol. 82, No. EM-1, 1956, pp. 1–9.

2 Y. K. Lin, "Coupled Bending and Torsional Vibrations of Restrained Thin-Walled Beams," see this issue of the JOURNAL OF APPLIED MECHANICS, pp. 739–740.

3 P. R. Miller, "Free Vibrations of a Stiffened Cylindrical Shell," Aeronautical Research Council Paper No. 19338, University of Southampton, May, 1957.

4 A. Powell, "On the Fatigue Failure of Structures Due to Vibrations Excited by Random Pressure Field," *Journal of the Acoustical Society of America*, vol. 30, 1958, pp. 1130–1135.

5 J. M. Hedgepeth, B. Budiansky, and R. W. Leonard, "Analysis of Flutter in Compressible Flow of a Panel on Many Supports," *Journal of the Aeronautical Sciences*, vol. 21, 1954, pp. 475–486.

On a Class of Nonlinear Axisymmetric Plate Problems[1]

F. ESSENBURG
Associate Professor of Mechanics, Illinois Institute of Technology, Chicago, Ill., Assoc. Mem. ASME

The validity of the classical treatment of problems involving axisymmetric plates, partially constrained from deflection by the presence of a smooth, rigid, plane surface, is re-examined, and both the practical and conceptual advantages of carrying the analysis within the scope of the E. Reissner plate theory are illustrated by means of an example.

This paper is concerned with a class of problems involving uniform axisymmetric circular plates, portions of which are constrained from deflection by the presence of a smooth, rigid, plane surface parallel to the undeformed middle plane of the plate. Since, for such problems, the deflection is not proportional to the magnitude of the loading (for loading of sufficient magnitude to cause a portion of the plate to contact the constraining surface) and the circular boundary of the region contacting the constraining surface is determined from a transcendental equation, such problems are called "nonlinear" even though the analysis is within the scope of a linear plate theory. Within the limitations of the Poisson-Kirchhoff plate theory, examples of problems of this type have been considered by Girkmann [1][2] and Hofmann [2] and are discussed in [3].

In accordance with the classical-theory analysis, in the region contacting the constraining surface, the deflection is constant, and consequently, the plate is free from stress in that region. Continuity requirements as regards the slope and radial bending couple are satisfied at the boundary of the region contacting the constraining surface, and the discontinuity in the shear-stress resultant is justified only by assuming that, at that boundary, the constraining surface exerts a line load on the plate. Moreover, in accordance with the classical theory prediction, the only conclusion which can be drawn regarding the force distribution on the constraining surface is that the surface traction on the face of the plate contacting the constraining surface is equal to the surface traction on the opposite face. Thus in the case of a plate which is free from surface load, it is concluded that the surface traction on the constraining surface is everywhere zero.

The physical inconsistencies of such conclusions suggest the desirability of re-examining the validity of the classical treatment and carrying the analysis within the scope of E. Reissner's plate theory [4, 5] which accounts for the effects of both transverse shear deformation and transverse normal stress and which stipulates the satisfaction of a system of natural edge-boundary conditions consistent with the physical boundary conditions at the edge of the plate. In this connection it is pertinent to recall the application of Reissner's theory to plates on an elastic foundation carried out by Naghdi and Rowley [6] and Frederick [7].

In the present paper, by including the effect of transverse shear deformation, expressions are deduced for the stresses and displacement (radial rotation) which are valid for the region of constant deflection. At the boundary of the region contacting the constraining surface, continuity requirements for the shear-stress resultant as well as the radial bending couple and the displacements are satisfied. In addition, a physically consistent expression for the force field on the constraining surface is obtained. As a specific example, a simply supported circular plate, loaded uniformly at its top surface and constrained from deflection by a smooth, rigid, plane surface, situated a small distance below its (undeformed) bottom surface, is considered. Numerical results afford a means of comparison of the classical theory prediction with the present treatment and indicate the significance of the inclusion of the effect of the transverse normal stress in addition to the effect of transverse shear deformation.

Region of Constant Deflection

In terms of the dimensionless radius $\rho = r/b$, where r is the radial co-ordinate, and b is conveniently chosen as the radius of circular boundary of the region of the plate contacting the constraining surface,[3] the basic equations of the Reissner plate theory (in polar co-ordinates and under the assumptions of axial symmetry) are

$$M_r' + \frac{M_r - M_\theta}{\rho} = bV \qquad (\rho V)' = b(p_2 - p_1)\rho \tag{1}$$

$$M_r = \frac{D}{b}\left(\beta' + \nu\frac{\beta}{\rho}\right) - \frac{c\nu h^3}{10(1-\nu)}(p_2 - p_1)$$

$$M_\theta = \frac{D}{b}\left(\frac{\beta}{\rho} + \nu\beta'\right) - \frac{ch^3}{10(1-\nu)}(p_2 - p_1) \tag{2}$$

$$\beta = -\frac{w'}{b} + \frac{12(1+\nu)}{5Eh}V$$

where $D = Eh^3/[12(1-\nu^2)]$ and prime denotes differentiation with respect to ρ. In equations (1) and (2), M_r and M_θ are, respectively, the radial and circumferential bending moments; V is the radial shear-stress resultant; p_1 and p_2 are the surface loading at the top and bottom surfaces, respectively; β and w are the radial rotation and deflection of the middle plane, respectively; h is the thickness of the plate; E is Young's modulus; and ν is Poisson's ratio. The co-ordinate system is chosen so that the deflection is positive when measured downward, and the parameter c is a dimensionless tracer, identifying the inclusion of the

[1] The results presented here were obtained in the course of research sponsored by the National Science Foundation Grant G-9175.

[2] Numbers in brackets designate References at end of paper.

Presented at the West Coast Conference of the Applied Mechanics Division, Pasadena, Calif., June 27–29, 1960, of THE AMERICAN SOCIETY OF MECHANICAL ENGINEERS.

Discussion of this paper should be addressed to the Secretary, ASME, 29 West 39th Street, New York, N. Y., and will be accepted until January 10, 1961, for publication at a later date. Discussion received after the closing date will be returned.

Manuscript received by ASME Applied Mechanics Division, December 3, 1959. Paper No. 60—APMW-7.

[3] In problems of the type of the example considered in the next section, the radius b is an unknown parameter of the problem.

effect of the transverse normal stress in the stress-strain relations, which is either unity or zero according to whether this effect is to be included or excluded in the course of the development. It also should be recalled that the edge-boundary conditions consistent with the foregoing set of equations are (i) either M_r specified or β specified, and (ii) either V specified or w specified.

In the region contacting the constraining surface, the deflection w is constant. It then follows, through appropriate substitution into the first of equations (1), that the shear stress resultant V is governed by the modified Bessel equation

$$V'' + \frac{1}{\rho} V' - \left(k^2 + \frac{1}{\rho^2}\right) V = 0 \tag{3}$$

where

$$k^2 = \frac{10(1-\nu)}{2-c\nu}\left(\frac{b}{h}\right)^2$$

It then readily follows that

$$V = AI_1(k\rho) + BK_1(k\rho)$$

$$p_2 - p_1 = \frac{k}{b}\left[AI_0(k\rho) - BK_0(k\rho)\right]$$

$$\beta = \frac{12(1+\nu)}{5Eh}\left[AI_1(k\rho) + BK_1(k\rho)\right]$$

$$M_r = \frac{h^2}{5b}\left\{A\left[\frac{(2-c\nu)}{2(1-\nu)}\,kI_0(k\rho) - \frac{1}{\rho}\,I_1(k\rho)\right] - B\left[\frac{(2-c\nu)}{2(1-\nu)}\,kK_0(k\rho) + \frac{1}{\rho}\,K_1(k\rho)\right]\right\} \tag{4}$$

$$M_\theta = \frac{h^2}{5b}\left\{A\left[\frac{(2-c)\nu}{2(1-\nu)}\,kI_0(k\rho) + \frac{1}{\rho}\,I_1(k\rho)\right] - B\left[\frac{(2-c)\nu}{2(1-\nu)}\,kK_0(k\rho) - \frac{1}{\rho}\,K_1(k\rho)\right]\right\}$$

where $I_n(k\rho)$ and $K_n(k\rho)$ are modified Bessel functions of order n. The arbitrary constants of integration, A and B, are determined by the specification of either M_r or β at the circular edges of the region under consideration.[4]

An Example

As an example let us consider a simply supported circular plate of radius a subjected to a uniform load $p_1 = p_0$ (where p_0 is a constant) at its top surface and constrained from deflection by a smooth, rigid, plane surface situated a distance δ below the undeformed bottom surface as shown in Fig. 1. With the value of p_0 for which the center of the plate just contacts the constraining surface denoted by p_0^*, it is apparent that for $p_0 > p_0^*$ a circular region of radius b, i.e., $0 \leq \rho \leq 1$, will contact the constraining surface. It is convenient to introduce the dimensionless parameter $m = b/a$. It is clear that in the region $1 \leq \rho \leq 1/m$ the stresses and displacements are given by the solution of equations (1) and (2) with $p_2 = 0$ and $p_1 = p_0$ subject to the appropriate edge boundary conditions at $\rho = 1/m$ and continuity conditions $\rho = 1$. It should be noted that m (and hence b) is an unknown parameter of the problem. For the region $0 \leq \rho \leq 1$ the solution is given by equations (4), and, in view of the requirement that the stresses and displacements remain finite at the origin, the constant B in equations (4) must be zero.

[4] The second of the edge boundary conditions is satisfied since the deflection w is prescribed.

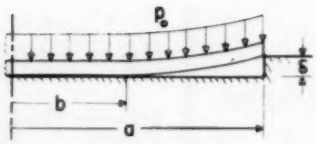

Fig. 1 Deformed plate

For the region $1 \leq \rho \leq 1/m$, the solution of equations (1) and (2) may be written

$$V = -\frac{bp_0}{2}\left[\rho + \frac{C_1}{4\rho}\right]$$

$$\beta = -\frac{b^2p_0}{16D}\left[\rho^3 + C_1\left(\rho\log\rho - \frac{\rho}{2}\right) + C_2\rho + \frac{C_3}{\rho}\right]$$

$$M_r = -\frac{b^2p_0}{16}\left\{(3+\nu)\rho^2 + C_1\left[(1+\nu)\log\rho + \frac{1-\nu}{2}\right] + (1+\nu)C_2 - \frac{(1-\nu)}{\rho^2}\,C_3 - \frac{c\nu\lambda}{m^2}\right\} \tag{5}$$

$$M_\theta = -\frac{b^2p_0}{16}\left\{(1+3\nu)\rho^2 + C_1\left[(1+\nu)\log\rho - \frac{1-\nu}{2}\right] + (1+\nu)C_2 + \frac{1-\nu}{\rho^2}\,C_3 - \frac{c\nu\lambda}{m^2}\right\}$$

$$w = \frac{b^4p_0}{16D}\left[\frac{\rho^4-1}{4} + \frac{C_1}{2}\left(\rho^2\log\rho - \rho^2 + 1\right) + \frac{C_2}{2}\left(\rho^2 - 1\right) + C_3\log\rho - \frac{\lambda}{2m^2}\left(\rho^2 - 1 + \frac{C_1}{2}\log\rho\right)\right]$$

where

$$\lambda = \frac{8}{5(1-\nu)}\left(\frac{h}{a}\right)^2$$

and C_1, C_2, and C_3 are arbitrary constants of integration.[5]

The arbitrary constants, A, C_1, C_2, and C_3, together with an expression specifying the unknown parameter, m, are obtained from the continuity requirements on M_r, β, and V at $\rho = 1$ together with the boundary conditions

$$M_r\Big|_{\rho=\frac{1}{m}} = 0 \qquad w\Big|_{\rho=\frac{1}{m}} = -\delta \tag{6}$$

It is convenient to introduce a function

$$F = \frac{2}{bp_0}\,AI_1(k) \tag{7}$$

in which case

$$C_1 = -4[1+F]$$

$$C_2 = -2 + \frac{c\lambda\nu}{2m^2} - \frac{2-c\nu}{4m^2}\,F\,\frac{\lambda kI_0(k)}{I_1(k)}$$

$$C_3 = -1 - \frac{c\lambda\nu}{2m^2} + F\left[\frac{2-c\nu}{4m^2}\,\frac{\lambda kI_0(k)}{I_1(k)} - 2 - \frac{\lambda}{m^2}\right]$$

$$F = \left\{\frac{3+\nu}{m^2} - 4 + (1-\nu)m^2 + 4(1+\nu)\log m\right. \tag{8}$$

[5] In equations (5) a fourth constant of integration arising in the solution of equations (1) and (2) has been evaluated from the condition $w|_{\rho=1} = 0$.

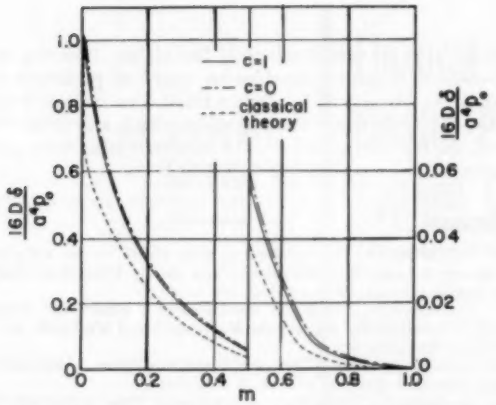

Fig. 2 Variation of radius of region contacting constraining surface with load intensity

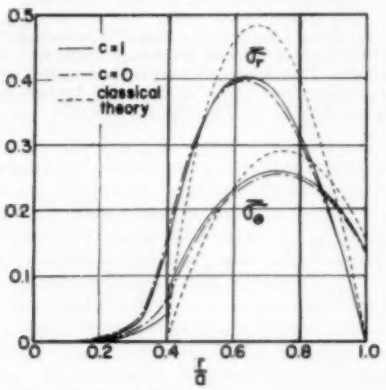

Fig. 3 Distribution of normal components of stress

$$- \frac{c\lambda\nu}{2m^2}(1-\nu)(1-m^2)\Bigg\}\Bigg\{2(1-\nu)(1-m^2) - 4(1+\nu)\log m - \lambda(1-\nu) + \frac{2-c\nu}{4}\left[\frac{1+\nu}{m^2}+1-\nu\right]\frac{\lambda k I_0(k)}{I_1(k)}\Bigg\}^{-1}$$

$$\frac{16D}{a^4}\frac{\delta}{p_0} = -\frac{1-m^4}{4} - m^2(1-m^2) - (2+m^2)m^2\log m + \lambda\left(1-\frac{c\nu}{2}\right)\left(\frac{1-m^2}{2}+m^2\log m\right) + F\Bigg\{\frac{2-c\nu}{4}\left(\frac{1-m^2}{2}+m^2\log m\right)\frac{\lambda k I_0(k)}{I_1(k)} - 2m^2[(1+m^2)\log m + 1 - m^2]\Bigg\} \quad (9)$$

The value of p_0^*, obtained by putting $m = 0$ in equation (9), is given by

$$\frac{16D}{a^4}\frac{\delta}{p_0^*} = -1/4 + \frac{(3+\nu)}{2(1+\nu)} + \frac{\lambda}{2}\left(1-\frac{c\nu}{1+\nu}\right) \quad (10)$$

It may be noted that as the thickness h approaches zero, the foregoing solution approaches the solution of the classical theory. The expressions appropriate to the classical treatment may be obtained by putting terms containing λ equal to zero in equations (5), (8), (9), and (10), and setting the right-hand side of each of equations (4) equal to zero.[6]

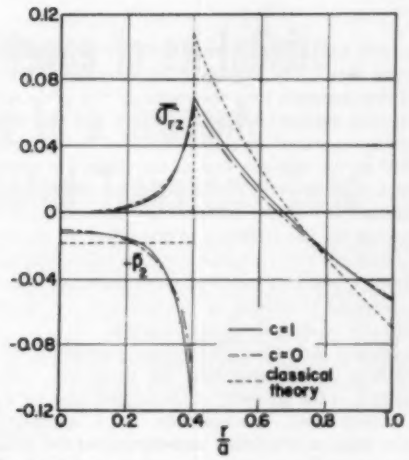

Fig. 4 Distribution of transverse shear stress and surface traction on constraining surface

In order to evaluate the practical significance of the modifications from the classical treatment introduced in this analysis, let us consider a specific numerical example in which $\nu = 1/3$ and $h/a = 1/10$. A curve of $(16D/a^4)(\delta/p_0)$ as a function of m is shown by the solid line in Fig. 2. The same results for the case where the effect of the transverse normal stress has been neglected is shown by the broken line, and the classical theory prediction is shown by the dotted line. It will be observed that while the present treatment provides considerable improvement over the classical theory prediction, the result of the inclusion of the effect of the transverse normal stress is negligible, at least from a practical point of view. From a comparison of abscissa values corresponding to the same ordinate value, it should be noted that this improvement is very substantial for small values of m. For the particular case of $m = 0.4$, the distribution of the stress, together with the force field on the constraining surface, is shown by the solid line in Figs. 3 and 4 in terms of the dimensionless parameters

$$\bar{\sigma}_r = \frac{a}{\delta E}\sigma_r\Big|_{z=\frac{h}{2}} \qquad \bar{\sigma}_\theta = \frac{a}{\delta E}\sigma_\theta\Big|_{z=\frac{h}{2}}$$

$$\bar{\sigma}_{rz} = \frac{a}{\delta E}\sigma_{rz}\Big|_{z=0} \qquad \bar{p}_z = \frac{a}{\delta E}p_z$$

Again, the case where the effect of the transverse normal stress has been neglected is identified by the broken line, and the classical theory prediction is shown by the dotted line. It is apparent that the maximum value of each of the components of stress is substantially lower than the value indicated by the classical theory prediction, but that the result of the inclusion of the effect of the transverse normal stress is practically negligible. Moreover, the present treatment predicts a physically consistent force field on the constraining surface, while the classical treatment prescribes a line load at the periphery of the region contacting the constraining surface.

Conclusions

It is apparent that in the analysis of axisymmetric circular plates, partially constrained from deflection by the presence of a smooth, rigid, plane surface, the utilization of the E. Reissner

[6] If $h \to 0$, then $\lambda \to 0$, $A \to 0$ and $k \to \infty$. However, $\lambda k I_0(k)/I_1(k) \to 0$ and F is defined by the fourth of equations (8).

plate theory is advantageous from both a conceptual and practical point of view. The physical inconsistencies of the classical treatment requirements that the region of the plate contacting the constraining surface be free from stress, and that the surface traction on the constraining surface be equal to the surface traction applied at the opposite face of the plate, are overcome by employing a plate theory which includes the effect of transverse shear deformation. It also appears that the additional improvement obtained by the inclusion of the effect of the transverse normal stress in the stress-strain relations is sufficiently small that, at least from a practical point of view, adequate improvement over the classical treatment is accomplished by including the effect of transverse shear deformation alone.

On the basis of the numerical example considered, the classical treatment errs in overestimating the maximum value of the stresses as well as the intensity of the applied load for a specified state of deformation. Alternatively, for a specified load intensity, the classical prediction underestimates the radius of the region contacting the constraining surface, and for load intensities for which this radius is small the error is particularly marked.

Since the predictions of the shear-deformation theory approach those of the classical treatment as the thickness of the plate approaches zero, it follows that the errors resulting from the neglect of the effect of transverse shear deformation will be less appreciable in the case of extremely thin plates. However, since the classical treatment provides no means of predicting adequately the intensity of the surface traction on the constraining surface, it follows that if this surface traction is a quantity of interest, the inclusion of the effect of transverse shear deformation is essential even in the case of very thin plates.

References

1 K. Girkmann, "Formänderung eines kreisförmigen auf ebener Unterlage aufruhenden Bahälterbodens durch Flüssigkeitsdruck," *Der Stahlbau*, vol. 4, 1931, pp. 205–209.

2 R. Hofmann, "Über ein nichtlineares Problem der Plattenstatik," *Zeitschrift für angewandte Mathematik und Mechanik*, vol. 18, 1938, pp. 226–232.

3 S. P. Timoshenko, "Theory of Plates and Shells," McGraw-Hill Book Company, Inc., New York, N. Y., 1940.

4 E. Reissner, "The Effect of Transverse Shear Deformation on the Bending of Elastic Plates," JOURNAL OF APPLIED MECHANICS, vol. 12, 1945, TRANS. ASME, vol. 67, pp. A-69-77.

5 E. Reissner, "On a Variational Theorem in Elasticity," *Journal of Mathematics and Physics*, vol. 29, 1950, pp. 90–95.

6 P. M. Naghdi and J. C. Rowley, "On the Bending of Axially Symmetric Plates on Elastic Foundations," Proceedings of the First Midwestern Conference on Solid Mechanics, 1953, pp. 119–123.

7 D. Frederick, "On Some Problems in Bending of Thick Circular Plates on an Elastic Foundation," JOURNAL OF APPLIED MECHANICS, vol. 23, TRANS. ASME, vol. 78, 1956, pp. 195–200.

Flexural Stress Waves in an Infinite Elastic Plate Due to a Suddenly Applied Concentrated Transverse Load[1]

JULIUS MIKLOWITZ[2]
Associate Professor of Applied Mechanics, California Institute of Technology, Pasadena, Calif.
Mem. ASME

The problem solved is that of an infinite plate subjected to a suddenly applied concentrated transverse shear load. The solution is derived from a plate theory that incorporates, in addition to bending, the effect of shear force and rotatory inertia on the deflection. These added effects give the present theory true wave character along with greater accuracy in the waves predicted. Numerical evaluation of the solution brings out the effects of dispersion and distortion on the moment and shear-force response of the plate. A criterion is developed for judging the accuracy of this response. It is based on a comparison, employing the stationary phase method, of the present approximate and exact (three-dimensional) theories.

THE problem treated in the paper is that of a thin elastic plate, infinite in extent, subjected to a step concentrated transverse shear load at its center, Fig. 1. The classical Lagrange theory could be employed for this problem. However, it is known that this theory does not give very accurate response information for sharp inputs; i.e., in having an infinite velocity associated with its leading disturbance, it is basically nonwave in nature. A more accurate displacement equation of motion was contributed by Uflyand [1][3] whose plate theory is the analog of the Timoshenko beam theory and which, in a similar manner, includes the effects of shear force and rotatory inertia.

Both of these theories have a bounding wave velocity, and wave information from the beam theory has been shown to compare favorably with experimental results involving reasonably sharp inputs. Unfortunately, Uflyand did not contribute the correct boundary conditions for his theory; however, these were supplied in a later and more complete analysis by Mindlin [2]. Mindlin also showed how much more favorably the plate, incorporating shear force and rotatory-inertia physics, compared with the three-dimensional theory of elasticity on the basis of phase velocities.

Uflyand [1] was the first to derive a solution for the present problem in accord with his higher order bending theory. He employed the Laplace transform and a contour integration-inversion method. The afore-mentioned erroneous boundary conditions, however, led to an invalid result. A correct mathematical solution for the problem was contributed by Lubkin [3] who worked with the nonhomogeneous equations of the present approximate theory. Lubkin's input was created by defining a limiting unit, disk loading in the neighborhood of $r = 0$, having impulsive time character (delta function). The response to the step is then obtained through a convolution.

As will be shown later, a somewhat simpler analysis results if the homogeneous equations and boundary conditions (at $r = 0$) of the theory are used for the problem. Further, the method could be used for other plate problems involving boundaries. On the other hand, Lubkin's analysis offers possibilities for solutions to plate problems that involve distributed loadings. It will be seen that the mathematical solution arrived at here is in agreement with Lubkin's. It is evaluated numerically and discussed for the first time here.

Statement of Problem

The method used by the author [4, 5] to derive traveling-wave solutions from the Timoshenko beam theory will also yield analogous solutions from this related plate theory and, in particular, the solution to the problem of interest here, Fig. 1.

Using a transformation analogous to that used in [4]

$$w = w_b + w_s, \quad \psi_x = -\frac{\partial w_b}{\partial x}, \quad \psi_y = -\frac{\partial w_b}{\partial y} \tag{1}$$

applied to Mindlin's equations [equation (36) and the third of equations (16) in reference 2], the governing equations for the plate can be written in a form similar to the Timoshenko beam equations in [4]; i.e., for the homogeneous case (plate normal pressure, $q = 0$)

$$\left.\begin{aligned} \left(-D\nabla^2\cdot\nabla^2 + \frac{\rho h^3}{12}\frac{\partial}{\partial t^2}\cdot\nabla^2\right) w_b - \kappa^2 Gh\nabla^2 w_s = 0 \\ \kappa^2 Gh\nabla^2 w_s - \rho h\frac{\partial^2}{\partial t^2}(w_b + w_s) = 0 \end{aligned}\right\} \tag{2}$$

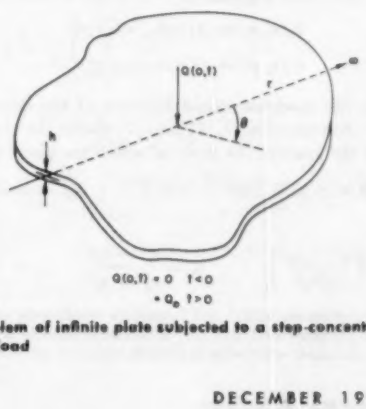

Fig. 1 Problem of infinite plate subjected to a step-concentrated, transverse-shear load

[1] This paper has been abstracted from Space Technology Laboratories Report TR-59-0000-00701, EM 9-10, June 5, 1959.

[2] Also, Consultant, Space Technology Laboratories, Inc.

[3] Numbers in brackets designate References at end of paper.

Presented at the West Coast Conference of the Applied Mechanics Division, Pasadena, Calif., June 27–29, 1960, of THE AMERICAN SOCIETY OF MECHANICAL ENGINEERS.

Discussion of this paper should be addressed to the Secretary, ASME, 29 West 39th Street, New York, N. Y., and will be accepted until January 10, 1961, for publication at a later date. Discussion received after the closing date will be returned.

Manuscript received by ASME Applied Mechanics Division, January 15, 1960. Paper No. 60—APMW-11.

where w_b and w_s are, respectively, the bending and shear components of the total displacement w, and ∇^2 is the two-dimensional Laplacian for the axially symmetric case; D is given by $Eh^3/12(1-\nu^2)$; κ^2, a correction factor relating to Rayleigh surface waves, is given by $0.76 + 0.3\nu$; G is the shear modulus equal to $E/2(1+\nu)$; ν is Poisson's ratio, ρ is the material density, and h the plate thickness. It should be emphasized that the second two equations of (1) are valid transformations in Mindlin's theory only in the special case where the plate rotation (in plane of plate) is zero; i.e., the rotation potential H of equations (52) in [2] is zero. Hence (1) and (2) apply only in the one-dimensional (Timoshenko beam) and axially symmetric cases.

For the present problem, it can be shown that the appropriate initial conditions are

$$w_b(r, 0) = w_s(r, 0) = \frac{\partial w_b(r, 0)}{\partial t} = \frac{\partial w_s(r, 0)}{\partial t} = 0, \quad r > 0 \tag{3}$$

and the boundary conditions at $r = 0$

$$\lim_{r \to 0}\left[r\frac{\partial w_s(r, t)}{\partial r}\right] = \lim_{r \to 0}\left[r\frac{Q_r(r, t)}{\kappa^2 Gh}\right] = \frac{Q(0, t)}{2\pi\kappa^2 Gh} \tag{4}$$

$$\lim_{r \to 0}\left[\frac{\partial^2 w_b(r, t)}{\partial t \partial r}\right] = 0, \qquad t > 0 \tag{5}$$

where $Q(0, t)$ is the step function

$$Q(0, t) = 0 \qquad t < 0$$
$$= Q_0 \qquad t > 0$$

The conditions at infinity are

$$\lim_{r \to \infty}[w_b(r, t)] = 0, \qquad \lim_{r \to \infty}[w_s(r, t)] = 0 \tag{6}$$

Equations (3), (4), (5), and (6) are consistent with the requirements of the theory as stated in [2].[4] Hence information in the present shear problem lies in the solution of the boundary-value problem given by (2), (3), (4), (5), and (6).

Solution of Problem

Following the earlier method [4] based on the Laplace transform, the governing equations (2), subject to the initial conditions (3), transform to

$$\left.\begin{aligned}\left(-D\nabla^2\cdot\nabla^2 + \frac{\rho h^3}{12}p^2\nabla^2\right)\bar{w}_b - \kappa^2 Gh\nabla^2\bar{w}_s = 0\\ \kappa^2 Gh\nabla^2\bar{w}_s - \rho h p^2(\bar{w}_b + \bar{w}_s) = 0\end{aligned}\right\} \tag{7}$$

where the bar indicates the transformed variable and p the transformation parameter. A possible solution of this set of ordinary differential equations is given by

$$\left.\begin{aligned}\bar{w}_b(r, p) = A(p)K_0[n(p)r]\\ \bar{w}_s(r, p) = B(p)K_0[n(p)r]\end{aligned}\right\} \tag{8}$$

where K_0 is the modified Bessel function of the second kind of order zero. Substitution of (8) into (7) yields the characteristic equation of the system, the roots of which are given by

$$n_j = \pm M\sqrt{p[p \mp N(p^2 - a^2)^{1/2}]^{1/2}}, \qquad (j = 1, 2, 3, 4) \tag{9}$$

where

$$M = \frac{\sqrt{2}}{2}\left(\frac{v_1^2 + v_2^2}{v_1^2 v_2^2}\right)^{1/2}, \qquad N = \frac{v_1^2 - v_2^2}{v_1^2 + v_2^2}, \qquad a = \frac{2\sqrt{V}\,v_1^2 v_2^2}{v_1^2 - v_2^2},$$

$$V = \frac{12}{h^2 v_1^2}, \qquad v_1^2 = \frac{E}{\rho(1-\nu^2)}, \qquad v_2^2 = \frac{\kappa^2 G}{\rho}, \quad v_1 > v_2$$

v_1 is the so-called "plate velocity," v_2 the Rayleigh surface wave velocity [respectively, c_p and κc_s in [2], where c_s is the shear-wave velocity $(G/\rho)^{1/2}$].

Hence the general solution to (7) is given by

$$\left.\begin{aligned}\bar{w}_b(r, p) = \sum_{j=1}^{4} A_j K_0(n_j r)\\ \bar{w}_s(r, p) = \sum_{j=1}^{4} \phi_j A_j K_0(n_j r)\end{aligned}\right\} \tag{10}$$

where

$$\phi_j = \left(\frac{p^2}{v_1^2} - n_j^2\right)\Big/ v_2^2 V$$

The conditions (6) transform to

$$\lim_{r \to \infty}[\bar{w}_b(r, p)] = 0, \qquad \lim_{r \to \infty}[\bar{w}_s(r, p)] = 0 \tag{11}$$

Applying this to (10), taking into account the behavior of $K_0(n_j r)$ for large argument (see Erdelyi [6]),

$$K_0(n_j r) = \left(\frac{\pi}{2n_j r}\right)^{1/2} e^{-n_j r} \tag{12}$$

it is seen that the general solutions in the present infinite medium problem reduce to

$$\left.\begin{aligned}\bar{w}_b(r, p) = A_1 K_0(n_1 r) + A_2 K_0(n_2 r)\\ \bar{w}_s(r, p) = \phi_1 A_1 K_0(n_1 r) + \phi_2 A_2 K_0(n_2 r)\end{aligned}\right\} \tag{13}$$

where n_1 and n_2 are the positive roots in (9), agreeing with

$$Re\, n_j > 0 \tag{14}$$

which is imposed by (11) and (12). A_1 and A_2 are evaluated by transforming and applying the boundary conditions (4) and (5) to (13); i.e.,

$$A_1 = -A_2 = -\frac{Q_0}{2\pi D p(n_2^2 - n_1^2)} \tag{15}$$

With prime interest here in the stresses, solutions for the moments and shear force were needed. In the present theory, the expressions for M_θ and M_r are given by

$$\left.\begin{aligned}M_\theta = -D\left[\nu\frac{\partial^2 w_b}{\partial r^2} + \frac{1}{r}\frac{\partial w_b}{\partial r}\right]\\ M_r = -D\left[\frac{\partial^2 w_b}{\partial r^2} + \frac{\nu}{r}\frac{\partial w_b}{\partial r}\right]\end{aligned}\right\} \tag{16}$$

and that for Q_r by

$$Q_r = \kappa^2 Gh\frac{\partial w_s}{\partial r} \tag{17}$$

where M_θ and M_r are moments per unit length, acting on radial and circumferential sections, respectively, and Q_r is shear force per unit length acting on a circumferential section. Maximum stresses differ from M_θ, M_r, and Q_r only by a constant as in the elementary bending theory.

[4] See the section on initial and boundary conditions, and note that the third boundary condition in the present case is automatically satisfied by the axial symmetry involved.

Substitution of (13) into (16) and (17) give the transformed solutions for the moments and shear force. They are

$$\bar{M}_\theta(r, p) = -D\left\{A_1\left[\nu n_1^2 K_0(n_1 r) - \frac{(1-\nu)}{r} n_1 K_1(n_1 r)\right] + A_2\left[\nu n_2^2 K_0(n_2 r) - \frac{(1-\nu)}{r} n_2 K_1(n_2 r)\right]\right\} \quad (18)$$

$$\bar{M}_r(r, p) = -D\left\{A_1\left[n_1^2 K_0(n_1 r) + \frac{(1-\nu)}{r} n_1 K_1(n_1 r)\right] + A_2\left[n_2^2 K_0(n_2 r) + \frac{(1-\nu)}{r} n_2 K_1(n_2 r)\right]\right\} \quad (19)$$

and

$$\bar{Q}_r(r, p) = -\kappa^2 Gh[\phi_1 n_1 A_1 K_1(n_1 r) + \phi_2 n_2 A_2 K_1(n_2 r)] \quad (20)$$

The solutions for M_θ, M_r, and Q_r are obtained by inverting (18), (19), and (20). Since the Laplace transform pairs for these complicated functions do not exist in tables, appeal must be made to the complex inversion integral and contour integration. As Uflyand [1] pointed out, the analysis is considerably reduced, however, by noting that the characteristic equation of the present transformed plate equations is, except for constants, the same as that associated with the Timoshenko beam equations. In comparison the reader will note that if v_1, the plate velocity, were replaced by the bar velocity $c_1 = (E/\rho)^{1/2}$, and the constant V by the analogous $C = A/Ic_1^3$, where A and I are the area and moment of inertia of the beam section, respectively, the roots given by (9) would be those associated with the Timoshenko beam theory. Velocity c_2 is also taken equal to v_2.

This equivalence in characteristic equations means that the contour and related analysis, used to obtain the solutions for the Timoshenko beam, also may be used to invert (18), (19), and (20). In this work, this was done by drawing upon the contour analysis and results in the author's earlier work on beams [5]. That analysis in turn was shown to be in agreement with Uflyand's work.

On the basis of the existing work [1, 5] much of the detail of the inversion method employed here can be omitted. Briefly, then, use of the Mellin inversion theorem leads to the solution statements

$$M_\theta(r, t) = M_{\theta 1}(r, t) + M_{\theta 2}(r, t) = \frac{1}{2\pi i}\int_{\mathrm{Br}_1} [\bar{M}_{\theta 1}(r, p) + \bar{M}_{\theta 2}(r, p)]e^{pt}dp \quad (21)$$

$$M_r(r, t) = M_{r1}(r, t) + M_{r2}(r, t) = \frac{1}{2\pi i}\int_{\mathrm{Br}_1} [\bar{M}_{r1}(r, p) + \bar{M}_{r2}(r, p)]e^{pt}dp \quad (22)$$

$$Q_r(r, t) = Q_{r1}(r, t) + Q_{r2}(r, t) = \frac{1}{2\pi i}\int_{\mathrm{Br}_1} [\bar{Q}_{r1}(r, p) + \bar{Q}_{r2}(r, p)]e^{pt}dp \quad (23)$$

where Br_1 is the Bromwich contour in the right half of the p-plane (see McLachlan [7]) and where, from (18), (19), and (20) in which $j = 1, 2$,

$$\bar{M}_{\theta_j}(r, p) = -DA_j\left[\nu n_j^2 K_0(n_j r) - \frac{(1-\nu)}{r} n_j K_1(n_j r)\right]$$

$$\bar{M}_{r_j}(r, p) = -DA_j\left[n_j^2 K_0(n_j r) + \frac{(1-\nu)}{r} n_j K_1(n_j r)\right]$$

$$\bar{Q}_{r_j}(r, p) = -\kappa^2 Gh\phi_j A_j n_j K_1(n_j r)$$

Completing the contour Br_1 to the right, and employing Cauchy's theorem and Jordan's lemma, it is readily shown that

$$\left.\begin{aligned} M_{\theta_j}(r, t) &= 0 \\ M_{r_j}(r, t) &= 0 \\ Q_{r_j}(r, t) &= 0 \end{aligned}\right\} \quad \text{for} \quad t < \frac{r}{v_j} \quad (24)$$

stemming from the fact that the singularities of the integrals appearing in (21), (22), and (23) lie to the left of Br_1 and that

$$\lim_{|p|\to\infty} n_j = \frac{p}{v_j} \quad (25)^{\S}$$

Equations (24) establish the wave character of the solutions (21), (22), and (23).

For $t > r/v_j$, inversion of the integrals in (21), (22), and (23) was accomplished by integrating along a contour completed to the left of Br_1. Introducing Uflyand's transformation $p = aq$, and noting the common structure of terms composing $\bar{M}_{\theta_j}$ and $\bar{M}_{r_j}$ in (21) and (22), the solutions for M_θ, M_r, and Q_r in terms of the dimensionless q-plane become

$$\left.\begin{aligned} \frac{M_\theta(r, t)}{Q_0} &= 0 && 0 < t < \frac{r}{v_1} \\ &= -D\left[\nu\alpha_1 - \frac{(1-\nu)}{r}\beta_1\right] && \frac{r}{v_1} < t < \frac{r}{v_2} \\ &= -D\left[\nu(\alpha_1 + \alpha_2) - \frac{(1-\nu)}{r}(\beta_1 + \beta_2)\right] && t > \frac{r}{v_2} \end{aligned}\right\} \quad (26)$$

$$\left.\begin{aligned} \frac{M_r(r, t)}{Q_0} &= 0 && 0 < t < \frac{r}{v_1} \\ &= -D\left[\alpha_1 + \frac{(1-\nu)}{r}\beta_1\right] && \frac{r}{v_1} < t < \frac{r}{v_2} \\ &= -D\left[\alpha_1 + \alpha_2 + \frac{(1-\nu)}{r}(\beta_1 + \beta_2)\right] && t > \frac{r}{v_2} \end{aligned}\right\} \quad (27)$$

$$\left.\begin{aligned} \frac{hQ_r(r, t)}{Q_0} &= 0 && 0 < t < \frac{r}{v_1} \\ &= -\kappa^2 Gh\gamma_1 && \frac{r}{v_1} < t < \frac{r}{v_2} \\ &= -\kappa^2 Gh(\gamma_1 + \gamma_2) && t > \frac{r}{v_2} \end{aligned}\right\} \quad (28)$$

where use has been made of (24), and where

$$\alpha_j(r, t) = \frac{(-1)^j H}{i}\int_{\mathrm{Br}_1} \frac{z_j K_0(n_j r)e^{aqt}dq}{q(q^2-1)^{1/2}}$$

$$\beta_j(r, t) = \frac{(-1)^j J}{i}\int_{\mathrm{Br}_1} \frac{\sqrt{z_j}\, K_1(n_j r)e^{aqt}dq}{q^{3/2}(q^2-1)^{1/2}}$$

$$\gamma_j(r, t) = \frac{(-1)^j L}{i}\int_{\mathrm{Br}_1} \frac{[q - v_1^2 M^2 z_j]\sqrt{z_j}\, K_1(n_j r)e^{aqt}dq}{\sqrt{q}(q^2-1)^{1/2}}$$

and where

$$n_j = P\sqrt{q}\sqrt{z_j}, \qquad z_j = q + (-1)^j N(q^2-1)^{1/2}$$

§ The behavior of $K_0(n_j r)$ and $K_1(n_j r)$, in the right half plane for large $|p|$, is given by the right-hand side of (12).

$$P = Ma, \qquad H = \frac{1}{8\pi^2 DN}, \qquad J = \frac{H}{P}, \qquad L = \frac{Hha}{Mv_1^2 v_2^2 V}$$

The integrand singularities of α_j, β_j, and γ_j are the branch points

$$q = 0, \qquad q = \pm 1, \quad \text{and} \quad q = \pm i\alpha \tag{29}$$

where

$$\alpha = \frac{N}{(1 - N^2)^{1/2}}$$

The first of these is a branch point of $\sqrt{q}$, hence of $q^{1/2}$, n_j, $K_0(n_j r)$, and $K_1(n_j r)$. The second are branch points of $(q^2 - 1)^{1/2}$, hence of z_j, n_j, $K_0(n_j r)$ and $K_1(n_j r)$. The last are branch points of $\sqrt{z_1}$, and hence only of n_1, $K_0(n_1 r)$, and $K_1(n_1 r)$. Further consideration must be given to the multivaluedness of the K-functions in their own right, due to their logarithmic behavior (see the series definition in [6]). Since their multivaluedness depends directly on that of

$$\log n_j r = \log |n_j r| + i \arg (n_j r) \tag{30}$$

hence on that of n_j, it can be seen that single valuedness is obtained for the K-functions through the single valuedness of the n_j-functions.

The cuts and contours used for the Timoshenko beam solution, shown in Fig. 2, are sufficient to render the integrals defining α_j, β_j, and γ_j single valued and led to their evaluation. In order to use these contours to get a convergent inversion for α_j and β_j in the present case, however, they first had to be written in terms of the convolution theorem; a necessity imposed by the contribution from the small circle about $q = 0$. According to the theorem the inversion integral can be written as

$$\frac{1}{2\pi i} \int_{\mathrm{Br}_1} \phi_1(aq)\phi_2(aq)e^{aqt}d(aq)$$

which has its inverse in

$$\int_0^t f_1(t - \tau)f_2(\tau)d\tau$$

where ϕ_1 and f_1, ϕ_2 and f_2 are transform pairs. In the case of α_j and β_j, ϕ_1 was taken as $1/aq$ and ϕ_2 as the rest of the integrand. Since the inverse $f_1(t - \tau)$ is the unit function, α_j and β_j may be written as

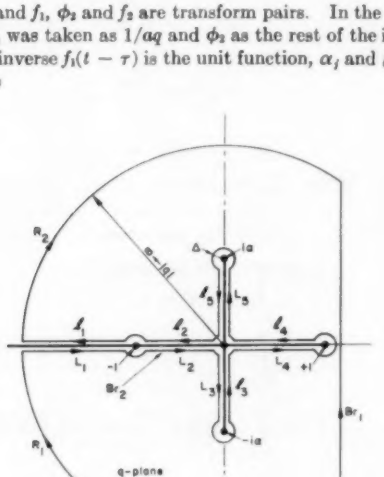

Fig. 2 Integration contours used in evaluating inverse transforms

$$\alpha_j(r, t) = \frac{(-1)^j Ha}{i} \int_{\frac{r}{v_j}}^{t} \left[\int_{\mathrm{Br}_1} \frac{z_j K_0(n_j r)e^{aq\tau}}{(q^2 - 1)^{1/2}} \, dq \right] d\tau$$

$$= \frac{(-1)^j Ha}{i} \int_{\frac{r}{v_j}}^{t} \alpha_j^*(r, \tau)d\tau \tag{31}$$

and

$$\beta_j(r, t) = \frac{(-1)^j Ja}{i} \int_{\frac{r}{v_j}}^{t} \left[\int_{\mathrm{Br}_1} \frac{\sqrt{z_j} K_1(n_j r)e^{aq\tau}}{\sqrt{q}(q^2 - 1)^{1/2}} \, dq \right] d\tau$$

$$= \frac{(-1)^j Ja}{i} \int_{\frac{r}{v_j}}^{t} \beta_j^*(r, \tau)d\tau \tag{32}$$

It remains, then, to carry out the contour integration of the inner integral in (31) and (32) (i.e., evaluate α_j^* and β_j^*) over the paths shown in Fig. 2 and subsequently, the simple outer τ-integration. γ_j in (28) is evaluated directly by contour integration.

Making use of (12) and (25) it may be shown that the paths R_1 and R_2 do not contribute to the solutions for α_j, β_j, and γ_j, since on these paths as $|q| \to \infty$ the integrands of α_j^*, β_j^*, and γ_j behave as

$$\frac{\exp\left[aq\left(\tau - \frac{r}{v_j}\right)\right]}{\sqrt{q}}, \qquad \frac{\exp\left[aq\left(\tau - \frac{r}{v_j}\right)\right]}{q^{3/2}},$$

$$\frac{\exp\left[aq\left(\tau - \frac{r}{v_j}\right)\right]}{\sqrt{q}}$$

respectively, (see [7], page 77). The replacement of contour Br_1 with Br_2 in Fig. 2 (composed of the linear paths L_1, L_2, L_3, l_3, L_4, l_4, L_5, l_5, l_2, and l_1, and the small circles about the branch points) follows from Cauchy's theorem.

The integrals on these component paths are written by employing the same technique as used in [1, 5]. Briefly then, particular branches of the multivalued integrands of α_j^*, β_j^*, and γ_j are selected to agree with $Re\, q > 0$, and the condition $Re\, n_j > 0$ (14). These branches are then continued analytically to, and on Br_2. The use of basic geometrical variables (complex vectors emanating from the branch points) to write the integrands, which are composed of these variables, and the use of the binomial theorem to obtain representations in the vicinity of the branch points, facilitates the continuation. The table in [5], giving the resultant values of these integrand elements on each of the lineal paths comprising Br_2, has been used to construct on these paths the integrals of α_j^*, β_j^*, and γ_j. A limiting process, similar to that in the Appendix of [5] which used for the integrand elements on the small circles, the limiting end point values of the adjacent lineal paths, showed that the small circles contributed nothing to α_j^* and β_j^*. This was also true of γ_j, with the exception of a contribution from the small circle around $q = 0$, reflecting the boundary condition of the step input in shear. Hence it remains to consider the possible contributions from just the lineal paths of Br_2.

Let us consider α_1^* on l_1. The table in [5] shows this is

$$[\alpha_1^*]_{l_1} = \frac{Ha}{i} \int_1^{\infty} \frac{\gamma^2 K_0(Pr\sqrt{\rho}\gamma e^{\pi i})e^{-a\rho\tau} \, d\rho}{(\rho^2 - 1)^{1/2}} \tag{33a}$$

ρ being the real variable $|q|$, and $\gamma = [\rho - N(\rho^2 - 1)^{1/2}]^{1/2}$ representing $|\sqrt{z_1}|$ on the path. Similarly on L_1

$$[\alpha_1^*]_{L_1} = \frac{Ha}{i} \int_{\infty}^{1} \frac{\gamma^2 K_0(Pr\sqrt{\rho}\gamma e^{-\pi i})e^{-a\rho\tau} \, d\rho}{(\rho^2 - 1)^{1/2}} \tag{33b}$$

These integrals combine since we have the relation (given in [6], page 80),

$$K_n(ze^{im\pi}) = e^{-im n\pi}K_n(z) - i\pi m(-1)^{n(m+1)}I_n(z) \quad (34)$$

where $I_n(z)$ is the modified Bessel function of the first kind of order n, m and n are integers, and z is a complex variable. Equation (34) applied to (33a) and (33b) combines these integrals into the single real definite integral

$$[\alpha_1^*]_{l_1+L_1} = -2Ha\pi \int_1^\infty \frac{\gamma^2 I_0(Pr\sqrt{\rho}\gamma)e^{-a\rho\tau}\,d\rho}{(\rho^2-1)^{1/2}} \quad (35)$$

Similarly, contributions of this type from the paths l_1 and L_1 are obtained for α_2^*, β_j^*, and γ_j.[6]

Consider next α_1^* on l_2. The table in [5] shows that this integral can be written as

$$[\alpha_1^*]_{l_2} = Ha \int_0^1 \frac{(\rho + i\delta)K_0[Pr\sqrt{\rho}e^{i\pi}(\lambda + i\mu)]e^{-a\rho\tau}\,d\rho}{(1-\rho^2)^{1/2}} \quad (36)$$

where $(\lambda + i\mu)e^{i\pi/2}$ represents $\sqrt{z_1}$ on the path in terms of the rectangular real variables

$$\lambda = \left(\frac{\Delta+\rho}{2}\right)^{1/2}, \qquad \mu = \left(\frac{\Delta-\rho}{2}\right)^{1/2},$$

$$\Delta = (1-N^2)^{1/2}(\rho^2+\alpha^2)^{1/2}$$

and $-(\rho + i\delta)$ represents z_1 on the path, where $\delta = 2\lambda\mu$. Similarly, α_1^* on L_2 is given by

$$[\alpha_1^*]_{L_2} = Ha \int_1^0 \frac{(-\rho + i\delta)K_0[Pr\sqrt{\rho}e^{-i\pi}(\lambda - i\mu)]e^{-a\rho\tau}\,d\rho}{(1-\rho^2)^{1/2}} \quad (37)$$

where $(\lambda - i\mu)e^{-i\pi/2}$ represents $\sqrt{z_1}$, and $-\rho + i\delta$ represents z_1 on the path.

Since $K_0(\bar{z}) = \overline{K_0(z)}$, after an interchange of the limits on this last integral it may be seen that its integrand is the complex conjugate of that in (36). Hence using (34) again and the complex conjugate character of the integrands in (36) and (37), they combine to give

$$[\alpha_1^*]_{l_2+L_2} = 2Ha \int_0^1 Re\{z_a[K_0(z_b) - i\pi I_0(z_b)]\}\,\frac{e^{-a\rho\tau}\,d\rho}{(1-\rho^2)^{1/2}} \quad (38)$$

where $z_a = \rho + i\delta$, and $z_b = Pr\sqrt{\rho}(\lambda + i\mu)$.

Similar considerations for the paths l_4 and L_4 produce the result

$$[\alpha_1^*]_{l_4+L_4} = -2Ha \int_0^1 Re[z_a K_0(z_b)]\,\frac{e^{a\rho\tau}\,d\rho}{(1-\rho^2)^{1/2}} \quad (39)$$

so that adding there results the real definite integral

$$[\alpha_1^*]_{l_2+L_2+l_4+L_4} = -2Ha \int_0^1 \{2\sinh a\rho\tau Re[z_a K_0(z_b)] + \pi e^{-a\rho\tau}Re[iz_a I_0(z_b)]\}\,\frac{d\rho}{(1-\rho^2)^{1/2}} \quad (40)$$

The analysis for α_2^*, β_j^*, and γ_j is quite similar, producing contributions like (40) for these integrals.

Consider finally the α_1^* on l_3. The table in [5] gives

$$[\alpha_1^*]_{l_3} = Ha \int_\alpha^0 \frac{\omega^2 K_0(Pr\sqrt{\rho\omega}e^{i\pi})e^{ia\rho\tau}\,d\rho}{(\rho^2+1)^{1/2}} \quad (41)$$

where $\omega = [N(\rho^2+1)^{1/2} - \rho]^{1/2}$ represents $|\sqrt{z_1}|$ on the path. Likewise the integral α_1^* on L_3 is given by

$$[\alpha_1^*]_{L_3} = Ha \int_0^\alpha \frac{\omega^2 K_0(Pr\sqrt{\rho\omega})e^{ia\rho\tau}\,d\rho}{(\rho^2+1)^{1/2}} \quad (42)$$

Using (34) again, (41) and (42) combine to give

$$[\alpha_1^*]_{l_3+L_3} = \pi Ha \int_0^\alpha \frac{\omega^2 I_0(Pr\sqrt{\rho\omega})ie^{ia\rho\tau}\,d\rho}{(\rho^2+1)^{1/2}} \quad (43)$$

Considering the paths l_5 and L_5 in the same way then, results in

$$[\alpha_1^*]_{l_5+L_5} = -\pi Ha \int_0^\alpha \frac{\omega^2 I_0(Pr\sqrt{\rho\omega})ie^{-ia\rho\tau}\,d\rho}{(\rho^2+1)^{1/2}} \quad (44)$$

Equations (43) and (44) combine to give the real definite integral

$$[\alpha_1^*]_{l_3+L_3+l_5+L_5} = -2\pi Ha \int_0^\alpha \frac{\omega^2 \sin a\rho\tau I_0(Pr\sqrt{\rho\omega})\,d\rho}{(\rho^2+1)^{1/2}} \quad (45)$$

Here, analogous results are similarly produced for β_1^* and γ_1, but α_2^*, β_2^*, and γ_2 give a zero contribution on these paths since $q = \pm i\alpha$ are branch points only of $\sqrt{z_1}$ (and not of $\sqrt{z_2}$), as noted earlier.

Adding the results in (35), (40), and (45), and performing the simple outer integration indicated in (31), we have

$$\alpha_1(r,t) = 2\pi H\left\langle \int_1^\infty \frac{X_1\gamma^2 I_0(Pr\sqrt{\rho}\gamma)\,d\rho}{\rho(\rho^2-1)^{1/2}} - \int_0^1 \left\{\frac{2}{\pi}Y_1 Re[z_a K_0(z_b)] - X_1 Re[iz_a I_0(z_b)]\right\}\frac{d\rho}{\rho(1-\rho^2)^{1/2}} + \int_0^\alpha \frac{\omega^2 Z_1 I_0(Pr\sqrt{\rho\omega})\,d\rho}{\rho(\rho^2+1)^{1/2}}\right\rangle \quad (46)$$

and similarly, in light of the previously discussed development for α_2^*, β_j^*, and γ_j, we have

$$\alpha_2(r,t) = -2\pi H\left\langle \int_1^\infty \frac{X_2\beta^2 I_0(Pr\sqrt{\rho}\beta)\,d\rho}{\rho(\rho^2-1)^{1/2}} - \int_0^1 \left\{\frac{2}{\pi}Y_2 Re[z_a K_0(z_b)] + X_2 Re[iz_a I_0(z_b)]\right\}\frac{d\rho}{\rho(1-\rho^2)^{1/2}}\right\rangle \quad (47)$$

$$\beta_1(r,t) = -2\pi J\left\langle \int_1^\infty \frac{X_1\gamma I_1(Pr\sqrt{\rho}\gamma)\,d\rho}{\rho^{3/2}(\rho^2-1)^{1/2}} + \int_0^1 \left\{\frac{2}{\pi}Y_1 Re[z_c K_1(z_b)] + X_1 Re[iz_c I_1(z_b)]\right\}\frac{d\rho}{\rho^{3/2}(1-\rho^2)^{1/2}} + \int_0^\alpha \frac{\omega Z_1 I_1(Pr\sqrt{\rho\omega})\,d\rho}{\rho^{3/2}(\rho^2+1)^{1/2}}\right\rangle \quad (48)$$

$$\beta_2(r,t) = 2\pi J\left\langle \int_1^\infty \frac{X_2\beta I_1(Pr\sqrt{\rho}\beta)\,d\rho}{\rho^{3/2}(\rho^2-1)^{1/2}} + \int_0^1 \left\{\frac{2}{\pi}Y_2 Re[z_c K_1(z_b)] - X_2 Re[iz_c I_1(z_b)]\right\}\frac{dp}{\rho^{3/2}(1-\rho^2)^{1/2}}\right\rangle \quad (49)$$

$$\gamma_1(r,t) = -2\pi L\left\langle \int_1^\infty \frac{\Gamma\gamma I_1(Pr\sqrt{\rho}\gamma)e^{-a\rho t}\,d\rho}{\rho^{3/2}(\rho^2-1)^{1/2}} + \int_0^1 \left\{\frac{2}{\pi}\cosh a\rho t Re[z_c z_* K_1(z_*)]\right.\right.$$

[6] In agreement with Lubkin's findings. Uflyand erroneously concluded that these paths contributed nothing.

$$+ e^{-a\rho t} Re[iz_o z_s I_1(z_b)] \Big\} \frac{d\rho}{\rho^{1/2}(1-\rho^2)^{1/2}}$$

$$- \int_0^a \frac{\Omega\omega \cos(a\rho t) I_1(Pr\sqrt{\rho}\omega)\, d\rho}{\rho^{1/2}(\rho^2+1)^{1/2}} \Big\rangle - \frac{1}{4\pi\kappa^2 Gr} \quad (50)$$

$$\gamma_3(r,t) = 2\pi L \Big\langle \int_1^\infty \frac{B\beta I_1(Pr\sqrt{\rho}\beta) e^{-a\rho t} d\rho}{\rho^{1/2}(\rho^2-1)^{1/2}}$$

$$+ \int_0^1 \Big\{ \frac{2}{\pi} \cosh a\rho t Re[z_o z_s K_1(z_b)]$$

$$- e^{-a\rho t} Re[iz_o z_s I_1(z_b)] \Big\} \frac{d\rho}{\rho^{1/2}(1-\rho^2)^{1/2}} \Big\rangle - \frac{1}{4\pi\kappa^2 Gr} \quad (51)$$

where

$$X_1 = e^{-a\rho t} - e^{-a\rho r/v_1}, \qquad X_2 = e^{-a\rho t} - e^{-a\rho r/v_2}$$

$$Y_1 = \cosh a\rho t - \cosh a\rho \frac{r}{v_1}, \qquad Y_2 = \cosh a\rho t - \cosh a\rho \frac{r}{v_2}$$

$$Z_1 = \cos a\rho t - \cos a\rho \frac{r}{v_1}$$

$$\beta = [\rho + N(\rho^2-1)^{1/2}]^{1/2}, \qquad \Gamma = (1 - v_1^2 M^2)\rho + v_1^2 M^2 N(\rho^2-1)^{1/2}$$

$$\Omega = \rho + v_1^3 M^2 \omega^2, \qquad B = (1 - v_1^2 M^2)\rho - v_1^2 M^2 N(\rho^2-1)^{1/2}$$

$$z_o = \frac{z_b}{Pr\sqrt{\rho}} = \lambda + i\mu, \qquad z_s = (1 - v_1^2 M^2)\rho - iv_1^2 M^2 \delta$$

Equations (26) to (28) together with (46) to (51) give the complete mathematical solutions for the dimensionless moments and shear in the present problem.

Numerical Evaluation and Discussion of Solution

Figs. 3 to 5 present the results that were derived from (26) to (28) and (46) to (51) by numerical integration.[7] They represent the response of the infinite plate to a (*a*) step (solid and dashed line) and (*b*) rectangular pulse (solid line) input of concentrated shear load at $r = 0$.

The latter was obtained from the former by simple graphical addition according to

$$[M_r(r,t)]_{RP} = [M_r(r,t)]_S - [M_r(r,t-k)]_S \quad (52)$$

for the moment M_r, for instance, where RP stands for the response to the rectangular pulse and S the step input.

It will be noted that three dimensionless stations r/h (ratio of station r to plate thickness) are represented in Figs. 3 to 5. Consistent generality is contained in the abscissa variable in these curves, $(1/h)(t - r/v_1)$. This is a modified "time after arrival of first wave front" which yields an absolute time for a particular plate thickness. The ordinate variables are all dimensionless. The material constants represented in these figures are $E = 28 \times 10^6$ psi $\nu = 0.3$, and density, $\rho = 7.41$ lb-sec^2/in^4, reflecting a high-strength stainless steel.

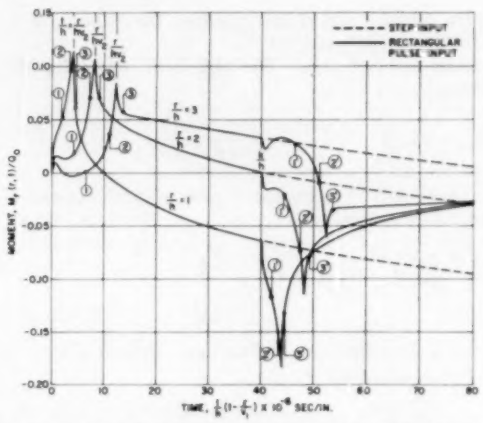

Fig. 3 Moment $M_r(r,t)/Q_0$ response of plate at various stations r/h due to step and rectangular pulse inputs of concentrated shear load at $r = 0$

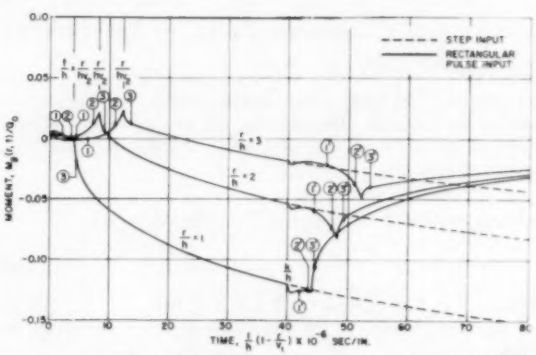

Fig. 4 Moment $M_\theta(r,t)/Q_0$ response of plate at various stations r/h due to step and rectangular pulse inputs of concentrated shear load at $r = 0$

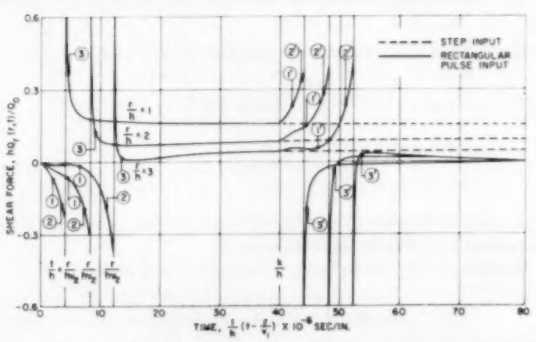

Fig. 5 Shear force $hQ_r(r,t)/Q_0$ response of plate at various stations r/h due to step and rectangular pulse inputs of concentrated shear load at $r = 0$

[7] The numerical integration of the integrals appearing in (46) to (51) was carried out on an 1103A Univac scientific computer. The integration scheme employed a high-order polynomial and a sufficient number of points to represent the integrand in all cases. The modified Bessel functions appearing in these equations were represented in series form for both real and complex arguments. In the case of the latter this meant a series composed of both real and imaginary parts, enabling an evaluation of the $\int_0^1$ integrals in (46) to (51) in the form shown rather than reduce them further. Convergence of an integration to an acceptable numerical value was based on a sufficiency criterion in the number of points used to represent the integrand in the full range of integration; that is, when the number of points used reached a value such that a significant increase in this number did not make a significant change in the numerical integration result, this evaluation was accepted. An even stronger check on results is given through wave-front expansion terms, which are established independently of the solution given in (26) to (28) and (46) to (51). These expansions are derived from the inversion integral-solution statements (21) to (23) for $t > r/v_j$ by letting $|p| \to \infty$ in these integrals and then imposing $t \to r/v_j$ on the resultant inversion which can be found in transform tables. The terms in the present case may be found in the report from which this paper was abstracted [8] along with numerical comparisons with the present integral solution which show good agreement.

Focusing attention first on the curves in Figs. 3 to 5, representing the plate response to the step excitation, it may be seen that consistent with the solution statements, (26) to (28), two resultant waves are involved, the fronts of these waves propagating with the velocities v_1 and v_2, as in a Timoshenko beam. It may be noted in the present case that the concentrated step shear excitation causes no discontinuities in the moment-response curves, although there are discontinuities at the wave fronts in the moment-time derivatives. In the case of the shear force there is no discontinuity associated with the first wave front but an infinite discontinuity occurs at the second wave front (shear front). Hence the step concentrated shear load at $r = 0$ becomes in propagation a more severe discontinuity. It should be emphasized, however, that these wave-front characteristics, although a property of the solution, are not to be considered as accurate information since they represent the very short waves and very high frequencies in the present theory. As Mindlin [9] points out, this theory is good only up to moderately short waves and moderately high frequencies as a comparison with the three-dimensional theory shows (see Fig. 5.071 in this reference).

Considering next the long-time behavior of the moment solutions shown in Figs. 3 and 4 for the step input, it may be seen that the response of both moments at a particular station r/h increases indefinitely with time. In the limit, this long-time behavior should be equivalent to that for the static problem of an infinitely large circular plate subjected to a concentrated load at $r = 0$. It may be shown that the solution for a problem of this type according to the present theory is the same as in the elementary theory. Timoshenko [10] gives the solution for the case of built-in outer edge as

$$\left.\begin{aligned} \frac{M_r}{Q_c} &= \frac{1}{4\pi}\left[(1+\nu)\log\frac{a}{r} - 1\right] \\ \frac{M_\theta}{Q_c} &= \frac{1}{4\pi}\left[(1+\nu)\log\frac{a}{r} - \nu\right] \end{aligned}\right\} \tag{53}$$

where a is the plate radius. Since the stations close to $r = 0$ will be independent of the type of boundaries at large r, this solution suffices to show that for fixed r the moments in an infinitely large plate ($a \to \infty$) are infinite, in agreement with the long-time character exhibited in Figs. 3 and 4. In turn, the long-time shear-load solution should be just $Q_r = Q_0/2\pi r$ or

$$\frac{hQ_r}{Q_0} = \frac{h}{2\pi r} \tag{54}$$

Letting $r/h = 1$ there results $hQ_r/Q_0 = 1/2\pi = 0.159$, in agreement with the long-time limit of the relative curve in Fig. 5. It may be noted that (54) results from just the two nonintegral terms in (50) and (51), added according to the third of (28).

Consider next the curves in Figs. 3 to 5 corresponding to the rectangular pulse input (of duration k/h). In the limit, as t becomes large, the long-time response of the plate (at a station r/h) to the rectangular pulse input should be equivalent to that for the static problem of an unloaded infinitely large circular plate; i.e., zero moments and shear force. Figs. 3 to 5 exhibit this character which follows from (52) and the related equations for M_θ and Q_r.

Of importance in the present problem is the influence of the spacial variable r on the response amplitudes. Before this kind of information can be deduced from the curves in Figs. 3 to 5, however, it is necessary to have some criterion for judging their accuracy. This is necessary since as pointed out earlier the solution given here is derived from a theory that is a good approximation only when limited to moderately short waves and moderately high frequencies. Therefore what is needed is a guide that will establish what parts of the curves in Figs. 3 to 5 are composed predominantly of the longer and lower frequency waves in the theory. Such a guide is contained in a comparison of the predominant period T_p versus time of occurrence t-relations from the exact and the present approximate theories that result from applying Kelvin's stationary phase method to the problem of an infinite plate, subjected initially to a shear load that is infinite at $r = 0$ and zero elsewhere. In the method this initial distribution of shear load is expressed as a Fourier integral. Physically the input might be thought of as the superposition of an infinite number of sinusoidal wave trains, agreeing in phase at the origin at time $t = 0$, but interfering to give zero shear load elsewhere. At time t later, the result at a station r is obtained by summing the contributions due to all the waves, which have traveled ct (where c is the phase velocity). The main effect at station r is due to a small group of waves that have nearly equal phase velocities, periods, and wave lengths, and that are in phase at the station at time t.

The $T_p - t$ relation can be derived from the phase velocity–wave number relation of the theory, related group velocity c_g–wave-number relation, and the stationary phase condition $r - c_g t = 0$. It is convenient to introduce dimensionless variables similar to those used by Davies [11] who first used the present scheme in an analysis of the elastic rod. In the present case the dimensionless predominant period and time of occurrence are

$$\frac{c_s T_p}{h} = \frac{\Lambda c_s}{hc} \quad \text{and} \quad \frac{c_s t}{r} = \frac{c_s r}{r c_g} = \frac{c_s}{c_g} \tag{55}$$

where Λ is wave length.

The phase velocity-wave number relations from the exact (three-dimensional theory) and present approximate theories for the free elastic plate are given in [2]. Use of the well-known $c_g - c$ relation yields the group velocity-wave number relations for the two theories. A particular dimensionless wave number h/Λ, then, yields the dimensionless variables given by (55). The numerical results are given in Fig. 6.[8]

First it should be noted that Fig. 6 reflects the important features of the group velocity-wave number relations of the two theories and their comparison. It shows that as the wave length decreases (accompanying frequency gets higher and period shorter) the

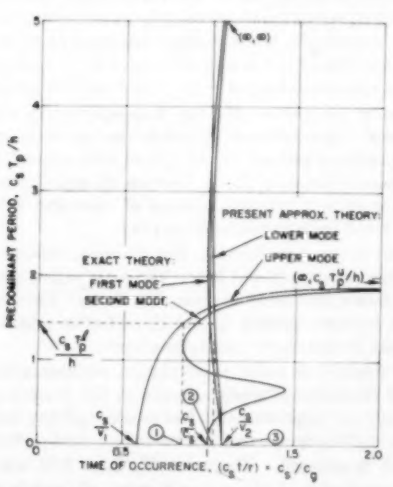

Fig. 6 Comparison of predominant period-time of occurrence curves in present and exact theories ($\nu = 0.3$)

[8] For the present purposes, only this figure is necessary. The phase and group velocity-wave number relations for the first two modes from the exact theory are given in a paper by Tolstoy and Usdin [12].

group velocity of the second mode of the exact theory goes through a maximum and a minimum before reaching its limiting short-wave velocity c_s. On the other hand, the group velocity from the corresponding mode of the approximate theory increases monotonically to its limiting short-wave velocity v_1 which for $\nu = 0.3$ is about 70 percent greater than c_s.

The first mode in the present approximate theory is seen to have excellent agreement with the exact theory for all periods. This, of course, was shown in the phase velocity-wave number comparison in [2]. Fig. 6 shows that there is also excellent agreement of the two theories for the second mode of wave transmission from the upper bound on periods $c_sT_p^u/h$ (an inverse cut-off frequency) down to moderately short periods. The lower bound on second-mode periods $c_sT_p^l/h$ is taken as that predominant period of the approximate theory that occurs at the same time as the related period from the exact theory. The dashed lines in the figure indicate this. The corresponding initial time of interest in Figs. 3 to 5 is based on this criterion then; i.e., the initial dimensionless time will be taken as that marked ① in Fig. 6. This criterion says that for dimensionless times earlier than ① there will be no representation in the second mode of the approximate theory that corresponds to the second mode of the exact theory.[9] For all times later than ① then, as far as their long period (and accompanying low frequency and long wave-length) character is concerned, the solutions (in Figs. 3 to 5 for the step-input case) should be good approximations; i.e., Fig. 6 shows in this region of time good agreement between the present approximate and exact theories for long period waves. Note that the initial time ① has been indicated in Fig. 3 to 5 for each station r/h. It is arrived at easily by noting that the time of occurrence in Fig. 6 can be written as

$$\left(\frac{h}{h}\right)\frac{c_s t}{r} = \frac{c_s}{c_g} \quad \text{hence} \quad \frac{t}{h} = \frac{(r/h)}{c_s}\left(\frac{c_s}{c_g}\right)$$

pointing out the linear dependence the time of occurrence has on the station position.

One further thing must be taken into account in our criterion for judging the accuracy of the curves in Figs. 3 to 5. This is a means for dealing with the discontinuity that occurs in the shear force at $t = r/v_2$, and its coupled effect on the moments occurring at the same time. The literature contains enough conclusive evidence that in bounded elastic media, such as beams and plates, no propagating discontinuities are present. It follows that no such character would be expected from the exact theory. Hence aside from being of interest in pointing out the limitations of the present approximate theory, information from the vicinity of the wave front at $t = r/v_2$ in the present problem will be excluded.[10] The stationary phase solution in Fig. 6 can give no fixed means of deciding on a region about $t = r/v_2$ to exclude in the solutions given by Figs. 3 to 5; i.e., it offers no means of judging amplitudes. It does, however, offer a seemingly logical approximation in this direction.

The scheme is as follows: The lower bound on upper-mode periods $c_sT_p^l/h$ is also taken as the lower bound on the lower-mode periods. The time of occurrence of this period is marked in Fig. 6 as ③, arrived at by extending the dashed horizontal line through $c_sT_p^l/h$ to the right until it intersects the lower-mode curve of the approximate theory. Then if it is assumed that the discontinuity affects the same region before c_s/v_2 as after, the excluded region is taken as that between ③ and ③'; i.e.,

$$c_s/v_2 + c_s/v_2 - ③ = ③'$$

Hence the scheme amounts to imposing the same limitations on both modes of the theory; i.e., periods less than $c_sT_p^l/h$ are not recognized. It should be noted that this lower-bound period limitation is consistent with the upper bound on frequencies argued in [9].

The times ①, ②, and ③ indicated in Figs. 3 to 5 refer to the step-input curves. On each of the curves this criterion means that the disturbance in advance of ① and between ② and ③ is not recognized. This, however, is not a severe limitation on the solution since it may be seen that most of the response curve is acceptable. The same remark applies to the rectangular pulse-input curves where this criterion only adds another set of the same limitations delayed by k/h, indicated by the primed times ①', ②', and ③'. It should be remarked that this stationary phase criterion is best suited to large time analysis. Hence use of it in judging basically short-time results, like those in Figs. 3 to 5 (i.e., r/h stations are in close), may be subject to criticism. However, the author has found, in some earlier work with waves in an elastic rod employing an approximate theory quite similar to that used here, that results from the stationary phase and integral-solution analysis agree very well even for stations close in [14].

The character of the spatial influence in the present solutions is amply demonstrated by the results in Figs. 3 to 5, in spite of the limitations on numerical evaluation at larger r/h stations. Consider the curves representing the response to the rectangular pulse input. The mean of the moment M_r, Fig. 3, in the "valid" region between ① and ② decays very rapidly with r/h, going from $M_r/Q_0 \leqq 0.075$ at $r/h = 1$ to ~ 0.018 at $r/h = 3$. In the region between ③' and k/h the three curves exhibit nearly equal values for the mean moment, although the maximum value in this region is the lowest for the $r/h = 3$ station. The later "valid" regions between primed ① and ② and after primed ③', both show sharp decays in the mean moments with the r/h increase. It may be noted that the tail of the disturbance exhibits rather sizable moment values that seem to decay rather slowly with time. It must be pointed out, however, that the extent of absolute time represented in Figs. 3 to 5 is rather short, an $h = {}^1/_4$-in. plate, for instance, is represented by just $\sim 18 \times 10^{-6}$ sec in these figures.

The mean of the moment M_θ, Fig. 4, decays rapidly with r/h in the important region between ③ and k/h and in the later regions of validity between primed ① and ② and after primed ③'. The mean moment in the early region between ① and ② is relatively unimportant from a magnitude point of view and exhibits no particular trend in its dependence on r/h.

The mean of the shear force Q_r, Fig. 5, decays rapidly with r/h in the region between ③ and k/h. The early region between ① and ② exhibits a slow decay in mean shear force. The later region of validity between primed ① and ③ and after primed ③' also exhibit rapid decays in the mean shear force.

It is of interest to make a calculation representative of the outer fiber (maximum) tensile stresses in the present problem. Since the present approximation has greater validity with larger distance from the origin, a moment value representing the $r/h = 3$ station will be selected. The value $M_r/Q_0 = 0.05$ will be used being representative of the region between ③ and k/h, Fig. 3. It is also representative of the M_θ/Q_0 response at $r/h = 3$ for the

[9] It should be emphasized that ① signifies the earliest arriving disturbance, governed by the exact theory, only when the lowest two modes are considered. Actually when higher modes of transmission are taken into account they govern, as Tolstoy and Usdin [13] have shown, earlier arrival times (larger c_g) than the second mode. These higher modes become more important as the impact becomes sharper and of shorter duration.

[10] It should be noted that this is still consistent with the results in Fig. 6. Even though the predominant periods are in agreement at c_s/v_2 it does not necessarily follow that amplitudes there have to have like agreement. In particular an approximate theory, based on "plane sections remain plane," such as the present one, would not be expected to give reliable information based on its very short-wave character.

later region after primed ③, Fig. 4. The outer fiber stresses then are given by

$$\sigma_{\theta 0} = \sigma_{r0} = \frac{0.3Q_0}{h^2} \tag{56}$$

With say a load Q_0 of 5000 lb and a plate thickness h of $^1/_4$ in. (56) gives stresses of 24,000 psi.

Figs. 3 to 5 bring out another interesting point worth mentioning. They indicate that, if the pulse time k is made smaller, the magnitudes of the moment response becomes less. Figs. 3 to 5 bring this out with a shift of the k/h point to the left which cuts off the long-time step response earlier. Hence with a shorter pulse it appears that the stresses are reduced. Said in other words, the longer pulse with its relatively longer wave influence excites the higher stresses. It appears that the shear force Q_r is not as sensitive to this effect.

Acknowledgments

Acknowledgment is due Mr. Francis Welsh, Jr., of the Computing Center at Space Technology Laboratories, Inc., who contributed the numerical evaluation work contained herein.

References

1 Ya. S. Uflyand, "The Propagation of Waves in the Transverse Vibrations of Bars and Plates," Akad. Nauk, *USSR Prikladnaya Matematika i Mekhanika*, vol. 12, 1948, pp. 287–300.

2 R. D. Mindlin, "Influence of Rotary Inertia and Shear on Flexural Motions of Isotropic, Elastic Plates," JOURNAL OF APPLIED MECHANICS, vol. 18, TRANS. ASME, vol. 73, 1951, pp. 31–38.

3 J. L. Lubkin, "Propagation of Elastic Impact Stresses," ONR Progress Report No. 5, Contract No. Nonr-704(00), April, 1954.

4 J. Miklowitz, "Flexural Wave Solutions of Coupled Equations Representing the More Exact Theory of Bending," JOURNAL OF APPLIED MECHANICS, vol. 20, TRANS. ASME, vol. 75, 1953, pp. 511–514.

5 J. Miklowitz, "Flexural Waves in Beams According to the More Exact Theory of Bending," NAVORD Report No. 2049, NOTS, China Lake, Calif., September, 1953.

6 A. Erdelyi, W. Magnus, F. Oberhettinger, and F. G. Tricomi, "Higher Transcendental Functions," Bateman Project, McGraw-Hill Book Company, Inc., New York, N. Y.,1953, p. 86.

7 N. W. McLachlan, "Complex Variable Theory and Transform Calculus," Cambridge University Press, Cambridge, England, second edition, 1953, p. 65.

8 J. Miklowitz, "Flexural Stress Waves Generated by the Sudden Punching Process in a Stretched Elastic Plate," Space Technology Laboratories, Inc., Report No. TR-59-0000-00701, June 5, 1959, pp. 28–29.

9 R. D. Mindlin, "An Introduction to the Mathematical Theory of Vibrations of Elastic Plates," U. S. Army Signal Corps Engineering Laboratories Monograph, Fort Monmouth, N. J., 1955, pp. 5.25–5.29.

10 S. Timoshenko, "Theory of Plates and Shells," McGraw-Hill Book Company, Inc., New York, N. Y., 1940, p. 75.

11 R. M. Davies, "A Critical Study of the Hopkinson Pressure Bar," *Philosophical Transactions of The Royal Society of London*, series A, vol. 240, 1948, pp. 375–457.

12 I. Tolstoy and E. Usdin, "Dispersive Properties of Stratified Elastic and Liquid Media: A Ray Theory," *Geophysics*, vol. 18, 1953, pp. 844–870.

13 I. Tolstoy and E. Usdin, "Wave Propagation in Elastic Plates: Low and High Mode Dispersion," *Journal of the Acoustical Society of America*, vol. 29, 1957, pp. 37–42.

14 J. Miklowitz, "The Propagation of Compressional Waves in a Dispersive Elastic Rod," JOURNAL OF APPLIED MECHANICS, vol. 24, TRANS. ASME, vol. 79, 1957, pp. 231–239.

A. KALNINS
Assistant Professor of Civil Engineering, Yale University, New Haven, Conn.
Assoc. Mem. ASME

P. M. NAGHDI
Professor of Engineering Science, University of California, Berkeley, Calif.
Mem. ASME

Propagation of Axisymmetric Waves in an Unlimited Elastic Shell[1]

This investigation is concerned with the propagation of axisymmetric stress waves in unlimited thin shallow elastic spherical shells. In particular, a solution is obtained for an unlimited shallow spherical shell subjected to a harmonically oscillating concentrated load at the apex. This solution, exact within the scope of the linear theory of shallow shells, has an outward propagating wave character in the entire range of forcing frequency. Appropriate expressions for the mechanical impedance and the energy input are derived, and numerical results are obtained for the axial displacement corresponding to various forcing frequencies.

In a recent investigation [1],[2] the general problem of elastokinetics in the theory of thin shallow elastic shells was reduced to a system of simultaneous differential equations in terms of the axial displacement of the shell and a stress function. This system of equations, upon linearization and the neglect of the entire effect of longitudinal inertia, reduces to that given by E. Reissner [2] for *transverse* vibrations of shallow shells.[3] More recently, with the use of the exact linearized equations given in [1], the natural frequencies and amplitude ratios for free axisymmetric vibrations of a spherical shell segment with various edge conditions have been obtained in [3], where in particular the case of a shell segment with a free edge is treated in detail.

The present paper, utilizing the exact system of linearized differential equations derived in [1], is primarily concerned with the propagation of axisymmetric stress waves in an unlimited[4] shallow elastic spherical shell, which are generated by an oscillating concentrated normal load at the apex of the shell. The solution, in terms of the axial displacement and a stress function, is exact within the scope of the classical theory of shallow shells and describes the character of the stress waves emanating from the apex. In addition, expressions for the mechanical impedance, the power input, and the work done over a cycle are deduced, and an interesting comparison is drawn with the corresponding results predicted by the differential equations for *transverse* motion of shallow shells.

It is relevant to recall here that the radially symmetric wave propagation in a flat plate subjected to an oscillating point load has been treated by H. and L. Cremer [4], while the mechanical impedance for a thin elastic plate is discussed in references [4–8]. Furthermore, a solution for an unlimited shell with an oscillating point load at the apex has been obtained in [9] with the use of the approximate kinetic equations for shallow shells (valid for *transverse* vibrations), where the effect of longitudinal inertia is neglected. If ω is the forcing frequency, R the radius of curvature of the middle surface, E the Young's modulus, and ρ the mass density, then it is concluded in [9, Secs. 6 and 7] that sufficiently far from the point of application of the load, the solution in the high-frequency range $[\omega > (E/\rho)^{1/2}/R]$ represents outward traveling waves, while in the low-frequency range $[\omega < (E/\rho)^{1/2}/R]$ the solution is of a standing-wave type with fixed nodes.

The solution obtained here reduces directly to the appropriate results for an infinite plate under an oscillating point load [4] and a shallow spherical shell subjected to a static concentrated load at the apex [10]. In contrast to the conclusions drawn in [9] with the use of the kinetic equations for *transverse* motion, the solution given here possesses a traveling-wave character in the entire forcing-frequency range, and at no time do standing waves occur. Morever, the expression for the work done by the point load over a cycle is shown to be nonzero for all forcing frequencies; this latter conclusion is in accord with the corresponding result in [4], but differs from that predicted by the equations for *transverse* motion of shallow shells [9].

It may be pointed out that although attention is confined here to the response of unlimited shallow shells subjected to harmonically oscillating loads, the treatment of related axisymmetric problems with the same system of differential equations is also possible. Thus the extension to a more general type of axisymmetric loading, as well as to shallow shell segments, offers no fundamental difficulties and may be carried out with the use of integral transforms in a manner similar to that for elastic plates [5] and *transverse* vibrations of shallow viscoelastic spherical shells [11].

Solution of Differential Equations for Axisymmetric Motion of Shallow Spherical Shells

With reference to polar co-ordinates, it is shown in [3] that the exact linearized system of kinetic equations, deduced as a special case of the general formulation in [1], for torsionless axisymmetric deformation of shallow spherical shells, and in the absence of surface loads, may be written as

$$\left[\nabla^2 - \frac{\rho(1-\nu^2)}{E}\frac{\partial^2}{\partial t^2}\right] F - \frac{Eh}{R} w = 0 \qquad (1a)$$

[1] The results presented here were obtained in the course of research sponsored by The Office of Naval Research under Contract Nonr-222(69), Project NR-064-436, with the University of California, Berkeley, Calif.

[2] Numbers in brackets designate References at end of paper.

[3] See [1] for an historical account of the subject. Reference [1], in addition to the exact system of nonlinear equations, contains two other systems for nonlinear vibrations, only one of which when linearized reduces to that in [2].

[4] Recall that here the use of the term "unlimited" implies that the (outer) edge of the shell is sufficiently far removed from the shallow region so that no reflection occurs.

Contributed by the Applied Mechanics Division and presented at the Winter Annual Meeting, New York, N. Y., November 27–December 2, 1960, of The American Society of Mechanical Engineers.

Discussion of this paper should be addressed to the Secretary, ASME, 29 West 39th Street, New York, N. Y., and will be accepted until January 10, 1961, for publication at a later date. Discussion received after the closing date will be returned.

Manuscript received by ASME Applied Mechanics Division, March 7, 1960. Paper No. 60—WA-22.

$$\left[\nabla^2\nabla^2 + \frac{\rho h}{D}\frac{\partial^2}{\partial t^2}\right] w + \frac{1}{DR}\left[\nabla^2 - \frac{2\rho(1+\nu)}{E}\frac{\partial^2}{\partial t^2}\right] F = 0 \tag{1b}$$

where w is the axial displacement of the middle surface; F is a stress function; E, ρ, and R are as defined before; ν is Poisson's ratio; t denotes time; h is the thickness of the shell;

$$D = \frac{Eh^3}{12(1-\nu^2)}, \quad \text{and} \quad \nabla^2 \equiv \frac{\partial^2}{\partial r^2} + \frac{1}{r}\frac{\partial}{\partial r}$$

The stress-resultants $\{N_r, N_\theta\}$ are given by

$$N_r = \left[\frac{1}{r}\frac{\partial}{\partial r} - \frac{\rho(1+\nu)}{E}\frac{\partial^2}{\partial t^2}\right] F \tag{2a}$$

$$N_\theta = \left[\frac{\partial^2}{\partial r^2} - \frac{\rho(1+\nu)}{E}\frac{\partial^2}{\partial t^2}\right] F \tag{2b}$$

and the remaining relevant quantities may be obtained in terms of F and w from the usual relations of the theory of shallow shells and are given in detail in [3]. Since they will be necessary in the sequel, we also record here the expressions for the transverse shear stress-resultant Q_r and the meridional displacement u, i.e.,

$$Q_r = -D\frac{\partial}{\partial r}(\nabla^2 w) \tag{3}$$

$$u = -\frac{1+\nu}{Eh}\frac{\partial F}{\partial r} \tag{4}$$

It should be noted that while the system of equations (1) is exact within the scope of the classical theory of shallow shells, the omission of terms involving time derivatives of F in (1) and (2)[5] leads to the system of equations for *transverse* vibrations of shallow shells [9], in which case F becomes an Airy stress function.

In the following, we consider the steady-state solution of the system of equations (1) when the dependent variables vary harmonically with time; i.e.,

$$w = \mathrm{Re}\{w^* \exp(i\omega t)\}, \quad F = \mathrm{Re}\{F^* \exp(i\omega t)\} \tag{5}$$

where the symbol Re denotes the "real part of" and $i = \sqrt{-1}$. Thus the general solution of (1) for our present purposes may be conveniently expressed in terms of Hankel functions in the form[6]

$$w^* = \sum_{\alpha=1}^{3}\left[A_\alpha H_0^{(1)}\left(\mu_\alpha \frac{r}{l}\right) + B_\alpha H_0^{(2)}\left(\mu_\alpha \frac{r}{l}\right)\right] \tag{6a}$$

$$F^* = \frac{Eh l^2}{R}\sum_{\alpha=1}^{3}\left[\left(\frac{1-\nu^2}{12}\right)^{1/2}\frac{h}{R}\Omega^2 - \mu_\alpha^2\right]^{-1}\left[A_\alpha H_0^{(1)}\left(\mu_\alpha \frac{r}{l}\right) + B_\alpha H_0^{(2)}\left(\mu_\alpha \frac{r}{l}\right)\right] \tag{6b}$$

where the parameters μ_α in (6) are the roots of

$$\mu^6 - \left(\frac{1-\nu^2}{12}\right)^{1/2}\frac{h}{R}\Omega^2\mu^4 - (\Omega^2 - 1)\mu^2 + \frac{h}{R}\Omega^2\left(\frac{1-\nu^2}{12}\right)^{1/2}\left(\Omega^2 - \frac{2}{1-\nu}\right) = 0 \tag{7a}$$

given by

$$\left.\begin{aligned}
\mu_1^2 &= A + B + \frac{1}{3}\left(\frac{1-\nu^2}{12}\right)^{1/2}\frac{h}{R}\Omega^2 \\
\begin{Bmatrix}\mu_2^2 \\ \mu_3^2\end{Bmatrix} &= -\frac{1}{2}(A+B) + \frac{1}{3}\left(\frac{1-\nu^2}{12}\right)^{1/2}\frac{h}{R}\Omega^2 \pm i\frac{\sqrt{3}}{2}(A-B) \\
\begin{Bmatrix}A \\ B\end{Bmatrix} &= \left[-\frac{n}{2} \pm \Delta^{1/2}\right]^{1/3} \\
\Delta &= \left(\frac{n}{2}\right)^2 + \left(\frac{m}{3}\right)^3 \\
m &= -\frac{1}{36}\left[(1-\nu^2)\left(\frac{h}{R}\right)^2\Omega^4 + 36(\Omega^2 - 1)\right] \\
n &= -\frac{1}{27}\frac{h}{R}\Omega^2\left(\frac{1-\nu^2}{12}\right)^{1/2}\left[\left(\frac{h}{R}\right)^2\frac{1-\nu^2}{6}\Omega^4 - 18\Omega^2 + \frac{54}{1-\nu} - 9\right]
\end{aligned}\right\} \tag{7b}$$

$$l^4 = \frac{R^2h^2}{12(1-\nu^2)} \qquad \Omega^2 = \frac{\rho\omega^2R^2}{E} \tag{7c}$$

The form of the solution (6) is particularly suited for the study of radially symmetric two-dimensional wave propagation,[7] since, for μ_α real, the terms involving $H_0^{(1)}$ in (6a) represent incoming waves moving toward the apex, while the terms involving $H_0^{(2)}$ represent outgoing waves emanating from the apex.

Stress Waves in an Unlimited Shallow Spherical Shell

In what follows, by way of application of the foregoing solution, we consider the propagation of axisymmetric stress waves in an unlimited shallow spherical shell subjected to an oscillating normal concentrated load $P = P^*e^{i\omega t}$ at the apex $r = 0$. The regularity requirements at the apex of the shell demand that

$$\lim_{r\to 0} 2\pi r Q_r = P \tag{8a}$$

$$\left\{w, \frac{\partial w}{\partial r}, F, \frac{\partial F}{\partial r}, \frac{\partial^2 F}{\partial r^2}\right\} \text{ are finite at } r = 0 \tag{8b}$$

and the boundary conditions at infinity require the vanishing of the displacement vector, which for axisymmetric deformation of shallow spherical shells is characterized by

$$\left\{w, \frac{\partial w}{\partial r}, u\right\} \to 0 \quad \text{as} \quad r \to \infty \tag{9}$$

It follows from (7b) that μ_1 is always real and positive, and further examination of (7b) reveals that the remaining roots of (7a) may be written in the form $\mu_2 = \rho_2 \exp(i\alpha_2)$, $\mu_3 = \rho_3 \exp(-i\alpha_3)$, where $(\rho_2, \rho_3) \geq 0$, and $0 \leq (\alpha_2, \alpha_3) \leq \pi/2$. Recalling that for large values of the argument the Hankel functions have the asymptotic form

$$\left.\begin{aligned}
H_0^{(1)}(\rho e^{\pm i\alpha}) &\simeq \left(\frac{2}{\pi\rho}\right)^{1/2} e^{\mp\rho\sin\alpha}\, e^{i\left(\rho\cos\alpha \mp \frac{\alpha}{2} - \frac{\pi}{4}\right)} \\
H_0^{(2)}(\rho e^{\pm i\alpha}) &\simeq \left(\frac{2}{\pi\rho}\right)^{1/2} e^{\pm\rho\sin\alpha}\, e^{-i\left(\rho\cos\alpha \pm \frac{\alpha}{2} - \frac{\pi}{4}\right)}
\end{aligned}\right\} \tag{10}$$

[5] The omission of these terms in (1) and (2) is equivalent to the neglect of the effects of longitudinal inertia.

[6] This solution may be utilized for free vibrations of shallow spherical shell segments as well as wave propagation problems, which are of main concern here. In the former case, the form of solution as used in [3] is more convenient. For notation and other relations concerning Hankel functions see [12].

[7] Reference [13], vol. 2, p. 1371.

then with the aid of (10), it is easily concluded that the solution (6) meets (9) provided $B_2 = A_3 = 0$. Moreover, the requirement that the propagated wave be divergent, which is equivalent to Sommerfeld's radiation condition[8]

$$\lim_{r\to\infty} r^{1/2}\left[\frac{\partial w^*}{\partial r} + i\,\frac{\mu_1}{l}\,w^*\right] = 0,$$

leads to $A_1 = 0$, and the solution (6) reduces to

$$w^* = B_1 H_0^{(2)}\left(\mu_1 \frac{r}{l}\right) + A_2 H_0^{(1)}\left(\mu_2 \frac{r}{l}\right) + B_3 H_0^{(2)}\left(\mu_3 \frac{r}{l}\right)$$

$$F^* = \frac{Ehl^2}{R}\left\{\frac{B_1 H_0^{(2)}\left(\mu_1 \frac{r}{l}\right)}{\left(\frac{1-\nu^2}{12}\right)^{1/2}\frac{h}{R}\,\Omega^2 - \mu_1^2} + \frac{A_2 H_0^{(1)}\left(\mu_2 \frac{r}{l}\right)}{\left(\frac{1-\nu^2}{12}\right)^{1/2}\frac{h}{R}\,\Omega^2 - \mu_2^2} + \frac{B_3 H_0^{(2)}\left(\mu_3 \frac{r}{l}\right)}{\left(\frac{1-\nu^2}{12}\right)^{1/2}\frac{h}{R}\,\Omega^2 - \mu_3^2}\right\}$$

Next, with the observation that

$$\lim_{\rho\to 0} H_1^{(1)}(\rho e^{i\alpha}) = -i \lim_{\rho\to 0}\frac{2}{\pi\rho}\,e^{-i\alpha}$$
$$\lim_{\rho\to 0} H_1^{(2)}(\rho e^{i\alpha}) = i \lim_{\rho\to 0}\frac{2}{\pi\rho}\,e^{-i\alpha} \qquad (11)$$

the conditions (8) yield the following nonhomogeneous system of equations

$$B_1 - A_2 + B_3 = 0$$
$$\frac{B_1}{\gamma_1} - \frac{A_2}{\gamma_2} + \frac{B_3}{\gamma_3} = 0 \qquad (12)$$
$$\mu_1^2 B_1 - \mu_2^2 A_2 + \mu_3^2 B_3 = i\Lambda$$

whose solution may be written in the form

$$B_1 = i\Lambda\Gamma_1 \qquad A_2 = -i\Lambda\Gamma_2 \qquad B_3 = i\Lambda\Gamma_3 \qquad (13a)$$

where

$$\Gamma_1 = \frac{\gamma_1}{(\gamma_3-\gamma_1)(\gamma_2-\gamma_1)},\quad \Gamma_2 = \frac{\gamma_2}{(\gamma_1-\gamma_2)(\gamma_3-\gamma_2)},$$
$$\Gamma_3 = \frac{\gamma_3}{(\gamma_2-\gamma_3)(\gamma_1-\gamma_3)} \qquad (13b)$$

$$\gamma_\alpha = \mu_\alpha^2 - \left(\frac{1-\nu^2}{12}\right)^{1/2}\frac{h}{R}\,\Omega^2,\quad \Lambda = {}^1\!/_4\,\frac{P^*R}{Eh^2}\,[12(1-\nu^2)]^{1/2} \qquad (13c)$$

Thus with $A_1 = A_3 = B_2 = 0$ and (13), the solution (6), for the problem at hand, finally becomes

$$w = \Lambda\,\mathrm{Re}\left\{\left[i\Gamma_1 H_0^{(2)}\left(\mu_1\frac{r}{l}\right) - i\Gamma_2 H_0^{(1)}\left(\mu_2\frac{r}{l}\right) + i\Gamma_3 H_0^{(2)}\left(\mu_3\frac{r}{l}\right)\right]\exp(i\omega t)\right\} \qquad (14a)$$

$$F = \frac{P^*R}{4}\,\mathrm{Re}\left\{\left[-\frac{i\Gamma_1}{\gamma_1}H_0^{(2)}\left(\mu_1\frac{r}{l}\right) + \frac{i\Gamma_2}{\gamma_2}H_0^{(1)}\left(\mu_2\frac{r}{l}\right) - \frac{i\Gamma_3}{\gamma_3}H_0^{(2)}\left(\mu_3\frac{r}{l}\right)\right]\exp(i\omega t)\right\} \qquad (14b)$$

[8] For a discussion of the radiation condition see [14], p. 189.

We now proceed to discuss the character of the solution (14) for two separate frequency ranges: (*a*) The "high"-frequency range $\Omega_0 \leq \Omega < \infty$; (*b*) the "low"-frequency range $0 \leq \Omega < \Omega_0$.

(*a*) The forcing frequencies that satisfy the relation $\Delta \leq 0$ fall within the range $\Omega_0 \leq \Omega < \infty$, where the value of Ω_0 corresponds to $\Delta = 0$ and is a function of both h/R and ν. In this range, since the phase of μ_2 is always $\pi/2$ and Γ_α are real, the real and imaginary parts of w^* in (14*a*) are easily separable; this is accomplished with the use of the identities

$$H_0^{(2)}\left(\rho e^{-i\frac{\pi}{2}}\right) = -H_0^{(1)}\left(\rho e^{i\frac{\pi}{2}}\right) = i\,\frac{2}{\pi}\,K_0(\rho),$$

where ρ is real and positive and $K_0(\rho)$ is the modified Bessel function. For frequencies $\Omega_0 \leq \Omega < \Omega^* = [2/(1-\nu)]^{1/2}$, the phase of μ_3 is $-\pi/2$, and (14*a*) permits a convenient representation in the form

$$w = \Lambda\,\mathrm{Re}\left\{\left[i\Gamma_1 H_0^{(2)}\left(\mu_1\frac{r}{l}\right) - \Gamma_2\frac{2}{\pi}K_0\left(\rho_2\frac{r}{l}\right) - \Gamma_3\frac{2}{\pi}K_0\left(\rho_3\frac{r}{l}\right)\right]\exp(i\omega t)\right\} \qquad (15)$$

For $\Omega^* < \Omega$ the phase of μ_3 is zero, and (14*a*) may then be written as

$$w = \Lambda\,\mathrm{Re}\left\{\left[i\Gamma_1 H_0^{(2)}\left(\mu_1\frac{r}{l}\right) - \Gamma_2\frac{2}{\pi}K_0\left(\rho_2\frac{r}{l}\right) + i\Gamma_3 H_0^{(2)}\left(\mu_3\frac{r}{l}\right)\right]\exp(i\omega t)\right\} \qquad (16)$$

The transition frequency Ω^*, which separates the solutions (15) and (16), is of a special significance. It may be seen from (7) that $\Omega = \Omega^*$ renders $\mu_3 = 0$, and consequently, the solutions (15) and (16) in the limit as $\Omega \to \Omega^*$ exhibit a logarithmic singularity, which is reminiscent of resonance phenomena in forced vibration problems. Similar resonance frequencies are also present in other problems of wave propagation in elastic media; for example, they occur in the corresponding solution of the problem considered here deduced by the differential equations for *transverse* motion [9] and in the solution of an infinite Timoshenko beam on an elastic foundation subjected to an oscillating load [15]. It should be added that inclusion of viscous damping in the governing differential equations would remove this resonance character, while addition of the effect of transverse shear deformation and rotatory inertia (in the absence of damping) will still yield the same resonance frequency as predicted by the differential equations (1).

(*b*) If the frequency satisfies the inequality $\Delta > 0$, then $\rho_2 = \rho_3$, $\alpha_2 = \alpha_3$, and $0 \leq \Omega < \Omega_0$. Since Γ_2, Γ_3 are complex conjugates, with the use of the relation

$$H_0^{(2)}\left(\rho e^{-i\alpha}\frac{r}{l}\right) = \overline{H}_0^{(1)}\left(\rho e^{i\alpha}\frac{r}{l}\right),$$

where $\overline{H}_0^{(1)}$ denotes the complex conjugate of $H_0^{(1)}$, it is seen that the last two terms of (14) are complex conjugates, and consequently, their sum is real. In this frequency range, by letting $\gamma_3 = \xi + i\zeta$, (14*a*) may be expressed as

$$w = \frac{\Lambda}{(\xi-\gamma_1)^2+\zeta^2}\,\mathrm{Re}\left\{\left[i\gamma_1 H_0^{(2)}\left(\mu_1\frac{r}{l}\right) + \frac{\xi\gamma_1 - \xi^2 - \zeta^2}{\zeta}\,\mathrm{Re}\,H_0^{(1)}\left(\mu_2\frac{r}{l}\right) - \gamma_1\,\mathrm{Im}\,H_0^{(1)}\left(\mu_2\frac{r}{l}\right)\right]\exp(i\omega t)\right\} \qquad (17)$$

where Im denotes the "imaginary part of."

Examination of the foregoing solutions reveals that the first term of (15) and (17) and the first and third terms of (16) represent (outward traveling) radially symmetric two-dimensional waves, while the remaining terms decay exponentially as $r \to \infty$. On account of the asymptotic behavior of Bessel functions with large real arguments, i.e.,

$$J_0\left(\mu \frac{r}{l}\right) \simeq \left(\frac{2l}{\pi\mu r}\right)^{1/2} \cos\left(\mu \frac{r}{l} - \frac{\pi}{4}\right)$$

$$Y_0\left(\mu \frac{r}{l}\right) \simeq \left(\frac{2l}{\pi\mu r}\right)^{1/2} \sin\left(\mu \frac{r}{l} - \frac{\pi}{4}\right)$$

the solution at a large distance from the apex (or large values of $\mu_\alpha r/l$) for $0 \leqq \Omega < \Omega^*$ may be obtained from either (15) or (17) and reads

$$w \simeq A\Gamma_1 \left(\frac{2l}{\pi\mu_1 r}\right)^{1/2} \cos\left(\mu_1 \frac{r}{l} - \frac{\pi}{4} - \omega t\right) \tag{18a}$$

while for $\Omega^* < \Omega$ by (16)

$$w \simeq A\left(\frac{2l}{\pi r}\right)^{1/2} \left[\frac{\Gamma_1}{\sqrt{\mu_1}} \cos\left(\mu_1 \frac{r}{l} - \frac{\pi}{4} - \omega t\right) + \frac{\Gamma_2}{\sqrt{\mu_2}} \cos\left(\mu_2 \frac{r}{l} - \frac{\pi}{4} - \omega t\right)\right] \tag{18b}$$

It should be noted that expressions (18) represent trains of harmonic waves which travel outward with a velocity $c_\alpha = \omega l/\mu_\alpha$ and wave-length $\lambda_\alpha = 2\pi l/\mu_\alpha$ [$\alpha = 1$ for (18a) and $\alpha = 1,2$ for (18b)]. Since the disturbance produced by the point load does not propagate without dispersion, the group velocity C_α of the wave trains is different from the phase velocity c_α and at a large distance from the apex is given by $C_\alpha = l(d\mu_\alpha/d\omega)^{-1}$. The amplitude of the wave profile decays as $r^{-1/2}$ with increasing r in the whole forcing frequency range $0 < \omega < \infty$. The latter conclusion is in accord with that reached in [4] for an infinite plate, but differs from the corresponding results for transverse vibrations [9], where for the lower frequency range the amplitude decay is exponential and no traveling wave is produced.

Reduction to Special Cases

In this section we consider the reduction of the solution (14) to the previously known special cases.

For the case of a plate, since $R = \infty$, it is necessary to modify the parameters occurring in (14) so that they do not involve R. Let $\eta_\alpha = \mu_\alpha/l$, then it follows from (7) that for a flat plate

$$\eta_1 = \left[\frac{\rho h\omega^2}{D}\right]^{1/4} \qquad \eta_2 = i\left[\frac{\rho h\omega^2}{D}\right]^{1/4} \qquad \eta_3 = \left[\frac{\rho(1-\nu^2)\omega^2}{E}\right]^{1/2} \tag{19a}$$

and (13) in the limit as $R \to \infty$, yields

$$A\Gamma_1 = \frac{1}{8}\frac{P^*}{k\omega D} \qquad A\Gamma_2 = -\frac{1}{8}\frac{P^*}{k\omega D} \qquad A\Gamma_3 = 0 \tag{19b}$$

where $k = [\rho h/D]^{1/4}$. Then the expression for the transverse displacement w as given by (14a) reduces to

$$w = \frac{P^*}{8k\omega D} \operatorname{Re}\{i[H_0^{(1)}\langle(k\omega)^{1/2}r\rangle + H_0^{(1)}\langle i(k\omega)^{1/2}r\rangle] \exp(i\omega t)\} \tag{20}$$

which is precisely the solution derived in [4].

To carry out the reduction of the solution (14) to the elastostatic case, let in (7) $\omega \to 0$ and obtain $\gamma_1 = 0$, $\gamma_2 = i$, and $\mu_2 = i^{1/2}$. With the aid of the relation

$$H_0^{(1)}\left(i^{3/2}\frac{r}{l}\right) = -\frac{2}{\pi}\operatorname{kei}\frac{r}{l} - i\frac{2}{\pi}\operatorname{ker}\frac{r}{l} \tag{21}$$

where kei and ker denote Kelvin functions, (14a) becomes

$$w = \frac{1}{2\pi}\frac{P^*R}{Eh^2}[12(1-\nu^2)]^{1/4} \operatorname{kei}\frac{r}{l} \quad . \tag{22}$$

which agrees with that given in [10].

Owing to the approximation of the neglect of the longitudinal inertia introduced in the system of equations for *transverse* vibrations of shallow spherical shells, the character of the solution in [9] is different from that of (14). While the foregoing reduction to the results in [4] and [10] is accomplished by assigning limiting values of the variable parameters R and ω, the neglect of the longitudinal inertia, on the other hand, demands setting $\omega = 0$ in some but not all terms of (7). Consequently, a direct reduction of (14) to the solution given in [9] is not possible, and it is necessary to return to the system of differential equations for *transverse* vibrations, which as pointed out earlier may be obtained from (1) by omitting the terms involving time derivatives of F.

The Driving-Point Impedance of a Shallow Spherical Shell and the Energy Input

The expression for the driving-point (mechanical) impedance Z for a shallow spherical shell under a concentrated normal load P at the apex ($r = 0$) may be written as the ratio of P to the velocity of the apex, i.e.,

$$Z = P\Big/\left(\frac{\partial w}{\partial t}\right)_{r=0} \tag{23}$$

The axial displacement and velocity at $r = 0$, by (14), are

$$w_0 = A\operatorname{Re}\left\{\left[\Gamma_1\left(\frac{2}{\pi}\log\mu_1 + i\right) + \Gamma_2\left\langle\frac{2}{\pi}\log\rho_2 - i\left(1 - \frac{2}{\pi}\alpha_2\right)\right\rangle + \Gamma_3\left\langle\frac{2}{\pi}\log\rho_3 + i\left(1 - \frac{2}{\pi}\alpha_3\right)\right\rangle\right]\exp(i\omega t)\right\} \tag{24a}$$

and

$$\left(\frac{\partial w}{\partial t}\right)_0 = A\omega\operatorname{Re}\left\{\left[-\Gamma_1\left(1 - i\frac{2}{\pi}\log\mu_1\right) + \Gamma_2\left(1 - \frac{2}{\pi}\alpha_2 + i\frac{2}{\pi}\log\rho_2\right) - \Gamma_3\left(1 - \frac{2}{\pi}\alpha_3 - i\frac{2}{\pi}\log\rho_3\right)\right]\exp(i\omega t)\right\} \tag{24b}$$

with the aid of which by (23)

$$Z^{-1} = {}^1/_4\frac{R}{Eh^2}[12(1-\nu^2)]^{1/4}\omega\left\{-\Gamma_1\left(1 - i\frac{2}{\pi}\log\mu_1\right) + \Gamma_2\left(1 - \frac{2}{\pi}\alpha_2 + i\frac{2}{\pi}\log\rho_2\right) - \Gamma_3\left(1 - \frac{2}{\pi}\alpha_3 - i\frac{2}{\pi}\log\rho_3\right)\right\} \tag{25}$$

It is of interest to note here that the axial displacement, as well as the velocity of the apex, is out of phase with the oscillating

force P, and that the phase difference is, in general, neither $\pi/2$ nor π. This observation differs from that for a flat plate [4], where the displacement and the velocity of the driving-point are out of phase with P by $\pi/2$ and π, respectively. On account of the phase difference between the velocity and P, the impedance (25) is neither independent of the forcing frequency nor real; it may be shown readily with the aid of (19) that for a flat plate (25) becomes real and independent of frequency—a result explicitly derived in [4]. As it turns out, for *transverse* vibrations of a shallow spherical shell the driving-point impedance is real in the high-frequency range and imaginary in the low-frequency range.

The instantaneous power input by the oscillating force at the apex as given by

$$L = \frac{1}{4}\frac{(P^*)^2R}{Eh^2}\,[12(1-\nu^2)]^{1/2}\omega\cos\omega t$$
$$\mathrm{Re}\left\{\left[-\Gamma_1\left(1-i\frac{2}{\pi}\log\mu_1\right)+\Gamma_2\left(1-\frac{2}{\pi}\alpha_2+i\frac{2}{\pi}\log\rho_2\right)\right.\right.$$
$$\left.\left.-\Gamma_3\left(1-\frac{2}{\pi}\alpha_2-i\frac{2}{\pi}\log\rho_2\right)\right]\exp(i\omega t)\right\} \quad (26)$$

represents the energy per unit time that is absorbed by the shell medium and propagates outward in the form of strain energy. Since the shell is elastic and there is no dissipative energy loss, then at any instant the same amount of energy per unit time as given by (26) is transmitted through any cylindrical surface $r = C$, C being a constant.

The work done by the point load at the apex over a cycle ($0 \leqq \leqq 2\pi/\omega$) is obtained from (26) and reads

$$W = \frac{\pi}{4}\frac{(P^*)^2R}{Eh^2}\,[12(1-\nu^2)]^{1/2}\,\mathrm{Re}\left\{-\Gamma_1+\Gamma_2\left(1-\frac{2}{\pi}\alpha_2\right)\right.$$
$$\left.-\Gamma_3\left(1-\frac{2}{\pi}\alpha_2\right)\right\} \quad (27)$$

Here it should be recalled that the corresponding expression in [9] predicts the work done by the concentrated force over a cycle in the low-frequency range [$\omega < (E/\rho)^{1/2}/R$] to be zero, which also implies that there is no net energy input at the apex, and no energy is transported away from the apex. This observation further illustrates the significance of the effect of longitudinal inertia and the necessity for a traveling-wave solution in the entire range of forcing frequencies.

Numerical Results

To illustrate the wave character of the response, with values of $\nu = 0.3$ and $h/R = 1/30$ the expression for the axial displacement is evaluated numerically at $t = 0$, $\pi/4\omega$, $\pi/2\omega$, and $3\pi/4\omega$. The distribution of w versus r is shown in Figs. 1, 2, and 3 for various forcing frequencies, while in Fig. 4 the axial displacement of the apex is plotted versus Ω at $t = 0$. In Figs. 1–3, the distribution of w at other values of time may be easily constructed by considering the mirror image about the line $w = 0$ of the curves shown.

For the purpose of comparison, the response predicted by the differential equations for *transverse* motion is also included in Figs. 1 and 4 by dashed curves. In view of the fact that (for all values of t) in the low-frequency range the behavior of the solution for *transverse* motion is of the standing-wave type, the amplitude of w as given in [9] is shown in Fig. 1 only at $t = 0$. The corresponding comparison between the predictions of the solution of the present paper and that of [9] is not made in Figs. 2 and 3, since in the high-frequency range the two solutions are of a similar character. Likewise, the comparison in Fig. 4, which also displays the resonance phenomena discussed earlier, is shown only at $t = 0$; the displacement of the apex for other values of t will have essentially the same features.

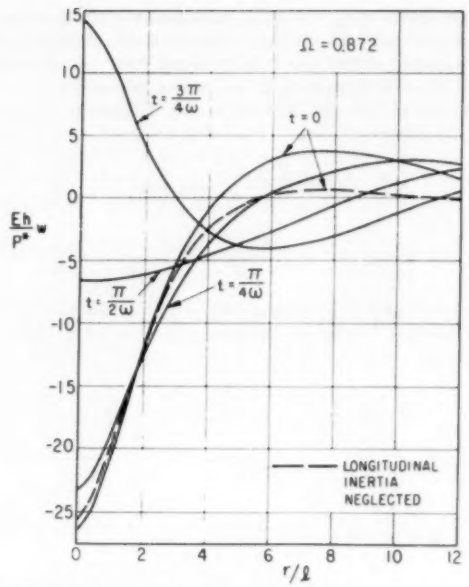

Fig. 1 Axial displacement versus r for $\Omega = 0.872$ at various values of time ($\nu = 0.3$, $h/R = 1/30$)

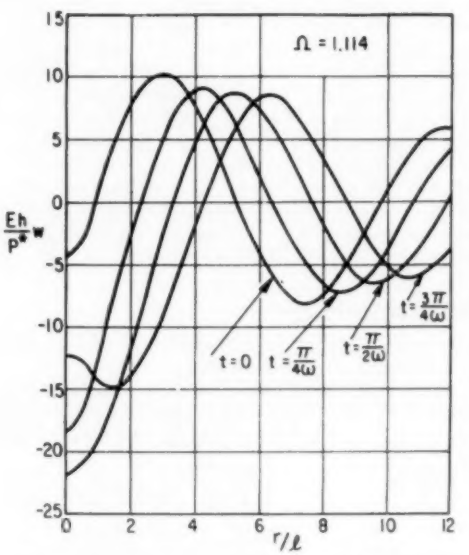

Fig. 2 Axial displacement versus r for $\Omega = 1.114$ at various values of time ($\nu = 0.3$, $h/R = 1/30$)

References

1 P. M. Naghdi, "On the General Problem of Elastokinetics in the Theory of Shallow Shells," Proceedings of the IUTAM Symposium on the Theory of Thin Elastic Shells (Delft, Netherlands, 1959), North-Holland Publishing Co., 1960, pp. 301–330.

2 E. Reissner, "On Transverse Vibrations of Thin Shallow Elastic Shells," *Quarterly of Applied Mathematics*, vol. 13, 1955, pp. 169–176.

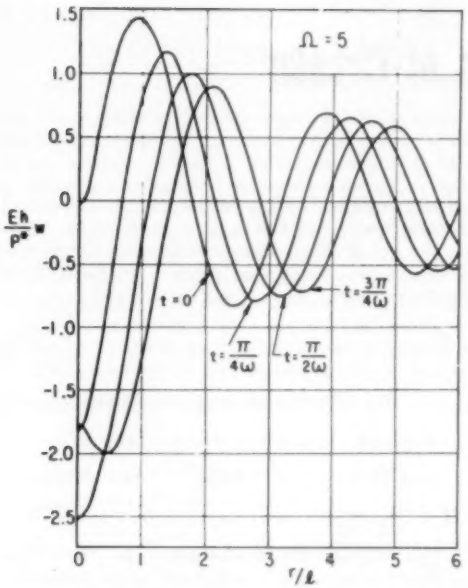

Fig. 3 Axial displacement versus r for $\Omega = 5$ at various values of time ($\nu = 0.3$, $h/R = 1/30$)

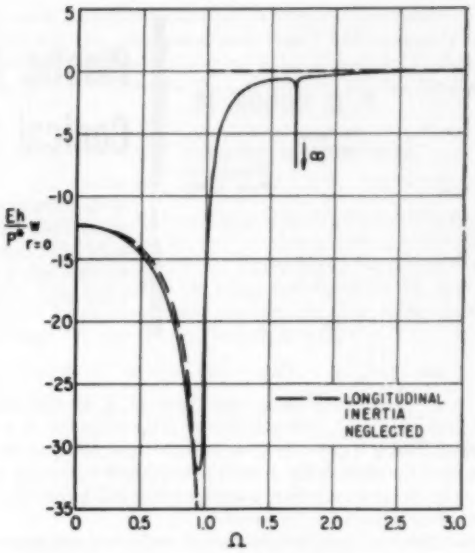

Fig. 4 Variation of axial displacement of the apex with frequency Ω at $t = 0$ ($\nu = 0.3$, $h/R = 1/30$)

3 A. Kalnins and P. M. Naghdi, "Axisymmetric Vibrations of Shallow Spherical Shells," *Journal of the Acoustical Society of America*, vol. 32, 1960, pp. 342–347.

4 H. Cremer and L. Cremer, "Theorie der Entstehung des Klopfschalls," *Frequenz*, vol. 2, 1948, pp. 61–72.

5 I. N. Sneddon, "The Symmetrical Vibrations of a Thin Elastic Plate," *Proceedings of the Cambridge Philosophical Society*, vol. 41, 1945, pp. 27–43.

6 M. J. Boussinesq, "Application des potentiels a l'étude de l'équilibre et du mouvement des solides élastiques," Gauthier-Villars, Paris, France, 1885.

7 R. C. Jones, "The Driving-Point Impedance of an Infinite Solid Plate," *Journal of the Acoustical Society of America*, vol. 17, 1947, pp. 334–336.

8 C. Zener, "The Intrinsic Inelasticity of Large Plates," *Physical Review*, vol. 59, 1941, pp. 669–673.

9 E. Reissner, "On Axi-Symmetrical Vibrations of Shallow Spherical Shells," *Quarterly of Applied Mathematics*, vol. 13, 1955, pp. 279–290.

10 E. Reissner, "Stresses and Small Displacements of Shallow Spherical Shells," *Journal of Mathematics and Physics*, vol. 25, 1945, pp. 279–300.

11 P. M. Naghdi and W. C. Orthwein, "Response of Shallow Viscoelastic Spherical Shells to Time-Dependent Axisymmetric Loads," *Quarterly of Applied Mathematics*, vol. 18, 1960, pp. 107–121.

12 N. W. McLachlan, "Bessel Functions for Engineers," Clarendon Press, Oxford, England, 1955.

13 P. M. Morse and H. Feshbach, "Methods of Theoretical Physics," McGraw-Hill Book Company, Inc., New York, N. Y., 1953.

14 A. Sommerfeld, "Partial Differential Equations in Physics," Academic Press, Inc., New York, N. Y., 1949.

15 S. H. Crandall, "The Timoshenko Beam on an Elastic Foundation," Proceedings of the Third Midwest Conference on Solid Mechanics, 1957, pp. 146–159.

P. G. HODGE, JR.
Professor of Mechanics,
Illinois Institute of Technology,
Chicago, Ill.
Mem. ASME

Plastic Analysis of Circular Conical Shells[1]

A right circular conical shell of edge angle α is subjected to a concentrated load Q directed along the axis. The collapse load is found to be $Q = 2\pi M_0 \cos^2 \alpha$, independently of the size or support conditions of the shell. Some solutions are also obtained for the case where the load is distributed over a finite area. Bounds are found on the collapse load of a general rotationally symmetric shell under a concentrated load.

It has previously been shown [1, 2, 3][2] that the collapse load of a rigid, perfectly plastic plate subjected to a concentrated load Q is given by $Q = 2\pi M_0$ independently of the size or shape of the plate or the manner in which it is supported at the edge. In the present paper, a similar result will be obtained for a conical shell, loaded at its vertex.[3]

It is difficult to make a direct formal analysis of a plate or shell subjected to a concentrated load since the resulting shear force at the point of load application is infinite. Therefore, after reviewing the necessary "Basic Equations," we consider a shell where the load is applied over a small but finite area. A complete solution is obtained for fairly flat shells and an upper bound is found for all shells. Complete solutions for shells which are of medium flatness are given in an Appendix.

In the section, "Solution for Concentrated Load," we pass to the limit as the loaded area tends to zero. Here it is shown that $Q = 2\pi M_0 \cos^2 \alpha$ is both an upper and a lower bound on the concentrated collapse load. Further, it is shown that the same result is obtained independently of the method of load application, support conditions of the shell, or shape of the yield surface.

The final section indicates how the problem of a general shell of revolution subjected to a concentrated load at its vertex may be attacked. The collapse load is shown to be between that of a flat plate and a circumscribed conical shell.

Basic Equations

The dimensions of the shell are shown in Fig. 1(a). The stress state is defined by the stress resultants N_θ, N_x, M_θ, M_x, and S, and the velocity state by two components V and W; sign conventions for positive resultants and displacements are shown in Fig. 1(b). We define the following dimensionless quantities:[4]

$$\begin{aligned} r &= R/L \qquad a = A/L \qquad v = V/L \\ w &= W/L \qquad n = N/N_0 \qquad m = M/M_0 \\ j &= (M_0 \cos^2 \alpha)/(LN_0 \sin \alpha) \qquad K = (M_0/N_0)\kappa \end{aligned} \tag{1}$$

$$q = Q/(2\pi L N_0 \sin \alpha) - j$$

Here N_0 and M_0 are the yield direct force and bending moment per unit length, respectively, and κ is the curvature of the middle surface.

The shell is assumed to be rigid perfectly plastic and to satisfy the two-moment limited interaction yield condition [4]

$$\max\left[|n_x|,\ |n_\theta|,\ |n_x - n_\theta|,\ |m_x|,\ |m_\theta|,\ |m_x - m_\theta|\right] \leq 1 \tag{2}$$

Since there are no forces applied to the surface of the shell, the condition of the vertical equilibrium can be trivially integrated to yield

$$2\pi R(N_x \sin \alpha - S \cos \alpha) = Q \tag{3}$$

The equations of equilibrium along a generator and moment equilibrium may then be written

$$(rn_x)' - n_\theta = 0 \tag{4}$$

$$j[(rm_x)' - m_\theta + 1] = rn_x - q \tag{5}$$

Here primes indicate differentiation with respect to the dimensionless horizontal distance r, dimensionless quantities are defined in equations (1), and the shear has been replaced by its value from equation (3).

The generalized strain rates corresponding to n_θ, n_x, m_θ, and m_x as generalized stresses are the unit extension rates, λ, and dimensionless curvature rates, K, of the middle surface. These, of course, may be expressed in terms of the velocities v and w, the results being

[4] Since quasi-static problems in perfect plasticity are independent of time scale, we can, without loss of generality, treat time as dimensionless.

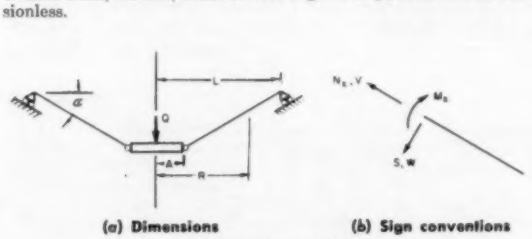

(a) Dimensions (b) Sign conventions

Fig. 1 Conical shell

[1] This investigation was sponsored by the Office of Naval Research.

[2] Numbers in brackets designate References at end of paper.

[3] Shortly after submitting this paper for publication, the author was informed of a similar study by E. T. Onat, "On the Plastic Analysis of Shallow Conical Shells" (DAM Report DA—4795/3, Brown University, Providence, 1959). Although this paper bears a similar title, the methods used and the problem considered are basically different. Onat's paper is concerned with a load applied over a finite area at the shell vertex, uses a nonlinear yield condition, obtains results for shallow shells only, and applies the solution to finite bending of a flat plate. This paper is concerned with a load applied over a vanishingly small area, uses a linear yield condition, obtains results for shells of any depth, and applies the solution to a concentrated load at the vertex of an axially symmetric shell.

Presented at the Summer Conference of the Applied Mechanics Division, University Park, Pa., June 20–22, 1960, of The American Society of Mechanical Engineers.

Discussion of this paper should be addressed to the Secretary, ASME, 29 West 39th Street, New York, N. Y., and will be accepted until January 10, 1961, for publication at a later date. Discussion received after the closing date will be returned.

Manuscript received by ASME Applied Mechanics Division, November 23, 1959. Paper No. 60—APM-31.

$$\mathbf{q} = (\lambda_\theta, \lambda_r, K_\theta, K_r)$$
$$= [(v \cos\alpha + w \sin\alpha)/r, v' \cos\alpha,$$
$$- jw' \sin\alpha/r, - jw'' \sin\alpha] \quad (6)$$

The plastic potential flow law states that if the stress point is in the interior of the yield surface (2), then $\mathbf{q} = 0$; if the stress point is in contact with one of the hyperplanes of the yield surface, then $\mathbf{q}$ is directed along the outward normal of that hyperplane; if the stress point is at the intersection of two or more hyperplanes, then $\mathbf{q}$ must be a linear combination with non-negative coefficients of the outward normals to the hyperplanes in question; the stress point can never be outside of the yield surface.

We consider, for definiteness, the case where the load is applied to a conical frustrum by means of a rigid punch, the cone being simply supported against normal motion as shown in Fig. 1(*a*). Therefore the boundary conditions are as follows:

At $r = a^-$

$$m_r = 0, \quad w = \delta \cos\alpha, \quad v = -\delta \sin\alpha \quad (7a)$$

At $r = 1$

$$m_r = 0, \quad n_r = 0, \quad w = 0 \quad (7b)$$

In addition, m_r, n_r, and w must always be continuous; w' must be continuous except possibly at a hinge circle where $|m_r| = 1$; v must be continuous unless $|n_r| = 1$.

In equation (7*a*), δ represents the dimensionless downward vertical velocity of the punch. Therefore the external rate of dissipation of energy is

$$D_e = QL\delta \quad (8a)$$

The internal rate of energy dissipation is obtained by integrating the product of stress and strain rate over the shell:

$$D_i = 2\pi N_0 L^2 \sec\alpha \int_{a^-}^{1} (n_\theta \lambda_\theta + n_r \lambda_r + m_\theta K_\theta + m_r K_r) r dr \quad (8b)$$

For any kinematically admissible velocity field, the equation $D_e = D_i$ may be solved to give an upper bound on Q.

Solution for Finite a

Experience with rotationally symmetric shell problems [4] has shown that the plastic flow mechanism is usually associated with at least two faces of the yield surface (2), one involving direct stresses and the other bending moments. Therefore we draw two two-dimensional projections of the four-dimensional yield surface, Fig. 2, and assume that the projections of the stress profile will lie on both curves. We consider first the direct stresses.

Since n_r is zero at $r = 1$ and positive at $r = a$, we expect it to be positive throughout. Since λ_θ as given by equation (6) is equal to $(1/r)$ times the outward horizontal component of velocity, we intuitively expect λ_θ to be negative. These two facts suggest a stress profile on side FA in Fig. 2(*a*). Equation (4) and the boundary condition (7*b*) on n_r then lead to $n_r = -\log r$.

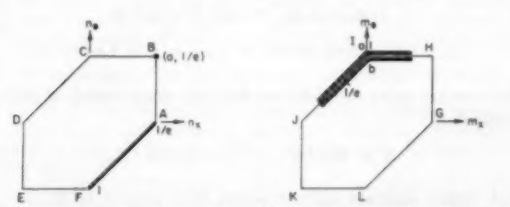

(a) Direct stress profile for all j (b) Moment profile for $0.632 \leq j$

Fig. 2 Stress profiles

However, this solution lies on the yield surface only for $r > 1/e$.

For $r < 1/e$, $-\log r$ is greater than 1 which suggests that the correct hypothesis is to set $n_r = 1$. Equation (4) then shows that $n_\theta = 1$. Therefore the proposed solution for direct stresses is

$$n_r = n_\theta = 1, \qquad a \leq r \leq 1/e$$
$$n_r = -\log r, \qquad n_\theta = -\log r - 1, \quad 1/e \leq r \leq 1 \quad (9)$$

To complete the stress solution by finding the bending moments, we observe that the case $j = \infty$ corresponds to a flat plate for which the solution is $m_\theta = 1$. This suggests that the entire stress profile is on side HI in the projection shown in Fig. 2(*b*). The moment distribution under this hypothesis is easily found from equations (5) and (9) and boundary conditions (7):

$$jm_r = (1/2)(r - a^2/r) - q(1 - a/r) \qquad a \leq r \leq 1/e$$

$$jm_r = (1/4)[-2r \log r + r - 1/r - 4q(1 - 1/r)] \qquad 1/e \leq r \leq 1$$

$$q = \frac{1 - 2a^2 - 1/e^2}{4(1 - a)}$$

However, for $a < 0.246$, m_r' is negative at $r = a$, which implies that $m_r < 0$ near $r = a$. Since $m_r < 0$ is not on side HI, the proposed solution is not statically admissible.

As is often the case, an incorrect hypothesis suggests the correct one shown in Fig. 2(*b*). The resulting moment distribution is

$$jm_r = r - a - q \log(r/a) \qquad a \leq r \leq 1/e \quad (10a)$$

$$jm_r = -(r + q) \log r + (b + q) \log b + r - b \qquad 1/e \leq r \leq b \quad (10b)$$

$$jm_r = (1/4)[-2r \log r + r - 4q - (1 - 4q)/r] \qquad b \leq r \leq 1 \quad (10c)$$

$$q = \frac{1 - b^2 + 2b^2 \log b}{4(1 - b)} = \frac{b(1 - \log b) - (a + 1/e)}{\log b/a} \quad (10d)$$

It is readily verified that equations (9) and (10) satisfy equations (4), (5), and (7) and provide continuous n_r and m_r.

To determine the range of static admissibility of equations (10) we consider the first and second derivatives of m_r to show the following facts: m_r decreases from zero at $r = a$ to a relative minimum at $r = q < 1/e$; m_r then increases through zero at $r = b$ to a relative maximum at $r = g$ defined by

$$4q = 1 - g^2 - g^2 \log g^2 \quad (11)$$

m_r then decreases back to zero at $r = 1$. Therefore it follows from Fig. 2(*b*) that the solution will be statically admissible provided

$$m_r(q) = (1/j)[q - a - q \log(q/a)] \geq -1 \quad (12a)$$

$$m_r(g) = (1/4j)[(2g^2 - 4g) \log g + g^2 - 1] \leq 1 \quad (12b)$$

With a given, b, q, and g can be numerically or graphically determined from equations (10*d*) and (11); inequalities (12) will then show the smallest j for which the solution is statically admissible. In particular, if a is very small, we may neglect all secondary terms in a and obtain the following results:

$$q \simeq (1 - 1/e)/(-\log a) \qquad b \simeq 1 - 2q \qquad g \simeq 1 - q$$
$$jm_r(q) \simeq -(1 - 1/e) \qquad jm_r(g) \simeq q^2/2 \quad (13)$$

Therefore, provided that

$$j > 1 - 1/e = 0.632 \quad (14)$$

equations (10) will be statically admissible for a sufficiently small.

To complete the foregoing solution we must exhibit a kinematically admissible velocity field. Applying the plastic-flow law to the stress profile shown in Fig. 2 and using the boundary conditions (7), we obtain

$$w = \delta \cos \alpha \frac{1 - b + b \log b/r}{1 - b + b \log b/a} \qquad a \leq r \leq b$$

$$v = -\delta \sin \alpha \frac{1 - b + b \log b/r}{1 - b + b \log b/a} \qquad a \leq r \leq 1/e$$

$$v = -\delta \sin \alpha \frac{1 - b/re + b \log b/r}{1 - b + b \log b/a} \qquad 1/e \leq r \leq b \quad (15)$$

$$w = \delta \cos \alpha \frac{1 - r}{1 - b + b \log b/a} \qquad b \leq r \leq 1$$

$$v = -\frac{\delta \sin \alpha}{2} \frac{2 - r + (b - 2/e)(b/r)}{1 - b + b \log b/a} \qquad b \leq r \leq 1$$

It is readily verified that the strain-rate vector in equation (6) is normal to the proper hyperplanes and that the plastic multipliers are all positive. Therefore equations (15) provide a kinematically admissible velocity field.

Equating the internal and external energy rates from equations (8) we are led to the collapse load

$$q = \frac{3b^2 - 4ab + 1 - 4b/e - 2b^2 \log b}{4[1 - b + b \log b/a]} \qquad (16)$$

Equation (16) will provide an upper bound for any choice of b. To find the best lower bound we set the derivative of q with respect to b equal to zero. With some manipulation, it can be shown that the resulting values of b and q are those defined by equations (10d). Therefore equation (10d) is the exact collapse load for j satisfying inequality (14) and a sufficiently small; it is an upper bound on the collapse load for all j and all $a < 1/e$.

Solution for Concentrated Load

Since the load defined by Equation (10d) is an upper bound for all j, we may obtain an upper bound for the concentrated load by letting a tend to zero in equation (10d). Thus $q = 0$ is an upper bound.

The foregoing kinematic problem cannot be considered directly, for, if we let a tend to zero in equations (15) we find that $w = v = 0$ except at $r = a$. However, by keeping a small but finite, we can obtain a kinematically admissible velocity field and an upper bound arbitrarily close to zero for all j.

The static problem, on the other hand, can be approached directly. Indeed, it is evident that the stress field

$$n_x = n_\phi = m_x = 0, \qquad m_\phi = 1, \qquad q = 0 \qquad (17)$$

satisfies equations (4) and (5), boundary conditions (7) and inequalities (2). Therefore it is statically admissible and hence furnishes a lower bound. Finally, since $q = 0$ is both an upper and a lower bound, it follows that it is the concentrated collapse load. Thus reverting to dimensioned quantities from equations (1), we obtain the concentrated collapse load

$$Q = 2\pi M_0 \cos^2 \alpha \qquad (18)$$

Equation (18) is also the collapse for other conditions of loading and support. If the rigid punch is rigidly attached to the conical frustrum, or equivalently, if it is applied to the complete conical shell, the boundary condition $m_x = 0$ at $r = a^-$ will be replaced by $w' = 0$. Since we have removed a stress-boundary condition, equations (17) are statically admissible in this case also, and $q = 0$ is still a lower bound.

The velocity fields of equation (15) may be used for an upper bound provided that the energy rate due to a discontinuity in slope rate at $r = a$ is included. However, it is easily shown that this energy rate tends to zero with a and hence does not affect the limit $q = 0$ as an upper bound. Therefore the collapse load is still given by equation (18).

The support conditions used to derive Equation (18) provide no constraints on v or w' at $r = 1$. The same velocity field may be used with other support conditions provided that account is taken of the energy rate dissipation due to discontinuities in v and/or w'. However, as a tends to zero, v (1) and $w'(1)$ each tend to zero, so that any discontinuity energy rate will also tend to zero. Therefore $q = 0$ will be an upper bound for any conditions of support at $r = 1$.

If the shell is rigidly clamped at $r = 1$, the stress field of equations (17) is still statically admissible, so that equation (18) gives the collapse load for a clamped shell.

On the other hand, if the shell is simply supported against vertical motion, then the condition of zero horizontal force, assuming that $q = 0$, leads to

$$\text{at } r = 1, \qquad n_x = j \sin^2 \alpha \qquad (19)$$

In this case, the stress field

$$n_x = n_\phi = j \sin^2 \alpha$$

$$m_x = 0, \qquad m_\phi = 1 - r \sin^2 \alpha, \qquad q = 0 \qquad (20)$$

is statically admissible provided $j \sin^2 \alpha \leq 1$. In view of equations (1), this restriction is satisfied in all cases which may reasonably be called shells.

The analysis leading to equation (18) was based on the two-moment limited interaction yield surface. However, the result may easily be shown to be valid for the exact yield surfaces of a uniform [5] or sandwich [6] shell based on the Tresca yield condition. Indeed, as shown in [4] the yield surface (2) circumscribes both of these other two; hence the exact collapse load based on inequalities (2) is an upper bound for either of the other theories. On the other hand, since the three yield surfaces all include the point $n_x = n_\phi = m_x = 0$, $m_\phi = 1$, equations (17) provide a statically admissible stress field according to any of the three theories. Thus the concentrated collapse load of a conical shell is also given by equation (18) according to either of the more exact theories.

Extension to Other Shells

With the experience gained in analyzing the conical shell, we may approach the concentrated load for a general rotationally symmetric shell more directly. As in the case of the cone, we may obtain one integral of the equilibrium equations and eliminate the shear. Thus equations (11-50a) of [6] may be replaced by

$$(r_0 n_\phi/\cos \phi)' = r_1 n_\theta + p \sec^2 \phi$$

$$k[(r_0 m_\phi)' - r_1 m_\theta \cos \phi] = r_1 \sec \phi (p - r_0 n_\phi \sin \phi) \qquad (21)$$

Here we are using the notation and sign conventions of [6]. In particular,

$$k = M_0/LN_0, \qquad p = Q/(2\pi L N_0) \qquad (22)$$

and primes indicate differentiation with respect to ϕ.

A simple solution of equations (21), and boundary conditions corresponding to equations (7) is

$$n_\phi = m_\phi = 0, \qquad n_\theta = -(p/r_1)\sec^2\phi$$
$$m_\theta = -(p/k)\sec^2\phi \tag{23}$$

This will be statically admissible if n_θ and m_θ are each less than 1 in magnitude. For the case of a shell cap which has a maximum slope of 2ω and designed so that $r_1 > k$ throughout, the lower bound is given by

$$p^- = k\cos^2\omega \tag{24}$$

To obtain an upper bound, we consider a velocity field which is concentrated in a central region $\epsilon \le \phi \le \beta$ of the shell. Further, we assume that $\lambda_\theta = K_\theta + K_\phi = 0$. This leads, then, to the velocity field

$$w = \delta\cos\phi\left[\frac{\int_\epsilon^\phi (r_1/r_0)\sec\phi\,d\phi}{\int_\epsilon^\beta (r_1/r_0)\sec\phi\,d\phi} - 1\right] \qquad \epsilon \le \phi \le \beta$$
$$v = w\tan\phi \tag{25}$$
$$w = v = 0 \qquad \beta \le \phi$$

Using the geometric relations

$$r_0 = r_2\sin\phi, \qquad dr_0 = r_1\cos\phi\,d\phi \tag{26}$$

we can write the upper bound obtained from the internal and external energies in the form

$$p^+ = \frac{\int_{a_0}^{b_0}\tan\phi\sec\phi\,dr_0 + k(1 + \log b_0/a_0)}{\int_{a_0}^{b_0}\sec^2\phi\,dr_0/r_0} \tag{27}$$

Here a_0 and b_0 are the values of r_0 at the inner edge $\phi = \epsilon$ and plastic boundary $\phi = \beta$, respectively.

Let us assume that the shape of the shell near the center is given by

$$z = Cr_0^n, \qquad n > 1 \tag{28}$$

Then, letting a_0 tend to zero we find the best value of the parameter b_0 to be such that b_0 tends to zero but b_0/a_0 becomes infinite. In such a limit, the value of p^+ in equation (27) approaches

$$p^+ = k \tag{29}$$

Therefore, in terms of dimensional quantities, it follows from equations (24) and (29) that

$$2\pi M_0\cos^2\omega \le Q \le 2\pi M_0 \tag{30}$$

In other words, the concentrated collapse load of a shell cap with continuous slope at $r = 0$ lies between that of a flat plate and a circumscribing cone.

References

1 D. C. Drucker and H. G. Hopkins, "Combined Concentrated and Distributed Load on Ideally-Plastic Circular Plates," *Proceedings*, Second U. S. National Congress of Applied Mechanics, 1954, Ann Arbor, Mich., 1955, pp. 517–520.

2 M. Zaid, "On the Carrying Capacity of Plates of Arbitrary Shape and Variable Fixity Under a Concentrated Load," JOURNAL OF APPLIED MECHANICS, vol. 25, TRANS. ASME, vol. 80, 1958, pp. 598–602.

3 W. Schumann, "On Limit Analysis of Plates," *Quarterly of Applied Mathematics*, vol. 16, 1958, pp. 61–71.

4 P. G. Hodge, Jr., "Yield Conditions for Rotationally Symmetric Shells Under Axisymmetric Loading," JOURNAL OF APPLIED MECHANICS, vol. 27, TRANS. ASME, vol. 82, series E, June, 1960, pp. 323–331.

5 E. T. Onat and W. Prager, "Limit Analysis of Shells of Revolution," *Proceedings Royal Netherlands Academy of Science*, vc' B57, 1954, pp. 534–548.

6 P. G. Hodge, Jr., "Plastic Analysis of Structures," McGraw-Hill Book Company, Inc., New York, N. Y., 1959, Section 11-5.

APPENDIX

We present here complete solutions for a finite but sufficiently small and $0.134 \le j \le 0.632$. The distribution of direct stresses is still given by equations (9) but the bending moments must be modified. For j slightly smaller than 0.632, we expect part of the stress profile to be on side JK as shown in Fig. 3(a). The resulting stress field gives m_θ discontinuous at $r = d$, but this discontinuity is permissible. The moment field is defined by equations (10a), (10b), and (10c), for $a \le r \le c$, $1/e \le r \le b$, and $b \le r \le 1$, respectively, together with

$$jm_\theta = q - r \qquad c \le r \le d \tag{31a}$$
$$jm_\theta = r - d - j - q\log(r/d) \qquad d \le r \le 1/e \tag{31b}$$

The load q and the geometric parameters b, c, and d are implicitly defined as functions of a by

$$q = c = (c - a + j)/\log(c/a) \tag{31c}$$
$$= [b(1 - \log b) - (d + j + 1/e)]/\log(b/d) \tag{31d}$$
$$= (1/4)(1 - b^2 + 2b^2\log b)/(1 - b) \tag{31e}$$

For very small a, equations (31c, d, e) lead to

$$q = c \simeq \frac{-j}{\log a}, \quad b \simeq 1 - 2\frac{j}{-\log a}, \quad d \simeq 1 - \frac{1}{e} - j \tag{32}$$

The only restrictions on static admissibility turn out to be $m_\theta(d) \ge -1$ and $d \ge a$ which lead in the limit to

$$0.316 = (1/2)(1 - 1/e) \le j \le 1 - 1/e = 0.632 \tag{33}$$

The stress profile in Fig. 3(a) can support only a rigid body motion for $c \le r \le d$. Intuitively we do not expect to find a ring of rigid material between plastically flowing material so that we are led to consider a velocity field corresponding to side IJ for $a \le r \le c$ and rigid for $c \le r \le 1$. Thus

$$w = \delta\cos\alpha\frac{\log c/r}{\log c/a}, \quad v = -\delta\sin\alpha\frac{\log c/r}{\log c/a} \qquad a \le r \le c$$
$$w = v = 0 \qquad c \le r \le 1 \tag{34}$$

In computing the internal energy rate from equations (34) it is necessary to include the energy rate due to a discontinuous slope rate at $r = c$. When this is done, the upper bound

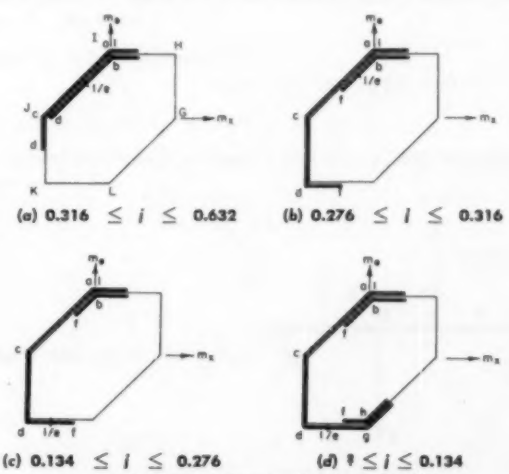

Fig. 3 Moment stress profiles for $j \le 0.632$

$$q = \frac{c + j - a}{\log c/a}$$

is obtained on the collapse load for any c. Obviously the best upper bound is that which minimizes q, thus leading to

$$q = c = \frac{c + j - a}{\log c/a} \tag{35}$$

Since this is the same value of q as that given by equations (31), we have found the exact collapse load for $0.316 \leq j \leq 0.632$, and an improved upper bound for all $j \leq 0.632$.

For all $j \leq 0.316$ we make the general hypothesis that the stress profile in the m-plane goes from I at $r = a$, along sides IJ and JK, that it somehow goes from K back to I for $r = b$, and that it is on side IH for $b \leq r \leq 1$. It follows that q and c are still defined by equations (31c), b is defined by equation (31e), and the stress values for $a \leq r \leq d$ and $b \leq r \leq 1$ are the same as before. Further, the value of q is also an upper bound as shown by equation (35). Therefore the problem reduces to verifying that a statically admissible state of stress exists for $d \leq r \leq b$.

Three such profiles are shown in Figs. 3(b, c, d). The corresponding moment distributions are

$$jm_x = (1/2)(r - 4j + j^2/r) \qquad j \leq r \leq f$$

$$jm_x = r + (1/2f)(-f^2 - 4fj + j^2) \qquad f \leq r \leq 1/e$$

$$jm_x = -r \log r + r - 1 \qquad 1/e \leq r \leq 1 \tag{36}$$

$$f = (1 - 2j - 1/e) + [(1 - 2j - 1/e)^2 + j^2]^{1/2}$$

$$0.276 = [2 - (7 - 2e)^{1/2}]/e \leq j \leq (1/2)(1 - 1/e) = 0.316$$

and

$$jm_x = (1/2)(r - 4j + j^2/r) \qquad j \leq r \leq 1/e$$

$$jm_x = (1/4)[-2r \log r + r - 8j + (2j^2 - 1/e^2)/r] \qquad 1/e \leq r \leq f$$

$$jm_x = -r \log r + r - 1 \qquad f \leq r \leq 1 \tag{37}$$

$$2j^2 - 8fj + 2f^2 \log f + 4f - 3f^2 - 1/e^2 = 0$$

$$0.134 \leq j \leq 0.276$$

Here, for simplicity of exposition, we have written only the leading terms as a tends to zero. Thus

$$a = c = q = 0, \qquad d = j, \qquad b = 1$$

However, in each case the corresponding solution is valid for some range of finite a.

For $j = 0.134$ the stress profile touches point L for some value of r between $1/e$ and f. Solutions for smaller values of j thus become very complex and have not been attempted.

A. C. ERINGEN
Professor,
Division of Engineering Sciences,
Purdue University,
Lafayette, Ind.

J. W. DUNKIN
Instructor,
Division of Engineering Sciences,
Purdue University,
Lafayette, Ind.

The Elastic Half Plane Subjected to Surface Tractions With Random Magnitude or Separation[1]

First and second-order moments of the stress tensor are obtained for the elastostatic problem concerning the half-plane subjected to random boundary tractions. The cases treated include the following types of applied surface tractions: (a) A purely random Gaussian load (white noise); (b) concentrated loads of random magnitudes separated by equal intervals; (c) a concentrated load acting at a random location; and (d) concentrated loads of equal magnitudes separated by random intervals.

THE elastostatic problem of a half plane acted upon by boundary tractions on its straight boundary is classical.[2] However, when the surface tractions are random in magnitude or when they are randomly distributed, a novel problem arises which has not been treated to date.

Quite often, in many problems encountered in engineering, either the magnitude or the location of the surface tractions is not known precisely as, for example, when a random noise is applied to the surface. We may, however, have some knowledge of the mean and mean-square values of these loads or their locations, whichever is random. It may happen that we make certain mean-square errors in locating the loads; it would then be of interest to find what the mean-square error would be in the stresses. In such cases, the methods of deterministic analysis are not applicable, and so we must turn to a method such as the one presented in this paper for answers to these problems. The method used here is suggestive in that it applies to other types of problems in elasticity theory.

The problem, in essence, is to find the mean and mean-square values and cross correlations of stress components given either the same information for the surface tractions or else their probability density functions. When the magnitude of the tractions obeys the Gaussian law of distribution, the first two moments determine the distribution function for the stresses, since they are also distributed in a Gaussian fashion. This, however, is not generally the case when the intervals of separation of the loads are random. The latter case is nonetheless the more interesting of the two classes of problems, but in this case we must be satisfied with the determination of the second-order moments.

Formulation of the Problem

Components σ_{jk} of the stress tensor at a point (x, y) due to surface pressure $\sigma_{11} = p(y)$, $\sigma_{12} = 0$ acting on the boundary $x = 0$, Fig. 1, of a two-dimensional, homogeneous, isotropic, semi-infinite, plane elastic medium, are given by[2]

$$\sigma_{jk}(x, y) = \int_{-\infty}^{\infty} p(\xi)\bar{G}_{jk}(x, \xi)e^{-i\xi y}d\xi \tag{1}$$

where

$$\begin{aligned} 2\pi\bar{G}_{11}(x, \xi) &= (1 + |\xi|x)\exp(-|\xi|x) \\ 2\pi\bar{G}_{22}(x, \xi) &= (1 - |\xi|x)\exp(-|\xi|x) \\ 2\pi\bar{G}_{12}(x, \xi) &= ix\xi\exp(-|\xi|x) \end{aligned} \tag{2}$$

where a bar superposed on a letter represents the Fourier transform of the function; i.e.,

$$\bar{p}(\xi) = \int_{-\infty}^{\infty} p(y)e^{i\xi y}dy \tag{3}$$

$$p(y) = \frac{1}{2\pi}\int_{-\infty}^{\infty} \bar{p}(\xi)e^{-i\xi y}d\xi \tag{4}$$

Using the Fourier convolution theorem, (1) may also be written as

$$\sigma_{jk} = \int_{-\infty}^{\infty} p(\xi)G_{jk}(x, y - \xi)d\xi \tag{5}$$

where $G_{jk}(x, y - \xi)$ is the Green tensor, which is none other than the σ_{jk} at (x, y) due to a unit concentrated load acting at $x = 0$, $y = \xi$. We have

$$\begin{aligned} G_{11}(x, y) &= 2\pi^{-1}x^3(x^2 + y^2)^{-2}, \\ G_{22}(x, y) &= 2\pi^{-1}xy^2(x^2 + y^2)^{-2} \\ G_{12}(x, y) &= 2\pi^{-1}x^2y(x^2 + y^2)^{-2} \end{aligned} \tag{6}$$

A concentrated load P, acting at $x = 0$, $y = \eta_r$, may formally be represented by

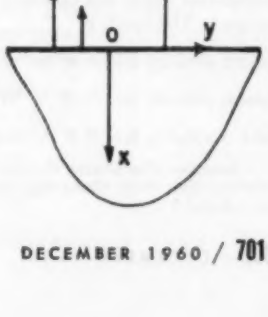

Fig. 1 Semi-infinite elastic plane

---

[1] This investigation was supported by the Office of Naval Research.

[2] I. N. Sneddon, "Fourier Transforms," McGraw-Hill Book Company, Inc., New York, N. Y., 1951, p. 405.

Presented at the West Coast Conference of the Applied Mechanics Division, Pasadena, Calif., June 27–29, 1960, of THE AMERICAN SOCIETY of MECHANICAL ENGINEERS.

Discussion of this paper should be addressed to the Secretary, ASME, 29 West 39th Street, New York, N. Y., and will be accepted until January 10, 1961, for publication at a later date. Discussion received after the closing date will be returned.

Manuscript received by ASME Applied Mechanics Division, August 31, 1959. Paper No. 60—APMW-10.

$$p(y) = P_r\delta(y - \eta_r) \tag{7}$$

where $\delta(u)$ is the Dirac delta function. Substitution of (7) into (5) gives

$$\sigma_{jk} = P_r G_{jk}(x, y - \eta_r) \tag{8}$$

If there are many concentrated loads acting at locations $x = 0$, $y = \eta_r$ $(r = 1, 2, \ldots)$, then we write

$$\sigma_{jk} = \sum_r P_r G_{jk}(x, y - \eta_r) \tag{9}$$

In all of the foregoing, the loads $p(\xi)$, P_r, and their locations $y = \xi$ or $y = \eta_r$ were nonrandom. In the following, we consider various cases in which either the loads or their locations are random. We distinguish the various cases as:

(a) A purely random Gaussian load (white noise).

(b) Concentrated loads of random magnitudes separated by equal intervals.

(c) A concentrated load acting at a random location.

(d) Concentrated loads of equal magnitudes separated by random intervals.

Purely Random Gaussian Load (White Noise)

In this case the correlation function for $p(y)$ is given by

$$\langle p(y)p(\eta)\rangle = H\delta(y - \eta) \tag{10}$$

where H is the spectral density of the white noise, $\delta(u)$ is the Dirac delta function, and $\langle\rangle$ represents the space mean. We shall assume that the *ergodic* hypothesis applies. According to this, the space mean is the same as the statistical mean. From (3), we have

$$\langle p(\xi)p(\eta)\rangle = \int_{-\infty}^{\infty}\int \langle p(y)p(z)\rangle \exp\,[i(\xi y + \eta z)]dy\,dz = 2\pi H\delta(\xi + \eta) \tag{11}$$

where we used (10). The mean and the cross-correlation functions for σ_{jk} are calculated from

$$\langle \sigma_{jk}(x, y)\rangle = \frac{1}{2\pi}\int_{-\infty}^{\infty} \langle p(\xi)\rangle \bar{G}_{jk}(x, \xi)e^{-i\xi y}d\xi \tag{12}$$

$$\langle \sigma_{jk}(x, y)\sigma_{mn}(x_1, y_1)\rangle = \frac{1}{4\pi^2}\int_{-\infty}^{\infty}\int \langle p(\xi)p(\eta)\rangle \bar{G}_{jk}(x, \xi)\bar{G}_{mn}(x_1, \eta) \exp\,[-i(\xi y + \eta y_1)]d\xi\,d\eta \tag{13}$$

If we use (11) in (13), we obtain

$$\langle \sigma_{jk}\sigma_{mn}\rangle = \frac{H}{2\pi}\int_{-\infty}^{\infty} \bar{G}_{jk}(x, \xi)\bar{G}_{mn}(x_1, -\xi) \exp\,[-i\xi(y - y_1)]d\xi \tag{14}$$

We now evaluate these integrals.

These integrals may be expressed as Fourier cosine and sine transforms which can be found among the integrals listed elsewhere.[3] The result is

$$\langle \sigma_{11}(x, y)\sigma_{11}(x_1, y_1)\rangle = \pi^{-1}a^{-1}H(A + B + xx_1a^{-2}C)$$

$$\langle \sigma_{22}(x, y)\sigma_{22}(x_1, y_1)\rangle = \pi^{-1}a^{-1}H(A - B + xx_1a^{-2}C)$$

$$\langle \sigma_{12}(x, y)\sigma_{12}(x_1, y_1)\rangle = \pi^{-1}Hxx_1a^{-3}C$$

[3] Bateman Manuscript Project, "Tables of Integral Transforms," McGraw-Hill Book Company, Inc., New York, N. Y., vol. 1, 1954, pp. 14 and 17.

$$\langle \sigma_{11}(x, y)\sigma_{22}(x_1, y_1)\rangle = \pi^{-1}a^{-1}H[A + (x - x_1)a^{-1}B - xx_1a^{-3}C] \tag{15}$$

$$\langle \sigma_{11}(x, y)\sigma_{12}(x_1, y_1)\rangle = -\pi^{-1}a^{-1}H(x_1a^{-1}B' + xx_1a^{-2}C')$$

$$\langle \sigma_{22}(x, y)\sigma_{12}(x_1, y_1)\rangle = -\pi^{-1}a^{-1}H(x_1a^{-1}B' - xx_1a^{-2}C')$$

where

$$A = [1 + (h/a)^2]^{-1}, \qquad B = [1 - (h/a)^2]A^2, \qquad C = 2[1 - 3(h/a)^2]A^3$$
$$B' = 2(h/a)A^2, \qquad C' = 2(h/a)[3 - (h/a)^2]A^3 \tag{16}$$
$$a = x + x_1, \qquad h = y - y_1$$

We notice that the stress correlations are functions of $y - y_1$, as well as x and x_1. Hence the output process is homogeneous in y. The mean-square values of σ_{ij} are obtained by taking $x = x_1$ and $y = y_1$ in (15). This gives

$$\langle \sigma_{11}^2\rangle = 5H/4\pi x, \qquad \langle \sigma_{22}^2\rangle = \langle \sigma_{12}^2\rangle = \langle \sigma_{11}\sigma_{22}\rangle = H/4\pi x$$
$$\langle \sigma_{11}\sigma_{12}\rangle = \langle \sigma_{22}\sigma_{12}\rangle = 0 \tag{17}$$

It is interesting to note that $\langle \sigma_{11}^2\rangle$ possesses five times as high a magnitude as the remaining nonzero mean-square stresses. Moreover, contrary to our expectations, σ_{11} and σ_{22} are correlated. It is also clear from (17) that the mean-square stresses die out hyperbolically away from the boundary $x = 0$. At the boundary the situation is, of course, chaotic since there, a white noise is present.

Concentrated Loads of Random Magnitude Separated by Equal Intervals

If a concentrated load P_r acts at $x = 0$, $y = rY$, $(r = 1, 2, \ldots)$, where Y is constant, then through (9) we have, Fig. 2

$$\sigma_{jk}(x, y) = \sum_r P_r G_{jk}(x, y - rY) \tag{18}$$

The means of the stress components are given by

$$\langle \sigma_{jk}(x, y)\rangle = \sum_r \langle P_r\rangle G_{jk}(x, y - rY) = P\sum_r G_{jk}(x, y - rY) \tag{19}$$

where for the mean of loads P_r we wrote

$$\langle P_r\rangle = P \tag{20}$$

The cross correlation function for any two components is

$$\langle \sigma_{jk}(x, y)\sigma_{mn}(x', y')\rangle = \sum_{r,\,s} \langle P_rP_s\rangle G_{jk}(x, y - rY)G_{mn}(x', y' - sY) \tag{21}$$

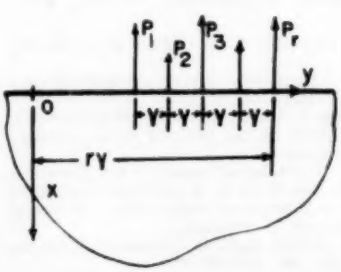

Fig. 2 Equally spaced loads of random magnitude

The correlation function of the loads may be expressed conveniently in terms of their means and the mean-square deviations if we write

$$P_r = p_r + P, \qquad P = \langle P_r \rangle, \qquad \langle p_r \rangle = 0 \tag{22}$$

Hence

$$\langle P_r P_s \rangle = \langle p_r p_s \rangle + P^2$$

If the load P_r is statistically independent of $P_s (s \neq r)$ then this can be expressed as

$$\langle P_r P_s \rangle = \sigma^2 \delta_{rs} + P^2 \tag{23}$$

where δ_{rs} is the Kronecker delta which is zero for $r \neq s$ and 1 for $r = s$ and σ^2 is the mean-square deviation; i.e.,

$$\sigma^2 = \langle (P_r - P)^2 \rangle \tag{24}$$

Equation (21) can now be written as

$$\langle \sigma_{jk}(x, y) \sigma_{mn}(x', y') \rangle = \sigma^2 \sum_r G_{jk}(x, y - rY) G_{mn}(x', y' - rY) + P^2 \sum_{r,s} G_{jk}(x, y - rY) G_{mn}(x', y' - sY) \tag{25}$$

The series appearing in (19) and (25) are summed as follows: Let

$$\sum_{r=-\infty}^{\infty} f(rY)$$

represent any of the summations encountered in this problem. As the first step consider the function $f(z) \cot (\pi z/Y)$ in which z is a complex variable; i.e., $z = u + iv$. In the z-plane the singularities of this function consist of a series of first-order poles at $z = rY (r = 0, \pm 1, \pm 2, \ldots)$ contributed by the cot $(\pi z/Y)$ and certain singularities contributed by $f(z)$. Let us examine the integral

$$\oint_{C^{(n)}} f(z) \cot (\pi z/Y)\, dz$$

where $C^{(n)}$ is a circle with radius R_n such that, Fig. 3,

$$|\pm n| Y < R_n < |\pm n \pm 1| Y \qquad (n = 0, 1, 2, \ldots)$$

For all series that arise in this paper $f(z)$ behaves in such a manner for large $|z|$ that

$$\lim_{R_n \to \infty} \oint_{C^{(n)}} f(z) \cot (\pi z/Y) dz = 0 \tag{26}$$

Therefore by deforming the infinite circle into a contour surrounding each of the singularities of $f(z) \cot (\pi z/Y)$ we obtain

$$\sum_{r=-\infty}^{\infty} \oint_{C_r} f(z) \cot (\pi z/Y) dz + \oint_{\substack{\text{all singularities} \\ \text{of } f(z)}} f(z) \cot (\pi z/Y) dz = 0$$

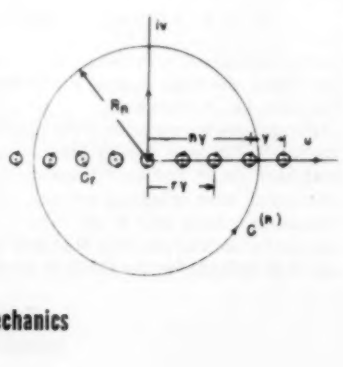

Fig. 3 Contours $C^{(n)}$ and C_r in the z-plane

where C_r is a contour enclosing only the one singular point rY of $f(z) \cot (\pi z/Y)$. The series of contour integrals on the left of this equation can be evaluated by means of residue theory. Thus

$$\oint_{C_r} f(z) \cot (\pi z/Y) dz = 2\pi i \operatorname*{Res}_{rY} f(z) \cot (\pi z/Y) = 2\pi i \lim_{z \to rY} [(z - rY) f(z) \cot (\pi z/Y)] = 2iY f(rY)$$

where we have used the notation

$$\operatorname*{Res}_{rY} f(z) \cot (\pi z/Y)$$

to mean the residue of $f(z) \cot (\pi z/Y)$ at $z = rY$. Substituting this result back into the preceding equation we get

$$\sum_{r=-\infty}^{\infty} f(rY) = -\frac{1}{2iY} \oint_{\substack{\text{all singularities} \\ \text{of } f(z)}} f(z) \cot (\pi z/Y) dz \tag{27}$$

As an example let us evaluate the series

$$\sum_{r=-\infty}^{\infty} [x^2 + (y - rY)^2]^{-2}$$

In this case $f(z)$ is

$$f(z) = [z - (y + ix)]^{-2} [z - (y - ix)]^{-2}$$

and its singularities consist of second-order poles at $z = y + ix$ and $z = y - ix$. Therefore according to (27)

$$\sum_{r=-\infty}^{\infty} [x^2 + (y - rY)^2]^{-2} = -\frac{\pi}{Y} \left\{ \operatorname*{Res}_{y+ix} \frac{\cot (\pi z/Y)}{[z - (y + ix)]^2 [z - (y - ix)]^2} + \operatorname*{Res}_{y-ix} \frac{\cot (\pi z/Y)}{[z - (y + ix)]^2 [z - (y - ix)]^2} \right\}$$

and upon carrying out the computations there results

$$\sum_{r=-\infty}^{\infty} [x^2 + (y - rY)^2]^{-2} = \pi (x^2 Y)^{-1} [1 - \cos (2\pi y/Y) \cosh (2\pi x/Y)] [\cosh (2\pi x/Y) - \cos (2\pi y/Y)]^{-2} - (2x^2)^{-1} \sinh (2\pi x/Y) [\cosh (2\pi x/Y) - \cos (2\pi y/Y)]^{-1} \tag{28}$$

Most of the summations in this and later sections are evaluated by calculating residues at poles of $f(z)$ just as in the foregoing example. However, in one of the later sections summations are encountered in which $f(z)$ possesses branch cuts. In one case the integrals around the cuts could be evaluated very simply while in the others they could not be evaluated. In none of the summations did any of the poles of $f(z)$ fall on the real axis except when $x \to 0$. If such were to happen when $y = rY$, then there would be a coincidence of poles of $f(z)$ and cot $(\pi z/Y)$ which would necessitate a special treatment of the $\pm n$th term in the series.

If the foregoing procedure is applied to the series occurring in (19) and (25) the following results are obtained for the means and correlation functions:

$$\langle \sigma_{11}(x, y) \rangle = 2PY^{-1}(B_1 - xB_2)$$

$$\langle \sigma_{12}(x, y) \rangle = 2PxY^{-1}B_2$$

$$\langle \sigma_{22}(x, y) \rangle = 2PY^{-1}(B_1 + xB_2)$$

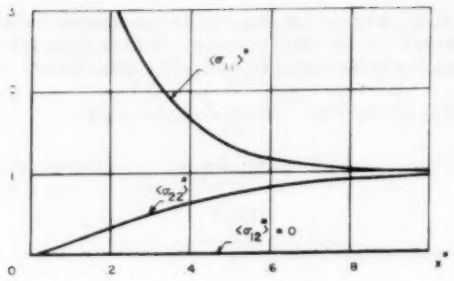

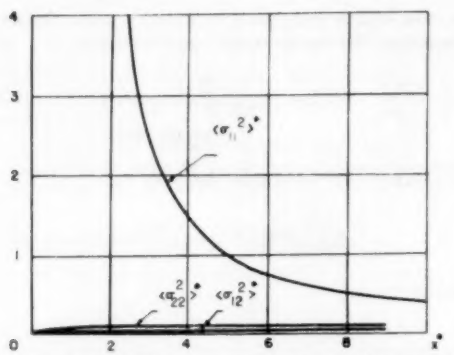

Fig. 4 Mean stresses and mean-square deviations of stresses for uniformly spaced concentrated loads of random magnitude; uniform distribution, $y^* = 0$

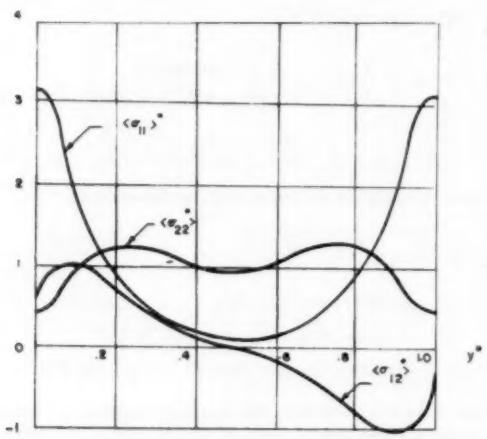

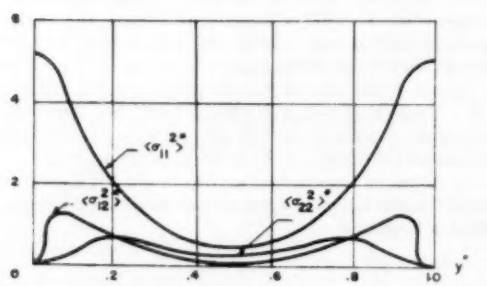

Fig. 5 Mean stresses and mean-square deviations of stresses for uniformly space concentrated loads of random magnitude; uniform distribution, $x^* = 0.2$

$$\langle\sigma_{11}(x,y)\sigma_{11}(x,y)\rangle = \sigma^2(2\pi Y)^{-1}[5x^{-1}B_1 - 5B_2 - 2xB_4 - (x^2/3)B_6] + 4P^2Y^{-2}(B_1 - xB_2)^2$$

$$\langle\sigma_{11}(x,y)\sigma_{12}(x,y)\rangle = \sigma^2(2\pi Y)^{-1}[B_3 - xB_5 + (x^2/3)B_7] + P^2 4xY^{-2}B_3(B_1 - xB_2) \quad (29)$$

$$\langle\sigma_{11}(x,y)\sigma_{22}(x,y)\rangle = \sigma^2(2\pi Y)^{-1}[x^{-1}B_1 - B_2 + (x^2/3)B_6] + P^2 4Y^{-2}(B_1^2 - x^2B_2^2)$$

$$\langle\sigma_{12}(x,y)\sigma_{12}(x,y)\rangle = \sigma^2(2\pi Y)^{-1}[x^{-1}B_1 - B_2 + (x^2/3)B_6] + P^2 4x^2Y^{-2}B_3^2$$

$$\langle\sigma_{22}(x,y)\sigma_{12}(x,y)\rangle = \sigma^2(2\pi Y)^{-1}[B_3 - xB_5 - (x^2/3)B_7] + P^2 4Y^{-2}xB_3(B_1 + xB_2)$$

$$\langle\sigma_{22}(x,y)\sigma_{22}(x,y)\rangle = \sigma^2(2\pi Y)^{-1}[x^{-1}B_1 - B_2 - 2xB_4 - (x^2/3)B_6] + P^2 4Y^{-2}(B_1 + xB_2)^2$$

where

$$B_1 = (1/2)D^{-1}\sinh(2\pi x/Y)$$

$$B_2 = \pi Y^{-1}D^{-2}[1 - \cosh(2\pi x/Y)\cos(2\pi y/Y)]$$

$$B_3 = \pi Y^{-1}D^{-2}\sinh(2\pi x/Y)\sin(2\pi y/Y)$$

$$B_4 = \pi^2Y^{-2}D^{-3}[-3\sinh(2\pi x/Y) + \cos(4\pi y/Y)\sinh(2\pi x/Y) + \cos(2\pi y/Y)\sinh(4\pi x/Y)]$$

$$B_5 = \pi^2Y^{-2}D^{-3}[3\sin(2\pi y/Y) - \sin(4\pi y/Y)\cosh(2\pi x/Y) - \sin(2\pi y/Y)\cosh(4\pi x/Y)] \quad (30)$$

$$B_6 = -6\pi^3Y^{-3}D^{-4}[\cos(4\pi y/Y)\cosh(4\pi x/Y) - 4\cos(2\pi y/Y)\cosh(2\pi x/Y) + 3] + 4\pi^3Y^{-3}D^{-3}[1 - \cos(2\pi y/Y)\cosh(2\pi x/Y)]$$

$$B_7 = -6\pi^3Y^{-3}D^{-4}[\sin(4\pi y/Y)\sinh(4\pi x/Y) + 4\sin(2\pi y/Y)\sinh(2\pi x/Y)] + 4\pi^3Y^{-3}D^{-3}\sin(2\pi y/Y)\sinh(2\pi x/Y)$$

$$D = \cosh(2\pi x/Y) - \cos(2\pi y/Y)$$

Sample calculations are carried out for the means and mean squares of the stresses for two situations:

(*a*) $y = 0;\ x = 0, 0.2Y, \ldots, 0.8Y$

(*b*) $x = 0.2Y;\ y = 0, 0.2Y, \ldots, Y$

These results are plotted in Figs. 4 and 5 in the form of normalized quantities defined by

$$\langle\sigma_{ij}\rangle^* = (Y/P)\langle\sigma_{ij}\rangle, \qquad \langle\sigma_{ij}^2\rangle^* = (Y^2/\sigma^2)\langle\sigma_{ij}^2\rangle$$

versus normalized co-ordinates $x^* = x/Y$ and $y^* = y/Y$. In calculating the mean squares it was assumed that the means of the loads, i.e., P, were zero.

Fig. 4 shows the variation of the mean stresses and mean-square deviation of stresses directly beneath one of the loads. Observe that both $\langle\sigma_{11}\rangle^*$ and $\langle\sigma_{11}^2\rangle^*$ become infinite at the boundary, whereas all other quantities are zero. The means of both normal stresses at infinity tend to the value P/Y, the mean of the load divided by the load spacing; that is to say, on the average a condition of uniform tension exists at infinity, the magnitude being

equal to the mean load per unit surface area. The mean-square deviations of stresses, on the other hand, tend to zero as $x^* \to \infty$.

In Fig. 5 the variation of these same quantities is shown over one load spacing at a depth equal to one fifth of a load spacing. The pertinent features of these curves are the following:

1 $\langle\sigma_{11}\rangle^*$ and $\langle\sigma_{11}^2\rangle^*$ reach maxima directly under the loads and they are significantly higher than the other quantities.

2 All other quantities are largest just to either side of the load.

3 $\langle\sigma_{12}\rangle^*$ is skew symmetric about the point directly beneath the load while $\langle\sigma_{12}^2\rangle^*$, of course, is always positive and hence is symmetric.

A Concentrated Load Acting at a Random Location

Let a single concentrated load P act at $x = 0$, $y = \eta$ where η is random, then we have

$$\sigma_{jk}(x, y) = PG_{jk}(x, y - \eta)$$

The mean and the cross correlations are now given by

$$\langle\sigma_{jk}(x, y)\rangle = P\langle G_{jk}(x, y - \eta)\rangle$$

$$\langle\sigma_{jk}(x, y)\sigma_{mn}(x', y')\rangle = P^2\langle G_{jk}(x, y - \eta)G_{mn}(x', y' - \eta)\rangle$$

These averages cannot be calculated by the same methods used in the foregoing since G_{jk} is not linear in the random variable η. Let $W_1(\eta)$ be the probability density function of first order, then

$$\langle\sigma_{jk}(x, y)\rangle = P\int_{-\infty}^{\infty} G_{jk}(x, y - \eta)W_1(\eta)d\eta$$

$$\langle\sigma_{jk}(x, y)\sigma_{mn}(x', y')\rangle = P^2\int_{-\infty}^{\infty} G_{jk}(x, y - \eta)G_{mn}(x', y' - \eta)W_1(\eta)d\eta$$

The integration is carried out for the following probability density functions:

(*a*) Uniform distribution

$$W_1(\eta) = \begin{cases} (2b)^{-1} & |\eta| < b \\ 0 & |\eta| > b \end{cases}$$

(*b*) Cauchy distribution

$$W_1(\eta) = \frac{b}{\pi(b^2 + \eta^2)}$$

The following results are given for $x_1 = x$ and $y_1 = y$:

(*a*) Uniform distribution

$$\langle\sigma_{11}\rangle = P(2b\pi)^{-1}(A_1^0 + xA_2^0)$$

$$\langle\sigma_{12}\rangle = P(2b\pi)^{-1}x^2A_3^0$$

$$\langle\sigma_{22}\rangle = P(2b\pi^{-1})(A_1^0 - xA_2^0)$$

$$\langle\sigma_{11}\sigma_{11}\rangle = P^2(b\pi^2)^{-1}[5(8x)^{-1}(A_1^0 + xA_2^0) + (5/12)x^2A_4^0 + (1/3)x^4A_6^0]$$

$$\langle\sigma_{11}\sigma_{12}\rangle = P^2(b\pi^2)^{-1}(1/3)x^5A_6^0 \qquad (31)$$

$$\langle\sigma_{11}\sigma_{22}\rangle = P^2(b\pi^2)^{-1}[(8x)^{-1}(A_1^0 + xA_2^0) + (1/12)x^2A_4^0 - (1/3)x^4A_6^0]$$

$$\langle\sigma_{12}\sigma_{12}\rangle = \langle\sigma_{11}\sigma_{22}\rangle$$

$$\langle\sigma_{22}\sigma_{12}\rangle = P^2(b\pi^2)^{-1}[-(1/3)x^5A_6^0 + (1/2)x^3A_7^0]$$

$$\langle\sigma_{22}\sigma_{22}\rangle = P^2(b\pi^2)^{-1}[(8x)^{-1}(A_1^0 + xA_2^0) - (7/12)x^2A_4^0 + (1/3)x^4A_6^0]$$

where

$$A_1^0 = \tan^{-1}[(b - y)/x] + \tan^{-1}[(b + y)/x]$$

$$A_2^0 = (b - y)[x^2 + (b - y)^2]^{-1} + (b + y)[x^2 + (b + y)^2]^{-1}$$

$$A_3^0 = [x^2 + (b - y)^2]^{-1} - [x^2 + (b + y)^2]^{-1}$$

$$A_4^0 = (b - y)[x^2 + (b - y)^2]^{-2} + (b + y)[x^2 + (b + y)^2]^{-2} \qquad (32)$$

$$A_5^0 = (b - y)[x^2 + (b - y)^2]^{-3} + (b + y)[x^2 + (b + y)^2]^{-3}$$

$$A_6^0 = [x^2 + (b - y)^2]^{-2} - [x^2 + (b + y)^2]^{-2}$$

$$A_7^0 = [x^2 + (b - y)^2]^{-2} - [x^2 + (b + y)^2]^{-2}$$

(*b*) Cauchy distribution

$$\langle\sigma_{11}\rangle = P(\pi b)^{-1}(2bx^2T_1 + b^2S_1 - 2b^2xS_3)$$

$$\langle\sigma_{12}\rangle = P(\pi b)^{-1}(2bx^2yT_1 + 2b^2x^2T_2 + 2b^2xS_4)$$

$$\langle\sigma_{22}\rangle = P(\pi b)^{-1}[2bx(y^2 - b^2)T_1 + 4b^2xyT_2 + 2b^2xS_5 + b^2S_1]$$

$$\langle\sigma_{11}\sigma_{11}\rangle = P^2(\pi^2b^2)^{-1}[4b^2x^2T_3 + (5/4)b^2x^{-1}S_1 - (5/2)b^2S_3 + b^2x(S_2 - 4S_4) - 2b^2x^2(S_7 - 2S_{11})]$$

$$\langle\sigma_{11}\sigma_{12}\rangle = P^2(\pi^2b^2)^{-1}[4b^2x^2yT_3 + 4b^2x^2T_4 + (1/2)b^2S_4 + (1/2)b^2x(S_5 - 4S_6) + 2b^2x^2(S_6 - 3S_{10})]$$

$$\langle\sigma_{11}\sigma_{22}\rangle = P^2(\pi^2b^2)^{-1}[4b^2x^2(y^2 - b^2)T_3 + 8b^2x^2yT_4 + (1/4)b^2x^{-1}S_1 - (1/2)b^2S_5 + 2b^2x^2(S_7 - 2S_{11})] \qquad (33)$$

$$\langle\sigma_{12}\sigma_{12}\rangle = \langle\sigma_{11}\sigma_{22}\rangle$$

$$\langle\sigma_{22}\sigma_{12}\rangle = P^2(\pi^2b^2)^{-1}[4b^2x^2y(y^2 - 3b^2)T_3 + 4b^2x^2(3y^2 - b^2)T_4 + (1/2)b^2S_4 + (1/2)b^2x(S_5 - 4S_6) - 2b^2x^2(S_6 - 3S_{10})]$$

$$\langle\sigma_{22}\sigma_{22}\rangle = P^2(\pi^2b^2)^{-1}\{4b^2x^2[(y^2 - b^2)^2 - 4b^2y^2]T_3 + 16b^2x^2y(y^2 - b^2)T_4 + (1/4)b^2x^{-1}S_1 - (1/2)b^2S_5 - b^2x(S_2 - 4S_6) - 2b^2x^2(S_7 - 2S_{11})\}$$

where

$$S_1 = (y^2 - x^2 + b^2)[(x^2 + y^2 - b^2)^2 + 4b^2y^2]^{-1}$$

$$S_2 = [(y^2 - x^2 + b^2)^2 - 4x^2y^2][(x^2 + y^2 - b^2)^2 + 4b^2y^2]^{-2}$$

$$S_3 = -4xy(y^2 - x^2 + b^2)[(x^2 + y^2 - b^2)^2 + 4b^2y^2]^{-2}$$

$$S_4 = y[(y^2 - x^2 + b^2)(x^2 + y^2 + b^2) - 2x^2(x^2 + y^2 - b^2)][(x^2 + y^2 - b^2)^2 + 4b^2y^2]^{-2}$$

$$S_5 = -x[(y^2 - x^2 + b^2)(x^2 + y^2 - b^2) + 2y^2(x^2 + y^2 + b^2)][(x^2 + y^2 - b^2)^2 + 4b^2y^2]^{-2}$$

$$S_6 = y\{(x^2 + y^2 + b^2)[(y^2 - x^2 + b^2)^2 - 4x^2y^2] - 4x^2(x^2 + y^2 - b^2)(y^2 - x^2 + b^2)\}[(x^2 + y^2 - b^2)^2 + 4b^2y^2]^{-3}$$

$$S_7 = -x\{(x^2 + y^2 - b^2)[(y^2 - x^2 + b^2)^2 - 4x^2y^2] + 4y^2(y^2 - x^2 + b^2)(x^2 + y^2 + b^2)\}[(x^2 + y^2 - b^2)^2 + 4b^2y^2]^{-3} \qquad (34)$$

$$S_9 = \{(y^2 - x^2)(y^2 - x^2 + b^2)[(y^2 - x^2 + b^2)^2 - 12x^2y^2] + 4x^2y^2[3(y^2 - x^2 + b^2)^2 - 4x^2y^2]\}[(x^2 + y^2 - b^2)^2 + 4b^2y^2]^{-3}$$

$$S_9 = 2xy\{(y^2 - x^2 + b^2)[(y^2 - x^2 + b^2)^2 - 12x^2y^2] - (y^2 - x^2)[3(y^2 - x^2 + b^2)^2 - 4x^2y^2]\}[(x^2 + y^2 - b^2)^2 + 4b^2y^2]^{-3}$$

$$S_{10} = y\{(y^2 - 3x^2)[(y^2 - x^2 + b^2)^2 - 24x^2y^2(y^2 - x^2 + b^2)^2 + 16x^4y^4] + 8x^2(3y^2 - x^2)(y^2 - x^2 + b^2)[(y^2 - x^2 + b^2)^2 - 4x^2y^2]\}[(x^2 + y^2 - b^2)^2 + 4b^2y^2]^{-4}$$

$$S_{11} = x\{(3y^2 - x^2)[(y^2 - x^2 + b^2)^2 - 24x^2y^2(y^2 - x^2 + b^2)^2 + 16x^4y^4) - 8y^2(y^2 - 3x^2)(y^2 - x^2 + b^2)[(y^2 - x^2 + b^2)^2 - 4x^2y^2]\}[(x^2 + y^2 - b^2)^2 + 4b^2y^2]^{-4}$$

$$T_1 = [(x^2 + y^2 - b^2)^2 - 4b^2y^2][(x^2 + y^2 - b^2)^2 + 4b^2y^2]^{-2}$$

$$T_2 = 4by(x^2 + y^2 - b^2)[(x^2 + y^2 - b^2)^2 + 4b^2y^2]^{-2}$$

$$T_3 = [(x^2 + y^2 - b^2)^4 - 24b^2y^2(x^2 + y^2 - b^2)^2 + 16b^4y^4)][(x^2 + y^2 - b^2)^2 + 4b^2y^2]^{-4}$$

$$T_4 = 8by(x^2 + y^2 - b^2)[(x^2 + y^2 - b^2)^2 - 4b^2y^2][(x^2 + y^2 - b^2)^2 + 4b^2y^2]^{-4}$$

In both cases calculations were made for mean and mean-square stresses for

(*a*) $y = 0;\ x = 0, b, \ldots, 5b$

(*b*) $x = b;\ y = 0, b, \ldots, 5b$

The results are plotted in Figs. 6, 7, 8, and 9 for normalized quantities

$$\langle \sigma_{ij} \rangle^* = \pi b P^{-1} \langle \sigma_{ij} \rangle, \qquad \langle \sigma_{ij}^2 \rangle^* = \pi^2 b^2 P^{-2} \langle \sigma_{ij}^2 \rangle$$

versus normalized co-ordinates $x^* = x/b$ and $y^* = y/b$.

The mean and mean-square stresses resulting from a single concentrated load at a random distance for the origin (uniform distribution) are shown in Figs. 6 and 7. The same quantities for a Cauchy distribution of the load are shown in Figs. 8 and 9. It is apparent that there is little difference in the two sets of mean and mean-square stresses corresponding to the two distributions.

In both cases for $y^* = 0$ we see that as $x^* \to 0$ the mean stresses remain finite but the mean-square stresses become infinite. This is roughly explained as follows: At one value of the random variable (the co-ordinate of the point of application of the concentrated load) we have infinite stress (a Dirac δ-function). In taking the mean we integrate out this singularity. However, in the calculation of mean-square stresses the integrand will contain a singularity of the form of the square of the δ-function.

The variation in the direction along the boundary but at $x^* = 1$ is just about what one might except after seeing the results in Fig. 5. In Figs. 7 and 9 one sees that $\langle \sigma_{11} \rangle^*$, $\langle \sigma_{11}^2 \rangle^*$, and $\langle \sigma_{12}^2 \rangle^*$ have maxima directly under the load while $\langle \sigma_{22} \rangle^*$, $\langle \sigma_{22}^2 \rangle^*$, and $\langle \sigma_{12} \rangle^*$ have extrema to either side of the load. All quantities tend to zero as either x^* or y^* become infinite.

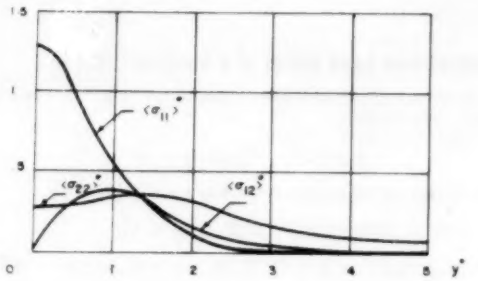

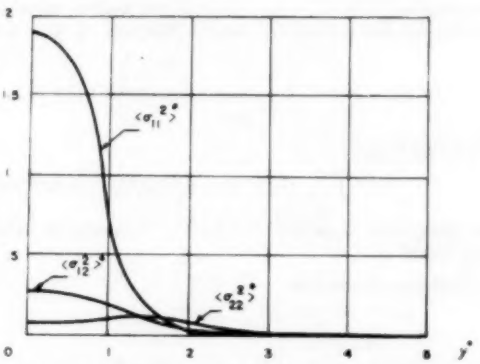

Fig. 7 Mean and mean-square stresses for a single concentrated load randomly located along boundary; uniform distribution, $x^* = 1$

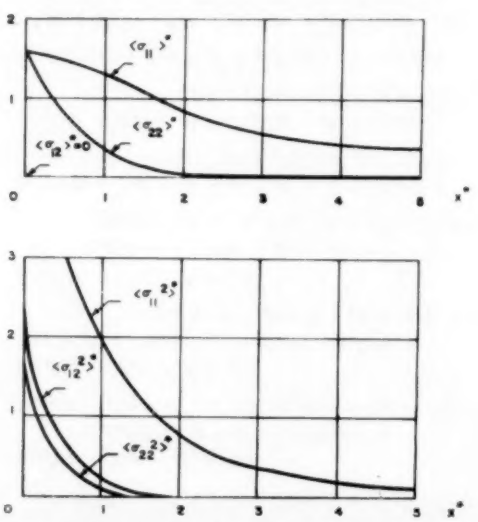

Fig. 6 Mean and mean-square stresses for a single concentrated load randomly located along boundary; uniform distribution, $y^* = 0$

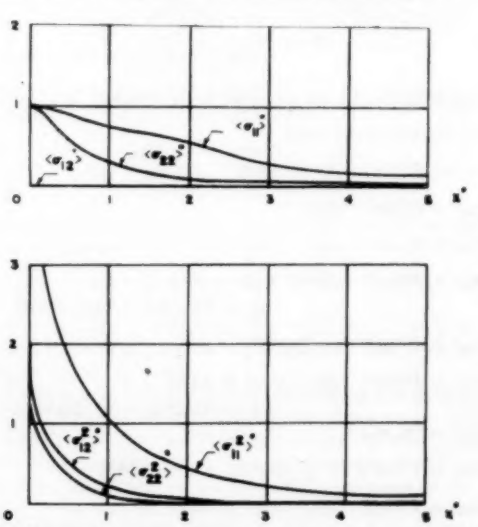

Fig. 8 Mean and mean-square stresses for a single concentrated load randomly located along boundary; Cauchy distribution, $y^* = 0$

Concentrated Loads of Equal Magnitudes Separated by Random Intervals

Let the deviation of the location of the rth load from the mean rY be γ_r, Fig. 10. Through (9) with $P_r = P$, $(r = 1, 2, \ldots)$, we have

$$\sigma_{jk} = P \sum_r G_{jk}(x, y - rY - \gamma_r)$$

The means and the correlation functions are therefore given by

$$\langle \sigma_{jk}(x, y) \rangle = P \sum_r \langle G_{jk}(x, y - rY - \gamma_r) \rangle$$

$$\langle \sigma_{jk}(x, y)\sigma_{mn}(x', y') \rangle = P^2 \sum_{r,s} \langle G_{jk}(x, y - rY - \gamma_r) G_{mn}(x', y' - sY - \gamma_s) \rangle$$

which may also be written as

$$\langle \sigma_{jk}(x, y) \rangle = P \sum \int_{-\infty}^{\infty} G_{jk}(x, y - rY - \gamma_r) W_1(\gamma_r) d\gamma_r$$

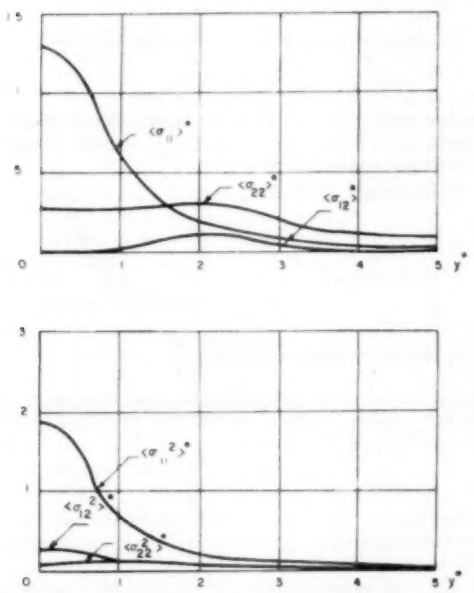

Fig. 9 Mean and mean-square stresses for a single concentrated load randomly located along boundary; Cauchy distribution, $x^* = 1$

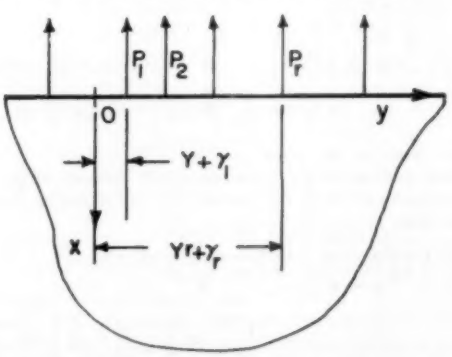

Fig. 10 Concentrated surface loads of equal magnitude and random spacing

$$\langle \sigma_{jk}(x, y)\sigma_{mn}(x', y') \rangle = P^2 \sum_{r \neq s} \iint_{-\infty}^{\infty} G_{jk}(x, y - rY - \gamma_r) G_{mn}(x', y' - sY - \gamma_s) W_2(\gamma_r, \gamma_s) d\gamma_r d\gamma_s + \sigma^2 \sum_r \int_{-\infty}^{\infty} G_{jk}(x, y - rY - \gamma_r) G_{mn}(x', y' - rY - \gamma_r) W_1(\gamma_r) d\gamma_r$$

We evaluate these averages for a uniform distribution; i.e.,

$$W_1(\gamma_r) = \begin{cases} (2b)^{-1} & |\gamma_r| < b \\ 0 & |\gamma_r| > b \end{cases}$$

$$W_2(\gamma_r, \gamma_s) = \begin{cases} (4b^2)^{-1} & |\gamma_r| < b, \quad |\gamma_s| < b \\ 0 & \text{either } |\gamma_r| > b \text{ or } |\gamma_s| > b \end{cases}$$

The results are given for $x_1 = x$ and $y_1 = y$:

$$\begin{aligned}
\langle \sigma_{11} \rangle &= P(2\pi b)^{-1}(A_1 + xA_2) \\
\langle \sigma_{12} \rangle &= P(2\pi b)^{-1} x^2 A_3 \\
\langle \sigma_{22} \rangle &= P(2\pi b)^{-1}(A_1 - xA_2) \\
\langle \sigma_{11}\sigma_{11} \rangle &= P^2(2\pi b)^{-2}[(A_1 + xA_2)^2 + 5b(2x)^{-1}(A_1 + xA_2) \\
&\quad + (5/3)bx^2 A_4 + (4/3)bx^4 A_5 - (A_8 + x^2 A_9 + 2xA_{11})] \\
\langle \sigma_{11}\sigma_{12} \rangle &= P^2(2\pi b)^{-2}[x^2 A_3(A_1 + xA_2) + (4/3)bx^5 A_6 \\
&\quad - x^2(A_{12} + xA_{13})] \\
\langle \sigma_{11}\sigma_{22} \rangle &= P^2(2\pi b)^{-2}[(A_1^2 - x^2 A_2^2) \\
&\quad + b(2x)^{-1}(A_1 + xA_2) + (1/3)bx^2 A_4 \\
&\quad - (4/3)bx^4 A_5 - (A_9 - x^2 A_9)] \\
\langle \sigma_{12}\sigma_{12} \rangle &= P^2(2\pi b)^{-2}[x^4 A_3^2 + b(2x)^{-1}(A_1 + xA_2) \\
&\quad + (1/3)bx^2 A_4 - (4/3)bx^4 A_5 - x^4 A_{16}] \\
\langle \sigma_{22}\sigma_{12} \rangle &= P^2(2\pi b)^{-2}[x^2 A_3(A_1 - xA_2) \\
&\quad - (4/3)bx^5 A_6 + 2bx^3 A_7 - x^2(A_{12} - xA_{13})] \\
\langle \sigma_{22}\sigma_{22} \rangle &= P^2(2\pi b)^{-2}[(A_1 - xA_2)^2 + b(2x)^{-1}(A_1 + xA_2) \\
&\quad - (7/3)bx^2 A_4 + (4/3)bx^4 A_5 - (A_8 + x^2 A_9 - 2xA_{11})]
\end{aligned} \tag{35}$$

where

$$A_1 = \tan^{-1}\{\sinh(2\pi x/Y)\sin(2\pi b/Y)[\cosh(2\pi x/y) \cos(2\pi b/Y) - \cos(2\pi y/Y)]^{-1}\}$$

$$A_2 = \pi Y^{-1}\{D_1^{-1}\sin[2\pi(y + b)/Y] - D_2^{-1}\sin[2\pi(y - b)/Y]\}$$

$$A_3 = \pi(xY)^{-1}\sinh(2\pi x/Y)(D_2^{-1} - D_1^{-1})$$

$$A_4 = \pi^2(xY^2)^{-1}\sinh(2\pi x/Y)\{D_1^{-2}\sin[2\pi(y + b)/Y] - D_2^{-2}\sin[2\pi(y - b)/Y]\}$$

$$\begin{aligned}
A_5 = {} & \pi^2(4x^2Y^2)^{-1}\sinh(2\pi x/Y)\{D_1^{-2}\sin[2\pi(y + b)/Y] \\
& - D_2^{-2}\sin[2\pi(y - b)/Y]\} + \pi^2(4x^2Y^2)^{-1} \\
& [[D_1^{-2}\{\sin[2\pi(y + b)/Y][\cosh(4\pi x/Y) - 3] \\
& + \sin[4\pi(y + b)/Y]\cosh(2\pi x/Y)\} \\
& - D_2^{-2}\{\sin[2\pi(y - b)/Y][\cosh(4\pi x/Y) - 3] \\
& + \sin[4\pi(y - b)/Y]\cosh(2\pi x/Y)\}]]
\end{aligned}$$

$$\begin{aligned}
A_6 = {} & \pi^2(4x^2Y^2)^{-1}[[D_1^{-2}\sinh(2\pi x/Y) \\
& \{\cos[4\pi(y + b)/Y] - 3\} \\
& + D_1^{-2}\cos[2\pi(y + b)/Y]\sinh(4\pi x/Y) \\
& - D_2^{-2}\sinh(2\pi x/Y)\{\cos[4\pi(y - b)/Y] - 3\} \\
& - D_2^{-2}\cos[2\pi(y - b)/Y]\sinh(4\pi x/Y)]]
\end{aligned}$$

$$+ 3\pi^3(4x^4Y^3)^{-1}[[D_1^{-2}\{1 - \cos[2\pi(y+b)/Y]\cosh(2\pi x/Y)\} - D_2^{-2}\{1 - \cos[2\pi(y-b)/Y]\cosh(2\pi x/Y)\}]] + 3\pi(8x^5Y)^{-1}\sinh(2\pi x/Y)(D_2^{-1} - D_1^{-1})$$

$$A_7 = 4\pi^2(x^2Y^2)^{-1}[[D_1^{-2}\{1 - \cos[2\pi(y+b)/Y]\cosh(2\pi x/Y)\} - D_2^{-2}\{1 - \cos[2\pi(y-b)/Y]\cosh(2\pi x/Y)\}]] + 4\pi(x^3Y)^{-1}\sinh(2\pi x/Y)(D_2^{-1} - D_1^{-1})$$

$$A_8 = \sum_{k=-\infty}^{\infty} \{\tan^{-1}[(b - y + kY)/x] - \tan^{-1}[(-b - y + kY)/x]\}^2 \tag{36}$$

$$A_9 = \pi^2Y^{-2}[[D_1^{-2}\{1 - \cos[2\pi(y+b)/Y]\cosh(2\pi x/Y)\} + D_2^{-2}\{1 - \cos[2\pi(y-b)/Y]\cosh(2\pi x/Y)\}]] + \pi(2b^2 + x^2)[2bY(b^2 + x^2)]^{-1}\{D_1^{-1}\sin[2\pi(y+b)/Y] - D_2^{-1}\sin[2\pi(y-b)/Y]\} + \pi^2b^2[2xY(b^2 + x^2)]^{-1}\sinh(2\pi x/Y)(D_1^{-1} + D_2^{-1})$$

$$A_{10} = -\pi^2(x^2Y^2)^{-1}[[D_1^{-2}\{1 - \cos[2\pi(y+b)/Y]\cosh(2\pi x/Y)\} + D_2^{-2}\{1 - \cos[2\pi(y-b)/Y]\cosh(2\pi x/Y)\}]] - \pi[2bY(b^2 + x^2)]^{-1}\{D_1^{-1}\sin[2\pi(y+b)/Y] - D_2^{-1}\sin[2\pi(y-b)/Y]\} + \pi^2b^2[2x^2Y(b^2 + x^2)]^{-1}\sinh(2\pi x/Y)(D_1^{-1} + D_2^{-1})$$

$$A_{11} = \sum_{k=-\infty}^{\infty} \{\tan^{-1}[(b - y + kY)/x] - \tan^{-1}[(b - y + kY)/x]\}\{(b - y - kY)[x^2 + (b - y + kY)^2]^{-1} - (-b - y + kY)[x^2 + (-b - y + kY)^2]^{-1}\}$$

$$A_{12} = \sum_{k=-\infty}^{\infty} \{\tan^{-1}[(b - y + kY)/x] - \tan^{-1}[(-b - y + kY)/x]\}\{[x^2 + (b - y + kY)^2]^{-1} - [x^2 + (-b - y + kY)^2]^{-1}\}$$

$$A_{13} = -\pi^3(xY^2)^{-1}\sinh(2\pi x/Y)\{D_2^{-2}\sin[2\pi(y-b)/Y] + D_1^{-2}\sin[2\pi(y+b)/Y]\} - \pi(4x^2Y)^{-1}\{D_2^{-1}\sin[2\pi(y-b)/Y] + D_1^{-1}\sin[2\pi(y+b)/Y]\} + \pi(2bxY)^{-1}\sinh(2\pi x/Y)(D_1^{-1} - D_2^{-1})$$

$$D_1 = \cosh(2\pi x/Y) - \cos[2\pi(y+b)/Y]$$

$$D_2 = \cosh(2\pi x/Y) - \cos[2\pi(y-b)/Y]$$

All of the quantities $A_1, A_2, \ldots, A_{13}$ first appeared as infinite series. The procedure explained in the section, "Concentrated Loads of Random Magnitude . . .," was applied for the evaluation of these summations where possible. Since the procedure is somewhat different when treating functions with singularities other than poles, we give some of the details involved in calculating A_1:

$$A_1 = \sum_{k=-\infty}^{\infty} \{\tan^{-1}[(b - y + kY)/x] - \tan^{-1}[(-b - y + kY)/x]\} \tag{37}$$

Following the summation procedure described in the foregoing section the function $f(z)$ here is defined as

$$f(z) = \tan^{-1}[(b - y + z)/x] - \tan^{-1}[(-b - y + z)/x]$$

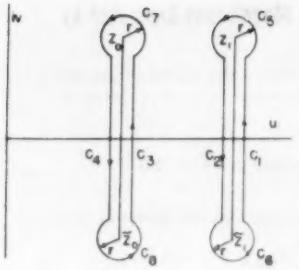

Fig. 11 Singularities of $f(z)$

where as before z is the complex variable $z = u + iv$. Employing the logarithmic definition of the complex arctangent and the notation z for the complex conjugate of z, $f(z)$ can be written as

$$f(z) = (i/2)\left(\log\frac{z - \bar{z}_0}{z_0 - z} - \log\frac{z - \bar{z}_1}{z_1 - z}\right)$$

and after adding $i\pi$ to the first log term, adding $-i\pi$ to the second, and factoring out a (-1), $f(z)$ becomes

$$f(z) = -(i/2)\left(\log\frac{z - z_0}{z - \bar{z}_0} - \log\frac{z - z_1}{z - \bar{z}_1}\right) \tag{38}$$

where $z_0 = y - b + ix$ and $z_1 = y + b + ix$.

The singularities of $f(z)$ consist of two branch cuts connecting $z_0, \bar{z}_0$ and $z_1, \bar{z}_1$, which are introduced, Fig. 11, in order to make the two logarithms single-valued.

At the right-hand cut we have

$$\log\frac{z - z_1}{z - \bar{z}_1} = \begin{cases} \log\left|\dfrac{z - z_1}{z - \bar{z}_1}\right| - i\pi & \text{on } C_1 \\ \log\left|\dfrac{z - z_1}{z - \bar{z}_1}\right| + i\pi & \text{on } C_2 \end{cases} \tag{39}$$

while on the left-hand cut we have

$$\log\frac{z - z_0}{z - \bar{z}_0} = \begin{cases} \log\left|\dfrac{z - z_0}{z - \bar{z}_0}\right| - i\pi & \text{on } C_3 \\ \log\left|\dfrac{z - z_1}{z - \bar{z}_1}\right| + i\pi & \text{on } C_4 \end{cases} \tag{40}$$

Note that $\log[(z - z_0)/(z - \bar{z}_1)]$ is continuous across the right-hand cut and that $\log[(z - z_1)/(z - \bar{z}_1)]$ is continuous across the left-hand cut.

We now can apply equation (27) for the evaluation of A_1. Thus in terms of line integrals along $C_1, C_2, \ldots, C_9$, which surround the singularities of $f(z)$, A_1 becomes

$$A_1 = \frac{1}{4Y}\oint_{C_3+C_4+C_7+C_9} \log\frac{z - z_0}{z - \bar{z}_0}\cot\frac{\pi z}{Y}\,dz - \frac{1}{4Y}\oint_{C_1+C_2+C_5+C_6} \log\frac{z - z_1}{z - \bar{z}_1}\cot\frac{\pi z}{Y}\,dz \tag{41}$$

The integrals along C_5, C_6, C_7, and C_9 tend to zero as $r \to 0$. The second integral, which for the moment will be denoted by I, therefore becomes

$$I = \int_{C_1}\left[\log\left|\frac{z - z_1}{z - \bar{z}_1}\right| - i\pi\right]\cot\frac{\pi z}{Y}\,dz + \int_{C_2}\left[\log\left|\frac{z - z_1}{z - \bar{z}_1}\right| + i\pi\right]\cot\frac{\pi z}{Y}\,dz$$

but

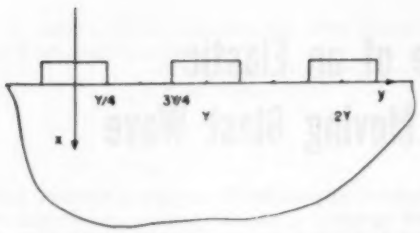

Fig. 12 Load probability distribution corresponding to the totality of $W_1(\gamma_r)$

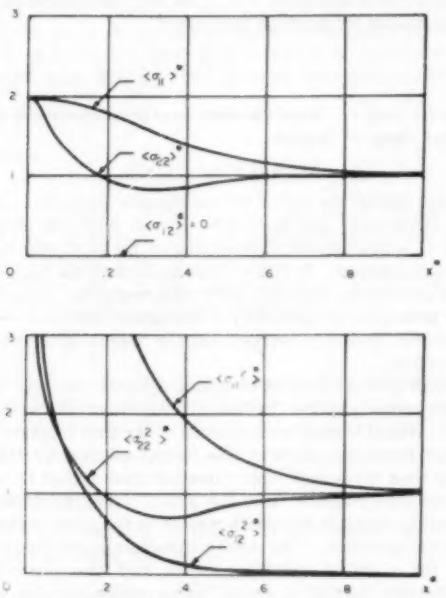

Fig. 13 Mean and mean-square stresses for concentrated surface loads of uniform magnitude and random spacing; uniform distribution, $y^* = 0$

$$\int_{C_1+C_2} \log\left|\frac{z-z_1}{z-\bar{z}_1}\right| \cot\frac{\pi z}{Y}\,dz = 0$$

and hence I reduces to

$$I = i\pi\int_{C_2}\cot\frac{\pi z}{Y}\,dz - i\pi\int_{C_1}\cot\frac{\pi z}{Y}\,dz = 2i\pi\int_{z_1}^{\bar{z}_1}\cot\frac{\pi z}{Y}\,dz$$

Finally, upon evaluating the last integral we find

$$I = 4Y\,Im\left(\log\sin\frac{\pi z_1}{Y}\right) \tag{42}$$

The first integral in (41) can be treated in the same way and with similar results. After combining the results of the two integrations, we obtain

$$A_1 = \tan^{-1}\frac{\sin(2\pi b/Y)\sinh(2\pi x/Y)}{\cos(2\pi b/Y)\cosh(2\pi x/Y) - \cos(2\pi y/Y)}$$

which agrees with the first of (36).

Quantities A_2, A_{11}, and A_{12} also have the branch cuts shown in Fig. 11 as at least part of the singularities of the $f(z)$ associated with them. However, the integrals along the cuts for these quantities are much more difficult to evaluate and, consequently,

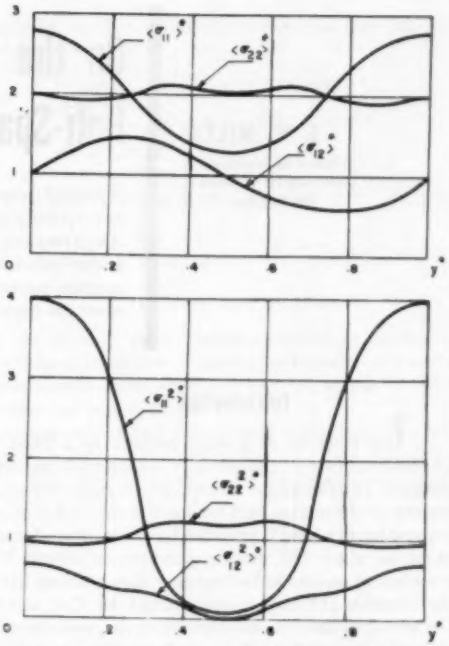

Fig. 14 Mean and mean-square stresses for concentrated surface loads of uniform magnitude and random spacing; uniform distribution, $x^* = 0.2$

these expressions were left in the series form.

As an example of the variation of the mean and mean-square stresses, calculations were made for the uniform distribution in which $b = Y/4$. The probability distribution for the load in this case is drawn in Fig. 12. Computations were made at the following positions:

(a) $y = 0;\quad x = 0, 0.2b, \ldots, 0.8b$

(b) $x = 0.2b;\quad y = 0, 0.1b, \ldots, 0.5b$

In Figs. 13 and 14 normalized quantities

$$\langle\sigma_{ij}\rangle^* = YP^{-1}\langle\sigma_{ij}\rangle \qquad \langle\sigma_{ij}{}^2\rangle^* = Y^2P^{-2}\langle\sigma_{ij}{}^2\rangle$$

are plotted versus $x^* = x/Y$ and $y^* = y/Y$.

The plots of mean and mean-square stresses as x^* increases and $y^* = 0$, Fig. 13, show several features similar to the case in which loads of random magnitude and regular spacing were considered. Thus a uniform mean tension exists for large x^* but in this case shows up in the mean-square normal stresses since here the square of the means are not subtracted off. However, in this case we observe that (a) the mean normal stresses have a finite, nonzero value at $x^* = 0$, $y^* = 0$; (b) $\langle\sigma_{22}\rangle^*$ and $\langle\sigma_{22}{}^2\rangle^*$ have minima just below the surface at the origin; and (c) all mean squares tend to infinity as $x^* \to 0$.

In examining Fig. 14 one should keep in mind that for $0 \le y^* < 0.25$ and $0.75 < y^* \le 1.0$ a vertical concentrated load can occur with equal probability at each point while a load never occurs for $0.25 < y^* < 0.75$. The principal differences between these curves and those in Fig. 5 seem to be associated with the jump from a condition of possible load to one of no load which occurs at $y^* = 0.25$ and $y^* = 0.75$. We see that the peaks in $\langle\sigma_{11}\rangle^*$ and $\langle\sigma_{11}{}^2\rangle^*$ are broadened, the extremal values in $\langle\sigma_{22}\rangle^*$, $\langle\sigma_{22}{}^2\rangle^*$, $\langle\sigma_{12}\rangle^*$, and $\langle\sigma_{12}{}^2\rangle^*$ are moved toward the interior of the interval, and inflection points are introduced at $y^* = 0.25, 0.75$ in some of the curves.

The authors wish to thank Mr. Sat Dev Sarna for his care and patience in performing the calculations and checking the analysis.

On the Response of an Elastic Half-Space to a Moving Blast Wave

J. W. MILES[1]
Professor of Engineering,
University of California,
Los Angeles, Calif.

A formal integral transform solution is obtained for the response of an elastic half-space to a radially symmetric pressure signature of variable pressure and variable velocity. An asymptotic approximation to this solution is developed and expressed in terms of the known solution for the response of a half-space to a two-dimensional pulse moving with constant velocity plus a correction that is important only if the blast-wave speed directly above the point of observation is close to the Rayleigh-wave speed.

Introduction

THE response of a solid medium to a blast wave moving over its surface is a problem of considerable importance in the design of blast-resistant structures. Perhaps the simplest model for this problem that still retains the essential features of wave propagation in a solid is provided by a two-dimensional load distribution, say $p(x - Ut)$, moving with uniform velocity U over the free surface of an elastic half-space. This problem has been solved by Sneddon [1][2] and, in more detail, by Cole and Huth [2]. The principal deficiencies of such a model, aside from those inherent in the assumption of an elastic medium, are that (*a*) the resulting displacements tend to infinity as U tends to γ, the Rayleigh-wave speed; and (*b*) these displacements contain an arbitrary constant and therefore are ambiguous as $t \to \infty$. The Rayleigh-wave infinities may be removed either by allowing for dissipation in the medium or by allowing U to vary with distance, as it must for a true blast wave. The ambiguities in the displacements are more or less intrinsic to two-dimensional wave phenomena and result from the absence of any upper bound on the travel time from remote points to the point of observation; fortunately, the displacements *per se* are unimportant in the majority of applications, while the arbitrary constants do not enter such quantities as velocity, acceleration, and stress.

We shall consider here, Fig. 1, the response of an elastic half-space ($z > 0$) to a radially symmetric pressure signature, say $p(r, t)$, for which both peak pressure and blast-wave speed decay with distance r from the epicenter. This model suffers from neither of the foregoing difficulties if the resulting boundary-value problem is solved exactly, but we shall seek only an asymptotic solution for large r. Now it is clear from dimensional considerations that "large r" implies

$$r \gg (\alpha, \beta, U)[t - t_0(r)], \tag{1}$$

where $t_0(r)$ denotes the arrival time at the blast front, and α and β denote dilatational and shear-wave speeds, with the choice of α, β, or U in the inequality depending on the particular feature under consideration. It follows that an asymptotic approximation in r may not be uniformly valid with respect to $t - t_0(r)$, and we may anticipate the possibility of ambiguous results as $t \to \infty$—in particular, arbitrary constants in the approximations to the displacements.

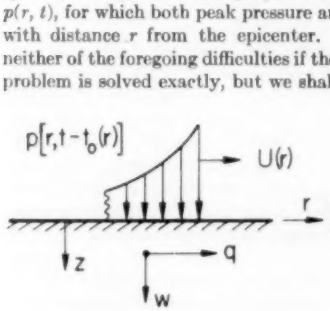

Fig. 1 Axisymmetric blast wave on elastic half-space

We shall proceed by first obtaining a formal solution to our boundary-value problem (which is formulated in Section 2) through integral transforms (Section 3). We then (Section 4) replace the Bessel functions in this formal solution by the first terms in their asymptotic approximations and neglect those disturbances that originate from the action of the blast wave at points in the opposite side (with respect to the point of observation) of the epicenter. The resulting problem is two-dimensional except for a radial weighting factor and the three-dimensional features implicit in $p(r, t)$; consequently, we may obtain results in the form of convolution integrals over the product of $p(r, t)$ with the known solution for the two-dimensional response to a unit impulse. Even these calculations would be quite involved, however, and we therefore impose (in Section 5) approximations on the pressure signature that are suggested by (but go beyond) G. I. Taylor's strong-shock approximation. The resulting integrals may be reduced (Section 6) to the two-dimensional results of [2], with U evaluated directly above the point of observation, plus a correction term for the Rayleigh-wave singularity, with the latter being important only if $U(r)$ approximates γ, where it renders the net solution of order

$$[t_0''(r)]^{-1/2}$$

Finally (in Section 7), we evaluate the displacements corresponding to the correction term and the total displacements for the special case $U(r) = \gamma$.

An alternative and more direct reduction of the asymptotic approximation developed in Section 4 may be obtained by a stationary phase approximation to the double integrals without posing special assumptions for the pressure signature. The results for the Rayleigh wave are less satisfactory, however, and we therefore relegate this solution to the Appendix, where it is used to obtain results for $U(r) > \alpha$ without imposing the restriction $z \ll r$ that is imposed in Section 6.

2 Mathematical Formulation

Following the notation of Ewing, Jardetzky, and Press [3] (subsequently abbreviated by EJP), we derive the radial q and

[1] Also, Consultant, Engineering Mechanics Department, Space Technology Laboratories, Inc., Los Angeles, Calif.

[2] Numbers in brackets designate References at end of paper.

Presented at the West Coast Conference of the Applied Mechanics Division, Pasadena, Calif., June 27–29, 1960, of THE AMERICAN SOCIETY OF MECHANICAL ENGINEERS.

Discussion of this paper should be addressed to the Secretary, ASME, 29 West 39th Street, New York, N. Y., and will be accepted until January 10, 1961, for publication at a later date. Discussion received after the closing date will be returned.

Manuscript received by ASME Applied Mechanics Division, November 3, 1959. Paper No. 60—APMW-9.

vertical (w, positive down) displacements from dilatational ϕ and shear ψ potentials according to

$$u = \phi_r + \psi_{rz}, \tag{2a}$$

$$w = \phi_z - r^{-1}(r\psi_r)_r$$

$$= \phi_z + \psi_{zz} - \beta^{-2}\psi_{tt} \tag{2b}$$

$$\alpha^2\nabla^2\phi = \phi_{tt} \qquad \beta^2\nabla^2\psi = \psi_{tt} \tag{3a, b}$$

where $\alpha = [(\lambda + 2\mu)/\rho]^{1/2}$ and $\beta = (\mu/\rho)^{1/2}$ (4a, b)

denote the dilational and shear-wave speeds, respectively; λ and μ denote Lamé's constants, and ρ the density. We note that $w \sim \phi_z - \psi_{rr}$, $r \to \infty$, so that in the subsequent, asymptotic calculations it is more direct to calculate ψ_r in place of ψ. We require solutions to (3a, b) subject to the boundary conditions

$$p_{zz} = \lambda\nabla^2\phi + 2\mu w_z = -p[r, t - t_0(r)], \qquad z = 0, \quad t > t_0(r) \tag{5a}$$

and

$$p_{rz} = \mu(u_z + w_r) = 0, \qquad z = 0 \tag{5b}$$

corresponding to the prescribed, compressive load and zero shear load at the free surface. The displacements (and therefore the potentials) also must vanish at infinity.

We observe that $t = t_0(r)$ defines the front of the blast wave and that the velocity at this front is given by

$$U(r) = 1/t_0'(r) \tag{6}$$

and must be positive. We also may assume $t_0''(r) > 0$, corresponding to the physical fact that $U(r)$ cannot increase with r. Asymptotically, $U(r)$ tends to the acoustic velocity (in air) and $t_0''(r)$ to zero.

3 Formal Solution

Let $\bar{f}(r, \omega)$ and $F(k, \omega)$ denote Fourier and Fourier-Bessel transforms according to

$$\bar{f}(r, \omega) = \int_{-\infty}^{\infty} e^{-i\omega t} f(r, t)dt, \tag{7a}$$

$$f(r, t) = \frac{1}{2\pi}\int_{-\infty}^{\infty} e^{i\omega t}\bar{f}(r, \omega)d\omega \tag{7b}$$

$$F(k, \omega) = \int_0^{\infty} \bar{f}(r, \omega)J_0(kr)r\,dr, \tag{8a}$$

$$\bar{f}(r, \omega) = \int_0^{\infty} F(k, \omega)J_0(kr)k\,dk \tag{8b}$$

where, for analytical convenience, ω may be assumed to have a small, negative imaginary part. Transforming (3a, b), (5a), and the r-integral of (5b) (the constant of integration is zero in virtue of the null conditions at infinity) with respect to both t and r, we obtain

$$\Phi_{zz} - (k^2 - k_\alpha^2)\Phi = 0, \qquad \Psi_{zz} - (k^2 - k_\beta^2)\Psi = 0 \tag{9a, b}$$

$$\mu(2k^2 - k_\beta^2)\Phi + 2\mu k^2\Psi_z = -P, \qquad z = 0 \tag{10a}$$

$$2\mu\Phi_z + \mu(2k^2 - k_\beta^2)\Psi = 0, \qquad z = 0 \tag{10b}$$

where

$$k_\alpha = \omega/\alpha, \qquad k_\beta = \omega/\beta \tag{11a, b}$$

We note that P is the Fourier-Bessel transform of

$$p(r, \omega)\exp\,[-i\omega t_0(r)],$$

where $p(r, \omega)$ denotes the Fourier transform of $p(r, t)$ (our notation is, to this extent, inconsistent, but there is no danger of ambiguity).

It may be verified by direct substitution that (cf. EJP, pp. 38–40 with $Z = -1$)

$$\Phi(k, z, \omega) = A(k, \omega)P(k, \omega)e^{-\nu z}, \tag{12a}$$

$$\Psi(k, z, \omega) = B(k, \omega)P(k, \omega)e^{-\nu' z} \tag{12b}$$

where

$$\nu = (k^2 - k_\alpha^2)^{1/2}, \qquad \nu' = (k^2 - k_\beta^2)^{1/2} \tag{13a, b}$$

and

$$A = -\frac{(2k^2 - k_\beta^2)}{\mu F(k, \omega)}, \qquad B = \frac{-2\nu}{\mu F(k, \omega)} \tag{14a, b}$$

$$F = (2k^2 - k_\beta^2)^2 - 4k^2\nu\nu' \tag{14c}$$

satisfy (9a, b) and (10a, b), while the boundary conditions at infinity will be satisfied if we choose the ν branches of ν and ν' that have non-negative real parts (see EJP for details on the appropriate choice of branch cuts).

We remark that A and B are homogeneous functions (of k and ω) of order -2 and have simple poles at $k = \pm\kappa = \pm\omega/\gamma$, where γ is the Rayleigh-wave speed. In the neighborhoods of these poles, we may write

$$k \to \pm\kappa = \pm\frac{\omega}{\gamma}$$

$$\begin{cases} A \to \dfrac{A_R}{k^2 - \kappa^2}, \qquad B \to \dfrac{B_R}{|\kappa|(k^2 - \kappa^2)} & (15a, b) \\ \nu \to \nu_R = |\kappa|\epsilon, \qquad \nu' \to \nu_R' = |\kappa|\epsilon' & (16a, b) \end{cases}$$

where A_R, B_R, ϵ, and ϵ' are frequency-independent constants given by

$$A_R = \frac{-2\kappa(2\kappa^2 - k_\beta^2)}{\mu(\partial F/\partial k)_{k=\kappa}}, \qquad B_R = \frac{\epsilon A_R}{1 - \frac{1}{2}(\gamma/\beta)^2} \tag{17a, b}$$

$$\epsilon = [1 - (\gamma/\alpha)^2]^{1/2}, \qquad \epsilon' = [1 - (\gamma/\beta)^2]^{1/2} \tag{18a, b}$$

We shall limit the subsequent, intermediate analysis to the dilatational potential ϕ; the corresponding results for the shear potential then can be established by analogy.

Inverting (12a) according to (8a, b) and noting that

$$\overline{p(r, t - t_0)} = e^{-i\omega t_0}\overline{p(r, t)} \tag{19}$$

we obtain

$$\bar{\phi}(r, z, \omega) = \int_0^{\infty} A(k, \omega)J_0(kr)e^{-\nu z}k dk \times \int_0^{\infty} e^{-i\omega t_0(\eta)}p(\eta, \omega)J_0(k\eta)\eta\,d\eta \tag{20}$$

Anticipating the asymptotic behavior of the Bessel functions, we find it convenient to rewrite this result in the form

$$\bar{\phi}(r, z, \omega) = r^{-1/2}\int_0^{\infty} \eta^{1/2}p(\eta, \omega)e^{-i\omega t_0(\eta)}\bar{g}(r, z, \omega;\ \eta)d\eta \tag{21}$$

$$\bar{g}(r, z, \omega;\ \eta) = (r\eta)^{1/2}\int_0^{\infty} A(k, \omega)J_0(kr)J_0(k\eta)e^{-\nu z}k\,dk \tag{22}$$

Inverting (21) with the aid of the convolution and shifting theorems, we then obtain

$$\phi(r, z, t) = r^{-1/2}\int_0^{\infty}\int_0^{\infty} \eta^{1/2}p(\eta, \tau)g[r, z, t - t_0(\eta) - \tau;\ \eta]d\eta\,d\tau \tag{23}$$

It appears impracticable, even by numerical procedures, to evaluate (21) and (23) without further approximation (compare the much simpler, point-load problem; see EJP, Sect. 2–7, for ref-

erences), and we shall proceed by first introducing asymptotic approximations for the Bessel functions and then investigating possible approximations to $p(r, \omega)$ and $t_0(r)$.

4 Asymptotic Approximation

Starting from the well-known approximation

$$J_0(x) \sim (2/\pi x)^{1/2} \cos (x - {}^1/_4\pi)[1 + O(x^{-1})], \qquad x \to \infty \quad (24)$$

we obtain directly

$$J_0(kr)J_0(k\eta) \sim (\pi k)^{-1}(r\eta)^{-1/2}[\cos [k(r - \eta)] + \sin [k(r + \eta)]] \quad (25)$$

Substituting this approximation in (22), we may place the result in the form

$$\bar{g}(r, z, \omega; \eta) = \bar{g}_-(r - \eta, z, \omega) + \bar{g}_+(r + \eta, z, \omega) \quad (26a)$$

$$\bar{g}_\mp(r, z, \omega) = \frac{1}{\pi} \int_0^\infty A(k, \omega)e^{-\nu z} \begin{matrix}\cos \\ \sin\end{matrix} (kr)dk \quad (26b)$$

Now it is intuitively clear that $\bar{g}_-$ comprises those disturbances that originate in the semicircle bisected by the radius from epicenter to the point of observation, whereas $\bar{g}_+$ comprises the antipodal disturbances, Fig. 2. If we were to admit a small absorption constant δ, the latter disturbances would be inferior to the former by a factor of order $\exp(-2\delta|k|r)$; accordingly, we shall neglect $\bar{g}_+$, even though it is of the same algebraic order within the hypotheses originally adopted for our model.[3]

We could obtain a less intuitive identification of the terms in our asymptotic approximation from the representation

$$J_0(kr)J_0(k\eta) = \frac{1}{2\pi} \int_{-\pi}^{\pi} J_0(kR)d\theta, \qquad R = (r^2 + \eta^2 - 2r\eta \cos \theta)^{1/2} \quad (27)$$

which exhibits the influence, at any point P on a circle of radius r, of all points Q on a circle of radius η, R being the distance between the first point and one of the latter points displaced azimuthally by the angle θ, Fig. 2. Approximating this integral by the method of stationary phase then establishes the allegations of the preceding paragraph (the points of stationary phase being 0 and π, respectively).

We may simplify $\bar{g}_-$ further by noting that A and ν are even functions of k; then, neglecting $\bar{g}_+$ in (26a) yields

$$\bar{g}(r, z, \omega; \eta) = \frac{1}{2\pi} \int_{-\infty}^{\infty} A(k, \omega)e^{-ik(r-\eta)-\nu z}dk \quad (28)$$

We remark that differentiations with respect to r and z may be conveniently carried out at this point. In keeping with the approximation (25), we may neglect the variation of the $r^{-1/2}$ factor in the r-differentiation, so that we may obtain $\bar{\phi}_r$ and $\bar{\phi}_z$ simply by inserting the respective factors $-ik$ and $-\nu$ in (28).

We now observe that the only vestiges of three-dimensionality in the approximation given by (21) and (28) appear implicitly through the prescription of $p(\eta, \tau)$ and explicitly through the factor $(\eta/r)^{1/2}$; a two-dimensional formulation (with r as a Cartesian co-ordinate) would yield identical results except for the absence of this factor. It follows that $g(r, z, t)$ constitutes the two-dimensional response to a unit-impulse, concentrated in both space ($r = 0$) and time ($t = 0$). This last problem has been studied extensively (see especially Sauter [4]; EJP, Sect. 2–3, gives other references), and explicit results have been obtained for the corresponding displacements. Numerical integration of (23), using these results, appears feasible, albeit lengthy, if only the Rayleigh-wave singularities be treated separately. It is doubtful that most applications would warrant the amount of work required, however, and we shall seek further simplifications.

Before discussing these further simplifications, we anticipate the possible consequences of the asymptotic approximations imposed in this section. We first observe that the representation (25) can be quantitatively accurate only if both kr and $k\eta$ are large, but it is qualitatively accurate except for rather small values of k, r, or η. The loss of accuracy for small r or η is likely to be trivial compared with the approximations already inherent in our model of an elastic medium for a strong explosion[4]; hence the principal deficiency of the asymptotic approximation is for small k. The final results imply integration over k (with a consequent reduction in error), however, and we may choose $k_\alpha = \omega/\alpha$ as an appropriate measure of k for the integrated result [if $U(r) \gg \alpha$, $k_0 = \omega/U$ would be a more significant measure, while $\kappa = \omega/\gamma$ would be preferable for the Rayleigh wave alone]. This, in turn, implies that our approximations may be deficient as $\omega \to 0$ and hence that g may be deficient as $\alpha[t - t_0(r)] \to \infty$. We conclude that the inequalities of (1) should be sufficient for quantitative validity of the asymptotic expansion and that these inequalities may not have to be very strong for qualitative validity.

5 Pressure Signature Approximations

The further simplification of the quasi-two-dimensional results represented by (23) in conjunction with equation (28) demands some more explicit statement as to the exact and/or approximate behavior of $p(r, t)$ and $t_0(r)$. We shall proceed by imposing (and defending) the approximations

$$\eta^{1/2}p(\eta, \omega) \doteqdot r^{1/2}p(r, \omega) \quad (29)$$

and

$$t_0(\eta) \doteqdot t_0(r) + t_0'(r)(\eta - r) + {}^1/_2t_0''(r)(\eta - r)^2 \quad (30)$$

The approximation (29) is suggested by G. I. Taylor's strong-shock theory [5], which yields the similarity expression

$$p(r, t) = r^{-2}f(r^{-1/2}t) \quad (31)$$

whence

$$r^{1/2}\bar{p}(r, \omega) = \bar{f}(\omega r^{3/2}) \quad (32)$$

Comparing (29) and (32), we conclude that the former approximates the frequency-scale in the spectral amplitude at all points (η) by that scale appropriate to the point of observation (r). This approximation evidently is least critical at low-frequencies,[5] but it breaks down at high frequencies; it also must break down for very large r, where p may be expected to exhibit the acoustic behavior $p(r, t) = r^{-2}f(t)$. Fortunately, either of these contingencies renders a stationary phase argument useful.

[3] We could strengthen the argument by noting that, for strong explosions, the most direct paths from the antipodal region must traverse the more highly absorbing neighborhood of the epicenter.

Fig. 2 The domains of $g_-(r - \eta)$ and $g_+(r + \eta)$; O is the epicenter and P the point of observation

[4] It might be thought that the asymptotic approximation could be seriously deficient as $\eta \to 0$ in consequence of the reduction (by $\eta^{1/2}$) of algebraic order, thereby overweighting the anticipated singularity in $\bar{p}(\eta, \omega)$. In fact, similarity considerations [see (32)] imply $\bar{p} = O(\eta^{-1/2})$ as $\eta \to 0$, so that the integrand of (21) remains bounded there despite the $\eta^{-1/2}$ singularity incorrectly imputed to $J_0(k\eta)$.

[5] A specific, representative example is $\bar{f}(\tau) = C \exp(-\alpha\tau)$, which yields $\bar{f}(\omega\tau^{3/2}) = C(\alpha + i\omega\tau^{3/2})^{-1}$.

The stationary phase argument (see Appendix for $U(r) > a$) leads to the conclusion that, provided $z \ll r$, the most important portion of the pressure signature is that for which $\eta \doteq r$ unless $U(r) < \gamma$; if $U(r) < \gamma$ the same conclusion holds for all components of the disturbance except the outwardly propagated Rayleigh wave, for which the neighborhood of $U(\eta) \doteq \gamma$ is the most important and for which (29) should be replaced by

$$(\eta/r)^{1/2}p(\eta, \omega) \doteq (\eta_R/r)^{1/2}p(\eta_R, \omega),\ U(\eta_R) = \gamma \quad (33)$$

Even in this instance, however, the approximation (29) is likely to be adequate.

Equation (30) approximates $t_0(\eta)$ by a parabola having the correct slope and curvature at $\eta = r$; which is to say that the blast-front is assigned both the correct velocity and acceleration directly above the point of observation. We may expect such an approximation to be entirely adequate at all points for which our model could be significant. In that region for which the blast-wave constitutes a strong shock Taylor's similarity theory [5] and the more accurate, real-gas theory of Brode [6] predict that $t_0(\eta)$ should be proportional to $\eta^{5/2}$ and $\eta^{21/8}$, respectively, either of which may be fitted very closely by a parabola at points reasonably removed from $\eta = 0$. At very great distances, on the other hand, the blast-front velocity tends to the (constant) velocity of sound, and the parabolic approximation is clearly satisfactory (the actual value of t_0'', in so far as it tends to zero, does not enter this limiting result). Finally, we observe that the approximation (30) arises naturally in the stationary phase argument, where $t_0(\eta)$ is approximated by a parabola through the point of stationary phase (see Appendix).

Invoking the approximations (29) and (30) in (21) and substituting (28) therein, we may place the results in the form

$$\bar{\phi}(r, z, \omega) = p(r, \omega)\bar{h}(r, z, \omega)e^{-i\omega t_0(r)} \quad (34)$$

$$\bar{h}(r, z, \omega) = \int_0^\infty \exp\left\{i\omega[t_0(r) - t_0(\eta)]\right\}\bar{g}(r, z, \omega;\ \eta)d\eta \quad (35a)$$

$$= \int_{-\infty}^{\infty} A(k, \omega)I(k, \omega, r)e^{-\nu z}dk \quad (35b)$$

$$I(k, \omega, r) = \frac{1}{2\pi}\int_0^\infty \exp\left\{-\tfrac{1}{2}i\omega t_0''(r)(\eta - r)^2 + i[k - \omega t_0'(r)](\eta - r)\right\}d\eta \quad (36)$$

We may evaluate the integral I, within the approximation already implied by the neglect of g_+ in Section 4, by replacing the lower limit of integration by $-\infty$; then, introducing the parameters

$$k_0 = \omega t_0'(r) = \omega/U(r), \qquad a = \tfrac{1}{2}[i\omega t_0''(r)]^{-1} \quad (37a, b)$$

we obtain

$$I \sim \frac{1}{2\pi}\int_{-\infty}^{\infty} \exp\left[-(4a)^{-1}(\eta - r)^2 + i(k - k_0)(\eta - r)\right]d\eta \quad (38a)$$

$$= (a/\pi)^{1/2}\exp\left[-a(k - k_0)^2\right] \quad (38b)$$

We add that $R|a > 0$ if (as assumed) $\operatorname{Im}\omega < 0$ and that

$$a = O(k_0^{-1}r),\ r \to \infty.$$

6 Stationary Phase Approximation

We consider now the evaluation of the integrals in (35a) on the basis of the assumptions

$$|ak_0^2| = \omega t_0'^2(r)/2t_0''(r) \gg 1 \quad \text{and} \quad z \ll r \quad (39a, b)$$

the first of which is equivalent to $k_0 r \gg 1$ (and therefore consistent with the asymptotic approximation of Section 4) if $t_0'' = O(r^{-1}t_0')$ and the second of which will be satisfied for points close to the surface. The assumption $|ak_0^2| \gg 1$ suggests a stationary phase approximation of the integral obtained by substituting (38b) in (35b); viz.,

$$\bar{h}(r, z, \omega) = \left(\frac{a}{\pi}\right)^{1/2}\int_{-\infty}^{\infty} A(k, \omega)\exp\left[-\nu z - a(k - k_0)^2\right]dk \quad (40)$$

while the assumption $z \ll r$ permits the neglect of the variation of νz compared with that of $a(k - k_0)^2$, thereby placing the point of stationary phase at $k = k_0$. The stationary phase approximation is not directly applicable to (40), however, in consequence of the Rayleigh-wave poles at $k = \pm\kappa$, and we therefore separate these poles out from (35b) by writing [see (15) and (16)]

$$\bar{h} = \bar{h}_R + \left(\frac{a}{\pi}\right)^{1/2}\int_{-\infty}^{\infty}\left[A(k, \omega)e^{-\nu z} - \frac{A_R e^{-\nu_R z}}{k^2 - \kappa^2}\right]\exp\left[-a(k - k_0)^2\right]dk \quad (41a)$$

$$\bar{h}_R = \frac{A_R e^{-\nu_R z}}{2\pi}\int_{-\infty}^{\infty}\int_{-\infty}^{\infty}(k^2 - \kappa^2)^{-1}\exp\left[-(4a)^{-1}(\eta - r)^2 + i(k - k_0)(\eta - r)\right]dk\,d\eta \quad (41b)$$

where I has been retained in the form of (38a), rather than (38b), in $\bar{h}_R$.

We may carry out the k-integration of (41b) by closing the path of integration in $\operatorname{Im}k \gtrless 0$ for $\eta \gtrless r$, thereby enclosing the poles at $k = \mp\kappa$, respectively, as shown in Fig. 3 (where $\operatorname{Im}\omega < 0$ implies $\operatorname{Im}\kappa < 0$). Invoking Cauchy's residue theorem, we then obtain

$$\bar{h}_R = \frac{a^{1/2}A_R e^{-\nu_R z}}{i\kappa}\left[e^{-a(\kappa + k_0)^2}\int_{ia^{1/2}(\kappa + k_0)}^{\infty\exp(i\pi/4)} e^{-x^2}dx + e^{-a(\kappa - k_0)^2}\int_{ia^{1/2}(\kappa - k_0)}^{\infty\exp(i\pi/4)} e^{-x^2}dx\right] \quad (42)$$

Now, within the approximations already imposed, we may replace the first of these two, complementary error integrals by its asymptotic approximation (which may be obtained by integration by parts)

$$\int_{x_1}^{\infty\exp(i\pi/4)} e^{-x^2}dx \sim \frac{e^{-x_1^2}}{2x_1}\left[1 + O(x_1^{-2})\right] \quad (43)$$

and (42) reduces to

$$\bar{h}_R \sim A_R e^{-\nu_R z}\left[\frac{-1}{2\kappa(\kappa + k_0)} + \frac{a^{1/2}e^{-a(\kappa - k_0)^2}}{i\kappa}\int_{ia^{1/2}(\kappa - k_0)}^{\infty\exp(i\pi/4)} e^{-x^2}dx\right] \quad (44)$$

Turning now to the integral of (41a), we may argue that the bracketed portion of the integrand is of bounded variation, while the oscillating factor $\exp\left[-a(k - k_0)^2\right]$ oscillates rapidly except in the neighborhood of $k = k_0$. Setting $k = k_0$ inside the brackets

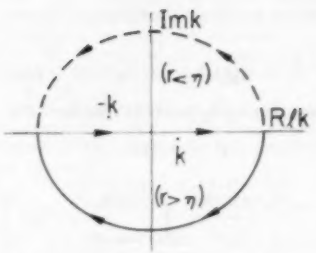

Fig. 3 Integration contours for (41b)

and carrying out the k-integration, we obtain the stationary phase approximation

$$\bar{h} \sim \bar{h}_R + A(k_0, \omega)e^{-\nu_0 z} - A_R(k_0^2 - \kappa^2)^{-1}e^{-\nu_R z} \quad (45)$$

where $\nu_0 = (k_0^2 - k_\alpha^2)^{1/2}$. Substituting $\bar{h}_R$ from (44), we have the end result

$$\bar{h} \sim A(k_0, \omega)e^{-\nu_0 z} + A_R e^{-\nu_R z}\left[\frac{1}{2\kappa(\kappa - k_0)} + \frac{a^{1/2}e^{-a(\kappa-k_0)^2}}{i\kappa}\int_{ia^{1/2}(\kappa-k_0)}^{\infty(i\pi/4)} e^{-x^2}dx\right] \quad (46)$$

If

$$R|[ia^{1/2}(\kappa - k_0)]| \gg 1$$

i.e., if $U(r)$ is larger than and not close to γ, the last integral may be approximated according to (43) and (46) reduces to

$$\bar{h} \sim A(k_0, \omega)e^{-\nu_0 z}, \qquad [\omega/t_0''(r)]^{1/2}[\gamma^{-1} - U^{-1}(r)] \gg 1 \quad (47)$$

a result we also could have obtained by a direct, stationary phase approximation of (40), as in the Appendix. We conclude that, within the approximations of (39), the pole at $k = -\kappa$, which represents a receding Rayleigh wave (i.e., a wave excited at points in $\eta > r$), has no effect on the stationary phase approximation, whereas the advancing Rayleigh wave associated with the pole at $k = \kappa$ may be important unless $U(r)$ is appreciably in excess of γ (which would imply that the blast-wave velocity could not have approximated the Rayleigh-wave speed in $\eta < r$); in the final analysis, however, we shall find that (47) also is valid if U is appreciably less than γ.

We obtain the error term for the approximation (46) by subtracting out from the integral of (41a) the value of the bracketed portion of the integrand at $k = k_0$, whence

$$\Delta = \left(\frac{a}{\pi}\right)^{1/2}\int_{-\infty}^{\infty}\left[A(k, \omega)e^{-\nu z} - A(k_0, \omega)e^{-\nu_0 z} + \frac{A_R(k^2 - k_0^2)e^{-\nu_R z}}{(k_0^2 - \kappa^2)(k^2 - \kappa^2)}\right]e^{-a(k-k_0)^2}dk \quad (48)$$

If k_0 is not too close to the branch points at k_α or k_β we may obtain the order of Δ by expanding the bracketed term in a power series about $k = k_0$; only the even terms contribute to the end result, and we obtain $\Delta = O(a^{-1}k_0^{-2})$, which is of the same order as terms already neglected. The radius of convergence of this power series is the smaller of $|k_0 - k_\alpha|$ or $|k_0 - k_\beta|$, however, and our estimate of Δ therefore is valid only if neither of these parameters is small compared with $|k_0|$; indeed, the critical term in the expansion yields

$$\Delta = O[a^{-1}|k_0^2 - k_\alpha^2|^{-1/2}|k_0^2 - k_\beta^2|^{-1/2}] \quad (49)$$

We could obtain a more general estimate of Δ by deforming the path of integration in the k-plane into paths along the branch cuts from $k = k_\alpha$ and $k = k_\beta$ (cf. EJP, Sect. 2–5) plus a path of steepest descent, but this would appear to be rather involved. If k_0 coincides with either k_α or k_β, however, we find

$$\Delta = O(a^{-1/4}k_0^{-1/2}), \qquad k_0 = k_\alpha \text{ or } k_\beta \quad (50)$$

which, for $t_0'' = O(r^{-1}t_0')$, is $O[(k_0r)^{-1/4}]$. This is of lower order than terms previously neglected, but even in this extreme case (46) gives the dominant term in the asymptotic approximation to $\bar{h}$ as $k_0r \to \infty$.

7 Calculation of Displacements

The calculation of the displacements from (2a, b) requires that we first calculate ψ, which we may obtain from the foregoing results simply by replacing A by B, ν by ν', and A_R by $|\kappa|^{-1}B_R$ [see (15b)]. The required r and z-differentiations then may be carried out according to the discussion following (28), and we may express the Fourier transforms of the displacements given by (2a, b) according to [cf. (34)]

$$\begin{matrix}\bar{q}\\ \bar{w}\end{matrix}(r, z, \omega) = p(r, \omega)\left[\begin{matrix}\bar{q}_1\\ \bar{w}_1\end{matrix}(r, z, \omega) + \begin{matrix}\bar{q}_2\\ \bar{w}_2\end{matrix}(r, z, \omega)\right]e^{-i\omega t_0(r)} \quad (51)$$

$$\begin{Bmatrix}\bar{q}_1\\ \bar{w}_1\end{Bmatrix} = \int_{-\infty}^{\infty}\begin{Bmatrix}-ik\\ -\nu\end{Bmatrix}A(k, \omega)I(k, \omega, r)e^{-\nu z}dk \quad (52a)$$

$$\begin{Bmatrix}\bar{q}_2\\ \bar{w}_2\end{Bmatrix} = \int_{-\infty}^{\infty}\begin{Bmatrix}ik\nu'\\ k^2\end{Bmatrix}B(k, \omega)I(k, \omega, r)e^{-\nu' z}dk \quad (52b)$$

We may invert $\bar{q}$ and $\bar{w}$, as given by (51), with the aid of the convolution theorem to obtain

$$\begin{matrix}q\\ w\end{matrix}(r, z, t) = \int_0^{\infty} p(r, \tau)\left\{\begin{matrix}q_1\\ w_1\end{matrix}[r, z, t - t_0(r) - \tau] + \begin{matrix}q_2\\ w_2\end{matrix}[r, z, t - t_0(r) - \tau]\right\}d\tau \quad (53)$$

We may obtain the stationary phase approximations to $\bar{q}_1, \ldots$ as in Section 6, and it follows by analogy that we need only multiply the first and second terms in (46) by the braced factors of (52a, b) with $k = k_0$ and κ, respectively. The end results are [see (16a, b) for ν_R and ν_R', with $|\kappa| = k \operatorname{sgn} \omega$]

$$\begin{Bmatrix}\bar{q}_1\\ \bar{w}_1\end{Bmatrix} = \begin{Bmatrix}-ik_0\\ -\nu_0\end{Bmatrix}A(k_0, \omega)e^{-\nu_0 z} + \begin{Bmatrix}1\\ -i\epsilon \operatorname{sgn} \omega\end{Bmatrix}A_R e^{-\nu_R' z}f(\kappa - k_0) \quad (54a)$$

$$\begin{Bmatrix}\bar{q}_2\\ \bar{w}_2\end{Bmatrix} = \begin{Bmatrix}ik_0\nu_0'\\ k_0^2\end{Bmatrix}B(k_0, \omega)e^{-\nu_0' z} + \begin{Bmatrix}-\epsilon'\\ i \operatorname{sgn} \omega\end{Bmatrix}B_R e^{-\nu_R' z}f(\kappa - k_0) \quad (54b)$$

$$f(k) = \frac{1}{2ik} - a^{1/2}e^{-ak^2}\int_{ia^{1/2}k}^{\infty \exp(i\pi/4)} e^{-x^2}dx \quad (55)$$

Now it may be established, by retracing the steps of our analysis, that the first terms on the right-hand side of (54a, b) are precisely the results for a two-dimensional unit impulse of pressure moving with the constant speed $U(r)$; their inverse transforms, as required in (53), are given in [2], and we therefore need consider further only the Rayleigh-wave terms. Designating the former by the superscript zero and inverting the latter according to (7b), we obtain

$$\begin{Bmatrix}q_1\\ w_1\end{Bmatrix} = \begin{Bmatrix}q_1^{(0)}\\ w_1^{(0)}\end{Bmatrix} + \frac{A_R}{2\pi}\int_{-\infty}^{\infty}\begin{Bmatrix}1\\ -i\epsilon \operatorname{sgn} \omega\end{Bmatrix}e^{i\omega t - |\omega|(\epsilon z/\gamma)} f\left[\omega\left(\frac{1}{\gamma} - \frac{1}{U}\right)\right]d\omega \quad (56)$$

and similarly for q_2 and w_2. We may write this result in the form

$$[q_1 - q_1^{(0)}] + i\epsilon^{-1}[w_1 - w_1^{(0)}] = A_R(\gamma^{-1} - U^{-1})^{-1}\chi[t + i(\epsilon z/\gamma)] \quad (58a)^{6}$$

where[7]

[6] Equation (57) has been deleted.

[7] The integral in (59) is improper, and only its finite part as the lower limit tends to 0 exp ($i\pi/2$) is to be retained. The subsequent analysis is, for this reason, heuristic.

$$\chi(\zeta) = \frac{1}{\pi}(\gamma^{-1} - U^{-1}) \int_0^\infty e^{i\omega\zeta} f\left[\omega\left(\frac{1}{\gamma} - \frac{1}{U}\right)\right] d\omega \quad (59)$$

Similarly,

$$\epsilon'^{-1}[q_2 - q_2^{(0)}] + i[w_2 - w_2^{(0)}] = -B_R(\gamma^{-1} - U^{-1})^{-1}\chi[t + i(\epsilon' z/\gamma)] \quad (58b)$$

It remains to evaluate χ. Substituting f in (59) from (55) and introducing the parameter

$$\theta = \theta(r) = [2t_0''(r)]^{-1/2}[\gamma^{-1} - U^{-1}(r)] \quad (60)$$

we obtain

$$\chi(\zeta) = \frac{1}{2\pi}\int_0^\infty \left[\frac{1}{i\omega} - \frac{2\theta e^{i\omega\theta^2}}{(i\omega)^{1/2}} \int_{(i\omega)^{1/2}\theta}^\infty e^{-x^2} dx\right] e^{i\omega\zeta} d\omega \quad (61)$$

The singularity at $\omega = 0$ renders this integral improper and leads to an arbitrary, additive constant in the end result, as anticipated in Section 1. We may determine the real part of this constant by integrating the singular term in the integrand of (56) for $q_1 - q_1^{(0)}$ along a path in Im $\omega < 0$ and requiring the result to agree with that given by (58a), but a similar integration for $w_1 - w_1^{(0)}$ is not possible because of the factor sign ω in the integrand.

Evaluating the integral of (61) in accord with the foregoing remarks, we obtain (see Appendix for details)

$$\chi(\zeta) = \frac{i}{2\pi}\left\langle (\log \zeta - i\pi) - \frac{\theta}{(\zeta + \theta^2)^{1/2}}\left\{\log\left[\frac{(\zeta + \theta^2)^{1/2} - \theta}{(\zeta + \theta^2)^{1/2} + \theta}\right] - i\pi\right\} + C\right\rangle \quad (62)$$

where C is a real constant, and the principal branch of the logarithm is implied (log $1 = 0$, $-\pi <$ arg log $\zeta \leq \pi$). We observe that

$$\chi \to (i/2\pi)\log(4\theta^2) + H(-\theta), \quad |\theta| \to \infty; \quad (63)$$

thus, since the displacements already contain arbitrary constants, we confirm the result (47).

A limiting case of special interest is $U(r) = \gamma$ or $\theta = 0$. The foregoing results are not convenient for a direct reduction, but, on substituting the result (62) in (58a, b) and then letting $U(r) \to \gamma$, we find that the contributions of the term $(i/2\pi)(\log \zeta - i\pi + C)$ in χ cancel the two-dimensional results within the approximations already imposed (the singular terms canceling exactly), while the remaining term in (62) yields

$$U(r) = \gamma \begin{cases} q_1 + i\epsilon^{-1}w_1 = -\frac{1}{2}A_R\left\{[2t_0''(r)][t + i(\epsilon z/\gamma)]\right\}^{-1/2} & (64a) \\ \epsilon'^{-1}q_2 + iw_2 = +\frac{1}{2}B_R\left\{[2t_0''(r)][t + i(\epsilon' z/\gamma)]\right\}^{-1/2} & (64b) \end{cases}$$

These last results tend to especially simple limits as $z \to 0+$, for then the phase of $\zeta^{-1/2}$ is 0 or $-\pi/2$ as $t > 0$ or $t < 0$, respectively, and substitution in (53) yields

$$q(r, z, t) = \frac{(-A_R + \epsilon' B_R)}{2[2t_0''(r)]^{1/2}} \int_0^t \frac{p(r, \tau)d\tau}{(t - \tau)^{1/2}} \quad (65a)$$

$$w(r, z, t) = \frac{(\epsilon A_R - B_R)}{2[2t_0''(r)]^{1/2}} \int_t^\infty \frac{p(r, \tau)d\tau}{(\tau - t)^{1/2}} \quad (65b)$$

for the free surface displacements at a point where the blast-front speed equals the Rayleigh-wave speed.

References

1 I. N. Sneddon, "Fourier Transforms," McGraw-Hill Book Company, Inc., New York, N. Y., 1951, pp. 447–449.

2 J. D. Cole and J. H. Huth, "Stresses Produced in a Half-Plane by Moving Loads," Journal of Applied Mechanics, vol. 25, Trans. ASME, vol. 80, 1958, pp. 433–436.

3 W. Ewing, W. Jardetzky, and F. Press, "Elastic Waves in Layered Media," McGraw-Hill Book Company, Inc., New York, N. Y., 1957, pp. 38–40.

4 F. Sauter, "Der elastiche Halbraum ber einer Mechanischen Beeinflussung seiner Oberflache (Zweidimensionales Problem)," *Zeitschrift für angewandte Mathematik and Mechanik*, vol. 30, 1950, pp. 203–215.

5 R. Courant and K. O. Friedrichs, "Supersonic Flow and Shock Waves," Interscience Publishers, Inc., New York, N. Y., 1948, p. 422.

6 H. L. Brode, "Point Source Explosion in Air," RAND Report RM-1824 AEC, Santa Monica, Calif., 1956.

7 E. T. Copson, "The Asymptotic Expansion of a Function Defined by a Definite Integral or Contour Integral," reference no. SRE/ACS 106, Department of Scientific Research and Experiment, The Admiralty, London, England, 1946, pp. 22–24.

8 G. A. Campbell and R. M. Foster, "Fourier Integrals for Practical Applications," Bell Telephone Monograph B-584, 1942.

APPENDIX

Direct Stationary Phase Approximation

We consider the double integral

$$\bar{\phi}(r, z, \omega) = \frac{r^{-1/2}}{2\pi}\int_0^\infty p(\eta, \omega)\eta^{1/2}d\eta \int_{-\infty}^\infty A(k, \omega) \exp[-i\omega t_0(\eta) - ik(r - \eta) - \nu z]dk \quad (66)$$

as obtained from (21) and (28). Introducing the transformations

$$k = \omega\xi = (\omega/\alpha)\sin\theta \quad (|\xi| < 1/\alpha) \quad (67a)$$

$$= \omega/c \quad (|\xi| > 1/\alpha) \quad (67b)$$

we may rewrite this integral in the form

$$\bar{\phi}(r, z, \omega) = \frac{\omega r^{-1/2}}{2\pi}\int_0^\infty p(\eta, \omega)\eta^{1/2}d\eta \times \left[\frac{1}{\alpha}\int_{-\pi/2}^{\pi/2} A\left(\frac{\omega}{\alpha}\sin\theta, \omega\right) e^{-i\omega T_a(t, \eta)}\cos\theta d\theta + \int_{-\alpha}^{\alpha} A\left(\frac{\omega}{c}, \omega\right) e^{-i\omega T_b(t, \eta) - \nu z}\frac{dc}{c^2}\right] \quad (68)$$

$$T_a = t_0(\eta) + \alpha^{-1}[(r - \eta)\sin\theta + z\cos\theta] \quad (69a)$$

$$T_b = t_0(\eta) + c^{-1}(r - \eta) \quad (69b)$$

We note that $c^{-2}\exp(-\nu z) \to 0$ as $c \to 0$, so that the integral is not singular there.

We may interpret the inverse transform of the first integral on the right-hand side of (68) as a packet of plane waves having normals inclined at the angle θ to be the z-axis and traveling at the constant speed α, Fig. 4, the individual wave excited by $p(\eta, \tau)$ arising at the point $(\eta, 0)$ at $t = t_0(\eta) + \tau$. Similarly, the second integral leads to a packet of radial surface waves moving with individual speed c and falling off exponentially with depth. We remark that the Rayleigh surface wave comprises those singular components of the latter packet that move with speed γ. The ray paths of typical plane and surface waves are sketched in Fig. 4.

We now seek a stationary phase approximation to $\bar{\phi}$ on the hypothesis $U(r) > \alpha$; we could extend the calculation to $U(r) < \alpha$ if $z \ll r$, but the method of Sections 5 and 6 then is more advantageous in handling the Rayleigh wave. We assume, in order to apply the stationary phase argument (see [7] for mathematical background), that ω is so large that T_a and T_b oscillate rapidly with respect to variations of both ξ and η; it is clear from dimensional considerations that the quantity relative to which ω must be large is $r^{-1}U(r)$, which is tantamount to the approxima-

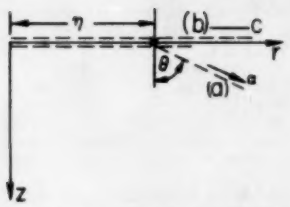

Fig. 4 Ray paths for plane waves (a) and surface waves (b)

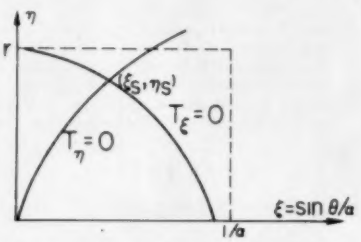

Fig. 5 Determination of point of stationary phase

tion already adopted in Section 4 (but we do not imply that the order of the approximations with respect to $k_0 r$ is necessarily the same).

The point of stationary phase, say (ξ_s, η_s), is determined by

$$T_\xi = T_\eta = 0 \ (\xi = \xi_s, \eta = \eta_s) \tag{70}$$

We find, on the hypothesis $U(r) > \alpha$, that only the first integral on the right-hand side of (68) has such a point; viz.,

$$\xi_s = \alpha^{-1} \sin \theta_s = t_0'(\eta_s) = 1/U_s \tag{71a}$$

$$\eta_s = r - z \tan \theta_s \tag{71b}$$

Expanding T_s about this point, introducing $x = \xi - \xi_s$ and $y = \eta - \eta_s$, and invoking the arguments that $\eta^{1/2}p$ and A vary only slowly compared with the exponential and that the range of integration may be extended over all x and y, we obtain

$$\bar{\phi} \sim \frac{\omega}{2\pi}\left(\frac{\eta_s}{r}\right)^{1/2} p(\eta_s, \omega) A\left(\frac{\omega}{U_s}\right) e^{i\omega T_s} \times \int_{-\infty}^{\infty}\int_{-\infty}^{\infty} \exp\left\{-\frac{i\omega}{2}\left[(T_{\xi\xi})_s x^2 + 2(T_{\xi\eta})_s xy + (T_{\eta\eta})_s y^2\right]\right\} dx\, dy \tag{72a}$$

$$= (\eta_s/r)^{1/2}[(T_{\xi\eta})_s^2 - (T_{\xi\xi})_s (T_{\eta\eta})_s]^{-1/2} \times A\left(\frac{\omega}{U_s}, \omega\right) p(\eta_s, \omega) e^{-i\omega T_s} \tag{72b}$$

where $T = T_s$, and the subscript s implies evaluation at $\xi = \xi_s$ and $\eta = \eta_s$; in particular,

$$T_s = t_0(\eta_s) + \alpha^{-1} R_s, \qquad R_s = [(r - \eta_s)^2 + z^2]^{1/2} \tag{73a, b}$$

Evaluating the second derivatives from (69a), we obtain

$$\bar{\phi} \sim \left[\frac{1 - (z/r)\tan\theta_s}{1 + \alpha z t_0''(\eta_s) \sec^3 \theta_s}\right]^{1/2} A\left(\frac{\omega}{U_s}, \omega\right) p(\eta_s, \omega) e^{i\omega T_s} \tag{74}$$

The curves defined by (70) are sketched in Fig. 5 assuming $t_0'(0) = 0$ and $t_0''(\eta) > 0$. We remark that the point of stationary phase given by (71a, b) exists for either $U(r) > \alpha$ or $U(r) < \alpha$, but in the latter case the second integral also has a point of stationary phase that provides the dominant contribution to the result if $z \ll r$. We also remark that if $U(r) > \alpha$ and $z \ll r$, $\eta_s \doteq r$ and (74) reduces to

$$\bar{\phi} \sim A(k_0, \omega) p(r, \omega) e^{i\omega t_0(r)}, \qquad z \ll r \tag{75}$$

in agreement with the results of Section 6 [since $U(r) > \alpha$ implies that $U(r)$ cannot be close to γ].

Evaluation of $\chi(\zeta)$

We require the integrals

$$\chi_1(\zeta) = \frac{1}{2\pi}\int_0^\infty \frac{e^{i\omega\zeta}}{i\omega}\, d\omega \tag{76}$$

$$\chi_2(\zeta) = \frac{-\theta}{\pi}\int_0^\infty (i\omega)^{-1/2} \exp\left[i\omega(\theta^2 + \zeta)\right] d\omega \int_{(i\omega)^{1/2}\theta}^\infty e^{-x^2} dx \tag{77}$$

where $\chi = \chi_1 + \chi_2$, as defined by (61).

To evaluate χ_1, we revert to (56), from which χ was derived. Comparing the contributions of the singular term in $f(k)$—viz., $(ik)^{-1}$—to (56) and (58a), we obtain

$$Rl\chi_1 = \frac{1}{4\pi}\int_{-\infty}^\infty e^{i\omega t - |\omega|(ez/\gamma)} \frac{d\omega}{i\omega} \tag{78a}$$

$$= \frac{1}{4\pi}\int_{-\infty}^\infty \left\{\frac{1}{i\omega} + \left[\frac{e^{-|\omega|(ez/\gamma)} - 1}{i\omega}\right]\right\} e^{i\omega t} d\omega \tag{78b}$$

where the path of integration lies in $\mathrm{Im}\ \omega < 0$. Carrying out the integration with the aid of a table of Fourier integrals [8], we obtain

$$Rl\chi_1(\zeta) = {}^1\!/_2 H(t) - \frac{1}{2\pi}\tan^{-1}(ez/\gamma t) \tag{79}$$

where $H(t)$ denotes Heaviside's step function, and $-\pi/2 < \tan^{-1}(ez/\gamma t) < \pi/2$. That function whose real part is given by (79) is

$$\chi_1(\zeta) = \frac{i}{2\pi}(\log \zeta - i\pi + C) \tag{80}$$

where C is any real constant.

Turning to χ_2, we introduce the change of variable $x = (i\omega)^{1/2} y$ and reverse the order of integration to obtain

$$\chi_2(\zeta) = -\frac{\theta}{\pi}\int_\theta^\infty dy \int_0^\infty \exp\left[i\omega(\zeta + \theta^2 - y^2)\right] d\omega \tag{81a}$$

$$= \frac{\theta}{i\pi}\int_\theta^\infty \frac{dy}{\zeta + \theta^2 - y^2} \tag{81b}$$

$$= -\frac{i\theta}{2\pi(\zeta + \theta^2)^{1/2}}\left\{\log\left[\frac{(\zeta + \theta^2)^{1/2} - \theta}{(\zeta + \theta^2)^{1/2} + \theta}\right] - i\pi\right\} \tag{81c}$$

where $Rl(\zeta + \theta^2)^{1/2} > 0$, and where we have invoked the requirement $\mathrm{Im}\ \zeta \geq 0$ in determining the phase of the logarithm.

Finally, we obtain (62) by adding χ_1 and χ_2.

WERNER GOLDSMITH
Professor of Engineering Mechanics,
University of California,
Berkeley, Calif.
Mem. ASME

PETER T. LYMAN
Associate in
Mechanics and Design,
University of California,
Berkeley, Calif.
Assoc. Mem. ASME

The Penetration of Hard-Steel Spheres Into Plane Metal Surfaces[1]

An experimental investigation was undertaken to determine the force-indentation relations governing the contact of hard-steel balls and plane surfaces of various metals both under static and dynamic conditions, the latter involving the Hopkinson-bar technique, with maximum elastic strain rates of 500 sec^{-1}. Excellent correlation was obtained between the measured permanent crater diameter at the contact point and that calculated from strain-gage data by means of an equation treating the bar as a one-dimensional member. A comparison also was effected between the static and dynamic force-indentation curves, the Hertz law of contact, and a relation based upon the concept of a constant flow pressure in the plastic regime.

Introduction

During the past decade, increasing attention has been focused on the problems attendant to the collision of a projectile and a target in the velocity regime where penetration of the striker is shallow and, while considerable plastic deformation at the point of contact exists, pulverization and shattering of both striker and target material are absent. For simple collision geometries, a mathematical analysis of such phenomena is feasible [1–7][2] provided a suitable relation, applicable under dynamic conditions, is stipulated which expresses the contact force between the two bodies as a function of the relative indentation. Such a relation provides the analog for an ordinary stress-strain curve of the two materials and constitutes the "equation of state" for the process. As a matter of convenience, almost all of the configurations treated consisted of the impact of two spheres or the collision of a sphere with a rod, beam, or plate. In the past, the majority of theoretical investigations concerned with such collision problems have postulated the existence of a completely elastic process at the contact point. Consequently, these derivations have utilized the well-known Hertz law of contact as the relevant equation of state, given by [8]

$$F = k_2\alpha^{3/2} \tag{1}$$

where F is the force of compression between the bodies, k_2 a constant dependent upon the contact geometry and the elastic properties of the bodies, and α the relative indentation. This procedure has been adopted even though some questions have been raised concerning the validity of equation (1) under dynamic, albeit elastic conditions. Furthermore, it has been demonstrated [9] that impacts at extremely low initial relative velocities involving materials with the highest possible surface hardness generate a permanent deformation at the contact point. The formation of such a crater, then, cannot logically be described by a relation based on a completely reversible, elastic process, derived only for equilibrium conditions, in spite of the fact that the use of the Hertz law in many impact problems has been surprisingly successful in correlating theoretical predictions with corresponding experimental results. Plastic static force-indentation relations for spheres in contact with plane surfaces have been determined experimentally by numerous investigators; the results of such tests have been summarized in [10]. The most universal and widely used equation determined from these experiments is the Meyer law [11], expressed as

$$F = k\alpha^n \tag{2}$$

with k and n as empirical constants. Equation (2) bears a close resemblance to the elastic Hertz law; it has furthermore been suggested [12, 13] that the Meyer law be applied to dynamic conditions involving plastic deformations at the contact point in a similar manner to the use of the Hertz relation for the corresponding elastic case.

For relatively shallow indentations, $\alpha \ll R$ where R is the radius of the indenting sphere, a special form of equation (2) is obtained by setting the constant n in equation (2) equal to unity. This form of the equation provides a fair correlation with test results derived from the static indentation of a hard-steel sphere into a number of metals, and corresponds to a condition of constant flow pressure p_0, since

$$F = p_0\pi a^2 \approx 2Rp_0\pi\alpha \text{ as } a^2 = 2R\alpha - \alpha^2 \approx 2R\alpha \tag{3}$$

where a is the radius of the boundary of the indentation.

The supposition of a constant pressure was utilized by Andrews [14, 15] in the construction of a theory of the collision of soft-metal spheres which encompassed three regimes; an initial elastic phase governed by equation (1), a further plastic deformation involving a central region deforming under a constant flow pressure p_0 and surrounded by an elastic annulus, and finally a restitution domain where the plastic zone recovered elastically. While the analysis is based on a number of postulates which have been subjected to criticism [10], satisfactory agreement was obtained between its predictions and experimental measurements derived from the impact of soft spheres at low velocities (maximum about 25 ips).

Equation (3) has been used by Crook [16] in a comparison with experimental results of the impact of crossed cylinders coupled with an elastic return described by equation (1), where now, however, the term α is replaced by the quantity $\alpha - \alpha_r$ where α_r represents the final value of the approach under no contact force. The theory so derived is also based on some questionable as-

[1] Work supported by U. S. National Science Foundation.

[2] Numbers in brackets designate References at end of paper.

Contributed by the Applied Mechanics Division and presented at the Winter Annual Meeting, New York, N. Y., November 27–December 2, 1960, of The American Society of Mechanical Engineers.

Discussion of this paper should be addressed to the Secretary, ASME, 29 West 39th Street, New York, N. Y., and will be accepted until January 10, 1961, for publication at a later date. Discussion received after the closing date will be returned.

Manuscript received by ASME Applied Mechanics Division, January 5, 1960. Paper No. 60—WA-15.

sumptions, but correlates very well with the data in the velocity range investigated (below 25 ips relative initial velocity). In still another investigation, an attempt to deduce a dynamic plastic force-indentation relation was made by measuring the height of fall and rebound of steel spheres striking a massive steel plate, and observing the permanent crater depth. With a number of assumptions, these data were then fitted to the Meyer law, equation (2), and the two types of assumed recovery processes; a restitution according to the modified form of Hertz's law, as described previously, and recovery as a linear spring [7]. The application of this method to mild-steel blocks did not indicate a completely constant flow pressure, although nearly so, and furthermore, provided no better prediction of the transverse impact process of a sphere against a simply supported beam than did the use of equation (1). However, the plastic dynamic force-indentation relation so derived, as well as the corresponding results obtained by Crook [16] and Tabor [10], indicated that a considerably greater force was required to produce the same permanent indentation under dynamic than under quasi-static conditions. This feature was partially attributed to the inertial effects present during the removal of the material from the crater and, speculatively, to the effects of strain rate.

It is thus evident that the question of a suitable dynamic plastic force-indentation relation for use in analyses involving impact problems has not been settled satisfactorily. While the excellent correlation obtained with the Hertz law may be rationalized in a velocity regime where elastic effects predominate over permanent deformation, its apparently satisfactory extrapolation into the realm of the formation of sizable permanent craters is puzzling. The concept of a constant flow pressure in the plastic regime appears to be only an approximation and does not appear too reasonable for materials exhibiting pronounced strain-hardening in the plastic portion of their stress-strain curves. Experimental evidence on this question is available only for crossed cylinders and, while apparently supporting the premise of a constant flow pressure [16], has been obtained only in the low-velocity region below 25 ips. Furthermore, such data have been obtained only from records in which the initial portion of the pulse was lost. The present investigation was designed to shed some further light on the question of the proper description of the material behavior to be applied to the theoretical analysis of impact processes involving spherical indenters.

Specificially, force-indentation relations were determined both under static and dynamic conditions for the relatively shallow penetration of $^1/_2$-in-diam steel ball bearings with a surface hardness of 67 Rockwell C into plane surfaces of various metals. In all instances, a substantial crater was produced at the contact point, but the maximum diameter of such indentations was limited to about one half the ball diameter. The target surfaces investigated were a tool steel, both in an annealed and a quench-hardened state, 2024-T4 aluminum, 1100-F aluminum, and extruded lead. The dynamic tests were performed by the Hopkinson-bar technique with impact velocities ranging from 25 to 300 fps, resulting in maximum elastic strain rates of about 500 sec^{-1}. The force-indentation relations obtained statically and dynamically were compared with each other and with the predictions of both the Hertz theory, equation (1), and the postulate of a constant flow pressure. Unfortunately, the results could not be compared directly with the data obtained by Crook [16] in view of the differences in the materials, collision geometry, and velocity range employed.

Apparatus and Instrumentation

The basic apparatus has been described in a previous paper [20]. Briefly, the tests were conducted with the aid of a $^1/_2$-in-diam Hopkinson bar, with an initial length of 30–36 in. clamped at one end, against which a $^1/_2$-in-diam steel sphere was fired by means of an air gun. The Hopkinson-bar technique of dynamic-force measurement has been used frequently in the past for the experimental investigation of wave phenomena in bars [16–20]. The initial and rebound velocities of the ball were obtained by means of a stroboscopic camera to an over-all accuracy of about 0.5 per cent. Strain-time records in the bar were obtained at a single station located from 2 to 8 in. from the impact point and sufficiently far removed from the clamp to avoid the return of reflected pulses on the records. Two resistance-foil gages were cemented to the bar at opposite ends of a diameter and connected so as to cancel antisymmetrical components of the pulse [20]. The gages were connected through a potentiometric circuit to a cathode-ray oscilloscope with a band pass from 1-$^1/_2$ cycles to 1 megacycle. The records so photographed were estimated to have an accuracy of ± 1 per cent.

Each trace was initiated by the grounding of a foil trigger, placed in front of the bars, by the passage of the ball. The force scale for each record was individually calibrated at the time of the test by using a shunt resistance on the gage circuit. After the completion of each shot, a portion of the bar at the impact end was cut off for measurement of the crater depth and the end of the bar was resurfaced for the next shot.

The craters were measured by a profilometer consisting primarily of a linear displacement transducer having an inherent accuracy of ± 1 per cent over the range of 0 to 0.040 in. Permanent deformation of the steel spheres, which occurred when using very hard targets, was measured with a supermicrometer.

Data Analysis

The technique of dynamic measurement described in the previous section consists essentially of the determination of force-time curves in a plane-ended Hopkinson bar consisting of the material to be studied. Fig. 1 shows the reproduction of a set of original oscillographic strain-time records for 2024-T4 aluminum, which are typical of all the recorded data when the gages were not subjected to a permanent set.

The conversion of the data to an experimental force-indentation relation was effected by means of the equation

$$\alpha = v_0 t - \frac{1}{\rho A c}\int_0^t F\,dt - \frac{1}{m}\int_0^t dt \int_0^t F\,dt \qquad (4)$$

which is based on a one-dimensional equation of motion of the bar. Here ρ, A, and c are the density, cross-sectional area, and

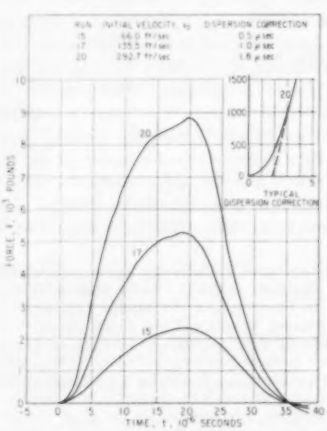
RUN INITIAL VELOCITY, v_0 DISPERSION CORRECTION
15 64.0 ft/sec 0.5 μ sec
17 135.5 ft/sec 1.0 μ sec
20 292.7 ft/sec 1.6 μ sec
FORCE, F, 10^3 POUNDS
TIME, t, 10^{-6} SECONDS
TYPICAL DISPERSION CORRECTION

Fig. 1 Typical force-time record. Material: 2024-T4, $^1/_2$-in-diam specimen.

"bar velocity" of the rod, respectively, m is the mass of the striking sphere, v_0 its initial velocity, and t is time. This relation, which can be applied stepwise over small time increments of the contact period, was originally suggested by Sears [4] and has been employed subsequently by numerous other investigators concerned with similar problems, including Crook [16]. Equation (4) neglects the vibrations of the striking sphere, a supposition the theoretical validity of which has been demonstrated by Rayleigh [21].

The use of equation (4) for the reduction of the data neglects, however, certain important approximations inherent in the relation. Since the force-time relation at the point of contact rather than at the measuring station is to be determined, direct application of equation (4) presumes that the pulse propagates along the bar without any change of shape whatsoever. However, it has been demonstrated repeatedly [18, 19, 22, 23, 24] that geometrical dispersion of a pulse prevails in any bar of finite diameter, the degree of such dispersion depending upon the ratio of pulse length to bar diameter, even if it is assumed that the internal friction of the material can be neglected completely. A previous investigation has indicated [24] that the major features of the pulse can be retained provided the ratio of pulse length to bar diameter is about 8 or greater; in the present series of tests this ratio was at least 10. An additional dispersive mechanism is represented by the character of the source. The pulse produced in the bar by the striking sphere is generated initially at a point; the source subsequently spreads across a portion of the area of the bar, but is never completely uniformly distributed over the entire cross section of the rod. Consequently, the initial shape of the pulse is a spherical dilatation wave, which is reflected from the lateral boundaries of the bar in such a manner as to produce a reasonably uniform stress across the entire section one or two diameters away from the contact point [20].

Both the initial spherical dilatation and the three-dimensional characteristics of the bar contribute to the dispersion experienced by the pulse. For pulses of sufficient length detected at stations removed several bar diameters from the contact point in materials with low internal damping, this dispersion is primarily manifested by a rounding of the initial and terminal slopes of the pulse, while the central, high-amplitude portion of the wave is relatively unaffected. The reason for this feature is the fact that the predominant high-energy groups travel at a rate indistinguishable from the rod velocity. This has been verified by a number of measurements of successive reflections of a single pulse produced in a freely suspended $^1/_2$-in-diam steel rod, 30 in. in length, where the peak amplitude decreased only about 5 per cent after more than 10 reflections. Only low-energy, high-frequency components can propagate at rates substantially different from the bar velocity.

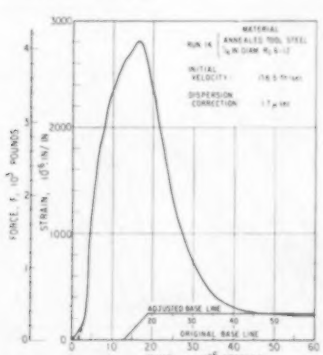

Fig. 2 Typical correction for impulse record displaying permanent plastic set of gage

When only the first mode of symmetric propagation in a three-dimensional bar is considered, the phase velocity of all high-frequency components is lower than the bar velocity which explains the dispersive features observed in the actual pulse at the tail end. The rounding at the initial rising portion of the wave is due, in part, to higher modes of the symmetric propagation; the existence of this feature has been demonstrated analytically by Skalak [25] and Curtis [23]. Alternately, this characteristic may also be produced by the initial spherical dilatation or higher antisymmetric propagation modes measured due to incomplete cancellation of this feature by the strain gages. Since complete centrality of the actual impact was difficult to achieve, and some slight curvature of the bar could not be eliminated, antisymmetrical components were, of course, present in the actual system. The elimination of the major portion of the antisymmetrical components was, of course, achieved by the coupled strain-gage transducer; but there is a possibility that the higher-frequency components observed at a given gage station arrived at slightly different times on the two sides of the bar, which might account for the presence of such components in the records.

The precise delineation of the force-indentation relation was found to be extremely sensitive to the exact location of the start of the pulse in the records such as shown in Fig. 1. Since the use of equation (4) in the reduction of the data assumes no change of shape of the pulse in its propagation from the contact point to the measuring station, serious errors are incurred in the position of the force-indentation curve relative to the indentation axis unless the dispersive characteristics are taken into account. If the pulse were applied uniformly across the entire impact end of the bar, the three-dimensional dispersive characteristics of the rod might conceivably be taken into account by synthesizing the measured pulse into harmonics of the various modes of longitudinal transmission and referring each component back to the contact point by means of the known dispersion diagram for a circular bar [26, 27].

In view of the actual initial spherical dilatation, however, even this tenuous process cannot be applied. Instead, the steeply rising portion of each pulse was extrapolated back to the base line in the manner shown in Fig. 1. This procedure provided close correspondence between the values of the calculated and measured terminal crater depth for virtually all test results (the only exception being four high-velocity runs where an additional correction, described later, was necessitated because of the existence of a permanent set of the strain gages), a situation which lends additional confidence in the acceptability of this correction. The loss of pulse area incurred by this process was found to have a negligible effect on the shape of the force-indentation relations; the procedure indicated just amounted to a translation of the calculated force-time relations to provide a much closer agreement of the calculated and measured terminal crater depths. Strictly speaking, a similar correction should have been applied at the tail of the pulse (and was, in some instances), but such corrections in this region of the pulse produced only very slight variations in the position of the force-indentation relations and, for the most part, could be neglected. It should be mentioned that, in almost all cases, the impulse determined from the wave shape checked the measured change of momentum of the ball within experimental error, about ± 2 per cent.

In some instances, particularly for very soft metals such as lead, the strain gages were subjected to a permanent set, such as illustrated in Fig. 2. It was then necessary to adjust the base line in accordance with the time span of the occurrence of this set on the record, which usually could be determined by inspection. This adjustment is indicated in the diagram.

With the foregoing modifications, the experimental data were converted into dynamic force-indentation relations whose general pattern now provided some very distinctive trends.

Table 1 Properties of materials tested

Target material	Modulus of elasticity 10^6 psi	Proportional limit, psi	Ultimate strength, psi	Poisson's ratio, μ	Rockwell hardness	Average alloy content, per cent				
						C	Mn	Cr	W	V
Tool steel, quench-hardened, 1/2-in-diam specimen	29.6	136000	180500	0.286	60–64 C	0.90	1.20	0.50	0.50	0.20
Tool steel, partially annealed, 1/2-in-diam specimen	29.6	...	...	0.286	17–32 C	0.90	1.20	0.50	0.50	0.20
Tool steel, fully annealed, 1/4-in-diam specimen	29.6	30000	95000	0.286	6–12 C	0.90	1.20	0.50	0.50	0.20
Aluminum, 2024-T4, 1/2-in-diam specimen	10.6	53000	69200	0.33	74 B	Cu 4.5	Mn 0.60	Mg 1.5		
Aluminum, 1100-F, 1/2-in-diam specimen	10.6	12000	19200	0.33	24 B	Commercially pure				
Lead, extruded, 1/2-in-diam specimen	3.43	...	...	0.45	...	Commercially pure				

Results

The static stress-strain diagrams for four of the materials tested are presented in Fig. 3, and the measured mechanical properties of all target materials investigated, whose values were subsequently employed in the reduction of the data, are listed in Table 1. The modulus of elasticity E for aluminum and steel as calculated from the slope of their respective stress-strain curves checked the value determined from wave-velocity measurements according to the relation $E = \rho c^2$ within 0.5 per cent. A stress-strain curve could not be obtained for lead but the modulus computed from wave measurements, while somewhat higher than published data for this material, provided a close agreement between the impulse produced in the bar and the measured change in momentum.

The static force-indentation curves were obtained from measurements of the slow compression of two 1/2-in-diam blocks, each 3/8 in. long and separated by the 1/2-in-diam steel sphere, in a standard universal test machine. The results represent the depth of the crater relative to the position of the edge of the loaded surface of each block under the applied force, so as to be completely comparable to the corresponding dynamic results. The dynamic force-indentation relations were computed from the Hopkinson-bar test results by the method described in the preceding section. Table 2 provides a summary of both the static and dynamic test results.

The static and the adjusted dynamic force-indentation relations have been plotted in Figs. 4–9 for the six rods investigated. The predictions of the Hertz law, equation (1), using the properties listed in Table 1, are also shown in each diagram. Fig. 10 presents a summary of the approach and recovery curves for all the materials; the compression process for any one substance, except for 2024-T4 aluminum, is represented by a single line denoting the mean value of the response of the material for the entire range of initial velocities used in the tests.

An additional analysis of the restitution process was ac-

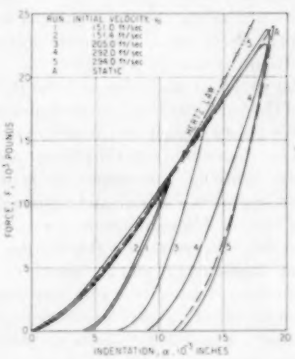

Fig. 4 Static and dynamic force-indentation curves for quench-hardened tool steel, R_c 60-64. Indenter: 1/2-in-diam hard-steel sphere.

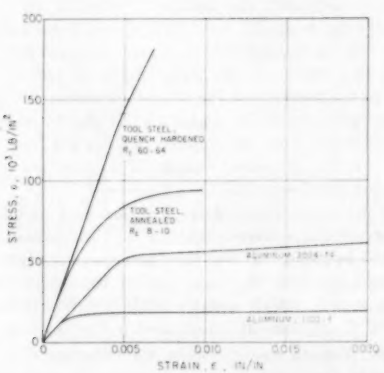

Fig. 3 Static stress-strain curves for test materials

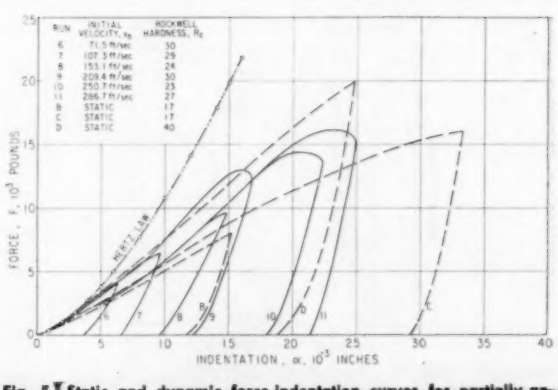

Fig. 5 Static and dynamic force-indentation curves for partially annealed tool steel. Indenter: 1/2-in-diam hard-steel sphere.

complished by plotting the function $\log_{10}(\alpha - \alpha_r)$ against the logarithm of the force for the range beyond the maximum indentation generated. Since very small changes in the calculated value of the permanent indentation produce very large changes in the character of such curves, the results of this analysis were not too satisfactory. Fig. 11 shows a diagram of such a curve for the various tests on hard steel; this figure is the most uniform of the entire sequence of tests. The slope of the Hertz curve, 3/2, is shown for comparison. It may be noted that all tests for this material, both static and dynamic, indicate a nearly linear relationship between the parameters plotted, with a slope close to that predicted by the modified form of equation (1), though slightly higher. For other materials, however, the corresponding restitution plots are not uniform straight lines, but curves with slopes ranging from 1 to about 3, although the average value would also be somewhat in excess of the predictions of a Hertzian restitution.

Discussion

A comparison of the location of the static and dynamic force-indentation curves presented in Figs. 3 to 9 indicated a virtual coincidence for quench-hardened tool steel, while a greater force, in varying degrees, appears to be required to produce the same indentation under dynamic conditions for the other materials. The maximum difference between the two sets of data is, however,

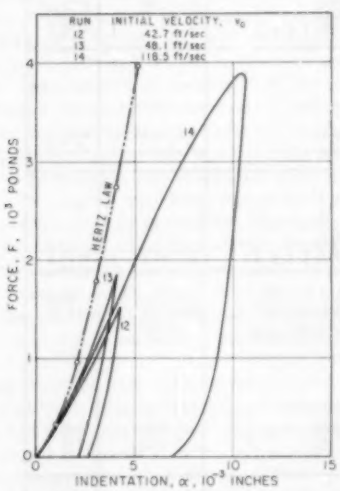

Fig. 6 Dynamic force-indentation curves for annealed tool steel. 1/2-in-diam specimen. Indenter: 1/2-in-diam hard-steel sphere.

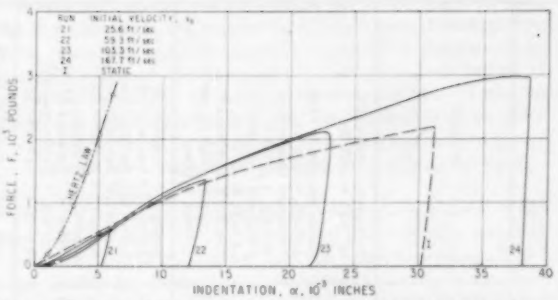

Fig. 8 Static and dynamic force-indentation curves for 1100-F aluminum. Indenter: 1/2-in-diam hard-steel sphere.

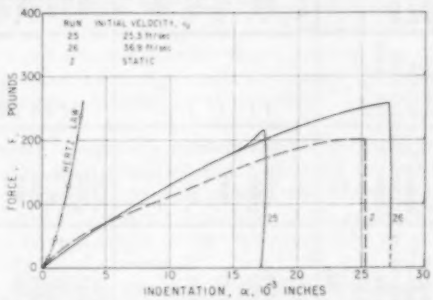

Fig. 9 Static and dynamic force-indentation curves for extruded lead. Indenter: 1/2-in-diam hard-steel sphere.

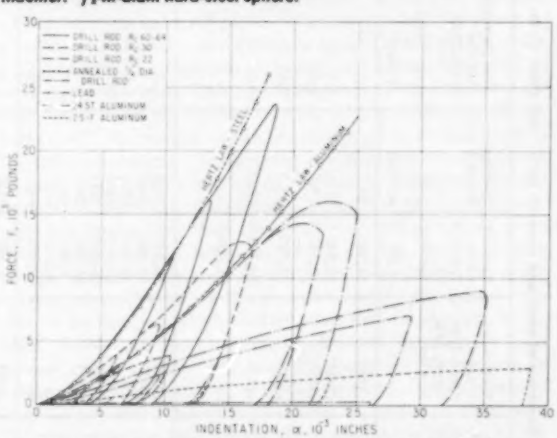

Fig. 10 Dynamic force-indentation curves for various metals under impact of a 1/2-in-diam hard-steel sphere

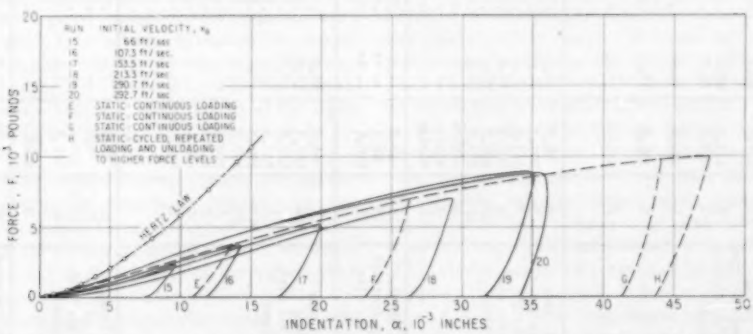

Fig. 7 Static and dynamic force-indentation curves for 2024-T4 aluminum. Indenter: 1/2-in-diam hard-steel sphere.

Table 2 Summary of static and dynamic tests. Ball diam 1/2 in. Material: Hardened steel, 67 Rockwell C.

Target Material	Run No.	Initial Velocity v_o ft/sec	Rebound Velocity v_f ft/sec	Measured Change of Momentum of ball Δmv lb-sec	Area under Original Force-Time Curve, $\int F dt$ Impulse lb-sec	Maximum Force Produced in Specimen lbs	Original Pulse Length microsec	Time Correction for Dispersion microsec	Maximum Approach Calculated after Adjustment in.	Permanent Approach Calculated after Adjustment α_r in.	Measured Maximum Approach for Static Tests in.	Measured Permanent Approach α_r in.	Comments
Tool Steel, Quench-Hardened 1/2 in. diam. specimen	1	151.0	63.7	.1228	.1263	11,850	20.5	0.4	.0109	.0044	—	.0045	Permanent compression of ball = .002 in.
	2	151.4	67.1	.1250	.1288	11,880	21.0	1.4	.0109	.0038	—	.0044	—
	3	205.0	84.8	.1653	.1659	16,310	19.6	1.08	.0135	.0067	—	.0065	Permanent compression of ball = .003 4 in.
	4	292.0	92.5	.2199	.2312	22,510	19.3	0.44	.0185	.0091	—	.0092	Permanent compression of ball = .0046 in.
	5	294.0	93.0	.2210	.2174	23,700	17.0	0.0	.0187	.0118	—	.0118	Permanent compression of ball = .0044 in.
	A	static	—	—	—	24,000	—	—	—	—	.0190	.0112	Permanent compression of ball = .0046 in. on each contact surface
Tool Steel, Partially Annealed 1/2 in. diam. specimen	6	71.5	26.8	.0563	.0570	4,130	26.0	1.8	.0064	.0038	—	.0038	Rockwell C Hardness 30
	7	107.3	34.6	.0812	.0817	6,360	24.0	2.3	.0097	.0067	—	.0067	Rockwell C Hardness 29
	8	153.1	42.4	.1119	.1208	9,600	26.0	2.4	.0148	.0096	—	.0090	Rockwell C Hardness 24
	9	209.4	52.3	.1500	.1519	12,890	23.5	3.3	.0168	.0123	—	.0125	Rockwell C Hardness 30
	10	250.7	50.2	.1722	.1745	14,280	25.3	3.5	.0224	.0182	—	.0175	Rockwell C Hardness 23
	11	286.7	48.4	.1928	.1945	16,000	24.0	3.0	.0250	.0219	—	.0213	Rockwell C Hardness 22
	B	static	—	—	—	8,000	—	—	—	—	.0152	.0115	Rockwell C Hardness 17-18
	C	static	—	—	—	16,000	—	—	—	—	.0333	.0293	Rockwell C Hardness 17-18
	D	static	—	—	—	20,000	—	—	—	—	.0249	.0190	Rockwell C Hardness 40
Tool Steel, Fully Annealed 1/4 in. diam. specimen	12	42.7	1.5	.0253	.0277	1,530	37.0	1.4	.0043	.0027	—	.0028	Tail end of record adjusted
	13	48.1	— **	.0275 *	.0317	1,860	31.8	1.55	.0041	.0022	—	.0025	Tail end of record adjusted
	14	118.5	— **	.0677 *	.0739	3,890	44.0	1.7	.0106	.0069	—	.0071	Plastic set occurred under gage
Aluminum, 2024-T4 1/2 in. diam. specimen	15	66.0	10.2	.0436	.0442	2,280	35.5	0.3	.0097	.0076	—	.0076	
	16	107.3	12.0	.0683	.0689	3,640	35.0	1.3	.0144	.0118	—	.0118	
	17	153.5	12.04	.0948	.0970	5,210	34.3	1.0	.0201	.0169	—	.0170	
	18	213.3	11.2	.1285	.1293	6,940	34.5	0.3	.0294	.0263	—	.0262	
	19	290.7	8.9	.1711	.1756	9,080	36.0	1.6	.0351	.0316	—	.0315	
	20	292.7	6.5	.1712	.1721	8,820	35.0	1.8	.0361	.0339	—	.0316	
	E	static	—	—	—	3,600	—	—	—	—	.0136	.0110	
	F	static	—	—	—	7,000	—	—	—	—	.0264	.0232	
	G	static	—	—	—	10,000	—	—	—	—	.0441	.0418	
	H	static	—	—	—	10,000	—	—	—	—	.0477	.0434	This data obtained by repeated loading and unloading to higher force levels
Aluminum, 1100-F 1/2 in. diam. specimen	21	25.6	3.4	.0168	.0167	580	51	1.0	.0059	.0052	—	.0052	
	22	59.3	— **	.0340 *	.0380	1,363	49	0.0	.0134	.0121	—	.0120	
	23	103.3	6.8	.0629	.0670	2,112	52	1.0	.0231	.0215	—	.0216	
	24	167.7	1.4	.0967	.0970	2,975	50	2.4	.0386	.0381	—	.0327	Plastic set occurred under gage
	I	static	—	—	—	2,200	—	—	—	—	.0311	.0302	Tail end of record adjusted
Lead, Extruded 1/2 in. diam. specimen	25	25.25	1.5	.0153	.0153	217	230	7.3	.0175	.0172	—	.0170	Plastic set occured under gage
	26	36.9	0.2	.0212	.0234	272	230	1.4	.0283	.0282	—	.0250	Plastic set occurred under gage
	J	static	—	—	—	200	—	—	—	—	.0254	.0254	

* Δmv based on zero final velocity of ball

** Terminal velocity negligible

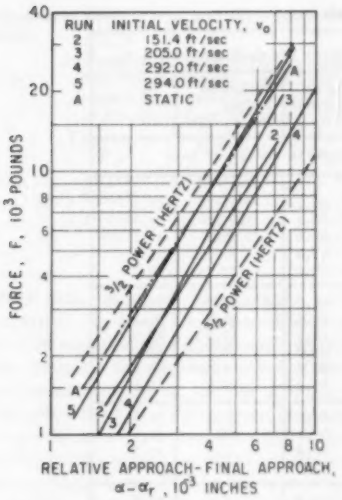

Fig. 11 Force vs. recovery for quench-hardened tool steel after penetration by a 1/2-in-diam hard-steel sphere

less than 25 per cent so that the static values could be employed in lieu of a dynamic relation as a first approximation within the margin of error. The results at low impact velocity for 2024-T4 aluminum fall below both the static force-indentation curve and the dynamic curve derived from the tests at the maximum impact velocity; this result is at variance with the indicated behavior of all other metals investigated and is believed to be an anomaly. The discrepancy between these curves is about 10 per cent, part of which may be attributed to experimental error. Since the static compressive and tensile test specimens were not detached from the original Hopkinson bar until after completion of the dynamic tests, it is also possible that the static compressive specimens were subjected to additional work-hardening relative to the dynamic specimens (particularly those at low velocity, which were conducted first), which may account for this difference. It also could be that individual variations in the material properties of various sections of the bar contributed to this effect.

An auxiliary series of tests on specimens of the various materials 1/4 in. and 1/2 in. long, backed up by a hardened steel bar, was conducted at three constant velocities to determine whether a significant plastic compression of the bar as a whole occurred. Such a feature might invalidate the measurement of the permanent crater depth by shifting the reference plane relative to the unindented portion of the impact end to which the crater indentation was referred. The maximum plastic compression of these specimens at the highest velocities investigated were found to be 0.0015 in., which is insufficient to change the character of the dynamic curves significantly. In most cases, this correction was found to be negligible. There is a possibility of some creep recovery of the crater before a measurement of its depth could be undertaken, but this contingency is believed to be remote.

It also may be observed from the diagrams presented that the dynamic plastic results during the compression phase for quench-hardened tool steel are in excellent correspondence with the predictions of the Hertz law for almost the entire range of velocities employed in the tests. Only in the vicinity of the highest load imposed on the specimens does the elastic relation predict too large a force for the production of a given crater depth. The percentage discrepancy between the two curves apparently will increase, however, if forces larger than those capable of being generated with the present equipment can be applied to the rod. The Hertz law in its original form is, of course, inapplicable during the recovery process, since it will not predict a permanent indentation, although the slopes of the recovery curves in Fig. 11 exhibit the same value as that for elastic restitution. It may be observed that the elastic recovery of this material is of the order of 50 per cent, which further indicates that the elastic behavior of the material has a significant influence on the hope of the dynamic force-indentation relation.

For all other materials, the Hertz law predicts a force whose magnitude becomes increasingly larger than actually required to produce a given indentation, and the percentage of elastic recovery is very much smaller. Consequently, the use of equation (1) would not appear to be a good substitute for an empirical dynamic force-indentation law.

It may be noted also that none of the metals involved in this investigation exhibited a linear force-indentation curve for the entire velocity range considered; thus a constant flow pressure does not prevail during the indentation process. A distinct upward curvature is exhibited for all materials at low values of the penetration; only hard steel subsequently exhibits a range during which a reasonably constant slope of the curve is maintained. The softer metals all show a distinctly downward concave curvature of the force-indentation relation, both statically and dynamically, for larger magnitudes of the approach. This curvature reversal cannot be expressed empirically by an equation of the form of equation (2).

From the previous discussion it is evident why the use of the Hertz law of contact should predict correctly the contact phenomena observed experimentally for the impact of the steel spheres on hardened steel plates or beams [28–30]. It is not so apparent why the same law should be equally applicable in specifying properly the response of beams and plates composed of other materials, when the present sequence of experiments indicates large variations of the dynamic plastic relation from the Hertz law. The answer to this question may lie in the choice of the materials tested. The present investigation was concerned primarily with materials which do not exhibit distinct yield-point phenomena and where the effects of strain rate are consequently much less pronounced than for a material such as a mild steel, which possesses a distinct yield point. In fact, the percentage increase in the required force under dynamic conditions for a given indentation as observed in the present series of tests is about the same as the increase determined by other investigators for stress-strain curves for these materials obtained dynamically and statically, respectively. For example, Campbell [31] reports an increase in the dynamic value of the stress at a given strain of about 15 per cent relative to the static value for an aluminum alloy similar to the 2024-T4 aluminum specimens utilized in the present investigation. Taylor [32] observed an increase in this parameter of about 20 per cent for a carbon-manganese steel having a static stress-strain curve very similar to that of the soft tool steel shown in Fig. 3. It would thus appear as though the mechanisms producing the dynamic effect in the stress-strain relations are operative to the same degree in the shifting of the corresponding force-indentation curves; this is, perhaps, expected, since the latter represent essentially an average value of total stress and strain at the crater surface.

On the other hand, materials with a distinct yield point, such as mild steel, exhibit dynamic stress-strain curves under impact conditions twice or more as large as the corresponding static relations [33, 34]. This characteristic is manifested by an extension of the elastic range to the new yield point; from this feature it is apparent that the impact behavior of such metals under high rates of strain is essentially elastic for a much longer range than for materials with less pronounced strain-rate sensitivity. As a consequence, it might be expected that a similar increase in the

Table 3 Energy distribution for tests

Target Material	Run No.	Kinetic Energy of Ball		Energy of Elastic Pulse in Bar	Energy for Crater Production		
		Initial	Final		During Approach	Recovered During Restitution	Net
		lb-in	percent of initial kinetic energy of ball				
Tool Steel, Quench-Hardened 1/2 in. diam. specimen	1	78.1	17.8	24.5	68.1	41.1	27.0
	2	78.5	19.6	25.9	69.2	43.9	25.3
	3	144.2	18.4	23.5	67.4	25.7	41.7
	4	292.0	10.0	23.3	63.4	27.6	35.8
	5	296.8	10.8	22.9	65.9	19.6	46.3
Tool Steel, Partially Annealed 1/2 in. diam. specimen	6	17.5	14.0	17.7	63.9	26.8	37.1
	7	39.5	10.4	17.7	67.6	16.2	51.4
	8	80.4	7.7	19.3	68.9	19.9	49.9
	9	150.6	6.2	17.3	62.8	14.7	48.1
	10	215.7	4.0	15.6	70.0	11.6	58.4
	11	282.0	2.8	15.0	75.2	10.6	64.6
Tool Steel, Fully Annealed 1/4 in. diam. specimen	12	6.2	12.3	35.7	49.6	15.3	34.3
	13	7.9	--*	38.3	55.2	24.1	31.1
	14	48.2	--*	32.5	42.4	8.5	33.9
Aluminum, 2024-T4 1/2 in. diam. specimen	15	14.9	2.4	25.4	55.3	9.6	45.7
	16	39.5	1.3	23.6	61.0	10.0	51.0
	17	80.6	0.6	25.3	66.5	14.0	52.5
	18	156.0	0.3	21.7	61.3	5.3	56.0
	19	290.0	0.1	20.7	62.6	3.8	58.8
	20	294.0	0.1	19.3	63.3	1.8	61.5
Aluminum, 1100-F 1/2 in. diam. specimen	21	2.3	1.6	16.3	69.8	4.9	64.9
	22	12.1	--*	15.1	69.4	5.5	63.9
	23	36.6	0.4	14.1	76.4	3.5	72.9
	24	96.4	0.6	11.9	74.1	0.9	73.2
Lead, Extruded 1/2 in. diam. specimen	25	2.2	0.4	4.9	97.2	--*	97.2
	26	4.7	--*	4.4	94.2	--*	94.2

* Negligible

force-indentation relation during the approach phase might be induced in such a material when subjected to a ball impact at a high velocity. This factor may be the explanation for the relatively excellent correlation obtained in previous investigations between a theory using the Hertz law and experimental data concerning the stresses, deflections, and durations of contact of spheres striking metal beams and plates, since the materials employed for the targets in physical tests were usually some form of mild steel [35, 30, 28, 7].

It would, of course, be extremely interesting to repeat this series of experiments with mild steel; attempts in this direction have not, thus far, been successful owing to the presence of magnetostrictive effects in the bar, also observed by other investigators [36, 20], which have introduced spurious signals in the strain-gage records. This factor was also present in the case of the soft tool steel, but was circumvented by quench-hardening the section of the bar around the gage location, while annealing the region near the impact end. The same procedure unfortunately could not be adopted in the case of mild steel.

To gain some impression of the relative importance of the role played in a theoretical analysis of an actual impact problem by the force-indentation relation, an approximate analysis based on energy considerations for the Hopkinson bar has been performed. Table 3 indicates the magnitude of the initial and rebound energy of the ball for the present series of runs, the energy required for producing the crater, taken as the area under the calculated force-indentation relation, and the energy present in the elastic pulse propagating down the bar. The latter was computed from the force-time records according to the equation

$$W = \frac{c}{2AE}\int_0^\tau F^2\,dt \qquad (5)$$

where τ is the pulse duration.

It may be observed that the energy required to form the crater is an appreciable fraction of the total energy; it has been demonstrated that this quantity represents about the same percentage of the total energy for transverse impact on beams [20]. It is thus not surprising that the crater depths for the two cases, as well as the maximum force produced for the same materials and initial velocities, is nearly the same regardless of whether a longitudinal collision with a rod or a transverse impact on a beam is effected. Failure to achieve a reasonable energy balance, manifested in Table 3, is ascribed to the crude manner of anaysis, involving neglect of other energies, as well as the high degree of sensitivity of the calculated parameters upon an exact determination of the peak force and crater depth.

When an average slope is determined for the force-indentation relations shown in Figs. 3 to 9, this information can be employed in comparison with the mean static and dynamic flow pressures cited by other investigators [10, 16]. Table 4 summarizes this information; in view of the differences in the properties of the materials actually employed and the variations in the size and initial velocity of the striking steel sphere, excellent correspondence between the respective values, particularly that of the ratio of the static to the dynamic flow pressure, may be noted.

It might be mentioned that the agreement obtained [16] for the calculated and measured permanent crater depth for the impact of crossed cylinders, with discrepancies up to 50 per cent, is not any more satisfactory than in the present series of tests when the uncorrected form of the strain-time diagram is employed. Furthermore, the earlier investigation was conducted at impact velocities two orders of magnitude below the present series of tests; in the present investigation, it was found that the correlation of calculated and measured permanent indentations, using

Table 4 Comparison of average flow pressures (determined from mean slopes of $F = \alpha$ curves) for present experiments with those determined by other investigators

	Present investigation: 1/2-in-diam steel ball striking plane ended rods; maximum velocity = 300 fps			Crook [16]: 1/4-in-diam steel ball bearing striking flat specimens, maximum velocity = 2 fps			Tabor [10]: 5-cm-diam ball dropped from a height of 300 cm onto a ball		
	Average flow pressure, psi			Average flow pressure, psi			Average flow pressure, psi		
Material	Dynamic P_D	Static P_S	P_D/P_S	Dynamic P_D	Static P_S	P_D/P_S	Dynamic P_D	Static P_S	P_D/P_S
Steel, hard	986000	952000	1.035	...	...	...	...	...	...
Steel, soft	588000	485000	1.212	...	...	...	...	...	1.00
Aluminum	175000	165000	1.065	362000	333000	1.085	...	...	1.10
Lead	6650	5200	1.275	8690	6950	1.25	8670	7820	1.11

the uncorrected data, improves considerably as the impact velocity is decreased. However, Crook's method of measurement using a short anvil mounted on a piezoelectric crystal backed up by a lead bar minimizes the dispersive effect of the Hopkinson bar and lends greater validity to the use of a one-dimensional theory; on the other hand, wave reflections generated at the interface of the crystal are not accounted for in his data reduction, and the calibration of the crystal neglected any three-dimensional effects of wave propagation. Furthermore, a serious question arises concerning the validity of his comparison of calculated and measured crater depth, since the start of the pulse cannot be obtained from the records, but must be determined by extrapolation. Consequently, any possible rounding of the record at the initial rise is completely lost. However, some further increase in the depth of the crater beyond the peak of the force, also observed by Crook, is evident in most of the present records.

Acknowledgment

The authors would like to express their sincere appreciation to Prof. D. M. Cunningham for his generous assistance and many helpful suggestions during the course of the investigation. Acknowledgment is also made to the aid rendered by Mr. Ching-Hsie Yew and Mr. William Sturgeon in the conduct of the experiments.

References

1 S. Timoshenko, "Zur Frage nach der Wirkung eines Stosses auf einen Balken," *Zeitschrift für Mechanik und Physik*, vol. 62, 1913, p. 198.

2 E. H. Lee, "The Impact of a Mass Striking a Beam," JOURNAL OF APPLIED MECHANICS, vol. 7, TRANS. ASME, vol. 62, 1940, pp. A-129-A-138.

3 W. H. Hoppmann, "Impact on a Multispan Beam," JOURNAL OF APPLIED MECHANICS, vol. 17, TRANS. ASME, vol. 72, 1950, p. 409.

4 J. E. Sears, "On the Longitudinal Impact of Metal Rods With Rounded Ends," *Trans. of the Cambridge Philosophical Society*, vol. 21, 1908, p. 49.

5 C. Zener and H. Feshbach, "A Method of Calculating Energy Losses During Impact," JOURNAL OF APPLIED MECHANICS, vol. 6, TRANS. ASME, vol. 61, 1939, p. A-67.

6 K. Karas, "Platten unter seitlichem Stoss," *Ingenieur-Archiv*, vol. 10, 1939, p. 237.

7 K. E. Barnhart and W. Goldsmith, "Stresses in Beams During Transverse Impact," JOURNAL OF APPLIED MECHANICS, vol. 24, TRANS. ASME, vol. 79, 1957, p. 440.

8 H. Hertz, "Über die Berührung fester elastischer Körper," *Journal für reine und angewandte Mathematik* (Crelle), vol. 92, 1881, p. 155.

9 R. M. Davies, "The Determination of Static and Dynamic Yield Stresses Using a Steel Ball," *Proceedings of the Royal Society of London*, series A, vol. 197, 1949, p. 416.

10 D. Tabor, "The Hardness of Metals," Clarendon Press, Oxford, England, 1951.

11 E. Meyer, "Untersuchungen über Härteprüfung und Härte," *Zeitschrift des Vereines Deutscher Ingenieure*, vol. 52, 1908, p. 645.

12 F. Berger, "Das Gesetz des Kraftverlaufs beim Stoss," F. Vieweg & Sohn, Braunschweig, Germany, 1924.

13 T. Pöschl, "Der Stoss," *Handbuch der Physik*, J. Springer, Berlin, Germany, vol. 6, 1926, chapter 7.

14 J. P. Andrews, "Experiments on Impact," *Proceedings of the Physical Society of London*, vol. 43, 1931, p. 8.

15 J. P. Andrews, "Theory of Collision of Spheres of Soft Metals," *Philosophical Magazine*, series 7, vol. 9, 1930, p. 593.

16 A. W. Crook, "A Study of Some Impacts Between Metal Bodies by a Piezoelectric Method," *Proceedings of the Royal Society of London*, series A, vol. 212, 1952, p. 377.

17 E. A. Ripperger, "Longitudinal Impact of Cylindrical Bars," *Proceedings of the Society for Experimental Stress Analysis*, vol. 10, no. 1, 1952, p. 209.

18 R. M. Davies, "A Critical Study of the Hopkinson Pressure Bar," Royal Society of London, *Philosophical Transactions*, series A, vol. 240, 1948, p. 375.

19 J. Miklowitz and C. R. Nisewanger, "The Propagation of Compressional Waves in a Dispersive Elastic Rod," JOURNAL OF APPLIED MECHANICS, vol. 24, TRANS. ASME, vol. 79, 1957, p. 240.

20 D. M. Cunningham and W. Goldsmith, "Short-Time Impulses Produced by Longitudinal Impact," *Proceedings of the Society for Experimental Stress Analysis*, vol. 16, no. 2, 1959, p. 153.

21 J. W. S. Rayleigh, "On the Production of Vibrations by Forces of Relatively Long Duration, With Applications to the Theory of Collisions," *Philosophical Magazine*, series 6, vol. 11, 1906, p. 283.

22 J. Miklowitz, "The Propagation of Compressional Waves in a Dispersive Elastic Rod," JOURNAL OF APPLIED MECHANICS, vol. 24, TRANS. ASME, vol. 79, 1957, p. 231.

23 C. W. Curtis, "Second Mode Vibrations of the Pochhammer-Chree Frequency Equation," *Journal of Applied Physics*, vol. 25, 1954, p. 928.

24 E. A. Ripperger, "The Propagation of Pulses in Cylindrical Bars—an Experimental Study," *Proceedings*, First Midwestern Conference on Solid Mechanics, 1953, p. 29.

25 Richard Skalak, "Longitudinal Impact of a Semi-Infinite Circular Elastic Bar," JOURNAL OF APPLIED MECHANICS, vol. 24, TRANS. ASME, vol. 79, 1957, p. 59.

26 D. Bancroft, "The Velocity of Longitudinal Waves in Cylindrical Bars," *Physical Review*, vol. 59, 1941, p. 588.

27 H. Kolsky, "Stress Waves in Solids," Clarendon Press, Oxford, England, 1953.

28 W. H. Hoppmann, "Impulsive Loads on Beams," *Proceedings of the Society for Experimental Stress Analysis*, vol. 10, 1952, p. 157.

29 M. Goland, P. D. Wickersham, and M. A. Dengler, "Propagation of Elastic Impact in Beams in Bending," JOURNAL OF APPLIED MECHANICS, vol. 22, TRANS. ASME, vol. 77, 1955, p. 1.

30 H. Mintrop, "Untersuchungen über den Stoss einer Kugel gegen eine ebene Platte," *Verein Deutscher Ingenieure*, Forschungsheft, vol. 12, 1941, p. 127.

31 J. D. Campbell, "An Investigation of the Plastic Behaviour of Metal Rods Subjected to Longitudinal Impact," *Journal of the Mechanics and Physics of Solids*, vol. 1, 1953, p. 113.

32 D. B. C. Taylor, "The Dynamic Straining of Metals Having Definite Yield Points," *Journal of the Mechanics and Physics of Solids*, vol. 3, 1954, p. 38.

33 G. I. Taylor, "The Use of Flat-Ended Projectiles for Determining Dynamic Yield Stress," *Proceedings of the Royal Society of London*, series A, vol. 194, 1948, p. 289.

34 J. D. Campbell and J. Duby, "The Yield Behaviour of Mild Steel in Dynamic Compression," *Proceedings of the Royal Society of London*, series A, vol. 236, 1956, p. 24.

35 R. N. Arnold, "Impact Stresses in a Freely Supported Beam," *Proceedings of The Institution of Mechanical Engineers*, vol. 137, 1937, p. 217.

36 I. Vigness, "Magnetostrictive Effects in Wire Strain Gages," *Proceedings of the Society for Experimental Stress Analysis*, vol. 14, no. 2, 1957, p. 139.

T. P. MITCHELL
Assistant Professor,
Department of Engineering Mechanics,
Cornell University,
Ithaca, N. Y.

J. A. WEESE
Lieutenant, Instructor,
U.S.A.F. Academy, Colo.

Stress Distributions Analyzed in Bispherical Co-Ordinates

Boussinesq-Papkovich potentials are used in conjunction with the bispherical co-ordinate system to analyze three problems in the classical theory of linear elasticity: (a) The extension of the Boussinesq point-load problem to that in which the half-space contains a spherical cavity; (b) the determination of the stress distribution in an eccentric spherical shell under uniform internal pressure; (c) the determination of the stress distribution in a half-space containing a uniformly pressurized spherical cavity. Numerical results are presented for representative configurations and load distributions in each case.

According to the theory of linear elasticity the displacement field, $\mathbf{u}$, in a homogeneous isotropic material, the body forces being zero, must satisfy the equation

$$(1 - 2\nu)\nabla^2\mathbf{u} + \nabla\nabla\cdot\mathbf{u} = 0 \tag{1}$$

in which ν is Poisson's ratio. A solution of this equation in terms of harmonic functions has been obtained by Boussinesq [1][1] and Papkovich [2]. This solution can be represented in the form

$$\mathbf{u} = \nabla(w + r\cdot\mathbf{B}) - 4(1 - \nu)\mathbf{B} \tag{2}$$

where w is a harmonic scalar, and $\mathbf{B}$ a harmonic vector, function. The expression (2) contains four harmonic scalar functions. The conditions under which one, or two, of these functions may be equated to zero are given in detail in [3]. It suffices to mention that for the axisymmetric, torsion-free problems to be studied here only two of the harmonic functions are required. Thus the displacement field is represented in Cartesian component form by

$$2Gu_i = z\psi_{,i} - \delta_{i3}(3 - 4\nu)\psi + \phi_{,i} \tag{3}$$

where ϕ and ψ are harmonic scalar functions. In expression (3) δ_{i3} is the Kronecker delta, a subscript comma denotes a partial derivative and the z-axis is the axis of symmetry.

The solution of the basic equations of linear elasticity in terms of the Boussinesq-Papkovich potentials has been employed by several authors to analyze three-dimensional stress distributions. A recent survey of their work is given in [4]. The method is utilized here (a) to extend the classical Boussinesq point-load problem to that in which the half space contains a spherical cavity symmetrically situated beneath the load; (b) to analyze the stress distribution in an eccentric spherical shell under uniform internal pressure; and (c) to consider the problem of a half-space containing a uniformly pressurized spherical cavity. In each case the material is assumed to be homogeneous and isotropic and the analysis is made within the limits of the linear theory. Numerical examples are provided.

[1] Numbers in brackets designate References at end of paper.

Presented at the West Coast Conference of the Applied Mechanics Division, Pasadena, Calif., June 27–29, 1960, of The American Society of Mechanical Engineers.

Discussion of this paper should be addressed to the Secretary, ASME, 29 West 39th Street, New York, N. Y., and will be accepted until January 10, 1961, for publication at a later date. Discussion received after the closing date will be returned.

Manuscript received by ASME Applied Mechanics Division, December 3, 1959. Paper No. 60—APMW-4.

Basic Equations

The geometrical configuration of the three problems outlined in the foregoing clearly indicates the use of the bispherical co-ordinate system. This system of co-ordinates, which is orthogonal, is defined in terms of the rectangular Cartesian co-ordinates x, y, z as follows:

$$x = \frac{ap}{q - p}\cos\gamma$$

$$y = \frac{ap}{q - p}\sin\gamma \tag{4}$$

$$z = -\frac{a\bar{q}}{q - p}$$

where

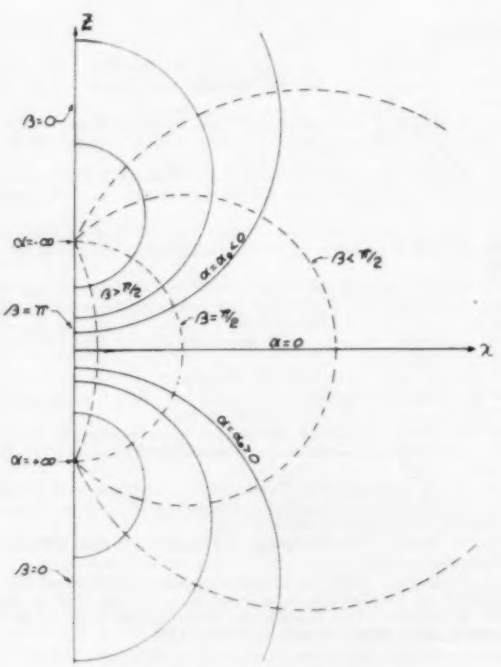

Fig. 1 The bispherical co-ordinate system

$$p = \cos\beta \qquad q = \cosh\alpha$$
$$\bar{p} = \sin\beta \qquad \bar{q} = \sinh\alpha \tag{5}$$

The entire three-dimensional space is covered by allowing the bispherical co-ordinates (α, β, γ) to range over the values

$$-\infty \leq \alpha \leq \infty$$
$$0 \leq \beta \leq \pi \tag{6}$$
$$0 \leq \gamma \leq 2\pi$$

The surface $\alpha = \alpha_0$ is the sphere of radius $a/\bar{q}_0$ with center at $x = 0, y = 0, z = -a \coth \alpha_0$. The surface $\alpha = 0$ thus represents the xy-plane and the infinite sphere. Fig. 1 provides a diagram of the co-ordinate system in the case $\gamma = 0$. Further details of the system which apparently was used for the first time in elasticity problems by Sternberg and Sadowsky [5] (whose notation is adopted here), are to be found, e.g., in [6].

The stresses in Cartesian co-ordinates can be written in terms of the two potential functions, ϕ and ψ, by the use of the stress-strain relationship in conjunction with equation (3). The stresses in the bispherical system, which are found by transforming from the Cartesian, are

$$\left.\begin{aligned}
\sigma_{\alpha\alpha} &= \frac{\mu^2}{a^2}\left[\mu^2\phi_{,\alpha\alpha} + \bar{q}\phi_{,\alpha} + \bar{p}^2\phi_{,p}\right] - \frac{1}{a}\left\{\mu^2\bar{q}\psi_{,\alpha\alpha}\right.\\
&\quad + \left.[\bar{q}^2 - 2(1-\nu)(1-qp)]\psi_{,\alpha} + (1-2\nu)\bar{q}\bar{p}^2\psi_{,p}\right\}\\
\sigma_{\beta\beta} &= \frac{\mu^2}{a^2}\left[\mu^2\bar{p}^2\phi_{,pp} - (\mu^2 p + \bar{p}^2)\phi_{,p} - \bar{q}\phi_{,\alpha}\right]\\
&\quad + \frac{1}{a}\left\{[\bar{q}^2 + 2\nu(1-qp)]\psi_{,\alpha} + [\mu^2\bar{q}p + (3-2\nu)\bar{q}\bar{p}^2]\psi_{,p}\right.\\
&\quad \left. - \mu^2\bar{q}\bar{p}^2\psi_{,pp}\right\}\\
\sigma_{\gamma\gamma} &= -\frac{\mu^2}{a^2}\left[\bar{q}\phi_{,\alpha} - (1-qp)\phi_{,p}\right]\\
&\quad + \frac{1}{a}\left\{[\bar{q}^2 + 2\nu(1-qp)]\psi_{,\alpha} + \bar{q}(2\nu\bar{p}^2 + qp - 1)\psi_{,p}\right\}\\
\sigma_{\alpha\beta} &= -\bar{p}\frac{\mu^2}{a^2}\left[\mu^2\phi_{,\alpha p} - \phi_{,\alpha} + \bar{q}\varphi_{,p}\right]\\
&\quad + \frac{\bar{p}}{a}\left\{\mu^2\bar{q}\psi_{,\alpha p} - 2(1-\nu)\bar{q}\psi_{,\alpha}\right.\\
&\quad + \left.[\bar{q}^2 - (1-2\nu)(1-qp)]\psi_{,p}\right\} \quad \sigma_{\alpha\gamma} = \sigma_{\beta\gamma} = 0
\end{aligned}\right\} \tag{7}$$

In the derivation of equations (7) the fact that the axisymmetric nature of the problems demands that ϕ and ψ be independent of γ has been utilized.

An examination of the forms of the solution of Laplace's equation in bispherical co-ordinates (see e.g., [6]) shows that the appropriate potential functions are

$$\phi = \sum_0^\infty \phi_n \qquad \psi = \sum_0^\infty \psi_n \tag{8}$$

where

$$\phi_n = \phi_n^0 + \phi_n^1 = \mu A_n^0 C_n(\alpha)P_n(p) + \mu A_n^1 S_n(\alpha)P_n(p) \tag{9}$$

and

$$\psi_n = \psi_n^0 + \psi_n^1 = \mu B_n^0 C_n(\alpha)P_n(p) + \mu B_n^1 S_n(\alpha)P_n(p) \tag{10}$$

In expressions (9) and (10)

$$\mu = (q-p)^{1/2} \qquad C_n(\alpha) = \cosh {}^1\!/_2 k\alpha$$
$$k = 2n+1 \qquad S_n(\alpha) = \sinh {}^1\!/_2 k\alpha$$

A_n^0, A_n^1, B_n^0, B_n^1 are constants, to be determined by boundary conditions, and P_n represents the Legendre polynomial of degree n with argument $\cos\beta$.

The determination of expressions for the stresses by using equation (7) in conjunction with equations (9) and (10) involves considerable algebraic manipulation and reduction. As the resulting expressions are quite lengthy only two of the stresses are given explicitly; the others are of a somewhat similar type.

The $\sigma_{\alpha\alpha}$ stress is

$$\sigma_{\alpha\alpha} = \mu^{-1}\sum_0^\infty f_n(\alpha)P_n(p) \tag{11}$$

where

$$\begin{aligned}
f_n(\alpha) &= -\frac{1}{a^2}A_{n-2}^0\frac{(k-1)(k-3)(k-5)}{32(k-2)}C_{n-2}\\
&\quad - \frac{1}{a^2}A_{n-2}^1\frac{(k-1)(k-3)(k-5)}{32(k-2)}S_{n-2}\\
&\quad + \frac{1}{a^2}A_{n-2}^0\frac{(k-1)(k-3)}{16(k-2)}[(3k-8)qC_{n-2} + 4\bar{q}S_{n-2}]\\
&\quad + \frac{1}{a^2}A_{n-2}^1\frac{(k-1)(k-3)}{16(k-2)}[(3k-8)qS_{n-2} + 4\bar{q}C_{n-2}]\\
&\quad - \frac{1}{a}B_{n-2}^0\frac{(k-1)(k-3)}{16(k-2)}[(k-2-4\nu)\bar{q}C_{n-2}\\
&\quad\quad - 4(1-\nu)(k-4)qS_{n-2}]\\
&\quad - \frac{1}{a}B_{n-2}^1\frac{(k-1)(k-3)}{16(k-2)}[(k-2-4\nu)\bar{q}S_{n-2}\\
&\quad\quad - 4(1-\nu)(k-4)qC_{n-2}]\\
&\quad + \frac{1}{a^2}A_{n-1}^0\left\{-\frac{(k-1)}{32(k^2-4)}(3k^3-4k^2-9k+18)C_{n-1}\right.\\
&\quad \left. - \frac{(k-1)}{8(k-2)}[(k-2)(3k-4)q^2 + 3\bar{q}^2]S_{n-1} - (k-1)q\bar{q}S_{n-1}\right\}\\
&\quad + \frac{1}{a^2}A_{n-1}^1\left\{-\frac{(k-1)}{32(k^2-4)}(3k^3-4k^2-9k+18)S_{n-1}\right.\\
&\quad \left. - \frac{(k-1)}{8(k-2)}[(k-2)(3k-4)q^2 + 3\bar{q}^2]C_{n-1} - (k-1)q\bar{q}C_{n-1}\right\}\\
&\quad + \frac{1}{4a}B_{n-1}^0(k-1)\left\{\frac{(k-2)^2 + (1-2\nu)(k-4)}{(k-2)}q\bar{q}C_{n-1}\right.\\
&\quad\quad \left. + 2\bar{q}^2S_{n-1} - 2(1-\nu)(1+q^2)S_{n-1}\right\}\\
&\quad + \frac{1}{4a}B_{n-1}^1(k-1)\left\{\frac{(k-2)^2 + (1-2\nu)(k-4)}{(k-2)}q\bar{q}S_{n-1}\right.\\
&\quad\quad \left. + 2\bar{q}^2C_{n-1} - 2(1-\nu)(1+q^2)C_{n-1}\right\}\\
&\quad + \frac{1}{8a^2}A_n^0\left\{2(k^2q^2 + 3\bar{q}^2)qC_n + \frac{(3k^4-9k^2-8)}{(k^2-4)}qC_n\right.\\
&\quad\quad \left. + 8kq^2\bar{q}S_n + 4k\frac{(k^2-3)}{(k^2-4)}\bar{q}S_n\right\}\\
&\quad + \frac{1}{8a^2}A_n^1\left\{2(k^2q^2 + 3\bar{q}^2)qS_n + \frac{(3k^4-9k^2-8)}{(k^2-4)}qS_n\right.\\
&\quad\quad \left. + 8kq^2\bar{q}C_n + 4k\frac{(k^2-3)}{(k^2-4)}\bar{q}C_n\right\}
\end{aligned}$$

$$- \frac{1}{8a} B_n^0 \left\{ 2(k^2 - 4 + 8\nu) q^2 \bar{q} C_n + \frac{k^2(k^2-3) - 4(1-2\nu)}{(k^2-4)} \bar{q} C_n + 2(7 - 8\nu) \bar{q}^2 C_n + 8k(\bar{q}^2 - 1 + \nu) q S_n + 4(1-\nu) k \frac{(k^2-3)}{(k^2-4)} q S_n \right\}$$

$$- \frac{1}{8a} B_n^1 \left\{ 2(k^2 - 4 + 8\nu) q^2 \bar{q} S_n + \frac{k^2(k^2-3) - 4(1-2\nu)}{(k^2-4)} \bar{q} S_n + 2(7 - 8\nu) \bar{q}^2 S_n + 8k(\bar{q}^2 - 1 + \nu) q C_n + 4(1-\nu) k \frac{(k^2-3)}{(k^2-4)} q C_n \right\}$$

$$+ \frac{1}{a^2} A_{n+1}^0 \left\{ - \frac{(k+1)}{32(k^2-4)} (3k^3 + 4k^2 - 9k - 18) C_{n+1} - \frac{(k+1)}{8(k+2)} [(k+2)(3k+4)q^2 + 3\bar{q}^2] C_{n+1} - (k+1) q \bar{q} S_{n+1} \right\}$$

$$+ \frac{1}{a^2} A_{n+1}^1 \left\{ - \frac{(k+1)}{32(k^2-4)} (3k^3 + 4k^2 - 9k - 18) S_{n+1} - \frac{(k+1)}{8(k+2)} [(k+2)(3k+4)q^2 + 3\bar{q}^2] S_{n+1} - (k+1) q \bar{q} C_{n+1} \right\}$$

$$+ \frac{1}{4a} B_{n+1}^0 (k+1) \left\{ \frac{(k+2)^2 - (k+4)(1-2\nu)}{(k+2)} q \bar{q} C_{n+1} + 2\bar{q}^2 S_{n+1} - 2(1-\nu)(1+q^2) S_{n+1} \right\}$$

$$+ \frac{1}{4a} B_{n+1}^1 (k+1) \left\{ \frac{(k+2)^2 - (k+4)(1-2\nu)}{(k+2)} q \bar{q} S_{n+1} + 2\bar{q}^2 C_{n+1} - 2(1-\nu)(1+q^2) C_{n+1} \right\}$$

$$+ \frac{1}{a^2} A_{n+2}^0 \frac{(k+1)(k+3)}{16(k+2)} [(3k+8) q C_{n+2} + 4\bar{q} S_{n+2}] + \frac{1}{a^2} A_{n+2}^1 \frac{(k+1)(k+3)}{16(k+2)} [(3k+8) q S_{n+2} + 4\bar{q} C_{n+2}]$$

$$- \frac{1}{a} B_{n+2}^0 \frac{(k+1)(k+3)}{16(k+2)} [(k+2+4\nu)\bar{q} C_{n+2} - 4(1-\nu)(k+4) q S_{n+2}]$$

$$- \frac{1}{a} B_{n+2}^1 \frac{(k+1)(k+3)}{16(k+2)} [(k+2+4\nu)\bar{q} S_{n+2} - 4(1-\nu)(k+4) q C_{n+2}]$$

$$- \frac{1}{a^2} A_{n+3}^0 \frac{(k+1)(k+3)(k+5)}{32(k+2)} C_{n+3} - \frac{1}{a^2} A_{n+3}^1 \frac{(k+1)(k+3)(k+5)}{32(k+2)} S_{n+3} \quad (12)$$

The $\sigma_{\alpha\beta}$ stress is

$$\sigma_{\alpha\beta} = p\mu^{-1} \sum_1^\infty g_n(\alpha) P_n'(p) \quad (13)$$

where

$$g_n(\alpha) = + \frac{1}{a^2} A_{n-2}^0 \frac{(k-3)(k-5)}{16(k-2)} S_{n-2} + \frac{1}{a^2} A_{n-2}^1 \frac{(k-3)(k-5)}{16(k-2)} C_{n-2}$$

$$- \frac{3}{8a^2} A_{n-2}^0 \frac{(k-3)}{(k-2)} [\bar{q} C_{n-2} + (k-3) q S_{n-2}] - \frac{3}{8a^2} A_{n-2}^1 \frac{(k-3)}{(k-2)} [\bar{q} S_{n-2} + (k-3) q C_{n-2}]$$

$$+ \frac{1}{8a} B_{n-2}^0 \frac{(k-3)}{(k-2)} [(k-4\nu)\bar{q} S_{n-2} - 2(1-2\nu) q C_{n-2}] + \frac{1}{8a} B_{n-2}^1 \frac{(k-3)}{(k-2)} [(k-4\nu)\bar{q} C_{n-2} - 2(1-2\nu) q S_{n-2}]$$

$$+ \frac{1}{a^2} A_{n-1}^0 \left[\frac{3(2k-5)}{4(k-2)} q \bar{q} C_{n-1} + {}^3/_4 (k-2) q^2 S_{n-1} + {}^3/_{16} \frac{(k^2-5)}{(k+2)} S_{n-1} \right]$$

$$+ \frac{1}{a^2} A_{n-1}^1 \left[\frac{3(2k-5)}{4(k-2)} q \bar{q} S_{n-1} + {}^3/_4 (k-2) q^2 C_{n-1} + {}^3/_{16} \frac{(k^2-5)}{(k+2)} C_{n-1} \right]$$

$$+ \frac{1}{4a} B_{n-1}^0 \left\{ 2 \frac{(1-2\nu)}{(k-2)} [(k-4) q^2 + k - 1] C_{n-1} - 3\bar{q}^2 C_{n-1} - (2k - 1 - 4\nu) q \bar{q} S_{n-1} \right\}$$

$$+ \frac{1}{4a} B_{n-1}^1 \left\{ 2 \frac{(1-2\nu)}{(k-2)} [(k-4) q^2 + k - 1] S_{n-1} - 3\bar{q}^2 S_{n-1} - (2k - 1 - 4\nu) q \bar{q} C_{n-1} \right\}$$

$$- \frac{1}{4a^2} A_n^0 \left\{ 3 \frac{(k^2-6)}{(k^2-4)} \bar{q} C_n + 6q^2 \bar{q} C_n + 3k \frac{(k^2-5)}{(k^2-4)} q S_n + 2kq^3 S_n \right\}$$

$$- \frac{1}{4a^2} A_n^1 \left\{ 3 \frac{(k^2-6)}{(k^2-4)} \bar{q} S_n + 6q^2 \bar{q} S_n + 3k \frac{(k^2-5)}{(k^2-4)} q C_n + 2kq^3 C_n \right\}$$

$$+ \frac{1}{4a} B_n^0 \left\{ 6q\bar{q} C_n - 2(1-2\nu) \frac{(3k^2-14)}{(k^2-4)} q C_n + \frac{k}{(k^2-4)} [2(1-2\nu) + (k^2-4)(1+q^2)] \bar{q} S_n \right\}$$

$$+ \frac{1}{4a} B_n^1 \left\{ 6q\bar{q} S_n - 2(1-2\nu) \frac{(3k^2-14)}{(k^2-4)} q S_n + \frac{k}{(k^2-4)} [2(1-2\nu) + (k^2-4)(1+q^2)] \bar{q} C_n \right\}$$

$$+ \frac{1}{a^2} A_{n+1}^0 \left[\frac{3(2k+5)}{4(k+2)} q \bar{q} C_{n+1} + {}^3/_4 (k+2) q^2 S_{n+1} + {}^3/_{16} \frac{(k^2-5)}{(k-2)} S_{n+1} \right]$$

$$+\frac{1}{a^2}A_{n+1}{}^1\left[\frac{3(2k+5)}{4(k+2)}q\bar{q}S_{n+1}\right.$$
$$\left.+\,{}^3/_4(k+2)q^2C_{n+1}+{}^3/_{16}\frac{(k^2-5)}{(k-2)}C_{n+1}\right]$$
$$+\frac{1}{4a}B_{n+1}{}^0\left\{2\frac{(1-2\nu)}{(k+2)}[(k+4)q^2+k+1]C_{n+1}\right.$$
$$\left.-3\bar{q}^2C_{n+1}-(2k+1-4\nu)q\bar{q}S_{n+1}\right\}$$
$$+\frac{1}{4a}B_{n+1}{}^1\left\{2\frac{(1-2\nu)}{(k+2)}[(k+4)q^2+k+1]S_{n+1}\right.$$
$$\left.-3\bar{q}^2S_{n+1}-(2k+1-4\nu)q\bar{q}C_{n+1}\right\}$$
$$-\frac{3}{8a^2}A_{n+2}{}^0\frac{(k+3)}{(k+2)}[\bar{q}C_{n+2}+(k+3)qS_{n+2}]$$
$$-\frac{3}{8a^2}A_{n+2}{}^1\frac{(k+3)}{(k+2)}[\bar{q}S_{n+2}+(k+3)qC_{n+2}]$$
$$+\frac{1}{8a}B_{n+2}{}^0\frac{(k+3)}{(k+2)}[(k+4\nu)\bar{q}S_{n+2}-2(1-2\nu)qC_{n+2}]$$
$$+\frac{1}{8a}B_{n+2}{}^1\frac{(k+3)}{(k+2)}[(k+4\nu)\bar{q}C_{n+2}-2(1-2\nu)qS_{n+2}]$$
$$+\frac{1}{a^2}A_{n+2}{}^0\frac{(k+3)(k+5)}{16(k+2)}S_{n+2}$$
$$+\frac{1}{a^2}A_{n+2}{}^1\frac{(k+3)(k+5)}{16(k+2)}C_{n+2} \quad (14)$$

It must be remembered that in applying equations (12) and (14) the constants B_{-2}, B_{-1}, A_{-2}, A_{-1} are to be taken as zero.

The Point-Load Problem

The formulation of the problem is as follows: A homogeneous isotropic half-space, defined by $z \geq 0$, contains a spherical cavity whose center lies on the z-axis. A point load, P, acts on the plane surface, directed along the z-axis. It is required to find the stress distribution in the solid. The configuration is shown in Fig. 2 which also bears the values of the co-ordinates to be used in the numerical example.

The stress distribution, σ^B, in the absence of the cavity is well known [7]. In bispherical co-ordinates it is given by

$$\left.\begin{aligned}
\sigma_{\alpha\alpha}{}^B &= \frac{P\mu^{-1}}{2\pi a^2}\{(1-2\nu)\bar{q}^2[\mu-\bar{q}(q+p)^{-1/2}]\\
&\qquad -3\bar{q}^2p^2(q+p)^{-5/2}\}\\
\sigma_{\beta\beta}{}^B &= \frac{P}{2\pi a^2}\{(1-2\nu)p^{-2}(1-qp)^2[1-\bar{q}(q^2-p^2)^{-1/2}]\\
&\qquad -3\bar{q}q^2p^2(q+p)^{-2}(q^2-p^2)^{-1/2}\}\\
\sigma_{\gamma\gamma}{}^B &= \frac{P(1-2\nu)}{2\pi a^2}\{-p^{-2}(q-p)^2[1-q(q^2-p^2)^{-1/2}]\\
&\qquad +\bar{q}(q-p)^{1/2}(q+p)^{-3/2}\}\\
\sigma_{\alpha\beta}{}^B &= \frac{P\mu^{-1}}{2\pi a^2}p\bar{q}\{(1-2\nu)p^{-2}(1-qp)\\
&\qquad [\mu-\bar{q}(q+p)^{-1/2}]-3q\bar{q}p(q+p)^{-5/2}\}
\end{aligned}\right\} \quad (15)$$

The term μ^{-1} has been factored out in the expressions for $\sigma_{\alpha\alpha}{}^B$ and $\sigma_{\alpha\beta}{}^B$ for convenience in a later stage of the analysis. To effect the solution in the presence of the cavity it is necessary to superpose on σ^B a complementary stress distribution, σ^c, which cancels the stresses arising from σ^B on the cavity wall $\alpha = \alpha_0$. The distribution σ^c must also be such that it does not introduce any stresses on the plane surface and that, being integrated over the infinite hemisphere $z \leq 0$, $r = (x^2+y^2+z^2)^{1/2} \to \infty$, it produces no resultant force. The first condition requires that

$$\sigma_{\alpha\alpha}{}^c = -\sigma_{\alpha\alpha}{}^B, \qquad \sigma_{\alpha\beta}{}^c = -\sigma_{\alpha\beta}{}^B \qquad \text{on} \qquad \alpha = \alpha_0 \quad (16)$$

The latter two are satisfied if

$$\sigma_{\alpha\alpha}{}^c = 0, \qquad \sigma_{\alpha\beta}{}^c = 0 \quad \text{on} \quad \alpha = 0 \quad (17)$$

Consideration of equations (12) and (14) indicates that in order to use the boundary conditions (16) it is necessary to expand the stresses $\sigma_{\alpha\alpha}{}^B$ and $\sigma_{\alpha\beta}{}^B$ on $\alpha = \alpha_0$ in Fourier-Legendre series. In fact, it is necessary to find the coefficients c_n and d_n in the expansions

$$\left.\begin{aligned}
\sigma_{\alpha\alpha}{}^B &= \mu_0{}^{-1}\sum_0^\infty c_nP_n(p)\\
\text{and}\qquad\\
\sigma_{\alpha\beta}{}^B &= p\mu_0{}^{-1}\sum_1^\infty d_nP_n{}'(p)
\end{aligned}\right\} \quad \text{on} \quad \alpha = \alpha_0 \quad (18)$$

where $\mu_0 = (q-p)^{1/2}$ evaluated on $\alpha = \alpha_0$. The values of these coefficients can be ascertained by using the generating functions for the Legendre polynomials; viz.,

$$(1-2pw+w^2)^{-1/2} = \sum_0^\infty w^nP_n(p) \quad (19)$$

The substitution $w = e^{-\alpha_0/2}$ immediately leads to

$$\mu_0{}^{-1} = \sqrt{2}\sum_0^\infty e^{-\frac{k}{2}\alpha_0}P_n(p) \quad (20)$$

and a subsequent simple change in sign provides the formula

$$(q_0+p)^{-1/2} = \sqrt{2}\sum_{n=0}^\infty(-1)^ne^{-\frac{k}{2}\alpha_0}P_n(p) \quad (21)$$

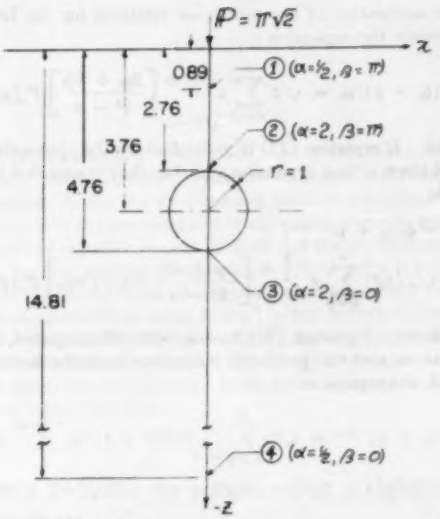

Fig. 2 Point load acting on half space containing a spherical cavity

By the application of the recurrence relations for the Legendre polynomials the expansion

$$\mu_0 = (q_0 - p)/\mu_0 = \sqrt{2} \sum_{n=0}^{\infty} e^{-\frac{k}{2}\alpha_0} \left[\frac{2q_0 + k\bar{q}_0}{k^2 - 4}\right] P_n(p) \quad (22)$$

is found. If equation (21) is multiplied by the appropriate factor and the resulting expansion added to that in equation (22) the formula

$$\bar{q}_0^2[\mu_0 - \bar{q}_0(q_0 + p)^{-1/2}]$$
$$= -\sqrt{2}(\bar{q}_0^2) \sum_{n=0}^{\infty} e^{-\frac{k}{2}\alpha_0} \left[\frac{2q_0 + k\bar{q}_0}{k^2 - 4} + (-1)^n \bar{q}_0\right] P_n(p) \quad (23)$$

is obtained. Equation (21) having been differentiated with respect to α_0 and the pertinent recurrence formulas having been applied, the expansion

$$3\bar{q}_0^2 p^2 (q_0 + p)^{-1/2} = \sqrt{2} \sum_{n=0}^{\infty} (-1)^n (k^2 - 4)^{-1} e^{-\frac{k}{2}\alpha_0} [k^4 \bar{q}_0 q_0^2$$
$$+ 2k^3 q_0(1 - 2\bar{q}_0^2) - k^2 \bar{q}_0(3 + q_0^2) + 2kq_0(-3 + 8\bar{q}_0^2)$$
$$- 12\bar{q}_0^3] P_n(p) \quad (24)$$

completes the determination of c_n. In addition, it is clear that

$$c_n = -\frac{\sqrt{2}P}{2\pi a^2} e^{-\frac{k}{2}\alpha_0} \left\{(1 - 2\nu)\bar{q}_0^2 \left[\frac{2q_0 + k\bar{q}_0}{k^2 - 4} + (-1)^n \bar{q}_0\right]\right.$$
$$+ (-1)^n (k^2 - 4)^{-1} [k^4 \bar{q}_0 q_0^2 + 2k^3 q_0(1 - 2\bar{q}_0^2)$$
$$\left. - k^2 \bar{q}_0(3 + q_0^2) + 2kq_0(-3 + 8\bar{q}_0^2) - 12\bar{q}_0^3]\right\} \quad (25)$$

A somewhat similar, but a more lengthy and complex, process results in the determination of the coefficients d_n in the expansion (18). Since the intermediate steps possess no intrinsic interest the end result only is set down. It is

$$d_n = \frac{\sqrt{2}P}{2\pi a^2} \bar{q}_0 \left[(1 - 2\nu)e_n - 2(-1)^n \bar{q}_0 e^{-\frac{k}{2}\alpha_0} (kq_0 - 3\bar{q}_0)\right] \quad (26)$$

where

$$e_{2n+1} = \frac{-4n + 3}{8(n + 1)(2n + 1)}$$
$$\left\{\left[\frac{8n^2 + 8n + 3}{(4n + 1)(4n + 3)} - 1\right] e^{-\left(\frac{4n-1}{2}\right)\alpha_0}\right.$$
$$- \left[3 + \frac{16n^2 + 24n - 1}{(4n + 1)(4n + 3)(4n + 5)}\right] e^{-\left(\frac{4n+3}{2}\right)\alpha_0}$$
$$\left. - 4\frac{(n + 1)(2n + 1)}{(4n + 3)(4n + 5)} e^{-\left(\frac{4n+7}{2}\right)\alpha_0}\right\} \quad (27)$$

and

$$e_{2n+2} = \frac{4n + 5}{8(n + 1)(2n + 1)}$$
$$\left\{\left[\frac{8n^2 + 12n - 3}{(4n + 3)(4n + 5)} - 1\right] e^{-\left(\frac{4n+1}{2}\right)\alpha_0}\right.$$
$$+ \left[\frac{16n^2 + 40n + 15}{(4n + 3)(4n + 5)(4n + 7)} - 3\right] e^{-\left(\frac{4n+5}{2}\right)\alpha_0}$$
$$\left. - \frac{8(n + 1)(n + 2)}{(4n + 5)(4n + 7)} e^{-\left(\frac{4n+9}{2}\right)\alpha_0}\right\} \quad (28)$$

The information necessary to write the boundary conditions is now available. Equations (16), (17), (25), and (26) show that these conditions are

$$\left.\begin{aligned} f_n(\alpha = 0) &= 0 \\ g_n(\alpha = 0) &= 0 \\ f_n(\alpha = \alpha_0) &= -c_n \\ g_n(\alpha = \alpha_0) &= -d_n \end{aligned}\right\} \quad (29)$$

These equations constitute an infinite set of linear simultaneous equations. Owing to the complexity of the coefficient it is not possible to proceed to an analytic solution of equation (29). Each configuration of interest must be treated separately and the required number of the constants A_n^0, A_n^1, B_n^0, and B_n^1 computed numerically. Following the evaluation of the constants the stresses σ^c are calculated by direct substitution in equations (11), (13), and so on.

Numerical results have been obtained for the geometric configuration shown in Fig. 2. This situation was chosen because it provided a few simplifications in the computations. The surface of the cavity is defined by $\alpha_0 = 2$ and its radius is made equal to unity by setting $a = \bar{q}_0$; the center is thus 3.762 units below the plane surface. The value of P is $\pi\sqrt{2}$ and ν is taken to be 0.3. The points at which the stresses were calculated ($\alpha = 1/2$, $\beta = \pi$), ($\alpha = 2$, $\beta = \pi$), ($\alpha = 2$, $\beta = 0$), and ($\alpha = 1/2$, $\beta = 0$) are also marked in Fig. 2.

A check on the accuracy of part of the numerical mark is provided by the fact that it follows from equation (18) that

$$\sum_{n=0}^{\infty} f_n(\alpha_0) = -\mu_0 \sigma_{\alpha\alpha}{}^B \quad \text{on} \quad \beta = 0$$

$$\sum_{n=0}^{\infty} (-1)^n f_n(\alpha_0) = -\mu_0 \sigma_{\alpha\alpha}{}^B \quad \text{on} \quad \beta = \pi$$

$$1/2 \sum_{n=1}^{\infty} n(n + 1) g_n(\alpha_0) = -\mu_0 \rho^{-1} \sigma_{\alpha\beta}{}^B \quad \text{on} \quad \beta = 0$$

$$1/2 \sum_{n=1}^{\infty} (-1)^{n+1} n(n + 1) g_n(\alpha_0) = -\mu_0 \rho^{-1} \sigma_{\alpha\beta}{}^B \quad \text{on} \quad \beta = \pi$$

The values of some of the partial sums as compared with the infinite sums are presented in Tables 1 and 2. These tabulations demonstrate that if four terms of each series are used, none of the

Table 1

n	$\sum_0^n f_n(\alpha_0 = 2)$	$\sum_0^n (-1)^n f_n(\alpha_0 = 2)$
0	$+1.3041841\ 10^0$	$+1.3041841\ 10^0$
1	$-3.1303820\ 10^{-1}$	$+2.9754064\ 10^0$
2	$+3.0010356\ 10^0$	$+6.3434801\ 10^0$
3	$+1.8784104\ 10^0$	$+7.5661052\ 10^0$
4	$+2.1004145\ 10^0$	$+7.8881093\ 10^0$
Infinite sums	$+2.0449405\ 10^0$	$+7.9810948\ 10^0$

Table 2

n	$1/2 \sum_1^n n(n+1)g_n$ ($\alpha_0 = 2$)	$1/2 \sum_1^n (-1)^{n+1} n(n+1) g_n$ ($\alpha_0 = 2$)
1	$-6.3121757\ 10^{-1}$	$-6.3121747\ 10^{-1}$
2	$+4.0278149\ 10^0$	$-5.2902517\ 10^0$
3	$+1.6877731\ 10^0$	$-7.6302944\ 10^0$
4	$+2.4702908\ 10^0$	$-8.4128121\ 10^0$
5	$+2.2607583\ 10^0$	$-8.6223446\ 10^0$
Infinite sums	$+2.2827955\ 10^0$	$-8.6223446\ 10^0$

partial sums differs from the infinite sum by more than 8.5 per cent. While an increase in the number of terms in the partial sums would most likely represent a gain in accuracy it would also substantially increase the number of simultaneous equations to be solved. Thus only four terms were used in each sum and the corresponding sixteen simultaneous equations were solved for the coefficients A_n^0, A_n^1, B_n^0, and B_n^1. The stresses were calculated directly. It should be noted that all points at which the stresses were calculated lie on the z-axis on which $\sigma_{\alpha\beta} = 0$ and $\sigma_{\beta\beta} = \sigma_{\gamma\gamma}$.

It was found that all of the series for the stresses showed decreasing terms which indicated convergence. As might be expected, the series for the stresses on the cavity converge more slowly than these at points removed some distance from it. The values of the stresses are given in Table 3.

Table 3 Stresses in the half-space, containing a spherical cavity, under the action of a point load

Stress	Location	σ^c	σ^B	$\sigma^B + \sigma^c$
$\sigma_{\alpha\alpha}$	1	$-2.63\ 10^{-4}$	$-2.69\ 10^{0}$	$-2.69\ 10^{0}$
$\sigma_{\beta\beta}$	1	$-3.77\ 10^{-4}$	$-1.79\ 10^{-1}$	$-1.80\ 10^{-1}$
$\sigma_{\alpha\alpha}$	2	...	...	0
$\sigma_{\beta\beta}$	2	$-8.97\ 10^{-2}$	$-1.85\ 10^{-3}$	$-1.08\ 10^{-1}$
$\sigma_{\alpha\alpha}$	3	...	...	0
$\sigma_{\beta\beta}$	3	$-1.85\ 10^{-2}$	$-6.24\ 10^{-4}$	$-2.47\ 10^{-3}$
$\sigma_{\alpha\alpha}$	4	$-3.03\ 10^{-3}$	$-9.67\ 10^{-4}$	$-9.64\ 10^{-3}$
$\sigma_{\beta\beta}$	4	$-2.63\ 10^{-3}$	$-6.50\ 10^{-4}$	$-6.76\ 10^{-4}$

That the stress distribution is significantly changed in the immediate vicinity of the cavity is clear from the tabulated results. However, at large distances it reverts to distribution, σ^B, which exists in the absence of the cavity. It should be noted that the stress at the uppermost point of the cavity wall is over five times larger (5.84) than the stress σ^B there and that at the lowest point of the wall it is slightly less than four times as large (3.93). It is to be expected that the increase in stress at the lower point should be less than the increase at the upper point.

The Eccentric Spherical Shell

The problem of interest here is that of finding the stresses in a shell bounded by two nonconcentric spheres which is subjected to an uniform internal pressure Q. The configuration and the values to be used in the numerical example are shown in Fig. 3.

The two spherical surfaces are defined by constant values of α, $\alpha_o > 0$ for the outer and $\alpha_i > \alpha_o$ for the inner. The radii of the inner and outer spheres are $r_i = a/\bar{q}_i$ and $r_o = a/\bar{q}_o$; the distance between the centers is

$$d = a(\bar{q}_i\bar{q}_i - \bar{q}_i\bar{q}_o)/\bar{q}_o\bar{q}_i$$

The equations developed earlier are applicable because the situation is rotationally symmetric and torson free. The boundary conditions are

$$\sigma_{\alpha\alpha} = 0, \quad \sigma_{\alpha\beta} = 0 \quad \text{on} \quad \alpha = \alpha_o \tag{30}$$

$$\sigma_{\alpha\alpha} = -Q, \quad \sigma_{\alpha\beta} = 0 \quad \text{on} \quad \alpha = \alpha_i \tag{31}$$

It is readily seen that

$$\sigma_{\alpha\alpha} = \sqrt{2}\,(Q\mu_i^{-1}) \sum_{n=0}^{\infty} e^{-\frac{k}{2}\alpha_i}(2q_i + k\bar{q}_i)(k^2 - 4)^{-1}P_n(p)$$

$$= \mu_i^{-1} \sum_{n=0}^{\infty} a_n P_n(p) \tag{32}$$

on the surface $\alpha = \alpha_i$. In view of equations (11), (13), and (32), equations (30) and (31) can be written as follows

$$f_n(\alpha_o) = 0$$

$$g_n(\alpha_o) = 0$$

$$f_n(\alpha_i) = a_n \tag{33}$$

$$g_n(\alpha_i) = 0$$

These equations constitute an infinite set of simultaneous linear equations. As mentioned previously, an analytic solution is not to be hoped for and the development must be numerical.

In order to avoid excessive additional calculations the geometry was chosen to coincide, in part, with that of the previous problem; see Fig. 3. The internal pressure, Q, is $1/\sqrt{2}$ and ν is 0.3. The values of the partial sums, as compared with the infinite sums, in the boundary-condition series at the top and bottom of the inner surface are registered in Table 4. The tabulation shows that the series converges very rapidly and that if only two terms are taken in each series the partial sums differ from the infinite sums by not more than 1 per cent.

Table 4

n	$\sum_0^n a_n(\alpha_i = 2)$	$\sum_0^n (-1)^n a_n(\alpha_i = 2)$
0	$-1.3674388\ 10^{0}$	$-1.3674388\ 10^{0}$
1	$-1.1841729\ 10^{0}$	$-1.5507047\ 10^{0}$
2	$-1.1759402\ 10^{0}$	$-1.5424720\ 10^{0}$
3	$-1.1752763\ 10^{0}$	$-1.5431359\ 10^{0}$
Infinite sums	$-1.1752012\ 10^{0}$	$-1.5430806\ 10^{0}$

Equations (33) with $\alpha_i = 2$ and $\alpha_o = 1/2$ were used to calculate the unknown coefficients. Since two terms were used in each series the calculation involved the solution of eight simultaneous equations. The points at which the stresses were evaluated lie along the z-axis and on the boundaries. These points were chosen because (a) they demonstrate the variation of this stress distribution from that of the concentric shell, and (b) they possess some computational advantages.

The stresses were computed in a manner similar to that used previously. By virtue of the boundary conditions $\sigma_{\alpha\beta}$ is zero at

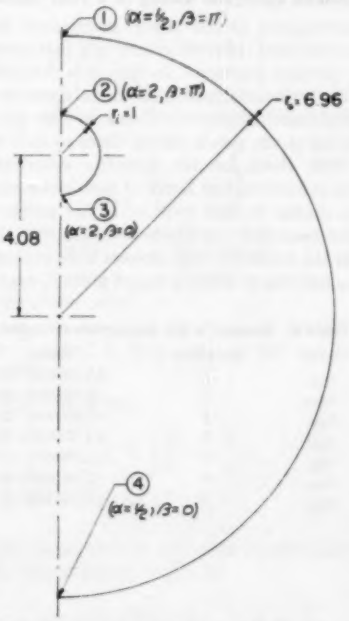

Fig. 3 Eccentric spherical shell under internal pressure

the points 1, 2, 3, and 4. $\sigma_{\alpha\alpha}$ is zero at the points 1 and 4 and is $-1/\sqrt{2}$ at the points 2 and 3. Therefore the only values which remain to be calculated are the $\sigma_{\beta\beta}$ stresses at points 1, 2, 3, and 4. These values are given in Table 5.

Table 5 Stresses in the spherical shell

Stress	Location	Value
$\sigma_{\beta\beta}$	1	$+2.2017185\ 10^{-2}$
$\sigma_{\beta\beta}$	2	$+1.3285205\ 10^{0}$
$\sigma_{\beta\beta}$	3	$+6.3065916\ 10^{-1}$
$\sigma_{\beta\beta}$	4	$+6.3870207\ 10^{-4}$

It is interesting to compare these results with these calculated for the case in which the surfaces are concentric. The stresses in the concentric shell are [7],

$$\sigma_{rr} = Qr^{-3}r_i^3(r_o^3 - r_i^3)^{-1}(r^3 - r_o^3) \tag{34}$$

and

$$\sigma_{\theta\theta} = \frac{Q}{2} r^{-3}r_i^3(r_o^3 - r_i^3)^{-1}(2r^3 + r_o^3) \tag{35}$$

radially and tangentially; where r_o and r_i stand for the outer and inner radii, respectively. Thus the values

$$\sigma_{\theta\theta} = 3.567 \times 10^{-1} \quad \text{on} \quad r = r_i$$

$$\sigma_{\theta\theta} = 3.155 \times 10^{-2} \quad \text{on} \quad r = r_o$$

are found if r_i and r_o are substituted in equation (35). These values may be compared with those for $\sigma_{\beta\beta}$ in Table 5. At point 2 the $\sigma_{\beta\beta}$ stress is 3.7 times larger than it would be if the shell were concentric, while at point 3 it is 1.8 times greater. Although the stress at point 1 is much larger proportionately than it is in the concentric case (6.8 times larger) this is not of such importance since the stress is much lower there than it is at point 2. This comparison shows that there is an important change in the stress distribution for large eccentricities and that the maximum stress is considerably increased.

The Pressurized Spherical Cavity in a Half-Space

The determination of the stress distribution surrounding a uniformly pressurized spherical cavity in a half-space is a special case of the previous problem. In fact, it is obtained by putting $\alpha_o = 0$ in the equations applicable to the eccentric shell.

The configuration adopted is shown in Fig. 4. The stresses were computed at the points shown there so that they could be compared with those for the eccentric spherical shell. The computation procedure, two terms of each series again being employed, was similar to that outlined in the previous cases. By virtue of the boundary conditions and the fact that all of the points lie on the z-axis the only stresses to be evaluated are $\sigma_{\beta\beta}$ at point 1, $\sigma_{\alpha\alpha}$ and $\sigma_{\beta\beta}$ at point 2, $\sigma_{\beta\beta}$ at point 3, $\sigma_{\beta\beta}$ at point 4, and

Table 6 Stresses in the degenerate spherical shell

Stress	Location	Value
$\sigma_{\beta\beta}$	1	$+5.4326382\ 10^{-3}$
$\sigma_{\alpha\alpha}$	2	$-8.5666697\ 10^{-4}$
$\sigma_{\beta\beta}$	2	$+1.6474441\ 10^{-3}$
$\sigma_{\beta\beta}$	3	$+1.1353586\ 10^{0}$
$\sigma_{\beta\beta}$	4	$+2.0958315\ 10^{-1}$
$\sigma_{\alpha\alpha}$	5	$-1.2918988\ 10^{-4}$
$\sigma_{\beta\beta}$	5	$+2.0811562\ 10^{-4}$

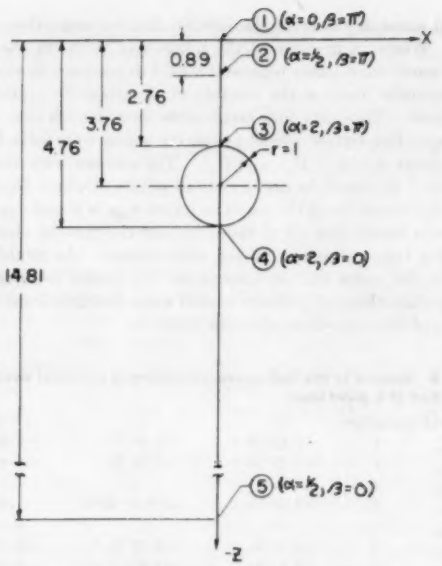

Fig. 4 Pressurized spherical cavity in a half-space

$\sigma_{\alpha\alpha}$ and $\sigma_{\beta\beta}$ at point 5. The values of these stresses are given in Table 6.

The trend of these stresses agrees quite closely with those of the spherical shell. The stress at the top of the cavity is somewhat less than that in the case of the shell, which is to be expected, the section being thicker in the present configuration. The stresses at points farther removed from the cavity decrease at a rate somewhat faster than those calculated for the eccentric spherical shell.

Acknowledgment

While the work reported in this paper was being carried out, one of the authors, J. A. Weese, held a Standard Oil Foundation Fellowship in the Department of Engineering Mechanics at Cornell University.

References

1 J. Boussinesq, "Applications des Potentiels," Gauthier-Villars, Paris, 1885.

2 P. F. Papkovich, "Solution Générale des Équations Différentielles Fondamentales d'Élasticite Éxprimée par Trois Fonctions Harmoniques," *Comptes Rendus de l'Academie des Sciences*, vol. 195, 1932, pp. 513–515, 754–756.

3 R. A. Eubanks and E. Sternberg, "On the Completeness of the Boussinesq-Papkovich Stress Functions," *Journal of Rational Mechanics and Analysis*, vol. 5, 1956, pp. 735–746.

4 E. Sternberg, "Three-Dimensional Stress Concentrations in the Theory of Elasticity," *Applied Mechanics Reviews*, vol. 2, 1958, pp. 1–4.

5 E. Sternberg and M. A. Sadowsky, "On the Axisymmetric Problem of the Theory of Elasticity for an Infinite Region Containing Two Spherical Cavities," JOURNAL OF APPLIED MECHANICS, vol. 19, TRANS. ASME, vol. 74, 1952, pp. 19–27.

6 P. M. Morse and H. Feshbach, "Methods of Theoretical Physics," McGraw-Hill Book Company Inc., New York, N. Y., 1953, Part Two, pp. 1298–1301.

7 S. Timoshenko and J. N. Goodier, "Theory of Elasticity," McGraw-Hill Book Company Inc., New York, N. Y., 1951.

Journal of APPLIED MECHANICS

Design Data and Methods

It is important that the data contained in technical papers be made readily available to design engineers. In order to satisfy these needs of industry, this section of the Journal includes a concise presentation of data and information drawn chiefly from papers previously published by the Applied Mechanics Division of The American Society of Mechanical Engineers.

Elastic-Plastic Bending of Curved Bars of Constant and Variable Thickness

H. D. CONWAY[1]

Because of its relative simplicity and practical importance, the problem of the elastic-plastic bending of curved bars by pure couples has recently been the subject of a number of theoretical investigations. For example, the plane-stress problem of a curved bar of constant thickness has been discussed in considerable detail by Swida [1][2] and the corresponding plane-strain case by Shaffer and House [2]. It is proposed to compare here some results from these investigations with those for curved bars having a particular thickness variation. Other recent studies on the elastic-plastic bending of curved bars have appeared under the authorship of Hill [3], Lubahn and Sachs [4], and Shepherd and Gaydon [5].

Considering a rectangular cross section of external radius b, internal radius a, and thickness H, subjected to equal and opposite end couples M, the problem divides naturally into three stages: (a) completely elastic, (b) plastic zone extending only from the inner radius, and (c) plastic zones extending from both the inner and outer radii culminating in complete plasticity. Assuming the maximum shearing stress or Tresca yield criterion, Swida showed, for example, that the moment M_{ult} corresponding to complete plasticity in the plane-stress case is

$$\frac{M_{ult}}{Ha^2\sigma} = \frac{1}{4}\left(2 + \alpha^2 - \frac{2\rho}{a} - \frac{\rho^2}{a^2}\right) \tag{1}$$

where σ is the yield point of the material in simple tension and $\alpha = b/a$. The radius ρ at which the two plastic zones coincide was found to be

$$1 - a/\rho = \log b/\rho \tag{2}$$

The moment M_{yp} at which plasticity just begins at $r = a$ is well known from elasticity theory to be

$$\frac{M_{yp}}{Ha^2\sigma} = \frac{(\alpha^2 - 1)^2 - 4\alpha^2(\log_e \alpha)^2}{4(1 - \alpha^2 + 2\alpha^2 \log_e \alpha)} \tag{3}$$

The plane-strain case discussed by Shaffer and House, with the same yielding criterion, gave somewhat simpler results:

$$\frac{M_{ult}}{Ha^2\sigma} = \frac{1}{4}(\alpha - 1)^2 \tag{4}$$

$$\rho^2 = ab \tag{5}$$

$$\frac{M_{yp}}{Ha^2\sigma} = \frac{(\alpha^2 - 1)^2 - 4\alpha^2(\log_e \alpha)^2}{4(1 - \alpha^2 + 2\alpha^2 \log_e \alpha)} \tag{6}$$

Quite recently, it has been shown by the writer [6] during a discussion of elastic plane-stress with variable thickness that, for the particular thickness variation $h = h_0/r^2$, the absolute values of the circumferential stresses at the inner and outer faces of the bar are the same. From this investigation, the moment M_{yp} which will first cause simultaneous yielding at these faces is:

$$\frac{M_{yp}}{Ha^2\sigma} = \frac{(\alpha^{\lambda/2} + \alpha^{-\lambda/2})\lambda \log_e \alpha - 2\alpha^{\lambda/2} + 2\alpha^{-\lambda/2}}{\lambda^2(\alpha^{\lambda/2} - \alpha^{-\lambda/2})} \tag{7}$$

where $H = h_0/a^2$ is now the thickness at the inner radius a and $\lambda^2 = 2(1 + \nu)$. It is interesting to compare this moment (assuming $\nu = 0.28$), the radius ρ at which the plastic zones coincide, and the fully plastic moment M_{ult} for this case, with the results given, respectively, by equations (1)–(6).

To investigate the plastic bending of a bar of variable thickness, subjected to couples decreasing the curvature, the equation of equilibrium for the outer portion is, with the Tresca yield criterion:

$$r\frac{d}{dr}(h\sigma_r) = h(\sigma_\theta - \sigma_r) = -h\sigma \tag{8}$$

Writing $h = h_0/r^2$, integrating and finding the constant of integration from $\sigma_r = 0$ at $r = b$, the stresses in the outer plastic zone are

$$\sigma_r = \frac{\sigma}{2}\left(1 - \frac{r^2}{b^2}\right)$$
$$\sigma_\theta = -\frac{\sigma}{2}\left(1 + \frac{r^2}{b^2}\right) \tag{9}$$

For the inner plastic zone

$$r\frac{d}{dr}(h\sigma_r) = h(\sigma_\theta - \sigma_r) = h(\sigma - \sigma_r) \tag{10}$$

which, on integrating, gives

$$\sigma_r = \left(\frac{r}{a} - 1\right)$$
$$\sigma_\theta = \sigma \tag{11}$$

Equating the values of σ_r in equations (9) and (11), the radius ρ at which the plastic zones coincide is

$$\frac{\rho}{a} = \alpha[(\alpha^2 + 3)^{1/2} - \alpha], \qquad \alpha = \frac{b}{a} \tag{12}$$

---

[1] Professor of Mechanics, Cornell University, Ithaca, N. Y.

[2] Numbers in brackets indicate References at end of paper.

Discussion of this paper should be addressed to the Secretary, ASME, 29 West 39th Street, New York 18, N. Y., and will be accepted until January 10, 1961, for publication at a later date. Discussion received after the closing date will be returned.

Manuscript received by ASME Applied Mechanics Division, April 12, 1960.

Table 1 Comparison of moments for elastic-plastic bending of curved bars bent by pure couples

$\frac{M_{yp}}{Ha^2\sigma} = k_1, \frac{M_{ult}}{Ha^2\sigma} = k_2$

$\alpha = b/a$		3	2	1.5	1.25
Plane stress (constant thickness)					
	k_1	0.436	0.129	0.036	0.0096
	k_2	0.926	0.237	0.060	0.0153
	k_2/k_1	2.12	1.84	1.67	1.62
	ρ/a	1.88	1.45	1.24	1.12
Centroid/inner radius ratio $(\alpha + 1)/2$		2.00	1.50	1.25	1.25
Plane strain	k_1	0.436	0.129	0.036	0.0096
	k_2	1.000	0.250	0.063	0.0156
	k_2/k_1	2.29	1.94	1.74	1.62
	ρ/a	1.73	1.41	1.22	1.12
Centroid/inner radius ratio $(\alpha + 1)/2$		2.00	1.50	1.25	1.125
Plane stress (variable thickness)					
	k_1	0.1915	0.0786	0.0275	0.0081
	k_2	0.230	0.109	0.041	0.012
	k_2/k_1	1.20	1.38	1.48	1.51
	ρ/a	1.39	1.29	1.19	1.11
Centroid/inner radius ratio $\alpha \log \alpha(\alpha - 1)$		1.65	1.39	1.22	1.12

The fully plastic moment M_{ult} is then

$$M_{ult} = -\int_a^\rho hr\sigma\, dr + \int_\rho^b \frac{\sigma h r}{2}\left(1 + \frac{r^2}{b^2}\right) dr \qquad (13)$$

which, with equation (12), can be evaluated in the form

$$\frac{M_{ult}}{Ha^2\sigma} = \frac{1}{2}\left[\alpha(\alpha^2 + 3)^{1/2} - \alpha^2 - 1\right]$$

$$- \frac{1}{2}\log \alpha^2\left[(4\alpha^2 + 3)(\alpha^2 + 3)^{1/2} - 4\alpha^2 - 9\alpha\right] \qquad (14)$$

As might be expected, the total force

$$\int_a^\rho h\sigma\, dr - \int_\rho^b \frac{h\sigma}{2}\left(1 + \frac{r^2}{b^2}\right) dr$$

on any radial section is zero, if ρ is given by equation (12).

Values of $k_1 = M_{yp}/Ha^2\sigma$, $k_2 = M_{ult}/Ha^2\sigma$, k_2/k_1 and ρ/a for the three cases have been calculated for four values of the radius ratio b/a, and are presented in Table 1 for the purpose of comparison.

It is seen from Table 1 that the radius ρ at which the two plastic zones coincide is a little less than the radius of the centroid of the cross section in all three cases. As would be expected, ρ approaches $(a + b)/2$ as the radius ratio b/a approaches unity. In the plane-stress (constant-thickness) and plane-strain cases, the values of $k_2/k_1 = M_{ult}/M_{yp}$ increase with increase of b/a, whereas they decrease in the plane-stress (variable-thickness) case.

References

1 W. Swida, "Die elastisch-plastische Biegung des krummen Stabes," *Ingenieur-Archiv*, vol. 16, 1948, p. 357.

2 B. W. Shaffer and R. N. House, Jr., "The Elastic-Plastic Stress Distribution Within a Wide Curved Bar Subjected to Pure Bending," JOURNAL OF APPLIED MECHANICS, vol. 22, TRANS. ASME, vol. 77, 1955, p. 305.

3 R. Hill, "The Mathematical Theory of Plasticity," Oxford University Press, London, England, 1950, p. 287.

4 J. D. Lubahn and G. Sachs, "Bending of an Ideal Plastic Metal," TRANS. ASME, vol. 72, 1950, p. 201.

5 W. M. Shepherd and F. A. Gaydon, "Plastic Bending of a Ring Sector by Couples," *Journal of the Mechanics and Physics of Solids*, vol. 5, 1957, p. 296.

6 H. D. Conway, "Analysis of Plane Stress in Polar Co-Ordinates," JOURNAL OF APPLIED MECHANICS, vol. 26, TRANS. ASME, vol. 81, Series E, 1959, p. 437.

Journal of APPLIED MECHANICS

Brief Notes

On the recommendation of the Executive Committee of the ASME Applied Mechanics Division, it was decided to initiate a section devoted to brief notes on technical matters in mechanics. These notes must not be longer than 750 words (about 2½ double-spaced typewritten pages, including figures) and will be subject to the usual review procedure prior to publication. After approval such notes will be published as soon as possible, normally in the next issue of the Journal. The notes should be submitted to the Technical Editors of the Journal of Applied Mechanics.

Graphical Investigation of Geometric Aspects of the Hertz Problem

D. C. GAZIS[1]

THE HERTZ solution of the problem of contact stresses [1][2] begins with a consideration of the geometry of two quadratic surfaces in the neighborhood of the center of contact. This consideration provides information regarding the applicability of the Hertz solution and the principal directions of the elliptic area of contact under pressure.

This note presents a discussion of the geometric aspects of the Hertz solution by means of a simple graphical construction. Such an investigation can, of course, be carried out in terms of the analytical relationships available. However, the graphical construction presented here provides an easy and complete visual investigation of the geometric aspects involved for any position which the two solids in contact may assume after a relative rotation about the axis of contact.

It will be convenient to give the appropriate relationships using tensor notation and the indicial notation of summation and differentiation. The two surfaces are referred to the co-ordinate systems x_1, x_2, x_3', and x_1, x_2, x_3'', respectively, with x_1, x_2 on the common tangent plane and x_3', x_3'' along the normal through the center of contact, on the two opposite sides of the tangent plane. The ordinates x_3' and x_3'' in the neighborhood of the center of contact are expressed as quadratic functions of x_1 and x_2, after expansion in Taylor series and truncation, according to the equations

$$x_3' \approx \left(\frac{1}{2}\right) x_i A_{ij} x_j,$$

$$x_3'' \approx \left(\frac{1}{2}\right) x_i B_{ij} x_j, \qquad i, j = 1, 2 \tag{1}$$

where A_{ij} and B_{ij} are the curvature tensors of the two surfaces given by

$$A_{ij} = x_3'_{,ij}, \qquad B_{ij} = x_3''_{,ij}. \tag{2}$$

The relative distance of the two surfaces is also given, in general, by a quadratic function of x_1 and x_2, namely,

$$x_3 = \left(\frac{1}{2}\right) x_i C_{ij} x_j, \tag{3}$$

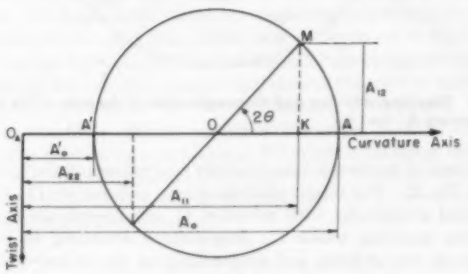

Fig. 1 Mohr's circle for the curvature tensor

where

$$C_{ij} = A_{ij} + B_{ij}. \tag{4}$$

The tensor C_{ij} provides two answers regarding the Hertz problem. First, it indicates whether or not the Hertz solution is applicable from geometric considerations alone. This is so only if the eigenvalues of C_{ij} are both positive or, equivalently, if the relative indicatrix [2]

$$x_i C_{ij} x_j = \text{const} \tag{5}$$

is an ellipse. And second, the eigenvectors of C_{ij} define the principal directions of the elliptic area of contact given by the Hertz solution.

Two graphical representations of quadratic surfaces come to mind, namely, the method of the "Dupin indicatrix" [3] and the method of the "Mohr circle" [4]. Dupin's description, although very illustrative, does not appear to yield a simple graphical investigation of the geometry of the Hertz problem, but Mohr's method is more promising. The representation of a curvature tensor by a Mohr circle is shown in Fig. 1. As is well known, the components of a tensor such as A_{ij} with respect to an arbitrary system x_1, x_2 are given in terms of its eigenvalues A_0 and A_0' and the angle θ measured from the direction associated with A_0 to the direction x_1, according to

$$A_{11} = \left(\frac{1}{2}\right)(A_0 + A_0') + \left(\frac{1}{2}\right)(A_0 - A_0') \cos 2\theta$$

$$A_{22} = \left(\frac{1}{2}\right)(A_0 + A_0') - \left(\frac{1}{2}\right)(A_0 - A_0') \cos 2\theta, \tag{6}$$

$$A_{12} = -\left(\frac{1}{2}\right)(A_0 - A_0') \sin 2\theta,$$

where the angle θ is positive counterclockwise. A simple graphical diagonalization of a tensor may be obtained on the basis of Equations (6), see ref. [5]. The graphical investigation of the Hertz problem may now be accomplished as follows: The tensors A_{ij} and B_{ij} are diagonalized and represented by Mohr circles whose axes make an angle 2ϕ, where ϕ is the angle between the

---

[1] Research Laboratories, General Motors Corporation, Warren, Mich.

[2] Numbers in brackets indicate References at end of Note.

Discussion of papers in Brief Notes should be addressed to the Secretary, ASME, 29 West 39th Street, New York, N. Y., and will be accepted until January 10, 1961, for publication at a later date. Discussion received after the closing date will be returned.

Manuscript received by ASME Applied Mechanics Division, March 18, 1960.

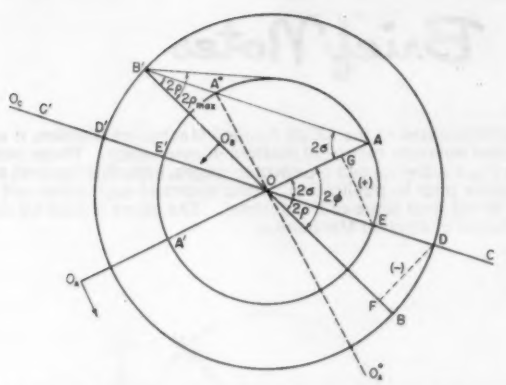

Fig. 2 Graphical addition and diagonalization of the sum of the curvature tensors A_{ij} and B_{ij}

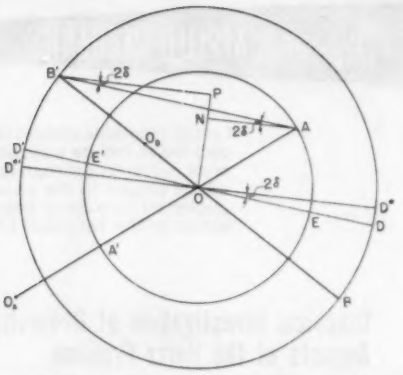

Fig. 3 Graphical demonstration that diagonalization yields stationary values for diagonal terms

directions of maximum (algebraically) curvatures of the two surfaces, Fig. 2. The tensor addition shown in Equation (4) can be executed graphically with reference to any co-ordinate system, and the resulting tensor C_{ij} diagonalized according to Fig. 1. However, the addition and diagonalization can be accomplished in one operation. It is observed that the components A_{12} and B_{12}, referred to the principal co-ordinate system of C_{ij} must satisfy the relationship

$$A_{12} = -B_{12}. \tag{7}$$

Thus the axis of the Mohr circle for C_{ij} will be a line $D'D$, Fig. 2, such that

$$(EG) = (DF) \tag{8}$$

or

$$\begin{aligned} (OA) \sin 2\sigma &= (OB) \sin 2\rho, \\ (OA)/\sin 2\rho &= (OB)/\sin 2\sigma, \end{aligned} \tag{9}$$

where σ and ρ are the angles of the principal axis of C_{ij} corresponding to OD with the axes of maximum curvature of A_{ij} and B_{ij}, respectively. Equations (8) and (9) lead to the construction of $D'D$ as the line through O parallel to the line $B'A$, where B' is the point of minimum curvature of the larger Mohr circle and A the point of maximum curvature of the smaller Mohr circle. The eigenvalues of C_{ij} can be obtained by performing the addition of the tensors A_{ij} and B_{ij} with respect to the principal system of C_{ij}, with the result

$$\begin{aligned} C_0 &= \frac{1}{2}(I_c + C_t), \\ C_0' &= \frac{1}{2}(I_c - C_t), \end{aligned} \tag{10}$$

where

$$\begin{aligned} I_c &= (A_0 + A_0' + B_0 + B_0'), \\ C_t &= 2(B'A) = [(A_0 - A_0') \cos 2\sigma + (B_0 - B_0') \cos 2\rho]. \end{aligned} \tag{11}$$

It is seen that the direction of maximum eigenvalue for C_{ij} is obtained between the directions of maximum eigenvalue for A_{ij} and B_{ij}. The preceding construction is always possible and yields a complete description of the relative indicatrix of the two surfaces under consideration. If both $C_0 = (O_cC)$ and $C_0' = (O_cC')$ are positive, then this indicatrix is an ellipse, the Hertz solution is applicable, and the eigenvectors of C_{ij} define the principal directions of the elliptic area of contact. It is interesting to note that if the body with the greater variation of curvature, B_{ij}, is kept fixed and the other one, A_{ij}, is rotated about the axis of contact, there are, in general, two different positions of the body A_{ij} which yield the same principal directions for C_{ij}, although not the same eigenvalues. These two positions are the one corresponding to O_AA, and one which may be defined as its "conjugate position," corresponding to $O_A{}^*A^*$, Fig. 2. To this conjugate position correspond the eigenvalues of C_{ij} given by

$$\begin{aligned} C_0 &= \left(\frac{1}{2}\right)(I_c + C^*_t), \\ C_0' &= \left(\frac{1}{2}\right)(I_c - C^*_t), \end{aligned} \tag{12}$$

where

$$C^*_t = 2(B'A^*) = [-(A_0 - A_0') \cos 2\sigma + (B_0 - B_0') \cos 2\rho]. \tag{13}$$

It is also observed that the maximum possible angle of OD with OB corresponds to a relative position of the two bodies such that the line $B'A$ is tangent to the smaller Mohr circle, in which case the two conjugate positions of the body A_{ij} with respect to B_{ij} coincide. The angle ρ_{max}, Fig. 2, is given by

$$\rho_{max} = \left(\frac{1}{2}\right) \sin^{-1} \frac{A_0 - A_0'}{B_0 - B_0'} \leq \frac{\pi}{4}. \tag{14}$$

One last remark regarding what might be regarded as a graphical differentiation: It is possible to show graphically that the construction of Fig. 2 yields stationary values for the diagonal terms of C_{ij}. Consider, for example, a direction OD^* making a small angle 2δ with OD, Fig. 3. The addition of the tensors A_{ij} and B_{ij} with respect to a co-ordinate system corresponding to $D^*{}'OD^*$ yields, for the diagonal terms of C_{ij},

$$\begin{aligned} C_{11} &= \frac{1}{2} I_c + [(AN) + (B'P)], \\ C_{22} &= \frac{1}{2} I_c - [(AN) + (B'P)], \end{aligned} \tag{15}$$

where OP is perpendicular to AN and $B'P$.

It is seen that

$$(AN) + (B'P) < (B'A) \tag{16}$$

hence C_0 and C_0' are stationary values of the diagonal terms of C_{ij}.

References

1 H. Hertz, "Ueber die Berührung Fester Elastischer Körper," *Journal für die reine und angewandte Mathematik* (Crelle), vol. 92, 1882, pp. 156–171. See also S. Timoshenko and J. N. Goodier, "Theory of Elasticity," McGraw-Hill Book Company, Inc., New York, N. Y., 1951, p. 372.

2 A. E. H. Love, "A Treatise on the Mathematical Theory of Elasticity," Dover Publications, New York, N. Y., 1944, p. 194.

3 Gino Loria, "Die Hauptsächlisten Theorien der Geometrie" (translated by F. Schütte), B. G. Teubner, Leipzig, 1888, p. 49.

4 Otto Mohr, "Ueber die Darstellung der Spannungszustandes und des Deformationszustandes eines Koerperelementes und ueber die Anwendung derselben in der Festigkeitslehre," *Zivilingenieur*, vol. 28, 1882, pp. 113–156.

5 See, for example, S. Timoshenko, "Theory of Plates and Shells," McGraw-Hill Book Company, Inc., New York, N. Y., 1940, p. 38.

The Effect of Axial Constraint on the Instability of Thin Circular Cylindrical Shells Under External Pressure[1]

J. SINGER[2]

Nomenclature

A, B, C = parameters
C_p = critical pressure coefficient defined by Equation (17)
D = diameter of shell
E = modulus of elasticity
h = thickness of shell
k = spring constant of axial elastic restraint
K = constant defined by Equation (6)
L = length of shell
p = hydrostatic pressure
R = radius of shell
t = number of circumferential waves
u = axial displacement
u_1 = axial displacement due to lateral pressure p only
u_2 = axial displacement due to axial stresses resulting from the pressure p on the end bulkheads and the restraining forces
v = circumferential displacement
w = radial displacement
Z = geometric parameter defined by Equation (18)
$\alpha = \beta L/2$ = constant defined by Equation (8)
β = constant defined by Equation (7)
γ = constant defined by Equation (5)
ν = Poisson's ratio
$\bar{\sigma}_x, \bar{\sigma}_\phi, \bar{\tau}_{x\phi}$ = membrane stresses prior to buckling
ϕ = circumferential co-ordinate

THE USUAL analysis of the stability of simply supported thin cylindrical shells under external pressure implies free warping normal to the curved edges (see, for example, [1]).[3] When there is some axial restraint, it is generally assumed that its effect on the buckling stresses can be neglected (see, for example, [2]). This assumption, however, is based only on physical considerations and on inference from analysis for the case of torsion. For this latter case, Donnell [3] discusses over-all axial constraint and shows that it makes no difference whether or not the ends are free to move as a whole; whereas Batdorf [4] compares results calculated under the customary simple support assumption $u \neq 0, v = 0$ with those of Leggett [5], for $u = 0, v = 0$, and finds very close agreement. The physical argument is presented clearly by Batdorf [4] stating that since the only difference between the buckling behavior of a cylindrical shell and that of a flat plate is due to the effect of the circumferential stresses caused by the buckling deformations, axial restraint, requiring application of axial stresses, will have but small effect on the buckling stresses.

To determine the effect of axial restraint from analysis rather than by physical argument, the instability of a cylindrical shell under hydrostatic pressure is analyzed by a Rayleigh-Ritz approach.

Two types of axial elastic restraints can be envisaged: (*a*) Restraints which are active from the beginning of loading, and (*b*) restraints which come into action only at the onset of buckling. Restraints of type (*a*) first reduce the axial stress applied to the cylinder by the external pressure, and then at the onset of buckling their effect is identical to that of restraints of type (*b*). The analysis therefore actually considers the effect of axial elastic restraints which come into action at the onset of buckling for two states of prebuckling stress. However, it will be shown that the difference in the axial prebuckling stress has only a very small influence on the critical pressure.

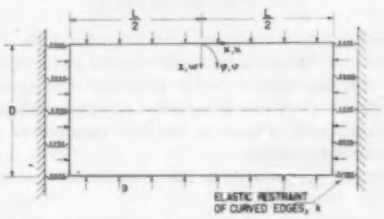

Fig. 1 Cylindrical shell under hydrostatic pressure with elastic restraint along curved edges

For a thin cylindrical shell under hydrostatic pressure, Fig. 1, with restraints of type (*b*), the stress state prior to buckling is given by the usual membrane stresses

$$\bar{\sigma}_x = -(pR/h) \tag{1}$$

$$\bar{\sigma}_\phi = -(pR/2h) \tag{2}$$

$$\bar{\tau}_{x\phi} = 0 \tag{3}$$

For restraints of type (*a*), which are active also during the loading process, the hoop stress and shear stress are as above, but the axial prebuckling stress is changed from Equation (1) to

$$\bar{\sigma}_x = -\gamma(pR/2h) \tag{4}$$

where

$$\gamma = 1 - K\{(1 - 2\nu) + (2\nu/\beta L)[(\sinh 2\alpha + \sin 2\alpha)/(\cosh 2\alpha + \cos 2\alpha)]\} \tag{5}$$

$$K = [1 + (2E/kL)]^{-1} \tag{6}$$

$$\beta^4 = 3(1 - \nu^2)/R^2h^2 \tag{7}$$

$$\alpha = \beta L/2 \tag{8}$$

To derive Equation (4), one notes that the axial displacement u is composed of u_1 due to the lateral pressure p only, and u_2 due to the superposed axial stress resulting from the pressure p on the end bulkheads and the restraining forces. From [6] one obtains, after integration, u_1 at the boundary

$$(u_1)_{L/2} = (\nu pR/2\beta Eh)[\beta L - (\sinh 2\alpha + \sin 2\alpha)/(\cosh 2\alpha + \cos 2\alpha)] \tag{9}$$

[1] This work was sponsored in part by the European Office, Air Research and Development Command, U. S. Air Force, under Contract AF 61 (052)-123, through the Technion Research and Development Foundation.

[2] Senior Lecturer, Department of Aeronautical Engineering, Israel Institute of Technology, Haifa, Technion City, Israel.

[3] Numbers in brackets indicate References at end of Note.

Manuscript received by ASME Applied Mechanics Division, February 16, 1960.

Integration of the axial strain caused by the pressure on the end bulkheads and the restraints yields

$$u_1 = (1/E)[-(xpR/2h) - xk(u)_{L/2}] \tag{10}$$

The total axial displacement at the boundary is therefore

$$(u)_{L/2} = [(u_1)_{L/2} - (pRL/4Eh)]/[1 + (kL/2E)] \tag{11}$$

now

$$\partial_x = -(pR/2h) - k(u)_{L/2} \tag{12}$$

and Equation (4) is arrived at after some manipulation.

The analysis is now carried out for restraints of type (a), bearing in mind that the results reduce to those for restraints of type (b) if one sets $\gamma = 1$.

The displacement boundary conditions of the problem are

$$\begin{aligned} w &= 0 \\ v &= 0 \end{aligned} \qquad \text{at} \quad x = \pm L/2 \tag{13}$$

Hence the usual displacement functions for the case of hydrostatic pressure,

$$\begin{aligned} u &= A \sin t\phi \sin (\pi x/L) \\ v &= B \cos t\phi \cos (\pi x/L) \\ w &= C \sin t\phi \cos (\pi x/L) \end{aligned} \tag{14}$$

satisfy these boundary conditions and are admissible.

Substitution of the assumed displacement functions, Equations (14), into the appropriate total potential energy expression (Equation (1) of [7]), which includes the prebuckling stresses, and minimizing with respect to the free parameters yields the usual stability determinant.

Hence the critical pressure in the presence of axial constraints is

$$p_k = [2hE/(1 - \nu^2)R][\gamma(\pi/L)^2 + 2(t/R)^2]^{-1}$$

$$\left\{(h^2/12)[(\pi/L)^2 + (t/R)^2]^2 + \frac{(1 - \nu^2)(\pi/LR)^2[(\pi/L)^2 + (4k/LE)]}{[(\pi/L)^2 + (t/R)^2]^2 + [4(1 + \nu)k/LE][2(t/R)^2 + (1 - \nu)(\pi/L)^2]}\right\} \tag{15}$$

In the absence of axial constraints, $k = 0$ and the critical pressure becomes

$$p_0 = [2hE/(1 - \nu^2)R]\ [(\pi/L)^2 + 2(t/R)^2]^{-1}$$

$$\{(h^2/12)[(\pi/L)^2 + (t/R)^2]^2$$

$$+ [(1 - \nu^2)/R^2](\pi/L)^4[(\pi/L)^2 + (t/R)^2]^{-2}\} \tag{16}$$

Equation (16) is equivalent to that derived by von Mises [8].

In Equations (15) and (16) the integral value of t (the number of lobes) which makes p a minimum must be used. For the case without axial constraint, a method for the determination of the correct value of t is given in [9]. In the presence of axial constraint, the number of lobes for minimum p depends also on k and may be larger than the t found from [9], since the energy absorbed by the elastic restraint decreases with increasing t.

The critical pressure in the presence or absence of axial elastic restraint has been calculated from Equations (15) and (16), for an extensive range of relative length (L/D), for four values of elastic restraint of type (a), (k/E) = 0.001, 0.01, 0.02, and 0.05; and three values of relative thickness (h/D) = 0.001, 0.003, 0.005.

General curves are obtained by transformation of the results to the parametric form suggested by Batdorf [4]. All relative thicknesses are then included in one curve. After a number of cases have been computed from Equations (15) and (16) and the typical ripples are smoothed out, the ratio of pressure parameters, C_{pk} to C_{p0}, is plotted versus the geometric parameter Z, Fig. 2. where

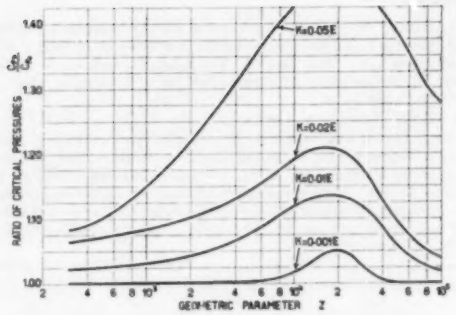

Fig. 2 Increase in critical pressure due to axial elastic restraint

$$C_p = \left(\frac{p_c}{E}\right)(1 - \nu^2)\left(\frac{6}{\pi^2}\right)\left(\frac{L}{D}\right)^2\left(\frac{D}{h}\right)^2 \tag{17}$$

and

$$Z = 2\sqrt{1 - \nu^2}\left(\frac{L}{D}\right)^2\left(\frac{D}{h}\right) \tag{18}$$

These curves represent design curves for the estimation of the effect of axial elastic restraint on cylindrical shells under hydrostatic pressure.

Now, since the entire effect of the restraint on the axial displacements prior to buckling is included in γ, the effect of γ on p_k will indicate the difference between the critical pressures for the two types of restraint.

It can be shown from Equation (15), however, that the effect of γ on p_k is very small indeed. Since $(\pi/L)^2 \ll 2(t/R)^2$, the term $[\gamma(\pi/L)^2 + 2(t/R)^2]$ will hardly differ from $[(\pi/L)^2 + 2(t/R)^2]$ even when γ is as low as 0.5 (the lowest possible practical value toward which γ would tend: for a very short shell of $L/D = 0.2$ and $k \to \infty$). It may be noted that the relation $(\pi/L)^2 \ll 2(t/R)^2$ will be preserved over the entire (L/D) range, since t becomes very large for small (L/D) ratios.

Numerical calculations which were carried out in order to obtain a more accurate estimate of the order of magnitude of the effect of γ on p_k [7] show that the contribution of γ is always less than 1 per cent, and in most cases even much less than 0.1 per cent. It can therefore be concluded that for practical purposes the difference is negligible, and that the effect of axial elastic restraints which are active from the beginning of loading is nearly identical to that of restraints which come into action only at the onset of buckling. Fig. 2 represents, therefore, the effect of axial restraint of both types on the critical pressure.

The instability of a cylindrical shell under uniform external lateral pressure only can be analyzed in a similar manner [7].

Acknowledgment

The author would like to express his gratitude to Professor N. J. Hoff of Stanford University, Stanford, Calif., for suggesting the analysis and for his helpful advice.

References

1 S. Timoshenko, "Theory of Elastic Stability," McGraw-Hill Book Company, Inc., New York, N. Y., 1936, p. 448.

2 G. Gerard and H. Becker, "Handbook of Structural Stability, Part 3, Buckling of Curved Plates and Shells," NACA TN 3783, 1957.

3 L. M. Donnell, "Stability of Thin-Walled Tubes Under Torsion," NACA Report No. 479, 1933.
4 S. B. Batdorf, "A Simplified Method of Elastic Stability Analysis for Thin Cylindrical Shells," NACA Report No. 874, 1947.
5 D. M. A. Leggett, "The Initial Buckling of Slightly Curved Panels Under Combined Shear and Compression," R & M 1972, British ARC, 1943.
6 S. Timoshenko, "Theory of Plates and Shells," McGraw-Hill Book Company, Inc., New York, N. Y., 1940, pp. 391 and 400.
7 J. Singer, "The Effect of Axial Constraint on the Instability of Thin Circular Cylindrical Shells Under External Pressure," Technion, Israel Institute of Technology, Department of Aeronautical Engineering, Report No. 2, May, 1959. Also Technical Note No. 1, Contract AF 61 (052)-123, September, 1959.
8 R. von Mises, "Der kritische Aussendruck für allseits belastete zylindrischer Rohre," Fest. zum 70 Geburtstag von Prof. Dr. A. Stodola, Zurich, 1929, pp. 418–432.
9 D. F. Winderburg and C. T illing, "Collapse by Instability of Thin Cylindrical Shells Under External Pressure," TRANS. ASME, vol. 56, 1934, pp. 819–825.

Coupled Bending and Torsional Vibrations of Restrained Thin-Walled Beams

Y. K. LIN[1]

IN A former paper,[2] coupled bending and torsional vibrations were discussed for open thin-walled beams with boundary restraints at the end sections only. Beams of this type are often used as stiffeners in aircraft structures and are rigidly attached to the skin. The additional restraints along the length of a beam due to such an attachment greatly alter its dynamic characteristics. The skin provides very large resistance along the line of attachment against movement in the plane of the skin, but only small resistance in the direction perpendicular to the skin. In the following discussions, the problem can be idealized such that the movement in the plane of the skin is zero at the beam-skin attachment.

In line with the nomenclature[3] used in the previous paper, and the additional symbols specified in Fig. 1, the equations of coupled vibration can be written according to d'Alembert's principle as the following:

$$\left.\begin{aligned} &EI_\eta w^{IV} + EI_{\eta\zeta} v^{IV} = -mA(\ddot{w} + c_y\ddot{\phi}) - h_z \\ &EI_\zeta v^{IV} + EI_{\eta\zeta} w^{IV} = -mA(\ddot{v} - c_z\ddot{\phi}) \\ &EC_w\phi^{IV} - GC\phi'' = -mI_p\ddot{\phi} - mA(\ddot{w} + c_y\ddot{\phi})c_y \\ &\qquad\qquad + mA(\ddot{v} - c_z\ddot{\phi})c_z - h_z s_y \end{aligned}\right\} \quad (1)$$

The centroidal axes η, are perpendicular and parallel to the skin in the present case, and they are not necessarily the principal axes. As implied in Fig. 1(*c*), the significant restraining forces from the skin are assumed to be distributed in the plane of the skin in the formulation of Equations (1). The restraining forces perpendicular to the skin and the restraining twisting moment from the skin are both neglected. This is reasonable when the bending stiffness of the skin is much smaller than the twisting stiffness of the beam, and when the spacings between the beams are large.

[1] Assistant Professor of Aeronautical Engineering, University of Illinois, Urbana, Ill.

[2] J. M. Gere and Y. K. Lin, "Coupled Vibrations of Thin-Walled Beams of Open Cross Section," JOURNAL OF APPLIED MECHANICS, vol. 25, TRANS. ASME, vol. 80, 1958, pp. 373–378.

[3] C_w = warping constant with respect to shear center, 0; C = torsion constant; I_p = centroidal polar moment of inertia; m = mass density; and so on.

Manuscript received by ASME Applied Mechanics Division, June 11, 1959; final draft received December 28, 1959.

By hypothesis, there is no displacement in the z-direction at the attachment to the skin, therefore,

$$w + s_y\phi = 0 \quad \text{or} \quad w = -s_y\phi \quad (2)$$

By eliminating w and h_z, Equations (1) are reduced to two simultaneous equations:

$$\left.\begin{aligned} &EI_\zeta v^{IV} - EI_{\eta\zeta} s_y \phi^{IV} + mA\ddot{v} - mAc_z\ddot{\phi} = 0 \\ &EC_{ws}\phi^{IV} - GC\phi'' - EI_{\eta\zeta} s_y v^{IV} + mI_s\ddot{\phi} - mAc_z\ddot{v} = 0 \end{aligned}\right\} \quad (3)$$

where

$I_s = I_p + A(s_y - c_y)^2 + Ac_z^2$
= the polar moment of inertia of the section with respect to S, the intersection line of the x-y plane and the skin

$C_{ws} = C_w + I_\eta s_y^2$
= the warping constant of the section with respect to S

It is seen that the additional restraint at the skin changes a triple-coupling problem to a double-coupling one in which only the vibrations in the v and ϕ directions are coupled with one another. Thus solution of Equations (3) follows the same procedure outlined in the previous paper for the double-coupling case. In actual application of the theory, however, it is reasonable to include effective widths of the skin in computing the area and bending stiffness for the beam cross section. The numerical solution of Equations (3) becomes quite laborious for beams which are not simply supported at both ends. An energy method is sometimes advantageous for computing the approximate natural frequencies for such cases. In agreement with the restraint condition specified by Equation (2), the strain and kinetic energies of a vibrating beam are, respectively,

$$U = \tfrac{1}{2}\left[EI_\zeta \int_0^l v''^2\,dx - 2EI_{\eta\zeta} s_y \int_0^l v''\phi''\,dx + GC\int_0^l \phi'^2\,dx + E\int_0^l \phi''^2\,dx\right] \quad (4)$$

$$T = \frac{mA}{2}\left[\int_0^l \dot{v}^2\,dx - 2c_z\int_0^l \dot{v}\dot{\phi}\,dx\,\frac{I_s}{A}\int_0^l \dot{\phi}\,dx\right] \quad (5)$$

Each of the deformations, v and ϕ, can be written as the product of an arbitrary amplitude, an assumed normal function of x satisfying the boundary conditions, and a harmonic time function. Following the Rayleigh-Ritz procedure outlined in the previous paper,[2] an expression for the squared values of natural frequencies, p_n^2, can be written by equating the maximum kinetic and strain energies. This expression is then minimized with

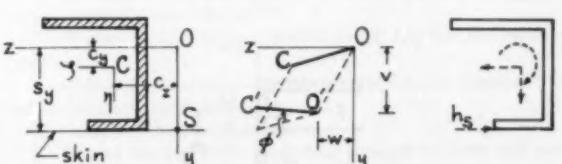

(a) Coordinates (b) Displacements (c) Dynamic Loads

Fig. 1 Thin-walled beam attached to skin in one direction

respect to the arbitrary amplitudes, and the following equation is obtained:

$$\left(\frac{p_n^2}{p_y^2}\right)^2\left(1-\alpha\frac{Ac_y^2}{I_n}\right)-\left(\frac{p_n^2}{p_y^2}\right)\left\{1+\left(\frac{p_\phi^2}{p_y^2}\right)-\gamma\frac{2EI_{\eta\zeta}s_yc_z}{mI_n p_y^2}\right\}+\left(\frac{p_\phi^2}{p_y^2}\right)-\delta\left(\frac{1}{AI_n}\right)\left(\frac{EI_{\eta\zeta}s_y}{mp_y^2}\right)^2=0 \quad (6)$$

where

$$\alpha=\frac{\left(\int_0^l X_y X_\phi dx\right)^2}{\int_0^l X_y^2dx\int_0^l X_\phi^2dx}=\text{a factor, dimensionless}$$

$$\gamma=\frac{\int_0^l X_y''X_\phi''dx\int_0^l X_yX_\phi dx}{\int_0^l X_y^2dx\int_0^l X_\phi^2dx}=\text{a factor, [length]}^{-2}$$

$$\delta=\frac{\left(\int_0^l X_y''X_\phi''dx\right)^2}{\int_0^l X_y^2dx\int_0^l X_\phi^2dx}=\text{a factor, [length]}^{-4}$$

$$p_y=\left(\frac{EI_\phi\int_0^l X_y''^2dx}{mA\int_0^l X_y^2dx}\right)^{1/2}=\text{uncoupled frequency in the } y\text{-direction}$$

$$p_\phi=\left(\frac{EC_{ws}\int_0^l X_\phi''^2dx+GC\int_0^l X_\phi'^2dx}{mI_n\int_0^l X_\phi^2dx}\right)^{1/2}=\text{uncoupled frequency in the } \phi\text{-direction}$$

X_y, X_ϕ = assumed normal functions, representing mode shapes

It is interesting to note that Equation (6) reduces to a form identical to Equation (21) in the previous paper when η and ζ are principal axes.

If the beam is attached to the skin in two perpendicular directions, as shown in Fig. 2, the beam is forced to rotate about the axis M. The motion is a noncoupled torsional vibration represented by:

$$EC_{ws}\phi^{IV}-GC\phi''+mI_m\ddot{\phi}=0 \quad (7)$$

The natural frequencies of the system can be readily computed:

$$p_n=\left\{\frac{EC_{ws}\int_0^l(X_\phi'')^2dx+GC\int_0^l(X_\phi')^2dx}{mI_m\int_0^l X_\phi^2dx}\right\}^{1/2} \quad (8)$$

In the foregoing expressions,

I_m = polar moment of inertia of the section with respect to M

C_{ws} = warping constant of the section with respect to M.

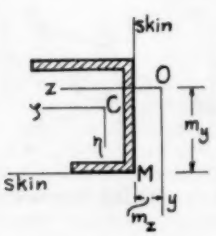

Fig. 2 Thin-walled beam attached to skin in two directions

Energy Absorption of Aluminum Tubing

L. D. MUTCHLER[1]

Nomenclature

- b = element width
- D = outside diameter of tube
- M = final bending moment on element
- M_H = bending moment at horizontal axis of symmetry
- M_V = bending moment at vertical axis of symmetry
- P = applied crushing load
- R = mean radius of undeflected tube
- r = radius of element when loaded
- S = arc length
- t = thickness
- y = co-ordinate of tube wall measured from mean radius
- ϵ = strain or elongation
- ϵ_1 = extreme fiber strain on the inside
- σ = stress
- $d\phi$ = angle subtended by arc length ΔS

Devices which are commonly used for absorbing energy are mechanical springs, hydraulic or pneumatic cylinders, or rubber shock absorbers. These appliances are normally designed for repeated application of the load. Tubing, being crushed by diametrically opposed forces, is a means for absorbing energy which is relatively simple and economical. A tube when used in this manner could be loaded beyond the proportional limit, provided replacement is economically feasible.

Fig. 1

The problem investigated is an approximate solution of a thin-walled tube when crushed between two unyielding, frictionless surfaces as shown in Fig. 1. For high energy-absorbing capacity, the stresses must be high enough to produce considerable yielding. The inherent difficulty in mathematically expressing the stress-strain relationship for a given material necessitates the development of a numerical procedure.

For the first approximation, a condition of plane stress is assumed instead of the usual condition of plane strain. The equations are based on the general assumptions associated with the elementary theory. According to this theory the strain in a ring of unit width, Fig. 2, at a distance y from the neutral axis is given by the expression

$$\epsilon=\frac{y}{R}\frac{\Delta d\phi}{d\phi} \quad (1)$$

where y is small compared to R. The radius after deformation is

$$r=\frac{dS}{d\phi-\Delta d\phi}\text{ where }d\phi=\frac{dS}{R}$$

Combining these expressions with equation (1) the final radius of curvature is

[1] Senior Group Engineer, McDonnell Aircraft Corporation, St. Louis, Mo.

Manuscript received by ASME Applied Mechanics Division, January 28, 1960.

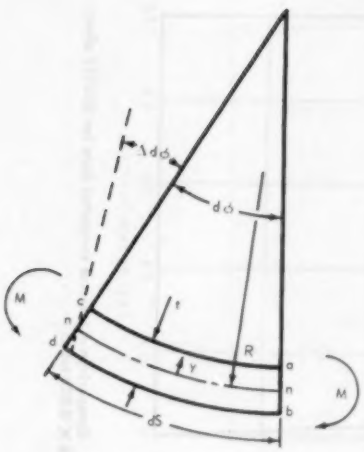

Fig. 2

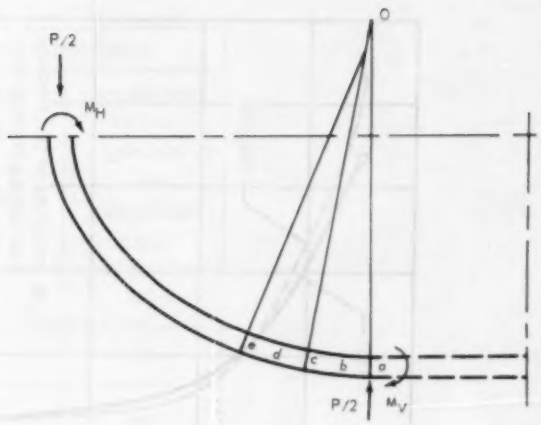

Fig. 4

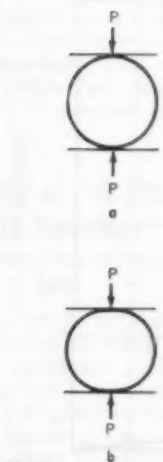

Fig. 3

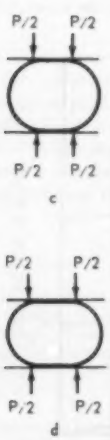

$$r = \frac{Rt}{t - 2\epsilon_1 R} \tag{2}$$

The applied bending moment M is

$$M = b\int_{-t/2}^{t/2} \sigma y dy = 2b\int_0^{t/2} \sigma y dy \tag{3}$$

and using equation (1)

$$M = \frac{bt^2}{2} \cdot \frac{1}{\epsilon_1^2}\int_0^{\epsilon_1} \sigma \epsilon d\epsilon \tag{4}$$

The integral in this equation represents the moment of the area under the stress-strain curve about the origin. This is a standard expression used in calculations involving deformations beyond the proportional limit.

The foregoing information is sufficient to plot the load deflection curve for a tube of a given size and material. A simple integration of the load deflection curve will give the absorbed energy.

To develop the numerical procedure, consider the loading sequence as shown in Fig. 3. Fig. 3(*a*) shows the tube in the initial no load position. Fig. 3(*b*) depicts the tube at the start of yielding. Fig. 3(*c*) presents the tube when the stresses are well into the plastic range, and Fig. 3(*d*) shows the tube at the end of the loading cycle. At this point it has reached its limiting load and any further application of load would result in fracture. The assumption is made that the portion of the tube on the vertical axis is flat leading to the condition that the initial load P has divided into two loads. The bending moment in the flat portion of the tube is defined by equation (4).

The following steps outline the numerical procedure for obtaining a solution to the problem (Fig. 4):

1 Assume a value for $P/2$.

2 Compute the value of M_V.

3 Project forward from *a*, normal to Oa, and find the bending moment at *b*.

4 Obtain the average radius of curvature of the element from *a* to *c* using equations (2) and (4).

5 Compute the co-ordinate at *c*.

6 Repeat the procedure projecting forward from Oc and continuing until a vertical tangent is reached.

7 The deflection of the tube can now be calculated and one point on the load deflection curve is established.

8 Repeat the procedure of steps 1 through 7 assuming other values for $P/2$.

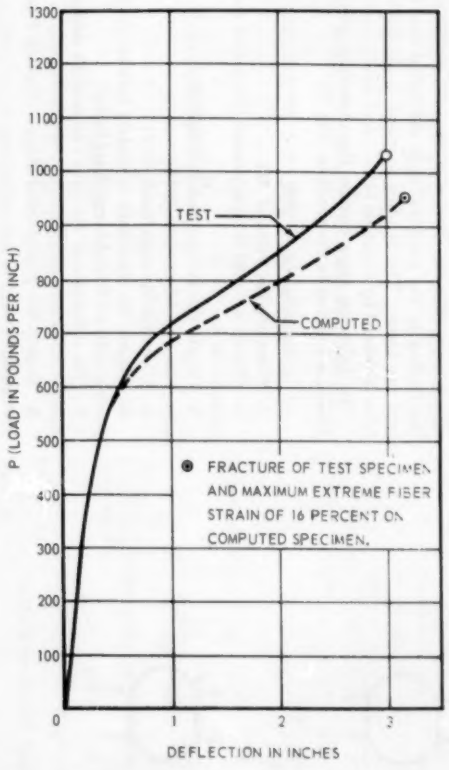
P (LOAD IN POUNDS PER INCH)
DEFLECTION IN INCHES
TEST
COMPUTED
FRACTURE OF TEST SPECIMEN AND MAXIMUM EXTREME FIBER STRAIN OF 16 PERCENT ON COMPUTED SPECIMEN.

Fig. 5 Comparison of test and computed data for 2024T4 aluminum (6 X 0.190 tube)

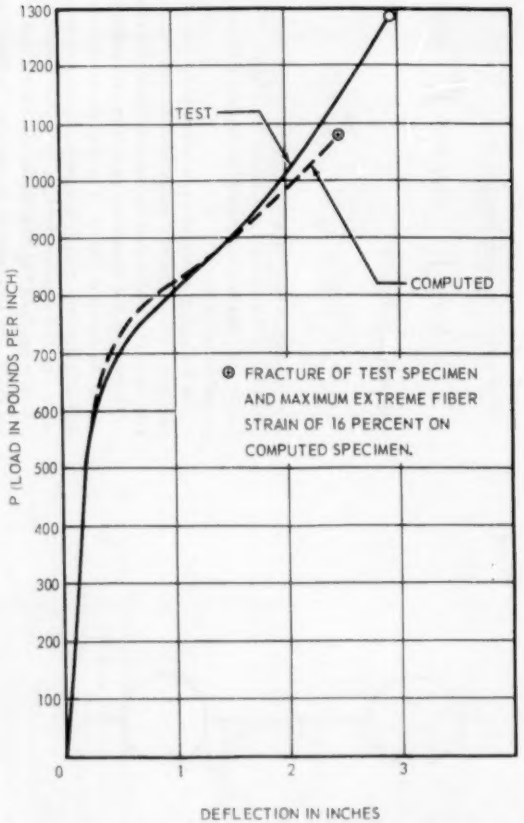
P (LOAD IN POUNDS PER INCH)
DEFLECTION IN INCHES
TEST
COMPUTED
FRACTURE OF TEST SPECIMEN AND MAXIMUM EXTREME FIBER STRAIN OF 16 PERCENT ON COMPUTED SPECIMEN.

Fig. 6 Comparison of test and computed data for 2024T4 aluminum (5 X 0.184 tube)

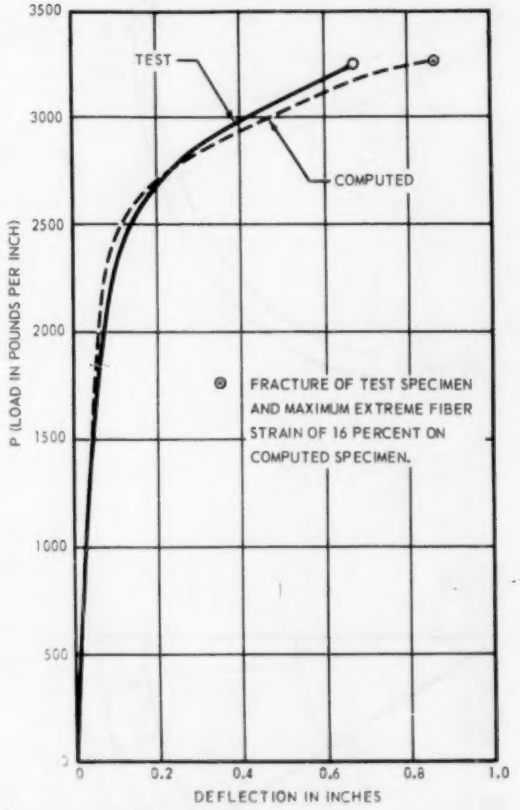
P (LOAD IN POUNDS PER INCH)
DEFLECTION IN INCHES
TEST
COMPUTED
FRACTURE OF TEST SPECIMEN AND MAXIMUM EXTREME FIBER STRAIN OF 16 PERCENT ON COMPUTED SPECIMEN.

Fig. 7 Comparison of test and computed data for 2024T4 aluminum (3 X 0.252 tube)

Table 1

TUBE SIZE D x t (INCHES)	ENERGY IN INCH POUNDS	
	INTEGRATION OF THE TEST LOAD DEFLECTION CURVE	INTEGRATION OF THE COMPUTED LOAD DEFLECTION CURVE
6 x .190	2410	2260
5 x .184	2040	2040
3 x .252	2500	2480

The elements can be taken as small as required to achieve the desired accuracy.

The maximum strains will always be at the horizontal axis of symmetry. The maximum permissible extreme fiber strains were determined from tests and found to be 0.16 in. per in. for the aluminum tubing illustrated. Load deflection curves, computed by the method outlined here, are presented as dashed lines in Figs. 5, 6, and 7. Actual test data are presented by the solid lines.

A simple integration of the curves of Figs. 5, 6, and 7 gives the absorbed energy. The results of the integration are presented in Table 1. The energy computed by the method presented here is generally less than the actual energy, indicating that the procedure is conservative.

Vibrations of Thin Paraboloidal Shells of Revolution

Y. K. LIN[1] **and F. A. LEE**[2]

RECENTLY, Saunders and Paslay[3] have used the inextensional vibration modes of spherical and conical thin shells[4] in the study of a sphere-cone shell combination which may be considered as the nose cone of a missile. In their analysis, the values for slopes along the sphere-cone joint computed from the spherical-shell expressions are different from those computed from the conical-shell expressions, thereby causing disturbing discontinuties. In the present note, these discontinuities are avoided through use of a paraboloidal shell of revolution as an alternative model.

Analysis

The governing equations for normal modes of vibrations are obtained by equating to zero the normal and shearing strains of the middle surface of the shell. Love[5] has given the general expressions for the strains at the middle surface. If the surface is a paraboloid of revolution, and when the co-ordinates shown in Fig. 1 are used, the governing equations for the normal modes reduce to:

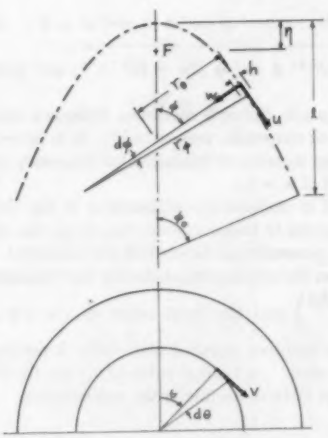

Fig. 1 Geometry, co-ordinates, and deflections of a thin paraboloidal shell of revolution. h = thickness, l = length, η = focal length of shell.

$$\frac{\partial u}{\partial \phi} - w = 0$$

$$\frac{\partial v}{\partial \theta} + \frac{u}{\sec \phi} - v \sin \phi = 0 \qquad (1)$$

$$\tan \phi \frac{\partial v}{\partial \phi} + \sec^2 \phi \frac{\partial u}{\partial \theta} - v \sec^2 \phi = 0$$

General solutions of Equations (1) involve two constants of integration. One of the constants is set equal to zero in order to exclude the singularity at $\phi = 0$. The other constant remains arbitrary, and the desired solutions for Equations (1) are the following:

[1] Assistant Professor of Aeronautical Engineering, University of Illinois, Urbana, Ill.

[2] Structural Dynamics Group, Structures Research Unit, Boeing Airplane Company, Transport Division, Renton, Wash.

[3] H. Saunders, and P. R. Paslay, "Inextensional Vibrations of a Sphere-Cone Shell Combination," *Journal of the Acoustical Society of America*, vol. 31, 1959, pp. 579–583.

[4] Lord Rayleigh, "Theory of Sound," vol. 1, Dover Publications, New York, N. Y., 1945.

[5] A. E. H. Love, "The Mathematical Theory of Elasticity," Dover Publications, New York, N. Y., 1944.

Manuscript received by ASME Applied Mechanics Division, April 28, 1960.

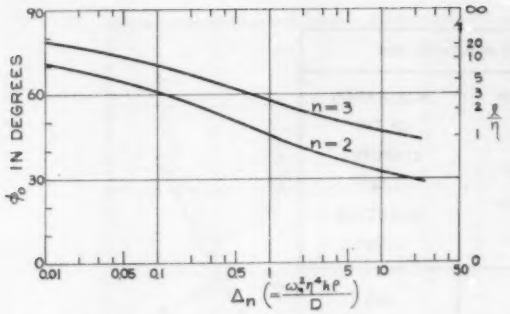

Fig. 2 Relation between the frequency parameter and the boundary co-ordinate ϕ_0

$$\begin{aligned} u_n &= a_n \sin\phi \tan^n\phi \cos n\theta \\ v_n &= a_n \tan^{n+1}\phi \sin n\theta \\ w_n &= a_n \tan^n\phi \,(\cos\phi + n \sec\phi) \cos n\theta \end{aligned} \tag{2}$$

where n is an integer representing physically the number of circumferential waves for the corresponding mode shape.

By equating the maximum kinetic and potential energies of the vibrating system, the natural frequencies of vibration can be obtained as follows:

$$\omega_n = \left\{ \frac{n^2(n^2-1)^2 E}{12(1-\nu^2)(2\eta)^4 \rho} \frac{\int_0^{\phi_0} h^3 \tan^{2n-2}\phi \sec^3\phi (\cos^2\phi + \sec^2\phi + 2 - 4\nu) d\phi}{\int_0^{\phi_0} h \tan^{2n+1}\phi \sec^3\phi \,[2n + (n^2+1)\sec^2\phi] d\phi} \right\}^{1/2} \tag{3}$$

where E, ν, ρ are Young's modulus, Poisson's ratio, and mass density of shell materials, respectively. It is interesting to note that the lowest nonzero or fundamental frequency corresponds to $n = 2$ instead of $n = 1$.

If the shell is uniform in thickness or if the thickness is expressible in terms of trigonometric functions, the integrations in Equation (3) generally can be worked out explicitly.

Fig. 2 shows the relationship between the frequency parameter $\Delta_n \left(= \frac{\omega_n^2 \eta^4 h \rho}{D}\right)$ and the limit angle ϕ_0 (or l/η ratio) at the boundary for uniform, paraboloidal shells of revolution made of aluminum or steel. A typical value of 0.3 for the Poisson's ratio is assumed for both materials in the calculations.

A Note on the Lowest Natural Frequency of Elastic Arcs

E. VOLTERRA[1] and J. D. MORELL[2]

In a well-known paper[3] Professor J. P. Den Hartog applied the Rayleigh-Ritz method for finding the lowest natural frequency of circular arcs with clamped ends and of vibrations occurring in the plane of initial curvature of the arc.

Den Hartog's results can be extended to elastic arcs having the center lines in the form of a cycloid, of a catenary, or of a parabola. With reference to Figs. 1 and 2, the following expressions are used for the potential energy U and the kinetic energy T of the arc:

$$U = \frac{EI}{2} \int_0^L \left[\frac{\partial^2 u}{\partial s^2} + \frac{1}{R} \frac{\partial w}{\partial s} \right]^2 ds + \frac{E\Omega}{2} \int_0^L \left[\frac{\partial w}{\partial s} - \frac{u}{R} \right]^2 ds \tag{1}$$

$$T = \frac{\rho\Omega}{2} \int_0^L \left[\left(\frac{\partial u}{\partial t} \right)^2 + \left(\frac{\partial w}{\partial t} \right)^2 \right] ds \tag{2}$$

ρ being the density of the material of the arc, EI its flexural rigidity, and Ω the cross-section area of the curved bar which is supposed to be circular.

For extensional vibrations the boundary conditions are:

$$u = w = \frac{\partial u}{\partial s} = 0 \quad \text{for} \quad s = \begin{cases} = 0 \\ = L \end{cases} \tag{3}$$

Suitable analytical expressions for the displacements satisfying equations (3) are:

$$\left.\begin{aligned} u &= A \left(1 - \cos\frac{2\pi s}{L}\right) \sin\omega t \\ w &= B \sin\frac{2\pi s}{L} \sin\omega t \end{aligned}\right\} \tag{4}$$

By inserting equations (4) into equations (1) and (2), one obtains:

$$\left.\begin{aligned} U_{max} &= \frac{E\Omega L}{4} \frac{1}{L^2} [A^2 k + B^2 m + 2AB n] \\ T_{max} &= \frac{\rho\Omega L}{4} \omega^2 [3A^2 + B^2] \end{aligned}\right\} \tag{5}$$

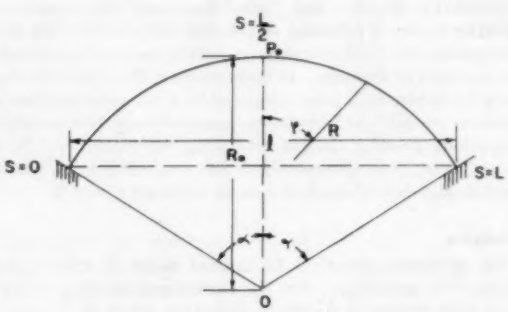

Fig. 1

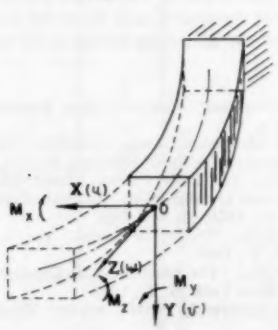

Fig. 2

[1] Professor of Engineering Mechanics, The University of Texas, Austin, Texas. Mem. ASME.

[2] Graduate student, Department of Engineering Mechanics, The University of Texas, Austin, Texas.

[3] J. P. Den Hartog, "The Lowest Natural Frequency of Circular Arcs," *Philosophical Magazine*, vol. 5, Series 7, 1928, pp. 400–408.

Manuscript received by ASME Applied Mechanics Division, May 10, 1960.

with:

$$k = \delta^2(2\pi)^4 + \frac{2}{L}\int_0^L \left(\frac{L}{R}\right)^2 ds +$$

$$\frac{2}{L}\int_0^L \left(\frac{L}{R}\right)^2 \left(\cos\frac{2\pi s}{L}\right)^2 ds - \frac{4}{L}\int_0^L \left(\frac{L}{R}\right)\cos\frac{2\pi s}{L}\, ds$$

$$m = \delta^2(2\pi)^2 \frac{2}{L}\int_0^L \left(\frac{L}{R}\right)^2 \left(\cos\frac{2\pi s}{L}\right)^2 ds + (2\pi)^2$$

$$n = \delta^2(2\pi)^3 \frac{2}{L}\int_0^L \left(\frac{L}{R}\right)\left(\cos\frac{2\pi s}{L}\right)^2 ds$$

$$- (2\pi)\frac{2}{L}\int_0^L \left(\frac{L}{R}\right)\cos\frac{2\pi s}{L}\, ds$$

$$+ (2\pi)\frac{2}{L}\int_0^L \left(\frac{L}{R}\right)\left(\cos\frac{2\pi s}{L}\right)^2 ds \qquad (6)$$

From the condition that

$$U_{max} = T_{max}$$

it follows that:

$$\Phi^2[3A^2 + B^2] = A^2k + B^2m + 2ABn \qquad (7)$$

where $\delta = \frac{r}{L}$

$\left(r = \sqrt{\frac{I}{\Omega}}\right.$ being the radius of gyration of the cross section of the curved bar$\left.\right)$

and

$$\Phi^2 = \frac{\rho\omega^2 L^2}{E}$$

Table 1 Values of the constant Φ

R_0/r \ α	5°	10°	15°	20°	25°	30°	35°	40°	
20	6.166	3.418	2.195	1.635	1.457	1.351	1.331	1.365	circle
	6.171	3.743	2.219	1.732	1.502	1.377	1.348	1.360	cycloid
	6.162	3.223	2.147	1.644	1.400	1.308	1.317	1.400	catenary
	6.160	3.206	2.124	1.617	1.374	1.291	1.321	1.432	parabola
30	4.343	2.184	1.499	1.296	1.107	1.102	1.123	1.240	circle
	4.349	2.203	1.515	1.230	1.138	1.106	1.145	1.209	cycloid
	4.332	2.159	1.469	1.180	1.084	1.099	1.186	1.319	catenary
	4.327	2.152	1.454	1.165	1.074	1.103	1.210	1.370	parabola
40	3.262	1.650	1.160	1.043	0.954	1.000	1.086	1.193	circle
	3.266	1.658	1.240	0.995	0.979	0.994	1.065	1.158	cycloid
	3.256	1.636	1.139	0.965	0.948	1.016	1.136	1.290	catenary
	3.250	1.626	1.129	0.957	0.947	1.029	1.169	1.347	parabola
50	2.612	1.331	0.963	0.897	0.874	0.951	1.053	1.171	circle
	2.615	1.337	0.970	0.864	0.896	0.937	1.026	1.124	cycloid
	2.605	1.319	0.947	0.847	0.879	0.975	1.112	1.276	catenary
	2.602	1.312	0.940	0.844	0.882	0.993	1.149	1.336	parabola
75	1.745	0.912	0.716	0.735	0.787	0.896	1.019	1.148	circle
	1.747	0.918	0.720	0.713	0.805	0.878	0.990	1.098	cycloid
	1.740	0.905	0.709	0.739	0.804	0.933	1.089	1.262	catenary
	1.738	0.901	0.706	0.714	0.812	0.956	1.129	1.326	parabola
100	1.312	0.710	0.607	0.667	0.754	0.876	1.007	1.348	circle
	1.314	0.712	0.608	0.652	0.770	0.855	0.972	1.096	cycloid
	1.309	0.574	0.604	0.658	0.778	0.918	1.080	1.257	catenary
	1.307	0.693	0.603	0.665	0.787	0.987	1.122	1.322	parabola

By expressing that:

$$\frac{\partial[\Phi]^2}{\partial A} = \frac{\partial[\Phi]^2}{\partial B} = 0$$

The following frequency equation:

$$3\Phi^4 - \Phi^2(k + 3m) + (km - n^2) = 0 \qquad (8)$$

is obtained.

In Table 1 the values of the lowest root Φ of equation (8) are given for the arcs of the circle, cycloid, catenary, and parabola for values of the ratio R_0/r varying from 20 to 100 and the angle α varying from 5 deg to 40 deg.

Following Den Hartog, it is more convenient in the case of small angles α to express the results under the form:

$$\omega = \frac{C}{l^2}\left[\frac{EI}{\rho\Omega}\right]^{1/2} \qquad (9)$$

where l is the length of the chord subtending the arc (see Fig. 1).

The numerical values of the constant C for the cycloid, catenary, and parabola are given, respectively, in Figs. 3, 4, and 5.

These values are compared in each figure with the corresponding values of the circle.

The following relationships are easily verified:

For the circle:

$$k = 16\pi^4\delta^2 + \frac{3L^2}{R_0^2}$$

$$m = 4\pi\left(1 + \delta^2\frac{L^2}{R_0^2}\right)$$

$$n = \frac{2\pi L}{R_0}(1 + 4\delta^2\pi^2)$$

$$C = \frac{2\sin^2\alpha}{\alpha}\Phi\frac{R_0}{r}$$

For the cycloid:

$$R = R_0\cos\varphi$$

$$s = R_0(\sin\varphi + \sin\alpha)$$

$$L = 2R_0\sin\alpha$$

$$l = R_0\left(\alpha + \frac{\sin 2\alpha}{2}\right)$$

$$C = \frac{\alpha + \frac{\sin 2\alpha}{2}}{2\sin\alpha}\Phi\frac{R_0}{r}$$

For the catenary:

$$R = \frac{R_0}{\cos^2\varphi}$$

$$s = R_0(\tan\varphi + \tan\alpha)$$

$$L = 2R_0\tan\alpha$$

$$l = R_0\ln\left(\frac{1 + \sin\alpha}{1 - \sin\alpha}\right)$$

$$C = \left\{\frac{\ln\frac{1 + \sin\alpha}{1 - \sin\alpha}}{2\tan\alpha}\right\}\Phi\frac{R_0}{r}$$

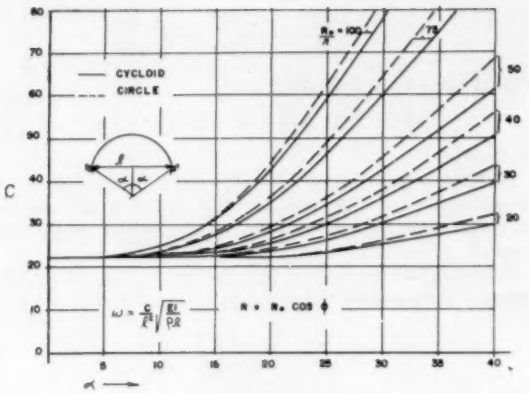

Fig. 3

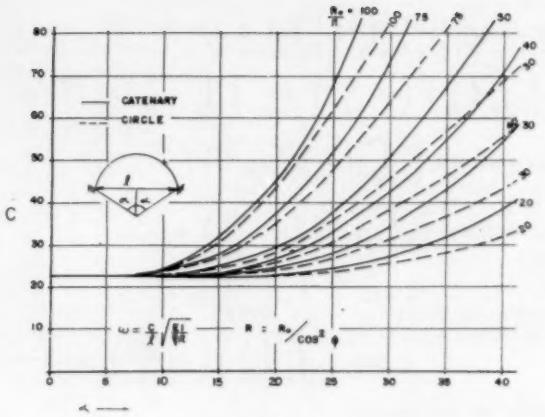

Fig. 4

For the parabola:

$$R = \frac{R_0}{\cos^2 \varphi}$$

$$s = \frac{1}{2} R_0 \left[\frac{\sin \varphi}{\cos^2 \varphi} + \frac{1}{2} \ln \left(\frac{1 + \sin \varphi}{1 - \sin \varphi} \right) \right.$$

$$\left. + \frac{\sin \alpha}{\cos^2 \alpha} + \frac{1}{2} \ln \left(\frac{1 + \sin \alpha}{1 - \sin \alpha} \right) \right]$$

$$L = R_0 \left[\frac{\sin \alpha}{\cos^2 \alpha} + \frac{1}{2} \ln \left(\frac{1 + \sin \alpha}{1 - \sin \alpha} \right) \right]$$

$$l = 2R_0 \tan \alpha$$

$$C = \frac{4 \tan^2 \alpha}{\left[\frac{\sin \alpha}{\cos^2 \alpha} + \frac{1}{2} \ln \left(\frac{1 + \sin \alpha}{1 - \sin \alpha} \right) \right]} \Phi \frac{R_0}{r}$$

It should be pointed out that, although the expressions (4) for the components of the displacements are the same as those used by Den Hartog, the method outlined in the present Note leads to lower values for the frequencies than in the Den Hartog paper. This is apparent from Table 2 where the values of the constant C for the circular bar are compared, the values for C given by Den Hartog being indicated by C_D.

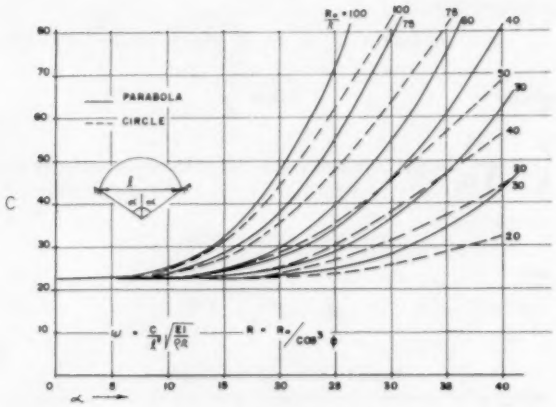

Fig. 5

Acknowledgment

This Note is written as a result of research at The University of Texas sponsored by the National Science Foundation under Grant No. G.4544.

Table 2

R_0/r \ α		5 deg	10 deg	15 deg	20 deg	25 deg	30 deg	35 deg	40 deg
20	C_D	22.722	22.578	22.550	22.923	24.000	25.000	28.907	32.646
	C	22.470	22.499	22.469	22.354	23.871	24.813	28.678	32.323
30	C_D	22.729	22.685	23.075	24.462	27.312	31.754	37.587	44.454
	C	22.683	22.649	23.025	23.888	27.208	31.584	37.326	44.058
40	C_D	22.738	22.834	23.790	26.468	31.370	38.405	47.108	57.016
	C	22.718	22.809	23.749	25.858	31.257	83.213	46.812	56.522
60	C_D	22.750	23.024	24.678	28.843	35.921	45.552	57.096	69.925
	C	22.738	23.005	24.642	28.183	35.797	45.454	56.721	69.327
75	C_D	22.793	23.674	27.542	35.889	48.514	64.485	82.872	102.859
	C	22.787	23.659	27.507	35.074	48.353	64.176	82.336	101.989
100	C_D	22.852	24.553	31.113	43.893	61.986	84.113	109.173	136.186
	C	22.847	24.539	31.070	42.898	61.777	83.715	108.501	125.781

An Accurate Expression for Gas-Pressure Drop in High-Speed Subsonic Flow With Friction and Heating[1]

R. H. FOX[2]

An approximate solution is derived for the pressure ratio in high-speed subsonic flow through constant-cross-section circular tubes with friction and heating. The results are compared with those obtained from an accurate numerical calculation. The gas used is air. A wide range of variables such as temperature ratio, exit Mach number (up to 0.90), tube length-to-diameter ratio, and shape of the power distribution function is examined. The derived expression is found to be quite accurate in all cases.

IN DESIGN studies of high-power-density gas-cooled reactors accurate calculation of the pressure drop is very important. Now, the momentum equation for the flow of gases through holes with friction and heating is nonintegrable. Therefore for work in this area numerical methods are normally used. These calculations are done very rapidly on digital computers and may include inlet effects, variation of the gas properties, and use of average film temperature for obtaining the gas local heat-transfer coefficient. In spite of the speed and accuracy obtained, there are also certain disadvantages. For example, the results are usually obtained several days after the problem is specified. Also, numerical calculations are sometimes not very convenient for estimating the results of parameter variations. As a result, a successful attempt has been made to obtain an analytic solution. Although this solution is not exact, it is surprisingly accurate and at the same time quite simple.

We start out with the exact momentum equation in the form given by Shapiro.[3]

$$\frac{dp}{p} = \frac{-\gamma M^2}{1 - M^2}\left\{\left[1 + \frac{\gamma - 1}{2} M^2\right]\frac{dT_0}{T_0} + \left[1 + (\gamma + 1)M^2\right] f\frac{dx}{a}\right\} \quad (1)$$

where

γ = gas specific heat ratio
f = the friction factor
T_0 = gas stagnation temperature
a = tube radius (constant)
p = gas free stream pressure
x = distance from the inlet

M, T_0, f are variable with x.

Since

$$M^2 = \frac{(\rho u)^2 R T_0}{\gamma p^2\left(1 + \frac{\gamma - 1}{2} M^2\right)}$$

this may be written in the form

$$(1 - M^2)pdp = -(\rho u)^2 R\left\{dT_0 + \frac{1 + (\gamma - 1)M^2}{1 + \frac{(\gamma - 1)}{2} M^2} T_0 z d\epsilon\right\} \quad (2)$$

where

$z = fL/a$, $\epsilon = x/L$, and L is the tube length

Now, for all the cases of interest to us the flow was turbulent. Therefore most of the pressure drop occurred near the exit where f changes very slowly. As a result, we can approximate

$$z(\epsilon) \cong z_2 \quad (3)$$

The subscripts 1 and 2 will indicate inlet and exit quantities, respectively. Further, assume that the factor on the right side involving M^2 is unity. Since ρu is constant, we may now integrate

$$\frac{-(p_2^2 - p_1^2)}{2} + \int_{p_1}^{p_2} M^2 pdp = (\rho u)^2 R\left[T_{0_2} - T_{0_1} + z_2\int_0^1 T_0 d\epsilon\right] \quad (4)$$

Now, we are mainly interested in reactor power sources. We can therefore assume that the axial power distribution is known. Let us write it in the form

$$P(\epsilon) = g(\epsilon)\int_0^1 P(\epsilon)d\epsilon$$

$g(\epsilon)$ is thus the normalized power distribution function. If T_{0_1} and T_{0_2} are the inlet and outlet stagnation temperatures, then we can easily show that

$$T_0(\epsilon) = T_{0_1} + (T_{0_2} - T_{0_1})\int_0^\epsilon g(\epsilon')d\epsilon'$$

Thus the integral on the right side of (4) is

$$\int_0^1 T_0 d\epsilon = T_{0_1} + (T_{0_2} - T_{0_1})\int_0^1 d\epsilon\int_0^\epsilon g(\epsilon')d\epsilon'$$

It is interesting to note that

$$b = \int_0^1 d\epsilon\int_0^\epsilon g(\epsilon')d\epsilon'$$

is just the distance of the centroid of $g(\epsilon)$ from the exit measured in units of x/L. In order to do the integral on the left side of (4), let us write the integrand in the form

$$M^2 pdp = \frac{(\rho u)^2 RT}{\gamma}\frac{dp}{p},$$

where

T is the gas free-stream temperature

Now this term is important only near the exit where M rapidly approaches the exit value M_2. In this region T, γ do not change much in most cases so that the use of the approximations

$$\gamma \cong \gamma_2, \qquad T \cong T_2 \quad (5)$$

seems reasonable. Then

$$\frac{(\rho u)^2 RT}{\gamma} \cong \frac{(\rho u)^2 RT_2}{\gamma_2} = M_2^2 p_2^2 \quad (6)$$

and the value of the integral is

$$\int_{p_1}^{p_2} M^2 pdp \cong M_2^2 p_2^2 \ln(p_2/p_1).$$

The complete integral of the differential equation (1) is then

$$p_1^2 - p_2^2 = 2(\rho u)^2 R\{T_{0_2}(1 + bz_2) + T_{0_1}[z_2(1 - b) - 1]\} + 2M_2^2 p_2^2 \ln(p_1/p_2)$$

Using (6) this may be put in the particularly convenient form

---

[1] This work was done under the auspices of the U. S. Atomic Energy Commission.

[2] Assistant Division Leader for Reactor Research and Advanced Concepts, Nuclear Propulsion Division, Lawrence Radiation Laboratory, University of California, Livermore, Calif.

[3] A. H. Shapiro, "The Dynamics and Thermodynamics of Compressible Fluid Flow," Ronald Press Co., New York, N. Y., 1953, vol. 1, p. 231 (Table 8.2, 6th item).

Manuscript received by ASME Applied Mechanics Division, March 29, 1960.

Table 1 Comparison of equation (7) with the results of numerical calculations for subsonic flow with heating and friction

$g(\epsilon)$, b	Problem No.	p_1/p_2 calc'd by Floss	p_1/p_2 calc'd by Eq. (7)	γ_2	M_2	deg K T_2	deg K T_{02}	deg K T_{01}	z_2
No power	0-10	2.23867	2.175	1.40340	0.900	257.854	300	300	0.934929
	0-11	3.65735	3.588	1.40340	0.900	257.854	300	300	3.70530
	0-12	4.84768	4.782	1.40340	0.900	257.854	300	300	7.30736
	0-13	1.37003	1.359	1.40215	0.500	285.604	300	300	0.941951
	0-14	2.04298	2.025	1.40215	0.500	285.604	300	300	3.73313
	0-15	2.64676	2.628	1.40215	0.500	285.604	300	300	7.36224
$\frac{\pi}{2}\sin \pi\epsilon$, $b = 1/2$	0-16	2.40247	2.381	1.31325	0.90	1333.11	1500	300	0.939230
	0-17	3.21509	3.184	1.31325	0.90	1333.11	1500	300	3.72235
	0-18	3.98859	3.961	1.31325	0.90	1333.11	1500	300	7.34097
	0-19	1.46128	1.454	1.30730	0.500	1445.34	1500	300	0.943648
	0-20	1.84153	1.835	1.30730	0.500	1445.34	1500	300	3.73986
	0-21	2.222781	2.224	1.30730	0.500	1445.34	1500	300	7.37550
$2(1-\epsilon)$, $b = 2/3$	0-22	1.48025	1.479	1.32560	0.500	1153.82	1200	300	0.920324
	0-23	1.93649	1.906	1.32560	0.500	1153.82	1200	300	3.64742
	0-24	2.38433	2.381	1.32560	0.500	1153.82	1200	300	7.19321
	0-25	2.47707	2.444	1.33240	0.900	1059.90	1200	300	0.924492
	0-26	3.42967	3.395	1.33240	0.900	1059.90	1200	300	3.66394
	0-27	4.32427	4.294	1.33240	0.900	1059.90	1200	300	7.22578
$g(\epsilon) = 1$, $b = 1/2$	F-19	1.45904	1.454	1.30730	0.500	1445.34	1500	300	0.943648
	F-20	1.83941	1.835	1.30730	0.500	1445.34	1500	300	3.73986
	F-21	2.22471	2.224	1.30730	0.500	1445.34	1500	300	7.37550
	F-22	2.39028	2.381	1.31325	0.900	1333.11	1500	300	0.939299
	F-23	3.20091	3.184	1.31325	0.900	1333.11	1500	300	3.72262
	F-24	3.96717	3.961	1.31325	0.990	1333.11	1500	300	7.34151

$$(p_1/p_2)^2 = 1 + \frac{^2\gamma_2 M_2^2}{T_2}\{T_{0_2}(1 + bz_2) + T_{0_1}[z_2(1 - b) - 1]\} + 2M_2^2 \ln (p_1/p_2) \quad (7)$$

Equation (7) turns out to be rather useful in gas-cooled reactor design calculations. Usually, M_2 is determined by the exit configuration and T_{0_2} and T_{0_1} are given by performance requirements and inlet conditions. b is given once and for all by the shape of the power distribution. z_2 is a rather insensitive function of flow conditions. The unknown variable, p_1/p_2, can be found to 3-place accuracy with two or three iterations. If a large parameter survey is required, the solution can readily be carried out on a small computer. See Table 1.

Conclusions

In over two and a half years of use, no cases have yet occurred where equation (7) was seriously in error in p_1/p_2 when compared with our Floss heat-transfer digital-computer code, Table 2. Apparently the approximations (3) and (5) nearly cancel each other. As a check, a series of 24 problems was computed and compared with Floss results. The input quantities used were: $M_2 = 0.50$ or 0.90; $T_{0_1} = 300$ deg K; $T_{0_2} = 300$, 1200, or 1500 deg K; $z_2 = 1$, 4, or 8. For the power distribution function we used $g(\epsilon) = 0$, $\frac{\pi}{2}\sin \pi\epsilon$, $2(1 - \epsilon)$, or 1.00 which give for the parameter b the values, respectively: indeterminate, 1/2, 2/3, 1/2. The gas used was air. Auxiliary parameter values were: radius 0.5 cm, length 163–1272 cm, power 0–590 kw, flow rate 148–439 gm/sec. In the Floss calculations, a correction near the tube inlet for boundary-layer buildup is included, the gas properties are variable, and the average film temperature is used for obtaining the local heat-transfer coefficient and friction factor. The agreement in p_1/p_2 was better than 1 per cent in 17 cases, 1–2 per cent in 6 cases, and 2.5 per cent in 1 case ($M_2 = 0.90$, $T_{0_2} = 300$ deg K, $z_2 = 1$).

Equation (7) predicts that the pressure drop depends only on the position of the centroid (value of b) of the power distribution rather than on its detailed shape. This was verified to 1/2 per cent for the sine and flat power distributions.

Equation (7) also predicts that if the equation

$$z_2(1 - b) = 1$$

is satisfied, then the pressure ratio p_1/p_2 is independent of the inlet temperature. This prediction was also verified to 1/2 per cent.

Table 2 Auxiliary problem parameters obtained from Floss code results. Tube radius is 0.50 cm.

Problem No.	gas flow, gm/sec	p_2, psia	length, cm	power, kw
0-10	156.624	73.8207	163	...
0-11	156.624	73.8207	646	...
0-12	156.624	73.8207	1274	...
0-13	148.758	132.880	163	...
0-14	148.758	132.880	646	...
0-15	148.758	132.880	1274	...
0-16	439.841	487.280	163	590.419
0-17	439.841	487.280	646	590.419
0-18	439.841	487.280	1274	590.419
0-19	421.459	877.100	163	565.743
0-20	421.459	877.100	646	565.743
0-21	421.459	877.100	1274	565.743
0-22	421.459	778.241	163	413.233
0-23	421.459	778.241	646	413.233
0-24	421.459	778.241	1274	413.233
0-25	421.459	413.327	163	413.233
0-26	421.459	413.327	646	413.233
0-27	421.459	413.337	1274	413.233
F-19	421.459	877.100	163	565.743
F-20	421.459	877.100	646	565.743
F-21	421.459	877.100	1274	565.743
F-22	439.679	487.100	163	590.201
F-23	439.679	487.100	646	590.201
F-24	439.679	487.100	1274	590.201

Flow of Liquid Metal Past a Porous Flat Plate

G. HORVAY[1]

A simple boundary-layer approximation formula is derived for the temperature distribution in liquid metal which flows past a porous flat plate at zero incidence at velocity U and is sucked into it at velocity V.

Introduction

We consider liquid metal of temperature T_∞ flowing at velocity U past a porous flat plate of temperature T_f, and being sucked

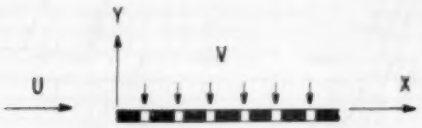

Fig. 1

into it at velocity V, $V/U \ll 1$, see Fig. 1. We seek to determine the heat-transfer coefficient

$$h \equiv \frac{k}{T_\infty - T_f}\left[\frac{\partial T}{\partial Y}\right]_{Y=0} \tag{1a}$$

Its fully developed value

$$XV^2/4\kappa U \gg 1\colon\ h = Vk/\kappa = \gamma c V \tag{1b}$$

can be readily obtained on the basis of physical arguments, and has in fact been used in the analysis of freezing processes; see, e.g. [1],[2] where k = conductivity, c = specific heat, γ = specific weight, and κ = diffusivity = $k/\gamma c$. In the vicinity of $X = 0$ the entrance conditions modify this value. We shall show below that

$$\frac{h}{k} = \frac{V}{2\kappa}\left[1 + \operatorname{erf}\sqrt{\frac{XV^2}{4\kappa U}}\right] + \sqrt{\frac{U}{\pi\kappa X}}\exp\left\{-\frac{XV^2}{4\kappa U}\right\} \tag{2a}$$

or, in dimensionless units

$$\mathfrak{N} = \text{Nusselt number} = ha/k = p[1 + \operatorname{erf}(p\sqrt{\tau})] + (\pi\tau)^{-1/2}e^{-p^2\tau} \tag{2b}$$

where

p = Péclet number for vertical flow = $aV/2\kappa$
P = Péclet number for horizontal flow = aU/κ
a = reference length (arbitrary)
τ = dimensionless time = $\kappa X/Ua^2 = X/aP$

Formulas (2) are based on two vital assumptions: (*a*) slug flow, i.e., precisely zero viscosity; (*b*) boundary-layer theory. The former assumption has been frequently used for liquid metals of low Prandtl numbers, and has been shown by Grosh and Cess [2], Morgan, Pipkin, Warner [3], Sparrow and Gregg [4] to be a good representation of actual conditions.[3] Assumption (*b*) merely expresses the supposition that the temperature gradient varies in the Y-direction much faster than in the X-direction. This is undoubtedly also true. Then the problem reduces to solution of the equation

$$U\frac{\partial T}{\partial X} - V\frac{\partial T}{\partial Y} = \kappa\frac{\partial^2 T}{\partial Y^2} \tag{3}$$

subject to the boundary conditions

$$\begin{aligned} X = 0\colon&\ T = T_\infty \\ Y = \infty\colon&\ T = T_\infty \\ Y = 0\colon&\ T = T_f \end{aligned} \tag{4a, b, c}$$

Analysis

We place, for simplicity

$$T_\infty = 0, \qquad T_f = -1 \tag{5}$$

and Laplace transform (3, 4). We obtain

$$\kappa\bar{T}'' + V\bar{T}' - U\lambda\bar{T} = 0;\ \bar{T}(0) = -1/\lambda,\ \bar{T}(\infty) = 0 \tag{6}$$

where

$$\bar{T} \equiv \mathfrak{L}T \equiv \int_0^\infty e^{-\lambda X}T\,dX, \qquad \bar{T}' \equiv d\bar{T}/dY \tag{7}$$

One finds

$$\bar{T} = -\frac{1}{\lambda}\exp\left\{-\frac{VY}{2\kappa} - \left[\frac{U\lambda}{\kappa} + \frac{V^2}{4\kappa^2}\right]^{1/2}Y\right\} = e^{-VY/2\kappa}\,\frac{\exp\{-Y[(\lambda + V^2/4\kappa U)U/\kappa]^{1/2}\}}{(\lambda + V^2/4\kappa U) - V^2/4\kappa U} \tag{8}$$

Correspondingly, using the well-known translation theorem

$$\mathfrak{L}^{-1}\{\bar{T}(\lambda + b)\} = e^{-bX}\,\mathfrak{L}^{-1}\{\bar{T}(\lambda)\} \tag{9}$$

we obtain

$$T = \exp\left\{-\frac{VY}{2\kappa} - \frac{V^2X}{4\kappa U}\right\}\mathfrak{L}^{-1}\left\{\frac{e^{-Y\sqrt{U\lambda/\kappa}}}{\lambda - V^2/4\kappa U}\right\} \tag{10}$$

But by Erdélyi [5], p. 246, #10,

$$2\mathfrak{L}^{-1}\left\{\frac{e^{-\sqrt{\alpha\lambda}}}{\lambda + \beta}\right\} = e^{-\beta X}\left[e^{i\sqrt{\alpha\beta}}\operatorname{erfc}\left(\frac{1}{2}\sqrt{\frac{\alpha}{X}} + i\sqrt{\beta X}\right) + e^{-i\sqrt{\alpha\beta}}\operatorname{erfc}\left(\frac{1}{2}\sqrt{\frac{\alpha}{X}} - i\sqrt{\beta X}\right)\right] \tag{11}$$

Accordingly

$$T = -\frac{1}{2}e^{-VY/\kappa}\operatorname{erfc} \mathrm{I} - \frac{1}{2}\operatorname{erfc} \mathrm{II}$$

$$\left.\begin{matrix}\mathrm{I}\\ \mathrm{II}\end{matrix}\right\} = \frac{1}{2}\left(Y \mp \frac{XV}{U}\right)\sqrt{\frac{U}{\kappa X}} \tag{12}$$

and

$$\frac{\partial T}{\partial Y} = \frac{V}{2\kappa}e^{-VY/\kappa}\operatorname{erfc} \mathrm{I} + \frac{1}{2}e^{-VY/\kappa}\sqrt{\frac{U}{\pi\kappa X}}\,e^{-\mathrm{I}^2} + \frac{1}{2}\sqrt{\frac{U}{\pi\kappa X}}\,e^{-\mathrm{II}^2} \tag{13}$$

---

[1] General Electric Company, Research Laboratory, Schenectady, N. Y.

[2] Numbers in brackets indicate References at end of Note.

[3] For example, it is seen in [4] that for flow past an impermeable isothermal plate the heat-transfer prediction based on inviscid flow is 15 per cent high compared with the boundary-layer prediction for Pr = 0.03.

Manuscript received by ASME Applied Mechanics Division, January 12, 1960.

On taking this derivative at $Y = 0$, we obtain the right side of Equation (2a).

In Fig. 2 we plot $\mathfrak{N}$ versus τ for various p. It is seen that, except at very small times, i.e., except for the vicinity of the entrance region, where horizontal convection effects dominate, the vertical convection has an overwhelming effect already for moderately large suction rates. We find the asymptotic behavior

$$\tau \gg 1: \qquad \mathfrak{N} \to \begin{cases} 2p & \text{for } p > 0 \\ 0 & \text{for } p < 0 \end{cases} \tag{14}$$

The result for $p = 0$ was discussed previously, in [2].

References

1 G. Horvay, "Freezing of a Growing Liquid Column," *Journal of Heat Transfer*—TRANS. ASME, Series C, vol. 82, February, 1960, pp. 37–47.

2 R. J. Grosh and R. D. Cess, "Heat Transfer to Fluids With Low Prandtl Numbers," TRANS. ASME, vol. 80, 1958, p. 667.

3 G. W. Morgan, A. C. Pipkin, and W. H. Warner, "On Heat Transfer in Laminar Boundary-Layer Flows of Liquids Having a Very Small Prandtl Number," *Journal of the Aeronautical Sciences*, vol. 25, 1958, p. 173.

4 E. M. Sparrow and J. L. Gregg, "Details of Exact Low Prandtl Number Boundary-Layer Solutions for Forced and Free Convection," NASA Memo 2-27-59E, 1959.

5 A. Erdélyi, W. Magnus, F. Oberhettinger, and F. G. Tricomi, "Tables of Integral Transforms," vol. 1, McGraw-Hill Book Co., Inc., New York, N. Y., 1954.

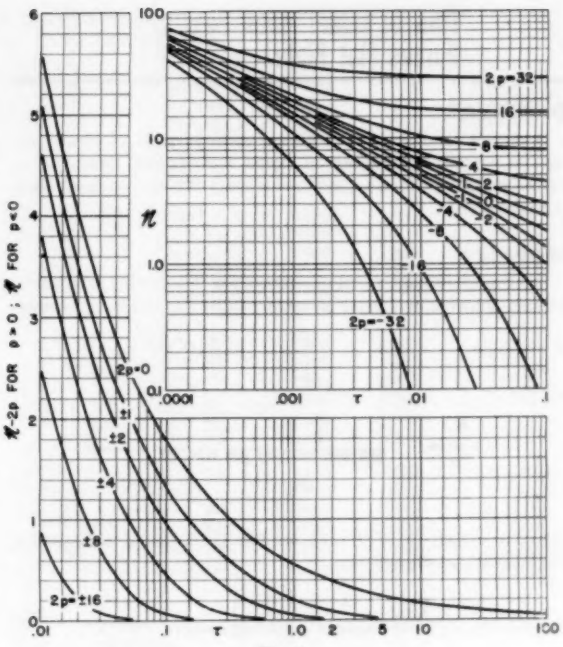

Fig. 2

The Elastic-Plastic Response of Thin Spherical Shells to Internal Blast Loading[1]

P. G. HODGE, JR.[2] There are certain questions which arise from the author's valuable treatment of this interesting problem. The first of these concerns the phenomenon of unloading. According to the analysis as given, the stress rises to a value σ_1 in an elastic and plastic response and then oscillates between $\pm\sigma_1$ elastically. For a perfectly plastic material, $\sigma_1 = \sigma_y$, and this analysis is theoretically correct. However, for a strain-hardening material, $\sigma_1 > \sigma_y$ and the unloading will be elastic only in the case of isotropic strain-hardening without any Bauschinger effect. If there is any Bauschinger effect, there would be plastic compressive behavior during the first unloading and possibly further plastic flow during subsequent oscillations. This phenomenon could easily be treated within the framework of the linear analysis and it would be interesting to compare the results with those of the author.

That this point may be of more than theoretical interest is suggested by the author's statement, ". . .maximum strains were recorded . . . before failure. . ." This statement seems to imply that failure occurred subsequent to reaching the maximum stress. This result is difficult to explain on the basis of the author's analysis, but could be a natural consequence of the further plastic flow resulting from a Bauschinger effect.

In the interpretation of the data, an objection may be raised to the author's adoption of one standard deviation as a "confidence limit." The distribution of measurements is far from a normal one so that the theoretical significance of the standard deviation is questionable. Indeed, the scatter between the two plastic tests is so great that one should hesitate to draw any qualitative conclusions from either test.

As a final point, one might mention that standard methods may be used to reduce the nonlinear equation (15) to a solution by quadrature in the particular case where p = const. In particular, such a solution would be applicable for a step pulse or for the phase $p = 0$ of any pressure wave.

Author's Closure

The author appreciates the careful consideration given the paper by Dr. Hodge. He is quite correct in pointing out that the Bauschinger effect has been neglected in the analysis for a strain-hardening material. The analysis presented in the paper could be easily extended to a stress-strain law which included this effect, as long as the law was represented by linear segments. Although this effect could explain failure occurring after maximum strains were recorded at several locations on the shell, the author believes that the delayed failure can probably be attributed to the propagation of tears in the shell from localized weak points which failed at stresses considerably below the maximum values which were recorded at locations distant from these points.

The author does not agree with Dr. Hodge's statement that "the distribution of measurements is far from a normal one." If one plots the data of Table 3 in the form of histograms and fits normal distribution curves to these histograms, he can see that the fits are quite good. Although the data in Table 4 have a much larger spread, they also fit a normal curve reasonably well. So, the assumption of normal distribution, implied in the paper, appears to be reasonable. However, association of the words "confidence limits" with one standard deviation *is* questionable, as the author intended to convey when he used quotation marks.

As Dr. Hodge indicated in his comment on qualitative conclusions from the plastic response tests, one cannot decide which of the theories presented in the paper should be used to obtain close agreement with experiment. But, despite their shortcomings, the plastic experiments yield response measurements of the same order of magnitude as those predicted from either theory, assuring one that there are no gross disagreements with theory.

The author wishes to thank Dr. Hodge for noting that standard methods can be used to solve equation (15) for a step increase in pressure. This case is of some interest, although it does not apply to the blast loading problem. For example, one can show that the shell motion is unstable for a sufficiently intense step of pressure.

[1] By W. E. Baker, published in the March, 1960, issue of the Journal of Applied Mechanics, vol. 27, Trans. ASME, vol. 82, Series E, pp. 139–144.

[2] Professor of Mechanics, Illinois Institute of Technology, Chicago Ill. Mem. ASME.

A Unified Criterion for the Degree of Constraint of Plane Kinematic Chains[1]

T. P. GOODMAN.[2] The clarification of the concept of constraint which this paper accomplishes is a welcome contribution to the literature of kinematics. The criterion of constraint based on velocities, as given in Section 2 of the paper, is particularly simple and easy to use.

Using the notation of the paper, this criterion may be stated as

$$x = (n - 1) - 2L \tag{1}$$

which is merely a rearrangement of equation (10) of the paper.

Section 4 of the paper may be interpreted as a demonstration of the equivalence between this constraint criterion and the conventional constraint criterion given by equation (9) of the paper. A simpler proof of this equivalence may be obtained by deriving equation (1) of this discussion directly from equation (9) of the paper in the following way:

1 Define the number of pairs in the mechanism as

$$p = \sum_i (i - 1) j_i \tag{2}$$

[1] By B. Paul, published in the March, 1960, issue of the JOURNAL OF APPLIED MECHANICS, vol. 27, TRANS. ASME, vol. 82, Series E, pp. 196–200.

[2] Kinematics Engineer, General Engineering Laboratory, General Electric Company, Schenectady, N. Y. Assoc. Mem. ASME.

i.e., a joint connecting two links is considered as a single pair, a joint connecting three links is considered as two pairs, and so on. Then equation (9) of the paper can be rewritten

$$x = 3(n - 1) - 2p = (n - 1) - 2[p - (n - 1)] \quad (3)$$

2 Define an open kinematic chain as a chain of links, connected by lower pairing, having no closed loops. In such a chain, there are as many pairs as movable links; i.e.,

$$n - 1 = p \quad (4)$$

This is also the number of degrees of freedom, x, as may be verified by substituting equation (4) in equation (3).

3 Each closure of the chain, accomplished by joining together two links of the open chain with a lower pair, forms an independent loop; therefore

$$L = p - (n - 1) \quad (5)$$

Equation (1) follows directly by substituting equation (5) in equation (3).

From this derivation, the underlying reason for the equivalence of the two constraint conditions may be expressed as follows: For a planar kinematic chain having only lower pairs, each pair in excess of the number of movable links forms an independent loop, and the number of constraints (two) introduced by a pair is equal to the number of equations provided by an independent loop.

The derivation of equation (4) of the paper can be simplified slightly by noting that in a sliding-pair chain a movable link has only two degrees of freedom, since no rotation of links is possible, and each sliding pair introduces one additional constraint. With this line of reasoning, equation (4) can be written directly from equation (9).

The analysis of independent loops is important not only in kinematic analysis but also in the kinematic synthesis of mechanisms to fulfill prescribed motion requirements. In general, a problem in kinematic synthesis can be expressed analytically by writing down a set of simultaneous equations of the form of equations (1) of the paper. The desired positions, velocities, and accelerations of the linkage are included in these equations as known constants, and the link dimensions are included as unknowns. The number N of precision points[3] for which a given mechanism can be synthesized can be readily determined from the loop equations in the following way: Let c be the number of unknown constants and v the number of unknown variables in the loop equations. For N precision points of a planar mechanism, there are $2NL$ equations which can be solved for $2NL$ unknowns; hence

$$2NL = c + Nv \quad (6)$$

from which

$$N = c/(2L - v) \quad (7)$$

The corresponding equation for a spatial linkage is

$$N = c/(3L - v) \quad (8)$$

For the synthesis of a prescribed functional relationship between input and output angles using a four-bar linkage, $c = 5$ (three link-length ratios; initial values of input and output angles), $v = 1$ (angle between coupler and frame), $L = 1$; hence by equation (7), $N = 5$, in agreement with Freudenstein's result.[3] Similarly it can be shown that for the same synthesis problem using two four-bar linkages in series, $N = 9$; using a six-bar, two-pivot or coupler-drive linkage, $N = 11$; and using a seven-bar linkage with two inputs and one output, $N = 13$.

[3] F. Freudenstein, "Structural Error Analysis in Plane Kinematic Synthesis," *Journal of Engineering for Industry*—TRANS. ASME, Series B, vol. 81, 1959, pp. 15–22.

Using L as defined by the author and N as found from equation (7) or (8) of this discussion, the general problem of kinematic synthesis may be stated as the simultaneous solution of $2NL$ (for a planar mechanism) or $3NL$ (for a spatial mechanism) equations in $c + Nv$ unknowns. The complexity of these equations is usually so great, however, that all available engineering insights into the problem must be exploited to make a solution economically feasible, even with high-speed digital computers.

FERDINAND FREUDENSTEIN.[4] The author is to be commended for his fresh and able approach to an old subject. The proof of the number of independent loops given in the Appendix is believed to be the first application of topological ideas to kinematics, and as such is noteworthy It may be mentioned also that the original formula often ascribed to Gruebler (1883) goes back to Chebichev (1869–1870) in his article "On Parallelograms" (1870; see his Collected Works, Part II, St. Petersburg, 1907), which fact was acknowledged by Gruebler in his original articles.

Author's Closure

The author appreciates the kind remarks of Drs. Goodman and Freudenstein. In particular, he found Dr. Goodman's alternate "equivalence proof" highly instructive. The derivation of the number of precision points (or collocation points) available for a given class of plane or spatial mechanisms is also of great interest. However, the author would like to offer a word of caution concerning the extension of results obtained for planar mechanisms to space mechanisms. It has been shown in the paper that, in the nonsingular case, the number of independent loops uniquely fixes the degree of freedom of a plane closed lower paired linkage. In the case of spatial linkages, however, this result is not generally true. It may be necessary, in certain cases, to supplement the 3L "loop equations" by certain auxiliary equations. These auxiliary equations depend upon the nature of the various joints in the linkage. For example, Fig. 1 of this closure shows a spatial linkage with three moving members. Apart from the rotation of the bar e about its own axis, there are six variable co-ordinates designated by S_1, S_2, Φ_f, Φ_e, θ_e, Φ_d. There is one obvious independent loop giving rise to the three scalar equations

$$\Sigma x = a - S_1 - S_2 - e \sin \Phi_e \cos \theta_e - f \sin \Phi_f = 0$$

$$\Sigma y = c - d \sin \Phi_d - e \sin \Phi_e \sin \theta_e - S_2 = 0$$

$$\Phi z = b + d \cos \Phi_d - e \cos \Phi_e - f \cos \Phi_f = 0$$

In addition to these three equations, one must append the auxiliary equation

$$S_1 = p\Phi_d$$

where p is the pitch of the screw. It is now evident that if two of

[4] Professor and Chairman, Department of Mechanical Engineering, Columbia University, New York, N. Y. Assoc. Mem. ASME.

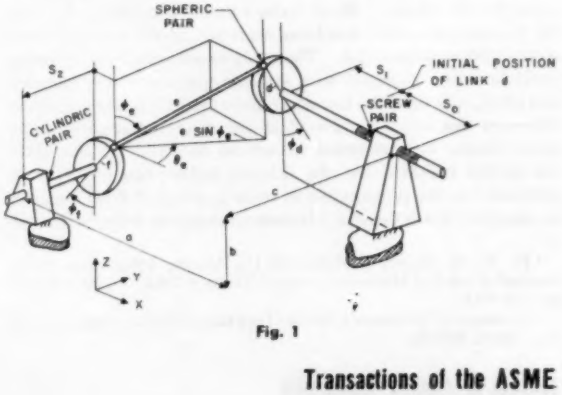

Fig. 1

the variables are specified the four foregoing equations will, in general, define the remaining four variables so that, apart from the rotation of bar e about its own axis, the system has two degrees of freedom.

It is not to be inferred, however, that the loop equations are never sufficient for solving a spatial system. If the pitch of the screw is made zero, the foregoing three loop equations are sufficient to find the three remaining variables in terms of two chosen independent variables.

The author feels that a systematic study of spatial mechanisms from the independent loop point of view, together with a study of the various types of auxiliary equations which can arise, may be very profitable.

The Motion and Loading of a Hinged Ramp Which Supports a Sliding Mass[1]

E. E. POSTEL.[2] It is well known that sudden application of a load to a linear spring will produce exactly twice static deflection. The curves in Fig. 3 of the paper show that the result of leaving out the Coriolis term can give twice the deflection given by the more exact equation at certain sliding velocities of the load, although for the velocities shown it does not reach twice static for either calculation.

In this particular case the size of the dynamic load factor is probably not of great significance from an engineering standpoint, but the fact that it may be varied considerably by the choice of parameters and the way in which it depends on these parameters indicate that this is a phenomenon whose advantage or disadvantage must be assessed in each application where accurate description is required.

To deflect the spring to more than twice static, more energy is required than is available from lowering the cargo through this distance. By virtue of the rearward velocity of the cargo, the additional energy could have been obtained by catapulting the cargo over the hinge point in an upward trajectory. A similar action might possibly occur at each bounce as the cargo traverses the length of the ramp. In the practical case this could also have been caused by irregular motions of the airplane. This implies that the ramp and cargo may assume positions higher than the static position of the ramp alone and that clearance and provision for upward travel and upward loads may be required. It is not clear whether the ramp would always follow the cargo to those higher positions or whether separation would occur. (No provision was made in the given equations for such separation.)

The study shows a practical situation requiring application of nonlinear mathematics and points to considerable additional study that would be of academic interest and could be of some practical importance.

Author's Closure

The case analyzed by the writer is somewhat idealized. However, as is the case for many problems in the literature involving formidable mathematics, the procedure for solution is, initially, to first idealize so that solvability of the equations can be assessed.

Mr. Postel's criticism is, from the practical viewpoint, meritorious and deserves future investigation.

[1] By B. Saelman, published in the March, 1960, issue of the JOURNAL OF APPLIED MECHANICS, vol. 27, TRANS. ASME, 82, Series E, pp. 177–181.

[2] Lockheed Aircraft Corporation, Burbank, Calif.

Stresses in a Circular Cylinder Having an Infinite Row of Spherical Cavities Under Tension[1]

CHIH-BING LING.[2] The present solution, as mentioned in the paper, was obtained by extending the writer's previous solution of a circular cylinder having a single spherical cavity.[3] The method of superposition was used. The required functions were expressed as infinite series of the corresponding functions for a single cavity. The question of convergency generally arises from such infinite series. It appears that in the two fundamental functions (3) and (4), the infinite series

$$\sum_{q=-\infty}^{\infty} \frac{a^3}{2} \log \frac{1+\mu_q}{1-\mu_q} \quad \text{and} \quad \sum_{q=-\infty}^{\infty} a^3 p_q$$

are both divergent and so also are certain expansions that follow. However, the divergency in the first series can be removed if the function U_0 defined by the writer in a recent paper[4] is used. When expressed in the present notation, it is as follows:

$$a^3 U_0 = -\frac{a^3}{2} \log \times \left\{ \frac{1+\mu}{1-\mu} \prod_{q=1}^{\infty} \frac{(1+\mu_q)(1+\mu_{-q})}{(1-\mu_q)(1-\mu_{-q})} \exp\left(-\frac{4z}{q\beta}\right) \right\} \quad (1)$$

in which the exponential factor $\exp(-4z/q\beta)$ is introduced for the sake of convergence.

The divergency in the second series cannot be so removed. Nevertheless, since this series is not directly used in the analysis, the following function V_0 may be used instead:

$$a^3 V_0 = a^3 \left\{ \mu + \sum_{q=1}^{\infty} (\mu_q + \mu_{-q}) \right\} \quad (2)$$

which is also defined in the writer's paper.[4] This function is formally the partial derivative of the second series with respect to z and becomes convergent when it is so arranged.[5]

[1] By Akira Atsumi, published in the March, 1960, issue of the JOURNAL OF APPLIED MECHANICS, vol. 27, TRANS. ASME, vol. 82, Series E, pp. 87–92.

[2] Director, Institute of Mathematics, Academia Sinica, Taiwan, China.

[3] Chih-Bing Ling, "Stresses in a Circular Cylinder Having a Spherical Cavity Under Tension," *Quarterly of Applied Mathematics*, vol. 13, 196, pp. 381–391.

[4] Chih-Bing Ling, "Stresses in a Stretched Slab Having a Spherical Cavity," JOURNAL OF APPLIED MECHANICS, vol. 26, TRANS. ASME, vol. 81, Series E, 1959, pp. 235–240.

[5] It may also be mentioned that certain functions in two other papers by the same author are divergent too, namely, the functions (1) and (2) in the paper, "Stresses in a Plate Under Tension and Containing an Infinite Row of Semi-Circular Notches," *Journal of Applied Mathematics and Physics* (ZAMP), vol. 8, 1957, pp. 466–477; and also the functions (4) and (12) in the paper, "Stress Concentrations in the Strip Under Tension and Containing an Infinite Row of Semi-Circular Notches," *Quarterly Journal of Mechanics and Applied Mathematics*, vol. 11, 1958, pp. 478–490. Consequently, modifications should be made to remove the divergency in these functions. Besides, in the latter paper the expressions (15) should be read as follows:

$$I_k = \frac{2^k}{k!} \int_0^{\infty} \frac{u^k}{\sinh 2u + 2u} \left(1 + 2\sum_{q=1}^{\infty} \cos q u\beta\right) du,$$

$$J_k = \frac{2^k}{k!} \int_0^{\infty} \frac{u^k e^{-2u}}{\sinh 2u + 2u} \left(1 + 2\sum_{q=1}^{\infty} \cos q u\beta\right) du.$$

Furthermore, it seems that owing to the periodicity along the z-axis the analysis can be simplified considerably if the sets of biharmonic functions are constructed by using Fourier series directly. Consider two fundamental biharmonic functions in the following form:

$$\chi_0 = a^3U_0 + a^3\sum_{n=1}^{\infty}\{\psi_1(n)I_0(nkr) + \psi_2(n)\,nkr\,I_1(nkr)\}\sin nkz \tag{3}$$

$$\chi_0' + a^3V_0 + a^3\sum_{n=1}^{\infty}\{\psi_3(n)I_0(nkr) + \psi_4(n)\,nkr\,I_1(nkr)\}\sin nkz$$

where $k = 2\pi/\beta$. It can be shown that they satisfy the boundary condition of no normal and tangential stresses on the surface $r = 1$ provided that

$$\psi_1(n) = \frac{2}{n\pi}\frac{n^2k^2I_0(nk)K_0(nk) + \{n^2k^2 + 2(1-\nu)\}I_1(nk)K_1(nk)}{n^2k^2I_0^2(nk) - \{n^2k^2 + 2(1-\nu)\}I_1^2(nk)} - 2(1-\nu)\psi_2(n)$$

$$\psi_2(n) = -\frac{2k}{\pi}\frac{I_1(nk)K_0(nk) + I_0(nk)K_1(nk)}{n^2k^2I_0^2(nk) - \{n^2k^2 + 2(1-\nu)\}I_1^2(nk)}$$

$$\psi_3(n) = \{n^2k^2 - 2(1-\nu)(1-2\nu)\}\psi_2(n) \tag{4}$$

$$\psi_4(n) = \psi_1(n) + 4(1-\nu)\psi_2(n)$$

These results are obtained by applying Fourier transforms with the aid of the relation

$$\sum_{q=-\infty}^{\infty}\int_{-\beta/2}^{\beta/2}\frac{\cos nkz\,dz}{\{1+(z-q\beta)^2\}^{(2p+1)/2}} = \int_{-\infty}^{\infty}\frac{\cos nkz\,dz}{(1+z^2)^{(2p+1)/2}} = \frac{2(p!)}{(2p)!}(2nk)^pK_p(nk) \tag{5}$$

Now, define χ_{2s} and χ_{2s}' in a slightly different manner as follows, for $s \geq 1$:

$$\chi_{2s} = \frac{1}{(2s-1)!}\frac{\partial^{2s}\chi_0}{\partial z^{2s}}, \quad \chi_{2s}' = \frac{4s+1}{(2s+1)!}\frac{\partial^{2s}\chi_0'}{\partial z^{2s}} \tag{6}$$

The stress function may be constructed in the same form as in (24), i.e.,

$$\chi = \chi_{00} + T\sum_{s=0}^{\infty}(A_{2s}\chi_{2s} + B_{2s}\chi_{2s}') \tag{7}$$

The parametric coefficients involved are adjusted accordingly so as to satisfy the remaining boundary conditions on the surfaces of the cavities.

It can be shown that in the stress function thus constructed the series of χ_{2s} and χ_{2s}' contributes an axial tension of amount

$$4\pi a^2T(A_0 + 3B_0 - 2\nu B_0)/\beta$$

to the cylinder. Therefore an additional biharmonic function, say χ_{00}' must be added to the stress function to annul this axial tension. Here

$$\chi_{00}' = -\frac{2Ta^3}{3(1+\nu)\beta}(A_0 + 3B_0 - 2\nu B_0)\{3\nu r^2z + (1-2\nu)z^3\} \tag{8}$$

In the paper, the axial tension contributed by the stress function in (24) was not investigated. This has immediate consequence to the values of the stresses for they now only represent those due to an average unit axial tension acting in the cylinder, which, as will be inferred later, is numerically less than T.

It is thought that the present problem is physically significant not only as it is, but also in that it gives at the same time the stresses in a finite circular cylinder having a symmetrical spherical cavity when the cylinder is compressed axially between two parallel rigid plates. It is thus interesting to investigate the effect of the cavity on the axial deformation in such a finite cylinder. Let the cylinder be of length βa with its ends at $z = -\beta/2$ and $z = \beta/2$. It can be shown that the functions χ_{2s} and χ_{2s}' contribute no axial deformation to the cylinder, the function χ_{00}' contributes an amount

$$-4aT(A_0 + 3B_0 - 2\nu B_0)/E,$$

and the function χ_{00} contributes an amount $\beta aT/E$. Here E is the modulus of elasticity of the material of the cylinder. Therefore the fractional increase in the axial deformation owing to the presence of the cavity is equal to

$$-4(A_0 + 3B_0 - 2\nu B_0)/\beta$$

Author's Closure

The author wishes to express his thanks to Dr. Ling for his kind comment. The first comment paying much attention to the expressions of the stress functions in the present or some of my other papers would be appreciated, but for brevity some of the constant terms or the terms linear in one co-ordinate were omitted, respectively, as they contribute nothing to the stresses. The second comment regarding an axial tension of the stress function (24) in the author's paper may be partly contributed in consequence of which the discusser neglects each term of my fundamental stress functions χ_0 and χ_0' in Equations (10). That is the term of the first limit of the form $\lim_{k\to 0}\frac{\pi}{2}f(k)$ which enters of itself into χ_0 and χ_0', respectively, in Equations (10) while it did not appear in the discusser's Equation (3), when expanded by using Dirichlet's integral. The method of the integral is adopted; so that the problem is considered in this paper as the particular case when the number of cavities is very large and tends to infinity, and the axial tension obtained from each first limit is taken into consideration.

Subharmonic Oscillations of a Pendulum[1]

T. K. CAUGHEY.[2] The authors are to be congratulated on a very interesting and illuminating paper which should stimulate further interest in the study of nonlinear systems.

The analysis presented by the authors is quite simple, but the solution is complicated by the fact that high-order algebraic equations must be solved in order to achieve the necessary accuracy. In the interests of simplifying the analysis, the writer would like to present a solution which achieves a higher accuracy without having to solve high-order algebraic equations.

Writing equation (2) of the paper as:

$$\theta'' + 2k\theta' + (a - n^2q\cos nz)\sin\theta = 0 \tag{1}$$

Assume a solution of the form

$$\theta = A\cos(z + \sigma) \tag{2}$$

[1] By Richard Skalak and M. I. Yarymovych, published in the March, 1960, issue of the JOURNAL OF APPLIED MECHANICS, vol. 27, TRANS. ASME, vol. 82, Series E, pp. 159–164.

[2] Associate Professor of Applied Mechanics, California Institute of Technology, Pasadena, Calif.

Now

$$\sin\theta = \sin[A\cos(z+\sigma)]$$

$$= 2\sum_{i=0}^{\infty}(-1)^i J_{2i+1}(A)\cos(2i+1)(z+\sigma) \quad (3)^3$$

Substitute (2) and (3) into (1) and equate the coefficients of cos $(z+\sigma)$ and sin $(z+\sigma)$ to zero. From the resulting equations it is easy to show that

$$\left(\frac{\omega}{\omega_0}\right)_n^2 = \frac{2J_1(A)}{A \pm [J_{n-1}(A) - J_{n+1}(A)]} \cdot \left[(n^2q^2)^2 - \left(\frac{2kA}{J_{n-1}(A) + J_{n+1}(A)}\right)^2\right]^{1/2} \quad (4)$$

and

$$\sin n\sigma = \frac{2kA}{n^2q[J_{n-1}(A) + J_{n+1}(A)]} \quad (5)$$

$$n = 2, 4, 6, \ldots .$$

It is instructive to take the case where $n = 2$ and to compare it with the authors' results. This has been done for $q = 0.05$ and $k = 0.01$, the results are shown in Fig. 1 of this discussion. It will be seen that the present results agree almost exactly with the experimental data.

Stability. The authors use the method of Andronow and Witt to discuss the stability of their solutions. This method is quite adequate to discuss instabilities of the same type as the assumed solution, but cannot cover all the possible modes of instability. It is therefore instructive to examine the stability of the system by perturbing equation (1).

Let $$\theta = \theta_0 + \xi \quad (6)$$

where

$\theta_0 = A\cos(z+\sigma)$ is the steady-state solution
ξ = a small perturbation

Substituting (6) into (1) and retaining only the linear terms in ξ:

For simplicity set $k = 0$; thus

$$\xi'' + (a - n^2q\cos nz)\cos\theta_0\xi = 0 \quad (7)$$

Now

$$\cos[A\cos(z+\sigma)] = J_0(A) + 2\sum_{i=1}^{\infty}(-1)^i J_{2i}(A)\cos 2i(z+\sigma) \quad (8)$$

If (8) is substituted into (7), a Mathieu-Hill equation results. For $n = 2$, $A < \pi$ this equation may be approximated by the Mathieu equation

$$\xi'' + [\alpha + 2\beta\cos 2z]\xi = 0 \quad (9)$$

where $$\alpha = \frac{A + 4q[J_1(A) - J_3(A)]\cos 2\sigma}{2J_1(A)} \cdot [J_0(A)] + 4qJ_2(A)\cos 2\sigma \quad (10)$$

and

$$\beta = 2qJ_0(A) + \frac{A + 4q[J_1(A) - J_3(A)]\cos 2\sigma}{2J_1(A)} \cdot [J_2(A)\cos 2\sigma] \quad (11)$$

From equation (5), if $k = 0$ and $n = 2$

$$\sin 2\sigma = 0 \quad \text{or} \quad \cos 2\sigma = \pm 1 \quad (12)$$

Fig. 2, herewith, shows a plot of α and β in the stability chart for the Mathieu equation[4] for several values of q. It will be seen that branch of the curve, $\cos 2\sigma = 1$ (this corresponds to the lower branch of the authors' curve in Fig. 3) is unstable for all values of A. The branch $\cos 2\sigma = -1$ (this corresponds to the upper branch of the curve in Fig. 3 of the paper) is stable for small values of A, but as A is increased, a point is reached at which the system becomes unstable. For $q = 0.05$, the representative point enters region 1 for sufficiently large A, and the system becomes unstable as $\xi = e^{\alpha z}\cos z$. For $q \geq 0.25$, the representative point enters region 2 for sufficiently large A, and the system becomes unstable as $\xi = e^{\beta z}$. This type of instability suggests that a large amplitude solution of the form $\theta = z + c$ might be possible. The writer[5] has investigated quasi-steady rotational solutions of this type, both theoretically and experimentally, and has found that such solutions do exist, and indeed, for an appropriate choice of the initial conditions, may exist over a wide range of exciting frequencies.

[3] L. Pipes, "Applied Mathematics for Engineers and Physicists," McGraw-Hill Book Company, Inc., New York, N. Y., 1946.

[4] N. W. McLachlan, "Theory and Applications of Mathieu Functions," The Oxford Press, New York, N. Y., 1947.

[5] T. K. Caughey, "Hula Hoop—An Example of Heteroparametric Excitation," *American Journal of Physics*, vol. 28, February 1960, pp. 104–109.

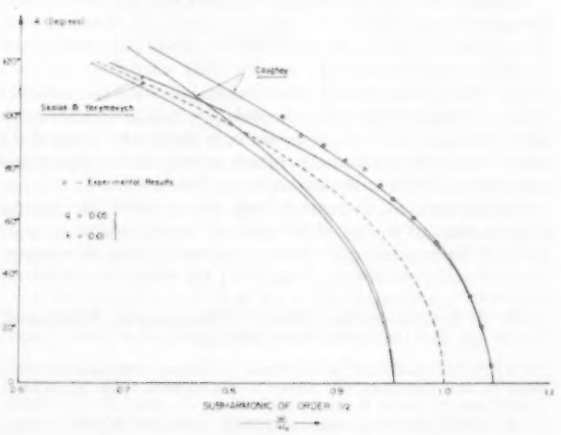

Fig. 1

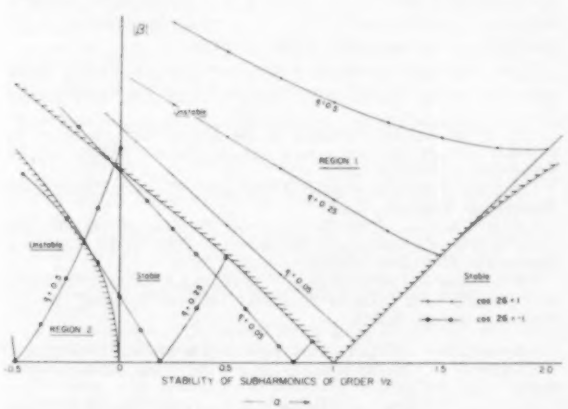

Fig. 2

Steady-State Undamped Vibrations of a Class of Nonlinear Discrete Systems[1]

T. K. CAUGHEY.[2] The author is to be congratulated on a very interesting paper which should stimulate interest in the field of nonlinear vibrations.

The writer was particularly interested in the examples given by the author, since the writer's doctoral thesis[3] was on the subject of forced oscillations in multidegree-of-freedom nonlinear systems. The writer[3] examined the stability of the steady-state solutions and showed that a necessary, but not in general sufficient, condition for stability was that the solutions lie outside the region enclosed by the locus of vertical tangency. By particularizing to a two-degree-of-freedom undamped system, the writer was able to show that the foregoing condition was also a sufficient one. Inspection of the author's response curves graphically illustrates this result.

Author's Closure

The author would like to thank Dr. T. K. Caughey for his comments. The author in his paper was primarily concerned with demonstrating the effect of the values of the natural frequencies corresponding to the linear part of the system on the qualitative nature of the solutions.

It is interesting that although the theory in the reference given by Dr. Caughey, due to its restrictions on the linear natural frequencies, does not strictly apply to examples given by the author, the conclusions arrived at by Dr. Caughey agree with the experimental results of the author.

A study of stability of steady-state solutions of a class of nonlinear problems more restricted as to the nature of the nonlinear terms than those discussed by Dr. Caughey, but with much weaker restrictions on the values of the linear natural frequencies, is the subject of a report by Mr. S. T. Chow and the author.[4]

Effect of the Wall on Two-Phase Turbulent Motion[1]

J. L. LUMLEY.[2] The authors' paper is interesting as a first attack, perhaps casting qualitative light, on a very difficult problem. There are, however, basic simplifying assumptions in the statement of which this writer feels the authors have not been sufficiently explicit, and which cause serious reservations in the quantitative interpretation of their results.

Most important, perhaps, is the fact that the fluid velocity appearing in the authors' equations must be at the instantaneous location of the particle; the fluid velocity that the particle sees is dependent on its position (which is dependent on the velocity it sees). Since the two (particle position, and fluid velocity at the particle position) are so strongly related to each other, it is not sufficient to say that a "stationary (i.e., without considering the probability for a particle to be at a certain state at any time, but considering what would happen if it is there) solution is attempted. . ." The solution obtained by the authors is equivalent to assuming the velocity field to be spatially uniform (a function of time only) or that the velocity seen by the particle and the particle position are statistically independent, which violates the dynamics. The consequences of this assumption are particularly serious in an inhomogeneous field.

A related difficulty is brought up by the use of the Lagrangian power spectrum for the power spectrum of the velocity seen by the particle. This will be accurate only if the particle follows the fluid motion perfectly, in which case the complicated dynamical equations used are not necessary. For a particle which nearly follows the fluid, the use of the Lagrangian velocity may be justified for short diffusion times, but a definite relation between particle parameters and Lagrangian scales must be presented to validate this. In particular, the problem as a whole can probably be formally validated as a first approximation for particles that almost follow the fluid motion, and this should be done. Again, such a validation is particularly necessary in the case of an inhomogeneous field, in which the particle after a time wanders into a region with different statistical properties.

It may be remarked in passing that an expansion such as the authors' equation (19) is formally invalid for a stationary random function[3] such as the Lagrangian velocity; indeed, the question of whether, in a nonhomogeneous flow, the Lagrangian velocity is stationary deserves some discussion.

Mechanics of the Sheet-Bending Process[1]

J. M. ALEXANDER.[2] The authors are to be congratulated for having tackled this complex problem and for having presented their analysis in such a concise manner. In studying the allied problem of the moderate bending of wide sheet referred to in the paper, the writer found that there is little or no theoretical consideration of the important problem of springback. For this reason, the authors' contribution is of great value and is to be commended to the consideration of both users and designers of sheet-metalworking equipment.

Basically, the problem of estimating the residual stresses (and consequently the elastic recovery) in a plastically deformed component is fairly simple, as may be seen from the few fundamental equations of equilibrium and compatibility set out at the start of the paper. The complexity arises mainly from the difficulty of establishing a meaningful nomenclature to cope with the addition of elastic and plastic stress states in the several zones of the sheet. It is believed that the authors have dealt with this aspect very clearly in that their notation is easy to follow.

Another example of metal deformation in which the residual stresses may attain values sufficient to cause yielding is to be found in the expanding of a hole in a plate by uniform pressure. In collaboration with Prof. Hugh Ford, the writer has considered

---

[1] By P. R. Sethna, published in the March, 1960, issue of the JOURNAL OF APPLIED MECHANICS, vol. 27, TRANS. ASME, vol. 82, Series E, pp. 187–195.

[2] Associate Professor of Applied Mechanics, California Institute of Technology, Pasadena, Calif.

[3] T. K. Caughey, "The Existence and Stability of Periodic Motions in Forced Non-Linear Oscillations," PhD thesis, California Institute of Technology, Pasadena, Calif., 1954.

[4] S. T. Chow and P. R. Sethna, "Steady State Damped Vibrations and Stability of a Class of Nonlinear Discrete Systems," WADC Technical Report 59-543.

[1] By S. L. Soo and C. L. Tien, published in March, 1960, issue of the JOURNAL OF APPLIED MECHANICS, vol. 27, Trans. ASME, vol. 82, Series E, pp. 5–15.

[2] Assistant Professor of Engineering Research, The Pennsylvania State University, University Park, Pa.

[3] G. K. Batchelor, "The Theory of Homogeneous Turbulence," Cambridge, The University Press, 1956, pp. 29, 30.

[1] By B. W. Shaffer and E. E. Ungar, published in the March, 1960, issue of the JOURNAL OF APPLIED MECHANICS, vol. 27, TRANS. ASME, vol. 82, Series E, pp. 34–40.

[2] Reader in Plasticity, Imperial College of Science and Technology, University of London, London, England.

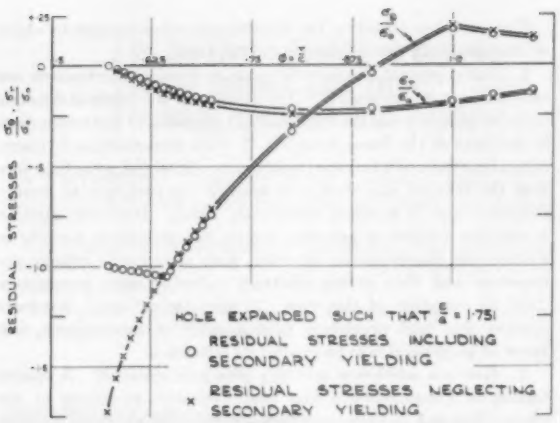
RESIDUAL STRESSES
HOLE EXPANDED SUCH THAT a/a = 1.751
RESIDUAL STRESSES INCLUDING SECONDARY YIELDING
RESIDUAL STRESSES NEGLECTING SECONDARY YIELDING

Fig. 1

this problem in some detail, and an estimate of the "relaxation" of the residual stresses resulting from this "secondary" yielding was reported in a paper published some time ago.[8] Fig. 1 herewith is a reproduction of Fig. 10 of that paper and illustrates how the residual stresses were reduced by this secondary yielding below those found if secondary yielding was neglected. The authors might be interested to note the similarity in their method of attack. In particular, Prof. Ford and the writer simulated the release of the expanding pressure by adding a tensile stress at the periphery of the hole to give the superimposed elastic stresses during recovery, much in the same way as the authors have superimposed a bending moment of opposite sign in the problem under discussion.

Authors' Closure

The authors wish to thank Dr. Alexander for his kind comments, which are particularly welcome in view of his own significant contribution to the solution of an allied problem dealing with bending of wide plates and with residual stresses. It should be noted that Dr. Alexander's and the present plate analyses provide solutions for different aspects of the same problem and thus tend to complement each other.

Approximate Synthesis of Spatial Linkages[1]

D. P. ADAMS.[2] The authors refer to their method as being a generalization of that of Freudenstein, but it would appear that it could stand completely on its own merits. Freudenstein's contribution lay primarily in obtaining equation (1) as the simplest possible equation for the four-bar linkage. It was an important advance, but a comparable development does not appear to have been necessary for the authors. The authors' system of linear equations is so basic an attack that the parallelism with Freudenstein appears as an inevitable result rather than a motivating factor.

The importance of such an approach cannot be overemphasized in view of advances in computing techniques, machining processes, and materials in recent years. With respect to the first of these, the authors have acknowledged their indebtedness for facilities and programming suggestions. It is doubtful that such a paper would have been considered practical 15 years ago. Today the authors are able to include specific results, and the paper is able to illumine clearly the very great possibilities of the general technique which they have already set forth in earlier publications of which the present paper presents such good examples. Clearly for the kinematician, as for so many engineers and scientists, the computer has become a way of life.

One of the great advantages of the plane four-bar mechanism is its simplicity of manufacture and operation. The corresponding lower-pair space mechanisms retain much of this simplicity. The spherical is the most difficult of the six motions, yet with modern materials, tooling, and lubrication, the possibility of good three-point contact is available by a linear, compensable adjustment, and its potentialities loom greater than ever before.

Perhaps the major difficulty with these mechanisms is due to binding. There may be situations in which vibration of suitable magnitude and frequency can be introduced whenever binding registers to create forces especially adapted to relieve it.

The authors are to be congratulated on such a stimulating paper. In addition to its direct utility, it offers the immediate possibility of corresponding optimizing programs plus the extensions where feasible to higher orders of agreement between the desired and derived functions. Each moving member can be regarded as an extended body and the path of one of its points synthesized into approximate agreement with some desired path. An effective pattern in two dimensions for expression in three dimensions has recently been set up for several of these projects by papers from Columbia University.[3, 4, 5]

FERDINAND FREUDENSTEIN.[6] The authors are to be commended for this further substantial contribution in the field of three-dimensional kinematics, in which field they have already established themselves by previous work on matrix notation and analysis. This is believed to be the first American paper—and one of the first anywhere—on three-dimensional *synthesis*, and the methods described appear to be well suited to the use of programmed computers.

R. A. BEYER.[7] Both authors, well known for their research work done in the analysis and synthesis of plane and spatial mechanisms—in Europe and particularly in Germany—have made an excellent contribution in this paper. It is of high caliber, not only as to its contents concerning progress in kinematical topics, but also in connection with the general point of view applied in their investigations and by the skillfulness of their methods. In these they derive properties of 3-D mechanisms and spherical mechanisms from those of plane mechanisms. They choose the "four-bar linkage of plane kinematics" as the starting-point for

[8] J. M. Alexander and Hugh Ford, "On Expanding a Hole From Zero Radius in a Thin Infinite Plate," Proceedings of the Royal Society, Series A, vol. 226, 1954, pp. 543–561.

[1] By J. Denavit and R. S. Hartenberg, published in the March, 1960, issue of the JOURNAL OF APPLIED MECHANICS, vol. 27, TRANS. ASME, vol. 82, Series E, pp. 201–206.

[2] Associate Professor of Mechanical Engineering, Massachusetts Institute of Technology, Cambridge, Mass.

[3] F. Freudenstein and G. N. Sandor, "Synthesis of Path-Generating Mechanisms by Means of a Programmed Digital Computer," *J. Engineering for Industry*—TRANS. ASME, vol. 81, Series B, 1959, pp. 159–168.

[4] G. N. Sandor and F. Freudenstein, "Kinematic Synthesis of Path-Generating Mechanisms by Means of the IBM 650 Computer," IBM Program Library File no. 9.5.003, obtainable from Applied Programming Publications, IBM Corp., 590 Madison Ave., New York, N. Y.

[5] F. Freudenstein, "Structural Error Analysis in Plane Kinematic Synthesis," *J. Engineering for Industry*—TRANS. ASME, vol. 81, Series B, 1959, pp. 15–22.

[6] Professor and Chairman, Department of Mechanical Engineering, Columbia University, New York, N. Y. Assoc. Mem. ASME.

[7] Professor, Olching near Munich, Germany.

generalization of the displacement equations to the solutions of 3-D-problems.

The results which the authors obtain in their practical applications for function generation, for angular velocities and for angular accelerations, and so on (programmed moreover for computer use) indicate that the authors are on the right track for continuing further research work in this direction.

With respect to these general remarks the American reader perhaps will be interested in some research made by the discusser concerning similar problems in three-dimensional kinematics:

(*a*) "Research About Dead-Positions of a Spatial Four-Bar Linkage," *Maschinenbau/Betrieb*, vol. 19, 1940, pp. 265–267.

(*b*) "Constructions for the Spatial Slider-Crank Mechanism," *Maschinenbau/Betrieb*, vol. 23, 1944, p. 133.

(*c*) "Synthesis of the Spatial Slider-Crank Mechanism," *Maschinenbau/Betrieb*, vol. 23, 1944, p. 199.

(*d*) "Synthesis of Plane and Spatial Crank Mechanisms," *VDI Forschungsheft* No. 394, Berlin, VDI-Verlag, 1939.

Additional references on the subject are to be found in R. Beyer and E. Schörner, "Raumkinematische Grundlagen," Munich, Barth, 1953.

Summarizing, it will be observed that this paper represents a remarkable step forward toward knowledge about the synthesis of spatial mechanisms and toward interesting the designer in applying these methods.

T. P. GOODMAN.[8] The straightforwardness of the authors' approach to this formidable problem and the accuracy of their results, as shown in Examples (*b*) and (*c*), are indeed impressive. In view of the great generality of their method, it would be of interest to know whether any general statement can be made at this time as to which additional mechanisms are susceptible to this approach; i.e., which additional mechanisms have displacement equations which can be put in the form of equation (2) of the paper.

To obtain additional accuracy points, it appears that either the analysis could be extended in the hope of finding a spatial analog for Freudenstein's five-point synthesis of four-bar linkages, or a scanning procedure could be used to repeat the computer solution while systematically varying the arbitrary parameters such as starting angles. It would be of interest to have the authors' opinion as to which of these alternatives seems more promising.

A third matter on which the authors' comments would be of interest is the range of transmission angles encountered in the spatial mechanisms which the authors have designed. If the transmission angles are favorable in the mechanisms of Examples (*b*) and (*c*), these might well be the first two entries in an atlas of spatial linkages.

Authors' Closure

We wish to thank the several discussers for their interest, kind remarks, and informative contributions.

It is true, as Professor Adams notes, that binding may be a problem with spatial linkages, especially those with cylinder pairs. Recent developments in ball-bushings and ball-splines may eliminate most of the anticipated difficulties; the ball-bearing screw is already a very useful kinematic pair.

[8] Kinematics Engineer, General Engineering Laboratory, General Electric Company, Schenectady, N. Y. Assoc. Mem. ASME.

The questions raised by Dr. Goodman involve matters to which we can give only partial answers at this time.

1 *Can a general statement be made as to which mechanisms are susceptible to this approach?* The success of the method depends on being able to write the displacement equation of the mechanism in the form of the linear equation (2) with n coefficients k, themselves functions of n linkage parameters. It would seem therefore that the method can always be applied—in principle at least—provided that n is taken sufficiently small. However, since n is also the number of accuracy points, the procedure consists in writing the displacement equation with all possible linkage parameters and then giving arbitrary values to some parameters until an equation of the type (2) may be written. We have applied this trial procedure to a number of mechanisms, but know of no general rule to predict its outcome.

2 *How can additional accuracy points be obtained?* A spatial analog of Freudenstein's four and five-point syntheses of the planar four-bar linkage may in some cases be obtained without too much difficulty. For example, a four-revolute spherical mechanism may be designed with four accuracy points if μ_1 (then initial crank angle) is taken as a design parameter. In this case, a second-degree compatibility equation is required, but the problem may be handled on a desk calculator. In other cases, however, a higher-degree compatibility equation, or more than one compatibility equation, may be required. Although less elegant, the scanning procedure in which a solution is repeated while systematically varying an arbitrary parameter has two advantages. It uses a simpler, and therefore cheaper, computer program, and provides a family of solutions from which the designer may choose, not only from the viewpoint of accuracy but also that of practicability. It must not be forgotten that while the present method yields mathematically exact results, these results may be completely impractical. We have, for example, had experience with a problem involving a logarithmic function generator of the two-revolute, two-spheric pair type in which the coupler was to be 150 times the length of the crank! With a different initial follower angle, more acceptable dimensions were obtained.

3 *What are the transmission angles in Examples (b) and (c)?* The exact meaning of the transmission angle in the case of spatial linkages seems difficult to define at this time, and we would prefer to keep our statement somewhat vague and to speak of force transmission qualities. Using breadboard components, a model of the mechanism of Example (*c*) was built and operates within its useful range without binding or excessive errors. No model was built of the mechanism of Example (*b*), but drawings in different positions indicate that good force transmission may also be expected of this mechanism.

When the crank of a planar four-bar linkage has a specified position, the mechanism may be closed for two different positions of the follower, forming either an "open" or a "crossed" linkage. Should the linkage proportions be such that only one follower position is possible, the transmission angle is then either zero or 180 deg, and no force may be transmitted from the crank to the follower. For other linkage proportions, there is a relation between the transmission angle and the two possible follower angles. It seems that a similar property holds for spatial linkages, the problem being more involved since there may be more than two ways of closing a spatial linkage. We feel that a rigorous study of the force transmission properties of spatial linkages is one of the most challenging problems in kinematics today.

On the Elastic Bending of Columns Due to Dynamic Axial Forces Including Effects of Axial Inertia[1]

N. F. SPRAGGINS.[2] Contrary to the statements made by the author, investigators in the past have considered axial-inertial effects in the solution of equations of dynamic column loading; e.g., Lubkin and Stoker[3] as well as the writer's thesis work in 1947. In both of these instances, we were able to include the effects of "axial inertia" by resorting to Mathieu equation solution. In fact, these solutions bring out some very interesting phenomena in the "stability bands" of column geometry. It is the writer's belief that, if some of the results of the Mathieu solution were coupled with the computer data now possible, the art of calculating dynamic columns would be greatly expanded.

It is hoped that in his future work the author will consider some of the possible combinations in his endeavors in this field.

[1] By Eugene Sevin, published in the March, 1960, issue of the JOURNAL OF APPLIED MECHANICS, vol. 27, TRANS. ASME, vol. 82, Series E, pp. 125–131.

[2] Mechanical Engineering Division, Atlantic Research Corporation, Alexandria, Va. Mem. ASME.

[3] S. Lubkin and J. J. Stoker, "Stability of Columns and Strings Under Periodically Varying Forces," *Quarterly of Applied Mathematics*, vol. 1, 1943, pp. 215–236.

Journal of APPLIED MECHANICS — Book Reviews

Fluid Mechanics

Advances in Applied Mechanics, Volume 6. By H. L. Dryden, Th. von Kármán, and G. Kuerti, Editors. Academic Press, Inc., New York, N. Y., 1960. Cloth 6¼ × 9¼ in., x and 294 pp. $9.00.

REVIEWED BY J. KESTIN[1]

THE sixth volume of the well-known and well-appreciated series of "Advances" continues the high standards of its predecessors. It contains five concise, highly informative, and well-written contributions, each of them dealing with some aspect of Fluid Mechanics. "They range"—to quote the Preface—"from a short review of recent experimental work on vortex sheets to a treatment of the flow of a gas in a boundary layer under extreme conditions which give rise to dissociation of the gas. In order to describe such a flow adequately, it is necessary to consider the underlying physical principles of the kinetics of gases and to apply the concepts of statistical mechanics.

"The major article in the volume is an extensive survey of similarity methods in aerodynamics, constituting a textbook in miniature on this important subject."

The first contribution, entitled "The Theory of Unsteady Laminar Boundary Layers," by K. Stewartson, is an intensely mathematical treatment of this fascinating, and in the reviewer's opinion, very important topic. Emphasis is placed mainly on impulsive motion in an attempt to develop an intuitive feeling for the essential characteristics of the relevant solutions of the Navier-Stokes equations under the circumstances, without, evidently, possessing the solutions themselves. Incidentally, on a matter of nomenclature, the reviewer recently verified that the problem which the author, along with many others, describes as "Rayleigh's problem" (impulsive start of an infinite flat plate in a viscous fluid) was first solved by Stokes, and that Lord Rayleigh fully acknowledged the fact in his later contribution.

In discussing fluctuating boundary layers, the author, in this reviewer's opinion, unduly concentrates on series expansions and somewhat neglects the very important investigation of secondary, steady flows which nearly always accompany oscillations. It is true that secondary flow is "higher order," but there seems to be ample evidence to suggest that it plays a dominant part in the physical process, particularly in the middle frequency range. Inadequate emphasis is placed on the circumstances that calculating flow fields "to first order" is physically equivalent to neglecting secondary flows. An excellent insight into the importance of this aspect of fluctuating boundary layers can be gained from C. C. Lin's admittedly incomplete, theory (Proc. 9th Intern. Congress of Applied Mechanics, Brussels, vol. 4, p. 155), and it is regrettable that an account of it has not been included in the article.

The second contribution by G. Ludwig and M. Heil on "Boundary Layer Theory With Dissociation and Ionization" plunges the reader into the mysteries of the Maxwell-Boltzmann equation and very heavy mathematics which the reviewer does not pretend to be familiar with, except for the conviction that he would like to see better agreement with measurements in the more modest ranges of temperature before accepting the results of extrapolating the method to exalted ranges of temperature and to complex mixtures of species.

The third article by W. Chester on "The Propagation of Shock Waves Along Ducts of Varying Cross Section" delivers exactly what is promised in the title, just as does the contribution by K. Oswatitsch on "Similarity and Equivalence in Compressible Flow"—the textbook in miniature mentioned earlier.

The volume concludes with a very interesting, very short, and very informative article by R. Wille on recalcitrant "Kármán Vortex Sheets."

[1] Division of Engineering, Brown University, Providence, R. I.

Droplet Evaporation

Evaporation and Droplet Growth in Gaseous Media. By N. A. Fuchs. Translated from the Russian by J. N. Pratt. Pergamon Press, New York, N. Y., 1959. Cloth, 8¾ × 5¾ in., 72 pp. $5.50.

REVIEWED BY R. H. SABERSKY[1]

THE above-mentioned book represents a rather thorough survey of the work which has been done in the specialized field of droplet evaporation. The survey includes references published in the early 1950's. The book is short, about 70 pages, and its content is subdivided into three chapters. In the first and longest (37 pages) a detailed discussion is given of the evaporation of a motionless droplet excluding the effects of free or forced convection. Maxwell's theory of evaporation is presented and several extensions of this theory are discussed. Among these are the effects of the convection current induced by diffusion (the so-called Stefan current), the influence of confining walls, the role of the concentration gradient in the immediate neighborhood of the droplet surface (within a distance of the order of a mean free path), and the corrections required for nonspherical droplet shapes. An analysis of the temperature profile is also given. In

[1] Associate Professor, Division of Engineering, California Institute of Technology, Pasadena, Calif.

order to be able to interpret experimental results, the effect of suspension filaments and thermocouple wires on the temperature is analyzed. Chapter I closes with a careful interpretation of available experimental results, and the author concludes that ". . . . Maxwell's theory of droplet evaporation can be considered as supported by experiment. . . ."

The second chapter is devoted to work in which moving droplets are considered. This problem is not nearly as well understood as that involving a stationary droplet. Several attempts at an analytical solution are discussed and some experimental results are presented. The experiments by Frössling are emphasized. The author points to the differences in results obtained for low Reynolds numbers and states that ". . . the problem of evaporation of droplets at small Reynolds numbers can by no means be considered as solved."

In the third chapter the nonstationary effects of evaporation are considered. The analysis for a motionless droplet is again given in some detail and the author finds that for small drops the quasi-stationary approximation is often sufficient. Approximations to the characteristic times for the evaporation of moving droplets are mentioned briefly.

The book will be of value to those interested in the specialized field in question. To avoid disappointment, the prospective buyer should know that this book has been reproduced by photo-offset from a typewritten manuscript.

Aerodynamics

Incompressible Aerodynamics. By Bryan Thwaites, Editor. Oxford University Press, New York, N. Y., 1960. Cloth, 6 × 9 in., xx and 636 pp. $12.

REVIEWED BY R. E. MEYER[3]

It is difficult to imagine now the full sensation in fluid dynamics and aeronautical engineering caused by the appearance of Durand's "Aerodynamic Theory" in the 1930's. It presented with sudden clarity a whole new chapter of science previously known to only the few who had created and reported it in a confusion of dispersed and unconnected papers. The collective account not only boosted aerodynamic research and engineering, it also encouraged the early publication of further collective works in the new fields explored during the sweeping surge of fluid dynamics which followed, from "Modern Developments" in 1938 to the "Princeton Series" still in progress of publication. Meanwhile, however, a gap has appeared in the serried ranks of the monograph series because the original Aerodynamic Theory has gone rather out of date.

It is into this gap that Thwaites has stepped with his "synthesis of original contributions" by 16 among the foremost British aerodynamicists. It presents a comprehensive, up-to-date account of the aerodynamics of wings and related bodies in steady flight at low Mach number and high Reynolds number. Actually, the book was not conceived as a new version of Durand's great series, but rather as the third volume of a new version of Goldstein's "Modern Developments." Accordingly, it is an account, not only of theory, but equally of experiment. Moreover, a great deal of attention has been devoted to some design aspects of the subject in order to avoid, as far as possible, even the appearance of a gap between pure science and engineering.

So comprehensive a purpose would have been ambitious even for a series of a dozen volumes. To achieve it in 570 pages has required considerable sacrifices. The bulk of the book consists of a string of what common parlance calls (so inappropriately) "digests" of original papers and groups of such papers. Collectively, they are made to tell a consistent and comprehensive story, but individually, they are too brief to be fully understandable. There is no room for the painstaking explicitness of a Goldstein in explaining the limitations of the evidence on which the theoretical or experimental results rest. The account must restrict itself almost entirely to the presentation of the best available results. Only too often, of course, the best available is merely tentative and preliminary. In many instances, these shortcomings will presumably be made good in the first two volumes of the series, but in others no redress is in sight.

The scope and purpose of the book would seem to remove it far from the ranks of the textbooks. In this reviewer's opinion, however, it occupies an outstanding place among them because of the passionate determination of the Editor to relate every sentence to physical reality. Rather than fail in this purpose, he exposes himself to the occasional charge of recklessness and of letting emphasis verge on dogmatism.

It cannot be counted as a criticism that the book will be found unsatisfactory by all the readers approaching it from a single point of view, whether it be the experimenter's, the theoretician's, designer's, or student's. Its primary purpose and merit lie in providing information, prodigious amounts of information, which is not only authoritative and useful, but the very existence of which was in many cases nearly impossible to discover from the normally published literature. The 37 pages of references alone would have constituted a valuable publication. If a substantial part of your work is in fluid mechanics, you will need this book.

[3] Division of Applied Mathematics, Brown University, Providence, R. I.

Linear Viscoelasticity

The Theory of Linear Viscoelasticity. International Series of Monographs on Pure and Applied Mathematics, vol. 10. By D. R. Bland. Pergamon Press, New York, N. Y., 1960. Cloth, 5½ × 8½ in., vi and 124 pp. $7.50.

REVIEWED BY WILLIAM PRAGER[4]

This introduction to the concepts and methods of linear viscoelasticity could well serve as a text for a one-semester course at the beginning graduate level. The exposition is very concise but clear. The mathematical background required from the reader unavoidably includes some familiarity with transform techniques.

The first two chapters are concerned with the mathematical description of linear viscoelastic behavior under uniaxial stress (Chap. I) and under combined states of stress (Chap. II). The treatment in Chap. II closely follows that in a recent paper of the author (*Proc. Roy. Soc.*, A, 250 (1959) 524). The next three chapters deal with problems of stress analysis in linearly viscoelastic bodies. Chap. III is concerned with problems involving sinusoidally varying stresses and strains, Chap. IV with quasi-static problems in which all inertia effects can be neglected, and Chap. V with dynamic problems. The fitting of simple models to measured values of the complex modulus or compliance is discussed in Chap. VI.

Since so much has been packed into the 124 pages of the text, the absence of a subject index is to be regretted.

[4] L. Herbert Ballou University Professor, Brown University, Providence, R. I. Mem. ASME.

Journal of APPLIED MECHANICS

Information for Authors

• Manuscripts should be submitted in final form to the Technical Editors. Each manuscript must be accompanied by a statement that it has not been published elsewhere nor has it been submitted for publication elsewhere. A paper which would occupy more than five pages of the Journal may be returned to the author for abridgment.

• The author should state his business connection, the title of his position, and his mailing address. A short abstract (50 to 100 words) should be included on the first page immediately preceding the introductory paragraph of the paper.

• Three copies of the manuscript are required. One of these must be a carefully prepared printer's copy, typed in double spacing, on one side of the page only, with wide margins, on $8^1/_2$ by 11-in. opaque white paper. Mimeographed manuscripts, if prepared with exceptional care, can be accepted provided they are completely edited.

• As far as possible, all mathematical expressions should be typewritten. Greek letters and other symbols not available on the typewriter should be carefully inserted in ink. Care should be taken to distinguish between capital and lowercase letters, between zero (0) and the letter (*O*), between the numeral (1) and the letter (*l*), etc. A letter representing a vector cannot be printed with an arrow above or below it. The letter should be underscored with a single wavy line, wherever it appears in the text, to designate boldface type. A list of symbols carefully marked for the use of the editor (thus: κ, Greek l.c. kappa), if it has not been included in the body of the paper, should accompany the manuscript on a separate page.

• Before preparing a manuscript the author should study printed articles in the Journal, with special attention to the form and style of mathematical expressions, tables, footnotes, references, and abstract. Numbers that identify mathematical expressions should be enclosed in parentheses. Numbers that identify references at the end of the paper should be enclosed in brackets. Care should be taken to arrange all tables and mathematical expressions in such a way that they will fit into a single column when set in type. Equations that might extend beyond the width of one column (fractions that should not be broken or long expressions enclosed in parentheses) should be rephrased to go on two or more lines within column width. Fractional powers are preferred to root signs and should always be used in more elaborate formulas. The solidus should be used instead of the horizontal line for fractions wherever possible.

• A normal paper should not exceed five pages in the Journal. It is about 6000 words or twenty to twenty-five double-spaced typewritten pages inclusive of drawings. A Brief Note should not exceed 750 words or about one column in the Journal inclusive of drawings.

• Originals and two copies of figures must accompany the manuscript. Line drawings should not be larger than $8^1/_2 \times 11$ inches and should be planned for reduction to column width. Lettering should be large enough to be clearly legible when the illustration is reduced. The originals of line drawings must be in India ink on white or pale blue tracing paper or tracing cloth. Photographs of equipment or test specimens must be glossy prints and should be used sparingly. Captions for figures should be typed double-spaced and included as the last page of the manuscript. The figure number and author's name should be written in the margin or on the back of each illustration.

• Titles of papers should be brief.

• Authors can obtain copies of the ASME Manual MS-4, "An ASME Paper," from the Technical Editors and are urged to do so before drafting their papers in final form.

• Papers published in the Journal of Applied Mechanics must be presented at a Meeting, either in person or by title. Scheduling of papers is in the hands of the Secretary of the Applied Mechanics Division. Authors should indicate their preference in this respect to the Technical Editors when submitting a paper.

• An author is entitled to 25 preprints free of charge (in the case of two authors, 15 each; three or more authors, 10 each). Larger quantities of preprints or reprints can be ordered from Editorial Department, The American Society of Mechanical Engineers. 29 West 39th Street, New York 18, N. Y. Quotations will be sent on request.

ASME Publications Committee

Please address all communications to:

Technical Editors

Journal of Applied Mechanics, ASME

Division of Engineering

Brown University

Providence 12, R. I.

Proceedings of Symposia and Conferences Sponsored by ASME Applied Mechanics Division

SHOCK AND STRUCTURAL RESPONSE

Presents specific, useful information on the methods and the scope of procedures developed for determining shock and structural responses

The coverage includes the nature and origin of shock loading with examples from several fields; the different kinds of shock spectrum, their characteristics and applications, techniques and instruments used for shock measurement; and the presentation of data for engineering applications. Also dealt with are the responses of single-degree-of-freedom systems to shock and the various ways of presenting information for design application and for indicating the requirement for shock-testing machines to simulate conditions occurring in actual service; modal method of analysis for the determination of the response of complicated systems to shock spectra; and the applications of methods discussed throughout the book to some of the problems of missile bases designed to withstand ground shock produced by detonations.

Published 1960 **$4.50***

MECHANICAL IMPEDANCE METHODS FOR MECHANICAL VIBRATIONS

A reference for engineers specializing in vibration analysis and control

This book shows how impedance methods apply to lumped and continuous systems of simple and moderate complexity, reviews measurement techniques, demonstrates the power of digital computers by comparing the calculated and measured characteristics of a highly symmetrical system of moderate complexity, gives measured values of typical structures of large size and high complexity, discusses the importance of the impedance in influencing shock and vibration spectra measured in field service, indicates how to apply impedance methods to the calculation of vibration isolator effectiveness, treats impedance of some disordered systems, shows how impedance methods may be used to find the response to random excitation, and describes a dynamic stiffness method that has proved useful in predicting critical speeds of steam turbines.

Published 1958 **$5.50***

THERMODYNAMIC AND TRANSPORT PROPERTIES OF GASES, LIQUIDS, AND SOLIDS

A valuable survey of data and techniques on the thermal properties of important materials of engineering

The methods and important experimental findings in this book are based on the work of the foremost authorities in the field. They include a survey of the present theoretical and experimental state of the science; a large amount of new data on current experimental and theoretical techniques. These data cover thermodynamic and transport properties, PVT data and equation of state, some experimental transport properties, and high thermodynamic properties of gases. The forty-two papers in this book were originally presented at an ASME Symposium on Thermal Properties.

Published 1959 **$12.50***

SHOCK AND VIBRATION INSTRUMENTATION

Gives the principal results of research and development programs sponsored by various agencies

Random vibration, effect of nonrigid structures on vibration isolation, hysteresis and slip damping, vibration and shock testing, design approaches, and analog methods are some of the subjects covered. Emphasis is placed throughout on applicable basic principles rather than on explicit problems of only passing interest.

Contents: The Evaluation of Mounts Isolating Nonrigid Machines from Nonrigid Foundations. Experimental Study of the Effects of Foundation Resilience on Vibration Isolation. Effect of Material and Slip Damping on Resonance Behavior. Shock and Vibration Environments. Mechanical Design for Random Vibration and Shock. Influence of Electrical and Motional Impedance on the Control and Performance of Some Vibration Machines. Shock Testing Machines and Procedures. Damaging Potential of Shock and Vibration. High Speed Computing Methods for Shock and Vibration Problems.

Published 1956 **$5.00***

STRUCTURAL DAMPING

Provides a wealth of information useful in engineering design

This book discusses such structural damping techniques as interfacial slip damping, viscoelastic laminate damping, and coulomb or viscoelastic junction damping. The information has been written by authorities in the field.

Contents: Energy Dissipation Mechanisms in Structures, with Particular Reference to Material Damping. A Review of Progress in Analysis of Interfacial Slip Damping. Damping of Plate Flexural Vibrations by Means of Viscoelastic Laminae. Vibrational Energy Dissipation at Structural Support Junctions. Measurement of Damping. Material Design for Resonant Members. Selected Bibliography on Structural Damping.

Published 1959 **$4.25***

DESIGN DATA AND METHODS

Replete with data, procedures and solutions—all in a form most useful to design engineers

Here in forty-one contributions and 200 pages are data applying to the stresses and deflections of engineering structures, fluid mechanics problems, bearing design, vibration, and balancing.

Contents: Formulas and Methods of Calculating Stresses in Beams, Plates, and Shafts. Stress Component and Formulas. Design Data on Press- and Shrink-Fitted Assemblies. Design Data for Piping. Working Stresses. Numerical Values of Tangential Stress in Thick-Walled Cylinders. Numerical Solution of Gas Flow Problems. Procedures for Method of Characteristics for Two-Dimensional Supersonic Flow. Chart for Oblique Shock Waves under Water. Bearing Calculations. Methods of Solving Vibration and Balancing Problems.

Published 1953 **$4.00***

Proceedings, 3rd U.S. NATIONAL CONGRESS OF APPLIED MECHANICS

Presents the findings of original researches and discusses the current approach to problems

Within this 904-page volume are reports of important studies in the fields of dynamics, vibration, elastic waves, elasticity, elastic structures, plasticity, viscoelastic flow, fracture, fluid flow, aerodynamics, and heat transfer. There are also discussions of new concepts and methods, and a large amount of new data which will aid in generating new ideas and new approaches toward solving other problems of the applied mechanics field.

Published 1958 $20.00 to members and nonmembers

***20% discount to ASME members.** **NOTE: Save handling and mailing charges by including remittance with order.**

THE AMERICAN SOCIETY OF MECHANICAL ENGINEERS

29 West 39th Street New York 18, N. Y.